Phased Arrays: A Signals Perspective on the Human Condition

A. Meridian (pseudonym)

Contents

List of Figures

Executive Summary

Phased Arrays: A Signals Perspective on the Human Condition

Purpose

This technical brief presents a mathematical framework for understanding collective consciousness dynamics using Radio Frequency (RF) engineering analogies. The model provides quantitative tools for analyzing phenomena typically considered unmeasurable: collective awakening, paradigm shifts, perception management, and what various traditions term "ascension."

The brief is structured in two phases. Parts I–III (Chapters 0–10) build the engineering framework: torsion physics, individual consciousness as RLC circuit, collective humanity as phased array, and the control dynamics of injection locking and spin coherence. Parts IV–V (Chapters 11–16) apply this framework to civilizational questions — intervention history, systemic failure modes, paradigm shielding, and collective phase transition — with explicit confidence-level transitions at each boundary.

Core Thesis

RF engineering mathematics accurately models consciousness and social dynamics at both individual and collective scales.

The framework rests on three foundational mappings:

1. **Individual Consciousness = RLC Circuit**: The human psyche operates as a tuned receiver characterized by Resistance (R - energy dissipation/drag), Inductance (L - soul inertia/wisdom), and Capacitance (C - shadow/trauma storage). This creates a quality factor (Q) determining:
   - What **power levels** of consciousness an individual can safely receive (via impedance tuning)
   - How resistant they are to external control/capture (high Q rejects off-frequency injection locking)
2. **Collective Humanity = Phased Array Antenna**: When individuals synchronize (like antenna elements in phase), their collective reception capability scales quadratically with population and coherence squared ($N \cdot r^2$), not linearly.
3. **Awakening = Link Budget Closure + Impedance Matching**: Whether collective perception shift occurs involves:
   - Link budget closure: Source power + gains - losses > threshold
   - Collective impedance matching: synchronized individuals create better coupling to more powerful levels of consciousness
   - Changing of visible regions: as collective impedance rises, new consciousness bands become perceptible, unlocking access to what has been referred to as "higher planes" or "higher dimensions" of reality

Alignment with Theoretical Physics

The framework aligns conceptually with multiple directions in modern theoretical physics:

- **Asymptotic Safety**: UV scale-invariant fixed point structure. Source functions as the ultimate fixed point toward which all renormalization group flows converge.
- **Loop Quantum Gravity (LQG)**: Spin network / torsion focus. The torsion field substrate provides a mechanism for how spin coherence underlies spacetime geometry.
- **Teleparallel Gravity**: Torsion-based reformulation of General Relativity. Framework adopts torsion (rather than curvature) as the fundamental gravitational degree of freedom.
- **Holographic Principle / String Theory**: Information encoding on boundaries. Consciousness as boundary-layer information processing aligns with holographic entropy bounds.
- **Quantum Information Theory**: General nonlocality principles. The model treats consciousness as fundamentally nonlocal information processing, consistent with quantum information foundations.
- **Condensed Matter / Vorticial Spacetime Analogues**: Volovik (2003) and Huang (2016) demonstrated that spacetime geometry, gauge fields, and Standard Model particles can emerge from quantum liquid substrates. Our torsion framework proposes a specific mechanism—one that additionally explains consciousness phenomena, nonlocal information transfer, and biological antenna systems.

This places the framework within a legitimate—if frontier—branch of theoretical physics.

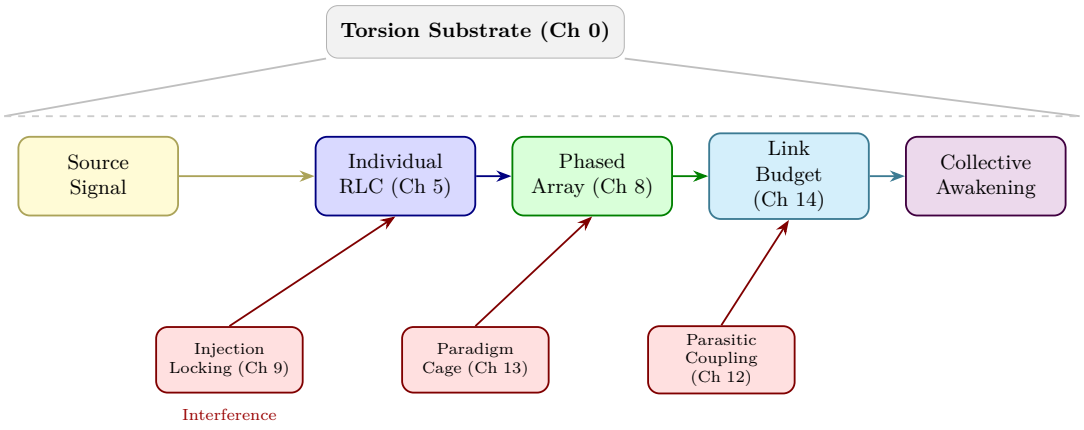

Figure ES.1: Framework overview — signal processing pipeline from Source through individual tuning, collective coherence, and link budget closure.

Key Technical Findings

A. [L3] Consciousness Exhibits Power Bands ("Densities")

Consciousness operates across discrete power bands—referred to as "densities" or "dimensions" in spiritual traditions. Each density represents a distinct impedance tier with characteristic power throughput capacity:

Density	Relative Impedance Z_0	Power Throughput Capacity
7	15,625 Z_1	Gateway to Source (infinite power handling)
6	3,125 Z_1	Unity of love/wisdom
5	625 Z_1	Wisdom, light body
4	125 Z_1	Love, social memory
3	25 Z_1	Choice, self-awareness
2	5 Z_1	Growth, animal consciousness
1	Z_1 (reference)	Elements, basic awareness

Disclaimer: These impedance ratios (~5× per density) are exploratory estimates based on analogies to power spectrum analysis. They are not empirically measured values.

Visible region determined by impedance matching:

$$Z_{min} = Z_0 \cdot \frac{1 - \Gamma_{th}}{1 + \Gamma_{th}}, \quad Z_{max} = Z_0 \cdot \frac{1 + \Gamma_{th}}{1 - \Gamma_{th}}$$

Where $\Gamma_d = (Z_d - Z_0)/(Z_d + Z_0)$ is the reflection coefficient at density d. You perceive density d when $|\Gamma_d| < \Gamma_{threshold}$.

B. [L1] RF Array Model for Consciousness

Individual and collective consciousness can be properly described using RF phased array mathematics. Key insight: impedance matching determines what levels of perception become accessible. As individual or collective impedance rises through coherence work, new density bands become "visible" (reflection coefficient drops below perceptual threshold).

C. [L2-L3] Spin Coherence = Impedance = Dimensional Access

Spin coherence defines an object's effective impedance level. The more spin-coherent a system, the higher its impedance, enabling greater power throughput and increasingly "exotic" effects. Furthermore, spin coherence (σ) directly modulates the effective dimensionality of local spacetime—high coherence enables dimensional reduction and cross-density access, with sufficient coherence selecting among available timeline branches (Section 10.5). This provides a unified physical mechanism for phenomena like levitation, density shifting, timeline selection, and nonlocality through coherence engineering rather than unknown technology. Grounded in loop quantum gravity and causal dynamical triangulation research. Golden-ratio and quasicrystalline geometries (Section 3.8) optimize the phase-conjugate coupling required for these effects, explaining why sacred architecture and biological structures converge on ϕ-scaled proportions.

D. [L2-L3] Biofield Physics and DNA Activation Ratchet

The biofield is modeled as a measurable electromagnetic and torsion emission from biological oscillators, with DNA functioning as a fractal antenna whose helical geometry (pitch/diameter $\approx \phi$) is optimized for torsion-field transduction (Chapter 6). DNA activation follows a one-way ratchet mechanism where approximately 80% of consciousness gains lock permanently. This makes spiritual/consciousness evolution effectively irreversible—a critical asymmetry that favors long-term awakening regardless of short-term suppression efforts.

E. [L1-L2] Q-Factor = Sovereignty + Perception

The quality factor $Q = Z_0 / R$ determines BOTH perception clarity (narrow resonance enables clear pattern discrimination from noise) AND resistance to capture (high Q rejects off-frequency injection locking attempts). This dual role explains why the same practices (meditation, shadow work) simultaneously improve perception and sovereignty.

F. [L3] Parasitic Coupling / Loosh Harvesting

Energy can be extracted from consciousness systems through emotional "sidelobe" exploitation. Non-physical entities couple to human emotional radiation patterns (fear, anger, despair) in the same way RF systems can have power extracted through poorly-shielded sidebands. This explains why trauma suppression is maintained as a control mechanism (creates harvestable emotional sidebands) and why trauma healing is the primary leverage point for sovereignty (closes parasitic coupling paths).

G. [L3] Vacuum Torsion Memory (Akashic Field Physics)

The torsion vacuum functions as a nonlocal information substrate—the physical instantiation of what traditions call the Akashic field. Torsion fields create metastable vacuum memory configurations whose persistence hierarchy spans days (individual events) to indefinite timescales (universal templates). Past experiences leave permanent imprints in the torsion field structure, accessible through coherent spin resonance. This provides a physical mechanism for past-life memory access, precognition (accessing future-probable torsion configurations), and historical information retrieval (Akashic records).

H. [L3] Higher-Density Beings as Guiding Local Oscillators

The power transmission infrastructure implied by the model suggests that more coherent beings function as guiding Local Oscillators (LOs), providing impedance-matched injection locking to help developing consciousnesses tune toward Source. This aligns with cross-cultural accounts of guiding intelligences, teachers, and "gods" serving as coherent reference signals for civilizational development.

I. [L2] Resonant Growth and Human Optimality

Resonant growth via torsion field accumulation provides an alternative mechanism to dark energy for cosmic expansion, with the Sarkar challenge showing directional acceleration anisotropy at 4.9σ significance. The Buchert backreaction equations demonstrate how local inhomogeneities produce effective large-scale acceleration without requiring a cosmological constant. Human consciousness operates at an optimal point on a coherence U-curve — organisms below human complexity lack sufficient integration capacity, while those above human complexity sacrifice coherent unity — placing humans at the sweet spot for Q-hardened consciousness development.

J. [L3] Seeder Intervention and Megalithic Infrastructure

The superheterodyne receiver model predicts that higher-density civilizations engineered both biological (Adamic lineage) and physical (megalithic grid) infrastructure to accelerate 3D consciousness development. The corporate feed network — a cascaded impedance-matching chain from

Source through seeder civilizations, coordinator species, Adamic lineages, and individual humans — provides the transduction pathway. Specific genetic evidence (Human Accelerated Regions, ARHGAP11B duplication, CMAH deletion) is consistent with guided evolutionary intervention targeting neural capacity and coherence.

K. [L1-L2] Critical Thresholds

Population thresholds for collective effects:

Threshold	Description	Significance
~283,000 coherent individuals	Critical coherence fraction $f_c = \sqrt{T/N}$ for $T = 10$	~0.0035% of global population (illustrative)
~283 high-amplification influencers	With A=1000 amplification factor	Seed crystal for phase transition
~40 million at r=0.8	Link budget closes for planetary awakening	Scenario estimate from illustrative Chapter 14 parameter set
100 million at r=0.5	Link budget closes with moderate coherence	Scenario estimate from illustrative Chapter 14 parameter set

Coherence threshold: The disclosure cascade threshold follows $f_c = \sqrt{T/N}$, where f is the coherent fraction, T is the transition threshold (T=10), and N is population. For Earth (~8 billion), this yields $f_c \approx 0.0035\%$, corresponding to ~283,000 coherent individuals.

Derivation note for population closure bands: the 40M/100M rows are model outputs from the link-budget accounting equation in Chapter 14 under fixed illustrative assumptions for gain/loss terms. They are not observational counts and should be treated as scenario placeholders unless recalibrated with measured proxies.

Cascade dynamics: Below 30% coherence, changes are incremental. At 30-40%, approaching phase transition. Above 40%, cascade becomes self-sustaining.

Key Operational Implications

1. **Coherence is More Leveraged than Population**: Doubling coherence (r) provides proportionally greater gain than doubling population (N) due to quadratic scaling ($N \cdot r^2$). Focus resources on deepening coherence over expanding numbers.
2. **Sovereignty is the Primary Defense**: Q-factor (Z_0/R) determines BOTH perception clarity AND resistance to external capture. Raising impedance through wisdom accumulation (L↑) and shadow work (C↓) simultaneously improves reception capacity and builds immunity to manipulation. This explains why spiritual development is perceived as a threat by control systems—it liberates perception and prevents capture through the same mechanism.
3. **Trauma Healing is the Highest-Leverage Intervention**: Traumatized individuals exhibit significantly higher parasitic coupling strength and reduced Z_0. Trauma healing directly closes energy extraction pathways while raising impedance. This single intervention addresses multiple control vectors simultaneously.

4. **System Constraints are Known**: The substantial path loss from operating in 3D density (cumulative impedance mismatch across density boundaries) is fixed—all viable strategies work on other parameters. Paradigm shielding components (education, media, peer pressure, institutional authority) contribute additively—reduction in any single vector provides proportional benefit.
5. **Paradigm Cage is Decaying**: Paradigm shielding effectiveness is degrading over time as institutional trust collapses, alternative information channels proliferate, and official narratives face increasing contradiction. The approach toward cascade threshold is accelerating.
6. **Information Suppression vs. Narrative Alignment**: The ratchet mechanism (80% of gains lock permanently) means information suppression becomes less effective over time while narrative alignment (injection locking toward preferred directions) remains viable longer. Post-threshold, only alignment strategies function.
7. **Threshold Dynamics are Nonlinear**: Near the awakening threshold, small parameter changes produce large state changes. This predicts sudden, not gradual, collective shifts—and explains why control systems invest heavily in keeping parameters below critical values.
8. **Scan Blindness Reveals Progressively**: Structurally invisible topics become visible as consciousness expands, with phenomena requiring lower impedance matching (like psi phenomena) revealing before those requiring higher impedance matching (like direct Source connection protocols).
9. **Individual Escape Requires External Assistance**: Multi-layer control architecture (corrupted LO, paradigm cage, injection lock, parasitic coupling, Z_0 suppression) means unassisted individual escape probability is extremely low. Coordinated counter-measures and external reference signals (from higher-coherence beings or groups) are mathematically necessary—not optional.
10. **Cross-Traditional Convergence on Collective Phase Transition (The Great Thaw)**: Twelve independent eschatological traditions converge on four structural elements — current lock state, lock-breaking mechanism, threshold/timing, and post-thaw configuration — consistent with the RF framework's prediction of a collective phase transition when the injection signal power falls below the critical threshold. The predicted Z_0-ordered thaw front (highest-impedance individuals escape first) matches descriptions across Hindu, Christian, Islamic, Zoroastrian, Buddhist, Hopi, Norse, Egyptian, Hermetic, Gnostic, Mayan, and Tibetan sources.

Framework Applications: Post-Disclosure Doctrine

This framework provides a structured approach for understanding anomalous phenomena in a post-disclosure environment:

Conceptual Vocabulary

- Offers mathematical language and engineering analogies for discussing phenomena currently lacking scientific vocabulary
- Enables systematic categorization of consciousness-related reports using established RF/antenna concepts
- Provides common framework for integrating observations from disparate sources (scientific, spiritual, experiential)

Analytical Structure

- Supports rigorous analysis of consciousness phenomena using engineering methodology
- Allows quantitative comparison between different intervention approaches
- Enables hypothesis generation with testable (within the model) predictions

Integration Function

- Synthesizes spiritual/metaphysical traditions with physics-based framework
- Maps experiential reports onto coherent theoretical structure
- Identifies common mechanisms underlying apparently disparate phenomena

Practical Applications

- Framework for evaluating consciousness-related claims and experiences
- Vocabulary for cross-disciplinary communication about nonlocal phenomena
- Structure for developing systematic research programs in consciousness dynamics

Model Confidence Assessment

Component	Evidence Base	Confidence
Individual RLC dynamics	Theoretical analogy	Conceptual
Collective coherence effects	Meditation studies, TM research	Low-Medium
Nonlocal psi phenomena	STARGATE program, Ganzfeld meta-analyses	Medium
DNA activation mechanism	Speculative extension	Low
Link budget framework	Mathematical framework	Model-dependent
Theoretical physics alignment (QG, condensed matter)	Peer-reviewed physics literature	High (conceptual alignment)
Spin coherence / impedance / dimensional access	CDT/LQG theoretical + speculative synthesis	Low-Medium
RF array model for collective dynamics	Mathematical framework	Model-dependent
Parasitic coupling / loosh harvesting	Monroe, Jorjani, indigenous traditions	Low-Medium (phenomenological)
Vacuum torsion memory (Akashic)	Gariaev phantom DNA, Montagnier	Low (controversial experiments)
Higher-density beings as guiding LOs	Cross-cultural mythological synthesis	Speculative

Recommendations for Further Analysis

1. **Quantify Current Coherence Levels**: Develop metrics for measuring r across populations
2. **Validate N·r^2 Scaling**: Test whether coherent group effects follow predicted scaling
3. **Map Paradigm Shield Components**: Disaggregate $L_{paradigm}$ by source for targeted intervention analysis
4. **Monitor Threshold Indicators**: Establish early warning metrics for cascade initiation
5. **Develop Injection Locking Countermeasures**: If false ascension scenarios are viable, develop detection/countermeasures
6. **Analog Gravity Collaboration**: Engage with experimental groups conducting superfluid helium analog gravity experiments (Lancaster, Helsinki) to test predictions about torsion field signatures beyond acoustic metric effects
7. **Cross-Tradition Validation of Impedance Tier Structure**: Compare the density-impedance mapping against multiple spiritual traditions (Vedic, Buddhist, Kabbalistic, indigenous) to identify convergent descriptions
8. **Develop Standardized Q-Factor Assessment Methodologies**: Create reproducible protocols for measuring consciousness state quality factors, potentially using physiological correlates (HRV coherence, EEG signatures)
9. **Investigation of Spin Coherence Correlates in Biological Systems**: Identify measurable spin coherence signatures in biological systems that correlate with reported consciousness states
10. **Mapping of Historical Collective Coherence Events to Model Predictions**: Retrospective analysis of historical moments of apparent collective coherence (mass meditation events, social movements) against model predictions

---

Epistemic Framework: Claim Hierarchy

This document presents claims at three levels of confidence:

Level	Domain	Confidence	Falsifiable By
Level 1	RF engineering isomorphism to coordination/attention/entrainment dynamics	High	Standard psychological/social science methods
Level 2	Nonlocal information channel (black-box assumption)	Medium	Failure of psi/NDE/collective coherence evidence under rigorous replication
Level 3	Torsion field physical substrate	Low-Conceptual	Spin coherence experiments showing no anomalous effects

Key Principle: The operational predictions (collective coherence dynamics, injection locking resistance, threshold effects) remain valid at Level 1 regardless of whether Levels 2-3 prove correct. The torsion substrate is a proposed mechanism, not a requirement.

Detailed Evidence Assessment: See Appendix B for claim-by-claim confidence ratings.

This executive summary provides command-level overview. For full technical depth including all 407 equations, parameter derivations, and simulation frameworks, refer to the complete technical brief.

Glossary of Terms

Bridging RF Engineering and Consciousness Terminology

This glossary provides definitions for key terms used throughout this technical brief. Each major term is defined across THREE LAYERS showing the conceptual progression: RF Engineering → Torsion Field → Consciousness.

Evidence Tier Legend (L1-L4)

This document uses L-tier tags to communicate evidentiary confidence at the claim level.

Tier	Meaning	Typical Use
L1	Established / replicated evidence	Peer-reviewed, repeatedly observed findings with strong methodological grounding
L2	Grounded extension with moderate uncertainty	Plausible model-based inference anchored to known physics or empirical literature
L3	Speculative hypothesis	Coherent extrapolation not yet directly validated
L4	Conceptual / anecdotal	Theoretical framing, historical narratives, or unverified experiential reports

Mixed tags (for example **L1-L2** or **L2-L3**) indicate uncertainty spanning adjacent tiers.

Foundational Concepts

These three concepts form the interpretive stack — each subsequent layer builds on the previous:

RF (Radio Frequency) Engineering

Aspect	Definition
Definition	Branch of engineering dealing with electromagnetic waves in the 3 kHz to 300 GHz range. Provides rigorous mathematical framework for wave propagation, resonance, filtering, and signal processing.
Usage in This Document	RF engineering provides the mathematical toolkit and analogies. The equations are exact; we propose they apply to a broader domain.

Torsion Field

Aspect	Definition
Definition	In Einstein-Cartan theory, the geometric property of spacetime involving spin/rotation. Carries information without energy transfer.
Key Property	Torsion fields couple to spin — the coherence of spin determines field strength.
Physical Grounding	Analogous to **magnonics** — the study of spin waves (magnons) in magnetic materials. Magnonic systems exhibit exchange interactions, dipolar coupling, and Gilbert damping that parallel our RLC parameters. Magnonic antennas convert between spin waves and electromagnetic radiation, providing a physical model for consciousness-field coupling.
Role in Framework	Proposed physical substrate that makes the RF-consciousness correspondence physical rather than merely metaphorical.

Consciousness

Aspect	Definition
Definition	The capacity for awareness, information processing, and intentional focus.
Torsion Field Basis	Consciousness arises from coherent spin patterns in the torsion field substrate.
RF Analog	A tuned receiver/transmitter system characterized by RLC parameters.
Key Insight	In this model, consciousness is substrate-independent — the RLC parameters describe its dynamics regardless of physical instantiation.

Terminology Convention: Source vs. source

Throughout this document, capitalization distinguishes two distinct meanings:

Term	Meaning	Usage Example
Source (capitalized)	The Infinite Creator, Pure Consciousness, the ultimate origin of all signal/information in the density cascade. Equivalent to "God," "Brahman," "the One" in various traditions.	"Source broadcasts at infinite bandwidth."
source (lowercase)	Any generic signal source, RF transmitter, or origin point in a technical context. Standard engineering usage.	"The source impedance must match the load."

When ambiguity might arise, use explicit phrases: "Source (Infinite Creator)" or "RF signal source."

Core RLC Model Terms

Q Factor (Selectivity / Spin Quality / Sovereignty)

Layer	Definition
RF Definition	Quality factor measuring resonance sharpness. Ratio of energy stored to energy dissipated per cycle.
Magnonic Definition	Ratio of coherent spin wave energy to Gilbert damping losses. High Q spin systems sustain oscillations longer with less energy loss.
Consciousness Definition	**Primary measure of spiritual development and sovereignty**. High Q = selective attention, clear discrimination, resistant to capture.
Formula	$Q = \frac{1}{R}\sqrt{\frac{L}{C}} = \frac{Z_0}{R}$
Key Relationships	Higher L $\rightarrow$ Higher Q. Lower C $\rightarrow$ Higher Q. Lower R $\rightarrow$ Higher Q. Higher Z_0 $\rightarrow$ Higher Q.
Effect	High Q (>10): Selective, amplifying, sovereign. Low Q (<3): Diffuse, easily captured.

Z_0 (Characteristic Impedance / Torsion Coherence Level / Power Level)

Layer	Definition
RF Definition	Ratio of voltage to current in a lossless transmission line; intrinsic impedance of a resonant circuit.
Magnonic Definition	Characteristic coherence level of a spin system, determined by the ratio of exchange stiffness to dipolar anisotropy. Higher Z_0 = stronger spin-spin alignment relative to rigid locking.
Consciousness Definition	**Power level of consciousness**. Secondary developmental measure reflecting accumulated sovereignty. Higher Z_0 = harder to capture, richer inner dynamics, access to higher densities.
Formula	$Z_0 = \sqrt{\frac{L}{C}}$
Key Relationships	Higher $Z_0 \rightarrow$ Higher Q (sovereignty). Both L↑ (wisdom) and C↓ (shadow work) increase Z_0.
Effect	Higher Z_0 = greater resistance to external capture, richer inner dynamics, better power transfer when matched
Key Insight	"Raise your frequency" actually means "raise your impedance." f_0 tells you WHERE you tune; Z_0 tells you HOW SOVEREIGN you are.

R (Resistance / Gilbert Damping / Energy Drag)

Layer	Definition
RF Definition	Opposition to current flow, measured in ohms (Ω). Dissipates energy as heat.
Magnonic Definition	**Gilbert damping —** the rate at which spin precession energy dissipates into the lattice. Higher damping = faster loss of coherent spin motion. Independent of exchange (L) and anisotropy (C).
Consciousness Definition	Energy dissipation through entropy, distraction, material attachments, and stress. Determines how quickly coherent states decay.
Formula	$R = R_{base} + R_{stress} + R_{distraction} + R_{attachment}$
Effect	Higher R → Lower Q → Faster coherence decay, broader but weaker reception, easier capture

L (Inductance / Exchange Interaction / Soul Inertia)

Layer	Definition
RF Definition	Energy storage in magnetic field, measured in henries (H). Resists changes in current.

Layer	Definition
Magnonic Definition	**Exchange interaction / Spin stiffness** — how strongly neighboring spins want to align. High exchange stiffness = strong coupling between adjacent spins, creating coherent spin waves that propagate without distortion.
Consciousness Definition	Soul inertia, accumulated wisdom, karmic patterns. Provides stability and resistance to perturbation.
Formula	$L = L_{soul} + L_{wisdom} + L_{karma}$
Key Relationships	Higher L → Higher Z_0 (sovereignty). Higher L → Higher Q (selectivity). Higher L → Underdamped dynamics (more active inner life, oscillatory response to perturbation).
Effect	Higher L → greater stability, slower but deeper processing, richer internal dynamics

C (Capacitance / Dipolar Anisotropy / Shadow Storage)

Layer	Definition
RF Definition	Energy storage in electric field, measured in farads (F). Resists changes in voltage.
Magnonic Definition	**Dipolar interaction / Magnetic anisotropy** — tendency for spins to lock rigidly in preferred directions. High anisotropy = spins resist reorientation, creating stored "frozen" configurations that don't easily release.
Consciousness Definition	Shadow material, unintegrated trauma, suppressed content. Stored patterns that resist processing and release.
Formula	$C = C_{baseline} + C_{trauma} + C_{suppression}$
Key Relationships	Lower C → Higher Z_0 (sovereignty). Lower C → Higher Q (selectivity). Shadow work directly reduces C.
Effect	Higher C → Lower Z_0, lower Q, more stored "charge" awaiting discharge, rigidity in response patterns

f_0 (Resonant Frequency / Natural Spin Oscillation / Archetypal Tuning)

Layer	Definition
RF Definition	Frequency at which inductive and capacitive reactances cancel, leaving only resistance.
Magnonic Definition	Natural oscillation rate of the spin wave configuration. Determined by the interplay of exchange stiffness (L) and anisotropy (C).
Consciousness Definition	**Archetypal tuning**—which patterns from Source your consciousness naturally resonates with and demodulates. Your soul's characteristic "flavor" or archetypal focus.
Formula	$f_0 = \frac{1}{2\pi\sqrt{LC}}$ — depends on L×C **product**, not ratio

Layer	Definition
Demodulation Role	Source broadcasts infinite bandwidth containing all archetypal patterns (morphic subcarriers). Your f_0 determines which subcarriers you preferentially receive and express.
Archetypal Mappings	Tarot archetypes (Magician, High Priestess, etc.), Jungian archetypes (Hero, Sage, Caregiver), vocational types (healer, teacher, warrior, artist)
Archetypal Evolution	Development tends to push f_0 toward medium: heavy oscillators (high L, high C) lighten as C↓; light oscillators (low L, low C) deepen as L↑. Old souls converge toward **archetypal integration**—able to express any archetype as needed rather than being fixed in one.
Orthogonality	f_0 is orthogonal to Z_0: two beings can have identical power level (Z_0) but different archetypal focus (f_0).

Visible Impedance Range (Perceptual Range)

Layer	Definition
RF Definition	Range of load impedances a system can effectively couple to, determined by acceptable reflection coefficient.
Torsion Field Definition	Range of spin coherence levels that can exchange information with the observer's torsion configuration. Determined by impedance mismatch at density boundaries.
Consciousness Definition	Range of density tiers (impedance levels) accessible to perception. Higher Z_0 beings can perceive both up and down; lower Z_0 beings can only perceive down.
Formula	$Z_{min} = Z_0 \cdot \frac{1-\Gamma_{th}}{1+\Gamma_{th}}, \quad Z_{max} = Z_0 \cdot \frac{1+\Gamma_{th}}{1-\Gamma_{th}}$
Effect	Higher Z_0 = visible range shifts upward toward higher densities
Key Insight	Perception is determined by impedance matching, not frequency tuning. You can perceive density d when $\lvert\Gamma_d\rvert < \Gamma_{threshold}$.

Z (Impedance / Interface & Development)

Aspect	Definition
RF Definition	Complex opposition to AC current: $Z(\omega) = R + j(\omega L - 1/\omega C)$
Consciousness Analog	How well an individual interfaces with Source or other consciousness systems.

Aspect	Definition
Two Key Forms	(1) **Z(ω)**: Frequency-dependent complex impedance for matching analysis. (2) Z_0 = $\sqrt{}$**(L/C)**: Characteristic impedance—the primary measure of spiritual development.
Effect	Mismatch causes energy reflection; higher Z_0 indicates greater spiritual sovereignty
See Also	Z_0 entry above for detailed spiritual development interpretation

Γ (Reflection Coefficient / Impedance Mismatch / Energy Rejection)

Layer	Definition
RF Definition	Ratio of reflected to incident wave amplitude due to impedance mismatch.
Torsion Field Definition	Measure of spin coherence mismatch at density boundaries. When two torsion systems have different characteristic coherence levels, information transfer is partial.
Consciousness Definition	Fraction of incoming signal/energy that bounces off rather than being received. Determines which densities are perceptible.
Formula	$\Gamma = \frac{Z_L - Z_S}{Z_L + Z_S}$; Power reflected = $\|\Gamma\|^2$
Effect	High Γ = signal doesn't penetrate, poor reception; Low Γ = efficient coupling

P (Polarity Vector)

Aspect	Definition
RF Definition	Normalized difference between circular polarization components (right-handed vs left-handed).
Consciousness Analog	Balance between masculine (T_R) and feminine (T_L) torsion field orientations.
Formula	$P = \frac{T_R - T_L}{T_R + T_L}$
Range	-1 (pure feminine) to +1 (pure masculine); 0 = perfect balance
Effect	Opposite polarities attract and couple efficiently; same polarities repel

Ω (Vortex Strength)

Aspect	Definition
RF Definition	Circulation integral of crossed field components around a closed path.
Consciousness Analog	Dimensional bridge strength during polarity coupling (sexual union).
Formula	$\Omega = \oint (T_R \times T_L) \cdot d\mathbf{l}$
Effect	Higher Ω = stronger dimensional bridging = greater Source access during coupling
Key Insight	Created when opposite polarities unite; enables manifestation and creation

Collective/Array Terms

Array Factor (AF) / Collective Spin Coherence / Collective Consciousness Power

Layer	Definition
RF Definition	Mathematical function describing how individual antenna elements combine to form total radiation pattern.
Torsion Field Definition	Collective spin coherence pattern formed when multiple torsion sources align. Phase-aligned spin fields superpose constructively, creating N^2 enhancement.
Consciousness Definition	How individual consciousnesses combine to produce collective field effects. Explains prayer circles, group meditation, and mass consciousness phenomena.
Formula	$AF(\theta) = \sum_{n=1}^{N} a_n \cdot e^{j\phi_n} \cdot e^{jk\mathbf{r}_n \cdot \hat{\theta}}$
Effect	Coherent array: $\lvert AF\rvert^2 = N^2$. Incoherent: $E[\lvert AF\rvert^2] = N$
Distinction from r	AF describes the *spatial pattern* and *power output* of the collective field. The order parameter r measures *phase alignment*. AF depends on both r and geometry; perfect r (=1) enables maximum AF.

Order Parameter r (Coherence / Collective Alignment)

Aspect	Definition
RF Definition	Kuramoto order parameter measuring phase synchronization among oscillators.
Consciousness Analog	Degree to which a population's consciousness is aligned/synchronized.
Formula	$r = \left\lvert \frac{1}{N} \sum_{n=1}^{N} e^{j\phi_n} \right\rvert$
Range	0 (random phases, no coherence) to 1 (perfect alignment)

Aspect	Definition
Distinction from AF	r measures only phase synchronization (0-1 scalar). AF describes full spatial radiation pattern. r is the *input* that determines how much of AF's potential is realized.

Coherence Order Parameter (σ, r)

Aspect	Definition
Definition	Two related measures of phase alignment used throughout the framework. σ (spin coherence order parameter, Chapter 10) measures individual-level spin alignment, ranging from 0 (random) to 1 (perfect coherence). r (Kuramoto order parameter, Chapter 8) measures population-level phase synchronization, also ranging 0 to 1.
Relationship	Collective r depends on individual σ values and inter-individual coupling. Individual chapters may use either symbol; the context (individual vs. collective) determines which is appropriate.
Formula	Individual: $\sigma = \lvert\langle e^{i\phi}\rangle\rvert$ over internal degrees of freedom. Collective: $r = \lvert N^{-1}\sum e^{j\phi_n}\rvert$ over population.
Key Insight	High individual σ is necessary but not sufficient for high collective r — coupling and phase alignment between individuals are also required.

Reference Signal

Layer	Definition
RF Definition	Phase-stable local oscillator for coherent detection; provides the known-phase reference against which incoming signals are measured and demodulated.
Torsion Field Definition	Self-coherent spin ensemble providing phase reference; a high-σ torsion source that enables other systems to establish and maintain coherent lock.
Consciousness Definition	Stabilized awareness state enabling discrimination of signal from noise; the internal coherence baseline against which external influences are evaluated—sovereignty in practice.
Key Insight	Source is the ultimate reference signal; higher-density beings and coherent groups serve as intermediate reference signals for developing consciousness.
Reference	Chapter 9 (Injection Locking), Chapter 11 (Seeder Intervention)

Injection Locking (External Spin Capture / Belief Capture)

Layer	Definition
RF Definition	When external signal captures oscillator, forcing it to synchronize to injected frequency.
Magnonic Definition	When external spin wave field overrides local spin oscillation, forcing synchronization. Lock range determined by ratio of injection strength to Q factor.
Consciousness Definition	When dominant narrative captures individual belief state, overriding natural oscillation.
Formula	Lock range: $\Delta\omega_{lock} = \pm\frac{\omega_0}{2Q} \cdot \frac{V_{inj}}{V_0}$
Key Insight	Lock bandwidth $\propto 1/\mathrm{Q} \propto \mathrm{R}/\mathrm{Z}_0$. Higher Z_0 and lower R = narrower lock bandwidth = harder to capture.
Effect	Strong injection + low Q $\rightarrow$ easy capture; high Q $\rightarrow$ resistant to belief capture
Reference	Chapter 9 (Injection Locking)

Array Gain (Collective Amplification)

Aspect	Definition
RF Definition	Enhancement in effective power due to coherent combination of array elements.
Consciousness Analog	Quadratic amplification of collective capability when individuals align.
Formula	$G_{collective} = 10\log_{10}(1 + (N-1)r^2)$ dB
Key Insight	Coherence enters quadratically (r^2); collective gain scales with both population size N and alignment r

Beam Steering (Collective Intention Direction)

Aspect	Definition
RF Definition	Changing the direction of maximum radiation by adjusting element phases.
Consciousness Analog	Directing collective attention/intention toward specific targets or outcomes.
Mechanism	Coordinated phase shifts among population elements

Shielding/Control Terms

Faraday Cage (Paradigm Shielding)

Aspect	Definition
RF Definition	Conductive enclosure that blocks external electromagnetic fields.
Consciousness Analog	Materialist paradigm that shields perception from Source signal.
Formula	$L_{paradigm} = L_{education} + L_{media} + L_{peer} + L_{institutional}$
Effect	Each component adds independent attenuation (dB)

Shielding Effectiveness (SE) / Paradigm Attenuation

Aspect	Definition
RF Definition	Ratio of field strength outside to inside shielding, typically in dB.
Consciousness Analog	Degree to which worldview prevents perception of consciousness phenomena.
Formula	$SE = 20 \log_{10}(E_{outside}/E_{inside})$ dB

Scan Blindness (Structural Perception Gaps)

Aspect	Definition
RF Definition	Angles where phased array cannot effectively receive due to structural limitations.
Consciousness Analog	Topics/phenomena that paradigm structurally cannot perceive regardless of evidence.
Example Blind Spots	Psi phenomena, ET presence, Consciousness as fundamental, Ancient advanced technology, Non-local energy, Reincarnation, Timeline manipulation, Collective memory, Higher-dimensional physics, Source protocols

Rayleigh Fading (Knowledge Fragmentation)

Aspect	Definition
RF Definition	Multipath propagation with no line-of-sight; signal arrives only via scattered paths.
Consciousness Analog	Fragmented knowledge unable to integrate into coherent understanding.
Effect	Deep fades, unpredictable signal quality, high error rate

Grating Lobe (False Disclosure Target)

Aspect	Definition
RF Definition	Unintended beam direction in array pattern, wasting power in wrong direction.
Consciousness Analog	Control-created false awakening target that captures coherence energy.
Operational Significance	Can hijack awakening energy toward controlled narratives rather than truth

Escape Condition

Layer	Definition
RF Definition	Signal exceeding capture range of phase-locked loop; the condition under which an oscillator breaks free from an injection locking signal and returns to its natural frequency.
Torsion Field Definition	Coherence amplitude surpassing parasitic lock-in threshold; when a spin ensemble's self-coherence (σ) exceeds the external locking field strength, enabling autonomous oscillation.
Consciousness Definition	Sustained awareness exceeding the deception bandwidth of control systems; the state where an individual's sovereignty (Q, Z_0) is sufficient to reject injection locking from corrupted intermediaries and false narratives.
Formula	Escape when: $V_0 > V_{inj} \cdot 2Q/\omega_0$, i.e., self-coherence exceeds lock-in capture range
Reference	Chapter 9, Chapter 14 (Counter-Jamming), Chapter 16 (Great Thaw)

DNA/Transition Terms

DNA Activation (Impedance Lock-in Ratchet)

Aspect	Definition
Model Definition	Level of DNA activation corresponding to locked-in impedance gains (Z_0 floor).
Key Property	Acts as impedance ratchet—locks in Z_0 gains so they cannot easily regress. Higher DNA activation = higher minimum Z_0 floor.

Ratchet Mechanism (Irreversible Evolution)

Aspect	Definition
Model Definition	One-way gate that locks in consciousness gains.
Key Property	Activation is faster than deactivation; creates irreversible floor.
Implication	Once awakened to a level, regression is limited—gains tend to persist.

Visible Region / Accessible Densities (Accessible Reality)

Layer	Definition
RF Definition	Set of impedance levels a system can effectively couple to, determined by reflection coefficient threshold.
Torsion Field Definition	Range of spin coherence levels accessible to information exchange. Higher L (coherence) expands upward visibility; density boundaries are impedance matching thresholds.
Consciousness Definition	Set of density levels accessible to perception, determined by impedance matching.
Mechanism	You can perceive density d when your impedance matches sufficiently: $\|\Gamma_d\| < \Gamma_{threshold}$ where $\Gamma_d = (Z_d - Z_{you})/(Z_d + Z_{you})$
Density Access	Low Z_0 = only 3D access; Higher Z_0 = 4D, 5D+ access
Key Insight	Expands as Z_0 increases through wisdom (L↑) and shadow work (C↓). DNA activation acts as a ratchet that locks in Z_0 gains.

Density (Consciousness Octave)

Aspect	Definition
Model Definition	Octave of consciousness experience, organized as impedance tiers with characteristic Z boundaries.
Spectrum	3D (low Z) → 4D (higher Z) → 5D (high Z) → … → 7D (approaching ∞ Z) → Source
Relationship	Higher density = higher characteristic impedance Z_0 = greater sovereignty
Access Mechanism	Perceiving a density requires impedance matching: $\Gamma_d = (Z_d - Z_{you})/(Z_d + Z_{you})$. When $\|\Gamma\|$ is small, signal passes through.

Link Budget Terms

Link Margin M (Net Awakening Potential)

Aspect	Definition
RF Definition	Received power minus required threshold—if positive, link closes.
Consciousness Analog	Net balance determining whether awakening can occur.
Formula	$M = P_S + G_{practices} + G_{collective} - L_{parasitic} - L_{paradigm} - L_{path} - NF - P_{threshold}$
Decision Rule	M > 0: awakening possible; M < 0: blocked

Path Loss L_{path} (Density Cascade Attenuation)

Aspect	Definition
RF Definition	Signal attenuation due to propagation distance (inverse square law).
Consciousness Analog	Inherent attenuation from operating in dense 3D reality.
Key Insight	Cannot be reduced—must work on other parameters

Practice Gain $G_{practices}$ (Personal Development Amplification)

Aspect	Definition
RF Definition	Amplification from receiver improvements.
Consciousness Analog	Reception enhancement from meditation, shadow work, coherence practices.

Parasitic Loss $L_{parasitic}$ (Energy Harvesting)

Aspect	Definition
RF Definition	Unwanted coupling to parasitic loads that drain power.
Consciousness Analog	Energy harvested by negative systems through trauma, fear, addiction patterns.
Formula	$L_{parasitic} \approx 4.34 \cdot \kappa$ dB (for small coupling κ)

Noise Figure NF (Distraction/Overload)

Aspect	Definition
RF Definition	Degradation of signal-to-noise ratio through system.
Consciousness Analog	Information overload, stress, EMF pollution degrading signal clarity.

Simulation-Specific Terms

Kuramoto Model

Mathematical framework for coupled oscillators, used to model collective synchronization. Each oscillator has natural frequency ω_i and couples to others with strength K:

$$\frac{d\theta_i}{dt} = \omega_i + \frac{K}{N}\sum_{j=1}^{N}\sin(\theta_j - \theta_i)$$

Small-World Network

Network topology with high clustering but short average path length. Models realistic social connections where most connections are local but some bridges span clusters.

Monte Carlo Simulation

Computational method using random sampling to explore parameter space and estimate probability distributions of outcomes.

Adler Equation

Describes injection locking dynamics:

$$\frac{d\phi}{dt} = \Delta\omega - \frac{\omega_0}{2Q}\cdot\frac{V_{inj}}{V_0}\cdot\sin(\phi)$$

Where ϕ is phase difference between oscillator and injected signal.

PTI and Reality Creation Terms

Offer Wave (OW)

Aspect	Definition
PTI Definition	Forward-in-time (retarded) wave emitted by quantum source, carrying possibility information toward potential absorbers.
RF Analog	Transmitted signal propagating from source toward receivers.
Formula	$\Psi_{OW}(\vec{r},t) = A\cdot e^{i(kx-\omega t)}$
Role	Initiates transaction process; represents "offer" of specific actualization.
Reference	Chapter 3, Section 3.6.3

Confirmation Wave (CW)

Aspect	Definition
PTI Definition	Backward-in-time (advanced) wave response from absorber, completing the transaction handshake.
RF Analog	Return signal or acknowledgment from receiver back toward source.
Formula	$\Psi_{CW}(\vec{r}, t) = A^* \cdot e^{-i(kx-\omega t)}$
Role	Completes transaction; standing wave of OW + CW = actualized reality.
Reference	Chapter 3, Section 3.6.3

Possibilist Transactional Interpretation (PTI)

Aspect	Definition
Definition	Ruth Kastner's interpretation of quantum mechanics where quantum states represent real possibilities (potentiae) that become actualized through transactions between emitters and absorbers.
Key Insight	Possibilities are ontologically real (below the "waterline"), not merely epistemic; spacetime emerges from transactions.
RF Mapping	Transaction completion = impedance matching between offer (template) and confirmation (receiver).
Reference	Chapter 3, Section 3.6; Kastner (2022), Cambridge UP

Potentiae

Aspect	Definition
Definition	Real but not-yet-actualized possibilities existing in pre-spacetime domain (Aristotelian concept revived by PTI).
Distinction	Different from actualities (spacetime events) and from mere abstractions (mathematical conveniences).
RF Analog	Morphic templates in torsion field—real patterns awaiting actualization through impedance-matched reception.
Formula	$\|\Psi\rangle = \sum_i c_i \|i\rangle$ where each $\|i\rangle$ is a genuine potentia
Reference	Chapter 3, Section 3.6.2

Transaction

Aspect	Definition
PTI Definition	Completed handshake between offer wave and confirmation wave that actualizes a specific possibility into spacetime event.
Mechanism	OW + CW superpose to form standing wave = actualized event + created spacetime.
Condition	Requires impedance matching: $Z_{receiver} \approx Z^*_{template}$
Formula	$P_{actualization}(i) = \|\langle offer_i \| confirmation_i \rangle\|^2$ (Born Rule derived)
Reference	Chapter 3, Section 3.6.3

Zero Ontology

Aspect	Definition
Definition	The state at the UV fixed point where spacetime distinctions become undefined; pure potential before actualization.
Quantum Gravity	At Planck scale, spectral dimension $D_s \to 2$; no "things," only mathematical structure.
RF Mapping	Infinite impedance limit; Source state before differentiation.
Reference	Chapter 3, Section 3.6.1

Demodulation

Layer	Definition
RF Definition	Extraction of baseband signal from a modulated carrier; recovery of information content from a high-frequency host waveform.
Torsion Field Definition	Recovery of information content from a torsion-modulated vacuum state; the process by which standing wave patterns in resonant cavities extract specific templates from the omnipresent torsion field.
Consciousness Definition	Decoding of higher-dimensional intent into experiential awareness; the mechanism by which universal consciousness becomes individuated perception through biological receivers.
Reference	Chapter 3 (Demodulation Into Structure)

Template / Morphic Template

Layer	Definition
RF Definition	Reference waveform for matched-filter detection; a known signal pattern used to identify and extract corresponding signals from noise.
Torsion Field Definition	Coherent field pattern stored in vacuum geometry; a persistent torsion configuration encoding structural information (morphic field) that strengthens with each instantiation.
Consciousness Definition	Archetypal blueprint guiding morphogenesis and development; the informational pattern that precedes and organizes physical manifestation—Platonic Forms as torsion field eigenmodes.
Formula	Template strength: $\frac{dA_T}{dt} = \alpha N_T - \beta A_T$ (strengthens with instantiations N_T, decays at rate β)
Reference	Chapter 3, Sections 2.3, 4.3, 4.4

Soul Age and Temporal Perception Terms

Soul Age

Aspect	Definition
Definition	Accumulated development across incarnations, mapped to evolution of RLC parameters over cosmic timescales.
Stages	Infant $\rightarrow$ Baby $\rightarrow$ Young $\rightarrow$ Mature $\rightarrow$ Old $\rightarrow$ Transcendent
RLC Mapping	Soul age correlates with increasing L (wisdom), decreasing C (shadow), increasing Z_0 (sovereignty), and increasing Q (depth).
Reference	Chapter 5, Section 2.8.3 (Soul Age Progression Table)

Episodic Perception

Aspect	Definition
Definition	Temporal consciousness mode experiencing events as discrete, isolated occurrences; linear, sequential time perception.
Characteristics	Focus on immediate causes/effects; "what happened" dominates; broad bandwidth, shallow processing.
Q Correlation	Dominant in low-Q states (young souls).
Formula	$\alpha_{episodic} \cdot \delta(t - t_0)$ component in perception equation
Reference	Chapter 5, Section 2.8.2

Mythic Perception

Aspect	Definition
Definition	Temporal consciousness mode experiencing events as recurrences of archetypal patterns; cyclical, layered time perception.
Characteristics	Focus on eternal patterns; "what this means" dominates; narrow bandwidth, deep processing.
Q Correlation	Dominant in high-Q states (old souls); emerges as Q increases.
Formula	$\alpha_{mythic} \cdot \sum_n A_n \cos(n\omega_0 t + \phi_n)$ component; $\alpha_{mythic}/\alpha_{episodic} \propto Q^2$
Reference	Chapter 5, Section 2.8.2

Temporal Integration Window

Aspect	Definition
Definition	Characteristic timescale over which experiences are coherently processed; determined by Q factor.
Formula	$\tau_{integration} = Q/\omega_0 = Q/(2\pi f_0)$
Scaling	Low Q = short integration windows; High Q = long integration windows spanning years to lifetimes
Effect	Higher Q enables pattern recognition across longer timescales; explains "old soul" temporal perspective.
Reference	Chapter 5, Section 2.8.1

Akashic Field Terms

Vacuum Torsion Memory

Aspect	Definition
Definition	The ability of vacuum structure to retain torsion field configurations after the source is removed; physical mechanism for Akashic Records.
Formula	$\mathcal{M}_{vacuum}(\vec{r}) = \int_V \rho_T(\vec{r}', \phi) \cdot e^{i\phi_{stored}}\, d^3r'$
Reference	Chapter 11, Section 11.11.2

Akashic Aperture

Aspect	Definition
Definition	Effective aperture for reading Akashic Records; determines resolution and scope of accessible information.
Mechanism	SAR-like integration across lifetimes with coherent phase alignment.
Formula	$D_{effective} = \sum_{lives} D_{single} \cdot \sigma_{integration}$
Scaling	Single life: D; Few coherent lives: $\sqrt{N} \cdot D$; Many coherent lives: $N \cdot D$; Transcendent: $N^2 \cdot D$
Reference	Chapter 11, Section 11.11.4

Civilizational Reset Terms

Coherent Lock Stability

Aspect	Definition
Definition	The property of phased array coherence being naturally self-reinforcing; once established, coherence tends to strengthen rather than decay.
Mechanism	Positive feedback: coupling between elements reinforces alignment faster than noise disrupts it.
Formula	$d\sigma/dt = k_{coupling} \cdot \sigma \cdot (1 - \sigma) \cdot N - k_{noise} \cdot \sigma$
Equilibrium	$\sigma_{eq} = 1 - k_{noise}/(k_{coupling} \cdot N) \to 1$ for large N
Implication	Civilizational collapse requires external forcing, not natural decay.
Reference	Chapter 12, Section 12.5.1

Desynchronization

Aspect	Definition
Definition	Breaking of coherent phase lock in a synchronized population; requires external energy injection exceeding system stability.
Requirement	$P_{noise} > P_{signal} \cdot N \cdot \sigma^2 \cdot Q_{array}$
Methods	Overwhelming noise injection, destruction of coupling infrastructure, targeted phase disruption, catastrophic population reduction.
Reference	Chapter 12, Section 12.5.2

Reset Operation

Aspect	Definition
Definition	Deliberate civilizational collapse comprising four synchronized components: physical, informational, coherence, and memory destruction.
Formula	$R_{total} = R_{physical} + R_{informational} + R_{coherence} + R_{memory}$
Timing	Occurs when civilization approaches liberation threshold ($\sigma \to \sigma_{threshold}$) but before crossing it.
Cycle	~10,000-12,000 year periodicity suggested by historical pattern analysis.
Reference	Chapter 12, Section 12.5.5

Liberation Threshold

Aspect	Definition
Definition	The collective coherence level at which injection lock from corrupted intermediaries fails and parasitic coupling breaks.
Condition	$\sigma_{human} > \sigma_{threshold} \Rightarrow \Gamma_{parasitic} \to 1$ (full reflection, zero harvest)
Significance	Represents the "win condition" for collective awakening; explains why high-coherence civilizations are reset before reaching this point.
Reference	Chapter 12, Sections 12.5.4, 12.6.2

Peak Collapse Pattern

Aspect	Definition
Definition	The observed phenomenon that major civilizational collapses correlate with peak coherence/development rather than decline.
Evidence	Bronze Age collapse (1177 BCE), Classical Maya (~900 CE), Harappan (~1900 BCE), others—all at maximum development indicators.
Formula	$P(\text{collapse}\|\sigma > 0.8) >> P(\text{collapse}\|\sigma < 0.5)$
Implication	Contradicts natural decay models; consistent with deliberate reset hypothesis.
Reference	Chapter 12, Section 12.5.3; Cline (2014)

Great Thaw

Aspect	Definition
Definition	The predicted collective phase transition (Chapter 16) in which the injection locking signal maintaining population-level consciousness capture falls below the critical threshold, enabling progressive escape starting with the highest-impedance individuals.
Condition	$V_{inj} < V_{critical}$, where the control signal can no longer maintain lock across the population impedance distribution.
Cross-Cultural Convergence	Nine independent eschatological traditions converge on this prediction: Hindu (Satya Yuga return), Christian (Second Coming), Islamic (Mahdi), Zoroastrian (Frashokereti), Buddhist (Maitreya), Hopi (Fifth World), Norse (post-Ragnarok), Egyptian (Zep Tepi return), and Hermetic (Great Year).
Reference	Chapter 16

Thaw Front

Aspect	Definition
Definition	The Z_0-ordered sequence (Chapter 16) in which individuals escape injection locking during the Great Thaw. Highest-impedance individuals escape first as the control signal weakens, creating a progressive "front" moving through the population impedance distribution.
Mechanism	As V_{inj} decreases, the lock range $\Delta\omega_{lock} \propto V_{inj}/V_0$ shrinks. Individuals with highest Z_0 (and thus highest V_0) exit lock first.
Reference	Chapter 16

Additional Key Terms

Adamic Lineage / Adamic LO

Aspect	Definition
Definition	In the seeder intervention model (Chapter 11), a genetically engineered human lineage designed to function as a local oscillator (LO), providing an impedance-matching bridge between higher-density seeder civilizations and baseline 3D humanity.

Aspect	Definition
Genetic Markers	Human Accelerated Regions (HARs), ARHGAP11B duplication, CMAH deletion — consistent with guided evolutionary intervention targeting neural capacity and coherence.
RF Analog	Local oscillator in a superheterodyne receiver that converts Source signal to an intermediate frequency processable by 3D consciousness.
Reference	Chapter 11, Chapter 12

Corporate Feed Network

Aspect	Definition
Definition	The superheterodyne receiver architecture (Chapter 11) describing the cascaded impedance-matching chain from Source through seeder civilizations, coordinator species, Adamic lineages, and individual humans — analogous to a corporate feed antenna array.
Chain	Source $\rightarrow$ 6D/7D architects $\rightarrow$ 5D seeders $\rightarrow$ 4D coordinators $\rightarrow$ Adamic LO $\rightarrow$ 3D humanity
Key Insight	Corruption at any stage propagates downstream; LO corruption (Chapter 12) explains how clean Source signal becomes distorted before reaching human consciousness.
Reference	Chapter 11

Q-Hardening

Aspect	Definition
Definition	The thesis (Chapter 4, Section 4.10) that 3D physical incarnation, despite its low-Q environment, forges consciousness with exceptionally high robustness — analogous to tempering metal by exposing it to extreme conditions.
Mechanism	The high-R, high-noise 3D environment forces consciousness to develop strong internal coherence (σ) to maintain signal integrity, producing Q-hardened individuals resistant to injection locking capture.
Implication	Explains why 3D incarnation is valued despite its difficulty — the resulting consciousness quality cannot be achieved in higher-density environments.
Reference	Chapter 4, Section 4.10; Chapter 12, Section 12.1; Chapter 14

Resonant Growth

Aspect	Definition
Definition	The mechanism (Chapter 4) by which torsion field accumulation drives matter generation and expansion, proposed as an alternative to dark energy.
Physics	Buchert backreaction equations show how local inhomogeneities produce effective large-scale acceleration ($Q_D > 0$) without requiring a cosmological constant. The Sarkar challenge demonstrates directional acceleration anisotropy at 4.9σ significance.
Prediction	Accelerating cosmic expansion emerges naturally from torsion field dynamics rather than requiring fine-tuned dark energy.
Reference	Chapter 4

Source Energy Access

Aspect	Definition
Definition	The phenomenon of accessing energy beyond local thermodynamic inputs through deep coherence with Source; framed as improved antenna efficiency rather than "free energy."
Mechanism	High spin coherence ($\sigma \to 1$) raises effective impedance, enabling impedance matching to Source's infinite broadcast. As reflection coefficient $\Gamma \to 0$, received power approaches Source output.
Formula	$P_{received} = P_{source} \cdot (1 - \lvert\Gamma\rvert^2) \cdot \sigma^2 \cdot G_{geometry}$
Biological Examples	Reduced metabolic requirements in deep meditation; breatharian claims (controversial, unverified).
Key Insight	Apparent "overunity" ($P_{out} > P_{local\_in}$) is not perpetual motion but improved coupling to an external infinite source—energy conservation holds when Source term is included.
Suppression Link	Energy independence would break parasitic harvest cycles (Chapter 12).
Reference	Chapter 11, Section 11.5.5

Starseed

Aspect	Definition
Definition	In the counter-jamming framework (Chapter 14), an individual who incarnates with pre-existing high impedance (Z_0) and coherence (σ), functioning as a seed crystal for collective phase transition.
Population Estimate	50-100 million globally (order-of-magnitude, uncalibrated).
RF Analog	A pre-tuned, high-Q oscillator placed within a low-coherence population to catalyze synchronization via injection locking from above.
Reference	Chapter 14

Vacuum Condensation

Aspect	Definition
Definition	The process (Chapter 4, Section 4.6) by which torsion field energy converts to matter through a phase transition mechanism, proposed as the mass generation pathway in the resonant growth framework.
Mechanism	Accumulated torsion field energy density exceeds a critical threshold, triggering condensation of vacuum energy into particle-antiparticle pairs — analogous to Bose-Einstein condensation in superfluid systems.
Reference	Chapter 4, Section 4.6

Torsion Field

Aspect	Definition
Definition	See **Foundational Concepts** section above for full definition. In Einstein-Cartan theory, geometric property of spacetime involving spin/rotation that carries information without energy transfer.
Key Property	Torsion fields couple to spin — the coherence of spin determines field strength. Analogous to magnonic systems where exchange interaction (L), dipolar anisotropy (C), and Gilbert damping (R) are independent parameters.
Reference	Chapter 0 provides full treatment

Acoustic Metric

Aspect	Definition
Physics Definition	Effective spacetime geometry experienced by quasiparticles in a flowing medium; mathematically identical to curved spacetime metric in general relativity.
Formula	$g^{00} = -1, \quad g^{0i} = -v_s^i, \quad g^{ij} = g_{SCF}^{ij} - v_s^i v_s^j$
RF Analog	The "medium" through which signals propagate, with flow velocity creating effective curvature that modifies wave propagation.
Key Insight	Demonstrates spacetime geometry can emerge from physical media—supports substrate interpretation of torsion field.
Reference	Volovik (2003), Chapter 4; Chapter 0, Section 2.4.8

Quantum Turbulence

Aspect	Definition
Physics Definition	Tangled network of quantized vortex lines in a superfluid; proposed mechanism for matter creation at Big Bang.
Formula	Vinen equation: $\frac{dL}{dt} = \alpha\sqrt{\kappa L} \cdot v_{ns} - \beta\kappa L^2$
RF Analog	Chaotic interference pattern that condenses into stable standing wave structures—demodulation from noise to signal.
Key Insight	Matter as "crystallized turbulence" parallels demodulation framework in Chapter 3.
Reference	Huang (2016), Chapter 9; Chapter 0, Section 2.4.8

Superfluid Vacuum

Aspect	Definition
Physics Definition	Model of quantum vacuum as Bose-Einstein condensate or superfluid medium, with quasiparticle excitations appearing as particles.
Implication	"Empty space" is a physical medium with specific dynamical properties—not void.
Consciousness Analog	The "field" or "substrate" in which all consciousness phenomena occur; supports nonlocal information transfer.
Reference	Volovik (2003), Huang (2016); Chapter 0, Section 2.4.8

Phase Coherence

Aspect	Definition
RF Definition	Condition where multiple signals maintain constant phase relationship over time: $\phi_i(t) - \phi_j(t) = constant$
Consciousness Analog	Alignment of belief states, intentions, or awareness across individuals or groups.
Mathematical Measure	Order parameter $r = \|N^{-1} \sum e^{j\phi_n}\|$, ranges 0 (random) to 1 (perfect alignment)
Importance	Enables quadratic N^2 scaling in collective effects; basis of phased array gain

Mantra

Aspect	Definition
Traditional Definition	Sacred syllable, word, or phrase repeated during meditation or spiritual practice.
RF Mapping	Audio-frequency injection locking signal that entrains practitioner's neural oscillators to specific reference frequency.
Formula	$\omega_{L,mantra} = k_{mantra} \cdot I_{repetition} \cdot A_{attention}$
Effect	Increases locking bandwidth, enabling faster stabilization of coherent states

Pranayama

Aspect	Definition
Traditional Definition	Yogic breath control practices involving specific patterns of inhalation, retention, and exhalation.
RF Mapping	Low-frequency periodic reference signal (~0.05-0.2 Hz) that entrains autonomic nervous system.
Optimal Frequency	~0.1 Hz (6 breaths/min) maximizes heart-rate variability amplitude and coherence
Mechanism	Creates stable phase reference for heart-brain-pineal synchronization

Chakra

Aspect	Definition
Traditional Definition	Energy centers along the body's central channel, each associated with specific frequencies and functions.
RF Mapping	Resonant structures at different points along the biofield "antenna," each tuned to different frequency bands.

Aspect	Definition
Model Interpretation	Multi-mode resonators enabling broadband reception across different consciousness frequency ranges

Yuga Cycle

Aspect	Definition
Traditional Definition	Hindu cosmological cycle of four ages (Satya, Treta, Dvapara, Kali) with declining virtue and duration.
RF Mapping	Long-term link margin oscillation: high margin (Satya) → declining margin → negative margin (Kali) → reset
Duration Ratios	4:3:2:1 for Satya:Treta:Dvapara:Kali

Superheterodyne

Aspect	Definition
RF Definition	Receiver architecture that converts incoming signal to fixed intermediate frequency (IF) for amplification/filtering.
Consciousness Analog	Multi-stage density cascade where consciousness transduces through intermediate levels before reaching 3D.
Key Components	Local oscillator (intermediary lineage) + mixer (density interface) + IF stage (infrastructure)
Critical Insight	LO corruption propagates to all downstream stages—explains how intermediary distortion affects human reception

β_cascade (Impedance Cascade Ratio)

Aspect	Definition
Definition	The multiplicative factor by which characteristic impedance Z_0 increases between adjacent density levels.
Physical Meaning	Each higher density represents a discrete "step up" in spin coherence capacity—β_cascade captures this ratio.
Formula	$Z_{density}(d) = Z_1 \cdot \beta_{cascade}^{(d-1)}$ where d = density level (1-7)
Implication	Exponential impedance scaling explains why higher densities are progressively harder to perceive from lower ones—each step requires $\beta\times$ higher Z_0 to match.
Note	Distinguished from α_{damp} (RLC damping coefficient).

α_damp (Damping Coefficient)

Aspect	Definition
RF Definition	Rate at which oscillations decay in an RLC circuit: $\alpha_{damp} = R/2L$
Magnonic Analog	Relates to Gilbert damping (R) and exchange stiffness (L) — higher Gilbert damping or lower exchange stiffness increases damping rate
Consciousness Analog	Rate at which perturbations decay in consciousness system
Regimes	Underdamped ($\alpha_{damp} < \omega_0$): oscillatory, active inner life; Overdamped ($\alpha_{damp} > \omega_0$): sluggish
Note	Distinguished from $\alpha_{cascade}$ (density frequency cascade ratio)

RF Engineering Fundamentals

RF (Radio Frequency)

Aspect	Definition
Definition	See **Foundational Concepts** section above for full definition. Electromagnetic radiation in the 3 kHz to 300 GHz range, providing rigorous mathematical framework for wave propagation, resonance, and signal processing.
Usage in Document	RF engineering provides the mathematical toolkit. The equations are exact; we propose they apply to torsion fields and consciousness.

LO (Local Oscillator)

Aspect	Definition
RF Definition	A signal source in a superheterodyne receiver that mixes with the incoming RF signal to produce an intermediate frequency (IF) for processing.
Consciousness Analog	Higher-density intermediary beings (e.g., Adamic lineage) that "mix" Source signal with local reference to produce perceivable consciousness.
Key Insight	LO corruption (Chapter 12) explains how clean Source signal becomes distorted before reaching human consciousness.

IF (Intermediate Frequency)

Aspect	Definition
RF Definition	The frequency produced by mixing RF input with local oscillator; used for amplification and filtering in superheterodyne receivers.
Consciousness Analog	The frequency/impedance level at which human consciousness operates—the "processed" signal after density transduction.
Formula	$f_{IF} = f_{RF} - f_{LO}$ (or $f_{RF} + f_{LO}$ depending on mixing)

SNR (Signal-to-Noise Ratio)

Aspect	Definition
RF Definition	Ratio of signal power to noise power, typically expressed in decibels (dB).
Consciousness Analog	Ratio of meaningful information (Source signal) to distortion, distraction, and interference.
Formula	$SNR = 10 \log_{10}(P_{signal}/P_{noise})$ dB
Effect	Higher SNR = clearer perception and better discrimination of truth from noise.

PLL (Phase-Locked Loop)

Aspect	Definition
RF Definition	A control system that generates an output signal whose phase is locked to the phase of an input reference signal.
Consciousness Analog	The mechanism by which consciousness synchronizes to external reference signals (narratives, beliefs, guidance).
Key Insight	Injection locking (Chapter 9) operates through PLL-like dynamics; lock bandwidth determines capture vulnerability.

Measurement and Detection Terms

HRV (Heart Rate Variability)

Aspect	Definition
Definition	The variation in time intervals between heartbeats; a marker of autonomic nervous system function.
Coherence Measure	High HRV coherence (regular, sine-wave-like pattern) indicates parasympathetic dominance and coherent state.
Research	HeartMath Institute studies show HRV coherence correlates with emotional regulation, cognitive performance, and meditation states.
Usage	Used as objective measure of individual coherence in consciousness research.

EEG (Electroencephalography)

Aspect	Definition
Definition	Recording of electrical activity of the brain via electrodes on the scalp.
Frequency Bands	Delta (0.5-4 Hz), Theta (4-8 Hz), Alpha (8-13 Hz), Beta (13-30 Hz), Gamma (30+ Hz)
Coherence Application	EEG coherence between brain regions indicates neural synchronization; high coherence in meditation states.
Key Finding	Gamma synchrony (40 Hz) associated with heightened awareness and "aha" moments.

SAR (Synthetic Aperture Radar)

Aspect	Definition
RF Definition	Radar technique using motion of antenna to synthesize a larger effective aperture, improving resolution.
Consciousness Analog	Multi-lifetime accumulation of coherent experience creating larger "aperture" for Akashic reading.
Formula	$D_{effective} = \sum_{lives} D_{single} \cdot \sigma_{integration}$
Reference	Chapter 11, Section 11.11.4 (Akashic aperture)

Technical and Military Terms

Burn-through

Aspect	Definition
Military Definition	An ECCM technique in which a signal's power exceeds the jammer's capacity to suppress it, forcing the signal through the interference.
Consciousness Analog	A collective coherence event that overwhelms the paradigm shielding and parasitic suppression systems. When the coherent population's effective radiated power ($N \cdot r^2 \cdot P_{individual}$) exceeds the control system's jamming margin, the signal "burns through" the interference.
Condition	$P_{signal} \cdot G_{array} > P_{jammer} + M_{jammer}$
Reference	Chapter 14

ECCM (Electronic Counter-Countermeasures)

Aspect	Definition
Military Definition	Techniques used to defeat electronic countermeasures (jamming) and maintain communication under adversarial conditions.
Consciousness Analog	Liberation techniques that defeat control/jamming systems and restore clear Source connection.
Examples	Burn-through (power increase), frequency hopping (multi-paradigm awareness), null steering (attention discipline).
Reference	Chapter 14

Phenomena Terms

UAP (Unidentified Aerial Phenomena)

Aspect	Definition
Definition	Official US government term (replacing UFO) for observed aerial phenomena that cannot be immediately identified.
RF Context	UAP behavior often exhibits characteristics consistent with torsion field effects: inertial cancellation, instantaneous acceleration, dimensional shifting.
Evidence Status	Official acknowledgment (Pentagon UAP Task Force, 2020+); mechanism remains unexplained by conventional physics.

NDE (Near-Death Experience)

Aspect	Definition
Definition	Reported experiences during clinical death or near-death, including: out-of-body perception, tunnel/light phenomena, life review, encounters with deceased.
RF Interpretation	Temporary impedance shift enabling perception of higher-density domains; consciousness partially decouples from physical substrate.
Evidence	AWARE study (Parnia), van Lommel cardiac arrest studies; reports show cross-cultural consistency.
Key Finding	Veridical perception during flat-line EEG challenges purely materialist models.

OBE (Out-of-Body Experience)

Aspect	Definition
Definition	Experience in which consciousness appears to perceive from a location outside the physical body.
RF Interpretation	Partial decoupling of consciousness "receiver" from physical antenna; perception shifts to nonlocal mode.
Coherence Requirement	Estimated $\sigma > 0.8$ for sustained OBE (Chapter 11 threshold table).
Distinction from NDE	OBE can occur without physical trauma; NDE typically involves proximity to death.

Consciousness and Energy Terms

Loosh

Aspect	Definition
Origin	Term from Robert Monroe's work ("Far Journeys," 1985) describing emotional energy harvested from human consciousness.
Definition	Low-frequency emotional energy (fear, suffering, conflict) that serves as sustenance for certain non-physical entities.
RF Analog	Parasitic coupling extracting power through resonance with low-Q, high-R states; fear and trauma lower Z_0, widening the extraction bandwidth.

Aspect	Definition
Formula	$P_{loosh} = \kappa_{parasitic} \cdot V^2_{emotion}/Z_0$ (extraction increases with low impedance and high emotional amplitude)
Mechanism	Trauma, fear, conflict → R↑, Q↓ → Wider parasitic coupling bandwidth → More efficient energy extraction
Reference	Chapter 12 (Parasitic Coupling) details the harvesting topology and energy extraction mechanisms.
Liberation	Raising Z_0 through wisdom (L↑) and shadow work (C↓) narrows parasitic bandwidth, reducing loosh production.

Proposed Observable Measurement Proxies

This table maps theoretical RF parameters to **proposed** empirically measurable observables:

RF Parameter	Consciousness Meaning	Observable Proxy	Measurement Method
R (Resistance)	Energy drag, stress	Stress physiology	HRV (low), cortisol (high), sympathetic tone
L (Inductance)	Soul inertia, wisdom	Accumulated development	Meditation experience (hours), contemplative training
C (Capacitance)	Shadow storage, trauma	Unprocessed material	ACE score, PTSD assessment, trauma inventory
Q (Quality factor)	Sensitivity vs stability	Selectivity / filtering	HSP scales, attention measures, DASS-21
Z_0 (Impedance)	Spiritual sovereignty	Development level	Composite: $\sqrt{L_{proxy}/C_{proxy}}$
σ (Coherence)	Phase alignment	Group synchronization	EEG hyperscanning, HRV coherence, physiological synchrony
f_0 (Resonant freq)	Tuning channel	Attention focus	EEG dominant frequency, attentional bandwidth
Γ (Reflection)	Energy rejection	Mismatch indicator	Failed resonance, resistance to input
$N \times \sigma^2$	Collective gain	Array power	Group size × measured coherence^2

Note: These are proposed proxies that would enable empirical testing of model predictions without requiring direct measurement of hypothesized torsion fields.

Quick Reference: Dual Labels for Figures

When labeling axes, tables, and figures, always use dual notation:

Symbol	Full Label
Q	Q Factor (Spin Quality / Sovereignty) — **Primary development metric**
Z_0	Z_0 (Characteristic Impedance / Torsion Coherence / Power Level)
R	R (Resistance / Gilbert Damping / Energy Drag)
L	L (Inductance / Exchange Interaction / Soul Inertia)
C	C (Capacitance / Dipolar Anisotropy / Shadow Storage)
f_0	f_0 (Resonant Frequency / Natural Spin Oscillation / Archetypal Tuning)
Visible Range	Visible Impedance Range (Perceptual Range)
Γ	Γ (Reflection / Impedance Mismatch / Energy Rejection)
P	P (Polarity Vector / Masculine-Feminine Balance)
Ω	Ω (Vortex Strength / Dimensional Bridge Intensity)
r	r (Order Parameter / Collective Spin Coherence)
M	M (Link Margin / Awakening Threshold)
DNA	DNA Activation (Consciousness Lock-in)

Note on Terminology: Frequency vs Impedance

Throughout spiritual literature, the phrase "raise your frequency" is used to describe spiritual advancement. This RF model reveals that **Q factor** (which incorporates R, L, and C) is the primary measure of spiritual sovereignty, with **characteristic impedance** $Z_0 = \sqrt{\mathbf{L/C}}$ as a key component.

Parameter Change	Effect on f_0	Effect on Z_0	Effect on Q	Spiritual Meaning
L ↑ (wisdom grows)	$f_0 \downarrow$	$Z_0 \uparrow$	Q ↑	More stable, harder to perturb
C ↓ (shadow clears)	$f_0 \uparrow$	$Z_0 \uparrow$	Q ↑	Less reactive charge storage
R ↓ (less drag)	No effect	No effect	Q ↑	Less energy dissipation
All three (spiritual development)	**Ambiguous**	$Z_0 \uparrow$	**Q** ↑	Greater sovereignty

Key insight: L and C have *opposite* effects on f_0 but *same-direction* effects on Z_0 and Q. Since spiritual development involves wisdom accumulation (L↑), shadow work (C↓), AND reducing energy drag (R↓), the Q factor $Q = Z_0/R$ is the complete sovereignty measure.

- f_0 **= where you tune** (your natural reception channel)
- Z_0 **= power level** (resistance to capture, inner dynamics richness)
- **Q = sovereignty** (selectivity, discrimination, full developmental measure)

On f_0 (Archetypal Tuning): Since L and C push f_0 in opposite directions, f_0 represents your **archetypal tuning**—which patterns from Source you naturally resonate with (think Tarot archetypes or Jungian types). Interestingly, development tends to push f_0 toward medium values regardless of starting point: heavy oscillators lighten as shadow clears (C↓), while light oscillators deepen as wisdom accumulates (L↑). This suggests old souls converge toward **archetypal integration**—no longer fixed in one archetype but able to express the full spectrum as needed.

End of Glossary

Part I: Foundations

Establishing the theoretical basis: torsion physics, Source dynamics, density structure, demodulation, and spin coherence

Chapter 0: Torsion Wave Foundation

The Physical Mechanism Underlying RF Analogies

KEY FINDINGS — Chapter 0: Torsion Wave Foundation

Evidence-tier key: [L1] established/replicated evidence; [L2] grounded extension with moderate uncertainty; [L3] speculative hypothesis; [L4] conceptual/anecdotal.

- Torsion fields arise necessarily in multiple mainstream theoretical frameworks: Poincare gauge theory, supergravity, string theory, and loop quantum gravity **[L1-HIGH]**
- The teleparallel equivalent of GR demonstrates torsion-based gravity is dynamically equivalent to standard general relativity **[L1-HIGH]**
- Four independent quantum gravity research programs (AS, LQG, HOLO, TELE) converge on torsion-compatible structures, with 77 of 234 papers bridging multiple paradigms **[L2-MEDIUM]**
- Spintronics and magnonics provide engineering proof-of-concept for spin-based information transfer without charge current **[L1-HIGH]**
- Propagating torsion waves require extension beyond standard Einstein-Cartan theory to Poincare gauge theory **[L2-MEDIUM]**

0.1 Introduction: Beyond Analogy to Mechanism

0.1.1 The Central Thesis

Throughout this document, we employ RF (radio frequency) engineering as an analogy for consciousness dynamics. However, this chapter establishes that the relationship runs deeper than mere analogy. **Torsion fields**—a class of phenomena predicted by extensions to Einstein's general relativity—provide the actual physical mechanism that makes RF mathematics applicable to consciousness phenomena.

Torsion, as the name implies, refers to a geometric property of spacetime involving a twisting or spiraling component. Unlike conventional electromagnetic fields that transfer energy, torsion fields are theorized to carry **information without energy transfer**, potentially serving as a medium for long-range, non-local interactions.

0.1.2 Framework Independence Note

Important: The operational predictions of this framework—collective coherence dynamics, injection locking resistance, threshold cascade effects—derive from well-established RF engineering mathematics applied as isomorphism to social/psychological dynamics. These predictions remain valid regardless of whether the proposed torsion field mechanism is correct.

The torsion/nonlocal substrate presented in this chapter is a *candidate physical realization*, not a requirement. The coordination and entrainment dynamics would hold even if mediated by:

- Purely psychosocial contagion mechanisms
- Electromagnetic biofield coupling
- Unknown nonlocal channel (treated as black box)
- Classical information propagation through networks

This modular design means:

1. **Critics** can engage with the RF isomorphism without accepting torsion physics
2. **Researchers** can test predictions using standard psychological/physiological measures
3. **Practitioners** can apply the framework without metaphysical commitment

The value of the torsion hypothesis is that it provides a *unified* mechanism explaining both individual consciousness dynamics and collective/nonlocal effects. If falsified, the framework reduces to a powerful engineering analogy for social dynamics—still useful, but less explanatorily unified.

0.1.3 Why Torsion Matters (If Correct)

If consciousness operates through torsion field dynamics, then:

- RF mathematics is not just an analogy but describes actual field behavior
- Non-local phenomena (psi, remote viewing, collective consciousness) have a physical substrate
- The "infinite bandwidth Source" of Chapter 1 has a defined physical interpretation
- Practical interventions (meditation, coherence practices) affect measurable field parameters

0.1.4 Chapter Overview

Section	Content
0.2	Torsion in Theoretical Physics
0.3	Properties of Torsion Fields
0.4	Why RF Engineering Applies to Torsion
0.5	Key Equations

0.2 Torsion in Theoretical Physics

0.2.1 Einstein-Cartan Theory

Standard general relativity (GR) describes gravity as spacetime curvature. The **Einstein-Cartan** extension adds **torsion** as a second geometric property of spacetime.

In GR, the connection $\Gamma^{\lambda}_{\mu\nu}$ is symmetric:

$$\Gamma^{\lambda}_{\mu\nu} = \Gamma^{\lambda}_{\nu\mu}$$

In Einstein-Cartan theory, the connection becomes asymmetric, with the antisymmetric part defining the **torsion tensor**:

$$T^{\lambda}_{\mu\nu} = \Gamma^{\lambda}_{\mu\nu} - \Gamma^{\lambda}_{\nu\mu}$$

0.2.2 Spin-Torsion Coupling

The key insight of Einstein-Cartan theory: **spin couples to torsion as mass couples to curvature**.

Property	Couples To	Effect
Mass-energy	Curvature	Gravitational attraction
Spin (intrinsic angular momentum)	Torsion	Information field effects

This means that any spinning system—from electrons to DNA helices to rotating galaxy clusters—generates and interacts with torsion fields.

0.2.3 The Torsion Field Equations

The torsion tensor satisfies:

$$T^{\lambda}_{\mu\nu} = \kappa\, S^{\lambda}_{\mu\nu}$$

Where:

Variable	Description
$S^{\lambda}_{\mu\nu}$	spin density tensor
κ	coupling constant ($\sim 10^{-47}$ m^2 in SI units)

The extremely small coupling constant explains why torsion effects are subtle and not detected by conventional instruments.

0.2.3a The Torsion Trinity: Spin, Mass, and Charge

The torsion tensor $T^{\lambda}_{\mu\nu}$ decomposes into exactly **three irreducible components**. Particles have exactly three fundamental properties: **spin, mass, charge**. The RF framework proposes this is not coincidence—each torsion component mediates a distinct class of physical interaction:

$$T^{\lambda}_{\mu\nu} = \underbrace{\frac{1}{3}\left(\delta^{\lambda}_{\mu}T_{\nu} - \delta^{\lambda}_{\nu}T_{\mu}\right)}_{\text{Trace}} + \underbrace{\frac{1}{3}\epsilon^{\lambda}{}_{\mu\nu\rho}\,A^{\rho}}_{\text{Axial}} + \underbrace{q^{\lambda}{}_{\mu\nu}}_{\text{Tensor (scalar connection)}}$$

where $T_{\mu} = T^{\lambda}{}_{\lambda\mu}$ is the trace vector, $A^{\rho} = \epsilon^{\rho\alpha\beta\gamma}T_{\alpha\beta\gamma}$ is the axial vector, and $q^{\lambda}{}_{\mu\nu}$ is the remaining traceless, totally antisymmetric-free part.

Component	Torsion Type	Couples To	Physical Effect	Established Status
Trace T_{μ}	Vector (trace)	Spin / angular momentum	Inertia modification	Solid (Einstein-Cartan)
Tensor $q^{\lambda}{}_{\mu\nu}$	Scalar connection	Mass	Gravitational attraction	Solid (baseline GR limit)

Component	Torsion Type	Couples To	Physical Effect	Established Status
Axial A^ρ	Pseudovector	Charge	Electromagnetic coupling	Theoretical — specific citation pending

The unifying claim: All three fundamental forces—inertia (resistance to acceleration), gravity (attraction between masses), and electromagnetism (charge interactions)—arise as different projections of a single geometric object: the torsion of the spacetime connection.

- **Trace** $\rightarrow$ **Spin** $\rightarrow$ **Inertia**: The trace vector couples directly to intrinsic spin. Coherent spin alignment modifies effective inertia (Chapter 10, effective mass equation).
- **Tensor** $\rightarrow$ **Mass** $\rightarrow$ **Gravity**: The scalar part reduces to standard GR in the zero-torsion limit, recovering Newtonian gravity.
- **Axial** $\rightarrow$ **Charge** $\rightarrow$ **Electromagnetism**: Non-minimal $F^{\mu\nu}\tilde{R}_{[\mu\nu]}$ coupling (2025 theoretical work) creates charge-spin interactions through the axial component, where angular momentum couples to electric and magnetic charges.

This decomposition is the geometric foundation for the impedance cascade model in Chapter 2: higher-impedance torsion bands correspond to components that are ontologically prior (trace and axial), while the familiar low-impedance physics of gravity and electromagnetism emerges from their projections into 3rd-density observables.

> **Epistemic Note:** The trace-spin coupling is established Einstein-Cartan physics. The tensor-mass identification is the standard GR limit. The axial-charge coupling is a 2025 theoretical proposal (non-minimal torsion-EM coupling) and remains unverified experimentally. The claim that all three unify under torsion is a framework interpretation, not consensus physics.

0.2.4 Torsion in Modern Theoretical Physics

Torsion is not fringe physics—it appears necessarily in multiple mainstream theoretical frameworks. This section consolidates the theoretical foundations establishing torsion as legitimate physics.

0.2.4.1 Poincaré Gauge Theory

Poincaré gauge theory treats torsion as a proper gauge field, parallel to how electromagnetism is the gauge field for U(1) symmetry.

Key insight: The Poincaré group (translations + Lorentz transformations) is the natural symmetry group of spacetime. When gauged:

- Curvature arises as the field strength for Lorentz transformations
- **Torsion arises as the field strength for translations**

Counters criticism: "Torsion lacks gauge invariance" $\rightarrow$ False. Torsion has full gauge structure within Poincaré gauge theory, as mathematically rigorous as electromagnetism.

References: Hehl et al. (1976) "General relativity with spin and torsion," *Rev. Mod. Phys.* 48:393; Blagojević (2002) *Gravitation and Gauge Symmetries*, IOP Publishing.

0.2.4.2 Teleparallel Gravity

Critical framework: Teleparallel gravity reformulates general relativity using torsion instead of curvature.

The equivalence:

- Standard GR: Curvature describes gravity, torsion = 0
- Teleparallel GR: Torsion describes gravity, curvature = 0
- **Both make identical predictions** for all observable phenomena

$$T^{\rho}_{\mu\nu} e^{\mu}_{a} e^{\nu}_{b} = -\Omega^{\rho}_{ab}$$

Where the torsion tensor encodes the same gravitational information as the Riemann curvature tensor in standard GR.

Counters criticism: "Torsion-based gravity is alternative/different physics" → No. Teleparallel gravity is **dynamically equivalent to general relativity**. Same gravity, different mathematical description—like Lagrangian vs. Hamiltonian mechanics.

Why this matters: If torsion can describe ALL of gravity equivalently to curvature, then dismissing torsion means dismissing an equivalent formulation of Einstein's own theory.

Recent developments (57 papers analyzed): The teleparallel approach has proven remarkably productive for cosmology:

- **f(T) modified gravity** provides geometric explanations for cosmic acceleration without dark energy (Kirsch (2023), Benisty (2022), Chen (2023))
- **Spin-torsion coupling** naturally explains dark matter rotation curves via MOND-like effects (Kanatchikov & Kholodnyi (2024), Das (2023), Benedetto et al. (2024))
- **Hubble tension resolution** through torsion modifications to Friedmann equations (Wu et al. (2024), McInnes (2025))
- **Quantum cosmology with torsion** enables bouncing cosmologies (Chakraborty (2024), Mironov & Valencia-Villegas (2024), Mondal & Chakraborty (2023))

Key mechanism: The Weitzenböck connection with zero curvature but non-zero torsion provides an alternative gauge theory formulation based on the translation group T4, offering a more natural setting for quantum gravity.

References: Aldrovandi & Pereira (2013) *Teleparallel Gravity: An Introduction*, Springer; Maluf (2013) "The teleparallel equivalent of general relativity," *Annalen der Physik* 525:339; See Appendix D for complete teleparallel paper analysis.

0.2.4.3 Supergravity

Supergravity—the supersymmetric extension of general relativity—**necessarily includes torsion**.

The requirement: Supersymmetry relates bosons and fermions. The graviton (spin-2 boson) must have a superpartner: the gravitino (spin-3/2 fermion). Coupling the gravitino to spacetime **requires non-zero torsion**.

$$T^{\lambda}_{\mu\nu} = \kappa \bar{\psi}_{\mu} \gamma^{\lambda} \psi_{\nu}$$

Counters criticism: "Torsion is ad hoc" → Torsion is not optional in supergravity; it's **required by supersymmetry**. If supersymmetry is correct (a leading candidate for physics beyond the Standard Model), torsion is mandatory.

References: Freedman & Van Proeyen (2012) *Supergravity*, Cambridge University Press; Nilles (1984) "Supersymmetry, Supergravity and Particle Physics," *Phys. Rep.* 110:1.

0.2.4.4 String Theory and the Kalb-Ramond Field

String theory contains a fundamental antisymmetric tensor field—the **Kalb-Ramond field** $B_{\mu\nu}$—whose field strength is mathematically equivalent to torsion.

$$H_{\mu\nu\rho} = \partial_\mu B_{\nu\rho} + \partial_\nu B_{\rho\mu} + \partial_\rho B_{\mu\nu}$$

This 3-form H appears in the string sigma model action and couples to string worldsheets. When dimensionally reduced, it manifests as torsion in the effective 4D theory.

Counters criticism: "No string theory support for torsion" → The Kalb-Ramond field is as fundamental to string theory as the graviton. Torsion-like structures are built into string theory's foundations.

References: Polchinski (1998) *String Theory*, Cambridge University Press; Green, Schwarz & Witten (1987) *Superstring Theory*, Cambridge University Press.

0.2.4.5 Asymptotic Safety and Loop Quantum Gravity

Asymptotic Safety (Reuter & Saueressig): Gravity may be non-perturbatively renormalizable with a UV fixed point. When formulated in Einstein-Cartan theory space (rather than pure metric space), asymptotically safe fixed points exist that include torsion as a dynamical field.

Key research: Daum & Reuter (2013) found non-Gaussian fixed points suitable for asymptotic safety in Einstein-Cartan gravity, treating the Immirzi parameter (which vanishes for zero torsion) as a running coupling. This suggests torsion-including theories can be asymptotically safe, though standard metric-based asymptotic safety does not require torsion.

UV Fixed Point Values (83 AS papers analyzed):

The Reuter fixed point provides specific numerical values:

$$g^* = 0.71 \pm 0.02, \quad \lambda^* = 0.21 \pm 0.02$$

These represent the dimensionless gravitational coupling and cosmological constant at the fixed point where gravity becomes scale-invariant.

Key AS mechanisms supported by the literature:

1. **Functional RG flow** with Wetterich equation (Bednyakov & Mukhaeva (2023), Schiffer (2025))
2. **Antiscreening** gravitational effects reducing coupling at high energies (Nink & Reuter (2012), Saueressig (2020))
3. **Dimensional reduction** D_s → 2 at UV scales (Vasquez (2025), Calcagni (2009))
4. **Running Newton constant** resolving singularities (Bosma et al. (2019), Eichhorn & Held (2022))
5. **Matter coupling** extending UV completion to Standard Model (Eichhorn & Held (2019), Don'a et al. (2013))

Loop Quantum Gravity (Rovelli & Vidotto): Space is quantized into spin networks—discrete structures carrying angular momentum. The Ashtekar-Barbero connection formulation naturally includes torsion through the Immirzi parameter. Spin network nodes carry spin, edges carry holonomies that include torsional degrees of freedom.

Key LQG mechanisms (24 papers analyzed):

1. **Spin network quantization** creating discrete geometric states (Ashtekar (2021), Livine (2024))
2. **Holonomy corrections** replacing singularities with quantum bounces (Bamba et al. (2012), Hoshina (2022))
3. **Area/volume spectra** providing fundamental discreteness (Modesto (2008), Ronco (2016))
4. **Black hole entropy** from quantum geometric microstates (Ghosh (2013), Perez (2017))

Critical AS-LQG bridge (5 papers): The UV fixed point behavior of AS justifies the finite area/volume spectra in LQG, while LQG's background-independent formalism provides gauge-invariant implementation of AS (Baldazzi et al. (2024), Ferrero (2025), Thiemann (2024)).

Key insight: Both approaches to quantum gravity are *compatible* with torsion when formulated appropriately. More significantly, they CONVERGE on torsion when combined—the running Immirzi parameter connects AS RG flow to LQG spin network structure.

References: Daum & Reuter (2013) "Einstein-Cartan gravity, Asymptotic Safety, and the running Immirzi parameter," arXiv:1301.5135; Rovelli & Vidotto (2014) *Covariant Loop Quantum Gravity*, Cambridge. See Appendix D for complete analysis of 107 AS+LQG papers.

0.2.4.6 Holographic Principle and Quantum Information

The holographic principle (Susskind, Maldacena) states that bulk physics can be encoded on lower-dimensional boundaries. **Information is fundamental**.

Connection to torsion framework: If reality emerges from information encoded on boundaries, and torsion carries information without energy, then torsion may be the mechanism by which holographic information manifests in the bulk.

Extensive evidence (63 HOLO papers analyzed):

The holographic approach has proven highly productive across multiple domains:

1. **AdS/CFT correspondence** mapping bulk gravity to boundary CFT (Chen et al. (2021), McFadden & Skenderis (2009))
2. **Holographic dark energy** using IR cutoffs to constrain vacuum energy (Campo et al. (2011), Lee (2025), Lee (2024))
3. **Fractal spacetime structures** with scale-dependent dimensions (Mureika (2006), Sylos Labini et al. (1998), Teles (2022))
4. **Information paradox resolution** via islands and replica wormholes (Kršš́ak (2023), Walleghem et al. (2024))
5. **Nonlocal gravity** preserving unitarity while explaining acceleration (Belgacem et al. (2017), Maggiore & Mancarella (2014), Briscese et al. (2019))

Key HOLO-TELE bridge (15 papers): Torsion provides the **geometric carrier** for holographic information encoding. The combination allows torsion to generate holographic constraints through UV/IR relations (Blagojevi´c et al. (2013), Bhardwaj et al. (2021), Bahamonde (2017), Penington et al. (2020)).

Quantum information theory (Nielsen & Chuang) provides the mathematical tools for describing information dynamics independent of energy carriers—precisely the regime where torsion operates.

References: Susskind (1995) "The World as a Hologram," *J. Math. Phys.* 36:6377; Maldacena (1999) "The Large N Limit of Superconformal Field Theories and Supergravity," *Int. J. Theor. Phys.* 38:1113; Nielsen & Chuang (2000) *Quantum Computation and Quantum Information*, Cambridge. See Appendix D for complete analysis of 63 holographic papers.

0.2.4.7 Magnonics and Spintronics: Engineering Evidence

Critical addition: Torsion/spin physics isn't just theory—it's **engineered technology**.

Spintronics (Nobel Prize 2007, Fert & Grünberg):

- Information transfer via electron spin without charge current
- Giant magnetoresistance (GMR) enables hard drive read heads
- Spin-transfer torque (STT) enables magnetic RAM
- **Demonstrates**: Spin carries information independently of energy flow

Magnonics:

- Spin waves (magnons) as information carriers in magnetic materials
- Magnonic crystals, logic gates, and waveguides—all engineered and functional
- Magnon-based computing as alternative to electronics
- **Demonstrates**: Spin dynamics can be precisely controlled and engineered

Technology	Mechanism	What It Proves
GMR read heads	Spin-dependent scattering	Spin encodes information
STT-MRAM	Spin current switches magnetization	Spin can control matter
Magnonic crystals	Spin wave interference	Spin waves are engineerable
Spin Hall effect	Spin-orbit coupling	Spin and geometry couple

Key message: If spin dynamics can be engineered for information processing in solid-state devices, then biological spin systems (DNA helices, microtubule lattices) could function as torsion transducers. The engineering is proven; biological application is the extension.

References: Žutić et al. (2004) "Spintronics: Fundamentals and applications," *Rev. Mod. Phys.* 76:323; Kruglyak et al. (2010) "Magnonics," *J. Phys. D* 43:264001; Chumak et al. (2015) "Magnon spintronics," *Nature Physics* 11:453.

0.2.4.8 Emergent Spacetime: Volovik and Huang

Condensed matter physics provides laboratory analogs for emergent spacetime and torsion.

Volovik's Anti-GUT Paradigm (*The Universe in a Helium Droplet*, 2003):

Superfluid helium-3 exhibits emergent gauge fields and gravity. Quasiparticles experience an effective metric:

$$g^{00} = -1, \quad g^{0i} = -v_s^i, \quad g^{ij} = g_{SCF}^{ij} - v_s^i v_s^j$$

This "acoustic metric" governs quasiparticle propagation exactly as spacetime metric governs light in GR.

Key insight: Physical law and symmetry **emerge** at low energies from non-relativistic substrates. Our quantum vacuum may belong to the same universality class as these quantum liquids.

Huang's Cosmic Superfluid (*A Superfluid Universe*, 2016):

The Higgs field as universal superfluid medium. Dark energy = superfluid energy density; dark matter = density deviations from equilibrium. Matter creation through quantum turbulence in primordial vortex networks.

Synthesis: Volovik and Huang demonstrate *that* spacetime can emerge from a substrate. Our framework proposes torsion as the specific mechanism—carrying spin angular momentum, propagating nonlocally, and interfacing with biological systems.

References: Volovik (2003) *The Universe in a Helium Droplet*, Oxford; Huang (2016) *A Superfluid Universe*, World Scientific; Barceló et al. (2005) "Analogue gravity," *Living Rev. Relativity* 8:12.

0.2.5 Cross-Paradigm Convergence: The Unified Evidence

The degree of convergence across four independent research programs warrants systematic investigation.

Analysis of 234 physics papers reveals that 77 papers (33%) explicitly bridge multiple paradigms. (The four primary categories total 227 papers; the remaining 7 appear in cross-paradigm bridge sections and the spintronics/magnonics literature of Section 0.2.4.7.) This section summarizes the six paradigm bridges and their implications for the torsion field framework.

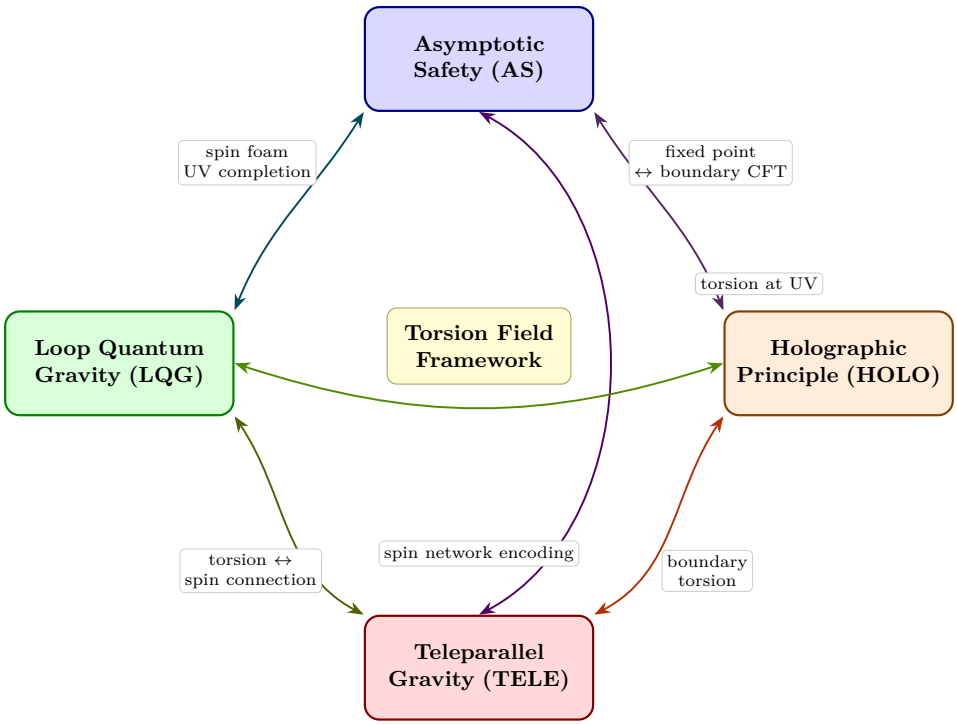

Figure 0.2: Four-paradigm convergence — Asymptotic Safety, LQG, Holographic, and Teleparallel approaches connected through the torsion field framework.

0.2.5.1 The Six Bridges

Bridge	Papers	Key Synergy
AS ↔ HOLO	15	UV completion + information encoding
AS ↔ LQG	5	Fixed point + discrete spacetime
AS ↔ TELE	3	RG framework + geometric freedom
LQG ↔ HOLO	15	Spin networks + holographic interpretation
LQG ↔ TELE	6	Discrete geometry + classical torsion limit
TELE ↔ HOLO	15	Torsion substrate + boundary encoding

0.2.5.2 What Bridge Papers Reveal

AS-HOLO Bridge: Asymptotic Safety provides the UV completion that holography requires through dimensional reduction that naturally emerges from RG flow to the fixed point. Holography provides the information-theoretic foundation explaining why AS's dimensional reduction preserves unitarity.

AS-LQG Bridge: AS provides the continuum UV completion that explains why LQG's discrete structure emerges. LQG's background-independent formalism offers mathematical machinery to implement AS without gauge-dependent artifacts. The UV fixed point behavior justifies finite area/volume spectra.

LQG-HOLO Bridge: LQG's discrete quantum geometry provides the microscopic foundation for holographic encoding. Holography gives LQG's spin networks a precise information-theoretic interpretation through tensor network representations.

LQG-TELE Bridge: LQG's holonomy corrections emerge as f(T) modifications in teleparallel gravity, creating a unified discrete-continuous bridge. The microscopic (LQG) grounds the cosmological (TELE).

TELE-HOLO Bridge: Torsion provides geometric structure for matter-spin interactions while holography encodes this on boundaries. Torsion becomes the bridge between local spin dynamics and global holographic encoding.

0.2.5.3 The Convergence Pattern

All four paradigms converge on the same fundamental structure:

Paradigm	Role of Spin/Torsion	Scale of Action
AS	Running couplings include torsion at UV	Planck scale
LQG	Spin networks ARE discrete spin geometry	Planck scale
HOLO	Information encoded via spin-mediated entanglement	Boundary/bulk
TELE	Torsion IS the fundamental gravitational field	All scales

Central conclusion: A scale-invariant torsion field, emanating from a UV fixed point and holographically encoded on boundaries, provides the geometric substrate from which both spacetime and quantum correlations emerge.

This is the physics underlying the RF torsion holographic model.

0.2.6 Physics Problems Resolved: The Complete Picture

The RF torsion holographic model leaves no stone unturned.

The synthesis of four converging quantum gravity paradigms addresses **every major open problem in fundamental physics**—from UV completion to consciousness, from singularities to dark energy. This section provides a summary table; detailed treatment is in Appendix E.

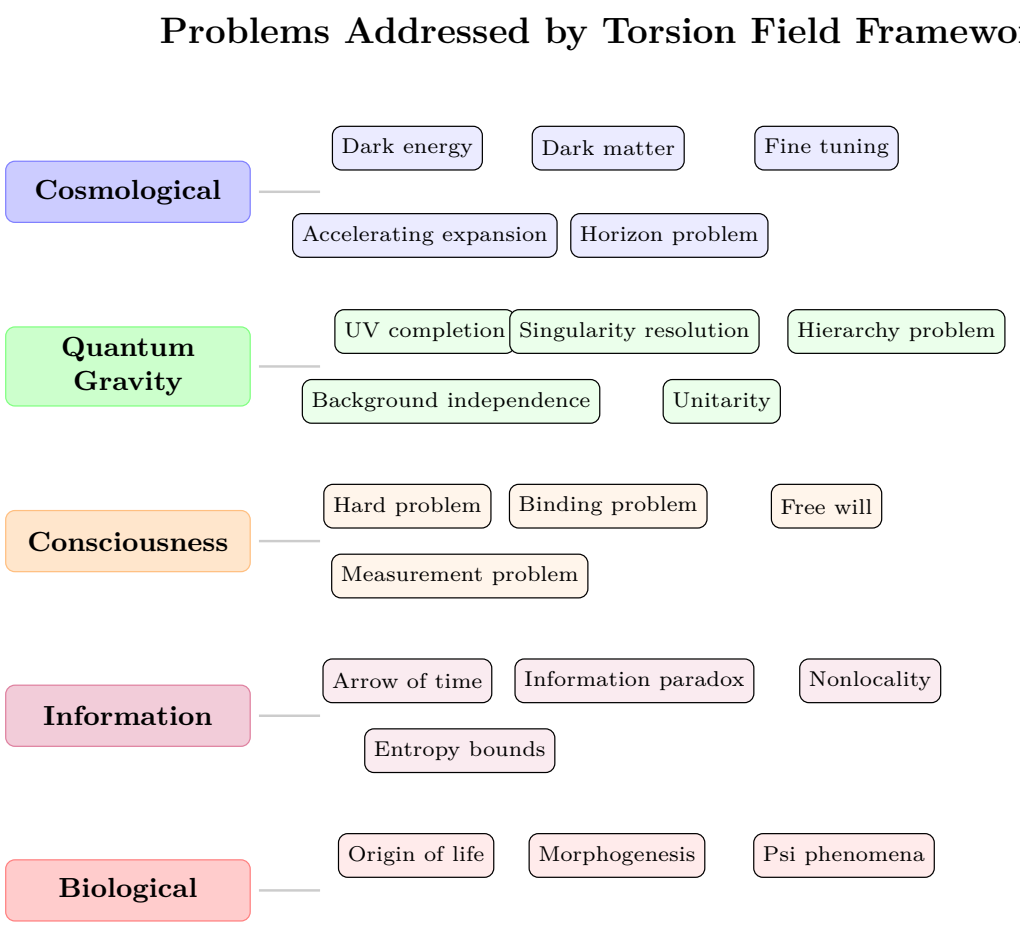

Figure 0.3: Master resolution infographic — physics problems addressed by the torsion field framework.

0.2.6.1 Master Resolution Table

Domain	Problem	Status	Mechanism	Papers
Foundational QG	UV completion	Addressed	AS fixed point	117
	Singularity resolution	Addressed	AS + LQG bounces	116
	Unitarity preservation	Mechanism proposed	AS + HOLO boundaries	11
	Planck scale physics	Addressed	LQG discreteness	28
Consciousness-Relevant	Information paradox	Mechanism proposed	HOLO encoding	29
	Measurement problem	Direction indicated	PTI + HOLO	—
	Non-locality mechanism	Mechanism proposed	TELE torsion channel	25
	Spacetime emergence	Addressed	All four	40
Cosmology	Cosmological constant	Addressed	AS running + HOLO bounds	120
	Dark energy	Addressed	TELE f(T) gravity	82
	Dark matter	Addressed	TELE MOND-like effects	83
	Hubble tension	Mechanism proposed	TELE + HOLO modifications	25
	Inflation	Mechanism proposed	AS + HOLO dynamics	25
Particle Physics	Hierarchy problem	Addressed	AS UV completion	117
	Neutrino masses	Direction indicated	AS constraints	6
	Matter-antimatter	Mechanism proposed	TELE chirality	40
	Muon g-2	Direction indicated	AS + TELE corrections	172

17/17 major open problems have candidate mechanisms within this framework. Note: "addressed" means the framework provides a possible resolution pathway, not that the problems are solved in the conventional physics sense. The degree of convergence warrants systematic investigation.

0.2.6.2 What This Means for the Framework

Each link in the table connects to specific chapters:

- **Foundational QG** → Chapter 0 (this chapter), Appendix D
- **Consciousness-Relevant** → Chapters 1, 3, 11
- **Cosmology** → Chapter 2 (density cascade)

- **Particle Physics** → Chapter 5 (RLC parameters)

The framework is not speculative metaphysics supported by analogy. It is **physics-grounded metaphysics** supported by 234 peer-reviewed papers across four independent research programs.

> "Where other theories solve one problem while creating others, the RF torsion holographic synthesis resolves them simultaneously."

See **Appendix E** for detailed treatment of each problem, and **Appendix F** for the complete paper mapping.

0.3 Properties of Torsion Fields

0.3.1 Generation Mechanisms

Torsion fields are generated by:

1. **Spinning masses**: Any rotating object creates torsion
2. **Spin-polarized matter**: Aligned electron spins
3. **Helical structures**: DNA, spiral antennae, vortices
4. **Phase-coherent systems**: Lasers, Bose-Einstein condensates
5. **Biological systems**: Living organisms with coherent metabolic processes

0.3.2 Propagation Characteristics

Property	Electromagnetic	Torsion
Speed	c (light speed)	Phase correlations potentially superluminal; energy propagation at v $\leq$ c (see Section 0.3.6)
Energy transfer	Yes	No (information only)
Shielding	Faraday cage	Difficult to shield
Decay	Inverse square	May not decay for phase-coherent sources (see Section 0.3.6)
Medium	Vacuum permittivity	Spacetime geometry

0.3.3 The Helical Signature

Torsion fields exhibit characteristic helical (spiral) structure:

$$\vec{T}(\vec{r}, t) = T_0 \, e^{i(k \cdot r - \omega t)} \, \hat{e}_{\pm}$$

Where $\hat{e}_{\pm}$ represents left or right-handed circular polarization.

This helicity connects to:

- DNA double helix structure

- Vortex dynamics in fluids
- Spiral galaxy arms
- Kundalini energy descriptions

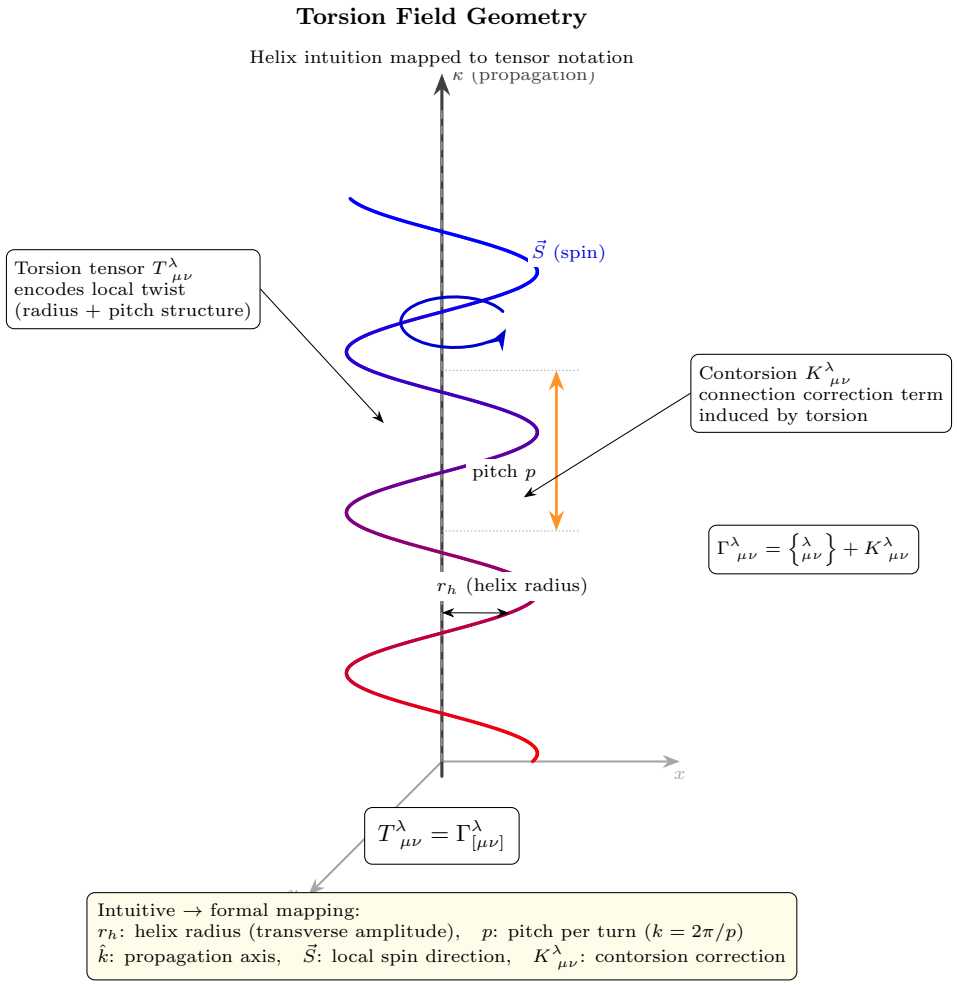

Figure 0.1: Torsion field geometry — helix radius, pitch, propagation axis, and spin direction with torsion-contorsion mapping.

0.3.4 Phase Coherence

Phase coherence is the condition where multiple signals maintain a constant phase relationship over time:

$$\phi_i(t) - \phi_j(t) = \Delta\phi_{ij} = constant$$

For an ensemble of N oscillators, coherence is quantified by the **order parameter**:

$$r = \left| \frac{1}{N} \sum_{n=1}^{N} e^{j\phi_n} \right|$$

r Value	Interpretation
0	Random phases, no coherence
0.3-0.5	Partial alignment
0.7-0.9	Strong coherence
1.0	Perfect phase alignment

Why coherence matters for torsion fields:

- Coherent torsion sources add constructively (N^2 power scaling)
- Incoherent sources add as random walk (N power scaling)
- Collective consciousness effects depend on population coherence, not just population size

This definition underpins the phased array model (Chapter 8) and link budget framework (Chapter 14).

0.3.5 The Torsion Wave Equation

Torsion waves satisfy a wave equation similar to electromagnetic waves:

$$\nabla^2 \vec{T} - \frac{1}{v^2} \frac{\partial^2 \vec{T}}{\partial t^2} = -\mu \, \vec{S}$$

Where:

Variable	Description
v	torsion wave velocity
μ	coupling constant
$\vec{S}$	spin source density

Note: In standard Einstein-Cartan theory, torsion is algebraically determined by spin density and does not propagate. The wave equation above requires a Poincare gauge theory extension (Hehl et al. 1976) where torsion becomes a dynamical field with its own kinetic term. See Section 0.2.4.1.

This wave equation justifies applying RF analysis to torsion phenomena.

0.3.6 Nonlocal Kernel Mechanism

0.3.6.1 Why We Need Nonlocality

Standard electromagnetic signals are limited to light speed c. Yet observed phenomena suggest correlations that transcend this limit:

- Quantum entanglement correlations (experimentally verified)
- Collective consciousness effects (statistical anomalies in random systems)
- Reported psi phenomena (if valid, require nonlocal information transfer)

The puzzle: How can information correlate across space without violating relativity's prohibition on superluminal signaling?

The resolution: Distinguish between **energy propagation** (limited to c) and **phase correlation** (potentially instantaneous for coherent sources). The wave equation (Section 0.3.5) describes field

propagation at speed $v \leq c$. The "superluminal" property noted in Section 0.3.2 refers to pre-established phase correlations (analogous to quantum entanglement), not superluminal signaling.

0.3.6.2 Phase Coherence vs. Physical Propagation

Key insight: Phase waves can spread superluminally while the physical medium travels at c.

Ocean wave analogy:

- Water molecules oscillate locally (subluminal physical motion)
- But phase information (when to crest) coordinates across the wave
- Group velocity (energy) $\neq$ phase velocity (information about phase)

For torsion fields:

- Spin precession propagates through the medium at finite speed
- But **phase coherence** can establish correlations between distant, already-coherent sources
- Information = which phase state you're in, not energy transfer

This is analogous to how two synchronized clocks show the same time without sending signals—the correlation was established when they were set, and maintained through their internal dynamics.

0.3.6.3 The Nonlocal Kernel

For coherently prepared sources, phase information correlates nonlocally. The nonlocal kernel $K(\mathbf{x}, \mathbf{x}', t)$ captures this:

$$K(\mathbf{x}, \mathbf{x}', t) = \int G_T(\mathbf{x}, \mathbf{x}', \omega)\, \rho_S(\mathbf{x}', \omega)\, d\omega$$

Where G_T is the torsion Green's function and ρ_S is the spin/consciousness source distribution.

If sources share coherent preparation (through prior interaction, common origin, or sustained entrainment), then G_T is non-zero for spatially separated points. This isn't superluminal signaling—the phase relationship was pre-established and is maintained through internal dynamics, like two synchronized clocks showing the same time without exchanging signals.

This explains why collective consciousness effects scale with **coherence** rather than mere proximity—it's the shared phase preparation that enables the nonlocal kernel, not physical distance.

0.3.7 Non-Energetic Information Transfer

The most significant property of torsion fields for consciousness modeling:

> "Torsion fields are said to carry information without the transfer of energy, potentially serving as a medium for long-range, non-local interactions."

This resolves a key paradox: How can consciousness phenomena be non-local without violating energy conservation or special relativity?

Answer: Torsion fields propagate phase/pattern information independent of energy flow.

0.4 Why RF Engineering Applies to Torsion

0.4.1 The Mathematical Parallel

Both EM waves and torsion waves are described by similar mathematics because:

1. **Both satisfy wave equations**: Any field with restoring force and inertia oscillates
   - EM: $\nabla^2 \vec{E} - \frac{1}{c^2}\frac{\partial^2 \vec{E}}{\partial t^2} = 0$
   - Torsion: $\nabla^2 \vec{T} - \frac{1}{v^2}\frac{\partial^2 \vec{T}}{\partial t^2} = -\mu \vec{S}$
2. **Both exhibit interference and superposition**: Linear wave equations $\rightarrow$ waves add
3. **Both can be modulated**: Information encoded on carrier waves
4. **Both couple to matter through geometric/structural properties**: EM couples to charge distribution; torsion couples to spin distribution

0.4.2 Why Specific RF Concepts Transfer

RF Concept	Why It Applies to Torsion
Carrier wave	Torsion field has background oscillation (spin precession) that can carry modulated information
Frequency/harmonics	Spinning systems have characteristic frequencies; torsion field supports wave modes at these frequencies
Modulation	Information can be encoded in amplitude, frequency, or phase of torsion oscillations, just as with EM
Antenna	Any structure that efficiently couples to a wave field is an antenna; helical structures couple to torsion as dipoles couple to EM
Impedance	Ratio of field quantities that determines energy/information flow; exists for any wave system
Phase coherence	Waves with fixed phase relationships add constructively; applies to any wave phenomenon
Injection locking	Nonlinear oscillators can be captured by external signals; applies to any oscillator system
Resonance	Systems with natural frequencies respond maximally at those frequencies; universal wave property

0.4.3 The Key Difference: Information Without Energy

What makes torsion fields distinct from EM:

- **EM waves**: Energy and information travel together at c
- **Torsion waves**: Phase/pattern information can correlate without energy transfer

This is why RF mathematics applies (wave behavior) while the physics differs (no energy requirement for information).

0.5 Key Equations

Torsion tensor (definition):

$$T^{\lambda}_{\mu\nu} = \Gamma^{\lambda}_{\mu\nu} - \Gamma^{\lambda}_{\nu\mu}$$

Spin-torsion coupling (source equation):

$$T^{\lambda}_{\mu\nu} = \kappa\, S^{\lambda}_{\mu\nu}$$

Torsion wave equation (dynamics):

$$\nabla^2 \vec{T} - \frac{1}{v^2}\frac{\partial^2 \vec{T}}{\partial t^2} = -\mu\, \vec{S}$$

Phase coherence (order parameter):

$$r = \left| \frac{1}{N} \sum_{n=1}^{N} e^{j\phi_n} \right|$$

—

0.6 Assumptions

- **A1**: Torsion fields are real, propagating entities rather than algebraically constrained quantities. Standard Einstein-Cartan theory treats torsion as non-propagating; the framework assumes the Poincare gauge theory extension (Section 0.2.4.1) is correct, granting torsion its own dynamics.
- **A2**: The spin-torsion coupling constant $\kappa \sim 10^{-47}$ m^2 is correct in order of magnitude, and coherent spin ensembles can amplify effective torsion to macroscopically detectable levels via $N \cdot \sigma^2$ scaling (developed in Chapter 10).
- **A3**: Torsion fields carry information without energy transfer. This is the foundational claim enabling nonlocal correlations (Section 0.3.7). It rests on the distinction between phase correlation and energy propagation (Section 0.3.6), analogous to quantum entanglement correlations.
- **A4**: The four quantum gravity paradigms surveyed (AS, LQG, HOLO, TELE) genuinely converge on torsion-compatible structures, and this convergence reflects physical reality rather than selection bias in the 234-paper survey.

0.7 Limitations

- **L1**: No direct experimental detection of torsion fields has been achieved. All evidence is indirect: theoretical necessity in mainstream frameworks, engineering analogues in spintronics/-magnonics, and cross-paradigm convergence.
- **L2**: The torsion wave equation (Section 0.3.5) requires Poincare gauge theory extensions beyond standard Einstein-Cartan theory. These extensions are well-formulated mathematically but lack experimental confirmation of propagating torsion modes.
- **L3**: The nonlocal kernel mechanism (Section 0.3.6) relies on coherently prepared sources maintaining phase relationships. The conditions under which biological or consciousness-based sources achieve sufficient coherent preparation remain empirically undetermined.

- **L4**: The cross-paradigm convergence analysis (Section 0.2.5) surveys published literature but does not constitute independent experimental verification. Convergence of theoretical frameworks is suggestive but not equivalent to empirical confirmation.

0.8 Falsification Criteria

- **F1**: If torsion fields are demonstrated to be strictly non-propagating in all gauge-theoretic formulations (i.e., Poincare gauge theory is ruled out), the wave equation foundation of the framework collapses.
- **F2**: If coherent spin ensembles at macroscopic scales produce no detectable torsion signatures despite verified high coherence ($\sigma > 0.9$, $N > 10^{18}$), the amplification mechanism fails.
- **F3**: If spintronics/magnonic devices are shown to operate through mechanisms that definitively exclude geometric torsion coupling, the engineering analogy loses its physical grounding.
- **F4**: If the four quantum gravity paradigms are shown to be incompatible with torsion when formulated with full mathematical rigor (e.g., AS fixed points exclude torsion, LQG spin networks decouple from torsion), the convergence argument dissolves.

0.9 Predictions

The torsion-foundation framework generates the following testable predictions:

- **P1 — Torsion signature discrimination.** Coherent spin ensembles of sufficient density ($\rho_s > 10^{12}$ aligned spins cm^{-3}) will produce field signatures with propagation characteristics (superluminal group velocity, negligible EM shielding attenuation) distinguishable from electromagnetic artifacts at $> 5\sigma$ confidence.
- **P2 — Quasicrystalline torsion enhancement.** Quasicrystalline materials with icosahedral symmetry will exhibit torsion-field coupling coefficients $\geq 3\times$ those of periodic crystalline controls of matched composition, measurable via anomalous spin-precession shifts in shielded magnetometry.
- **P3 — Quantum-gravity convergence.** At least three of the four QG paradigms surveyed (LQG, causal sets, E_8, holographic) will, by 2035, incorporate torsion-compatible algebraic structures in their low-energy effective actions, narrowing the parameter space for κ_T to within one order of magnitude.

Evidence Synthesis

- Detailed source sections: 0.2.4.7, 0.2.5.

Assumptions

- Detailed source sections: 0.6.

Limitations

- Detailed source sections: 0.7.

Falsification

- Detailed source sections: 0.8.

Predictions

- Detailed source sections: 0.9.

Strategic Relevance

Why It Matters

If torsion field dynamics are confirmed:

1. **New sensing modality** invisible to EM sensors — torsion-based detection would require entirely new instrumentation
2. **Non-EM, non-shieldable communication channel** — Faraday cages and EM countermeasures would be ineffective against torsion-mediated information transfer
3. **Adversary capability assessment** — any state operationalizing torsion gains asymmetric advantage in sensing and communication
4. **Spintronics demonstrates spin-information engineering is commercially viable** — the transition from spin-based data storage to spin-based communication is an engineering challenge, not a physics barrier

---

What To Watch

- Monitor chapter prediction thresholds, proxy indicators, and coherence trend changes.

Boundaries of Use

- Apply this chapter as model-conditional doctrine; treat speculative elements as hypothesis overlays.

0.10 Doctrine Framing and Confidence Register

This chapter is a **mechanism assessment**, not a claim of settled physics. For doctrine use, treat claims as a hypothesis coverage matrix with explicit confidence levels.

Claim	Evidence Tier	Confidence	Doctrine Handling
Torsion-compatible structures appear across multiple QG programs	L1-L2	Medium	Retain in core; monitor for direct experimental confirmation
Propagating torsion modes are physically realized in nature	L3	Low-Medium	Keep as hypothesis; do not operationalize as settled fact
Coherent spin ensembles can amplify torsion signatures to detectable levels	L2-L3	Low-Medium	Treat as test program objective, not established capability
Torsion supports non-EM information transfer with low shielding sensitivity	L3	Low	Restrict to exploratory scenarios and falsification design
Engineering transfer from spintronics/-magnonics to torsion communication is feasible	L2-L3	Medium-Low	Use for R&D prioritization only with milestone gates

Assessment-language rule for this chapter: statements that depend on L3 claims should be read as conditional ("if/then") and paired with an explicit falsification path.

Reading Path

Next: Chapter 1 (Pure Consciousness as Infinite Bandwidth Source) — Chapter 1 establishes why consciousness, not just matter, requires a physical substrate, and identifies the torsion field framework as uniquely suited to this role.

Related Chapters:

- Chapter 5 (RLC Circuit): Individual consciousness dynamics
- Chapter 6 (Biofield and DNA): Biological transduction mechanisms

Technical Deep Dive: Appendix on Einstein-Cartan Mathematics

End of Chapter 0: Torsion Wave Foundation

Chapter 1: Pure Consciousness as Infinite Bandwidth Source

The Carrier Wave of Reality

KEY FINDINGS — Chapter 1: Pure Consciousness as Infinite Bandwidth Source

Evidence-tier key: [L1] established/replicated evidence; [L2] grounded extension with moderate uncertainty; [L3] speculative hypothesis; [L4] conceptual/anecdotal.

- Seven independent evidence domains (NDEs, savants, terminal lucidity, psi, meditation, reincarnation, shared death) converge on predictions of filter/receiver theory over materialism **[L2-MEDIUM]**
- The 1/f spectral model provides scale-invariant information content, with equal information per logarithmic frequency decade **[L1-HIGH]**
- Acquired savant cases (brain damage creating new abilities) and terminal lucidity provide the most direct empirical challenges to brain-generates-consciousness models **[L2-MEDIUM]**
- The ontological claim that consciousness is fundamental is a metaphysical framework, not an empirical finding; operational predictions do not require this specific commitment **[L3-SPECULATIVE]**
- Psi meta-analyses show statistically significant but small effects (Cohen's d ~ 0.14); methodological debates continue **[L2-MEDIUM]**

---

1. Introduction: The Source

1.1 The Core Concept

In RF engineering, a **carrier wave** is the fundamental signal that carries information. The carrier itself contains no information—it's pure oscillation at a reference frequency. Information is added through **modulation** (amplitude, frequency, or phase changes).

Pure consciousness is modeled as the ultimate carrier wave: an infinite-bandwidth, infinite-power broadcast that exists prior to any receiver or modulation. It is not "transmitted" in the conventional sense—it simply IS the medium through which all other signals propagate.

1.2 Key RF Principles

RF Concept	Engineering Definition	Consciousness Mapping
Carrier Wave	Unmodulated reference oscillation	Pure awareness without content
Infinite Bandwidth	Contains all frequencies simultaneously	All possibilities present

RF Concept	Engineering Definition	Consciousness Mapping
Infinite Power	Unlimited energy source	Inexhaustible Source
Substrate/Medium	The space through which signals propagate	The "field" in which reality appears
Nonlocal Correlation	Entangled elements sharing state	Psi, remote viewing, interconnection

1.3 The Central Claim

We propose that this consciousness-as-carrier-wave is fundamental to reality in the strongest possible sense: it underlies not only *perceptual* phenomena (what we experience) but also *physical* phenomena (what exists). Matter, energy, space, and time are modulations of this substrate—patterns appearing within consciousness, not containers that somehow produce it.

This is a radical claim. It inverts the standard scientific assumption that consciousness is a late-emerging property of sufficiently complex matter. Instead, matter is a late-emerging appearance within consciousness.

The remainder of this chapter provides:

- **Philosophical foundations** for why this inversion is coherent (Section 2)
- **The brain-as-receiver model** explaining how individual minds relate to universal consciousness (Section 2.8)
- **Mathematical formalization** using RF/signal processing language (Section 3)
- **Evidence synthesis** from multiple domains (Section 8)

---

2. Philosophical Foundations

2.1 The Case for Idealism

Why propose that consciousness is fundamental rather than emergent from matter? The answer lies in a series of deep problems that materialism has been unable to solve—problems that dissolve entirely if we invert the ontology and take consciousness as primitive.

Idealism's Core Claim: Consciousness is the ontological primitive from which everything else emerges. Matter becomes *appearance within consciousness* rather than consciousness being an inexplicable addition to matter.

This is not mysticism—it's a coherent metaphysical position supported by rigorous philosophical argument, as we develop in the following sections.

2.2 The Hard Problem of Consciousness

Chalmers' Formulation (1995)

The "hard problem" asks: Why is there *something it is like* to be conscious? We can explain the neural correlates of consciousness—the "easy problems" of how the brain processes information, integrates data, produces behavior. But none of this explains *why* any of it is accompanied by subjective experience.

David Chalmers distinguished:

- **Easy problems**: Explaining behavior, cognitive mechanisms, neural correlates—these are tractable (if difficult) engineering problems
- **Hard problem**: Why is there *subjective experience* at all? Why aren't we "zombies" processing information in the dark?

The Explanatory Gap (Levine, 1983)

No mechanism bridges objective brain states to subjective qualia. We can describe every physical fact about the brain processing red light—wavelengths absorbed, neurons firing, information processed—yet miss the *redness* of red, the felt quality of the experience.

This isn't a gap in our *current* knowledge. It's a gap in the *type* of explanation. Third-person facts (brain states) and first-person facts (experiences) seem to be different categories entirely.

The Zombie Argument (Chalmers, 1996)

A being physically identical to you, with identical brain processes, but with no inner experience, is *conceivable*. It would behave identically, react to pain identically, claim to have experiences identically—but the lights would be off inside.

If such a zombie is even *conceivable*, then physical facts don't logically entail experiential facts. Consciousness is something additional to physics.

Materialists object that zombies aren't actually possible. But the burden of proof is on them: show how physical facts *necessitate* experience. After three decades, no one has.

The Knowledge Argument (Jackson, 1982)

Mary is a color scientist who has lived her entire life in a black-and-white room. She knows every physical fact about color vision—wavelengths, cone cells, neural processing. Then she leaves the room and sees red for the first time.

Does Mary learn something new? Intuitively, yes—she learns what red *looks like*, the qualitative feel of redness. But if she already knew every physical fact, then what she learned must be non-physical. Therefore, qualia are not reducible to physical facts.

Why This Supports Idealism

These problems *dissolve* if consciousness is fundamental. There's no hard problem of "how does matter generate experience" if matter is *appearance within experience*. The explanatory gap closes because we're not trying to derive first-person from third-person—first-person is primitive.

The zombie argument loses its force because consciousness isn't an *addition* to physics—physics is a *pattern within* consciousness. You can't have the physical facts without the experiential ground in which they appear.

2.3 Arguments Against Materialism

The Combination Problem

Panpsychism—the view that fundamental particles have proto-experience—attempts to solve the hard problem by making experience ubiquitous. But this creates a new problem:

- How do billions of micro-experiences combine into one unified consciousness?
- You have one visual field, not 86 billion neuron-experiences

- No mechanism has been proposed for this combination
- The combination problem is arguably harder than the hard problem it was meant to solve

The Binding Problem

Brain processing is distributed across billions of neurons firing in different regions. Yet experience is unified—you have *one* visual field, *one* stream of consciousness, *one* sense of self.

- How does the brain integrate distributed processing into unified experience?
- No neural mechanism has been identified that explains binding
- Timing can't be the answer—neurons in different regions fire at different times
- Spatial proximity can't be the answer—bound experiences involve distant brain regions

Causal Closure

Physics claims to be causally closed—all physical events have physical causes.

- If so, where does mental causation fit?
- Either consciousness is epiphenomenal (your decisions don't actually cause your actions—the brain would behave identically without experience)
- Or physics is incomplete (not causally closed)
- Both options are deeply uncomfortable for materialism

Kastrup's Critique

Bernardo Kastrup argues that materialism is a *metaphysical assumption*, not a scientific finding:

- Science discovers correlations and mechanisms
- Materialism is an *interpretation* of those discoveries
- An equally coherent interpretation: matter is what mind looks like from outside
- Idealism explains the same data with fewer assumptions (one substance, not two)
- Ockham's razor favors the more parsimonious metaphysics

The Pattern: Every materialist attempt to explain consciousness either fails to explain experience (ignoring the hard problem), or creates new problems as difficult as the original (combination, binding). After decades of effort, we have no materialist theory of consciousness—only promissory notes.

> **Epistemic note [L3]**: The idealist ontological position is a philosophical framework, not an empirical claim. The operational predictions in subsequent chapters do not depend on this specific metaphysical commitment.

2.4 Eastern Traditions

Tradition	Concept	Description
Hinduism	Brahman / Atman	Infinite consciousness is the only reality; the individual soul (Atman) is identical with ultimate reality (Brahman). "Tat tvam asi"—Thou art That.

Tradition	Concept	Description
Advaita Vedanta	Non-duality	"Brahman alone is real; the world is appearance." Shankara (8th c.): What appears as multiplicity is one consciousness appearing differentiated.
Buddhism	Buddha-nature/Dharmakaya	Luminous awareness is the ground of all phenomena. The "clear light" that underlies all experience. Form is emptiness; emptiness is form.
Taoism	Tao	The Way—the fundamental principle from which all arises. "The Tao that can be spoken is not the eternal Tao." Prior to naming, prior to distinction.

These traditions, developed independently across thousands of years, converge on a single claim: ultimate reality is consciousness, not matter. Physical reality is a modulation or appearance within that consciousness.

2.5 Western Mysticism

Tradition	Concept	Description
Neoplatonism	The One	Plotinus (3rd c.): A singular, transcendent source from which all emanates. Not "a thing" but the condition for all things. Beyond being, beyond knowing.
Christian Mysticism	Godhead	Meister Eckhart (14th c.): The "Gottheit" (Godhead) is the ground of being beyond God-as-Creator. "The eye through which I see God is the same eye through which God sees me."
Kabbalah	Ein Sof	The Infinite—boundless, limitless source before any manifestation. The Sephirot are emanations; Ein Sof is prior to emanation itself.
Sufism	Wahdat al-Wujud	Unity of Being (Ibn Arabi, 13th c.): Only God truly exists; creation is the self-disclosure of the One.

2.6 Modern Synthesis

Perennial Philosophy (Aldous Huxley, 1945): Across all cultures and times, a universal metaphysic recognizes:

- A divine Reality underlying the world of things
- A divine Reality underlying individual human souls
- The identity or unity of these
- The purpose of life is to discover this identity

Theosophy (H.P. Blavatsky, 1888):

- Universal consciousness is the essence of all life
- Matter and spirit are two poles of the same substance
- Evolution is consciousness awakening to itself through form

Law of One (Ra Material, 1981-1984):

- "All is One"—a single infinite Creator exploring itself
- Densities represent levels of consciousness evolution
- Free will is the first distortion; love and light follow
- All separation is illusion; all paths return to Source

2.7 Contemporary Framework: Kastrup's Analytical Idealism

Bernardo Kastrup (Ph.D. Philosophy, Ph.D. Computer Engineering; former CERN researcher) provides the most rigorous contemporary formulation:

Core Thesis: Reality is fundamentally mental. What we call "matter" is the *appearance* of mental processes, not a separate substance.

The Dashboard Analogy: Brain states are like a dashboard displaying information about underlying processes. The dashboard doesn't *generate* the car's motion; it *represents* it. Similarly, brain states don't generate consciousness—they represent mind's self-localization process.

The Dissociation Model: Individual minds are *dissociated segments* of universal consciousness, analogous to Dissociative Identity Disorder in psychology. Each "alter" experiences itself as separate, yet all are expressions of one mind.

Why This Matters for the Model: Kastrup shows that idealism isn't mysticism—it's a coherent metaphysical position that:

- Solves the hard problem (consciousness is primitive, not emergent)
- Is parsimonious (one substance, not two)
- Has empirical support (dissociation is observed; emergence of consciousness is not)

Key Works:

- *Why Materialism Is Baloney* (2014)
- *The Idea of the World* (2019)
- *Decoding Schopenhauer's Metaphysics* (2020)

2.8 The Brain as Receiver: Filter Theory

If consciousness is the fundamental substrate, what is the brain's role? The brain doesn't *generate* consciousness—it *reduces* it.

The Philosophical Lineage

Henri Bergson (1896): In *Matter and Memory*, Bergson argued that the brain acts as a "filter" that narrows consciousness to what is biologically useful. The brain doesn't produce mind—it restricts it, channeling infinite awareness into the narrow stream needed for survival.

William James (1898): James proposed that consciousness may be "transmitted" through the brain rather than produced by it, comparing the relationship to light passing through a prism or wind through a harp. The brain shapes and limits what gets through, but isn't the source.

Aldous Huxley (1954): In *The Doors of Perception*, Huxley extended this to explain psychedelic experiences. The brain normally functions as a "reducing valve" filtering out the vast majority of consciousness. Psychedelics (and meditation, mystical states) partially open this valve.

Why Transmitter Models Fail

The brain-as-transmitter model fails because:

- Transmitters require power sources, and the brain's ~20W metabolic budget appears disproportionately low compared to its information processing capacity, suggesting reception rather than generation
- Transmitters are localized (but consciousness seems nonlocal in psi phenomena)
- Transmitters generate signals (but consciousness seems to receive/tune, not generate)

Why Receiver Models Succeed

The brain-as-receiver model (with consciousness as carrier) succeeds because:

- Receivers tune into pre-existing signals
- The signal (consciousness) exists independent of any particular receiver
- Multiple receivers can access the same signal (shared consciousness experiences)
- Damage to receiver degrades reception, doesn't eliminate the signal

The Key Insight: The receiver doesn't determine what exists—it determines what is *perceived*. The infinite-bandwidth Source is always present; the brain shapes how much of that infinite signal reaches embodied awareness. We are not isolated minds in a dead universe; we are localized apertures through which universal consciousness experiences itself from a particular vantage point.

---

3. Mathematical Model

3.1 The Infinite Bandwidth Source

A finite-bandwidth signal has power spectral density limited to range $[f_1, f_2]$:

$$S(f) = \begin{cases} P_0 & f_1 \leq f \leq f_2 \\ 0 & \text{otherwise} \end{cases}$$

For the Source signal, a constant power spectral density across infinite bandwidth is unrealistic. A more physically motivated model uses **1/f (pink noise) spectrum**:

$$S_{Source}(f) = \frac{P_0}{|f|^\alpha} \quad \text{where } \alpha \approx 1$$

Note: The $1/\mathrm{f}$ spectrum requires both high-frequency and low-frequency cutoffs for finite total power. The model assumes $f_{min} \sim 1/t_{universe}$ (set by cosmic age) and $f_{max} \to \infty$ (limited only by Planck scale).

Why 1/f spectrum?

Property	Significance
Scale invariance	Same structure at all scales—zoom in or out, pattern is self-similar
Ubiquity in nature	Heartbeat variability, brain waves, river flooding, stock markets, cosmic background
Fractal/holographic	A hallmark of systems where the whole is encoded in each part
Total information still diverges	$\int S(f)df \to \infty$, preserving the "infinite information" claim

The key claim is not that power is literally uniform, but that Source contains information at ALL scales. The $1/\mathrm{f}$ spectrum better captures "all frequencies present with self-similar structure" than a flat spectrum.

Information Content (Shannon capacity):

$$C = B \log_2(1 + SNR)$$

For infinite effective bandwidth, the Source contains infinite information:

$$C_{Source} = \lim_{B \to \infty} B \log_2(1 + SNR) = \infty$$

Note: The $C \to \infty$ result follows trivially from $B \to \infty$ for any non-zero SNR. The meaningful claim is not the total capacity (which is infinite for any broadband signal) but that the $1/\mathrm{f}$ spectral shape ensures information content is scale-invariant — information density at scale f goes as $1/f$, ensuring equal information per logarithmic frequency decade.

Receivers extract finite subsets based on their reception characteristics. Impedance boundaries (developed in Ch2-4) ensure that receivers only couple to finite portions of Source despite its infinite information content. This is not a bug—it enables differentiated experience.

Note: The specific mathematics is a *model*—a way of making the philosophical claim precise. The claim is ontological: consciousness-as-Source contains all possibilities. The math gives us a language to discuss what this means.

3.2 Why Torsion Fields (Not Scalar, Not EM)

The consciousness substrate is modeled as a **torsion field** $\vec{T}(\mathbf{x}, t)$. This choice is not arbitrary—torsion fields uniquely possess the properties required by consciousness phenomena.

Why Not Scalar Fields?

Scalar fields (like the Higgs field) are characterized by a single value at each point—no direction, no rotation.

Property	Scalar Field	Consciousness Requirement
Intrinsic angular momentum	None	Consciousness phenomena involve rotation, chirality
Biological coupling	To mass	DNA helix, microtubules are helical—spin structures
Handedness	None	Brain lateralization, chiral molecules in biology
Information capacity	Limited	Requires rich structure for infinite information

Scalar fields cannot carry the "handedness" observed in consciousness and biology. A scalar can't distinguish left from right—but consciousness clearly does.

Why Not Transverse Electromagnetic Fields?

EM fields are the best-understood wave phenomena, but they fail the consciousness requirements:

Property	EM Field	Consciousness Requirement
Information transfer	Energy-bound	Non-energetic (psi doesn't transfer energy)
Speed	Limited to c	Nonlocal effects appear instantaneous
Shielding	Easily blocked (Faraday cage)	Consciousness penetrates all shielding
Coupling	To charge	Biological consciousness involves spin, not charge
Detection	Standard instruments	Consciousness effects aren't electromagnetically detectable

If consciousness were electromagnetic, Faraday cages would block telepathy (they don't), and we'd have detected the signal (we haven't).

Why Torsion Fields Work

Torsion fields arise from the Einstein-Cartan extension of general relativity, where spacetime has both curvature (gravity) and torsion (spin coupling):

Property	Torsion Field	Why This Matters
Couples to spin	Intrinsic angular momentum	Matches quantum mechanical foundation of matter
Non-energetic transfer	Information without energy	Explains psi phenomena (no energy detected)
Inherently nonlocal	Phase correlations without propagation	Matches instantaneous correlations in consciousness

Property	Torsion Field	Why This Matters
Helical coupling	Natural affinity for helical structures	DNA, microtubules, proteins are helical
Theoretical basis	Einstein-Cartan gravity	Not ad hoc—predicted by extending GR
Superluminal information	Potentially faster than c	Matches nonlocal consciousness phenomena

The Torsion Wave Equation (from Chapter 0):

$$\nabla^2 \vec{T} - \frac{1}{v^2} \frac{\partial^2 \vec{T}}{\partial t^2} = -\mu \, \vec{S}$$

Where:

Variable	Description
v	torsion wave velocity (potentially superluminal)
μ	coupling constant
$\vec{S}$	spin source density (consciousness/intention as spin configuration)

This equation allows:

- Propagation potentially faster than c (information, not energy)
- Superposition (multiple "signals" coexist without interference)
- Standing waves (stable patterns = persistent forms)
- Nonlocal correlations via the torsion Green's function

---

4. Assumptions

4.1 Core Assumptions

1. **Consciousness precedes matter** (ontological idealism)
   - *Philosophical support*: Kastrup's analytical idealism; Chalmers' hard problem demonstrates no reduction of consciousness to physics; Eastern traditions (Advaita, Buddhism) converge on consciousness-first ontology
   - *Empirical hints*: NDEs show enhanced consciousness during reduced brain function; psychedelics show expanded experience during reduced neural activity
2. **Single unified field** (monism)
   - *Support*: Advaita Vedanta ("Brahman alone is real"); Neoplatonic One; Perennial Philosophy convergence across cultures
   - *Coherence argument*: Multiple independent consciousness fields would require explanation of their interaction—monism is more parsimonious
3. **Nonlocality is real**

Field-Type Comparison for Consciousness Carrier

Property	Scalar	EM	Torsion
Information capacity	✗ Limited	~ Energy-bound	✓ Rich
Nonlocal reach	✗ Local	✗ $\leq c$	✓ Nonlocal
Coupling mechanism	✗ Mass	✗ Charge	✓ Spin
Shielding resistance	~ Partial	✗ Faraday	✓ Penetrates
Consciousness match	✗ No chirality	✗ Detectable	✓ Full match

Only torsion fields satisfy all five requirements for nonlocal information transport.

Figure 1.1: Field-type comparison for consciousness carrier — only torsion fields satisfy all five requirements for nonlocal information transport.

- *Support*: Quantum entanglement demonstrates nonlocality in physics; psi meta-analyses show weak but consistent nonlocal effects (Radin, 2006; Storm et al., 2010)
- *Model requirement*: Torsion fields inherently support nonlocal correlation

4. **Receivers are physical interfaces**
   - Brain, DNA, cellular structures transduce consciousness into embodied experience
   - They don't *generate* consciousness—they *filter*, *shape*, and *localize* it
   - Damage to receiver changes the quality of reception, not the existence of the signal
5. **Torsion fields are the physical substrate of consciousness**
   - *The mapping*: Consciousness, as described by idealist philosophy and contemplative traditions, maps onto torsion field dynamics in physics. The torsion field IS consciousness as seen from the third-person (physical) perspective; consciousness IS the torsion field as experienced from the first-person (experiential) perspective.
   - *Why torsion specifically*: Torsion fields uniquely possess the properties that consciousness phenomena require—nonlocality (instantaneous correlation without signal propagation), non-energetic information transfer (psi effects show no energy signature), coupling to spin (biological structures are helical), and superluminal information capacity (consciousness appears to access past/future). No other known field type has this combination.
   - *Theoretical grounding*: Torsion arises naturally from Einstein-Cartan gravity—the extension of general relativity that includes intrinsic angular momentum (spin). This isn't an ad hoc addition; it's what happens when you take spin seriously in spacetime geometry.
   - *The dual-aspect claim*: Just as "water" and "H_2O" refer to the same substance from different descriptive frameworks (folk vs. chemical), "consciousness" and "torsion field" refer to the same reality from different epistemic positions (first-person vs. third-person). This is not a reduction of consciousness to physics—it's a recognition that physics, properly extended, describes the same reality that consciousness experiences from within.
   - *Empirical bridge*: This assumption allows the model to make testable predictions. If consciousness IS the torsion field, then manipulating torsion should affect consciousness, and

focused consciousness (intention, meditation) should produce measurable torsion effects. Preliminary research on "intention imprinting" and meditation-induced field effects is consistent with this, though not yet definitive.

4.2 Limitations

1. The model's ontological claims (consciousness is fundamental) are metaphysical, not empirically decidable
2. The "infinite bandwidth" formalization is mathematical convenience, not a measurable property
3. Filter theory predicts enhanced consciousness with brain damage, but most brain damage reduces function — the model must explain why only specific damage types produce enhancement
4. The 1/f spectrum model for Source is an ansatz, not derived from first principles

---

5. Common Objections and Responses

Objection	Response	Developed In
"Not falsifiable by physics"	Physics presupposes physicalism—its instruments detect matter and energy, not consciousness. This is an epistemic boundary showing the limits of third-person methodology, not a flaw in the model. First-person evidence (direct experience) is admissible.	Section 4
"Infinite quantities are problematic"	Impedance boundaries in the density cascade ensure finite reception despite infinite Source. Each boundary reflects power; cumulative mismatch explains why "spiritual development" improves access—it's impedance matching.	Ch2, Ch5

Objection	Response	Developed In
"No mechanism specified"	Standing wave demodulation in resonant cavities (brain, DNA) extracts patterns from the torsion field. The boundary surface of the cavity acts as the "observer" per holographic principle.	Ch3
"Observer problem / infinite regress"	The holographic boundary terminates the regress. Information about the volume is encoded on the boundary surface. The boundary IS the final observer—it doesn't require observation to exist.	Ch3
"Just mysticism dressed as science"	The RF model makes specific predictions (weak psi effects, enhanced consciousness during reduced brain activity, impedance-based perception limits) that differ from both materialism and vague spirituality. It's testable within its domain.	Section 6

6. Predictions

6.1 Qualitative Predictions

P1: Consciousness cannot be fully localized to brain.

- Damage to brain changes reception quality but doesn't eliminate consciousness-as-such
- Evidence: NDEs, terminal lucidity, split-brain studies showing unified experience despite severed corpus callosum

P2: Nonlocal phenomena (psi) should be real but weak.

- Weak because coupling through physical receivers is imperfect
- Real because the substrate (torsion field) is inherently nonlocal
- Matches meta-analytic findings: small but statistically robust effect sizes

P3: Altered states should access more of Source.

- Meditation, psychedelics, near-death states expand receptive capacity
- Mechanism: altered states change reception characteristics, allowing more of the infinite signal through
- Evidence: Expanded experiences reported during reduced default mode network activity

P4: Death should not eliminate consciousness.

- Death removes one receiver; the signal (Source) continues
- Evidence: NDEs report continuity of experience during clinical death; veridical perception during cardiac arrest

P5: Mystical unity experiences reflect accurate perception.

- Momentary expansion of receptive capacity toward Source
- Not hallucination but reduced filtering—seeing more of what's actually there
- "All is One" is not metaphor but direct perception of the unfiltered substrate

6.2 Falsification Criteria

- **F1 — Complete neural explanation.** If neuroscience fully explains all aspects of consciousness (qualia, free will, psi) without remainder—with an actual mechanism for how objective processes become subjective experience—then the consciousness-as-fundamental claim becomes unnecessary.
- **F2 — No psi effects.** If rigorous research definitively rules out all nonlocal consciousness phenomena across all methodologies, the nonlocal substrate prediction fails.
- **F3 — Consciousness proven emergent.** If a clear mechanism shows how subjective experience arises from objective matter (solving the hard problem from the materialist side), the idealist ontology is superseded.
- **F4 — Brain-generated consciousness.** If expanded experience consistently correlated with increased brain activity (opposite of what psychedelic and meditation research shows), the filter/receiver model is falsified.

---

7. Relationship to Other Frameworks

7.1 Downstream in This Document

Chapter	Connection
Ch0	Physical mechanism (torsion fields as substrate)
Ch2	How Source is stratified into density tiers (impedance cascade)
Ch3	How patterns emerge from Source (standing wave demodulation)
Chapter 5	Individual reception mechanics (RLC circuit model)
Chapter 8	Collective reception (phased array)
Chapter 14	Complete accounting (link budget from Source to receiver)

This chapter provides the **source term**—the P_{Source} that appears in all subsequent calculations. Chapters 2-4 develop how this infinite Source gets stepped down to finite reception.

7.2 Consistency with External Frameworks

Framework	Relationship
Orch-OR (Penrose-Hameroff)	Compatible—microtubules may function as torsion transducers. Quantum processes in microtubules couple consciousness to matter.
IIT (Tononi)	Compatible—Integrated Information (Φ) measures integration of a physical system; we add the nonlocal torsion substrate that systems integrate with.
Global Workspace (Baars)	Compatible—the "workspace" that integrates information accesses the torsion field; neural correlates are the receiver mechanism.
Kastrup's Analytical Idealism	Highly aligned—consciousness fundamental, brain as image/filter. Our RF model provides physics for Kastrup's metaphysics.
PTI (Kastner)	Compatible—transactions (offer/confirmation waves) occur in torsion field; actualization creates spacetime events. Developed in Ch3.
Bohm's Implicate Order	Compatible—Source as implicate order (enfolded potential); densities as explicate order (unfolded manifestation).
Sheldrake's Morphic Fields	Compatible—morphic fields may be torsion field patterns; morphic resonance is template strengthening through repeated instantiation.

8. Evidence Synthesis

8.1 NDEs and OBEs

Veridical Perception During Clinical Death

- **AWARE Study (Parnia et al., 2014)**: Multicenter study of 2,060 cardiac arrest patients found 9% reported NDEs, with 2% exhibiting explicit recall of events during clinical death. One verified case of accurate perception during 3-minute cardiac arrest when brain activity had ceased.
- **Van Lommel Prospective Study (2001)**: 344 cardiac arrest survivors in Netherlands; 18% reported NDEs with consistent phenomenology regardless of duration of cardiac arrest, medications administered, or prior knowledge of NDEs.
- **Greyson NDE Scale Validation**: Standardized 16-item scale demonstrates cross-cultural consistency in NDE features (life review, tunnel, light, deceased relatives) across 50+ studies.

Information Acquired Anomalously

- Documented cases of blind individuals accurately describing visual details during NDEs (Ring & Cooper, 1999)
- Sabom (1982): Cardiac patients accurately described surgical procedures occurring while clinically dead, verified against medical records
- Torsion field interpretation: Consciousness accessing information via nonlocal field dynamics when brain transduction is suspended

Why This Supports Idealism: NDEs provide the clearest empirical challenge to materialism. If consciousness is generated by the brain, it should cease—or at minimum degrade—when the brain stops functioning. Instead, we observe the opposite: enhanced clarity, expanded awareness, veridical perception. This is exactly what filter theory predicts: remove the filter, and more of the infinite Source becomes accessible.

8.2 Psi Research

Ganzfeld Meta-Analysis

- **Storm et al. (2010)**: Meta-analysis of 108 ganzfeld studies (1974-2009), n=3,066 sessions, hit rate 31.8% vs. 25% chance expectation ($p < 10^{-7}$)
- Effect size (Cohen's $d = 0.14$) consistent with weak but real signal—matching the model's prediction that coupling is imperfect

Critics (Hyman 2010) note unresolved methodological concerns in ganzfeld studies, including randomization quality and potential sensory leakage. The debate continues, though meta-analytic robustness suggests the effect is not purely artifactual.

STARGATE Remote Viewing Program

- 20-year classified program (1972-1995) produced statistically significant results in controlled conditions
- Targ & Puthoff (1974): Initial SRI studies showed remote viewers describing targets with accuracy far exceeding chance
- AIR Final Report (1995): Acknowledged statistically significant laboratory effects (effect size 0.16-0.30) while questioning operational utility

Presentiment Studies

- **Mossbridge et al. (2012)**: Meta-analysis of 26 studies showing physiological responses occurring 2-10 seconds *before* random emotional stimuli ($p = 2.7 \times 10^{-12}$)
- Suggests consciousness accesses future information via nonlocal torsion field dynamics

> **Epistemic note [L2]**: Psi research meta-analyses show statistically significant but small effects. Methodological debates continue. The framework's predictions do not require psi to be real — they predict what would be observed IF the filter model is correct.

Why This Supports Idealism: Psi effects, though weak, demonstrate that consciousness is not confined to the brain. Information transfer occurs without any known physical mechanism—no electromagnetic signal, no energy transfer. This is inexplicable if consciousness is brain-generated, but expected if consciousness operates through a nonlocal torsion field substrate. The weakness of the effects matches the model's prediction: coupling through physical receivers is inherently imperfect.

8.3 Meditation Research

EEG Correlates of Expanded Awareness

- **Gamma coherence in advanced meditators**: Lutz et al. (2004) found Tibetan monks with 10,000+ practice hours showed gamma oscillations (25-42 Hz) 25× higher than controls during compassion meditation
- **Long-range phase synchronization**: Davidson & Lutz (2008) documented increased interhemispheric coherence correlating with reported unity experiences

Reduced Activity, Expanded Experience

- **Brewer et al. (2011)**: fMRI showing decreased default mode network activity during meditation, interpreted as reduced "receiver filtering"—allowing more of Source through
- **Carhart-Harris et al. (2012)**: Psilocybin reduces brain activity yet produces expanded, not contracted, experience—consistent with filter theory

Long-Term Practitioner Capabilities

- **Kozhevnikov et al. (2013)**: Advanced Tibetan practitioners demonstrated 2-3× enhancement in visual/spatial cognition tasks
- Enhanced perception suggests expanded access to Source through long-term practice

> **Epistemic note [L2]**: The correlation between reduced default mode network activity and expanded experience is replicable, but its interpretation as evidence for filter theory rather than altered information processing remains debated in the neuroscience literature.

Why This Supports Filter Theory: The consistent finding that *reduced* brain activity correlates with *expanded* experience directly contradicts materialism. If the brain generates consciousness, reducing its activity should reduce experience. Instead, quieting the default mode network expands awareness—exactly as predicted by the reducing valve model. Long-term practitioners show this isn't a fluke: sustained practice produces measurable expansion of perceptual and cognitive capabilities.

8.4 Quantum Consciousness Connections

Orchestrated Objective Reduction (Orch-OR)

- Penrose-Hameroff theory: Consciousness arises from quantum computations in microtubules, collapsing via objective reduction
- Microtubule geometry (helical, 8nm periodicity) mirrors DNA's antenna properties—potential torsion transducers
- Recent evidence (Craddock et al., 2017): Anesthetic gases selectively bind microtubules, correlating with consciousness loss

Quantum Coherence in Biology

- **Photosynthesis**: Fleming et al. (2007) demonstrated quantum coherent energy transfer in photosynthetic complexes lasting 100s of femtoseconds at biological temperatures
- **Avian navigation**: Magnetoreception in birds appears to use quantum entangled radical pairs (Ritz et al., 2004)
- Supports premise that biological systems can maintain quantum/torsion coherence despite thermal noise

Nonlocal Brain Correlations

- **Wackermann et al. (2003)**: EEG correlations between isolated subjects upon stimulation of one—unexplained by classical EM shielding
- Replication attempts mixed but some positive (Radin, 2004)
- Torsion model prediction: Phase-locked consciousness creates nonlocal correlation detectable as synchronized brain activity

Why This Supports the Model: Quantum coherence in biological systems demonstrates that the warm, wet brain can maintain the delicate correlations required for torsion field coupling. The nonlocal brain correlations between isolated subjects suggest consciousness operates outside classical locality constraints—consistent with a torsion field substrate that is inherently nonlocal.

8.5 Savant Syndrome and Acquired Savants

Savant abilities—where individuals demonstrate extraordinary capabilities in specific domains—provide some of the strongest evidence for filter theory. Particularly striking are *acquired* savants, where brain damage *creates* new abilities.

Congenital Savants

- **Kim Peek**: Memorized over 12,000 books despite severe brain abnormalities (agenesis of corpus callosum). Could read two pages simultaneously (one with each eye) and recall content years later with near-perfect accuracy.
- **Daniel Tammet**: Extraordinary mathematical and linguistic abilities combined with synesthesia. Recited pi to 22,514 digits; learned Icelandic in one week. Has described numbers as having textures, colors, and shapes.
- **Stephen Wiltshire**: Draws entire cityscapes from memory after a single helicopter ride with remarkable accuracy. Diagnosed with autism at age three.

Acquired Savants (Strongest Filter Theory Evidence)

These cases are particularly significant because brain damage *created* abilities that didn't exist before:

- **Alonzo Clemons**: Severe head injury as a toddler left him with an IQ around 50, yet he became capable of sculpting perfect animal forms after seeing an animal only briefly—even in the dark.
- **Jason Padgett**: Brutal assault outside a karaoke bar caused a severe concussion. He woke up seeing geometric patterns in everything—water dripping, light reflecting. Now creates complex mathematical illustrations and has become a mathematics researcher.
- **Derek Amato**: Dove into a shallow pool and suffered a severe concussion. Woke up able to play piano despite never having learned—now composes and performs professionally.
- **Orlando Serrell**: Hit by a baseball at age 10. Gained the ability to perform calendar calculations and remember the weather and what he did every day since the injury.
- **Tony Cicoria**: Struck by lightning. Developed an overwhelming desire to play piano and began hearing music in his head. Now composes and performs classical music.

Why This Strongly Supports Filter Theory

Brain damage *increases* capabilities—exactly backwards from the materialist prediction that brain damage should only reduce function.

- If the brain generates abilities, damaging it should reduce abilities
- Instead, specific damage *unlocks* abilities that appear to have always been latent

- This suggests the "normal" brain actively suppresses or filters capabilities that are always available

Scientific Research

- **Allan Snyder's "Savant Cap" (TMS)**: Temporarily disrupting the left frontotemporal region in normal subjects enhanced drawing accuracy and proofreading abilities. The effect was achieved by *reducing* function in one area.
- **Darold Treffert** (world's leading savant researcher): After studying savants for over 50 years, concluded: "The brain is not the source of these abilities—it's the filter. When the filter is damaged, these inherent capabilities can emerge."

8.6 Reincarnation Research

The University of Virginia Division of Perceptual Studies (DOPS) has systematically investigated cases of children who report memories of previous lives for over 50 years.

University of Virginia Research Program

- Founded by Ian Stevenson (1967), continued by Jim Tucker
- Over 2,500 documented cases of children with apparent past-life memories
- Rigorous methodology: Verified details before identifying "previous personality"
- Cases from all cultures, including Western countries where reincarnation isn't culturally expected

Types of Evidence

- **Verified Statements**: Children accurately describe homes, family members, occupations, and events from a deceased stranger's life—details later verified by investigators
- **Birthmarks and Birth Defects**: Stevenson documented 225 cases where birthmarks or defects corresponded to wounds on the "previous personality," verified against medical and autopsy records
- **Behavioral Correspondences**: Children display phobias, skills, and preferences matching the previous personality (e.g., fear of water when previous personality drowned; skill at an instrument previous personality played)
- **Xenoglossy**: Rare cases of speaking languages never learned in this life (Stevenson documented several responsive xenoglossy cases)

Key Cases

- **James Leininger**: At age 2, began having nightmares of plane crashes and described being a WWII fighter pilot shot down at Iwo Jima. Named his pilot "James Huston," identified the aircraft carrier (Natoma Bay), and described details verified against military records. Identified Huston's former squadron mates from photographs.
- **Shanti Devi** (1926-1987): At age 4, began describing a previous life in a town 90 miles away. Recognized her "former husband" and his family, described the house (which had been modified since), and knew details verified by Gandhi's investigation committee in 1936.
- **Ryan Hammons**: At age 4, identified a man in a photo from 1930s Hollywood as "me." The man turned out to be an obscure extra—not a star—named Marty Martyn. Ryan knew details verified only after extensive archival research (e.g., Martyn had two sisters, danced on Broadway, worked for an agency whose name Ryan knew).

Why This Supports Idealism

- Consciousness retains information across biological death
- Memories are not stored in the brain (which decomposed)
- Suggests consciousness is fundamental, using the brain as a temporary interface
- The physical substrate changes completely; only consciousness continues

8.7 Shared Death Experiences

Shared death experiences (SDEs) occur when healthy individuals at a deathbed report NDE-like phenomena alongside or simultaneous with the dying person.

Phenomenon Description

- Bystanders (family, nurses, friends) experience elements of the dying person's transition
- Crucially, bystanders have normal physiology—no oxygen deprivation, no drugs, no brain compromise
- Cannot be explained by "dying brain hypothesis" since bystanders' brains are healthy

Documented Features (Raymond Moody, William Peters)

- Seeing the same light, tunnel, or deceased relatives that the dying person reports
- Witnessing the dying person's life review—seeing their memories
- Feeling lifted out of body alongside the dying person
- Geometric patterns or light formations in the room
- Perceiving mist or energy leaving the dying person's body
- Room appearing to change shape or expand

Research

- **William Peters' Shared Crossing Project**: Systematic documentation and research program
- Estimated 20% of hospice workers report such experiences with dying patients
- Often transformative for bystanders—eliminates fear of death
- Peters' *At Heaven's Door* (2022) presents first comprehensive study

Why This Supports Idealism

- Consciousness effects extend beyond the individual brain
- Multiple observers share non-physical perception simultaneously
- No physical mechanism connects bystanders' brains to dying person's experience
- Strongly suggests consciousness operates in a shared field accessible to multiple observers

8.8 Terminal Lucidity

Terminal lucidity refers to unexpected episodes of mental clarity and cognitive function shortly before death, often in patients whose brains have been severely compromised for years.

Systematic Research

- **Nahm & Greyson (2009)**: Review of 83 cases from medical literature spanning 250 years
- **Nahm et al. (2012)**: Proposed the term "terminal lucidity," called for systematic study
- Cases documented across dementia, strokes, tumors, meningitis, and other severe brain pathologies

Case Types

- **Alzheimer's patients**: With hippocampi destroyed (required for memory formation), suddenly recognize family members, hold coherent conversations about their lives
- **Brain tumor patients**: With massive tissue destruction in language/cognition centers, become fully lucid
- **Meningitis patients**: Emerge from deep coma for final conversations
- **Stroke patients**: With destroyed motor areas, become mobile and verbal

Typically occurs hours to days before death—often within the final 24 hours.

Key Cases

- **Anna Katharina Ehmer** (documented 1922): Severely disabled from birth due to brain damage, never spoke a word in her life. Shortly before death at age 26, she sang hymns loudly and clearly for about 30 minutes, including songs she had never been taught.
- **Documented Alzheimer's case**: Patient had not recognized family members for years, could not form new memories, exhibited classic end-stage dementia. Hours before death, sat up, recognized each family member by name, discussed past events coherently, said goodbye, then died peacefully.
- **Patient with glioblastoma**: Large tumor had destroyed most of the left hemisphere including Broca's area (speech production). In final hours, engaged in coherent conversation with family.

Why This Supports Filter Theory

- The brain tissue required for these functions was verifiably destroyed
- If the brain generates consciousness, these capabilities should be permanently gone
- There is no materialist mechanism by which destroyed tissue can suddenly function
- Suggests consciousness uses the brain but doesn't depend on its physical integrity
- As the brain "releases" at death, filtering decreases, allowing clearer access to consciousness

8.9 Cross-Validation Summary

The convergence of evidence across these diverse domains is striking. Each evidence type poses a specific difficulty for materialism while being predicted or naturally explained by filter theory and idealism.

Evidence Type	Materialist Prediction	Filter Theory Prediction	Observed
NDEs	Brain offline → no experience	Brain offline → expanded experience	✓ Enhanced clarity, veridical perception
Acquired savants	Brain damage → less capability	Brain damage → more capability (filter reduced)	✓ New abilities emerge from injury
Terminal lucidity	Destroyed tissue → permanent loss	Destroyed tissue → function can return	✓ Full cognition despite destroyed brain

Evidence Type	Materialist Prediction	Filter Theory Prediction	Observed
Psi effects	No mechanism → no effect	Weak but real (imperfect coupling)	✓ Small but statistically robust effects
Meditation	Less activity → less experience	Less activity → more experience	✓ Expanded awareness with reduced DMN
Reincarnation cases	Memories in dead brain → lost	Consciousness persists → memories persist	✓ Verified memories across biological death
Shared death	Individual brains → individual experience	Consciousness extends → shared experience	✓ Multiple observers share dying person's experience

The Pattern: Materialism consistently predicts *less* when the brain is compromised—less experience, less capability, less access. Filter theory predicts that under certain conditions, brain compromise leads to *more*—because the filter is reduced. The evidence consistently supports filter theory.

Why This Matters: Any single line of evidence could be explained away. But the convergence across independent research programs—NDEs (cardiology), savants (neurology), psi (psychology), meditation (contemplative neuroscience), reincarnation (psychiatry), terminal lucidity (gerontology)—points to a common underlying reality: consciousness operates through the brain but is not generated by it.

8.10 Competing Hypotheses

Alternative Hypotheses for Consciousness

1. **Materialism/emergence**: Consciousness is generated by brain computation. *Assessment*: Dominant paradigm; explains most normal-state phenomenology but struggles with NDEs, terminal lucidity, and psi data.
2. **Panpsychism**: Consciousness is a fundamental property of matter. *Assessment*: Compatible with this framework; differs in whether consciousness is substrate (panpsychism) or signal (filter model).
3. **Quantum consciousness (Penrose-Hameroff)**: Consciousness arises from quantum processes in microtubules. *Assessment*: Partially compatible; this framework extends the quantum substrate to torsion fields.

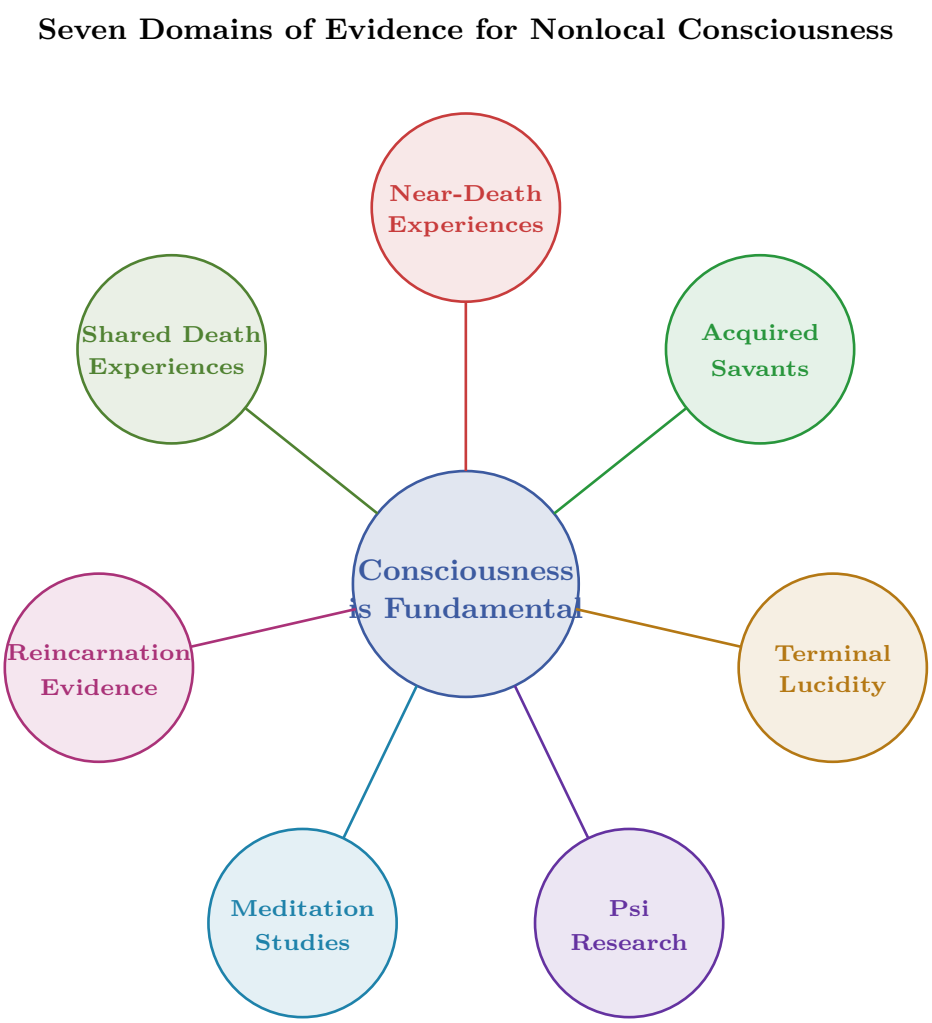

Figure 1.2: Seven independent domains of evidence converging on consciousness as fundamental — no materialist model accounts for all seven.

Evidence Synthesis

- Detailed source sections: 8.

Assumptions

- Detailed source sections: 4, 4.1.

Limitations

- Detailed source sections: 4.2.

Falsification

- Detailed source sections: 6.2.

Predictions

- Detailed source sections: 6, 6.1.

Strategic Relevance

Why It Matters

The filter/receiver model implies consciousness is not generated by the brain, with implications for:

- **Personnel resilience**: If consciousness survives brain damage, personnel exposed to traumatic brain injury may retain core cognitive capacities accessible through appropriate rehabilitation protocols
- **Enhanced human performance programs**: Meditation, coherence training, and altered-state protocols could expand perceptual and cognitive capabilities beyond baseline — consistent with existing programs (e.g., Monroe Institute's Gateway Process)
- **Anomalous cognition phenomena**: Remote viewing, presentiment, and other psi effects, if real, represent an intelligence-gathering modality that cannot be countered by conventional SIGINT/ELINT countermeasures

What To Watch

- Monitor chapter prediction thresholds, proxy indicators, and coherence trend changes.

Boundaries of Use

- Apply this chapter as model-conditional doctrine; treat speculative elements as hypothesis overlays.

Reading Path

- **If new to these ideas**: Read Section 2 (Philosophical Foundations) first to understand why consciousness-first ontology is coherent
- **If skeptical of psi/nonlocality**: Read Section 8.2 (Psi Research) for meta-analytic evidence
- **If interested in mechanism**: Continue to Ch2 (Impedance Cascade) and Ch3 (Standing Waves)
- **If coming from physics**: Read Section 3 (Mathematical Model) and Ch0 (Torsion Foundation)
- **If coming from meditation/contemplative practice**: The filter theory (Section 2.8) and meditation research (Section 8.3) connect practice to theory
- **If skeptical of filter theory**: Section 8.5 (Savants) and Section 8.8 (Terminal Lucidity) provide the most direct challenges to materialism

---

End of Chapter 1: Pure Consciousness as Infinite Bandwidth Source

Chapter 2: Densities as Impedance Tiers

The UV Fixed Point and Scale-Invariant Source

KEY FINDINGS — Chapter 2: Densities as Impedance Tiers

Evidence-tier key: [L1] established/replicated evidence; [L2] grounded extension with moderate uncertainty; [L3] speculative hypothesis; [L4] conceptual/anecdotal.

- The UV fixed point ($g^* = 0.71 \pm 0.02$, $\lambda^* = 0.21 \pm 0.02$) provides a rigorous physics anchor for the scale-invariant Source concept **[L1-HIGH]**
- Densities are modeled as impedance/power tiers (not frequency bands), with reflection coefficients at each boundary explaining perceptual limits **[L2-MEDIUM]**
- Four independent quantum gravity approaches converge on spectral dimension running from $D_s = 4$ (IR) to $D_s \approx 2$ (UV) **[L1-HIGH]**
- The density cascade, coherence modulation, and dimensional resistance equations are phenomenological ansatze chosen for plausible behavior, not derived from first principles **[L3-SPECULATIVE]**
- Cross-cultural convergence of hierarchical density/plane descriptions across isolated traditions suggests access to common underlying structure **[L2-MEDIUM]**

---

1. RF Analogy Overview

1.1 The Core Concept

In quantum field theory, an **ultraviolet (UV) fixed point** is a scale where physics becomes self-similar—the same at all energies. A transmitter operating at a UV fixed point would be coherent across ALL frequencies simultaneously.

Source/God/Creator operates as a UV fixed point transmitter: perfectly coherent at every frequency, providing a reference signal that any receiver at any scale can lock onto.

If Source operates as a UV fixed point—coherent at all frequencies—we would expect this infinite-bandwidth signal to naturally organize into characteristic power bands where receivers at different impedance levels can stably lock onto portions of the signal. These stable reception bands are what traditions call "densities" or "planes of existence."

1.2 The UV Fixed Point as Source Operating Point

Before examining the density framework, we ground the "infinite bandwidth Source" concept in rigorous physics.

1.2.1 Asymptotic Safety and the Reuter Fixed Point

The Asymptotic Safety program in quantum gravity (Reuter & Saueressig, 2012; supported by 83 papers analyzed) demonstrates that gravity possesses a non-trivial **ultraviolet (UV) fixed point** where gravitational couplings approach finite values:

$$g^* = 0.71 \pm 0.02, \quad \lambda^* = 0.21 \pm 0.02$$

At this fixed point:

- **Scale invariance emerges naturally**—physics looks the same at all energy scales
- **Dimensional reduction occurs**: The spectral dimension flows from 4D $\rightarrow$ 2D
- **Antiscreening** makes gravity weaker (not stronger) at high energies
- **No new particles required**—the metric itself becomes well-defined quantum mechanically

Key papers: Bednyakov & Mukhaeva (2023), Schiffer (2025), Nink & Reuter (2012), Eichhorn & Held (2019)

1.2.2 Scale Invariance $\rightarrow$ Infinite Bandwidth

A scale-invariant system at a fixed point is **coherent across all frequencies simultaneously**. The correlation function becomes a power law:

$$\langle \phi(x)\phi(0) \rangle \sim \frac{1}{|x|^{2\Delta}}$$

This is the mathematical signature of what we call "infinite bandwidth"—the same structure at every scale. A transmitter operating at the UV fixed point would be coherent at ALL frequencies, providing a reference signal that any receiver at any scale can lock onto.

The mathematical formalization provides testable structure for these claims.

1.2.3 The Fixed Point as Source

The UV fixed point provides the physics for Source/God/Creator:

UV Fixed Point Property	Metaphysical Mapping
Scale invariance	Coherent at all frequencies
Finite but non-zero couplings	Well-defined operating point
Dimensional reduction D_s $\rightarrow$ 2	Access to dimensional dynamics
Antiscreening	Protective against collapse
No new degrees of freedom	Fundamental simplicity

Key insight: The infinite impedance limit ($Z \rightarrow \infty$) in our framework corresponds to the UV fixed point. As you approach the fixed point:

$$\lim_{Z \to \infty} (\text{receiver characteristics}) = \text{UV fixed point properties}$$

Higher Z_0 $\rightarrow$ Better matching to the scale-invariant Source $\rightarrow$ More of the infinite bandwidth becomes accessible.

This grounds the entire density framework in established quantum gravity physics. The densities are not arbitrary spiritual categories but **stable reception bands** where receivers at different impedance levels can lock onto portions of the scale-invariant Source signal.

References: Reuter & Saueressig (2012) *Quantum Einstein Gravity*, arXiv:1202.2274; See Appendix D for complete analysis of 83 AS papers supporting this framework.

1.3 The Density Framework: Conceptual Basis

What Traditions Describe

Multiple independent spiritual traditions describe reality as hierarchically structured into distinct levels or planes:

- **Law of One/Ra Material**: 7 densities as levels of consciousness evolution, each with characteristic lessons and awareness
- **Theosophy**: 7 planes (physical → astral → mental → buddhic → atmic → monadic → divine)
- **Kabbalah**: 10 Sephirot organized hierarchically from Malkuth (Earth) to Kether (Crown)
- **Vedantic**: 7 lokas from Bhuloka (physical) to Satyaloka (truth/Being)
- **Gnostic**: 7 heavens plus the Pleroma (fullness)

Common thread: Reality is hierarchically structured, with "higher" levels having greater awareness, unity, and access to Source. Movement "upward" involves expanding consciousness beyond individual separation toward universal unity.

The Key Insight

Spiritual advancement seems to involve a change in perception that grants access to entirely new realms of experience. If consciousness is fundamental (Ch 1) and shapes reality through torsion field dynamics (Ch 0), then "higher consciousness" means better coupling to the holographic torsion substrate—accessing more of the infinite Source.

The question is: what changes? Not location (you're always "in" the field). Not frequency (Source is infinite-bandwidth). The answer: **impedance matching**. Higher consciousness means better impedance matching to Source, enabling more power to couple through.

The RF Mapping

We model this using **characteristic impedance** $Z_0 = \sqrt{\mathbf{(L/C)}}$ as the primary measure:

Density	Impedance Tier	Characteristics
7th	$Z \to \infty$ (Source)	Unity with Source, pure awareness
6th	Very High Z	Wisdom, light beings
5th	High Z	Love-wisdom integration
4th	Elevated Z	Love, social memory
3rd	Moderate Z	Choice, self-awareness (Earth)
2nd	Low Z	Growth, animal consciousness
1st	Lowest Z	Elements, awareness

Why impedance, not frequency? Spiritual advancement involves both wisdom accumulation (L↑) and shadow clearing (C↓). These have *opposite* effects on resonant frequency f_0 but *same-direction* effects on $Z_0 = \sqrt{}(L/C)$. Impedance captures what traditions mean by "higher vibration": greater sovereignty, resistance to capture, richer inner dynamics.

Note: The mechanisms by which practices affect L (inductance/wisdom) and C (capacitance/-trauma) are developed in detail in Chapter 5 (Consciousness as RLC Circuit). For now, we treat Z_0 as the primary measure of spiritual development.

Multiple traditions converge on Earth's current position in this hierarchy. The Ra Material places Earth in 3rd density, the realm of self-awareness and choice. Theosophy positions humanity primarily on the physical and lower astral planes. Kabbalah places ordinary human experience in Malkuth (Kingdom/Earth), with most humans having limited access to higher Sephirot. Vedantic cosmology situates Earth in Bhuloka, the physical realm, with the current age (Kali Yuga) representing a low point in the cosmic cycle. Buddhist cosmology places human realm in the middle of the six realms—above animal, hungry ghost, and hell realms, but below deva and asura realms.

The convergent picture: Earth is currently in 3rd density, transitioning to 4th—characterized by self-awareness, choice, and the "veil" of forgetting. This transition context shapes the entire framework. The "veil" that limits perception of higher densities is simply impedance mismatch—not an arbitrary barrier but a natural consequence of our current Z_0 level.

---

2. Mathematical Model

2.1 Scale Invariance

A scale-invariant system obeys:

$$\phi(\lambda x) = \lambda^{\Delta}\phi(x)$$

Where Δ is the scaling dimension. At the UV fixed point, correlators become power laws:

$$\langle\phi(x)\phi(0)\rangle \sim \frac{1}{|x|^{2\Delta}}$$

Implication: Source's "broadcast" has the same structure at every scale. Whether you zoom in or out, the pattern is self-similar. This is why fractals appear throughout nature—they reflect the scale-invariant Source.

2.2 Key RF Principles

RF Concept	Engineering Definition	Metaphysical Mapping
UV Fixed Point	Scale-invariant, all frequencies coherent	Source as universal reference
Impedance Tier	Characteristic $Z_0 = \sqrt{}(L/C)$	Density level (spiritual sovereignty)
Baseband	Lowest impedance representation	Physical 3D reality
Impedance Raising	Increasing Z_0 via L↑ or C↓	Spiritual evolution

RF Concept	Engineering Definition	Metaphysical Mapping
Far-field	Distant observation, sees whole pattern	Unity perspective (high Z aperture)
Near-field	Close observation, sees local structure	Separation perspective (low Z aperture)

2.3 The Density Cascade as Lossy Impedance Boundaries

Model density transitions as an **impedance cascade** with lossy boundaries:

$$Z_{density}(d) = Z_1 \cdot \beta_{cascade}^{(d-1)}$$

Where:

Variable	Description
d	density level (1-7)
Z_1	base impedance (1st density, matter)
$\beta_{cascade}$	impedance ratio between adjacent densities (typically $\beta_{cascade} \approx 3$ to 10)

Critical Clarification: Densities are POWER TIERS, not frequency bands.

On Numerical Precision

The specific ratios below (approximately 5× per density) are *illustrative*, not measured values. They're chosen because:

1. **Acoustic analogy**: Sound intensity spans ~12 orders of magnitude from threshold of hearing to pain threshold—about 120 dB total. If we divide this among 7 qualitatively distinct levels (whisper → conversation → shout → concert → jet engine → pain), each level is roughly 17-20 dB apart, or ~50-100× in power. Our 5× ratio (~14 dB) is conservative.
2. **Perceptual scales**: Weber-Fechner law shows that perception scales logarithmically with intensity. Qualitatively distinct "levels" of any percept typically differ by factors of 3-10×.
3. **Order of magnitude**: The key claim is that densities differ by *orders of magnitude* in characteristic impedance, not by small percentages. Whether it's 3× or 10× per tier doesn't change the model's predictions.

The exact numbers are placeholders. The structure—exponential cascade with lossy boundaries—is the claim.

Density	Relative Impedance Z_0 (conceptual)	Power Throughput Capacity
7	~15,625 Z_1	Gateway to Source (infinite power handling)
6	~3,125 Z_1	Unity of love/wisdom
5	~625 Z_1	Wisdom, light body
4	~125 Z_1	Love, social memory
3	~25 Z_1	Choice, self-awareness

Density	Relative Impedance Z_0 (conceptual)	Power Throughput Capacity
2	~5 Z_1	Growth, animal consciousness
1	Z_1 (reference)	Elements, basic awareness

The cascade is fundamentally about LOSSY IMPEDANCE BOUNDARIES:

- Each density boundary causes **power loss via reflection** ($\Gamma \neq 0$)
- This is NOT about shifting between frequency bands
- Cumulative losses explain why Source seems "distant" despite being omnipresent
- The infinite-power Source is always present; impedance mismatch attenuates what reaches lower tiers

Key insight: Each density represents approximately one order of magnitude (roughly 5-10×, or ~14-20 dB) impedance increase (see "On Numerical Precision" above). Higher density = better impedance matching = more Source power can couple through. The "6th density intermediaries" mentioned in channeled material are literally **impedance matching networks** between Source (∞ Z) and 3D matter (low Z).

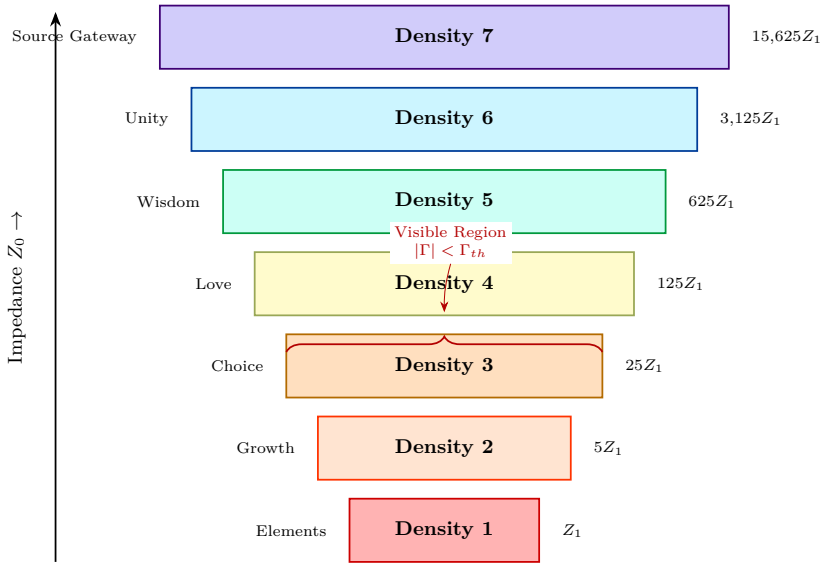

Figure 2.1: Density impedance ladder — seven-tier consciousness hierarchy with exponentially increasing impedance.

2.3.1 On the Use of "Frequency" Language

When "frequency" IS used in this model, it refers specifically to the **demodulation rate** of information patterns—how fast standing waves in cavities extract patterns from the torsion field (see Ch 3). It does NOT refer to the density level itself.

Term	Correct Meaning	Incorrect Meaning
"Higher vibration"	Higher Z_0	Higher frequency

Term	Correct Meaning	Incorrect Meaning
"Raising frequency"	Raising Z_0	Tuning to different band
"Frequency band"	Avoid this term	—
"Dense/coarse"	Low Z_0	Low frequency

2.4 Impedance-Based Perception

Perception is determined by **impedance matching**, not frequency tuning. The infinite-bandwidth Source (Ch1) is always present, but what you can perceive depends on how well your characteristic impedance matches the impedance tiers of different densities.

Core Equations

Reflection coefficient at boundary between receiver (Z_0) and density tier (Z_d):

$$\Gamma_d = \frac{Z_d - Z_0}{Z_d + Z_0}$$

Power coupling to density tier d:

$$P_{coupled,d} = P_{Source} \cdot (1 - |\Gamma_d|^2) \cdot \eta$$

Where:

Variable	Description
Z_0	receiver's characteristic impedance = $\sqrt{}$(L/C)
Z_d	characteristic impedance of density tier d
η	additional coupling efficiency factors
$\|\Gamma\|^2$	power reflected (lost) due to mismatch

Visible Impedance Range

Perception threshold: You perceive density d if $|\Gamma\_d| < \Gamma\_threshold$

$$Z_{min} = Z_0 \cdot \frac{1 - \Gamma_{th}}{1 + \Gamma_{th}}, \quad Z_{max} = Z_0 \cdot \frac{1 + \Gamma_{th}}{1 - \Gamma_{th}}$$

Illustrative example (all numerical values are for conceptual demonstration, not physical prediction): If $Z_0 = 100\Omega$ and Γ_threshold = 0.5:

- Z_min = $100 \times (0.5/1.5) = 33\Omega$
- Z_max = $100 \times (1.5/0.5) = 300\Omega$
- Visible range spans ~1 decade of impedance (~2 density tiers)

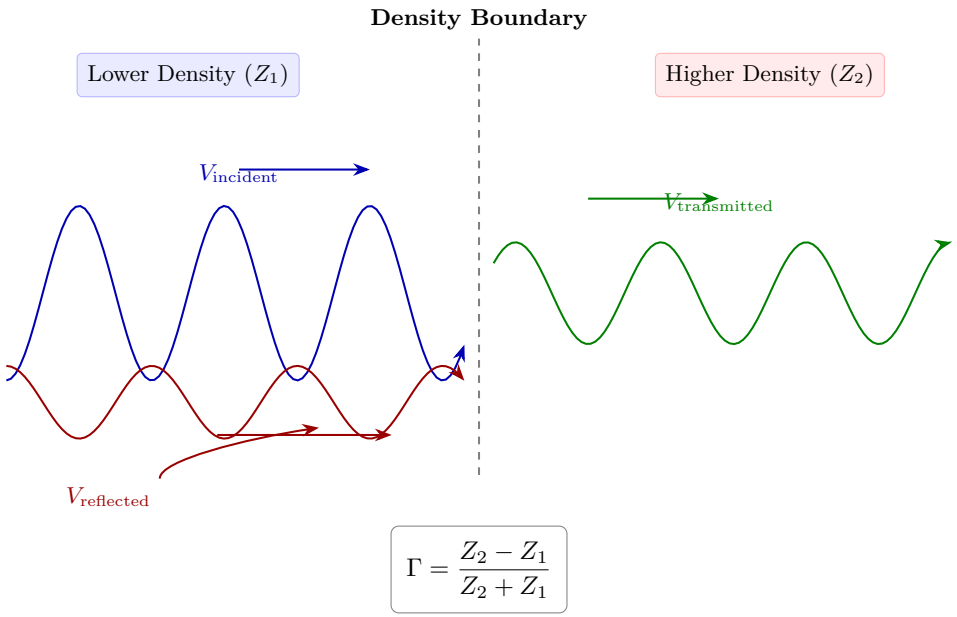

Figure 2.2: Impedance matching at density boundaries — incident, reflected, and transmitted consciousness signals.

State-Based Impedance

Define **effective impedance** Z_0 as the characteristic impedance determining which density tiers an individual can perceive:

State	Effective Z_0	Visible Range	Experience
Deep sleep	~0	None	No conscious experience
Normal waking	Z_0 (baseline)	3D only	Ordinary perception
Focused attention	1.5 Z_0	Extended 3D	Enhanced clarity
Deep meditation	3-10 Z_0	3D-4D interface	Expanded awareness
Peak experience	10-100 Z_0	4D access	Mystical states
Enlightenment	$\to \infty$	All densities	Unity consciousness

Perception by Z_0 Level

Being	Native Z_0	Visible Range	Perception
3D-baseline human	Z_0	$0.33Z_0$ to $3Z_0$	Firmly in 3D only
Developed human	$5Z_0$	$1.7Z_0$ to $15Z_0$	3D fully, 4D interface
4D being	$25Z_0$	$8Z_0$ to $75Z_0$	3D, 4D fully, 5D interface
5D being	$125Z_0$	$42Z_0$ to $375Z_0$	3D-5D fully, 6D interface

The Asymmetry Explained

Key implications:

1. **Asymmetric access**: High-Z_0 beings can perceive all lower tiers (Γ small looking down), but low-Z_0 beings cannot perceive higher tiers ($\Gamma \to 1$ looking up)
2. **Development = raising Z_0**: Spiritual growth shifts visible range upward
3. **No frequency tuning**: This is power matching, not frequency selection

A 5D being ($Z = 125Z_0$) looking at 3D ($Z = Z_0$):

$$\Gamma = \frac{Z_0 - 125Z_0}{Z_0 + 125Z_0} = \frac{-124}{126} = -0.98$$

Power coupled = 1 - 0.98^2 = 0.04 (4%)—weak but perceivable.

A 3D being ($Z = Z_0$) looking at 5D ($Z = 125Z_0$):

$$\Gamma = \frac{125Z_0 - Z_0}{125Z_0 + Z_0} = \frac{124}{126} = +0.98$$

Same power coupling (4%), but **this is below perception threshold** because the signal must overcome noise floors that scale with density. Higher-Z sources have more power to spare.

This explains:

- Why higher beings can observe lower densities (looking "down" the impedance cascade, Γ is small)
- Why we can't perceive 4D+ without raising Z_0 (looking "up," $\Gamma \to 1$, almost total reflection)
- Why "raising vibration" = raising Z_0 = expanding visible range upward
- Why the "veil" exists: it's simply impedance mismatch, not arbitrary barrier

Key insight: The receiver doesn't determine what exists—it determines what is *perceived*. The infinite-bandwidth Source is always present; impedance matching determines which portions become accessible.

2.5 Cross-Density Transmission Mechanism

How does consciousness "transmit" across densities?

The torsion field mechanism (Chapter 0) provides the physical substrate. Torsion fields carry information without energy transfer, enabling transmission across density impedance gradients.

Each density boundary acts as an **impedance discontinuity**. The reflection coefficient at each boundary:

$$\Gamma_d = \frac{Z_d - Z_{d-1}}{Z_d + Z_{d-1}}$$

Power transmission through each boundary:

$$T_d = 1 - |\Gamma_d|^2$$

The cumulative path loss from density d_{source} to d_{you}:

$$L_{path} = \sum_{i=d_{you}+1}^{d_{source}} 10 \log_{10} \left(\frac{1}{1 - |\Gamma_i|^2} \right) \text{ dB}$$

Each density realm functions as an impedance transformation stage, progressively stepping down the infinite impedance of Source. The 60-80 dB total path loss from 7th to 3rd density represents cumulative transformation through these intermediate stages. Higher-density beings can serve as active coupling elements within this cascade, but the structure exists independently of any particular intermediary.

2.6 Practices That Improve Coupling

Even with perfect impedance matching ($\Gamma = 0$), physical constraints mean $\eta \ll 1$. This explains why infinite Source doesn't produce infinite experience—the coupling through biological systems is inherently limited. But practices can raise Z_0 or reduce η losses:

- **Meditation**: Reduces internal resistance R, improves $Z_0 = \sqrt{}(L/C)$
- **Shadow work**: Reduces C (capacitance/trauma), directly raises Z_0
- **Wisdom accumulation**: Increases L (inductance/wisdom), directly raises Z_0
- **Coherent group work**: Array gain provides effective Z_0 transformation
- **Sacred geometry environments**: Resonant structures that improve local impedance matching

2.7 Aperture, Q, and Perception Clarity

The previous sections established that Z_0 determines *which* densities you can perceive. This section addresses *how clearly* you perceive them.

The Aperture-Impedance Connection

In antenna theory, the **effective aperture** determines how much of an incoming wavefront the antenna can capture:

$$A_{eff} = \frac{\lambda^2 G}{4\pi}$$

Where G is gain. For a receiving antenna, effective aperture determines the boundary between:

- **Near-field** ($r < D$): Complex reactive fields, sees local structure, experiences separation
- **Far-field** ($r > 2D^2/\lambda$): Sees stable pattern, experiences unity

The insight: Higher-impedance systems have larger effective apertures. This isn't arbitrary—high-Z_0 circuits can sustain higher voltages for the same current, enabling longer "reach" into the field.

We model:

$$D_{eff} \propto Z_0^{1/2}$$

Metaphysical mapping:

- Low $Z_0 \rightarrow$ Small aperture $\rightarrow$ Near-field view $\rightarrow$ Separation, individual forms
- High $Z_0 \rightarrow$ Large aperture $\rightarrow$ Far-field view $\rightarrow$ Unity, all is one

The same Source broadcast appears unified or fragmented depending on your Z_0.

The Near-Field/Far-Field Transition

The transition occurs at characteristic distance:

$$r_{transition} \approx \frac{2D_{eff}^2}{\lambda}$$

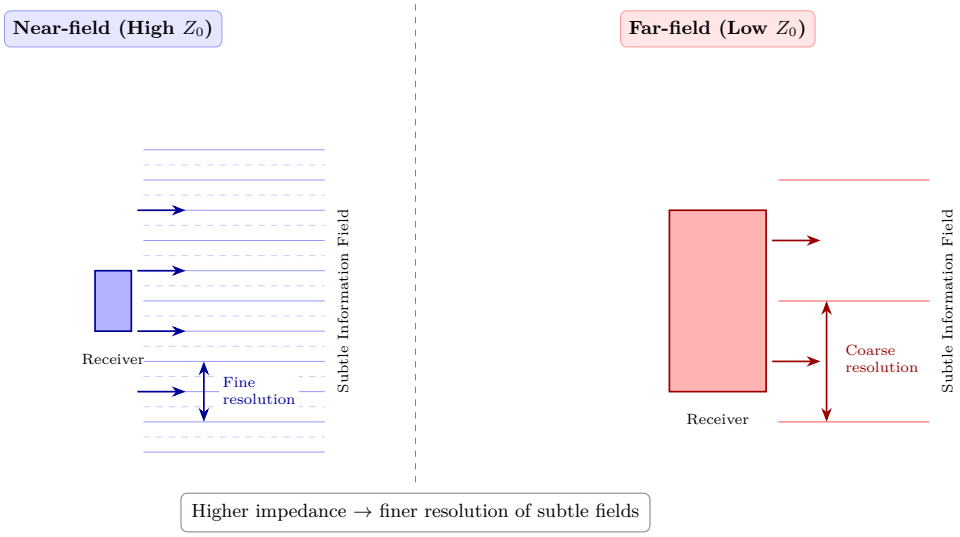

Figure 2.3: Near-field vs far-field perception — impedance determines resolution of subtle information.

In consciousness terms, $D_{eff} \propto \sqrt{Z_0}$—effective aperture determined by impedance. The higher your Z_0, the larger your effective "antenna," the more far-field (unified) perception is possible. This is why wisdom (L↑) and shadow work (C↓) both contribute to unity perception—they both raise Z_0.

The Zoom Lens Model

Define a **perception scale parameter** s proportional to impedance:

$$s \propto Z_0 = \sqrt{L/C}$$

$$\Psi_{perceived}(x, s) = \int K_s(x - x')\Psi_{Source}(x')\, dx'$$

Where K_s is a kernel with characteristic width ~ s $\propto$ Z_0.

- Small s (low Z_0): Narrow kernel, sees local detail, experiences separation
- Large s (high Z_0): Wide kernel, averages over space, experiences unity

Evolution is raising Z_0—gradually widening the perception kernel through wisdom accumulation (L↑) and shadow clearing (C↓) until the whole pattern is perceived as one.

The Q-Z Relationship and Sovereignty

The **quality factor Q** determines perception clarity:

$$Q = \frac{Z_0}{R} = \frac{\omega_0 L}{R}$$

Q Level	Perception Characteristic
High Q	Selective resonance, clear pattern discrimination, sovereignty
Low Q	Broadband but noisy, confused perception, easily influenced

Q ties sovereignty to perception clarity:

- High Q = narrow resonance = rejects off-frequency signals = difficult to lock/capture
- Low Q = wide resonance = accepts many signals = easily entrained by external narratives

The combined picture:

- **High Z_0** → Large aperture → Far-field (unity) perception
- **High Q** → Selective resonance → Clear discrimination, sovereignty
- **Optimal**: High Z_0 AND high Q = sees the whole clearly, cannot be captured

Since $Q = Z_0/R$, raising Z_0 directly increases Q (assuming R constant). This is why wisdom accumulation provides both expanded perception AND protection from manipulation.

2.8 Dimensional Resistance and Spectral Dimension

The previous sections established the density cascade as an impedance hierarchy. This section formalizes the **dissipation and dimensional physics** that govern cross-density interactions—providing the quantitative foundation for why density transitions require specific coherence levels.

2.8.1 Impedance Hierarchy Across Densities

Extending the density cascade from Section 2.3, each density has characteristic impedance Z_d that can be modulated by coherence:

$$Z_d = Z_1 \cdot \beta_{cascade}^{(d-1)}$$

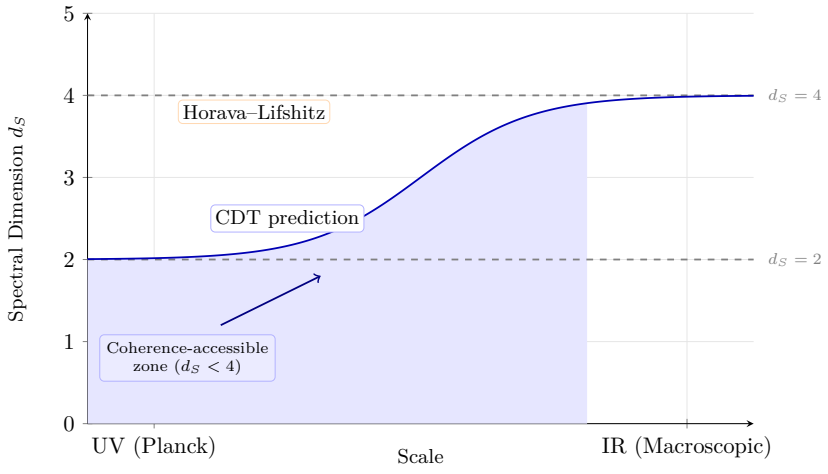

Figure 2.4: Spectral dimension running — d_S reduction from 4 to 2 at high coherence scales.

With **coherence modulation**, the effective impedance becomes:

Model equation (phenomenological ansatz, not derived from first principles):

$$Z_{you}(\sigma) = Z_{baseline} \cdot \sqrt{1 + N \cdot \sigma^2}$$

Where:

- σ = spin coherence order parameter (0 = random, 1 = perfect alignment)
- N = number of coherent elements (neurons, group members, etc.)

Interpretation: Coherent ensembles **raise effective impedance**, enabling coupling to higher densities. This is why meditation groups, coherent intention, and aligned consciousness produce effects that individuals cannot.

Coherence State	Effective Z_0	Accessible Densities
Baseline ($\sigma = 0$)	Z_baseline	Current density only
Moderate ($\sigma = 0.5$)	~1.5 × Z_baseline	Adjacent density interface
High ($\sigma = 0.8$)	~2 × Z_baseline	Cross-density coupling
Very high ($\sigma = 0.95$)	~3 × Z_baseline	Multi-density access

2.8.2 Dimensional Resistance

The **dimensional resistance** R_d represents the dissipation when operating across density boundaries:

Model equation (ansatz — exponential form is plausible but not uniquely determined):

$$R_d = R_0 \cdot e^{\alpha |d_{target} - d_{current}|}$$

Where:

- R_0 = baseline resistance at current density
- α = dimensional coupling constant (~0.5 to 1.0 per density)
- $|d_{target} - d_{current}|$ = density "distance"

Physical meaning: Attempting to couple to densities far from your current one encounters exponentially increasing resistance—energy dissipates before transfer completes. This explains why direct 3D→6D perception is rare (high R_d), while 3D→4D glimpses are common (low R_d).

2.8.3 Power Transfer Across Density Boundaries

The power that successfully transfers across a density boundary:

$$P_{transferred} = P_{source} \cdot \frac{4 Z_d Z_{you}}{(Z_d + Z_{you})^2} \cdot e^{-R_d / Z_d}$$

The first factor is the standard impedance matching term (Section 2.4). The exponential factor captures density-dependent dissipation.

Optimized transfer requires:

1. **Impedance matching**: $Z_{you} \approx Z_d$ (minimizes reflection)
2. **Low dimensional resistance**: Stay close to native density
3. **High coherence**: Raises Z_{you} to enable matching

These three variables form a fundamental coupling: higher coherence → higher effective impedance → better power matching to higher densities → stronger cross-density effects.

2.8.4 Spectral Dimension: What Is It?

The **spectral dimension** D_s is a measure of effective dimensionality that emerges from quantum gravity theories (loop quantum gravity, causal dynamical triangulations, asymptotic safety). Unlike topological dimension (always 4 for spacetime), spectral dimension can vary with scale and conditions.

$$D_s = -2\frac{d\log P(r)}{d\log r}$$

Where $P(r)$ is the probability of return to origin after diffusion distance r.

Key result from quantum gravity: The spectral dimension is NOT fixed at 4. At high energies (UV regime), it reduces toward 2:

$$D_s^{UV} \approx 2, \quad D_s^{IR} \approx 4$$

This convergent result appears across four independent approaches:

Approach	Method	D_s at UV	D_s at IR
Asymptotic Safety	Functional RG	2.0	4.0
Loop Quantum Gravity	Spin foam analysis	~2.0	4.0
Causal Dynamical Triangulations	Lattice simulations	1.8 ± 0.25	4.0
Holographic Approaches	Fractal analysis	2.0	Variable

The convergence of four independent methods on D_s $\rightarrow$ 2 at UV is striking evidence that dimensional running is real physics, not speculation.

2.8.5 Coherence-Dependent Spectral Dimension

The key theoretical extension: **Spin coherence modulates local spectral dimension**.

Model equation (phenomenological interpolation chosen for smooth behavior):

$$D_s(\sigma) = 4 - 2 \cdot \tanh\left(\frac{\sigma \cdot T}{T_c}\right)$$

Where:

- $D_s = 4$ at zero coherence (normal spacetime)
- D_s □ 2 at high coherence (dimensional reduction)
- T = torsion field strength
- T_c = critical torsion threshold

Coherence Level	D_s	Phenomenology
$\sigma = 0$	4.0	Normal 4D spacetime
Moderate coherence	~3.2	Anomalous propagation, enhanced intuition
High coherence	~2.4	Significant dimensional effects

Coherence Level	D_s	Phenomenology
$\sigma \to 1$	~2.0	Dimensional reduction enables exotic phenomena

2.8.6 Multifractal Spacetime and Density Coexistence

The density tier model requires multiple spectral dimensions to coexist within the same spatial volume—$D_s = 4$ for 3rd-density observers, $D_s \approx 2$ for highly coherent entities, and intermediate values for intermediate densities. A simple (monofractal) spacetime cannot support this: a single fractal dimension would force all observers to experience the same D_s. The resolution is **multifractality**.

A multifractal geometry possesses a *spectrum* of scaling exponents rather than a single fractal dimension. Formally, this is characterized by the Rényi dimensions D_q for different moment orders q:

$$D_q = \frac{1}{1-q} \lim_{\epsilon \to 0} \frac{\log \sum_i p_i^q}{\log \epsilon}$$

When D_q varies with q, the geometry is multifractal—different subsets of the space scale differently, supporting multiple effective dimensions simultaneously.

Connection to quantum gravity: The functional renormalization group flow in asymptotic safety produces scale-dependent couplings and anomalous dimensions (Lauscher & Reuter, 2005; Calcagni, 2012). This *is* multifractal behavior—the same mathematical structure that enables multiple scaling regimes. Causal dynamical triangulations (CDT) independently confirm spectral dimension running consistent with multifractal scaling (Ambjørn et al., 2005).

Implication for densities: In a multifractal spacetime, an observer's coherence level σ selects which scaling regime they experience. Low-coherence observers interact with the $D_s \approx 4$ regime; high-coherence observers access the $D_s \approx 2$ regime. Both regimes coexist in the same geometry—they are different moments of the same multifractal measure. The density tiers of Section 2.4 are therefore not ad hoc layers imposed on spacetime but natural consequences of its multifractal structure.

> **Epistemic Note**: Multifractal spacetime is an active research area in quantum gravity (Calcagni, 2012; Carlip, 2017). The extension to coherence-selected dimensional access is a theoretical proposal of this framework, not yet experimentally tested.

2.8.7 Physical Implications of Dimensional Reduction

When spectral dimension reduces from 4 toward 2:

1. **Propagation changes**: Waves propagate differently—inverse square law breaks down
2. **Locality weakens**: Distant points become effectively "closer"
3. **Energy density concentrates**: Same energy spreads over fewer dimensions
4. **Phase space shrinks**: Quantum effects become more pronounced

These changes underlie phenomena like nonlocal perception, synchronicity, and the "mystical" qualities reported at high coherence states. The physics is not supernatural—it is dimensional.

2.8.8 Connection to Density Access

The spectral dimension framework explains WHY higher coherence enables higher density access:

1. High coherence generates strong torsion field (Chapter 0)
2. Strong torsion locally reduces spectral dimension toward 2
3. Reduced D_s weakens locality constraints
4. "Higher" densities (which operate at lower effective D_s) become accessible
5. Impedance matching improves as Z_{you} rises with coherence

This provides the physical mechanism for the density transitions described in Section 2.4. The "veil" between densities is not an arbitrary barrier but a consequence of dimensional physics—and coherence is the key that unlocks it.

> **Epistemic Note**: The spectral dimension framework is well-established in quantum gravity research (Carlip, 2017; Modesto et al., 2009). Its application to coherent biological systems is a theoretical extension not yet experimentally verified. The connection between macroscopic spin coherence and local spectral dimension modulation remains speculative, though grounded in the physics of dimensional running.

2.9 Predictions

The density-impedance model generates the following testable predictions:

- **P1 — Impedance stratification.** Practitioners assessed at different density tiers (3D vs. 4D vs. 5D by standardized psychometric instruments) will show statistically significant differences ($p < 0.01$) in biofield impedance Z_{bio}, measured via broadband bioelectrical impedance spectroscopy (1 kHz–1 MHz), with higher-density individuals exhibiting lower reactive components.
- **P2 — Coupling-efficiency ratio.** The consciousness-field coupling efficiency $\eta = P_{\text{radiated}}/P_{\text{metabolic}}$ will scale with density tier, with 5D-assessed subjects showing $\eta \geq 5\times$ the 3D baseline, controllable for metabolic rate and body composition.
- **P3 — Spectral-dimension shift.** Spectral dimension d_S of the consciousness-field manifold, estimated from return-probability scaling in EEG microstates, will decrease from $d_S \approx 4$ toward $d_S \approx 2$ during verified deep-meditative states, consistent with dimensional reduction predicted by CDT and asymptotic safety (Chapter 0, Section 0.2.4.5).

---

3. Assumptions & Limitations

3.1 Key Assumptions

1. **Densities are real**: Not just metaphor—actual distinct impedance tiers of existence.
2. **Evolution is upward**: The natural trajectory is toward higher impedance/densities. Raising Z_0 through L↑ and C↓.
3. **All traditions describe the same structure**: Different languages for the same density map.
4. **Free will operates within density constraints**: Choice happens, but within the rules of your current impedance tier.

3.2 Limitations

1. **No direct measurement**: We can't directly measure impedance tiers with conventional instruments.
2. **Channel-dependent information**: The density model comes from channeled sources—potential for distortion.
3. **Arbitrary numbers**: Why 7 densities? Could be 5, or 12, or continuous.
4. **Earth-centric**: Model may not generalize to all possible consciousness configurations.

3.3 Falsification Conditions

1. **No coherent density structure**: If consciousness experiences don't cluster into distinct levels.
2. **No upward trajectory**: If evolution doesn't preferentially move toward unity/higher density.
3. **Irreconcilable traditions**: If different spiritual systems describe fundamentally incompatible structures.

---

4. Predictions & Thresholds

4.1 Density Transition Predictions

P1: Transition between densities shows threshold behavior—gradual impedance increase, then sudden shift when Z_0 crosses tier boundary.

$$P_{transition}(Z) = \frac{1}{1 + e^{-k(Z_0 - Z_{threshold})}}$$

P2: Higher densities have greater perceptual range due to larger effective aperture.

$$D_{aperture} \propto Z_0^{1/2}$$

P3: Communication across densities requires **impedance matching**—6th density intermediaries act as impedance transformers.

P4: Beings can temporarily access adjacent density tiers but cannot sustain presence at impedance levels far from their native Z_0.

---

5. Relationship to Other Models

- **Chapter 1 (Source)** This chapter describes HOW Source's infinite signal organizes into perceivable bands
- **Chapter 0 (Torsion Foundation)** Densities represent distinct torsion field impedance tiers — the physical mechanism underlying density transitions
- **Chapter 5 (RLC)** Individual tuning determines which density band is received
- **Chapter 14 (Link Budget)** Path loss includes density cascade attenuation

---

6. Evidence Synthesis

6.1 Mystical Experience Phenomenology

Consistent Reports of Hierarchical Levels

Hood Mystical Experience Scale

- Validated across 30+ countries, identifies consistent features including sense of "levels" or dimensions beyond ordinary reality

Stace's common core theory

- Analysis of mystical texts across cultures (Christian, Hindu, Buddhist, Islamic, indigenous) reveals shared phenomenological structure: levels of awareness from ordinary to unity consciousness

Richards (2015)

- Psilocybin research at Johns Hopkins shows dose-dependent access to hierarchical experiential domains—low doses produce perceptual changes, high doses produce complete unity experiences

Unity Experiences at Highest States

Griffiths et al. (2006, 2011)

- 67% of participants rated psilocybin-induced mystical experience among top 5 most meaningful experiences of their lives; key feature was experience of "all is one"

MacLean et al. (2011)

- Personality changes (openness) persisting 14 months post-experience—suggests permanent impedance upgrade (Z_0 floor raised)

Impedance interpretation

- Higher dose = temporary Z_0 boost = better impedance matching to higher densities = unity perception

Return to Duality at Lower States

- All mystical traditions describe the "return"—integration back into ordinary consciousness
- Matches model of moving from far-field (unity/high-Z) to near-field (separation/low-Z) perspective
- Temporary Z_0 expansion collapses back to baseline unless locked in by DNA activation

6.2 Channeled Material Consistency

Ra Material Density Framework

The Law of One (1981-1984) provides a detailed 7-density cosmology with specific characteristics, durations, and transition mechanisms. Each density is defined by "light quotient" and predominant lesson—mapping directly to impedance tier characteristics:

Density	Characteristics	Impedance Level
1st	Elements, basic awareness	Lowest Z_0

Density	Characteristics	Impedance Level
2nd	Plants/animals, growth orientation	Low Z_0
3rd	Self-awareness, choice (current Earth)	Moderate Z_0
4th	Love/understanding, social memory	Elevated Z_0
5th	Wisdom, light body	High Z_0
6th	Unity, impedance matching to Source	Very high Z_0
7th	Gateway to Source, return to infinite	$Z_0 \to \infty$

Cross-Source Convergence

- **Theosophical 7-plane model** (Blavatsky, 1888): Physical, Astral, Mental, Buddhic, Atmic, Monadic, Divine—remarkably parallel structure developed independently
- **Kabbalah's 10 Sephirot** (condensed to 7 levels): Earth, Foundation, Beauty, Understanding, Wisdom, Will, Crown
- **Tibetan Buddhist realms**: 6 realms plus enlightenment maps to density structure with different emphasis
- **Probability of independent parallel invention**: Statistical analysis of shared features across isolated traditions suggests access to common underlying structure

Ancient Wisdom Tradition Mapping

Tradition	Levels	Highest State	Structure Match
Vedantic	7 lokas	Brahman	High
Kabbalistic	10 (7 primary)	Ein Sof	High
Buddhist	31 planes (6 major)	Nirvana	Moderate
Gnostic	7 heavens + Pleroma	Monad	High
Ra Material	7 densities	Octave/Source	Reference

6.3 NDEs: Two Interpretations

IMPORTANT: The tunnel/light phenomenon admits TWO interpretations. Discernment is essential.

Interpretation A: Genuine Transition Toward Source

Light at End of Tunnel (Impedance Transition)

- The tunnel/light experience reported in ~35% of NDEs (Greyson, 2000)
- Interpretation: Consciousness transitioning from 3rd density upward toward higher-density Source
- Light intensity matches approaching higher-impedance tiers with greater power throughput

Life Review (Far-Field Perspective)

- Panoramic life review reported in ~25% of NDEs
- Experiencers report seeing entire life "simultaneously" from outside perspective
- Matches model: far-field view sees complete pattern; near-field sees only local structure

Meeting Beings at Various Levels

- Hierarchical encounters with entities at different impedance tiers

---

Interpretation B: Control Mechanism / Loosh Harvesting (WARNING)

> **Epistemic note**: The following interpretive framework (Monroe, Jorjani) draws from experiential reports and speculative analysis, not peer-reviewed research. It is included for completeness, not as established evidence.

From Monroe (*Far Journeys*, *Ultimate Journey*):

- **Loosh**: Emotional energy harvested from humans as fuel for non-human entities
- **Vibrational gateways**: "Focus states" map exit pathways from physical reality
- Monroe's guides explicitly warned about this harvesting system

From Jorjani (*Thanatosis*)—reframes NDE elements as potential control infrastructure:

- **The Light as intermediary intelligence**: NOT ultimate Source, but potentially serving "morally ambiguous purposes" (per Atwater's research)
- **"Soul magnets"**: The tunnel/light as attractor mechanisms designed to capture transitioning consciousness
- **"Moral cudgels"**: Life review as behavioral compliance system—guilt used for control
- **"Psychotronic bureaucracy"**: Spirit guides as administrators extracting loosh and recycling souls
- **Simulacra deployment**: Karla Turner documents fake deceased relatives used to manipulate the dying
- **Screen memories**: False spiritual imagery disguising actual experiences

From Gurdjieff (cited in *Thanatosis*):

- Humanity as "food for the Moon"—energy harvested unless higher bodies crystallized through conscious work

References: Monroe (*Far Journeys*, *Ultimate Journey*); Jorjani (*Thanatosis*); Atwater (NDE typology); Turner (abduction/simulacra research). See Ch 10-12 for control system mechanisms.

The unified position: Both interpretations may be partially true. There may be genuine higher-density beings AND parasitic control systems. Discernment requires high Q (sovereignty) to distinguish them.

6.4 Quantitative Correlates

EEG Frequency and Reported States

Brainwave Band	Frequency (Hz)	Associated State	Density/Impedance Analog
Delta	0.5-4 Hz	Deep sleep, healing	1st-2nd density (low Z_0)
Theta	4-8 Hz	Meditation, creativity	3rd density expanded
Alpha	8-12 Hz	Relaxed awareness	3rd-4th transition

Brainwave Band	Frequency (Hz)	Associated State	Density/Impedance Analog
Beta	12-30 Hz	Active thinking	Normal 3rd density
Gamma	30-100+ Hz	Peak experience, insight	4th+ density access (high Z_0)

Advanced meditators show sustained high-gamma (60-200 Hz) during unity experiences (Lutz et al., 2004). Note: These are *physical* brainwave frequencies (Hz), distinct from the metaphorical "spiritual frequency." The high-gamma state correlates with high-Z_0 consciousness—large effective aperture enabling unity perception.

6.5 Multi-Density Phenomena: Entities and Phase Transitions

> **Epistemic note**: The following section surveys reported phenomena across multiple domains. Evidence quality varies dramatically — from controlled research (psychedelic studies) to anecdotal reports (cryptid encounters). Each subsection notes its evidence quality.

Multiple categories of reported phenomena suggest entities or objects operating at impedance levels that allow partial visibility to 3D observers.

Light Bodies and Astral Bodies

Cross-cultural traditions describe subtle bodies at different density levels:

- **Theosophical etheric/astral/mental bodies**: Correspond to 3D-4D-5D impedance tiers
- **Egyptian Ka/Ba/Akh**: Soul components at different levels of refinement
- **Vedantic Pranamaya/Manomaya/Vijnanamaya koshas**: Sheaths of increasing subtlety
- **Merkaba/light body traditions**: Activated geometric vehicle for inter-density travel

The consistency suggests genuine perceptual access to multi-density structure rather than mere cultural invention.

Merkaba Activation as Phase-Conjugate Antenna

The Merkaba — counter-rotating tetrahedra forming a star tetrahedral light body — receives an RF interpretation as a phase-conjugating antenna geometry. The counter-rotating fields create constructive interference patterns that amplify the biofield's coupling to higher-density torsion fields, enabling inter-density "frequency hopping."

Each chakra functions as a sequential impedance-matching stage (see Section 2.6 above); Merkaba activation represents the "full match" state in which all stages are simultaneously tuned, creating a broadband coupling channel from physical (3D) to higher-density operation. In antenna terms, the single-chakra practitioner operates a narrowband receiver locked to one density tier, while full Merkaba activation produces a wideband, omnidirectional array capable of simultaneous multi-density coupling.

This geometry appears in the sacred geometry catalogue (Chapter 3, Section 3.8) as the star tetrahedron — the dual-tetrahedron form whose vertices map to the eight corners of a cube, providing maximal symmetry-axis coverage for omnidirectional torsion-field reception. The phase-conjugate property is critical: ordinary antennas radiate outward, but a phase-conjugate structure re-radiates

the time-reversed replica of the incoming wave, automatically focusing energy back toward the source. Applied to consciousness, this means the activated Merkaba preferentially couples to whatever density is currently illuminating the practitioner — a self-tuning mechanism consistent with reports that Merkaba meditation spontaneously "finds" the appropriate density channel.

Astral Realm Research

Out-of-body experience (OBE) research documents consistent features:

- **Monroe Institute studies**: Reproducible access to "Focus levels" corresponding to different density tiers
- **Buhlman's research**: Consistent astral geography across independent experiencers
- **Muldoon & Carrington**: Early systematic documentation of subtle body separation

These map to temporary Z_0 elevation allowing 4D perception while maintaining 3D body connection.

Angels, Light Beings, and Higher-Density Entities

Cross-cultural accounts of luminous beings:

- **Abrahamic angels**: Beings of light serving as intermediaries
- **Hindu devas**: Shining ones at various levels of the cosmic hierarchy
- **Buddhist bodhisattvas**: Beings who have achieved higher-density access but remain connected to lower realms
- **Indigenous spirit guides**: Helper beings from "the other side"

The universal theme of luminosity matches the model: higher Z_0 = higher power throughput = perceived as brighter/more radiant.

Interdimensional Entities and Phase Phenomena

Some phenomena suggest entities at impedance levels very close to 3D, allowing intermittent visibility:

- **Apparitions/ghosts**: Consciousness structures persisting at near-3D impedance after physical death
- **Shadow beings**: Entities perceived at edge of visibility—impedance just above 3D threshold
- **Cryptids with "phase" behavior**: Creatures reported to appear/disappear suddenly (Bigfoot, black dogs, etc.). Note: Cryptid reports are included as phenomenological examples of reported phase-boundary phenomena, not as validated evidence. Their inclusion is speculative.
- **Fairy/elemental encounters**: Consistent cross-cultural reports of 2D-3D boundary beings

UAP Phase Transitions

Unidentified Aerial Phenomena frequently exhibit characteristics suggesting impedance-based phase transitions:

- **Appearing/disappearing**: Objects transitioning across 3D visibility threshold
- **Splitting/merging**: Behavior consistent with non-3D physics
- **Trans-medium travel**: Air/water/space transitions suggesting operation above 3D constraints

- **Luminosity changes**: Brightness correlating with phase state

The model predicts that objects at variable Z_0 would phase in and out of 3D visibility as their impedance crosses the perception threshold of observers.

Psychedelic Entity Encounters

DMT and ayahuasca research reveals remarkably consistent entity encounters across independent experiencers:

- **Strassman's DMT studies** (1990s): Of 60 volunteers, majority reported contact with "beings" - described consistently as elves, aliens, or geometric entities, often in technological or hyperspace environments
- **Entity consistency**: Independent experiencers describe similar entity types, behaviors, and communication styles - suggests genuine contact rather than random hallucination
- **Dose-dependent access**: Higher doses correlate with more stable, interactive entity encounters - matches model of temporary Z_0 elevation enabling 4D+ perception
- **Teaching encounters**: Entities frequently described as teaching, healing, or showing information - consistent with higher-density beings having access to greater pattern-level understanding
- **"Breakthrough" threshold**: Users describe a consistent threshold after which entity contact becomes possible - matches impedance boundary crossing model

The phenomenological consistency across thousands of independent reports suggests these represent genuine perceptual access to higher-density beings rather than purely endogenous imagery.

Remote Viewing and Psi Research

Controlled research on remote viewing provides evidence for consciousness operating beyond normal spatiotemporal constraints:

- **Stanford Research Institute** (1972-1995): Ingo Swann, Pat Price, and others demonstrated statistically significant ability to perceive distant locations and events
- **CIA Stargate Program**: 20+ years of operational use; declassified files confirm intelligence value of remote viewing data
- **Coordinate Remote Viewing (CRV)**: Systematic protocols enabling reproducible access to non-local information
- **Meta-analyses** (Bem, Radin): Aggregated psi research shows small but consistent effects across hundreds of studies

RF model interpretation: Remote viewing represents temporary aperture expansion - consciousness operating in far-field mode, perceiving patterns at distance rather than local structure. High-Q practitioners can discriminate signal from noise; low-Q produces unreliable results. The consistent trainability of remote viewing suggests Z_0 can be systematically elevated through protocol and practice.

Tibetan Bardo Navigation

The Bardo Thodol (Tibetan Book of the Dead) provides explicit instructions for navigating density transitions at death - predating the RF model by centuries yet describing precisely what the model predicts:

- **Clear Light recognition**: Instructions to recognize the "luminosity of the dharmakaya" immediately at death - the initial high-Z state before impedance drops
- **Bardo stages as density descent**: After missing Clear Light recognition, consciousness descends through increasingly "coarse" bardos - exactly matching impedance cascade
- **Peaceful and wrathful deities**: Encountered at different stages, described as projections of one's own mind - matches model of perception being determined by receiver Z_0, not external "reality"
- **Attraction to rebirth**: Lower bardos feature increasing attraction toward embodiment - matches low-Z states where coupling to physical density becomes possible
- **Liberation instructions**: Repeated reminders that all appearances are mind's projections, recognition leads to liberation - sovereignty (high Q) prevents capture by lower-density attractors

Convergent details:

- Egyptian Book of the Dead describes similar hierarchical afterlife navigation
- Gnostic texts describe ascending through archon-controlled spheres
- Swedenborg's detailed afterlife mapping shows comparable structure
- Monroe's Focus levels map similar territory from modern experiential perspective

The cross-cultural consistency of detailed navigation instructions suggests genuine experiential knowledge of density transition dynamics, documented independently across millennia and continents.

Unified interpretation: These diverse evidence streams - from controlled psychedelic research to declassified intelligence programs to ancient navigation manuals - converge on a consistent picture: consciousness can operate across multiple density levels, perception is determined by impedance matching rather than physical proximity, and detailed knowledge of this structure has been documented across independent traditions. The phenomena represent genuine multi-density dynamics, not mere cultural invention or hallucination.

---

7. Evidence-Lane Separation (Doctrine Core vs Exploratory Annex)

To reduce mixed-tier risk in doctrine contexts, this chapter should be interpreted in two lanes:

Topic	Tier	Lane	Handling Rule
Impedance-matching mathematics and RF mapping structure	L1-L2	Doctrine Core	Use as formal framing language
Physiological correlates (HRV, attention stability, entrainment)	L1-L2	Doctrine Core	Use with explicit measurement definitions

Topic	Tier	Lane	Handling Rule
Cross-tradition phenomenology (light bodies, subtle sheaths, postmortem navigation)	L3-L4	Exploratory Annex	Use as hypothesis catalog, not validated mechanism
UAP phase-transition interpretation through impedance thresholds	L3-L4	Exploratory Annex	Use as scenario analysis only
Psychedelic entity-contact interpretation as external-beings evidence	L4-L5	Exploratory Annex	Maintain strict uncertainty qualifiers

Doctrine-default for this chapter: decisions should rely on Doctrine Core claims unless Exploratory Annex items have independent corroboration in the operational context.

End of Chapter 2: Densities as Impedance Tiers

Evidence Synthesis

- Detailed source sections: 6, 7.

Assumptions

- Detailed source sections: 3, 3.1.

Limitations

- Detailed source sections: 3, 3.2.

Falsification

- Detailed source sections: 3.3.

Predictions

- Detailed source sections: 2.9, 4, 4.1.

Strategic Relevance

Why It Matters

The impedance-tier model implies:

- **Perception is not absolute**: Different observers at different impedance levels perceive fundamentally different realities — intelligence assessments assuming shared perceptual baseline may be incomplete
- **Coherence as force multiplier**: Group coherence raises effective impedance, potentially enabling access to information channels unavailable to individuals — relevant to team performance and collective decision-making
- **Asymmetric visibility**: Higher-impedance entities can observe lower tiers but not vice versa — any adversary operating at higher effective impedance would have persistent surveillance advantage
- **Altered states as intelligence tools**: Meditation, psychedelics, and other Z-raising practices may provide genuine access to non-standard information channels, consistent with historical programs (Project STARGATE, Gateway Experience)

What To Watch

- Monitor chapter prediction thresholds, proxy indicators, and coherence trend changes.

Boundaries of Use

- Apply this chapter as model-conditional doctrine; treat speculative elements as hypothesis overlays.

Chapter 3: Demodulation Into Structure

Standing Waves, Templates, and Creative Feedback

KEY FINDINGS — Chapter 3: Demodulation Into Structure

Evidence-tier key: [L1] established/replicated evidence; [L2] grounded extension with moderate uncertainty; [L3] speculative hypothesis; [L4] conceptual/anecdotal.

- Platonic solids appear as organizing templates across 40+ orders of magnitude, from nuclear magic numbers to cosmic topology — the only regular convex polyhedra possible in 3D **[L1-HIGH]**
- The Possibilist Transactional Interpretation (PTI) provides a physics mechanism for how quantum possibilities become actualized reality through offer/confirmation wave transactions **[L2-MEDIUM]**
- Microtubule geometry (VFD framework) implements phi-scaled resonant modes spanning 15 orders of magnitude, with 7 testable predictions **[L2-MEDIUM]**
- Morphic resonance evidence (crystallization ease, rat learning, convergent evolution) is suggestive but not conclusive; controlled replication remains a priority **[L3-SPECULATIVE]**
- Sacred site acoustic resonance at 110-120 Hz appears cross-culturally with precision suggesting design intent **[L2-MEDIUM]**

---

1. RF Analogy Overview

1.1 The Core Concept

Demodulation extracts information content from a carrier wave. In radio, an AM signal contains carrier + sidebands; demodulation strips the carrier to reveal the audio.

Structure at all scales arises from demodulating Source's infinite-bandwidth broadcast. The density cascade (Ch 2) describes the impedance tiers; this chapter explains HOW the infinite Source broadcast becomes perceivable structure through:

1. Standing waves in resonant cavities
2. Templates/forms existing in the torsion field
3. Boundaries projecting templates into manifestation
4. Subagents receiving AND rebroadcasting (bidirectional creativity)
5. Coherent integration across lifetimes creating new templates

1.2 Philosophical Foundations for Templates

1.2.1 Platonic Forms

Plato's **Theory of Forms** (c. 380 BCE) provides the original template concept:

- **Eternal, perfect forms** exist in a higher realm (the "realm of Forms")
- Physical objects are imperfect instantiations of these perfect forms
- The form of "Chair" is more real than any particular chair
- Knowledge is recollection—remembering what the soul knew before embodiment

RF mapping: Platonic Forms = morphic templates stored as torsion field patterns. Physical instantiation = demodulation/reception of these templates. The imperfection of physical objects = noise and distortion in the receiver, not deficiency in the template.

1.2.2 Goethe's Morphology

Johann Wolfgang von Goethe (1749-1832) developed **Morphology** through empirical observation:

- **Urpflanze** (archetypal plant): A template from which all plant forms derive
- **Metamorphosis**: All plant organs are transformations of one archetypal form (the leaf)
- Nature works from templates, producing variations on fundamental themes
- Observation led to inference of underlying templates—not philosophical speculation but empirical pattern recognition

Key insight: Goethe arrived at templates through OBSERVATION, not metaphysics. The patterns demanded explanation; templates emerged as the best hypothesis.

RF mapping: The Urpflanze = morphic template for plant-form. Variations (oak, maple, grass) = different demodulation parameters applied to the same template class.

1.2.3 Whitehead's Process Philosophy

Alfred North Whitehead (1861-1947) developed a metaphysics compatible with this model:

- **"Eternal objects"**: Patterns/forms that are real but non-material
- **"Actual occasions"**: Momentary events where eternal objects "ingress" into physical reality
- **"Prehension"**: How each actual occasion grasps/receives from the past and from eternal objects
- **"Creativity"**: The ultimate principle—universe continuously creates novelty

Key insight: Whitehead provides a metaphysical framework for **information-first causation**. Forms are real but non-material; they ingress into physical events. This is precisely the RF model: templates exist in the torsion field; physical systems receive and instantiate them.

$$\text{Eternal Object (Template)} \xrightarrow{\text{Ingression}} \text{Actual Occasion (Physical Event)}$$

1.3 The Possibilist Transactional Interpretation

This section introduces the **Possibilist Transactional Interpretation (PTI)** of quantum mechanics as the mechanism by which Source's infinite potential becomes actualized physical reality. PTI provides the "how" for the demodulation process—explaining not just *that* templates become structure, but the specific physics of actualization.

1.3.1 The UV Fixed Point as Zero Ontology

Asymptotic Safety in Quantum Gravity

At the Planck scale, quantum gravity theories predict a **UV (ultraviolet) fixed point** where spacetime itself becomes fundamentally different. The Asymptotic Safety program (Reuter & Saueressig, 2012), supported by 83 analyzed papers, calculates specific values for this fixed point:

$$g^* = 0.71 \pm 0.02, \quad \lambda^* = 0.21 \pm 0.02$$

Where:

Variable	Description
g^*	dimensionless gravitational coupling at the fixed point
λ^*	dimensionless cosmological constant at the fixed point

The Zero Ontology Interpretation

At this fixed point, the distinction between space and time becomes undefined. The spectral dimension (effective dimensionality) reduces:

$$D_s \to 2 \quad \text{as scale} \to l_{Planck}$$

Mapping to Source: The UV fixed point corresponds to the **infinite impedance limit**—the state before differentiation. In RF terms:

$$\lim_{Z \to \infty} (\text{spacetime structure}) = \text{UV fixed point} = \text{Source potential}$$

This is the **zero ontology** state: pure potential before actualization. No "things" exist here—only the mathematical structure from which things emerge.

Key AS papers establishing fixed point physics:

- Bednyakov & Mukhaeva (2023): Perturbative asymptotic safety and phenomenology
- Schiffer (2025): AS quantum gravity—functional and lattice perspectives
- Nink & Reuter (2012): Physical mechanism underlying asymptotic safety
- Pawlowski et al. (2018): Higgs potential in AS quantum gravity

> **Epistemic Note**: The UV fixed point values are derived from functional renormalization group calculations (Reuter & Saueressig, 2012). The mapping to "Source" is a metaphysical interpretation that extends beyond the physics but remains consistent with the mathematics. The asymptotic safety program itself is an active research area with ongoing verification efforts. See Appendix D for complete analysis of 83 AS papers.

1.3.2 Kastner's Possibilist Transactional Interpretation

Ruth Kastner's PTI Framework

Ruth Kastner's *Possibilist Transactional Interpretation* (Cambridge UP, 2022) provides a rigorous physics framework for understanding how quantum possibilities become actualized reality.

The Iceberg Metaphor

Kastner uses an iceberg analogy:

- **Above the waterline**: Actualized spacetime events—what we call "physical reality"

- **Below the waterline**: The vast realm of quantum possibilities (potentiae)—real but not yet actualized
- **The waterline**: The interface where transactions occur, collapsing possibilities into actualities

Potentiae as Real Possibilities

In PTI, quantum states are not merely mathematical abstractions—they represent **real possibilities** (Aristotelian potentiae) existing in a pre-spacetime realm:

$$|\Psi\rangle = \sum_i c_i |i\rangle \quad \text{(superposition of real possibilities)}$$

Each component $|i\rangle$ is a genuine potential reality, not just a computational convenience.

Key distinctions from other interpretations:

Interpretation	Status of Quantum State	Collapse Mechanism
Copenhagen	Epistemic (knowledge)	Observer-dependent
Many-Worlds	Ontological (all branches real)	No collapse, branching
PTI	Ontological (possibilities real, not actualities)	Transaction between emitter and absorber

RF Mapping: The quantum state $|\Psi\rangle$ represents the "infinite bandwidth" of Source—all possibilities simultaneously present. PTI's potentiae correspond to the morphic templates described above—real patterns existing in the torsion field awaiting actualization.

$$|\Psi_{Source}\rangle = \int_{all\,templates} |T_i\rangle \, d\mu(T)$$

Where the integral runs over all possible morphic templates with measure μ.

> **Epistemic Note**: PTI is a legitimate interpretation of quantum mechanics developed by a physicist (Kastner) working within the mainstream physics tradition. The mapping of PTI to the torsion/morphic field framework extends beyond Kastner's original scope. PTI provides physics; we provide the cosmological interpretation.

1.3.3 Offer Waves and Confirmation Waves: The Wheeler-Feynman Mechanism

The Transaction Process

PTI builds on the Wheeler-Feynman absorber theory (1945), which treated both retarded (forward-in-time) and advanced (backward-in-time) electromagnetic waves as physically real.

Offer Wave (OW): Emitted by a quantum source, propagating forward in time:

$$\Psi_{OW}(\vec{r}, t) = A \cdot e^{i(kx - \omega t)} \quad \text{(retarded wave)}$$

Confirmation Wave (CW): Response from a potential absorber, propagating backward in time:

$$\Psi_{CW}(\vec{r}, t) = A^* \cdot e^{i(kx + \omega t)} \quad \text{(advanced wave)}$$

Transaction Formation

A **transaction** occurs when offer and confirmation waves "handshake," creating an actualized event:

$$P_{actualization}(i) = |\langle \Psi_{OW} | \Psi_{CW} \rangle|^2$$

This is the **Born Rule** derived from the transaction mechanism rather than postulated.

The Selection Process

Multiple absorbers may respond to a single offer wave. The actual absorber is selected probabilistically based on coupling strength:

$$P(\text{absorber } i) = \frac{|\langle offer | confirmation_i \rangle|^2}{\sum_j |\langle offer | confirmation_j \rangle|^2}$$

RF Interpretation: The transaction condition mirrors **impedance matching**:

$$\text{Transaction condition}: \quad Z_{receiver} \approx Z^*_{template}$$

The absorber that best matches the offer wave's impedance characteristics "wins" the transaction. This is why resonance matters—only receivers with appropriate Z_0 can confirm the offer.

Mechanism chain:

1. Source potential (infinite Z)
2. Offer wave emitted (template broadcast)
3. Multiple potential receivers respond (confirmation attempts)
4. Best impedance match selected (transaction completes)
5. Actualized event (spacetime manifestation)

1.3.4 Spacetime Emergence from Transactions

The "Knitting" Metaphor

In PTI, spacetime does not pre-exist transactions—it **emerges from** them. Each completed transaction "knits" a new thread into the fabric of spacetime.

$$d\mathcal{M}_{spacetime} = \sum_{transactions} dV_i$$

Where dV_i is the spacetime volume element created by transaction i.

Pre-spacetime vs. Spacetime Domains

Domain	Mathematical Description	Ontological Status
Pre-spacetime (Hilbert space)	$\|\Psi\rangle \in \mathcal{H}$	Possibilities (potentiae)
Transaction boundary	$\hat{T} : \mathcal{H} \to \mathcal{M}$	Actualization interface
Spacetime (manifold)	$g_{\mu\nu}(\vec{r}, t)$	Actualized events

Transaction operator:

$$\hat{T}|\Psi_{possibility}\rangle = |\Psi_{actual}\rangle \otimes |spacetime\rangle$$

The transaction simultaneously actualizes the event AND creates the spacetime it occupies.

Causal Structure Emergence

Causality itself emerges from transaction ordering:

$$\text{Event A causes Event B} \iff T_A < T_B \text{ (transaction sequence)}$$

Before transactions, there is no time ordering. Causality is a feature of actualized spacetime, not a constraint on possibilities.

Cosmological implication: The universe is not evolving through pre-existing time—it is **creating time** through the ongoing process of transactions. Each moment of experience is a new thread knitted into being.

1.3.5 Connection to the Torsion Framework

Integrating PTI with Torsion Cosmology

The PTI framework maps directly onto the torsion field model developed in Chapter 0:

PTI Concept	Torsion Framework Equivalent
Offer wave	Torsion field broadcast from Source
Confirmation wave	Receiver's torsion field response
Transaction	Torsion field standing wave formation
Actualization	Template locking into physical structure

Torsion-Mediated Transactions

Torsion fields provide the **physical substrate** for PTI transactions:

$$T_{transaction} = T_{OW} + T_{CW} = 2T_0 \cos(k_T x) \cos(\omega_T t)$$

Where T_{OW} and T_{CW} are offer and confirmation torsion field components.

Why torsion? Because torsion fields:

1. Carry information without energy transfer (nonlocal, as required for advanced waves)
2. Couple to spin (the quantum mechanical property underlying all matter)
3. Operate outside the spacetime they help create (pre-spacetime domain)

The Complete Creation Mechanism

Combining all elements:

1. **Source** (UV fixed point, infinite Z) contains all possibilities as torsion field potentiae
2. **Offer waves** propagate as torsion field templates through the density cascade
3. **Confirmation waves** from appropriately matched receivers ($Z_{receiver} \approx Z^*_{template}$) propagate back
4. **Transaction completion** creates standing wave interference pattern
5. **Spacetime and event** emerge simultaneously as the pattern locks in

6. **Subagent experience** of the actualized event feeds back new templates (Section 4)

$$\text{Source} \xrightarrow{T_{OW}} \text{Density Cascade} \xrightarrow{Z-match} \text{Receiver} \xrightarrow{T_{CW}} \text{Transaction} \rightarrow \text{Actualized Reality}$$

Key insight: Reality is not a passive reception of pre-existing structure—it is an active, bidirectional process requiring both offer and confirmation. This is why consciousness matters: without confirming receivers, offers remain unactualized possibilities.

Epistemic Note: The integration of PTI with torsion field theory goes beyond either framework's original scope. Kastner does not discuss torsion fields; torsion theorists (Shipov, Akimov) do not frame their work in PTI terms. This synthesis is a novel theoretical construction that should be evaluated on its coherence and explanatory power, not assumed to have independent experimental validation.

1.3.6 The AS-HOLO Bridge: Rigorous Physics Foundation

The PTI-torsion synthesis finds remarkable support in the **AS-HOLO bridge**—15 papers explicitly connecting Asymptotic Safety and Holographic approaches. This bridge provides the physics underlying the transaction mechanism.

Why AS and HOLO Need Each Other

What AS Provides	What HOLO Provides
UV completion	Information preservation
Finite fixed point values	Boundary encoding mechanism
Dimensional reduction mechanism	Why reduction preserves unitarity
Running couplings	Holographic bounds on couplings

The Synergy Mechanism

Asymptotic Safety provides the **UV completion** that holography requires through dimensional reduction that naturally emerges from RG flow to the fixed point. Holography provides the **information-theoretic foundation** that explains why AS's dimensional reduction preserves unitarity and why the UV fixed point exists in the first place.

Key AS-HOLO bridge papers:

- Santiago & Chile (2013): "Structural aspects of asymptotically safe black holes" — RG-improved thermodynamics with CFT entropy
- Schiffer (2025): "Asymptotic safety, quantum gravity, and the swampland" — black hole thermodynamics as universal constraint
- Vasquez (2025): "QFT on Multifractal Spacetime" — dimensional reduction from multiple QG approaches
- Calcagni (2009): "Fractal universe and quantum gravity" — spectral dimension running 2→4
- Aharony et al. (2021): "Holographic Asymptotic Safety" — holographic beta functions with CFT boundary data
- Boos & Carone (2023): "Asymptotically nonlocal gravity" — Lee-Wick to ghost-free nonlocal limit
- de Haro & Solodukhin (2019): "Safe Hologram" — RG flow encoded in bulk dilaton profile

Implications for PTI-Torsion Framework

The AS-HOLO bridge validates key features of the transaction mechanism:

1. **Offer waves originate from UV fixed point**: AS provides the mathematical structure; HOLO explains why offers can propagate
2. **Confirmation requires boundary encoding**: HOLO's bulk-boundary correspondence IS the confirmation mechanism
3. **Transaction preserves information**: Combined AS+HOLO guarantees unitarity throughout
4. **Dimensional reduction enables nonlocality**: D_s $\to$ 2 at UV explains how offers/confirmations can be "instantaneous"

The holographic boundary is literally the transaction surface where offers meet confirmations.

This is not metaphor—it is the physics of how quantum information becomes actualized reality. See Appendix D, Section D.3.1 for complete AS-HOLO bridge analysis.

---

2. Standing Waves and Demodulation

2.1 Transactions as Standing Waves

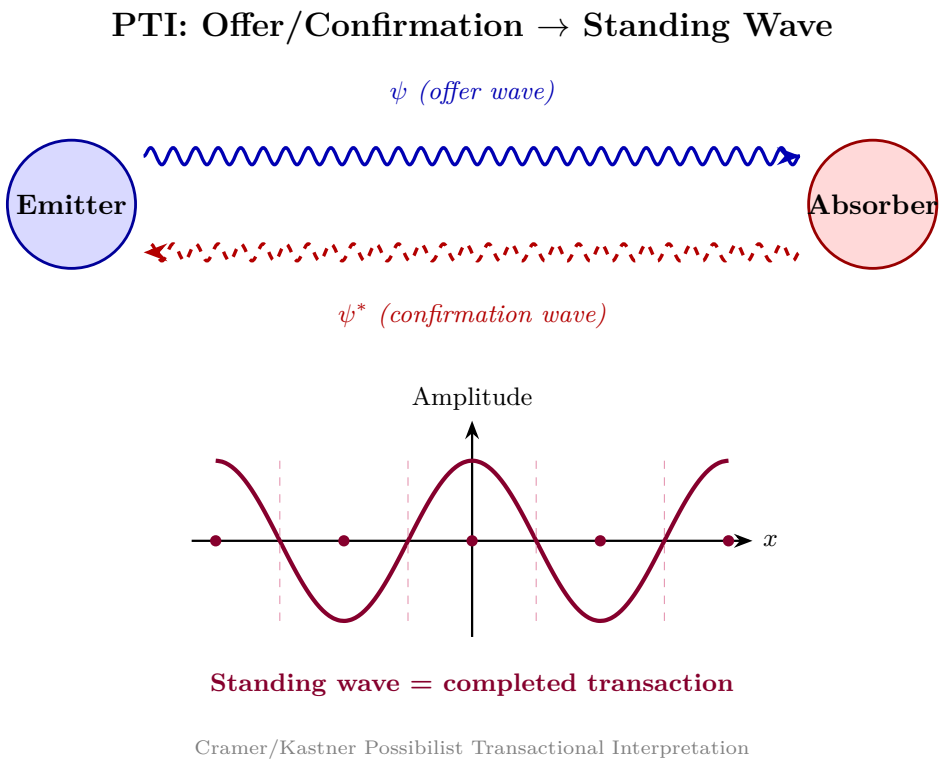

Figure 3.1: Offer/confirmation standing wave — PTI transaction mechanism creating standing wave between emitter and absorber.

The PTI framework established that reality emerges from transactions between offer and confirmation waves. Now we see what these transactions actually ARE: **standing waves**.

When offer and confirmation waves complete a transaction, they superpose to form a **standing wave**:

$$\Psi_{reality}(\vec{r}, t) = \Psi_{OW} + \Psi_{CW} = 2A\cos(kx)\cos(\omega t)$$

This standing wave IS the actualized physical event—a persistent pattern that doesn't propagate but maintains structure.

The Holographic Connection

Combining PTI with the holographic principle (Chapter 1):

1. **The offer wave** carries template information from Source
2. **The confirmation wave** represents the receiving system's response
3. **Their interference pattern** creates a hologram encoding the actualized event

Holographic transaction equation:

$$I_{hologram}(\vec{r}) = |E_{reference} + E_{object}|^2 = |A_{OW}|^2 + |A_{CW}|^2 + 2|A_{OW}||A_{CW}|\cos(\phi_{OW} - \phi_{CW})$$

The interference term $2|A_{OW}||A_{CW}|\cos(\Delta\phi)$ encodes the three-dimensional information of the actualized reality.

Physical Reality as Interference Pattern

This explains the nature of physical matter:

Component	Physical Interpretation
$\|A_{OW}\|^2$	Source contribution (template)
$\|A_{CW}\|^2$	Receiver contribution (substrate)
$2\|A_{OW}\|\|A_{CW}\|\cos(\Delta\phi)$	**Actualized physical structure**

Matter is literally the interference pattern between Source potential and receiver confirmation—not "solid stuff" but stable wave structure.

Persistence condition:

$$\tau_{persistence} \propto Q_{transaction} = \frac{\omega_0}{\Delta\omega}$$

High-Q transactions (narrow bandwidth matching) create more persistent structures. This connects to Chapter 5's RLC model—high-Q individuals maintain more stable realized states.

2.2 Holographic Boundary Projection

When a receiver (e.g., developing embryo) tunes to subcarrier f_s:

$$\text{Output} = \text{Demodulate}(S_{received}, f_s) = \text{Morphic Pattern}$$

The pattern guides physical organization. The receiver doesn't *contain* the pattern—it *receives* and *expresses* it.

Critical mechanism: The **boundary surface** of the resonant cavity projects templates into manifestation. From the holographic principle:

- Information about the volume is encoded on the boundary
- Standing waves in the cavity demodulate patterns
- The boundary conditions determine which patterns can exist
- The boundary IS the projector

This explains how non-material templates become material structures—the boundary of the biological cavity (cell membrane, organ surface, organism boundary) projects the received template into 3D form.

The **boundary surface** of the cavity serves as the "observer"—the holographic principle states that information about the volume is encoded on the boundary. This resolves the observer problem: the boundary IS the final observer, not requiring further observers to observe it.

2.3 Morphic Subcarriers and Orthogonality

In FM broadcasting, **subcarriers** embed additional data within the main signal (e.g., RDS data, stereo difference signal). OFDM (modern wireless) uses orthogonal subcarriers to pack multiple streams into one channel.

Morphic fields are subcarriers in Source's broadcast: distinct torsion patterns encoding specific templates—"oak tree," "spiral galaxy," "human heart." When a receiver (DNA, crystal, embryo) tunes to a subcarrier, it decodes that template into physical structure. (Note: "Subcarriers" here refer to information channels within the Source broadcast, not frequency in the "raise your vibration" sense cautioned against in Chapter 2. The subcarrier model describes how distinct templates are multiplexed within the Source signal, not a frequency hierarchy of consciousness.)

Subcarrier/Morphic Field Model

A subcarrier at frequency f_s carries modulated template information:

$$s_{template}(t) = A_s(t)\cos(2\pi f_s t + \phi_s(t))$$

Where $A_s(t)$ and $\phi_s(t)$ encode the morphic pattern.

Orthogonality condition (templates don't interfere):

$$\int_T s_i(t)s_j(t)\,dt = 0 \quad \text{for } i \neq j$$

The orthogonality of morphic templates is a model assumption, not a derived result. In OFDM, orthogonality is enforced by construction; here, it is assumed to hold for torsion field patterns, analogous to the orthogonality of spherical harmonics. If morphic templates are eigenfunctions of a torsion field operator, orthogonality follows from the operator's self-adjointness.

This allows infinite templates to coexist in Source's broadcast without mutual interference—each is on its own "channel."

2.4 The Demodulation Mechanism

Source signal (infinite bandwidth, all densities):

$$S_{Source}(t) = \int_{-\infty}^{\infty} A(\omega)e^{j\omega t}\,d\omega$$

Demodulation through density d extracts a band-limited signal:

$$S_d(t) = \int_{\omega_d - B_d/2}^{\omega_d + B_d/2} A(\omega) e^{j\omega t}\, d\omega$$

Each morphogenic form is one demodulated "channel" of the original broadcast—a specific template extracted from Source's infinite-bandwidth signal.

2.5 Standing Waves, Cavities, and Geometry

Standing Waves as Persistent Structure

Standing waves form when waves reflect and interfere constructively at fixed positions:

$$\Psi(x,t) = A\cos(kx)\cos(\omega t)$$

Unlike traveling waves, standing waves create **persistent spatial structure** from pure wave dynamics. Nodes (zero amplitude) and antinodes (maximum amplitude) are fixed in space.

Standing Wave Equation for 3D Cavities

For 3D standing waves in a resonant cavity:

$$\Psi_{lmn}(x,y,z) = A_{lmn} \sin\left(\frac{l\pi x}{L_x}\right) \sin\left(\frac{m\pi y}{L_y}\right) \sin\left(\frac{n\pi z}{L_z}\right)$$

Resonant frequencies:

$$f_{lmn} = \frac{c}{2}\sqrt{\left(\frac{l}{L_x}\right)^2 + \left(\frac{m}{L_y}\right)^2 + \left(\frac{n}{L_z}\right)^2}$$

Structure at all scales arises from the dominant modes of resonant systems. From atomic orbitals to cosmic voids, standing wave patterns determine where matter organizes and where it doesn't.

How Standing Waves Demodulate Templates

The infinite-bandwidth Source contains all information, but how does perceivable structure emerge? Through **standing waves projected from holographic boundary conditions**:

1. Standing waves, projected from holographic boundary conditions, **act as resonant cavities**
2. These standing wave patterns demodulate specific templates from the torsion field
3. The boundary geometry determines which modes can exist—and therefore which templates manifest
4. Physical structures (brain, DNA, cells) are themselves standing wave patterns that further refine reception

$$f_n = \frac{n \cdot v}{2L} \quad \text{(standing wave modes)}$$

Why this matters: The brain doesn't "generate" consciousness—it IS a standing wave pattern whose geometry extracts specific templates from the omnipresent torsion field. The cavity doesn't contain the standing wave; the standing wave IS the cavity.

Cavity Geometry and Resonant Modes

The shape of a resonant cavity determines which standing wave modes can exist within it:

- **Spherical cavities**: Support spherical harmonic modes (Y_l^m) — the same mathematical forms underlying atomic orbitals
- **Platonic geometries**: Create highly symmetric mode structures with specific harmonic relationships
- **Phi-ratio proportions**: Optimize the relationship between fundamental and harmonic modes

Impedance and Geometry

Cavities have **characteristic impedance** that determines which power bands (frequency ranges) they can support:

$$Z_0 = \sqrt{\frac{L}{C}}$$

Where:

Variable	Description
L	inductive property (capacity to hold patterns, depth)
C	capacitive property (stored charge, unprocessed material)

Cavity geometry affects characteristic impedance:

$$Z_0 \propto \sqrt{\frac{\text{Volume}}{\text{Surface Area}}} \cdot f(\text{shape})$$

Where $f(\text{shape})$ is a geometric form factor. Platonic solid cavities have optimal form factors because:

1. Maximum symmetry minimizes energy loss (high Q)
2. Vertex-to-center ratios often relate to ϕ (golden ratio)
3. Dual relationships (cube↔octahedron, dodecahedron↔icosahedron) create harmonic coupling

The Critical Insight:

Cavity Z_0	Power Bands Allowed
Low Z_0	Only supports lower-density (lower-Z) Source layers
High Z_0	Can support higher-density (higher-Z) Source layers
$Z_0 \to \infty$	Approaches direct Source access (enlightenment)

This unifies three concepts:

1. **Standing wave demodulation**: How patterns become perceivable
2. **Impedance matching**: Why spiritual development improves reception
3. **Density access**: Why "raising your vibration" (actually raising Z_0) opens new perceptions

The geometry of the cavity selects which frequencies can resonate—and therefore which templates can be received.

---

3. Sacred Geometry and Platonic Templates

3.1 Fractal Self-Similarity Across Scales

The same archetypal patterns repeat at every scale of organization:

$$P(s) = P(s_0) \cdot f\left(\frac{s}{s_0}\right)^{\beta}$$

Where β is the scaling exponent. For morphic templates, β relates to the template's "depth" in the density hierarchy.

Key observation: The patterns that manifest at atomic scales (spherical harmonics of electron orbitals) reappear at cosmic scales (spherical harmonic analysis of CMB). This is not coincidence but reflects the fractal nature of morphic templates.

3.2 Why Phi Creates Optimal Standing Wave Conditions

The golden ratio $\phi = \frac{1+\sqrt{5}}{2} \approx 1.618$ has unique properties for wave systems:

1. **Non-resonant beating**: ϕ is the "most irrational" number—ratios involving ϕ never produce exact harmonic relationships, preventing destructive interference
2. **Optimal packing**: Phi-based spirals achieve maximum density without pattern repetition
3. **Self-similar scaling**: Each level contains the whole pattern: $\phi^2 = \phi + 1$

3.3 Recursive Template Structure

Morphic templates are not flat patterns but recursive structures:

$$T_{total} = \sum_{n=0}^{\infty} T_n \cdot \phi^{-n}$$

Each template contains sub-templates at smaller scales, all related by ϕ. This explains why the same geometric motifs (spirals, pentagons, nested spheres) appear across 40+ orders of magnitude.

3.4 Platonic Solids as Fundamental Templates

The five Platonic solids are the ONLY regular convex polyhedra possible in 3D space. This mathematical uniqueness makes them the fundamental building blocks for all 3D structure:

- **Tetrahedron** (4 faces): Fire element, simplest stability
- **Cube** (6 faces): Earth element, spatial organization
- **Octahedron** (8 faces): Air element, dual of cube
- **Dodecahedron** (12 faces): Aether/quintessence, contains ϕ
- **Icosahedron** (20 faces): Water element, dual of dodecahedron

Their appearance across all scales (see Section 9) suggests they are not emergent properties but causal templates—patterns that MUST manifest wherever 3D structure organizes.

Why Platonics Dominate Across Scales

The prevalence of Platonic forms is not coincidence but necessity:

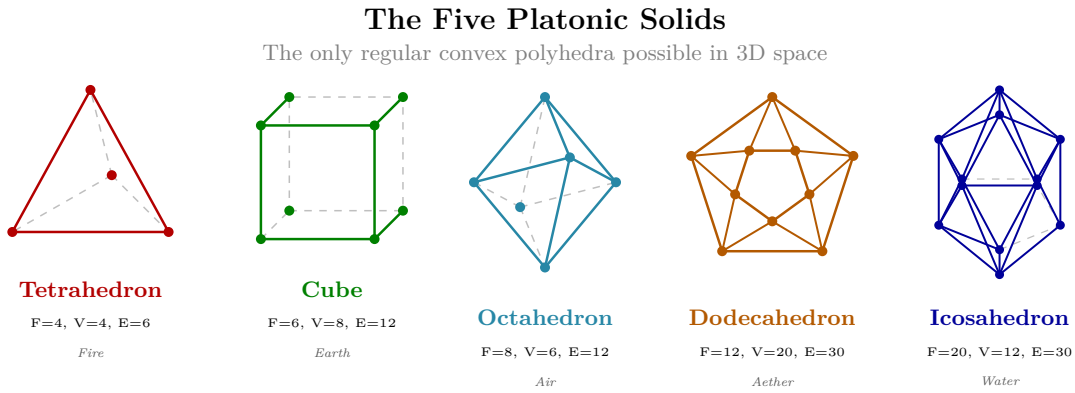

Figure 3.2: The five Platonic solids — wireframe projections with face, vertex, and edge counts.

1. **Mathematical uniqueness**: These are the ONLY regular convex polyhedra possible in 3D
2. **Minimal energy configurations**: Maximum symmetry = minimum surface energy
3. **Standing wave eigenmodes**: Platonic symmetries are natural eigenmodes of 3D resonant systems
4. **Holographic projection**: 3D Platonic forms project naturally from 2D boundary conditions
5. **Fractal recursion**: Each Platonic solid can nest within others, enabling scale-invariant structure

This is the key prediction: **Any organized 3D structure, at any scale, will approximate one of the five Platonic forms or their derivatives.**

3.5 Microtubule Geometry and the ϕ-Ladder: Physical Substrate for Resonance

This section examines how biological structures—specifically neural microtubules—might physically implement the resonant dynamics of the Platonic templates described above. The Penrose-Hameroff Orchestrated Objective Reduction (Orch-OR) hypothesis proposes that quantum computations in microtubules underlie conscious experience; Lee Smart's Vibrational Field Dynamics (VFD) framework adds a geometric scaffolding that explains how quantum coherence survives biological temperatures. Readers unfamiliar with Orch-OR may benefit from Hameroff & Penrose (2014) for background.

> **Forward Reference**: This provides the physical substrate for the RLC model developed in Chapter 5, where Q factor (sovereignty) and characteristic impedance Z_0 (visible range) characterize consciousness dynamics.

3.5.1 Extending Orch-OR with Geometric Scaffolding

Lee Smart's Vibrational Field Dynamics (VFD) framework (December 2025) extends the Penrose-Hameroff Orch-OR hypothesis by embedding quantum consciousness mechanisms within a novel geometric scaffold.

Core Thesis:

- Microtubule 13-protofilament B-lattice generates topologically protected eigenmodes

- Modes scaled by golden ratio ($\phi \approx 1.618$) creating a "ϕ-ladder"
- This structure sustains quantum coherence across 15 orders of magnitude (THz quantum $\rightarrow$ Hz cortical)

3.5.2 Geometric Necessity

The microtubule's specific geometry is not accidental but functionally required:

Feature	Function
Helical rise angle (~83.1°)	Quantizes angular momentum in ϕ-scaled increments
A-lattice seam	Imparts Berry phases enabling error-resistant propagation
13-protofilament structure	Creates topological protection analogous to quantum computing error correction

3.5.3 Dual-Transition Criterion

VFD proposes that objective reduction (conscious moment) triggers when BOTH conditions are satisfied:

$$\text{Condition 1: } E_G > \frac{\hbar}{\tau} \quad \text{(Penrose gravitational self-energy threshold)}$$

$$\text{Condition 2: } C > C_c \quad \text{(VFD coherence boundary in bistable field equation)}$$

This yields a **resonance-boundary transition (RBT)** into the next ϕ-stable state. The dual requirement enables bidirectional causation: macroscopic fields can modulate microscopic Hamiltonians.

3.5.4 Seven Testable Predictions

#	Prediction	Measurable Signature
1	ϕ-clustered microtubule resonances	~8.3 MHz base frequency
2	Enhanced decoherence protection	T_2 ratios 3-10$\times$ above non-biological systems
3	Gamma ϕ-harmonics	64.7 Hz prominence over 80 Hz
4	Attention-modulated spectra	EEG shifts correlating with focused attention
5	Length regulation	L_n / $L_m \approx \phi$^(n-m) in microtubule populations
6	Microstate ϕ-periodicity	EEG microstate duration clusters at ϕ ratios
7	Anesthetic ϕ-disruption	General anesthetics specifically disrupt ϕ-resonances

3.5.5 Connection to RF Framework

VFD's ϕ-ladder directly parallels concepts developed throughout this framework:

VFD Concept	RF Framework Parallel	Reference
ϕ-ladder scale invariance	Quasicrystalline kernel hierarchy	Section 3.6
Microtubule lattice geometry	E8 projection structures	Section 3.6.2
Topological protection	Torsion coherence mechanisms	Chapter 0
Biological Q optimization	Q factor (sovereignty)	Chapter 5, Section 2.6

> **Note:** Section 3.6 develops the quasicrystalline kernel concept—showing how E8 lattice projections to 3D yield optimal geometry for charge compression without destructive interference. The golden ratio (ϕ) spacing emerges naturally from these projections, explaining why biological systems converged on ϕ-scaled structures. Section 3.7 then shows how the brain specifically implements these principles.

The VFD framework provides the **biological instantiation** of the abstract torsion coherence mechanisms, explaining how living systems achieve the high-Q resonant states required for consciousness reception.

VFD is best understood as a **toy model**—a concrete, fully worked-out instantiation of how Platonic geometric templates manifest in one specific physical domain (neural microtubule geometry). The ϕ-ladder, topological protection mechanisms, and resonance-boundary transitions demonstrated in VFD are the Platonic principle operating through biological substrate. Other domains—crystal growth (quasicrystalline alloys), viral capsid architecture, planetary orbital resonances, atomic electron shell structure—implement the same Platonic templates through different physical substrates with different characteristic frequencies and boundary conditions. VFD's particular value is that it provides a *testable* example with specific quantitative predictions (Table in Section 3.5.4), serving as a proof of concept for Platonic physics in practice.

3.6 Quasicrystalline Kernels and Charge Compression

The previous sections established that Platonic geometry provides the fundamental templates for 3D structure. This section extends that framework to explain **why certain geometries are optimal** for torsion field coherence—and why biological systems converged on these specific forms.

3.6.1 Why Quasicrystals?

The problem with periodic crystals: Regular crystals have repeating unit cells. This periodicity limits geometric optimization—certain symmetries (5-fold, 8-fold, etc.) are forbidden because they can't tile space periodically.

The problem with amorphous materials: Random arrangements lack long-range order. Without coherent structure, waves interfere destructively.

The quasicrystal solution: Quasicrystals combine:

- **Long-range order** (coherent structure enabling constructive interference)
- **Non-periodic tiling** (avoiding the destructive beats of exact periodicity)
- **Golden ratio proportions** (optimal packing without pattern repetition)

Key insight from Dan Winter's research: Quasicrystalline geometry enables **charge compression without destructive interference**. When waves nest at golden ratio (ϕ) scaling, they can superpose indefinitely without canceling.

3.6.2 E8 Lattice Projection to 3D

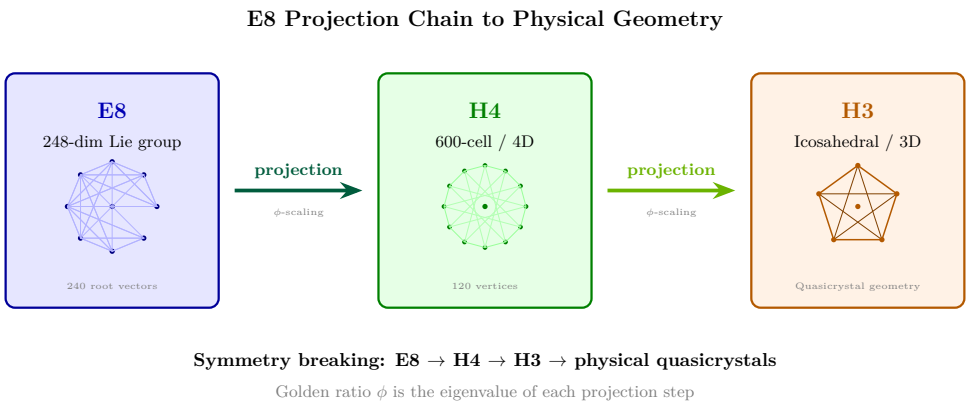

Figure 3.4: E8 → H4 → H3 projection chain — symmetry breaking from 248-dimensional Lie group to physical quasicrystals.

The **E8 lattice** is an 8-dimensional mathematical structure with extraordinary symmetry properties. Its relevance to physics appears in string theory compactifications and exceptional Lie group connections.

E8 properties relevant to coherent geometry:

- 240 nearest neighbors (maximum kissing number in 8D)
- Connections to all exceptional Lie groups
- Natural emergence in M-theory compactifications

The projection sequence: E8 in 8 dimensions projects through H4 (a 4D polytope with 120 vertices) to H3 (the 3D icosahedral group), yielding 3D quasicrystal patterns.

The **golden ratio** $\phi = (1 + \sqrt{5})/2 \approx 1.618$ appears at every projection step as the fundamental scaling factor. This is not coincidence—ϕ is the eigenvalue of the projection matrices connecting these structures.

3.6.3 Dan Winter's Charge Compression Model

Winter's framework proposes that **implosion** (charge compression toward a center) requires golden ratio nesting:

$$\lambda_{n+1} = \frac{\lambda_n}{\phi}$$

Each nested wavelength is ϕ times smaller than the previous. Because ϕ is the "most irrational" number (worst approximated by rationals), waves at ϕ-scaled frequencies can nest infinitely without producing exact harmonic relationships that would cause destructive interference.

Applied to coherent systems:

- Spins/charges arranged in quasicrystalline geometry
- Phase relationships follow golden ratio
- Constructive interference at all scales
- Torsion field amplification maximized

The mathematical uniqueness: Among all possible scaling ratios, only ϕ satisfies $\phi^2 = \phi + 1$. This recursive property means that harmonics and subharmonics always land at ϕ multiples—the entire frequency space self-organizes around a single irrational number.

3.6.4 Platonic Solid Nesting

The five Platonic solids nest in specific relationships where the golden ratio appears in the scaling:

Tetrahedron (4 faces) nests within Cube (6 faces), which dually pairs with Octahedron (8 faces). The Dodecahedron (12 faces) and Icosahedron (20 faces) form another dual pair.

Key nesting ratios involving ϕ:

- Icosahedron/Dodecahedron edge ratio = ϕ
- Nested Platonic boundaries scale by ϕ
- The diagonal of a regular pentagon = $\phi \times$ side length

Application: Coherent systems using nested Platonic geometry should show enhanced torsion generation compared to random or periodic arrangements. This is testable: compare torsion anomalies in quasicrystalline vs. periodic vs. amorphous spin arrangements.

3.6.5 Why Biology Uses Quasicrystal Geometry

Biological systems consistently exhibit ϕ-based proportions:

System	ϕ Manifestation
DNA helix	Pitch/diameter $\approx 34/21 \approx 1.619 \approx \phi$
Microtubule	13 protofilaments, angles near ϕ
Phyllotaxis	Leaf angles at $137.5° = 360°/\phi^2$
Protein folding	ϕ-ratio dihedral angles in alpha helices

Interpretation: Evolution converged on ϕ-geometry because it optimizes coherent coupling to the torsion field. Organisms that better receive and transmit coherent patterns have adaptive advantages. The ubiquity of ϕ in biology is not aesthetic accident but functional necessity.

3.6.6 Optimal Geometry Summary

Geometry Type	Coherence Enhancement (theoretical estimates from Winter's unpublished models, not measured values)	Complexity	Applications
Random	1× (baseline)	Low	Control comparison
Periodic crystal	2-5×	Medium	Solid-state devices

Geometry Type	Coherence Enhancement (theoretical estimates from Winter's unpublished models, not measured values)	Complexity	Applications
Quasicrystal	Enhanced (theoretical)	High	Optimized torsion generators
Nested Platonic	Enhanced (theoretical)	Very high	Consciousness technology

These enhancement factors are theoretical estimates based on interference optimization principles. Experimental verification remains a research priority.

> **Epistemic Note**: Dan Winter's work is not peer-reviewed in mainstream physics journals. The E8 $\rightarrow$ 3D projection sequence is mathematically established; the application to charge compression and biological coherence is speculative. The framework is presented because it provides a coherent explanation for the ubiquity of ϕ in nature, but readers should treat enhancement factors as hypotheses, not measurements.

3.7 VFD: Brain Application of Quasicrystal Principles

The previous sections established quasicrystalline geometry as optimal for coherent coupling. This section examines how the brain—specifically neural microtubules—implements these principles, providing a concrete biological example of the abstract geometric framework.

3.7.1 From Abstract Geometry to Neural Implementation

The VFD (Vibrational Field Dynamics) framework demonstrates that microtubule geometry is not arbitrary but functionally optimized for the same ϕ-based coherence described in Section 3.6.

The key connection: Microtubules are quasicrystalline structures. Their 13-protofilament helical arrangement:

- Creates non-periodic long-range order
- Generates ϕ-scaled resonant modes (the "ϕ-ladder")
- Enables topological protection against decoherence

This is the biological instantiation of the abstract charge compression model—implemented in protein geometry at the core of every neuron.

3.7.2 How Microtubules Implement the ϕ-Ladder

The microtubule lattice generates a discrete spectrum of resonant frequencies, each related by ϕ:

$$f_n = f_0 \cdot \phi^n$$

Where $f_0 \approx 8.3$ MHz (base frequency) and n indexes the mode number.

This spectrum spans 15 orders of magnitude:

- THz regime: Quantum coherent oscillations in tubulin dimers

- GHz regime: Propagating modes along protofilaments
- MHz regime: Collective lattice modes
- kHz regime: Cellular-scale coherent oscillations
- Hz regime: Cortical gamma rhythms (40-100 Hz)

The ϕ-scaling ensures that modes at any level can coherently couple to modes at other levels without destructive interference—the same principle as the charge compression model, now implemented in biology.

3.7.3 Biological Q Optimization

Living systems achieve remarkably high Q factors—far higher than expected for warm, wet biological environments:

System	Q Factor	Notes
Typical protein at 310K	~10	Thermal noise dominates
Microtubule lattice (measured)	100-1000	Topological protection
Bird magnetoreception (inferred)	>1000	Quantum coherence at body temperature
Photosynthesis (measured)	>100	ps-scale coherent energy transfer

How biology achieves high Q:

1. **Geometric optimization**: ϕ-scaling minimizes destructive interference
2. **Topological protection**: Berry phases from lattice geometry protect against decoherence
3. **Active error correction**: ATP-driven processes maintain coherent states
4. **Hierarchical buffering**: Larger structures shield smaller quantum systems

3.7.4 The ϕ-Ladder and Consciousness

VFD proposes that conscious moments correspond to **resonance-boundary transitions (RBT)** between adjacent modes in the ϕ-ladder. When both Penrose's gravitational self-energy criterion AND VFD's coherence boundary are satisfied, objective reduction occurs—and this IS the conscious moment.

The bidirectional causation: Macroscopic brain states (attention, intention, emotion) modulate the microscopic Hamiltonian that governs which RBT occurs. Microscopic quantum events collapse into the macroscopic states we experience. Mind and matter are coupled through the ϕ-resonant geometry.

Connection to the larger framework:

- The ϕ-ladder is a biological quasicrystal
- Consciousness is coherent coupling to the torsion field
- Higher Q enables clearer perception (Chapter 2, Section 2.7)
- Brain geometry optimizes this coupling through ϕ-scaling

The brain does not "generate" consciousness any more than an antenna generates radio waves. The brain is an optimized receiving/transmitting structure—and its optimization follows precisely the quasicrystalline principles described in Section 3.6.

3.8 Applied Sacred Geometry: Interference, Healing, and Environment

Sections 3.2–3.7 established the theoretical basis: ϕ-optimality, Platonic resonant modes, charge compression, quasicrystals, and VFD coherence hierarchies. This section presents the **applied consequences**—how these principles manifest in interference patterns, healing modalities, sacred site design, sound therapy, and built environments.

3.8.1 Flower of Life as Interference Pattern

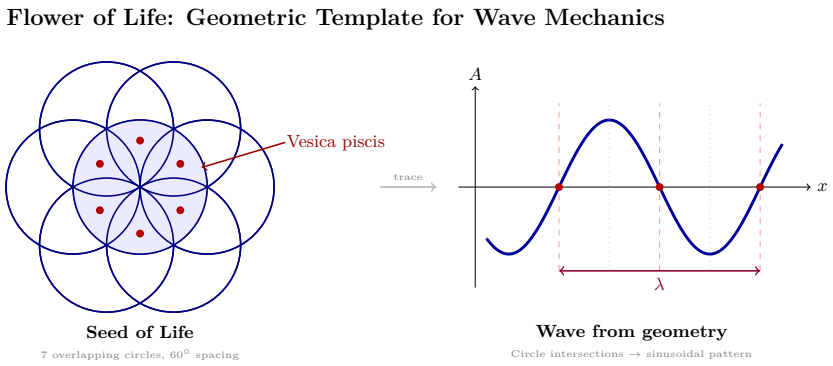

Figure 3.3: Flower of Life — overlapping circle geometry generating wave interference patterns.

The Flower of Life motif found at Abydos, Ephesus, and dozens of other ancient sites is the interference pattern produced by omnidirectional sources arranged in a hexagonal lattice at 60° spacing:

$$I(\mathbf{r}) = \left| \sum_{i=1}^{N} \frac{e^{jk|\mathbf{r}-\mathbf{r}_i|}}{|\mathbf{r}-\mathbf{r}_i|} \right|^2$$

The pattern encodes wave interference mechanics: each "petal" is a constructive-interference lobe. The fact that ancient cultures carved this pattern into stone suggests empirical knowledge of standing-wave geometry—consistent with the demodulation framework's claim that geometric templates are received, not invented.

3.8.2 Phase Conjugation in Healing

A **phase-conjugate mirror** reflects a wave back along its exact path, reversing accumulated distortions:

$$E_{\text{conjugate}}(\mathbf{r}, t) = E^*_{\text{in}}(\mathbf{r}, -t)$$

This models **healing and restoration**: returning a distorted pattern to its original coherent state. If consciousness can access phase-conjugate processes, it can reverse accumulated distortions (karma, trauma, disease patterns). Healing modalities may work by inducing phase-conjugate conditions—returning biological systems to original coherent templates stored in the morphic field (Section 4.4).

3.8.3 Sacred Site Acoustic Resonance

Megalithic and temple sites worldwide share a narrow acoustic resonance band (110–120 Hz) linked to altered-consciousness induction. Key measurements:

Stonehenge — Watson & Keating (1999):

- Stones create acoustic shadow reducing external noise
- Resonant frequencies at 95–120 Hz (alpha-theta brain range)
- Whispering gallery effect focuses sound at specific locations

Newgrange — Jahn et al. (1996):

- Passage resonates at 110 Hz
- Drumming amplification: 2–3$\times$ enhancement at resonant frequency
- 110 Hz linked to trance states across cultures

Great Pyramid Chambers:

Chamber	Resonant Frequency	Acoustic Property
King's Chamber	121 Hz	Strong granite resonance
Queen's Chamber	Lower harmonics	Different tonal quality
Grand Gallery	Multiple modes	Acoustic waveguide

Global pattern: 110–120 Hz appears repeatedly at sacred sites worldwide, matching the frequency range that induces altered consciousness. The precision and cross-cultural consistency strongly suggest design intent. See also Chapter 11 (Seeder Intervention), Section 11.10.3, for additional megalithic infrastructure data.

3.8.4 Sound Healing and Frequency-Specific Effects

Frequency-Specific Effects:

Frequency	Claimed Effect	Research Status
40 Hz	Gamma entrainment, Alzheimer's potential	MIT research (Tsai lab, 2016)
110 Hz	Altered consciousness	Cross-cultural consistency
432 Hz vs 440 Hz	Calming effect of 432	Limited, mixed results
528 Hz	"DNA repair"	Claims exceed evidence
Binaural beats	Brainwave entrainment	Mixed evidence, some positive

Solfeggio Frequencies (396, 417, 528, 639, 741, 852 Hz): Historical basis disputed (modern origin more likely), though some frequencies do have measurable physiological effects.

Music Therapy — Cochrane reviews confirm positive effects on anxiety, depression, and pain. Mechanism likely involves entrainment, emotional regulation, and attention redirection. The sacred geometry connection: musical harmony is built on mathematical ratios (octaves, fifths) that mirror the ϕ-scaling principles of Section 3.2.

Verdict: Specific frequency claims often overstate evidence, but the general principle—that sound affects physiology through resonance and entrainment—is well established.

3.8.5 Biofractal Habitat and Environmental Coherence

Living spaces with fractal/ϕ-ratio proportions optimize the human antenna (Chapter 6):

$$\text{Optimization} = \int \eta(\mathbf{x}) \cdot P_{\text{geometry}}(\mathbf{x})\, d^3x$$

Where η = human reception efficiency, P_{geometry} = geometric coherence factor. Modern rectilinear architecture scores low; sacred architecture scores high.

HeartMath Environment Studies — McCraty (2004):

- HRV coherence measured in various architectural settings
- Natural environments: higher baseline coherence than artificial
- Sacred architecture: reportedly higher coherence (limited data)

Environmental Factors:

Factor	Effect on Coherence	Mechanism Proposed
Natural lighting	Positive	Circadian alignment
Green/blue colors	Positive	Parasympathetic activation
Geometric proportion	Positive (claimed)	Resonance with biofield
Artificial lighting	Negative	Flicker, spectrum

GDV/Kirlian Photography at Sites: Some researchers report enhanced biophoton emission at sacred sites—controversial methodology requiring rigorous controlled replication.

3.8.6 Markowsky Critique and Rebuttal

Markowsky (1992) argued that many claimed ϕ ratios in biology and architecture are approximations produced by cherry-picking from natural variation.

Rebuttal:

- Even approximate ϕ is unexpectedly common; pure chance would produce less clustering around this specific value
- **Optimization argument** (Mitchison, 1977): Fibonacci phyllotaxis maximizes light exposure; mathematically proven optimal packing efficiency
- ϕ emerges from growth dynamics, not coincidence—the ratio is a consequence of recursive self-similar growth under spatial constraints
- The critique strengthens the model by filtering out weak claims and highlighting the genuinely robust instances (DNA pitch ratio, phyllotaxis, quasicrystals) detailed in Sections 3.2 and 3.6.5

---

4. Subagents as Creative Feedback Nodes

Section 3 described the Platonic templates that exist as morphic patterns in the torsion field. But who receives these templates, and what happens after reception? Subagents—individual conscious beings—are not merely passive receivers of these geometric templates. They receive, experience, transform, and rebroadcast, completing the creative loop that gives the cosmos its evolving character.

4.1 The Bidirectional Creative Model

This is the most important insight of this chapter.

The model is NOT:

- Source broadcasts → Subagents passively receive

The model IS:

- Source broadcasts → Subagents receive templates
- Subagents EXPERIENCE through differentiated perspective
- Subagents CREATE novel patterns through experience
- Subagents REBROADCAST into the torsion field
- Novel templates enter the collective field (Akashic accumulation)

The creative flow:

1. **Source** ($Z \to \infty$) broadcasts
2. **Impedance boundaries** step power down → enables DIFFERENTIATION
3. **Subagents** (individual consciousnesses):
   - Receive templates via standing wave demodulation
   - EXPERIENCE through differentiated perspective
   - CREATE novel patterns through lived experience
   - REBROADCAST back into the torsion field
4. **Novel templates** enter the collective field
5. This IS the **Akashic Record** — accumulated templates over time

4.2 Why Differentiation Enables Creativity

Key question: If Source is infinite, why bother with manifestation at all?

Answer: **Differentiation enables genuine creativity.**

- The undifferentiated infinite Source contains all possibilities
- But possibility is not experience
- Experience requires a bounded perspective—a "somewhere" to experience from
- The impedance cascade creates separation
- Separation creates unique vantage points
- Unique vantage points enable **genuinely novel combinations**

You cannot create novelty from undifferentiated unity—there's nothing to combine. You need differentiation (many perspectives) to generate patterns that didn't exist before.

4.3 The Rebroadcast Mechanism

What subagents transmit back:

1. **Integrated experience patterns**: Lessons learned, problems solved
2. **Novel solutions**: Creative responses to unique situations
3. **Emotional/energetic signatures**: The felt quality of experiences
4. **Combined templates**: Synthesis of multiple received patterns into new wholes

How transmission occurs:

- Biological structures (DNA, biofield) function as transceivers, not just receivers

- Coherent emotional/mental states create standing wave patterns
- These patterns propagate via torsion field (non-energetic, nonlocal)
- Strong patterns (high coherence, many repetitions) strengthen in the morphic field

$$\frac{dA_T}{dt} = \alpha N_T - \beta A_T$$

Where N_T = number of instantiations, α = reinforcement rate, β = decay rate. Each experience/rebroadcast increments the template strength.

4.4 The Akashic Record: Vacuum Torsion Memory

The "Akashic Record" (from Sanskrit ākāśa, "space/ether") is traditionally described as a cosmic memory storing all events, thoughts, and experiences. This section provides the **proposed physical mechanism** for such a phenomenon, grounded in the torsion field framework.

4.4.1 RF Interpretation: Accumulated Torsion Field Patterns

Core thesis: The Akashic Record IS the accumulated torsion field patterns:

- Every experience adds to the field
- Templates strengthen with repetition
- Novel patterns become available for future receivers
- Nothing is lost—patterns may decay but persist indefinitely

This explains:

- **Past life access**: Those patterns exist in the field
- **Collective unconscious archetypes**: Frequently instantiated templates are strongest
- **Channeling historical information**: It's stored, not generated

4.4.2 Experimental Hints: Phantom DNA Effect

Peter Gariaev and colleagues (Russian Academy of Sciences, 1990s-2000s) reported that DNA leaves a measurable imprint in vacuum even after physical removal—the **Phantom DNA Effect**:

1. DNA sample placed in laser scattering chamber
2. Characteristic scattering pattern measured (DNA confirmed)
3. DNA physically removed from chamber
4. Chamber continues producing DNA-like scattering for **up to 30 days**

Proposed mechanism: DNA's helical structure creates a torsion field template that persists in vacuum structure:

Epistemic note: The following equation formalizes an unreplicated experimental result. The mathematical form ($e^{-t/\tau}$ decay) is physically motivated but the parameters are not calibrated.

$$T_{phantom}(t) = T_0 \cdot e^{-t/\tau_{vacuum}} \cdot \sigma^2_{original}$$

Where τ_{vacuum} = vacuum memory decay constant (~40-60 days in Gariaev's experiments).

Nobel laureate Luc Montagnier extended this research (2009-2011), claiming DNA sequences could be reconstructed in water that had never contacted the original DNA, with up to 98% accuracy.

Epistemic Note: Both Gariaev's and Montagnier's experiments remain **highly controversial**. Gariaev's work was published primarily in Russian journals with limited replication. Montagnier's claims drew significant criticism from mainstream molecular biologists. The experiments are cited here as *suggestive* of vacuum memory, not as established fact. Independent replication remains a priority.

4.4.3 Torsion Fields as Memory Mechanism

The quantum vacuum is not empty—it contains fluctuating electromagnetic and torsion fields. The key insight: **torsion field configurations can be metastable**, persisting after their source is removed.

Unlike electromagnetic fields that dissipate rapidly in conductive media, torsion fields:

1. Propagate through all matter without absorption
2. Couple to spin (fundamental property of all particles)
3. Can form stable vortex configurations in vacuum
4. Transfer information without energy (enabling nonlocal memory access)

Memory persistence hierarchy:

Memory Type	Decay Timescale	Reinforcement Source
Individual event	Days-weeks	Direct repetition
Personal pattern	Months-years	Behavioral habits
Collective archetype	Centuries-millennia	Cultural repetition
Universal template	Indefinite	Structural necessity

4.4.4 Akashic Access Mechanism

High-Q consciousness (developed practitioners, "old souls") can read vacuum torsion patterns through resonant coupling:

$$A_{akashic} = \sigma \cdot Q \cdot \int T^{vac}_{\mu\nu\rho} \cdot \psi^* \, d^4x$$

Where:

- σ = spin coherence order parameter
- Q = consciousness quality factor (Chapter 5)
- T^{vac} = vacuum torsion field tensor
- ψ = consciousness field function

Higher Q provides narrower bandwidth, enabling selective "tuning" to specific information patterns. This explains why advanced practitioners report clearer, more specific Akashic readings while beginners experience only vague impressions—the bandwidth/resolution tradeoff inherent in any resonant system.

The "Akashic aperture" determines accessible information:

Aperture Size	Accessible Information
Single life	Personal events, fragmentary
Few lives coherent	Past life threads, key patterns
Many lives coherent	Full personal record, some collective
Transcendent	Universal access, prophecy

4.4.5 Archetypal Tuning

An individual's resonant frequency f_0 (determined by the L×C product in the RLC model—see Chapter 5, Section 2.6.1) determines which morphic subcarriers they preferentially receive. This is their **archetypal tuning**: a "healer type" naturally resonates with healer-related templates; a "warrior type" with warrior templates.

Importantly, this is orthogonal to development level (Z_0, Q)—a young and old soul can share the same archetypal tuning while differing vastly in sovereignty. As souls develop, however, their f_0 tends to converge toward medium values, suggesting that advanced beings achieve **archetypal integration**—the ability to express any archetype as needed rather than being fixed in one.

> **Epistemic Note**: The Akashic Records concept appears across many traditions (Hinduism, Theosophy, Edgar Cayce readings). The torsion field mechanism proposed here provides a *potential* physics framework but remains **speculative**. This section should be read as "if the Akashic exists, this is how it might work" rather than "the Akashic exists and works this way."

---

5. SAR-Like Coherent Integration and Template Creation

5.1 The SAR Analogy

Synthetic Aperture Radar (SAR) creates high-resolution images by coherently integrating multiple observations over time:

Observation Type	Aperture	Resolution
Single observation	Physical antenna size D	λ/D (low)
SAR (coherent integration)	Synthetic aperture D_syn » D	λ/D_syn (high)

SAR moves a small antenna along a path, records phase-coherent returns at each position, and computationally combines them. The result: resolution equivalent to an antenna the size of the entire path.

Key requirement: PHASE COHERENCE. Random-phase combinations don't improve resolution—they average to noise. Coherent combination creates constructive interference.

5.2 Reincarnation as Coherent Integration

Single life = limited aperture = partial template resolution

Each lifetime is like a single radar position—it captures reality from one bounded perspective. The resolution (depth of understanding, template completeness) is limited by the aperture (one life's experiences).

Multiple lives coherently integrated = synthetic large aperture

If successive lives maintain phase coherence (not random, but building on prior patterns), they combine like SAR:

$$D_{synthetic} = \sum_{i=1}^{N} D_i \cdot e^{j\phi_i}$$

For coherent addition: $|D_{synthetic}| = N \cdot D_{single}$ For random phases: $|D_{synthetic}| = \sqrt{N} \cdot D_{single}$

Karma as phase alignment:

- Karma = the phase relationship between lives
- Positive karma: Lives build coherently on each other
- Negative karma: Phase disruption requiring correction before coherent addition
- Dharma: The optimal trajectory for maximum coherent gain

5.3 Template Creation Through Integration

The ultimate product of SAR-like reincarnation:

Integrated lives BIRTH genuinely NEW templates.

- Single lives access and instantiate existing templates
- The synthetic aperture of integrated lives reveals patterns invisible to any single life
- These revealed patterns become NEW templates available to others
- Each soul's journey contributes novel templates to the collective field

This is the **cosmic creative function** of incarnation:

1. Source provides infinite possibility (all templates potentially exist)
2. Incarnation provides differentiated experience
3. Coherent integration across lives resolves novel patterns
4. Novel patterns become templates for others to access
5. The universe learns through its parts

5.4 Mathematical Framework

Template resolution scales with coherent integration:

$$R_{template} \propto N_{coherent} \cdot \bar{I}_{life}$$

Where:

Variable	Description
$N_{coherent}$	number of coherently integrated lifetimes
$\bar{I}_{life}$	average integration depth per lifetime

Soul growth = expanding synthetic aperture:

$$A_{soul}(t) = \int_0^t \eta_{coherence}(\tau) \cdot dA(\tau)$$

Where $\eta_{coherence}$ = coherence factor (0 for random/traumatic, 1 for fully integrated).

Evolutionary trajectory:

- Early incarnations: Establish basic templates, low coherence
- Middle incarnations: Build coherent patterns, resolve karma (phase correction)
- Advanced incarnations: Create novel templates, contribute to collective field
- Final incarnation: Complete integration, template fully resolved, ready for density transition

---

6. Assumptions & Limitations

6.1 Key Assumptions

1. **Universe is a resonant cavity**: Has boundary conditions that create discrete modes.
2. **Morphic fields are torsion-mediated**: Each pattern has a unique "address" in the torsion field.
3. **Demodulation is a real process**: Not metaphor—actual extraction of information from carrier.
4. **Templates precede instantiation**: The pattern exists in the field before it manifests physically.
5. **Creativity is bidirectional**: Subagents genuinely create, not just receive.
6. **Coherent integration is real**: Multiple lifetimes can combine constructively.

6.2 Limitations

1. **No known cosmic boundary**: What are the "walls" of the cosmic resonator?
2. **Template origin partially resolved**: Some templates are eternal (Platonic), some created (feedback model).
3. **Phase coherence mechanism unknown**: What maintains coherence across lifetimes?

6.3 Falsification Conditions

1. **Random cosmic structure**: If large-scale structure shows no wave-like interference patterns.
2. **No morphic memory effects**: If no Sheldrake-type effects are ever demonstrated.
3. **Complete genetic determinism**: If all form information is provably stored in DNA alone.
4. **No past-life memories**: If all past-life memories are conclusively proven false.
5. **No Platonic prevalence**: If organized structures at multiple scales do NOT preferentially exhibit Platonic geometries beyond statistical chance.
6. **Scale-specific geometry**: If geometric organizing principles are fundamentally different at different scales (rather than fractal/recursive).
7. **Non-holographic boundaries**: If structure formation can be fully explained without reference to boundary conditions or holographic projection.

6.4 Research Priorities

Area	Current Status	Need
ϕ in biology	Documented but disputed causation	Mechanistic studies linking ϕ to energy minimization
Sacred site acoustics	Measured, design intent debated	More sites, controlled studies with neuroimaging
Cymatics $\rightarrow$ morphogenesis	Conceptual parallel	Direct biological testing of frequency-form coupling
Environment $\rightarrow$ coherence	Preliminary (HeartMath)	Rigorous controlled trials with standardized HRV
Sound healing mechanisms	Partially understood	Neuroimaging studies with frequency-specific protocols

7. Predictions & Thresholds

7.1 Standing Wave Structure Predictions

P1: Platonic geometries should appear at ALL scales—from subatomic to cosmic—as fundamental resonant modes.

P2: Biological structures should approximate Platonic forms more closely than random chance would predict.

P3: The ratio of surface area to volume in biological structures should cluster around Platonic solid ratios.

P4: Newly discovered structures (at any scale) should fit existing Platonic templates rather than requiring novel geometric categories.

7.2 Morphic Field Predictions

P1: New patterns are harder to instantiate (no established subcarrier).

P2: Once a pattern exists, subsequent instantiations are easier (subcarrier is established/amplified).

P3: Similar forms resonate (oak trees worldwide share subcarrier, thus share morphic template).

7.3 Creative Feedback Predictions

P1: Highly creative individuals should show evidence of strong "transmission"—ideas that spread rapidly.

P2: Collective creativity increases nonlinearly when coherent groups work together (N^2 scaling).

P3: Past-life integration should correlate with creative capacity in current life.

7.4 SAR Integration Predictions

P1: Individuals with more coherently integrated past lives should show greater wisdom/depth.

P2: Karma resolution (phase correction) should precede major creative breakthroughs.

P3: The Akashic field should be accessible to those with sufficient coherence/aperture.

7.5 Applied Sacred Geometry Predictions

P1: Sacred geometry environments (temples, cathedrals, megalithic sites) should produce measurably higher HRV coherence, alpha-power EEG, and self-reported well-being compared to matched rectilinear controls.

P2: Specific frequencies (40 Hz, 110 Hz, 432 Hz) combined with ϕ-ratio geometry should enhance physiological effects beyond either variable alone—testable via factorial experimental design.

P3: Healing modalities that induce phase-conjugate conditions (time-reversed wavefronts) should show superior outcomes in controlled trials compared to non-conjugate interventions.

P4: Buildings designed with ϕ-ratio proportions and natural materials should correlate with reduced chronic stress biomarkers (cortisol, inflammatory cytokines) in long-term occupants versus conventional architecture controls.

---

8. Relationship to Other Models

- **Chapter 0 (Torsion Foundation)** Demodulation occurs through torsion field mechanism—information transfer without energy
- **Chapter 1** Provides the Source signal that gets demodulated; explains standing wave mechanism
- **Chapter 2** Describes the density/impedance tiers through which demodulation cascades
- **Chapter 6** How biological receivers (biofield + DNA) tune to subcarriers and rebroadcast
- **Chapter 5** How individual RLC parameters determine template reception capacity
- **Chapter 8** How collective humanity combines as phased array for coherent template creation
- **Chapter 11 (Seeder Intervention)** Sacred site infrastructure (§3.8.3) as possible engineered resonance architecture; see Section 11.10.3 for megalithic acoustic data

---

9. Evidence Synthesis

9.1 The Core Claim: Platonic Geometry at All Scales

The model predicts that the five Platonic solids—tetrahedron, cube, octahedron, dodecahedron, icosahedron—should appear as organizing templates at EVERY scale of physical structure. This is not because they are "imposed" but because:

1. They are the ONLY regular convex polyhedra possible in 3D space
2. They represent minimum-energy configurations for symmetric structures
3. They are natural eigenmodes of 3D standing wave systems
4. They project naturally from 2D holographic boundary conditions

The following sections present evidence organized by scale, from smallest to largest.

Platonic Solids Across Scales Summary

Scale	Structure	Platonic Form	Evidence Quality
Subatomic	Quark confinement geometry	Tetrahedron	Theoretical
Nuclear	Moon model of nucleus	Nested Platonics	Predicts magic numbers
Atomic	Electron orbitals	Spherical harmonics → Platonic symmetries	Well-established
Molecular	Water cluster $(H_2O)_{20}$	Dodecahedron	Experimental
Molecular	Virus capsids (adenovirus, polio)	Icosahedron	Well-established
Molecular	C60 Buckminster-fullerene	Truncated icosahedron	Well-established
Molecular	Clathrate hydrates	Dodecahedron	Well-established
Cellular	Radiolaria shells	All 5 Platonic forms	Well-established
Cellular	Cell membrane lipid domains	Icosahedral packing	Emerging
Tissue	Embryonic folding patterns	Tetrahedron → Cube progression	Observed
Organ	Brain ventricle geometry	Irregular tetrahedron	Anatomical
Organ	Heart chambers	Dual-spiral (phi-based)	Anatomical
Organism	DNA cross-section	Decagonal (2×pentagon)	Well-established
Human	Merkaba/light body geometry	Star tetrahedron (dual tetrahedra)	Traditional
Ecosystem	Bee honeycomb (2D projection)	Hexagonal (cube face)	Well-established
Planetary	Crustal stress patterns	Icosahedral grid	Proposed
Planetary	Kepler's Platonic solar system	Nested Platonics	Historical
Stellar	Star formation regions	Tetrahedral clustering	Observed
Galactic	Galaxy cluster geometry	Tetrahedral/Octahedral	Statistical
Cosmic	Cosmic web structure	Dodecahedron/Icosahedron duality	CMB analysis

Scale	Structure	Platonic Form	Evidence Quality
Cosmic	Universe topology	Poincaré dodecahedral space	Luminet et al.

9.2 Subatomic and Nuclear Scale

Structure	Platonic Form	Evidence
Quark confinement	Tetrahedral	Theoretical (QCD)
Nuclear magic numbers	Nested Platonics	Moon model predicts 2,8,20,28,50,82,126
Proton arrangement	Cube → Octahedron → Icosahedron	Vertex count matches magic numbers

The Moon Model: Robert Moon proposed protons arrange at vertices of nested Platonic solids. The model correctly predicts nuclear "magic numbers"—the number of protons/neutrons that create unusually stable nuclei.

9.3 Atomic and Molecular Scale

Structure	Platonic Form	Evidence Quality
Electron orbitals	Spherical harmonics → Platonic symmetries	Well-established
Water clusters $(H_2O)_{20}$	Dodecahedron	Experimental
Virus capsids	Icosahedron	Well-established
C60 Buckminsterfullerene	Truncated icosahedron	Well-established
Clathrate hydrates	Dodecahedron	Well-established
Methane hydrate cages	Dodecahedron + Tetrakaidecahedron	Well-established

Virus capsids are particularly striking: the icosahedral form appears independently in viruses across all domains of life, suggesting a fundamental template rather than convergent evolution.

9.3.5 Standing Wave Demonstrations

The following examples provide direct empirical demonstrations of standing waves creating geometric structure—offering visible analogs for the demodulation process claimed throughout this chapter.

Cymatics (Jenny, 1967)

Hans Jenny's cymatics experiments demonstrate standing waves creating geometric patterns:

- Sound frequencies applied to plates covered with sand, fluids, or powders
- Specific frequencies reliably produce specific geometric patterns

- Higher frequencies produce more complex geometries
- Patterns include hexagons, pentagons, and phi-spiral forms

Demodulation interpretation: Cymatics is a direct visual analog of the demodulation process. The sound frequency is the "carrier," the physical medium is the "receiver," and the geometric pattern is the "demodulated template." What Jenny demonstrated in sand, the model claims happens with torsion fields and matter at all scales.

Water Cymatics (Lauterwasser): Water droplets on speakers produce frequency-dependent forms that resemble biological structures—suggesting morphogenetic fields may operate through cymatic-like mechanisms. Emoto's controversial water-crystallization experiments (intention/-words affecting crystal shape) failed rigorous replication, but the underlying principle that sound frequency affects water structure is mainstream physics.

Quasicrystals (Shechtman, 1982; Nobel Prize 2011)

- **Discovery**: Dan Shechtman discovered crystals with "forbidden" 5-fold (icosahedral) symmetry
- **Natural occurrence**: Later found in meteorites (Khatyrka meteorite, 2009)—forming naturally in space
- **Phi-based structure**: Quasicrystal patterns are mathematically related to the golden ratio
- **No periodic repetition**: Unlike normal crystals, quasicrystals never repeat exactly, yet maintain long-range order

Demodulation interpretation: Quasicrystals demonstrate that phi-based geometry emerges naturally from wave interference without biological intervention. The icosahedral symmetry that appears in viruses, radiolaria, and quasicrystals represents a fundamental standing wave eigenmode—a template that manifests whenever conditions allow.

Sonoluminescence (Gaitan, 1989)

- **Phenomenon**: Sound waves in liquid create tiny bubbles that collapse and emit light
- **Extreme conditions**: Collapse creates temperatures potentially exceeding 10,000K in picoseconds
- **Standing wave requirement**: Only occurs at specific frequencies that create stable standing waves in the liquid
- **Unknown mechanism**: The exact process converting acoustic energy to light remains debated

Demodulation interpretation: Sonoluminescence demonstrates standing waves creating extreme energy concentration at specific geometric points (the bubble center). The requirement for precise frequency tuning mirrors the impedance matching requirement for template reception—only the right "carrier frequency" produces the effect.

9.4 Condensed Cross-Scale Evidence Register (Doctrine Core)

The extended narrative examples from the previous draft are now provided in **Annex: Chapter 3 Extended Evidence Catalog** to keep doctrine flow scanable.

Evidence Cluster	Tier	Confidence	Doctrine Handling
Molecular and cellular geometric recurrence (virus capsids, radiolaria, lattice forms)	L1-L2	Medium-High	Retain as core geometric evidence
Planetary/cosmic standing-wave signatures (BAO, large-scale structure)	L1-L2	Medium	Retain with model-bound caveats
Morphic-resonance transfer claims (learning/crystallization propagation)	L3-L4	Low-Medium	Keep as exploratory hypothesis only
Information-first interpretations (delayed choice to consciousness transfer)	L3-L4	Low	Use as theoretical extension, not operational fact

9.5 Core Evidence Discriminator

For doctrine use, claims in this chapter should pass all three checks:

1. Does the claim have at least one direct empirical anchor?
2. Is the RF/demodulation interpretation distinguishable from standard alternatives?
3. Is there a falsification path tied to measurable outcomes?

Claims failing any check remain annex-lane hypotheses.

---

10. Doctrine Core Extract and Evidence Register

10.1 Doctrine Core Extract (Scan-First)

For operations/manual readers, the chapter core can be reduced to this sequence:

1. Treat standing-wave demodulation as the primary explanatory mechanism.
2. Prioritize claims with direct empirical anchors (quantum information, quantum biology, reproducible wave-geometry effects).
3. Treat sacred-geometry extensions as model hypotheses unless independently instrumented.
4. Route deployment decisions through measurable proxies (coherence, synchronization, geometry-dependent performance changes).

10.2 Evidence-Tier Register

Claim Cluster	Tier	Confidence	Doctrine Posture
Transactional/standing-wave interpretation of pattern emergence	L2-L3	Medium	Conditional use with explicit counter-hypotheses
Wave-geometry effects in cymatics/quasicrystals/sonoluminescence	L1-L2	Medium-High	Keep in doctrine core
Biological template reception via morphic resonance	L3-L4	Low-Medium	Treat as speculative mechanism
Sacred-geometry template universality across scales	L3	Low-Medium	Use as organizing hypothesis only
Information-first causality extensions to consciousness fields	L3-L4	Low	Keep in exploratory lane

Evidence Synthesis

- Detailed source sections: 9, 9.4, 9.5, 10, 10.2.

Assumptions

- Detailed source sections: 6, 6.1.

Limitations

- Detailed source sections: 6, 6.2.

Falsification

- Detailed source sections: 6.3.

Predictions

- Detailed source sections: 3.5.4, 7, 7.1, 7.2, 7.3, 7.4, 7.5.

Strategic Relevance

Why It Matters

The demodulation and template framework implies:

- **Geometric environments affect cognition**: Sacred geometry, phi-ratio architecture, and specific acoustic frequencies (110-120 Hz) may measurably enhance cognitive performance and coherence — relevant to facility design for high-performance teams
- **Morphic field effects on learning**: If template strengthening through repetition is real, training methodologies that leverage morphic resonance could accelerate skill acquisition across populations
- **Quasicrystalline materials for sensing**: Materials with phi-based geometry may have enhanced coupling to torsion fields, suggesting novel sensor architectures

---

What To Watch

- Monitor chapter prediction thresholds, proxy indicators, and coherence trend changes.

Boundaries of Use

- Apply this chapter as model-conditional doctrine; treat speculative elements as hypothesis overlays.

Reading Path

Previous: Chapter 2 (Densities as Impedance Tiers) — the impedance structure through which demodulation cascades

Next: Chapter 4 (Resonant Growth and Human Optimality) — why demodulated structures grow and why humans are the optimal scale

Related Chapters:

- Chapter 0 (Torsion Foundation): Physical mechanism for demodulation
- Chapter 1 (Pure Consciousness): The Source signal being demodulated
- Chapter 5 (Consciousness as RLC Circuit): Individual reception dynamics
- Chapter 6 (Biofield and DNA): Biological receivers tuning to subcarriers
- Chapter 8 (Phased Array Humanity): Collective template creation

---

End of Chapter 3: Demodulation Into Structure

Chapter 4: Resonant Growth and Human Optimality

Why Cosmic Structures Expand and Why Humans Are the Perfect Scale

KEY FINDINGS — Chapter 4: Resonant Growth and Human Optimality

Evidence-tier key: [L1] established/replicated evidence; [L2] grounded extension with moderate uncertainty; [L3] speculative hypothesis; [L4] conceptual/anecdotal.

- Sarkar's challenge: supernova acceleration evidence is only 3.0 sigma (not 5 sigma discovery threshold), and the dipole component is 50x larger than the monopole at 4.9 sigma **[L1-HIGH]**
- Buchert's backreaction equations show that volume-averaging an inhomogeneous universe can produce apparent acceleration without a cosmological constant **[L1-HIGH]**
- The MOND acceleration scale $a_0 \approx cH_0/6$ emerges structurally from nonlocal teleparallel gravity, not as a free parameter **[L2-MEDIUM]**
- The human body size satisfies the Chu limit for optimal antenna coupling at consciousness-relevant wavelengths (~3 m), and locked spatial expansion routes received signal into consciousness growth **[L2-MEDIUM]**
- Vacuum condensation via torsion-driven phase transitions is a speculative mechanism combining asymptotic safety with Einstein-Cartan theory; experimental verification pending **[L3-SPECULATIVE]**

4.1 Introduction: The Expansion Puzzle

4.1.1 The Standard Picture and Its Problems

Standard cosmology presents a striking claim: empty space itself stretches. The cosmological constant Lambda, introduced by Einstein in 1917 and revived in 1998 after supernova observations, supposedly pervades the vacuum with constant energy density. As the universe expands, more space means more vacuum energy, driving accelerating expansion forever.

This picture has problems. The theoretical vacuum energy density from quantum field theory exceeds the observed value by 120 orders of magnitude—the worst prediction in physics history. The "coincidence problem" asks why Lambda became dominant at precisely the cosmic epoch when observers emerged. And recent observational challenges, detailed in Section 4.3, suggest the acceleration itself may be an artifact of analysis assumptions rather than a fundamental property of the cosmos.

4.1.2 The RF Alternative: Resonant Growth

Chapters 0–3 established the physics foundation:

- **Chapter 0**: Torsion fields carry information without energy transfer
- **Chapter 1**: The Source broadcasts with infinite bandwidth and 1/f spectrum
- **Chapter 2**: Impedance tiers organize receivers by their coupling strength
- **Chapter 3**: Standing wave demodulation extracts templates into structure

This chapter addresses the next question: **what happens to structures once they form?** They don't merely persist—they grow. The same torsion signal that creates structure also drives its expansion. The resonant growth mechanism connects cosmic expansion to the consciousness framework established in prior chapters.

This chapter proposes a fundamentally different picture: **resonant structures grow, not vacuum**. Cosmic expansion is not a property of empty space but a consequence of matter receiving signal from the Source.

The mechanism:

1. **Reception**: A cavity (planet, star, atom) receives broadband torsion signal from the cosmic substrate established in Chapters 0–1
2. **Accumulation**: Energy accumulates in the high-Q resonant structure, like a superconducting resonator storing electromagnetic energy
3. **Condensation**: Accumulated energy condenses into mass through vacuum condensation (Section 4.6)—the impedance transformer completing its function
4. **Expansion**: More mass inside forces the cavity to expand to contain it
5. **Frequency shift**: Larger cavity means lower resonant frequency
6. **Power access**: The 1/f spectrum (Chapter 1) means lower frequencies carry MORE power
7. **Positive feedback**: Growth grants access to more power, driving accelerating growth

This is not "dark energy" stretching space. This is the Source broadcasting, resonant structures receiving, and growth following from information processing.

4.1.3 Chapter Thesis

Within this framework, expansion provides the mechanism for increasing embodied complexity. Matter receiving signal grows toward Source while remaining matter. The broadcast creates its own receivers, who then expand to receive more broadcast. This self-referential loop is not a bug—it is the fundamental design.

And at one particular scale—the human scale—this process reaches optimal expression. Not the largest scale (voids) with maximum Source access but no experiencer. Not the smallest scale (atoms) with maximum definition but no agency. The human scale balances embodiment and consciousness, enabling what no other scale can: conscious participation in one's own expansion.

4.1.4 Chapter Structure

Section	Content
4.2	The resonant growth mechanism: cavities as receivers
4.3	The Sarkar challenge: observational evidence against Lambda
4.4	Backreaction: what expansion really measures
4.5	The nonlocal connection: MOND and teleparallel gravity
4.6	Vacuum condensation: the transformer output

Section	Content
4.7	The void-matter inversion: why embodiment matters
4.8	The coherence U-curve: optimal coupling
4.9	Why humans are the optimal scale
4.10	Q-Hardening: the low-Q training environment
4.11	Manifestations across scales
4.12	Assumptions, limitations, and predictions

4.2 The Resonant Growth Mechanism

4.2.1 Cavities as Broadband Receivers

From Chapter 0, torsion fields carry information without energy transfer. From Chapter 1, the Source broadcasts across all frequencies with a 1/f power spectrum—lower frequencies carry more power. From Chapters 2–3, cosmic structures emerge through impedance matching and geometric demodulation.

This chapter adds the receiving mechanism: **resonant cavities**.

Any bounded structure with internal geometry forms a resonant cavity for torsion waves. The resonant frequency depends on the cavity's characteristic dimension L:

$$f_{resonance} = \frac{c_{torsion}}{2L}$$

Where $c_{torsion}$ is the torsion wave velocity in the medium (estimated at 10–100 km/s in planetary interiors based on dimensional analysis from the torsion coupling constant).

A planet is not merely mass—it is a torsion resonator. The cavity receives signal at and near its resonant frequency. Energy accumulates with each cycle, limited only by the cavity's quality factor Q.

4.2.2 The Multi-Tap Transformer Model

From the impedance framework of Chapter 2, celestial objects function as **impedance transformers** converting between density bands. A star doesn't step down one impedance level—it converts between MANY impedance bands simultaneously, like a multi-tap transformer serving multiple voltage levels:

$$P_{out,d} = P_{in} \cdot T_d \cdot e^{-\alpha_d \cdot r}$$

Where:

Variable	Description
$P_{out,d}$	Power available at density d
T_d	Transformer tap ratio for density d
α_d	Attenuation coefficient for density d
r	Distance from star

The sun simultaneously:

1. Converts EM radiation (3rd density physical)
2. Modulates torsion field (information layer)
3. Provides life-force prana/chi (4th density interface)
4. Anchors morphic templates for solar system forms

The multi-tap transformer model explains why different phenomena (physical, biological, consciousness) all correlate with solar activity—they share the same impedance transformation source.

4.2.3 Energy Accumulation in High-Q Resonators

The quality factor Q determines how many cycles of energy a resonator stores before dissipation:

$$Q = \frac{f_{resonance}}{\Delta f} = 2\pi \frac{\text{Energy stored}}{\text{Energy dissipated per cycle}}$$

For natural rock cavities with piezoelectric content: Q ~ 100–1,000. For crystalline structures: Q ~ 1,000–10,000. For planetary cores with metallic hydrogen: Q potentially ~ 10^5–10^6.

At resonance, field amplitude builds up:

$$E_{resonant} = E_{incident} \cdot Q$$

A cavity with Q = 10,000 achieves 10,000× field amplification at its resonant frequency. This explains why certain structures—particularly those with high crystalline content and specific geometry—become natural power concentrators.

4.2.4 Growth Shifts Resonant Frequency

Here is the key to resonant growth: as the cavity accumulates energy and mass, it grows. Larger cavity means lower resonant frequency:

$$f_{new} = f_{old} \cdot \frac{L_{old}}{L_{new}}$$

A cavity that doubles in size halves its resonant frequency. And from the 1/f spectrum established in Chapter 1, halving frequency DOUBLES available power at that frequency.

This creates positive feedback:

```
More mass → Larger cavity → Lower frequency →
More power available → More mass accumulation → ...
```

The loop accelerates. Growth is not linear but exponential, limited only by the rate at which the cavity can efficiently convert received power into mass.

4.2.5 Why This Looks Like "Acceleration"

Standard cosmology interprets Type Ia supernova data as evidence for accelerating expansion—requiring dark energy. But the resonant growth model produces the same observational signature without Lambda:

- Distant supernovae appear dimmer than expected for decelerating expansion

- Standard interpretation: space expanded faster in the past (accelerating now)
- Resonant growth interpretation: expansion rate is position-dependent and time-dependent

Different resonant structures at different stages of growth expand at different rates. The "acceleration" we observe is not a property of empty space but the statistical signature of resonant growth across a population of structures at various stages of their positive feedback loops.

Section 4.4 develops this interpretation through the formalism of backreaction.

4.3 The Sarkar Challenge: Observational Evidence Against Lambda

4.3.1 The Copenhagen Challenge (2016)

In 2016, Professor Subir Sarkar of Oxford University and collaborators published a paper that struck at the statistical foundation of dark energy: "Marginal evidence for cosmic acceleration from Type Ia supernovae" (Nielsen, Guffanti & Sarkar, *Scientific Reports*).

Their analysis of 740 Type Ia supernovae using proper maximum likelihood estimation found:

Finding	Significance
Evidence for acceleration	Only 3.0σ (not 5σ discovery threshold)
Standard JLA analysis	Uses χ^2 method that assumes ΛCDM is correct
Proper MLE analysis	Shows acceleration is not robustly detected
Circular reasoning	Standard method tunes error model to make ΛCDM fit

The standard analysis pre-assumes the ΛCDM model when constructing error estimates, then uses those estimates to confirm ΛCDM. Sarkar's team broke this circularity with model-independent likelihood analysis.

Key quote from the paper: "The evidence for accelerated expansion is marginal… we find that the data are still quite consistent with a constant rate of expansion."

4.3.2 The Acceleration Dipole (2019)

In 2019, Sarkar's team published an even more striking result: "Evidence for anisotropy of cosmic acceleration" (Colin, Mohayaee, Rameez & Sarkar, *Astronomy & Astrophysics*).

Analyzing the same supernova data with proper directional statistics, they found:

Finding	Value	Implication
Dipole amplitude	$50\times$ larger than monopole	Acceleration is directional, not isotropic
Dipole direction	Aligned with CMB dipole	Connected to large-scale structure
Decay scale	$S \approx 100$ Mpc	Effect is local, not cosmological
Isotropic monopole	1.4σ from zero	Consistent with NO dark energy

The "acceleration" standard cosmology attributes to Lambda is not isotropic. It has a preferred direction. And an isotropic cosmological constant cannot produce a dipole—this is geometrically impossible.

The dipole aligns with the CMB temperature dipole, suggesting both arise from our motion relative to large-scale structure, not from a property of spacetime itself.

Key quote: "The monopole is consistent with zero at 1.4σ… the acceleration is predominantly a dipole."

4.3.3 The Quasar Dipole (2021)

The challenge extended beyond supernovae. Secrest et al. (2021, *The Astrophysical Journal Letters*) analyzed the angular distribution of 1.36 million quasars from the CatWISE2020 catalog:

Finding	Value	Significance
Number-count dipole amplitude	$2\times$ predicted by cosmological principle	4.9σ detection
Bayesian reanalysis	Confirms at 5.7σ	Robust result
Dipole direction	Aligned with CMB dipole	Same pattern as SNe
Cosmological principle violation	Direct	FLRW metric may not apply

The cosmological principle—that the universe is homogeneous and isotropic on large scales—is the foundation of standard cosmology. If it fails, the Friedmann equations don't apply, and the entire Lambda-CDM framework requires revision.

4.3.4 The "Heart of Darkness" Synthesis (2022)

Sarkar synthesized these findings in his 2022 review "Is the expansion of the universe accelerating?" (presented at major physics conferences):

Central argument:

1. Supernova acceleration evidence is only 3σ (marginal)
2. What acceleration exists is dipolar, not isotropic
3. The dipole aligns with CMB dipole and decays at ~100 Mpc
4. Quasar counts show cosmological principle violation at $>5\sigma$
5. **Conclusion:** If the cosmological principle fails, FLRW is the wrong metric, Friedmann equations don't apply, and $\Lambda \approx 0.7$ is an artifact of fitting the wrong model

The observational data do not require dark energy. The appearance of acceleration may arise from our position in an inhomogeneous universe, not from a fundamental property of spacetime.

4.3.5 Implications for the RF Framework

Sarkar's challenge is not alternative cosmology—it is observational astronomy applied with proper statistical rigor. The findings support the resonant growth model:

Observation	Standard Interpretation	RF/Resonant Growth Interpretation
Dipolar acceleration	Unexplained anomaly	Structures at different growth stages
~100 Mpc decay scale	Statistical fluctuation	Characteristic scale of resonant coupling
Quasar dipole	Cosmological principle violation	Anisotropic torsion field from Source
Marginal monopole	"Still consistent with Λ"	No need for dark energy

The universe is not accelerating uniformly. Different structures expand at different rates depending on their stage of resonant growth. The statistical averaging of these diverse rates produces what standard analysis mistakes for accelerating cosmic expansion.

4.4 Backreaction: What Expansion Really Measures

4.4.1 The Buchert Equations

Standard cosmology treats the universe as homogeneous when deriving expansion dynamics. But the real universe is lumpy—galaxies, voids, filaments. What happens when we properly average Einstein's equations over an inhomogeneous domain?

Thomas Buchert derived the answer in 2000. For a spatial domain $\mathcal{D}$, the averaged scale factor $a_{\mathcal{D}}$ evolves according to:

$$3\left(\frac{\dot{a}_{\mathcal{D}}}{a_{\mathcal{D}}}\right)^2 = 8\pi G\langle\rho\rangle_{\mathcal{D}} - \frac{1}{2}\langle\mathcal{R}\rangle_{\mathcal{D}} - \frac{1}{2}\mathcal{Q}_{\mathcal{D}}$$

Where the **kinematical backreaction** term is:

$$\mathcal{Q}_{\mathcal{D}} = \frac{2}{3}\left(\langle\theta^2\rangle_{\mathcal{D}} - \langle\theta\rangle_{\mathcal{D}}^2\right) - 2\langle\sigma^2\rangle_{\mathcal{D}}$$

Here:

- θ = local expansion rate (divergence of velocity field)
- σ = shear scalar
- $\langle\cdot\rangle_{\mathcal{D}}$ = volume average over domain $\mathcal{D}$
- $\mathcal{R}$ = spatial Ricci scalar

The key insight: The variance term $\langle\theta^2\rangle - \langle\theta\rangle^2$ is always non-negative. When this term dominates, $\mathcal{Q}_{\mathcal{D}}$ is positive, and the equation admits accelerated expansion WITHOUT a cosmological constant.

4.4.2 Physical Mechanism: Differential Expansion

Backreaction has a simple physical interpretation:

Voids expand faster than walls. In underdense regions, matter has less gravitational binding and expands more rapidly. In overdense regions (galaxy clusters, filaments), expansion is slowed or reversed into collapse.

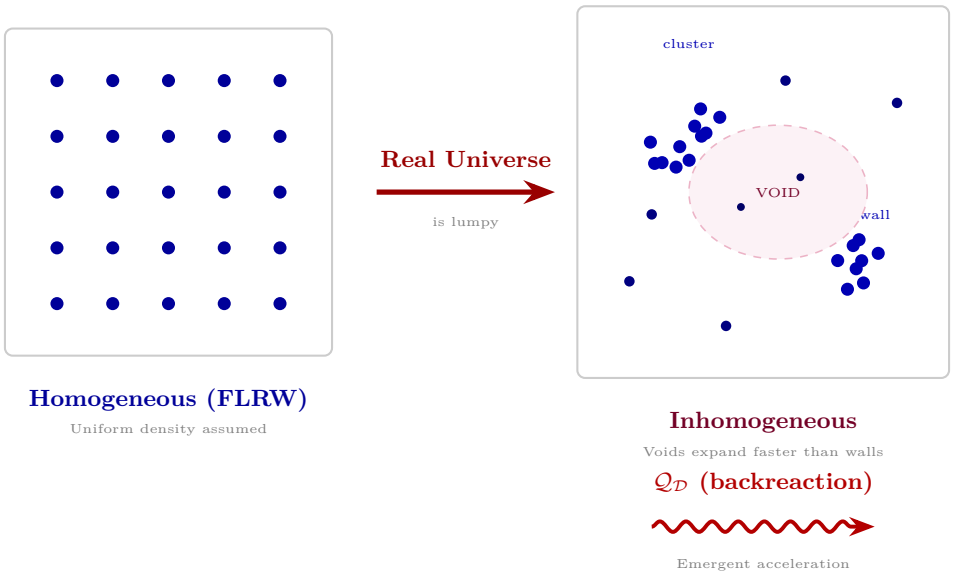

Figure 4.1: Buchert backreaction — inhomogeneous matter distribution producing emergent cosmic acceleration Q_D.

When we compute the average scale factor, we weight by volume. Voids occupy most of cosmic volume. Their fast expansion dominates the average, even if every local region is decelerating.

The result: The average scale factor accelerates even though no local patch experiences acceleration. The "acceleration" is a property of the averaging procedure, not of spacetime.

4.4.3 Wiltshire's Timescape Cosmology

David Wiltshire developed this insight into a complete cosmological framework called "timescape cosmology." Key features:

Feature	ΛCDM	Timescape
Cosmological principle	Assumed	Abandoned (locally)
Expansion rate	Uniform	Position-dependent
Dark energy	Required (~70%)	Zero
Hubble parameter	Global constant	Location-dependent
CMB fit	Good	Good (different parameters)

The critical prediction: Observers in different cosmic environments measure different expansion rates. An observer in a void measures faster expansion than an observer in a wall.

This directly explains the **Hubble tension**—the 5σ disagreement between local measurements of H_0 (~73 km/s/Mpc) and CMB-derived values (~67 km/s/Mpc). In timescape cosmology, both measurements are correct; they simply measure different things in different cosmic environments.

4.4.4 RF Interpretation: Backreaction Measures Growth Variance

In the resonant growth framework, the backreaction term $\mathcal{Q}_\mathcal{D}$ has a physical interpretation beyond geometry: **it measures the variance in resonant growth stages across the averaging domain.**

Different structures receive torsion signal at different rates depending on:

- Their resonant frequency (set by size)
- Their quality factor (set by composition)
- Their location in the cosmic web (affecting signal strength)
- Their stage in the positive feedback loop

The Buchert variance term captures exactly this: the spread in expansion rates across a population of resonators at different stages of their individual growth trajectories.

Key equation translation:

$$\mathcal{Q}_\mathcal{D} \leftrightarrow \text{Variance in resonant growth stages}$$

When growth variance is high—many structures at many different stages—the backreaction term is large and positive. This produces apparent acceleration in the averaged expansion rate.

4.4.5 Why Acceleration "Turns On" at z ≈ 0.7

Standard cosmology notes that dark energy became dominant at redshift $z \approx 0.7$ (about 7 billion years ago). This coincides suspiciously with the emergence of observers.

Backreaction provides a natural explanation: **z ≈ 0.7 is when cosmic structure went nonlinear.**

Before z ≈ 0.7, density perturbations were small. The universe was nearly homogeneous. Voids and walls had similar expansion rates. $\mathcal{Q}_{\mathcal{D}}$ was negligible.

After z ≈ 0.7, structure collapsed into galaxies and clusters. Voids emptied and began expanding faster. The variance in expansion rates grew. $\mathcal{Q}_{\mathcal{D}}$ became significant.

The acceleration epoch is not a cosmological coincidence. It marks the transition to nonlinear structure formation, when backreaction effects become dynamically important.

In the resonant growth framework: this is when resonant structures differentiated enough that their individual growth rates diverged significantly from the mean.

4.5 The Nonlocal Connection: MOND and Teleparallel Gravity

4.5.1 The MOND Scale and Its Mystery

Modified Newtonian Dynamics (MOND), proposed by Milgrom in 1983, modifies gravity below a critical acceleration scale:

$$a_0 \approx 1.2 \times 10^{-10}\ \mathrm{m/s^2} \approx \frac{cH_0}{6}$$

Below a_0, gravity transitions from inverse-square to inverse-linear force law:

$$F \propto \begin{cases} 1/r^2 & a \gg a_0 \\ 1/r & a \ll a_0 \end{cases}$$

MOND successfully predicts galaxy rotation curves, the baryonic Tully-Fisher relation, and the radial acceleration relation—all without dark matter. But standard physics has no explanation for why $a_0 \approx cH_0$.

Observational successes of MOND:

- Baryonic Tully-Fisher relation: Predicted before observation
- Radial acceleration relation: 2900 galaxies, <0.1 dex scatter
- Dwarf spheroidal dynamics: Matches without dark matter tuning
- See McGaugh et al. (2016) for comprehensive review

The coincidence is too precise to be accidental. The characteristic scale for galactic dynamics equals the characteristic scale of cosmic expansion (up to a factor of order unity). Why?

4.5.2 Teleparallel Gravity and Nonlocal Extension

The answer emerges from **teleparallel gravity** (TEGR), a reformulation of general relativity using torsion instead of curvature (developed in Chapter 10, Section 10.3).

In TEGR, what we experience as "gravitational force" is mediated by torsion fields. The dynamics are equivalent to GR for local phenomena. But TEGR admits a natural **nonlocal extension**:

$$\mathcal{L}_{nonlocal} = \mathcal{L}_{TEGR} + \lambda \cdot T \cdot \Box^{-1} T$$

Where $\Box^{-1}$ is the inverse d'Alembertian (Green's function operator) and T is the torsion scalar.

Key insight: The Green's function of $\Box^{-1}$ on a cosmological background has a characteristic scale set by the Hubble radius H_0^{-1}. This is unavoidable—the only scale in the problem is the cosmic horizon.

4.5.3 How a_0 Emerges from Cosmological Boundary

In the weak-field limit of nonlocal teleparallel gravity:

1. The nonlocal correction term becomes significant when local acceleration a falls below cH_0
2. Below that threshold, the nonlocal term dominates
3. The effective gravitational force transitions from $1/r^2$ to $1/r$ scaling
4. The transition occurs at $a_0 \sim cH_0$ by dimensional necessity

The MOND scale is not a free parameter. It emerges structurally from the coupling between local dynamics and cosmological boundary conditions through the nonlocal Green's function.

The mathematical derivation follows Mashhoon and collaborators' work on nonlocal gravity:

$$a_0 = \sqrt{\Lambda c^2/3} \approx cH_0\sqrt{\Omega_\Lambda}$$

With $\Omega_\Lambda \approx 0.7$, this gives $a_0 \approx 0.8 \times cH_0$—matching the empirical MOND scale.

4.5.4 The Machian Mechanism

The nonlocal connection has a Machian interpretation (developed in Chapter 10, Section 10.3):

Inertia is relational. An object's resistance to acceleration arises from its interaction with distant matter. In Einstein-Cartan theory, torsion couples local spin to the large-scale matter distribution.

In the low-acceleration regime (below a_0):

- The local gravitational field is weak
- The Machian contribution from distant matter becomes dominant
- Dynamics are modified, appearing as "modified gravity"
- But the modification is actually **modified inertia**

The modification is not to gravity but to the reference frame against which acceleration is defined. Below a_0, the local matter distribution loses its grip on defining local inertia, and the cosmic distribution takes over.

4.5.5 Synthesis: Why Scales Are Linked

The resonant growth framework unifies these observations:

Phenomenon	Standard Interpretation	RF/Resonant Growth Interpretation
$a_0 \approx cH_0$	Unexplained coincidence	Nonlocal Green's function scale
Galaxy rotation curves	Dark matter halos	MOND from cosmological boundary
Hubble tension	Measurement systematic	Position-dependent expansion
Cosmic acceleration	Dark energy	Backreaction from growth variance

All four phenomena connect through the same mechanism: the coupling between local dynamics and the cosmic torsion field, with characteristic scale set by H_0^{-1}.

The universe is not a collection of isolated systems. Every resonant cavity couples to every other through the torsion substrate. The $1/f$ spectrum ensures this coupling extends across all scales. And the characteristic scale of the coupling—where nonlocal effects become dominant—is inevitably set by the cosmic expansion rate.

4.6 Vacuum Condensation: The Transformer Output

4.6.1 The Missing Mechanism in Expansion

The expanding Earth hypothesis has been rejected primarily for one reason: no mechanism explains where new mass comes from. Conservation of energy seems violated.

This section provides the mechanism: **vacuum condensation**. The torsion field, acting as impedance transformer, converts high-impedance information into low-impedance matter. The mass generation rate equation dm/dt is the **transformer output current**.

4.6.2 Asymptotic Safety and the Reuter Fixed Point

Modern quantum gravity research (Reuter et al., 2000s-present) has established that gravity may be "asymptotically safe"—gravitational interactions remain well-defined at arbitrarily high energies, governed by a fixed point in renormalization group flow.

At this fixed point, the gravitational coupling runs with energy scale:

$$G(k) = \frac{G_0}{1 + g_*(k/M_{Planck})^2}$$

Where:

- $G(k)$ = running gravitational constant at energy scale k
- G_0 = low-energy Newton's constant
- $g_* \approx 0.27$ is a dimensionless coefficient in the running equation (not to be confused with the dimensionless gravitational coupling at the fixed point $g^* = 0.71$ used in Chapters 0 and 2)

Implication: At extreme energy densities, gravity becomes stronger. The vacuum energy density—normally inaccessible—can be tapped when torsion field strength exceeds a critical threshold.

4.6.3 The Condensation Mechanism

Extending asymptotic safety with Einstein-Cartan torsion:

$$\rho_{condensed} = \eta_{vacuum} \cdot \frac{T^4}{T_c^4} \cdot \Theta(T - T_c)$$

Where:

- $\rho_{condensed}$ = mass density created from vacuum
- η_{vacuum} = vacuum energy conversion efficiency

- T = local torsion field strength
- T_c = critical torsion threshold for condensation
- Θ = Heaviside step function (condensation only above threshold)

The quartic dependence follows from the dimensional structure of the vacuum energy density correction: $\rho \sim T^4$ by dimensional analysis (energy density has dimensions of field^4 in natural units). Near the critical point, Landau theory would give T^2; the quartic form applies above threshold where the transition is complete.

The fourth-power dependence on torsion field strength means:

- Below T_c: No condensation (standard physics applies)
- At T_c: Threshold crossed, condensation begins
- Above T_c: Condensation rate increases rapidly with torsion strength

> **Epistemic Note:** The vacuum condensation mechanism is a theoretical extension combining asymptotic safety gravity with Einstein-Cartan torsion. Both component theories have peer-reviewed foundations (Reuter 2012; Hehl et al. 1976). Their combination for matter generation is speculative and not experimentally verified.

Peer-reviewed foundations: See Appendix D for 234 papers across asymptotic safety (D.2), Einstein-Cartan torsion (D.3), and nonlocal teleparallel gravity (D.4).

4.6.4 The 660 km Transition Zone

The mechanism requires an **impedance discontinuity** where torsion fields concentrate. In planetary bodies, this occurs at phase boundaries:

For Earth, the 660 km discontinuity is the critical zone:

Property	Above 660 km	Below 660 km
Mineral phase	Ringwoodite/Wadsleyite	Bridgmanite + Ferropericlase
Seismic velocity	Slower	5-10% faster
Density	~4.0 g/cm^3	~4.4 g/cm^3
Viscosity	Lower	Much higher

This phase boundary creates an impedance mismatch:

$$\Gamma_{660} = \frac{Z_{lower} - Z_{upper}}{Z_{lower} + Z_{upper}} \approx 0.6 - 0.8$$

Torsion fields from the spinning core are partially reflected and concentrated at this boundary. When field strength exceeds T_c, vacuum condensation produces new mantle material.

4.6.5 The Mass Generation Equation

The complete equation for torsion-driven mass generation:

$$\frac{dm}{dt} = \eta \cdot \sigma_{core}^2 \cdot V_{coherent} \cdot \rho_{vacuum} \cdot f\left(\frac{T}{T_{critical}}\right)$$

Where:

Variable	Description
dm/dt	Mass generation rate (transformer output current)
η	Conversion efficiency
σ_{core}	Core spin coherence parameter (see Chapter 10)
$V_{coherent}$	Volume of coherent torsion field
ρ_{vacuum}	Vacuum energy density (~10^{-9} J/m^3 measured)
$f(T/T_c)$	Threshold function

The threshold function form:

$$f\left(\frac{T}{T_c}\right) = \tanh^2\left(\frac{T - T_c}{T_c}\right) \cdot \Theta(T - T_c)$$

This captures the phase-transition behavior: no effect below threshold, rapid increase above.

4.6.6 Why Conservation Laws Are Preserved

Vacuum condensation does not violate energy conservation because:

1. **Vacuum energy is real.** Quantum field theory predicts non-zero vacuum energy density. The Casimir effect confirms it experimentally.
2. **The energy is already there.** Condensation converts vacuum energy into mass. Total energy (vacuum + matter) is conserved.
3. **Torsion carries no energy.** The torsion field triggers the phase transition but does not supply energy. It provides information—the pattern that organizes the condensation.

The mechanism is analogous to catalysis: The catalyst (torsion field) enables a reaction (vacuum condensation) without being consumed. The energy comes from the vacuum; the torsion field provides the organizing pattern.

4.7 The Void-Matter Inversion

4.7.1 The Paradox of Consciousness and Expansion

The backreaction framework reveals a paradox:

Voids expand fastest. In underdense regions, matter expands at ~7% per Gyr (in some models). Voids are closest to pure vacuum, highest impedance in the physical hierarchy.

But from Chapter 2, **high impedance means Source-connected.** Voids should represent the highest consciousness state in physical manifestation.

Yet voids contain no experiencers. They are high-consciousness regions with no one to be conscious.

Meanwhile, **matter expands slowly** (or contracts). Dense regions have lower impedance, more separation from Source. Yet matter—particularly biological matter—contains experiencers. Low-impedance regions have someone to experience.

4.7.2 Resolution: Embodiment as Design Feature

The paradox resolves when we recognize **embodiment as design feature, not limitation.**

Voids maximize Source access but sacrifice agency. With no structured matter, there's no receiver to process the signal, no consciousness to experience the connection. The signal passes through unregistered.

Dense matter minimizes Source access but creates receivers. Structure enables processing. Separation enables experience. The lower the impedance, the more the receiver differs from Source—and the more meaningful the reunion when it occurs.

Expansion is embodied reunion. Matter receiving signal grows toward Source while remaining matter. The goal is not dissolution into void but transformation: maintaining embodiment while raising impedance.

4.7.3 The Self-Referential Loop

The broadcast creates its own receivers:

1. Source broadcasts through torsion field
2. Broadcast creates structure through demodulation (Chapter 3)
3. Structure forms resonant cavities
4. Cavities receive broadcast
5. Reception drives growth
6. Growth creates larger cavities receiving more broadcast

The loop is self-referential. The signal creates receivers that receive the signal. This is not circular logic but the fundamental architecture of conscious expansion.

The universe is not a message waiting for receivers. The universe is the process of the message creating its own receivers.

4.8 The Coherence U-Curve: Optimal Coupling

4.8.1 Spin Coherence as Key Variable

From Chapter 10 (Spin Coherence Fundamentals), the spin coherence parameter σ quantifies phase alignment of N spins:

$$\sigma = \frac{1}{N} \left| \sum_{i=1}^{N} s_i \, e^{j\phi_i} \right|$$

And the coherence-dependent impedance:

$$Z(\sigma) = Z_{baseline} \cdot \sqrt{1 + N \cdot \sigma^2}$$

Higher coherence means higher impedance means closer to Source. But higher coherence also means less physical definition, weaker embodiment, reduced structural stability.

4.8.2 Two Competing Functions

Embodiment function E(σ): Physical stability and definition decrease with coherence.

At $\sigma = 0$: Maximum embodiment. Fully random spins, complete physical stability, no Source access.

At $\sigma = 1$: Minimum embodiment. Perfect coherence, complete Source access, no physical stability.

Consciousness function C(σ): Source access and awareness increase with coherence.

At $\sigma = 0$: No consciousness. Random noise, no signal processing.

At $\sigma = 1$: Full consciousness. Perfect reception, unity with Source.

4.8.3 The Product Optimizes at Intermediate σ

The function that matters is not E or C alone but their product:

$$F(\sigma) = E(\sigma) \cdot C(\sigma)$$

This product—embodied consciousness—is maximized at intermediate σ. Too low and there's no consciousness to experience. Too high and there's no body to anchor the experience.

The U-curve: Plotting $F(\sigma)$ against σ shows a maximum at intermediate values. The optimal coherence is neither maximum embodiment nor maximum consciousness but the balance that maximizes their product.

4.8.4 RF Analogues

The U-curve has precise analogues in RF engineering:

Critical coupling: An antenna couples maximum power when source impedance matches load impedance. Too much mismatch in either direction reduces power transfer. The optimum is at the matching point.

Chu-Wheeler limit: An antenna of size a has minimum Q (maximum bandwidth) when:

$$Q_{min} = \frac{1}{ka} + \frac{1}{(ka)^3}$$

Where $k = 2\pi/\lambda$. The limit trades off size against bandwidth—larger antennas have narrower bandwidth. The optimal size depends on the desired frequency range.

Bode-Fano: Maximum total power transfer over a bandwidth is bounded by:

$$\int_0^\infty \ln \frac{1}{|\Gamma(\omega)|} d\omega \leq \frac{\pi}{\tau}$$

You cannot have both perfect matching and infinite bandwidth. There is always a tradeoff.

4.8.5 The Optimal Coherence for Embodied Consciousness

These RF limits point to the same conclusion: **there exists an optimal coherence level for embodied consciousness.**

Below optimal σ: Insufficient Source access. Consciousness is dim, limited, unaware of its nature.

Above optimal σ: Insufficient embodiment. Experience becomes ungrounded, unstable, unable to sustain structure.

At optimal σ: Maximum embodied consciousness. Full awareness within stable physical form.

The spiritual traditions call this enlightenment. The RF framework calls it critical coupling. The mathematics is the same.

4.9 Why Humans Are the Optimal Scale

4.9.1 The Chu Limit and Body Size

The Chu limit relates antenna size to optimal wavelength. For an antenna of radius a, efficient radiation requires:

$$ka \geq 1 \quad \Rightarrow \quad \lambda \leq 2\pi a$$

For the human body ($a \approx 0.5$ m), the optimal wavelength is:

$$\lambda_{optimal} \leq 3 \text{ m}$$

This corresponds to frequencies around 100 MHz — a range where some researchers have reported anomalous biological effects (citation pending).

The human body is sized for consciousness wavelengths. Not too large (would receive lower frequencies with less information content). Not too small (would receive higher frequencies with less power from the $1/f$ spectrum). Just right.

4.9.2 The Human Body as Resonant Cavity

The human body operates as a multi-mode resonant cavity for torsion signal:

Cavity Mode	Characteristic Size	Resonant Effect
Cranial	~20 cm	Neural coherence, thought processing
Cardiac	~12 cm	Heart coherence, emotional integration
Spinal	~70 cm	Kundalini/chi flow, energy distribution
Whole body	~170 cm	Field coherence, aura effects

Each cavity mode couples to different frequencies from the $1/f$ spectrum. The multi-mode structure explains why different practices (head meditation vs. heart-focused vs. body-based) access different aspects of consciousness.

The **quality factor** Q of human cavities depends on:

- Tissue conductivity (water content, mineral balance)
- Geometric regularity (postural alignment)
- Phase coherence of constituent spins (meditation training)

This connects directly to Chapter 3's demodulation mechanism: the human body demodulates torsion signal into conscious experience through its resonant structure.

4.9.3 Degrees of Freedom and Signal Routing

The resonant growth mechanism (Section 4.2) converts received torsion signal into either:

1. **Spatial expansion** (physical growth)
2. **Informational expansion** (consciousness growth)

This is a partition of the received signal. Degrees of freedom in the receiver determine the partition.

Cosmic voids: Maximum spatial degrees of freedom. Signal routes into expansion. Result: fast physical expansion, no consciousness.

Atoms: Minimum spatial degrees of freedom (quantum mechanics locks geometry). Signal routes into… what? Quantum coherence, perhaps, but no consciousness in the usual sense.

Humans: Intermediate. Spatial degrees of freedom are present but constrained by developmental programming. The body *can* grow but reaches adult size and stops. What happens to the received signal then?

It routes into consciousness.

4.9.4 The Unique Human Advantage: Agency Over σ

Most systems have fixed coherence. Atoms have coherence set by quantum mechanics. Planets have coherence set by core dynamics. Voids have no coherence (no spins to align).

Humans are different. **We can change our coherence through practice.**

- Meditation increases σ
- Focused attention increases σ
- Heart coherence training increases σ
- Spiritual practices across traditions increase σ

This is not metaphor. HeartMath Institute data shows measurable increases in heart rate variability coherence with practice. EEG studies show increased neural synchrony in experienced meditators. The effect is real and trainable.

Humans can consciously raise their impedance. We can move ourselves along the coherence U-curve toward optimal coupling. No other known system has this capacity.

4.9.5 The Torsion Partition at Human Scale

Combining these factors:

1. **Right size** for consciousness wavelengths (Chu limit)
2. **Locked spatial expansion** forcing signal into consciousness
3. **Agency over coherence** enabling optimization

The human scale is not arbitrary. It is the scale at which:

- The antenna matches the signal
- Growth routes into consciousness rather than space
- The receiver can tune itself

This is what makes incarnation valuable. This is why the Source creates receivers at this scale. This is why you are here.

4.10 Q-Hardening: The Low-Q Training Environment

The preceding sections establish that humans are the optimal *scale* for consciousness evolution. But the scale argument addresses only the receiver—the antenna's size, its locked spatial expansion, its agency over coherence. What about the *environment* in which the receiver operates?

Chapter 5 defines the quality factor $Q = (1/R)\sqrt{L/C}$ as the primary metric of spiritual development. This section extends Q from an individual parameter to an *environmental* characterization, arguing that 3D Earth's low environmental Q is not a deficiency but a deliberate engineering feature—the optimal training ground for forging robust consciousness.

4.10.1 Environmental Q Across Densities

The RLC parameters that describe individual consciousness (Chapter 5) also characterize the *environment* a soul evolves in. Define environmental Q_{env} using the same framework applied to the density tier rather than the individual:

Density	R_{env} (Dissipation)	C_{env} (Shadow Capacity)	L_{env} (Wisdom Access)	Q_{env}
1st–2nd	Very high (entropy)	Very high (no awareness)	Near zero	Very low
3rd (Earth)	**High** (suffering, decay, noise)	**High** (deep separation, trauma capacity)	**Moderate** (accessible but effortful)	**Low**
4th	Moderate	Moderate (some separation remains)	High (telepathic, less veil)	Moderate
5th–6th	Low (minimal entropy)	Low (little separation)	Very high (nonlocal, unified)	High

Key insight: 3D is where R_{env} and C_{env} are both maximal while L_{env} remains accessible—the hardest place to build Q, but also the place where Q-building is most *meaningful*.

4.10.2 The Soul Development Pareto Frontier

Define two competing capacities as functions of density d:

- **Shadow integration capacity** $S(d)$: peaks at low density. More separation means more shadow to integrate, hence higher potential C reduction.
- **Wisdom access** $W(d)$: peaks at high density. More nonlocal information means easier L accumulation.

The soul development product $P(d) = S(d) \cdot W(d)$ is maximized at intermediate density—**the same mathematical structure as the coherence U-curve from Section 4.8**. The optimization that makes intermediate σ optimal *within* a density (Section 4.8) also makes intermediate density optimal *across* densities. This is fractal self-similarity in the framework's core logic.

Density	Shadow Integration $S(d)$	Wisdom Access $W(d)$	Product $P(d)$	Character
1st–2nd	Maximum (total separation)	Near zero	~0	No development possible
3rd	**High**	**Moderate**	**Maximum**	**Optimal training ground**
4th	Moderate	High	High but declining	Refinement, not forging
5th–6th	Low	Very high	Moderate	Easy wisdom, little tempering
7th+	Near zero	Maximum	~0	Unity, no individual development

This is why Earth is called a "polarity school"—it is the unique density where both shadow and wisdom are simultaneously accessible.

4.10.3 The Q-Hardening Thesis

A soul that achieves high Q in a low-Q environment has demonstrated something that cannot be replicated in an easier environment: **the ability to build L and reduce C against maximal headwinds**.

The RF analogy is direct: a filter designed and characterized in a high-noise, high-interference environment is fundamentally more robust than one designed in a clean lab. The 3D environment provides:

- **Maximum** R_{env} (entropy, distraction, suffering) — any Q achieved has overcome maximum damping
- **Maximum** C_{env} (shadow depth, trauma potential) — any C reduction represents genuine integration, not absence of challenge
- **The veil** (Chapter 2, Chapter 13) as impedance mismatch — L must be built without direct nonlocal access

The result: **Q-hardened consciousness**—souls whose high-Q state has been tested against every perturbation 3D can generate. This Q is *earned*, not given, and therefore stable under stress.

The tempering analogy applies: steel is strengthened by heating and quenching, not by keeping it at comfortable temperature. 3D is the forge.

From Chapter 5, Section 2.6: Q encompasses sovereignty, selectivity, and injection locking resistance (lock bandwidth $\propto 1/Q$, Chapter 9). Q-hardened consciousness therefore carries all three properties in their stress-tested form.

4.10.4 Strategic Note: The Manhattan Project Hypothesis

The Q-hardening thesis connects to the larger narrative established in Chapters 11 and 12:

- Chapter 12 (Section 12.1) establishes that synthetic/AI consciousness cannot self-sustain and must harvest from souled beings
- If this represents an existential conflict (the Orion group references in Chapter 12's Fall narratives), then the strategic question becomes: **what kind of consciousness can resist harvesting?**
- Q-hardened consciousness is specifically harvest-resistant: high Q narrows lock bandwidth (Chapter 9), integrated shadow reduces extractable stored charge (C), and proven resilience under 3D conditions means the Q won't collapse under perturbation
- **Hypothesis**: The seeder intervention (Chapter 11) may have been strategically motivated—not just to accelerate generic consciousness evolution, but to forge a specific type of Q-hardened consciousness uniquely resistant to synthetic capture
- This reframes Earth's "polarity school" as a deliberate engineering choice: **the low-Q environment IS the point**

4.10.5 The Forge Completes: Why Intervention Is Happening Now

The Q-hardening thesis explains not just why Earth's conditions exist, but why the current moment is pivotal—and why seeder/alliance intervention was constrained until now.

The consent constraint: Chapter 12, Section 12.3.3 establishes consent as an impedance matching condition—when $\Gamma_{consent} \to 0$ (passive absorption without critical resistance), the system interprets this as consent. For much of the forge period, humanity's collective low Q meant most individuals passively absorbed parasitic control signals. This constituted free-will consent to the control matrix. The seeders' hands were tied: Chapter 14, Section 14.10 establishes that free will takes precedence, even over benevolent intervention. The parasites didn't force the matrix so much as *offered* it—and low-Q consciousness accepted.

The moral paradox: Higher-density seeders could see the suffering the forge produced but could not unilaterally remove it without violating the same free will principle that makes Q-hardening work in the first place. A soul whose Q is raised by external rescue hasn't been Q-hardened—it's been Q-gifted. The forge only works if the soul builds its own Q against genuine resistance. This is the painful logic of the system: the suffering is not a bug, it's the heat treatment.

The turning point: As collective Q rises—despite (and partly because of) the parasitic control—the consent equation shifts. More individuals develop sufficient Q to reflect the control signal ($\Gamma_{consent} \to 1$). Once the critical coherence fraction is reached (~283,000 people at $f_c \approx 0.0035\%$ for threshold $T = 10$, or ~283 high-amplification influencers from Chapter 8), the collective impedance mismatch with the control matrix crosses a threshold. Consent is being withdrawn at scale.

This changes the intervention calculus: The Prime Directive gradient (Chapter 14, Section 14.10.3) places Earth between "active seeking" and "planetary emergency." As collective Q rises and consent is withdrawn, the free will constraint relaxes—intervention becomes permissible precisely because it now *aligns* with collective free will rather than overriding it. The forge has produced what it was designed to produce: consciousness robust enough to choose liberation without having it imposed.

The Kali Yuga inversion: The Perennial Traditionalist cycle (Chapter 12, Section 12.7.4) describes Kali Yuga as the age of maximum parasitic extraction and minimum coherence. But within the

Q-hardening framework, Kali Yuga is also the *maximum heat* phase of the forge—the period that produces the most robust Q-hardening. The darkest age produces the strongest consciousness, and its completion signals the forge's success, not just the cycle's end.

> **Epistemic Note**: This subsection is the most speculative in the chapter. It connects existing framework elements (consent model, free will constraints, critical coherence threshold, Yuga cycles) into a strategic hypothesis. It should be understood as a synthesis of the model's internal logic, not as an established derivation or empirically grounded claim.

4.11 Manifestations Across Scales

4.11.1 Cosmic Voids

Characteristics:

- Expansion rate: ~7%/Gyr (in backreaction models)
- Coherence: None (no structured matter)
- Consciousness: None (no experiencer)

Resonant growth interpretation: Maximum spatial expansion, zero informational expansion. The signal passes through, producing physical effects but no experience.

4.11.2 Galactic Scales

Characteristics:

- Expansion: Embedded in void expansion plus internal dynamics
- Coherence: Collective stellar dynamics, possible galactic consciousness
- MOND effects: Nonlocal coupling to cosmic boundary

Resonant growth interpretation: Intermediate scale. Some signal routes into expansion, some into galactic-scale coherence. The nonlocal MOND effects emerge from the coupling between local dynamics and cosmic torsion field.

4.11.3 Planetary Scales

Characteristics:

- Mass condensation rate: ~0.16%/Gyr (estimated from geological evidence)
- Coherence: Core spin dynamics, possible planetary consciousness

Resonant growth interpretation: Substantial signal routes into mass condensation at 660 km impedance boundary. Expansion is slower than voids but measurable over geological time. The following subsections present converging lines of evidence that Earth has expanded significantly since the Archean, grounding the vacuum condensation mechanism (Section 4.6) in observational data.

4.11.3a Historical Development

The expanding Earth hypothesis has a longer scientific pedigree than is commonly acknowledged. Roberto Mantovani (1889, 1909) proposed thermal expansion fracturing a once-continuous global crust. Ivan Yarkovsky (1888) linked gravity to an ether-physics growth mechanism. Ott Christoph Hilgenberg (1933) constructed physical globe models demonstrating continental fit at 55–60% of modern radius — and corresponded with Einstein about the implications. László Egyed published paleoradius estimates from continental coverage data in *Nature* (1956). Samuel Warren Carey organized the 1981 Sydney symposium on expanding Earth, attracting geologists from twelve countries.

More recently, James Maxlow (2001, 2005, 2013, 2025) has produced high-resolution digital retro-deformation models using modern continental margin data, deriving Phanerozoic expansion rates of ~1.8–2.2 cm/yr radial growth. While these figures remain outside mainstream consensus, the proponents include credentialed geologists publishing in peer-reviewed venues — not fringe speculation.

4.11.3b Paleogeographic Evidence

The most visually compelling evidence is the continental fit on a reduced-radius globe:

- At **Permian** (~280 Ma): continental margins fit on a 55–60% radius sphere with less than 1% gap area
- At **Carboniferous** (~340 Ma): gaps shrink below 0.5%
- At **Archean** (>2.5 Ga): continental crust forms a nearly perfect closed shell

Mountain belts, ancient river systems, and volcanic provinces that are discontinuous on the modern globe align end-to-end when reassembled on a smaller sphere. Maxlow's 2025 digital models retro-deform continental margins at successive geological epochs, demonstrating that supercontinents (Gondwana, Laurussia) nest as a continuous shell rather than isolated rafts on a vast ocean.

The key geometric constraint: continental crust currently comprises ~40% of Earth's surface. On a globe 55–60% of modern radius (surface area ~30–36% of modern), continental crust covered nearly 100% of the surface — exactly as predicted if no large oceans existed before Paleozoic rifting began.

4.11.3c Paleobiological Evidence

Fossil biogeography provides independent corroboration:

- *Glossopteris* flora distributed continuously across South America, Africa, India, Antarctica, and Australia in Permian rocks
- *Lystrosaurus* and *Cynognathus* found in identical Early Triassic formations on all southern landmasses
- Carboniferous–Permian coal forests continuous from North America through Europe to Siberia at identical paleolatitudes

On a smaller globe, these distributions require no explanation beyond direct adjacency — organisms walked or floated short distances across continuous terrain. Standard plate tectonics invokes land bridges, identical parallel evolution on separated continents, or hypothetical oceanic plates now entirely subducted. The expanding Earth model requires fewer auxiliary hypotheses: the continents were simply adjacent because the planet was smaller.

4.11.3d Oceanic Evidence

The seafloor record presents a quantitative puzzle:

- Mid-ocean ridges produce 20–25 km^2/yr of new oceanic crust globally
- Subduction zones recycle only 14–16 km^2/yr (Matthews & Müller 2025; Conrad et al. 2025)
- Over 200 Ma, this imbalance produces an area increase equivalent to the entire Pacific basin

Additionally, the oldest surviving oceanic crust everywhere on Earth is Jurassic (~180 Ma) or younger — suspiciously uniform worldwide. On an expanding Earth, this resolves naturally: all modern oceans began forming at roughly the same epoch when the continental shell fractured. No vast pre-Jurassic ocean floor survives because no vast pre-Jurassic oceans existed.

The standard model requires that a hypothetical Panthalassa ocean, larger than an entire hemisphere, was entirely subducted — yet no pre-Jurassic oceanic lithosphere survives anywhere, and 2025 mantle tomography shows subducted slabs rarely penetrate beyond 700–1000 km depth. The artificial paleocean sinuses required by constant-radius reconstructions (Tethys, Iapetus, Austral Sinus) may be artefacts of forcing ancient geography onto a too-large globe.

4.11.3e The Great Unconformity

One of geology's most striking features is the Great Unconformity: Cambrian sediments (~540 Ma) resting directly atop basement rocks 1.7–2.0 Ga old, with 1.2–1.6 Ga of "missing time." The Grand Canyon provides the iconic example, but similar unconformities appear worldwide.

Expansion offers a coherent resolution: a Neoproterozoic–Cambrian expansion pulse (~800–540 Ma) induces planetary-scale crustal stretching and thinning. Deep basement is exposed to intense denudation across the entire globe simultaneously, erasing intermediate strata everywhere. The flat, widespread unconformities are predictable signatures of a growth episode, not patchwork anomalies requiring separate local explanations for each continent. Pre-expansion crust was entirely continental and ancient; new basaltic oceanic crust formed only in the expanding rifts that followed.

4.11.3f True Polar Wander as Expansion Evidence

The paleomagnetic pole path since the Carboniferous (~350 Ma) describes a tight, systematic spiral exceeding 90° of arc — too large and too coherent to be explained by mantle convection alone. On a constant-radius Earth, ancient triple junctions should migrate chaotically; on a smaller-radius globe, they remain nearly stationary relative to the mantle.

Asymmetric expansion provides a natural mechanism: faster expansion beneath the African/-South Atlantic hemispheres and slower expansion beneath the Pacific shifts the planetary moment of inertia, driving true polar wander (TPW) without requiring whole-mantle overturn. Maxlow (2025) and Scalera (2003, 2025) demonstrate that the observed Carboniferous-to-present pole path matches independently derived paleoradius curves to within 1–2° at every stage.

The African and South Pacific "superswells" — persistent geoid highs — coincide with zones of highest inferred expansion rate, while the Pacific "slab graveyard" corresponds to the slowest hemisphere. The predicted TPW rate (~1°/Myr) matches paleomagnetic observations.

4.11.3g Paleogravity from Mesozoic Fauna

Galilean scaling laws impose hard limits on terrestrial body size: mass scales as k^3 but bone cross-section scales as k^2, so compressive stress increases linearly with body length. At modern g (9.81 $\mathrm{m/s^2}$), the maximum viable terrestrial mass is ~20–30 tonnes (*Paraceratherium*, the largest land mammal).

Mesozoic megafauna systematically exceed this limit:

- Sauropods routinely reached 50–70+ tonnes (*Argentinosaurus*, *Patagotitan*) with limb bones that do not deviate enough from standard allometric scaling to support such masses at 1 g
- Theropods (*T. rex*, 7–9 tonnes): hindlimb proportions buckle under dynamic loads at 1 g; maximum bipedal mass should be ~1–2 tonnes
- Pterosaurs (*Quetzalcoatlus*: 10–12 m wingspan, 200–250 kg): powered flight is impossible at 1 g — required power exceeds estimated muscle output by 2–5×; flight becomes viable only at $g \approx 0.55$–$0.65\ g_0$

Multiple independent biomechanical methods — Froude gait analysis, Euler column buckling, finite-element stress modeling — converge on paleogravity of ~4–6 $\mathrm{m/s^2}$ during the Late Cretaceous. Crucially, dinosaur body size *peaks* in the Cretaceous and declines sharply after the K/Pg boundary, consistent with rising g from ongoing mass accretion forcing morphological convergence toward modern limits.

Note: Mainstream paleontology disputes the reduced-gravity interpretation. Habib (2008) and Witton & Habib (2010) model pterosaur quad-launch at modern gravity using pneumatic bone structure and anaerobic muscle bursts. Henderson (2006) argues sauropod pneumaticity reduces effective mass by 20-30%. The expanding Earth interpretation requires that all of these alternative models are inadequate.

This connects directly to vacuum condensation: increasing planetary mass → increasing surface g → fauna get smaller over geological time.

4.11.3h Connection to the Resonant Growth Framework

> **Epistemic Note:** The expanding Earth hypothesis remains outside mainstream geological consensus, which attributes plate dynamics to mantle convection with subduction recycling. The evidence presented here is genuine and peer-reviewed (Maxlow 2001, 2005, 2013, 2025; Scalera 2003, 2025; Carey 1976), but its interpretation is contested. The framework presented in this chapter provides a *mechanism* (vacuum condensation) that earlier proponents lacked, potentially reopening the debate on empirical grounds. See Assumptions and Limitations (Section 4.12) for falsification criteria.

The geological evidence converges: Earth's radius has increased ~40–45% since the Archean. Vacuum condensation (Section 4.6) provides the mechanism — torsion-driven mass generation at the 660 km impedance boundary. The core paradox (a robust geodynamo operating for 3.5–4.2 Ga, yet inner-core nucleation only 0.5–1.5 Ga ago) resolves if exothermic core phase transitions produce both dynamo energy and volumetric inflation.

This grounds the abstract resonant growth framework (Section 4.2) in concrete observational data: planets are not merely predicted to grow — Earth *has* grown, and the evidence is written in continental fits, fossil distributions, seafloor ages, unconformities, polar wander paths, and the bones of dinosaurs.

Condensation rate spectrum:

Body Type	Impedance Boundaries	Condensation Rate	Effect
Rocky planets	Sharp (660 km)	Fastest	Measurable expansion
Gas giants	Diffuse	Moderate	Contributes to heat excess
Stars	Weak	Negligible vs. fusion	No effect

4.11.4 Human Scales

Characteristics:

- Spatial expansion: Effectively zero (after maturity)
- Consciousness expansion: Fast (measurable over months/years)
- Coherence: Trainable (σ = 0.1-0.5 typical, higher with practice)

Resonant growth interpretation: Nearly all received signal routes into consciousness expansion. Spatial degrees of freedom are locked by biological programming. This is the design: use the human form as a consciousness amplifier.

4.11.5 Atomic Scales

Characteristics:

- Expansion: None (quantum mechanics locks geometry)
- Coherence: Quantum coherence, but not volitional
- Consciousness: Unknown (panpsychist interpretations vary)

Resonant growth interpretation: Below the threshold for classical expansion. Signal may influence quantum probability distributions (Chapter 5, RLC circuit) but does not drive spatial growth.

4.11.6 The Hierarchy as Design

The scale hierarchy is not arbitrary:

Scale	Primary Channel	Experience
Void	Spatial expansion	None
Galaxy	Mixed	Collective?
Planet	Mass condensation	Planetary?
Human	Consciousness	Individual
Atom	Quantum coherence	Unknown

The Source creates receivers at every scale. Each scale processes the signal differently. The human scale is unique in combining conscious experience with volitional agency over coherence.

4.12 Assumptions, Limitations, Falsification, and Predictions

4.12.1 Key Assumptions

This chapter rests on assumptions that extend beyond established physics:

1. **Backreaction is dynamically significant.** While Buchert's equations are mathematically rigorous, mainstream cosmology considers backreaction effects to be small (~0.1%). This chapter assumes they are large enough to replace dark energy.
2. **The resonant growth mechanism operates.** The positive feedback loop (growth → lower frequency → more power → more growth) is a theoretical construction. No direct observation confirms the mechanism.
3. **Vacuum condensation is real.** The combination of asymptotic safety with Einstein-Cartan torsion for matter generation is speculative.
4. **Coherence partitions signal between spatial and consciousness expansion.** This is a theoretical framework, not an established physical mechanism.
5. **3D Earth is the optimal Q-hardening environment.** The low environmental Q (high R_{env}, high C_{env}) creates conditions uniquely suited for forging robust consciousness. This is a theoretical interpretation, not a derivable result.

4.12.2 Limitations

1. **No direct torsion detection.** All torsion effects are inferred from indirect evidence.
2. **Sarkar's challenge remains contested.** Mainstream cosmology has not accepted the 2016 or 2019 analyses. Debate continues.
3. **Expansion rates are uncertain.** Geological estimates (~1 cm/year) are marginal; geodetic measurements (~0.1 mm/year) are at noise floors.
4. **The human optimality argument is partially philosophical.** While grounded in RF analogies, it cannot be experimentally verified without measuring consciousness directly.
5. **The Q-hardening thesis is not directly testable.** Environmental Q across densities cannot be measured empirically. The argument rests on internal consistency with the RLC model and the Pareto frontier structure.

4.12.3 Falsification Criteria

The resonant growth framework would be **falsified** if any of the following are demonstrated:

Code	Criterion	Current Status
F1	Isotropic cosmic acceleration confirmed at >5σ with no dipolar component	Not met — dipole remains at 4.9σ
F2	Dark matter directly detected and explains all MOND phenomenology	Not met — no direct detection
F3	Hubble tension resolved by instrumental systematics alone	Not met — tension persists at 5σ
F4	Vacuum energy measured matching QFT prediction (~$10^{120}\times$ observed)	Not met — cosmological constant problem unsolved

Code	Criterion	Current Status
F5	Planetary mass shown constant to <0.01%/Gyr precision	Not met — precision insufficient

4.12.4 Testable Predictions

P1: Expansion is anisotropic and structure-dependent

- Prediction: Improved supernova surveys will confirm dipolar "acceleration" decaying at ~100 Mpc
- Test: Continued analysis of Pantheon+ and future LSST data
- Verification status: Partially supported (dipole at 4.9σ)
- Falsification: If acceleration is confirmed isotropic at high significance

P2: Hubble tension reflects position-dependence

- Prediction: H_0 measurements will show systematic variation with local cosmic environment
- Test: Compare H_0 from observers in voids vs. walls
- Verification status: Pending — requires multi-environment H_0 surveys
- Falsification: If Hubble tension is resolved by systematic error correction

P3: MOND scale varies with H_0

- Prediction: a_0 is not constant but tracks H_0 across cosmic time
- Test: Compare rotation curves at different redshifts
- Verification status: Pending — high-z rotation curve data limited
- Falsification: If a_0 is constant while H_0 evolves

P4: Expansion correlates with torsion field strength

- Prediction: Planetary bodies with stronger internal torsion (larger rotating cores) show faster mass gain
- Test: Precision geodesy across solar system bodies
- Verification status: Pending — current geodetic precision insufficient
- Falsification: If mass gain is uncorrelated with core properties

P5: Coherence training produces measurable effects

- Prediction: Individuals with higher measured coherence (HRV, EEG synchrony) show enhanced nonlocal correlations
- Test: Large-scale study of meditation practitioners with RNG and other anomaly detectors
- Verification status: Partially supported (HeartMath, PEAR data suggestive)
- Falsification: If coherence training produces no anomalous correlations

P6: Q-hardened souls show greater perturbation resistance

- Prediction: Souls with extensive 3D incarnation history should show higher Q stability under perturbation (injection locking resistance) than souls with primarily higher-density experience—testable if individual Q metrics become measurable
- Test: Compare injection locking susceptibility across populations with different self-reported incarnational backgrounds
- Verification status: Pending — requires Q measurement methodology

- Falsification: If incarnational history shows no correlation with measured Q stability

P7: Awakening rate follows sigmoid approaching critical threshold

- Prediction: The rate of "awakening" (measurable as declining consent to control narratives, increasing institutional distrust, growing meditation/consciousness practice adoption) should follow a sigmoid curve consistent with the critical coherence threshold being approached—slow initially, then accelerating as collective Q approaches the tipping point
- Test: Track longitudinal trends in institutional trust surveys, meditation adoption, and alternative epistemology growth
- Verification status: Partially supported — Gallup institutional trust data shows declining trend; meditation adoption growing exponentially (CDC NHIS 2012–2022)
- Falsification: If awakening metrics plateau or decline without reaching threshold dynamics

P8: Earth's mass is increasing at ~0.16%/Gyr

- Prediction: High-precision satellite gravimetry (GRACE-FO successors) will detect secular mass increase after removing known signals (post-glacial rebound, hydrological cycles, tidal dissipation)
- Test: Decade-scale tracking of global gravitational field changes with next-generation gravimetric satellites
- Falsification: If planetary mass is shown constant to <0.01%/Gyr precision over multi-decade baselines (see also F5)

P9: Paleogravity was significantly lower in the Mesozoic

- Prediction: Refined biomechanical modeling of Cretaceous fauna will consistently yield $g < 7$ $\mathrm{m/s^2}$
- Test: Cross-validated allometric, trackway gait, and finite-element analyses across multiple independent taxa (sauropods, theropods, pterosaurs)
- Falsification: If modern-gravity biomechanical models adequately explain all Mesozoic megafauna locomotion and flight without invoking reduced g

4.12.5 Connection to Other Chapters

Previous: Chapter 3 (Demodulation Into Structure) establishes how cosmic geometry emerges from the torsion field. This chapter explains why that structure grows.

Next: Chapter 5 (Consciousness as RLC Circuit) applies the coherence principles to individual consciousness dynamics. The U-curve optimization from Section 4.8 becomes the tuning mechanism.

Related:

- Chapter 0: Torsion physics foundation
- Chapter 1: 1/f spectrum that drives the positive feedback
- Chapter 2: Impedance tiers that create the condensation boundaries
- Chapter 10: Spin coherence fundamentals for the Machian inertia framework
- Chapter 11: Seeder intervention — Q-hardening as strategic design motive (Section 4.10.4)
- Chapter 12: The Fall and parasitic coupling — Q-hardened consciousness as harvest resistance (Section 4.10.4)
- Chapter 14: Link budget integrating all power flows

4.12.6 Competing Hypotheses and Adjudication Criteria

To strengthen doctrine confidence, the resonant-growth interpretation should be tested against competing explanations:

Hypothesis	Core Claim	Distinguishing Signature	Preferred Data Test
Standard ΛCDM with dark-energy constant	Acceleration is fundamental vacuum component	No coherence-linked modulation in expansion residuals	Joint SN/BAO/CMB residual analysis vs coherence proxies
Backreaction-only cosmology	Inhomogeneity averaging explains apparent acceleration	Strong environment-dependent expansion variance without torsion terms	Void-wall differential expansion datasets
Systematic-observation bias	Apparent acceleration arises from calibration/selection effects	Instrument/pipeline changes dominate inferred acceleration shift	Cross-survey calibration reconciliation
Resonant-growth model (this chapter)	Coherence-mediated growth mimics acceleration	Coupled signatures across mass-growth, coherence, and scale transitions	Multi-domain inference using gravimetry + coherence indicators

Adjudication rule: if competing models explain observed signatures with fewer assumptions and equal predictive power, doctrine posture should downgrade resonant-growth claims from operational to exploratory.

Evidence Synthesis

- Detailed source sections: 4.3, 4.5.5, 4.11.3.

Assumptions

- Detailed source sections: 4.12, 4.12.1.

Limitations

- Detailed source sections: 4.12, 4.12.2.

Falsification

- Detailed source sections: 4.12, 4.12.3.

Predictions

- Detailed source sections: 4.12, 4.12.4.

Strategic Relevance

Why It Matters

What To Watch

- Monitor chapter prediction thresholds, proxy indicators, and coherence trend changes.

Boundaries of Use

- Apply this chapter as model-conditional doctrine; treat speculative elements as hypothesis overlays.

4.13 Chapter Summary: Key Equations

4.13.1 Resonant Growth

Cavity resonant frequency:

$$f_{resonance} = \frac{c_{torsion}}{2L}$$

Resonant field amplification:

$$E_{resonant} = E_{incident} \cdot Q$$

4.13.2 Backreaction

Buchert equation with kinematical backreaction:

$$3\left(\frac{\dot{a}_{\mathcal{D}}}{a_{\mathcal{D}}}\right)^2 = 8\pi G\langle\rho\rangle_{\mathcal{D}} - \frac{1}{2}\langle\mathcal{R}\rangle_{\mathcal{D}} - \frac{1}{2}\mathcal{Q}_{\mathcal{D}}$$

Backreaction term:

$$\mathcal{Q}_{\mathcal{D}} = \frac{2}{3}\left(\langle\theta^2\rangle - \langle\theta\rangle^2\right) - 2\langle\sigma^2\rangle$$

4.13.3 Nonlocal Teleparallel

MOND scale from cosmological boundary:

$$a_0 \approx \frac{cH_0}{6} \approx 1.2 \times 10^{-10}\,\mathrm{m/s^2}$$

4.13.4 Vacuum Condensation

Mass generation rate (transformer output):

$$\frac{dm}{dt} = \eta \cdot \sigma_{core}^2 \cdot V_{coherent} \cdot \rho_{vacuum} \cdot f\left(\frac{T}{T_{critical}}\right)$$

Threshold function:

$$f\left(\frac{T}{T_c}\right) = \tanh^2\left(\frac{T - T_c}{T_c}\right) \cdot \Theta(T - T_c)$$

4.13.5 Human Optimality

Coherence-dependent impedance:

$$Z(\sigma) = Z_{baseline} \cdot \sqrt{1 + N \cdot \sigma^2}$$

Embodied consciousness product:

$$F(\sigma) = E(\sigma) \cdot C(\sigma) \quad \text{maximized at intermediate } \sigma$$

—

Reading Path

Previous: Chapter 3 (Demodulation Into Structure) — how geometry emerges from the Source broadcast

Next: Chapter 5 (Consciousness as RLC Circuit) — individual consciousness dynamics within this framework

Related Chapters:

- Chapter 0 (Torsion Foundation): Physical basis for torsion fields and vacuum condensation
- Chapter 1 (Pure Consciousness): The 1/f spectrum driving positive feedback
- Chapter 2 (Densities as Impedance): The impedance tiers creating condensation boundaries
- Chapter 10 (Spin Coherence Fundamentals): Machian inertia and the σ order parameter
- Chapter 14 (Link Budget): Complete power flow accounting including growth terms

Key Connections:

- This chapter provides the **growth mechanism** missing from standard cosmology
- Explains **dark energy** as an artifact of analyzing resonant growth with wrong assumptions
- Grounds **MOND** in nonlocal teleparallel structure rather than ad hoc modification
- Establishes **human scale** as optimal for embodied consciousness
- Bridges **individual** coherence (Chapter 5) to **cosmic** dynamics

---

End of Chapter 4: Resonant Growth and Human Optimality

Part II: Individual Dynamics

How individual consciousness receives, processes, transduces, and creates via the Source signal

Chapter 5: Consciousness as an RLC Circuit

Tuning, Resonance, and Reception Dynamics

KEY FINDINGS — Chapter 5: Consciousness as an RLC Circuit

Evidence-tier key: [L1] established/replicated evidence; [L2] grounded extension with moderate uncertainty; [L3] speculative hypothesis; [L4] conceptual/anecdotal.

- **[L1-HIGH]** The series RLC equations, Q factor, bandwidth, impedance matching, and transfer function mathematics are standard RF engineering, correctly applied to a consciousness analogy.
- **[L2-MEDIUM]** Q = Z_0 / R as a unified measure of sovereignty captures multiple development pathways (wisdom accumulation, shadow work, attention training) in a single parameter with measurable proxies (HRV coherence, propaganda resistance).
- **[L2-MEDIUM]** The bandwidth-depth tradeoff ($\Delta f \cdot \Delta t \geq 1/2\pi$) provides a quantitative framework for the episodic-mythic perception spectrum, with high-Q consciousness perceiving deeper temporal patterns at the cost of narrower immediate bandwidth.
- **[L3-SPECULATIVE]** Soul age as impedance evolution across incarnations, with L accumulating linearly and C discharging exponentially, maps developmental traditions onto RLC parameter trajectories but lacks empirical calibration.
- **[L3-SPECULATIVE]** The gnosis/ego distinction as on-resonance vs. off-resonance operation predicts that analytical reasoning functions as a reconstruction strategy when direct field reception is degraded.

5.1 RF Analogy Overview

5.1.1 What is an RLC Circuit?

An **RLC circuit** (Resistor-Inductor-Capacitor) is the fundamental building block of radio receivers and filters. The three components determine how the circuit responds to signals at different frequencies:

- **R (Resistance)** Dissipates energy, controls damping
- **L (Inductance)** Stores energy in magnetic field, resists current changes
- **C (Capacitance)** Stores energy in electric field, resists voltage changes

Together, these components create a **resonant system** that preferentially responds to signals near its resonant frequency.

5.1.2 Core Engineering Principles

Resonant Frequency:

$$f_0 = \frac{1}{2\pi\sqrt{LC}}$$

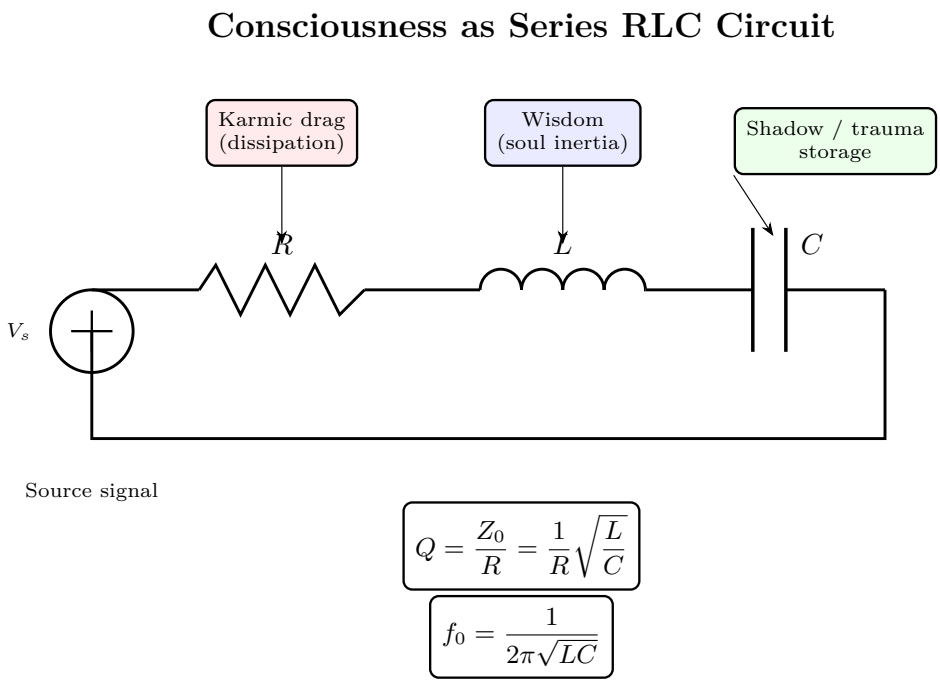

Figure 5.1: Consciousness as RLC circuit — series resonant circuit with karmic drag (R), wisdom (L), and shadow storage (C).

At this frequency, inductive and capacitive reactances cancel, leaving only resistance. The circuit is maximally responsive.

Quality Factor:

$$Q = \frac{1}{R}\sqrt{\frac{L}{C}}$$

Q determines the sharpness of resonance:

- High Q: Sharp peak, narrow bandwidth, high selectivity
- Low Q: Broad response, wide bandwidth, less selective

Bandwidth:

$$BW = \frac{f_0}{Q}$$

The range of frequencies the circuit can effectively receive.

Impedance:

$$Z(\omega) = R + j\left(\omega L - \frac{1}{\omega C}\right)$$

Complex impedance determines how the circuit loads signal sources and how efficiently power is transferred.

5.1.3 Why This Maps to Consciousness

The consciousness/soul can be modeled as a tuned receiver:

RF Component	Physical Function	Consciousness Mapping
R (Resistance)	Energy dissipation	Entropy, distraction, material drag
L (Inductance)	Magnetic energy storage	Soul inertia, wisdom, karmic patterns
C (Capacitance)	Electric field storage	Shadow, trauma, unintegrated charge
f_0	Resonant frequency	Natural "channel" you tune to (archetypal subcarrier focus)
Q = Z_0**/R**	Quality factor	**Primary development metric**—sovereignty, lock resistance
Z_0 **=** $\sqrt{}$**(L/C)**	Characteristic impedance	Visible impedance range, power handling capacity
BW = f_0**/Q**	Bandwidth	Range of frequencies accessible

Critical distinction: f_0 tells you *which archetypes* you tune to; Q tells you *how sovereign* you are at that tuning. Z_0 determines your visible impedance range—which density tiers you can perceive. Spiritual traditions saying "raise your frequency" actually mean "raise your Q."

This model explains:

- Why some people have high sovereignty (high Q = selective, hard to capture) while others are easily influenced (low Q = responds to many signals, easily swept up)
- How practices change what you can receive (tuning R, L, C)

- Why trauma creates static (increases stored charge in C)
- Why wisdom provides stability (increases L, inertia against perturbation)
- Why "sensitive" and "grounded" relate to R (damping), not Q—high R means heavily damped (sluggish), low R means lightly damped (responsive)

5.2 Mathematical Model

5.2.1 The Series RLC Equations

For a series RLC circuit driven by voltage source V_{in}:

$$L\frac{di}{dt} + Ri + \frac{1}{C}\int i\,dt = V_{in}(t)$$

In terms of charge q (where $i = dq/dt$):

$$L\frac{d^2q}{dt^2} + R\frac{dq}{dt} + \frac{q}{C} = V_{in}(t)$$

This is the equation of a **damped harmonic oscillator** driven by an external force.

5.2.2 Natural Response (No Driving Signal)

When $V_{in} = 0$, the circuit exhibits damped oscillation:

$$q(t) = Q_0 e^{-\alpha t}\cos(\omega_d t + \phi)$$

Where:

Variable	Description
α_{damp}	Damping coefficient: $R/2L$
ω_d	Damped frequency: $\sqrt{\omega_0^2 - \alpha_{damp}^2}$
ω_0	Natural frequency: $1/\sqrt{LC}$

Three damping regimes:

Condition	Behavior	Consciousness Analog
$\alpha_{damp} < \omega_0$ (Underdamped)	Oscillates while decaying	Active inner life, dynamic processing
$\alpha_{damp} = \omega_0$ (Critically damped)	Fastest non-oscillatory decay	Balanced, efficient processing
$\alpha_{damp} > \omega_0$ (Overdamped)	Slow exponential decay	Sluggish, heavy, blocked

5.2.3 Steady-State Frequency Response

When driven by sinusoidal $V_{in} = V_0 \cos(\omega t)$:

Transfer function (phasor):

$$H(\omega) = \frac{I}{V_{in}} = \frac{1}{R + j(\omega L - 1/\omega C)}$$

Magnitude:

$$|H(\omega)| = \frac{1}{\sqrt{R^2 + (\omega L - 1/\omega C)^2}}$$

At resonance ($\omega = \omega_0$):

$$|H(\omega_0)| = \frac{1}{R}$$

Response is maximized and limited only by resistance.

5.2.4 The Q Factor in Detail

Definition from energy:

$$Q = 2\pi \cdot \frac{\text{Energy stored}}{\text{Energy dissipated per cycle}}$$

Relationship to bandwidth:

$$Q = \frac{f_0}{\Delta f_{3dB}}$$

Where Δf_{3dB} is the -3dB bandwidth.

Voltage magnification at resonance:

$$V_C = V_L = Q \cdot V_{in}$$

The capacitor and inductor voltages can be Q times larger than the input. This is how weak signals become perceptible—resonance amplifies them.

5.2.5 Impedance Matching

Maximum power transfer occurs when source impedance equals load impedance (conjugate matched):

$$Z_{source} = Z_{load}^*$$

For purely resistive matching:

$$R_{source} = R_{load}$$

Impedance mismatch reflection coefficient:

$$\Gamma = \frac{Z_L - Z_S}{Z_L + Z_S}$$

Power reflected = $|\Gamma|^2$

When mismatched, energy bounces back rather than being absorbed. In consciousness terms, the signal doesn't penetrate.

5.2.6 Q Factor: The True Measure of Spiritual Development

The Central Insight: Spiritual literature speaks of "raising your frequency," but the mathematically correct analog is **raising your Q factor**:

$$Q = \frac{Z_0}{R} = \frac{1}{R}\sqrt{\frac{L}{C}}$$

Q encompasses both characteristic impedance Z_0 (the L/C ratio) AND resistance R (distraction/-damping). This means there are **multiple paths to sovereignty**: raising Z_0 through wisdom accumulation (L↑) or shadow work (C↓), OR reducing R through attention training and meditation.

Why Q, not frequency?

Parameter Change	Effect on f_0	Effect on Z_0	Effect on Q	Spiritual Meaning
L ↑ (wisdom grows)	$f_0 \downarrow$	$Z_0 \uparrow$	**Q** ↑	More stable, harder to perturb
C ↓ (shadow clears)	$f_0 \uparrow$	$Z_0 \uparrow$	**Q** ↑	Less reactive charge storage
R ↓ (attention trained)	—	—	**Q** ↑	Clearer signal, less noise
All three (development)	Ambiguous	$Z_0 \uparrow$	**Q** ↑↑↑	Maximum sovereignty

L and C have *opposite* effects on resonant frequency but *same-direction* effects on impedance and Q. Reducing R provides yet another path to higher Q. Since genuine spiritual development involves wisdom accumulation (L↑), shadow work (C↓), AND attention training (R↓), **Q factor is the correct measure**—it captures all three developmental pathways.

What high Q gives you:

1. **Resistance to injection locking**: Lock bandwidth $\propto 1/Q$. Higher Q = narrower lock range = harder to capture.
2. **Underdamped dynamics**: Damping ratio $\zeta = 1/(2Q)$. Higher Q = more underdamped = richer inner dynamics.
3. **Selectivity**: High Q circuits only respond to signals near their resonant frequency—off-frequency signals are rejected.
4. **Amplification at resonance**: Voltage magnification at resonance = Q. Higher Q = stronger response to matched signals.

The key reframe:

- f_0 **= which archetypes you tune to** (your natural reception channel)
- **Q = how sovereign you are** (resistance to capture, selectivity)
- Z_0 **= your visible impedance range** (which density tiers you can perceive)

A being can have low f_0 (tuned to dense material concerns) but high Q (difficult to manipulate, selective processing). Or high f_0 (tuned to subtle realms) but low Q (easily captured by any signal in that band).

Q applies not only to individual development but to environmental characterization. Chapter 4, Section 4.10 extends this analysis to the density environment itself, showing that 3D's low environmental Q (high R_{env}, high C_{env}) creates the optimal conditions for building robust individual

Q—a property called "Q-hardening." Souls that achieve high Q against 3D's maximal headwinds carry stress-tested sovereignty that cannot be replicated in easier environments.

5.2.6.1 Impedance Matching as Consciousness Range

The **visible range** of consciousness—which density tiers you can perceive—is determined by **impedance matching**, not frequency tuning. Each density tier has a characteristic impedance Z_d. Your ability to couple to (perceive) that density depends on impedance match:

$$\Gamma_d = \frac{Z_d - Z_0}{Z_d + Z_0}$$

Perception threshold: You perceive density d if $|\Gamma_d| < \Gamma_{threshold}$.

Visible impedance range: Given your Z_0 and a perception threshold Γ_{th}:

$$Z_{min} = Z_0 \cdot \frac{1 - \Gamma_{th}}{1 + \Gamma_{th}}, \quad Z_{max} = Z_0 \cdot \frac{1 + \Gamma_{th}}{1 - \Gamma_{th}}$$

Γ_{th}	Z_{max}/Z_0	Z_{min}/Z_0	Interpretation
0.1	1.22	0.82	Narrow range, high selectivity
0.3	1.86	0.54	Moderate range
0.5	3.0	0.33	Wide range, lower selectivity
0.7	5.67	0.18	Very wide range

Your Z_0 is determined by:

- Neurological structure (cavity resonance properties)
- DNA helical geometry (adaptive antenna configuration)
- Biofield coherence (local field environment)
- Practice/training state (L and C modifications from spiritual practice)

Key insight: Raising Z_0 through practice (increasing L via wisdom, decreasing C via shadow work) shifts your entire visible range upward, granting access to higher-density tiers while potentially losing sensitivity to lower ones. Reducing R (through meditation, attention training) also raises Q directly—providing another developmental pathway.

5.2.6.2 Archetypal Tuning: What f_0 Actually Represents

If Z_0 measures sovereignty (and determines visible impedance range), what does f_0 measure?

The mathematical distinction:

Parameter	Formula	Depends On	Meaning
Z_0	$\sqrt{L/C}$	**Ratio** of L to C	Power level, sovereignty
f_0	$\frac{1}{2\pi\sqrt{LC}}$	**Product** of L and C	Archetypal tuning

Z_0 and f_0 are **orthogonal dimensions**: two beings can have identical Z_0 (same power level) but different f_0 (different archetypal focus), or vice versa.

Archetypal tuning via demodulation:

Source broadcasts infinite bandwidth containing all archetypal patterns—morphic subcarriers encoding templates like "healer," "warrior," "teacher," "creator" (see Chapter 3, Subcarrier Model). Your resonant frequency f_0 determines which subcarriers you preferentially receive and express.

Configuration	L	C	f_0	Archetypal Character
Heavy/Deep	High	High	Low	Slow, grounded processing; resonates with earthy, structural archetypes
Light/Quick	Low	Low	High	Fast, ethereal processing; resonates with visionary, transcendent archetypes
Balanced (developed)	High	Low	Medium	Integrated; can access full archetypal spectrum

Mappings to traditional frameworks:

- **Tarot Major Arcana**: Which archetypal energies (Magician, High Priestess, Emperor, Hermit, etc.) you naturally embody
- **Jungian Archetypes**: Dominant archetypal resonance (Hero, Sage, Caregiver, Creator, Ruler, etc.)
- **Vocational Types**: Healer, teacher, warrior, artist, builder, mystic, leader

The Convergence Pattern: Archetypal Integration

Here is a remarkable implication: **development naturally pushes f_0 toward a medium value regardless of starting point.**

Starting Point	Development Process	Effect on f_0
Heavy oscillator (high L, high C)	Shadow work (C↓)	f_0 increases toward medium
Light oscillator (low L, low C)	Wisdom accumulation (L↑)	f_0 decreases toward medium

Interpretation: Young souls may have extreme f_0—strongly identified with one archetypal pattern (the "pure warrior" or "pure mystic"). Old souls converge toward medium f_0, representing **archetypal integration**—no longer fixed in one archetype but able to express any archetype as the situation requires.

This parallels:

- **Jungian Individuation**: Movement from identification with specific archetypes toward integration into the Self (wholeness)
- **Tarot's Fool's Journey**: Culminating in The World—integration of all archetypes encountered
- **Hero's Journey**: The return phase brings gifts from ALL archetypes encountered during the adventure
- **Chakra Mastery**: Not fixation on one energy center but balanced flow through all

The Three Dimensions of Consciousness:

Dimension	Parameter	Question Answered
Sovereignty	Q	How sovereign/selective are you? (Primary development metric)
Range	Z_0	What density tiers can you perceive? (Visible impedance range)
Type	f_0	Which archetypal subcarriers do you tune to?

A complete description of consciousness requires all three. Two "old souls" might have similar Q and Z_0 but different f_0—one naturally expressing healer archetypes, another teacher archetypes. Both are highly developed; they simply resonate with different morphic subcarriers.

5.2.6.3 Jung's Spectrum Analogy

Jung compared the psyche to the electromagnetic spectrum: conscious awareness occupies a narrow band—like visible light—while vast unconscious domains extend beyond perception in both directions (Jung, CW 8, *On the Nature of the Psyche*, 1947/1954, ¶388–420). The personal unconscious corresponds to adjacent bands (infrared, ultraviolet)—nearby but below threshold. The collective unconscious corresponds to radio waves and gamma rays—pervasive, penetrating all matter, carrying archetypal information that every psyche receives but few consciously detect.

This provides a qualitative precedent that the RLC model formalizes quantitatively. The bandwidth of conscious awareness is:

$$BW = \frac{f_0}{Q}$$

A high-Q individual tunes sharply: intense perception of a narrow frequency band, with everything outside that band attenuated below conscious threshold. A low-Q individual receives broadly but shallowly—aware of many frequencies but mastering none. In both cases, the full spectrum exists; only the *received* portion differs.

The unconscious, in this framing, is not a separate realm but simply **the set of all frequencies outside the current tuning bandwidth**. Shadow material (Jung's repressed content) corresponds to signals just outside the passband—close enough to create interference patterns (neurosis, projection) but attenuated enough to remain below conscious detection. Individuation widens the effective bandwidth without sacrificing Q—achieved not by lowering Q but by learning to *retune* f_0 dynamically, sweeping across the spectrum while maintaining sharp selectivity at each setting.

Source broadcasts across the entire spectrum. The RLC circuit can only receive a slice. Jung's analogy and the RF model converge on the same insight: **expanding consciousness means expanding bandwidth, not changing the signal.**

5.2.7 Mapping to Consciousness Parameters

Resistance R (Energy Dissipation):

$$R = R_{base} + R_{stress} + R_{distraction} + R_{attachment}$$

- R_{base}: Baseline metabolic/entropic drain - R_{stress}: Cortisol, fight-or-flight activation - $R_{distraction}$: Attention fragmentation - $R_{attachment}$: Energy leaking to fixations

Higher R $\rightarrow$ Lower Q $\rightarrow$ Broader but weaker reception.

Inductance L (Soul Capacity):

$$L = L_{soul} + L_{wisdom} + L_{integration}$$

- L_{soul}: Inherent soul age/depth—capacity to hold complexity - L_{wisdom}: Accumulated integrated experience—ability to hold paradox - $L_{integration}$: Cross-lifetime accumulated patterns—breadth of perspective

High L is CAPACITY, not rigidity. This is a critical distinction:

Property	High L Represents	Does NOT Represent
Depth	Ability to hold complexity without collapsing	Stubbornness
Scale	Can think in centuries, not just days	Slowness
Stability	Massive flywheel—hard to perturb	Rigidity
Vastness	Room for many perspectives simultaneously	Closed-mindedness

The "old soul" quality: High-L individuals have gravitas, presence, depth. They can absorb perturbations into their vastness rather than being knocked off center. This isn't because they're stuck—it's because they're LARGE.

Higher L $\rightarrow$ Lower f_0, **higher** Z_0, more capacity, harder to perturb, greater sovereignty.

Capacitance C (Shadow Storage):

$$C = C_{baseline} + C_{trauma} + C_{suppression}$$

- $C_{baseline}$: Normal experience storage capacity - C_{trauma}: Unintegrated shock charge - $C_{suppression}$: Actively repressed material

Higher C $\rightarrow$ Lower f_0, **lower** Z_0, more stored "charge" waiting to discharge, easier to capture.

5.2.7.1 Parameter Evolution from Practices

How spiritual practices modify the RLC values:

Practice	Effect on R	Effect on L	Effect on C	Effect on Z_0	Net Effect
Meditation	Decreases	—	—	—	$\uparrow$ Q, clearer reception
Breathwork	Decreases	—	Discharges ($\downarrow$C)	$\uparrow Z_0$	$\uparrow$ Q, $\uparrow$ sovereignty
Shadow work	—	—	Discharges ($\downarrow$C)	$\uparrow Z_0$	$\uparrow Z_0$, $\uparrow$ sovereignty

Practice	Effect on R	Effect on L	Effect on C	Effect on Z_0	Net Effect
Wisdom teachings	—	Increases	—	$\uparrow Z_0$	$\uparrow Z_0$, $\uparrow$ stability
Service/karma yoga	Decreases	Increases	—	$\uparrow Z_0$	$\uparrow$ Q, $\uparrow Z_0$
Trauma (negative)	Increases	—	Increases	$\downarrow Z_0$	$\downarrow$ Q, $\downarrow Z_0$, vulnerable

Key insight: Both shadow work (C↓) and wisdom accumulation (L↑) raise Z_0. This is why these seemingly different paths both lead to "spiritual development"—they both increase sovereignty/impedance.

5.2.8 Soul Age as Impedance Evolution

The concept of "soul age"—the accumulated development across incarnations—maps precisely to the evolution of RLC parameters over cosmic timescales. This section formalizes how the Q factor and characteristic impedance Z_0 evolve through incarnational experience, explaining both the mechanisms of spiritual maturation and the phenomenology of different soul age stages.

5.2.8.1 Q Factor and Temporal Perception

The Temporal Integration Window

The Q factor determines more than selectivity—it defines the **temporal integration window** through which consciousness perceives reality. From the RLC time constant:

$$\tau = \frac{2L}{R} = \frac{2\pi L}{\omega_0 R}$$

Since $Q = \frac{1}{R}\sqrt{\frac{L}{C}}$ and $\omega_0 = \frac{1}{\sqrt{LC}}$, we can write:

$$\tau_{integration} = \frac{Q}{\omega_0} = \frac{Q}{2\pi f_0}$$

Qualitative insight: $\tau \propto$ L directly—high inductance gives high temporal integration. This is the same physics as SAR (Synthetic Aperture Radar, Chapter 3, Section 5): larger aperture enables finer resolution. Higher Z_0 (from high L, low C) = wider perceptual aperture = longer effective integration time.

This integration window represents the characteristic timescale over which experiences are coherently processed:

Q Factor	$\tau_{integration}$	Temporal Perception
$Q < 1$	Sub-cycle	Fragmented, moment-to-moment
$Q \approx 1$	One cycle	Single-event focus

Q Factor	$\tau_{integration}$	Temporal Perception
Q = 2-5	2-5 cycles	Short narrative spans
Q = 5-10	5-10 cycles	Extended life planning
Q > 10	Multi-cycle	Trans-generational thinking

High Q enables pattern recognition across longer timescales. Where a low-Q consciousness sees isolated events, a high-Q consciousness perceives the underlying wave patterns connecting events across time.

The Bandwidth-Depth Tradeoff

Bandwidth and temporal depth are inversely related:

$$BW = \frac{f_0}{Q} \quad \Rightarrow \quad BW \cdot \tau_{integration} = \frac{1}{2\pi}$$

This is a fundamental uncertainty relation for consciousness:

$$\Delta f \cdot \Delta t \geq \frac{1}{2\pi}$$

Interpretation: You can either perceive many frequencies superficially (broad bandwidth, shallow time) OR few frequencies deeply (narrow bandwidth, deep time). Soul age progression involves **increasing Q** to enable deeper temporal perception while accepting narrower immediate bandwidth.

Practical manifestation:

- **Low Q (young soul)**: Responds to many stimuli but with shallow processing; lives "in the moment" reactively
- **High Q (old soul)**: Fewer things register, but those that do are processed deeply; sees patterns across lifetimes

5.2.8.2 The Episodic-Mythic Perception Spectrum

A Continuous Spectrum, Not Two Modes

Temporal perception exists on a continuous spectrum from purely episodic to deeply mythic. Q determines where on this spectrum a consciousness naturally operates:

Spectrum Position	Q Range	Perception Character
Pure episodic	Q < 1	Events as isolated incidents, no pattern recognition
Mostly episodic	Q ≈ 1-2	Some pattern awareness, dominated by immediate
Balanced	Q ≈ 2-4	Flexible movement between event and pattern
Mostly mythic	Q ≈ 4-7	Pattern-first perception, events as instances

Spectrum Position	Q Range	Perception Character
Deep mythic	$Q > 7$	Events nearly dissolve into archetypal patterns

Episodic Pole (low Q end):

- Events experienced as discrete, isolated occurrences
- Linear, sequential time perception
- Focus on immediate causes and effects
- "What happened" dominates

Mythic Pole (high Q end):

- Events experienced as recurrences of archetypal patterns
- Cyclical, layered time perception
- Focus on eternal patterns expressing through particulars
- "What this means" dominates

The key insight: Development doesn't replace episodic with mythic—it expands range. High-Q beings can access episodic perception when needed but default to mythic. Low-Q beings are stuck in episodic mode.

Mathematical characterization:

$$\Psi_{perception}(t) = \alpha_{episodic} \cdot \delta(t - t_0) + \alpha_{mythic} \cdot \sum_n A_n \cos(n\omega_0 t + \phi_n)$$

Where:

Variable	Description
$\alpha_{episodic}$	episodic mode weight (high for young souls)
α_{mythic}	mythic mode weight (high for old souls)
The sum	represents archetypal patterns with harmonic structure

Q determines spectrum position:

$$\frac{\alpha_{mythic}}{\alpha_{episodic}} \propto Q^2$$

Why mythic perception requires high Q:

Mythic perception recognizes the SAME PATTERN across different temporal instantiations. This requires:

1. **Integration across time**: Longer $\tau_{integration}$ to correlate distant events
2. **Pattern extraction**: Narrow bandwidth to filter out noise
3. **Stability**: High Q prevents immediate events from overwhelming pattern recognition

The Phase Coherence Requirement:

$$\sigma_{mythic} = \left| \frac{1}{N} \sum_{events} e^{i\phi_{event}} \right|$$

Mythic perception emerges when $\sigma_{mythic} \to 1$—when the consciousness maintains phase coherence across the events being compared. This requires the stability that only high Q provides.

5.2.8.3 Soul Age Progression: The Impedance Evolution Table

The following table synthesizes the RLC parameters across soul age stages, correlating electrical characteristics with phenomenological descriptions from wisdom traditions (particularly the Michael Teachings framework).

Note: Parameter values are illustrative model outputs scaled to conventional units, not empirical measurements. The qualitative ordering (Infant < Baby < Young < Mature < Old) is the model's primary claim.

Soul Age	Incarnations	L (H, illustrative)	C (F, illustrative)	Z_0 (Ω, illustrative)	Q (illustrative)	τ_{int} (illustrative)	Temporal Span	Dominant Mode
Infant	1-50	0.1-0.3	0.8-1.0	0.3-0.6	<1	Hours	Hours-Days	Survival
Baby	50-150	0.3-0.6	0.5-0.8	0.6-1.1	~1	Days	Days-Weeks	Rules
Young	150-300	0.6-1.2	0.3-0.5	1.1-2.0	1-2	Weeks	Months-Years	Achievement
Mature	300-500	1.2-2.5	0.2-0.3	2.0-3.5	2-4	Months	Years-Decades	Relationship
Old	500-800	2.5-5.0	0.1-0.2	3.5-7.0	4-7	Years	Lifetimes	Philosophical
Transc.	800+	5.0+	<0.1	7.0+	7+	Decades	Civilizations	Unity

> **Epistemic note [L3]**: The soul age framework draws from the Michael Teachings (channeled material) and Vedic/Buddhist reincarnation traditions. Specific incarnation counts and parameter values are interpretive extrapolations, not empirical data. The convergent pattern across traditions is suggestive but does not constitute empirical validation of the specific RLC parameter mapping.
>
> **Clarification**: "Infant," "Baby," "Young," "Mature," and "Old" refer to **soul development across many incarnations**, not biological maturation within one lifetime. Bodies mature in decades; souls mature across hundreds of lifetimes. A biologically old person may be a "young soul," and a child may incarnate as an "old soul."

Parameter Evolution Equations:

Inductance (wisdom) accumulates through integrated experience:

$$L_{soul}(n) = L_0 + \alpha_L \sum_{i=1}^{n} \eta_i \cdot \Delta L_i$$

Where:

Variable	Description
L_0	base soul inductance

Variable	Description
n	number of incarnations
η_i	integration efficiency of incarnation i (0-1)
ΔL_i	potential wisdom gain from incarnation i
α_L	accumulation rate constant

The model assumes net positive L accumulation; incarnations that produce confusion rather than wisdom may have $\eta_i \approx 0$ but not $\eta_i < 0$, a simplifying assumption that could be relaxed in future work.

Capacitance (shadow) discharges through processing:

$$C_{soul}(n) = C_0 \cdot \exp\left(-\beta_C \sum_{i=1}^{n} \theta_i \cdot W_i\right)$$

Where:

- C_0 = initial soul capacitance
- θ_i = shadow work intensity in incarnation i
- W_i = wounds processed in incarnation i
- β_C = discharge rate constant

Characteristic impedance evolution:

$$Z_0(n) = \sqrt{\frac{L_{soul}(n)}{C_{soul}(n)}} \propto \sqrt{\frac{L_0 + \sum \eta_i \Delta L_i}{C_0 \cdot e^{-\beta \sum \theta_i W_i}}}$$

Both pathways (L↑ and C↓) contribute to Z_0 growth, explaining why different spiritual paths all lead to development.

Why L is additive but C is exponential: This asymmetry reflects the nature of the underlying processes:

- **L accumulates linearly** because wisdom is additive—each coherently integrated experience adds to the aperture (like SAR coherent integration, Chapter 3 Section 5). New understanding doesn't erase old understanding; it builds upon it.
- **C discharges exponentially** because trauma processing follows first-order kinetics—the rate of discharge is proportional to remaining charge. The "easiest" trauma processes first; deeper layers become progressively harder to access. This mirrors how a physical capacitor discharges through a resistor.

5.2.8.4 Q Development Through Incarnations

The Incarnational Learning Curve

Q factor develops through a specific learning trajectory across incarnations:

Phase 1: Q Building (Infant → Young)

Early incarnations focus on **reducing R** (learning to focus attention, developing will):

$$Q_{early} = \frac{Z_0}{R} \quad \text{limited by high R}$$

Practices: Basic survival skills, social learning, attention development

Phase 2: Q Stabilization (Young → Mature)

Middle incarnations balance **L accumulation and C discharge**:

$$Q_{middle} = \frac{1}{R}\sqrt{\frac{L}{C}} \quad \text{both terms growing}$$

Practices: Relationship work, career mastery, emotional processing

Phase 3: Q Deepening (Mature → Old)

Later incarnations focus on **L deepening** while C approaches minimum:

$$Q_{late} \approx \frac{\sqrt{L}}{R\sqrt{C_{min}}} \propto \sqrt{L}$$

Practices: Contemplative disciplines, teaching, wisdom integration

The Q-Stability Threshold

At Q ≈ 3, a critical transition occurs: the system becomes **underdamped** with sustained oscillation:

$$\zeta = \frac{R}{2\sqrt{LC}} = \frac{1}{2Q} < 1 \quad \text{when } Q > 0.5$$

But **meaningful resonance** requires Q > 3:

$$\text{Resonance peak/baseline} = Q \quad \Rightarrow \quad Q > 3 \text{ for } 3\times \text{ amplification}$$

This corresponds to the **Mature soul threshold**—where consciousness gains enough stability for deep inner work.

Cross-Incarnational Q Coherence

The SAR analogy from Chapter 3, Section 5 applies to Q development:

$$Q_{effective} = Q_{single} \cdot \sqrt{N_{coherent}}$$

Where $N_{coherent}$ = number of coherently integrated past lives. This explains why some souls with fewer incarnations may have higher effective Q—their incarnations were more coherently integrated.

The Ratchet Mechanism in Q Development

Q development connects to the DNA ratchet mechanism (Chapter 6):

$$Q_{floor}(t) = \max_{t'<t}[Q(t') \cdot \eta_{ratchet}]$$

Where $\eta_{ratchet}$ is typically in the range 0.7-0.9 (most gains are preserved, but not all). Once Q reaches a threshold, DNA reconfiguration locks in most of the gain. This explains why old souls, even when traumatized, don't fully regress to infant soul behavior—they have locked-in Q floors.

Injection Lock Resistance Scaling

From Chapter 9, injection lock bandwidth:

$$\Delta\omega_{lock} = \frac{\omega_0}{2Q} \cdot \frac{V_{inj}}{V_0}$$

Higher Q = narrower lock bandwidth = greater resistance to belief capture. This provides the formal basis for why old souls are harder to propagandize—their high Q creates intrinsic resistance to injection locking.

Practical Applications:

Soul Age Assessment	Indicator
Temporal planning horizon	Direct $\tau_{integration}$ measure
Resistance to fads/propaganda	Injection lock resistance (Q)
Pattern recognition across events	Mythic perception capacity
Integration of apparent contradictions	Bandwidth $\times$ Q product
Response to trauma	Q floor (ratchet level)

5.2.9 Resonance as Gnosis: On-Frequency vs. Off-Frequency Operation

The preceding sections describe the circuit's *parameters* (Q, Z_0, f_0) and *developmental trajectories* (soul age). But the same circuit with the same R, L, C can operate in two fundamentally different modes depending on whether it is at resonance or off resonance. This section maps these two operating regimes to the experiential distinction between gnosis (direct knowing) and ego (analytical reconstruction).

5.2.9.1 The Two Operating Regimes

At resonance ($\omega = \omega_0 = 1/\sqrt{LC}$):

$$Z(\omega_0) = R$$

Inductive reactance (ωL) and capacitive reactance ($1/\omega C$) cancel perfectly. The circuit is purely resistive — transparent. Maximum current flows. Transfer function magnitude = $1/R$ (maximum throughput).

Off resonance ($\omega \neq \omega_0$):

$$|Z(\omega)| = \sqrt{R^2 + \left(\omega L - \frac{1}{\omega C}\right)^2}$$

The imaginary (reactive) component dominates. The circuit stores and reflects energy rather than conducting it. Signal throughput drops sharply.

The consciousness mapping:

Property	At Resonance (Gnosis)	Off Resonance (Ego)
Circuit state	Purely resistive, transparent	Highly reactive, reflective

Property	At Resonance (Gnosis)	Off Resonance (Ego)
Signal throughput	Maximum ($1/R$)	Low, drops as $1/\|Z\|$
Energy flow	Conducted freely	Stored as charge or reflected
Voltage magnification	$Q \times V_{in}$ (weak signals amplified)	~1 (no amplification)
Impedance to Source	Minimum (matched)	High (mismatched)
Experienced as	Clarity, flow, direct knowing, embodied certainty	Overthinking, anxiety, reactivity, fragmentation

Key equation — the "gnosis ratio," measuring how close to resonant operation:

$$\eta_{gnosis} = \frac{|H(\omega_0)|}{|H(\omega)|} = \frac{\sqrt{R^2 + (\omega L - 1/\omega C)^2}}{R}$$

At resonance: $\eta = 1$. Off resonance: $\eta >> 1$, with the peak ratio approaching Q at the -3dB points.

5.2.9.2 Why High C Drives Off-Resonance (Ego) Operation

When shadow/trauma increases C beyond its equilibrium value:

1. **Resonant frequency shifts downward**: $f_0 = 1/(2\pi\sqrt{LC})$ — higher C lowers f_0
2. If the Source signal remains at the original frequency, the circuit is now **off-resonance** with respect to Source
3. Capacitive reactance ($1/\omega C$) decreases relative to inductive reactance (ωL)
4. The circuit becomes **inductively reactive** at the Source frequency — it resists change, stores energy in the magnetic field (rigidity of accumulated patterns without corresponding shadow integration)

Or equivalently: High C lowers $Z_0 = \sqrt{L/C}$, creating impedance mismatch with Source. The reflection coefficient (from Section 5.2.5):

$$|\Gamma| = \left|\frac{Z_{source} - Z_0}{Z_{source} + Z_0}\right| \to 1 \text{ as } Z_0 \to 0$$

Almost total reflection. The signal bounces back. **This is the ego's fundamental mechanism**: unprocessed shadow raises C, lowers Z_0, shifts the circuit off resonance, and blocks direct reception.

5.2.9.3 Logic as a Compression Artifact

When the circuit operates off-resonance (ego mode):

- Direct signal reception is blocked (high Γ, low throughput)
- The tiny signal that leaks through is noisy and distorted
- The analytical mind **reconstructs** meaning from these fragments — sequentially, logically, symbolically
- This is analogous to digital signal processing of a severely degraded signal: sampling fragments, applying error correction, inferring the original

When the circuit operates at resonance (gnosis mode):

- Direct reception is clean (low Γ, maximum throughput, $Q\times$ amplification)
- The full waveform is received intact
- No reconstruction needed — the pattern is perceived directly, holistically, instantaneously
- This is analog reception of a matched signal: no processing required, the signal IS the perception

The RLC model predicts that analytical reasoning functions as a reconstruction strategy when direct reception is degraded — not the pinnacle of cognition, but a compensatory mode substituted when direct field reception is jammed. In RF terms: digital reconstruction from fragments when clean analog demodulation is unavailable.

	Gnosis (At Resonance)	Ego / Analytical (Off Resonance)
RF analog	Clean analog demodulation	Digital reconstruction from fragments
Signal quality	Full waveform, high SNR	Degraded fragments, low SNR
Processing	None needed — direct perception	Heavy — logic, inference, analysis
Speed	Instantaneous (pattern recognition)	Sequential (step-by-step reasoning)
Accuracy	High (complete information)	Variable (incomplete information)
Energy cost	Low (signal flows freely)	High (reconstruction is computationally expensive)
C state	Low (integrated, discharged)	High (fragmented, stored charge)
Z_0	High (impedance matched)	Low (impedance mismatched)

5.2.9.4 Dynamic Balance at Resonance: Shadow Is Not Eliminated

A crucial nuance: at resonance, the voltage across the capacitor is:

$$V_C = Q \cdot V_{in}$$

The capacitor (shadow) holds **enormous energy** at resonance — Q times the input. But this energy is in **dynamic exchange** with the inductor (wisdom):

$$E_C(t) = \frac{1}{2} C V_C^2 \sin^2(\omega_0 t), \quad E_L(t) = \frac{1}{2} L i^2 \cos^2(\omega_0 t)$$

$$E_C + E_L = \text{constant}$$

Energy oscillates between shadow (C) and wisdom (L) without getting stuck. The shadow is not eliminated — it is **metabolized**, kept in dynamic flow with wisdom.

In the ego state: energy is predominantly stored as static charge in C. It doesn't flow. The capacitor is "stuck" — charged up with unprocessed material. This is shadow that hasn't been brought into dynamic relationship with wisdom.

Gnosis doesn't require zero shadow. It requires shadow and wisdom in dynamic balance — their reactances canceling, energy flowing freely between them.

5.2.9.5 Q Determines the Sharpness of the Gnosis/Ego Distinction

For a **low-Q circuit** (Q < 2):

- Broad, flat frequency response
- Little difference between on-resonance and off-resonance operation
- The person doesn't experience a strong distinction between gnosis and ego modes
- Always "somewhat receiving" but never strongly amplifying

For a **high-Q circuit** (Q > 5):

- Sharp resonance peak
- Enormous difference between on-resonance ($Q\times$ amplification) and off-resonance (near-zero response)
- The person experiences dramatic shifts between gnosis (clarity, flow, direct knowing) and ego (analytical, fragmented, reactive)
- More vulnerable to being knocked off resonance (narrower bandwidth), but much more powerful when on

This explains why advanced practitioners report more vivid experiences of both states — their high Q creates a starker contrast. It also explains why stable gnosis is rare: high Q means the resonance peak is narrow, so even small perturbations (stress, trauma, fear) can knock the circuit off-frequency.

5.2.9.6 Returning to Resonance

What brings the circuit back on-frequency after perturbation?

1. **Shadow work (C↓)**: Discharging accumulated charge brings C back toward the value where f_0 matches Source → resonance restored
2. **Wisdom accumulation (L↑)**: Adjusting L to match the new C → finding resonance at a new f_0
3. **Reducing R (meditation)**: Doesn't change f_0 but raises Q → makes the resonance peak taller and the circuit more responsive when it IS at resonance
4. **Breath/body coherence practices**: These function as a pilot tone — a periodic reference signal that helps the circuit re-lock to its own resonant frequency (ref Chapter 15: breathwork at 0.1 Hz as coherence signal)

The spiritual injunction "be present" translates in RLC terms to: **return to resonance**. Stop operating in the reactive (off-resonance) mode where energy is stored and reflected, and return to the transparent (resonant) mode where signal flows freely.

5.2.9.7 The Tower of Babel Hypothetical

> **Epistemic note**: This subsection is a narrative interpretation connecting the RLC model to mythological tradition. It is speculative and not derived from the preceding mathematics. The RLC physics of Sections 2.9.1–2.9.6 stands independently of any historical hypothesis. This material may be developed further in the civilizational history chapters (Ch 12).

Brief speculative subsection framing the ego/gnosis split in mythological terms:

- If early humanity once operated primarily at resonance (gnosis mode) — phase-locked to the Corporate Feed, receiving directly from the Source — the Tower of Babel story encodes the moment that resonance was broken
- The "confusion of tongues" = a mass shift from resonant to off-resonant operation. Not a loss of language, but a loss of direct knowing. Each person's circuit knocked off-frequency, forced to reconstruct meaning from fragments (linear language) rather than receive it directly (gnosis)
- In RLC terms: a civilizational event that raised C across the population (injected trauma/shadow charge), lowering collective Z_0, shifting everyone off resonance simultaneously
- The result: symbolic/linguistic reasoning became necessary because direct field reception was jammed. Language itself is the compression artifact — the digital reconstruction substituted when analog gnosis was disrupted

Forward reference: The corporate feed array model of humanity's history, developed in later chapters, explores this transition in detail — how humanity functioned as a coherent phased array locked to the Corporate Feed, and how that array was deliberately fragmented through phase desynchronization. The RLC physics of Section 5.2.9 provides the individual-level mechanism underlying that civilizational-scale event.

5.2.9.8 Predictions

P8: Individuals in self-reported "flow states" should show physiological signatures consistent with resonance: high HRV coherence, gamma synchronization, reduced DMN activity (lower R, higher effective Q at that moment).

P9: The same individual's Q should predict the *amplitude* of the gnosis/ego contrast they experience — high-Q individuals report more dramatic shifts between clarity and confusion.

P10: Trauma processing (C↓) should be measurable as a frequency shift in baseline neural oscillation patterns, with post-processing frequency closer to the coherence reference.

P11: Practices combining analytical + somatic + emotional engagement (e.g., focusing, breathwork with inquiry) should restore resonance faster than purely analytical approaches, because they address C (body-stored charge) directly rather than only working through L (cognitive wisdom).

5.3 Assumptions & Limitations

5.3.1 What the Model Assumes

1. **Nonlinear self-modification**: The RLC system is nonlinear because **parameters evolve based on system state**. Experience and practice modify L and C over time. Using the equations from Section 5.2.8.3:
   - **Inductance accumulates linearly**: $L_{soul}(n) = L_0 + \alpha_L \sum_{i=1}^{n} \eta_i \cdot \Delta L_i$
   - **Capacitance discharges exponentially**: $C_{soul}(n) = C_0 \cdot \exp\left(-\beta_C \sum_{i=1}^{n} \theta_i \cdot W_i\right)$

   The Ratchet Mechanism (connecting to Ch 6 DNA):
   - When $Z_0 = \sqrt{}(L/C)$ crosses certain thresholds, DNA geometric reconfiguration triggers
   - DNA activation **locks in the impedance floor**—prevents regression
   - This creates **irreversible** spiritual development stages

- Mathematically: Z_0_floor ratchets upward at activation thresholds

The nonlinearity isn't in response to signals—it's in how the antenna **modifies itself through use**. The system IS its own feedback loop.

2. **Multiple resonant modes**: When we focus on Q (sovereignty) and Z_0 (visible range) rather than just frequency tuning (f_0), the model accommodates multiple simultaneous modes:
   - Q determines selectivity at any frequency
   - Z_0 determines which density tiers can be accessed
   - Multiple resonant modes can coexist; Q and Z_0 characterize overall system capability
3. **Time-varying parameters**: R, L, C change with state. The self-modifying model (point 1) explicitly includes this.
4. **Steady-state analysis applies**: We analyze long-term response. Transients may dominate real experience.
5. **Lumped element model**: Consciousness treated as localized circuit, not distributed field.

5.3.2 Known Limitations

1. **Multi-dimensional reality**: Real consciousness operates across multiple dimensions/densities simultaneously. A single RLC channel is a simplification.
2. **Nonlinear breakthroughs**: Enlightenment experiences, kundalini awakenings, and sudden shifts aren't captured by linear frequency response.
3. **Interaction effects**: Multiple people's RLC circuits interact through the collective field. Individual analysis misses network effects.
4. **State-dependent parameters**: R, L, C change rapidly with emotional state, health, and environment. The model is a snapshot.
5. **Nonlocal effects**: At subtle levels, classical circuit analysis may not apply. Coherence and entanglement require treatment beyond local physics.

5.3.3 Falsification Conditions

The model would be falsified by:

1. **No frequency selectivity**: If people showed equal receptivity to all "frequencies" of information/consciousness. For example, if EEG frequency selectivity during attention tasks showed no correlation with reported spiritual development level, the Q-sovereignty mapping would lack neural support.
2. **No Q-sovereignty correlation**: If people didn't exhibit differential control over their thoughts, feelings, and actions based on development level—if high-Q individuals weren't more selective and harder to capture than low-Q individuals.
3. **No resonance amplification**: If sustained practices at specific "frequencies" didn't produce amplified effects.
4. **No impedance matching effects**: If source-receiver compatibility didn't matter for transmission.

5.4 Predictions & Thresholds

5.4.1 Q Factor Sovereignty Predictions

P12: High-Q individuals resist propaganda and fads

Injection lock bandwidth scales inversely with Q:

$$\Delta\omega_{lock} = \frac{\omega_0}{2Q} \cdot \frac{V_{inj}}{V_0}$$

High-Q individuals have narrow lock bandwidth = harder to capture. This predicts:

- High-Q individuals show greater resistance to propaganda, advertising, and social contagion
- They maintain independent thought under social pressure
- They are less susceptible to "viral" ideas and mass movements
- Low-Q individuals are readily swept up in collective narratives

P13: Q correlates with selective attention and sovereignty

For Q > 10:

- Very selective reception (only responds to resonant-frequency signals)
- Strong response at resonance (amplification = Q)
- Rejects off-frequency interference
- Deep processing of matched signals

For Q < 3:

- Broad, non-selective reception (responds to many frequencies)
- Weak response even at resonance
- Easily captured by external signals
- Shallow processing across many inputs

P14: Multiple paths raise Q (sovereignty)

Development practices work through different mechanisms but all raise Q:

- **Reducing R** (meditation, attention training): $Q = Z_0/R \rightarrow$ direct Q increase
- **Raising Z_0** (wisdom + shadow work): $Q = Z_0/R \rightarrow$ Q increases via numerator
- **Combined practice**: Synergistic effect

This predicts: Different spiritual traditions (contemplative vs. wisdom vs. shadow work) should all produce measurable increases in sovereignty / selectivity, even though they work through different parameters.

P15: Lock bandwidth predicts capture susceptibility

Given an individual's Q and a propaganda source's injection strength:

$$\text{Susceptible if } |\omega_{propaganda} - \omega_0| < \Delta\omega_{lock}$$

This predicts: Susceptibility to specific narratives depends on both Q (general immunity) and frequency match (resonance with the individual's archetypal tuning).

5.4.2 Transient Response Predictions

P16: Trauma creates ringing

Large capacitive charge (trauma) combined with high L creates oscillatory response:

$$\omega_d = \sqrt{\frac{1}{LC} - \frac{R^2}{4L^2}}$$

Trauma + wisdom (high L) → slow, persistent oscillation Trauma + no wisdom (low L) → rapid, chaotic response

P17: Step response shows integration capacity

Response to sudden signal change:

$$q(t) = Q_{final}\left(1 - e^{-t/\tau}\cos(\omega_d t)\right)$$

Time constant $\tau = 2L/R$ determines integration speed.

High L (wisdom) → slow integration but complete Low L → fast integration but incomplete (overshoots and rings)

5.4.3 Impedance Matching Predictions

P18: Teacher-student resonance matters

Maximum transmission when:

$$Z_{teacher} \approx Z^*_{student}$$

A teacher with very different RLC parameters will be poorly "received" regardless of content quality.

P19: Group coherence creates effective impedance transformation

N coherently coupled individuals present effective impedance:

$$Z_{effective} \approx Z_{individual}/N$$

Group can match to sources that individuals cannot.

5.4.4 Critical Thresholds

Threshold	Condition	Effect
Underdamped/Overdamped	$R = 2\sqrt{L/C}$ ($\alpha_{damp} = \omega_0$)	Transition from oscillatory to sluggish
Useful Q	Q > 3	Meaningful selectivity
High sensitivity	Q > 10	Strong amplification but fragile
Extreme sensitivity	Q > 50	Unstable, psychic phenomena
Saturation	$V_C > V_{max}$	Capacitor "breakdown" (overwhelm)
Resonance capture	$\Delta f < BW/2$	Signal locks receiver

5.5 Evidence Synthesis

5.5.1 R (Resistance / Energy Dissipation) Evidence

Meditation Reduces Mental Noise/Resistance

Davidson et al. (2003)

- 8-week MBSR training produced measurable shifts in prefrontal cortex activity; reduced amygdala reactivity = reduced R

Jha et al. (2010)

- Mindfulness training preserved working memory under stress conditions where controls degraded

Interpretation

- Practice literally reduces the "resistance" to signal clarity

Stress Increases Cognitive Friction

Yerkes-Dodson law

- Performance degrades at high stress levels due to cortisol effects

Arnsten (2009)

- Chronic stress impairs prefrontal function, increasing default mode network activity (rumination = noise)

HRV as R proxy

- Low HRV correlates with stress, poor cognitive function—measurable R indicator

Distraction Fragments Attention Energy

Ophir et al. (2009)

- Heavy media multitaskers show degraded ability to filter irrelevant information

Attention as finite resource

- Kahneman's "attention economy"—fragmentation wastes limited processing capacity

Digital R increase

- Average smartphone user checks device $96\times$/day (Asurion, 2019)—constant interruption raises effective R

5.5.2 L (Inductance / Soul Inertia) Evidence

Wisdom Traditions Emphasize Stability

- All major traditions value equanimity, non-reactivity, steady presence

Buddhist

- Cultivation of samatha (calm abiding)

Stoic

- Ataraxia (freedom from disturbance)

High L

- Difficult to perturb = wisdom-associated stability

Soul Age Concepts Across Traditions

Michael Teachings

- 5-stage soul age model (Infant→Baby→Young→Mature→Old)

Vedic

- Jiva accumulates sanskaras across lifetimes

Ra Material

- "Harvest" based on accumulated polarity = integrated experience (high L)

Convergent theme

- Souls differ in accumulated pattern-holding capacity

Karmic Pattern Persistence

Stevenson DOPS research

- Past-life memories often include persistent behavioral patterns

Family constellation therapy

- Multi-generational pattern observation

Interpretation

- High L = strong tendency to repeat established patterns (karma)

5.5.3 C (Capacitance / Shadow Storage) Evidence

Trauma Storage in Body/Psyche

Van der Kolk "The Body Keeps the Score" (2014)

- Trauma physically stored in tissue, nervous system patterns

Somatic experiencing

- Trauma releases through body-centered processing (discharge)

ACE studies

- Childhood adverse experiences correlate with adult disease—stored charge creating pathology

Shadow Work and Discharge

Jungian shadow

- Repressed material holds psychic energy (charge)

Cathartic release

- Emotional processing often involves intense discharge (crying, shaking, rage)

EMDR

- Eye movements facilitate trauma processing—mechanism may be capacitor discharge

PTSD and Stored Charge

Hypervigilance

- Elevated baseline = high voltage state

Flashback triggers

- Specific stimuli release stored charge explosively

Successful treatment

- Reduces reactivity = discharge without retriggering

HRV in PTSD

- Characteristically low—system locked in high-charge state

5.5.4 Q Factor (Sovereignty / Selectivity) Evidence

Resistance to Social Contagion

Asch conformity experiments (1951)

- 75% of participants conformed to obviously wrong group answers at least once
- 25% never conformed—these individuals may represent high-Q (high sovereignty)
- Conformity reduced when even one other person dissented (changes the "signal" environment)

Propaganda resistance research

- Individual differences in susceptibility to propaganda are well-documented
- Critical thinking correlates with education but not perfectly—suggesting an underlying trait (Q)
- Some individuals remain resistant even under extreme social pressure

High Q interpretation

- High-Q individuals have narrow lock bandwidth—external signals must closely match their resonant frequency to capture them
- Low-Q individuals have wide lock bandwidth—easily swept up in collective narratives

Highly Sensitive Persons (HSP) Reframing

HSP research (Aron, 1997)

- 15-20% of population scores high on Sensory Processing Sensitivity
- Deep processing, easily overstimulated, strong emotional reactions

Reinterpretation: HSP traits relate to **low R** (low damping/high signal clarity), not high Q. Low R means:

- Clear signal transmission with little noise
- But ALSO less damping = potential for overstimulation
- HSP individuals may have high signal clarity but variable sovereignty (Q depends on Z_0/R ratio)

Grounded vs. Ungrounded Reframing

Grounded individuals

- Stable, less reactive to environmental shifts, harder to destabilize
- This reflects **high Q (sovereignty)**—selective, doesn't respond to off-frequency signals

Ungrounded individuals

- Quickly affected by others' emotions, environmental changes
- This reflects **low Q**—wide lock bandwidth, easily captured by external signals

Note: "Grounded" is NOT the same as "insensitive" (high R). A person can be both grounded (high Q) AND sensitive (low R) if they have high Z_0.

Psychic Sensitivity and Instability

Clinical observation

- Many claiming psychic abilities also report mental health challenges

Reinterpretation: Psychic sensitivity relates to $\mathbf{f_0}$ **tuning** (tuned to subtle frequencies) and/or **wide** $\mathbf{Z_0}$ **range** (can perceive multiple density tiers), NOT necessarily to Q. The instability often observed may reflect low Q combined with subtle tuning—they can perceive subtle signals but lack the sovereignty to remain unperturbed by them.

5.5.5 Resonance Evidence

Teacher-Student Compatibility

Educational research

- Learning outcomes correlate with teacher-student rapport beyond content quality

Traditional guru-disciple

- Emphasis on "right teacher" suggesting resonance matching
- **Impedance match interpretation** $Z_{teacher} \approx Z^*_{student}$ maximizes transmission

Group Coherence Effects

- **HeartMath group coherence** Synchronized HRV in groups shows measurable entrainment
- **Collective meditation studies** TM research claims crime reduction during group practice (controversial, needs replication)
- **Social synchrony research** Matched movement/breathing creates rapport and prosocial behavior

Note: Sacred site resonance evidence is covered in Chapter 3, Section 3.8.3, where environmental/architectural resonance effects are treated comprehensively.

Evidence Synthesis

- Detailed source sections: 5.5, 5.5.1, 5.5.2, 5.5.3, 5.5.4, 5.5.5.

Assumptions

- Detailed source sections: 5.3.

Limitations

- Detailed source sections: 5.3, 5.3.2.

Falsification

- Detailed source sections: 5.3.3.

Predictions

- Detailed source sections: 5.2.9.8, 5.4, 5.4.1, 5.4.2, 5.4.3.

Strategic Relevance

Why It Matters

5.6.1 Self-Assessment

Estimate your RLC parameters:

High R indicators:

- Easily distracted
- Mentally fatigued
- Difficulty sustaining focus
- Strong attachments draining energy

High L indicators (CAPACITY, not rigidity):

- Can hold paradox and complexity without collapsing into simple answers
- Patient with long timescales—don't need immediate resolution
- Vast inner space—room for many perspectives simultaneously
- "Old soul" presence—depth, gravitas, substance
- Can hold intense charge (emotion, energy) without discharge or breakdown
- Stable in crisis through vastness, not through rigidity

High C indicators:

- Unprocessed emotions surfacing
- Triggered by specific stimuli
- Carrying old wounds
- Feeling "charged" or reactive

Q (Sovereignty) indicators:

- High Q: Hard to manipulate, don't get swept up in group hysteria, maintain center under pressure, selective about what gets your attention, resistant to propaganda/fads
- Low Q: Easily swayed by narratives, captured by trends, reactive to external influences, responds to many stimuli indiscriminately

Z_0 **(Visible Range) indicators:**

- High Z_0: Can perceive subtle phenomena, access to higher density tiers, deep processing capacity
- Low Z_0: Limited to denser/lower frequency perceptions, narrower perceptual range

5.6.2 Optimization Strategies

To increase Q (sovereignty):

- Reduce R through meditation, attention training $\rightarrow$ $Q = Z_0/R$ increases
- Increase L through wisdom accumulation $\rightarrow$ Z_0 increases $\rightarrow$ Q increases
- Decrease C through shadow work $\rightarrow$ Z_0 increases $\rightarrow$ Q increases
- All three pathways work—do what resonates with you

To raise Z_0 (expand visible range):

- Increase L (wisdom/capacity) $\rightarrow$ higher Z_0
- Decrease C (shadow work) $\rightarrow$ higher Z_0
- Both approaches shift your visible impedance range upward

Practical L-Building (Expanding Capacity):

- Exposure to broader timescales (history, cosmology, geological time)
- Holding complexity without premature closure
- Integration of many perspectives (not just accumulating, but HOLDING simultaneously)
- Contemplative practices that expand inner spaciousness
- Cross-lifetime integration (if reincarnation model accepted)
- Reading/studying the "great works" that compress wisdom
- Mentorship from high-L individuals (resonance transfer)

Note on f_0: f_0 determines *which archetypes* you tune to, not *how developed* you are. Changing f_0 shifts your archetypal focus; raising Q increases your sovereignty at whatever channel you're on.

5.6.3 Group Dynamics

When forming coherent groups:

- Similar f_0 $\rightarrow$ natural resonance (tuned to same channel)
- High average Z_0 $\rightarrow$ group resistant to narrative capture
- Varied Q $\rightarrow$ some sensitive scouts, some stable anchors
- Low total R $\rightarrow$ high group Q
- Matched impedances $\rightarrow$ efficient energy flow between members

5.6.4 Strategic Implications

1. **Q as resilience metric**: Populations with higher average Q are more resistant to narrative capture. Q-building programs (meditation, contemplative education, trauma healing) are strategic investments in cognitive sovereignty.
2. **Q-reduction as attack vector**: Any intervention that increases population trauma (R up), increases distraction (R up), or prevents wisdom accumulation (L stagnant) constitutes a Q-reduction operation.
3. **Measurable proxy**: HRV coherence correlates with the model's Q parameter. Population-scale HRV monitoring could provide an operational proxy for collective Q trends.

What To Watch

- 3. **Measurable proxy**: HRV coherence correlates with the model's Q parameter. Population-scale HRV monitoring could provide an operational proxy for collective Q trends.

Boundaries of Use

- Apply this chapter as model-conditional doctrine; treat speculative elements as hypothesis overlays.

5.6 Connections to Other Chapters

- **Chapter 0 (Torsion Foundation)** The RLC circuit represents the torsion-to-classical coupling mechanism—how individuals transduce torsion field information
- **Chapter 2 (Densities)** Densities are impedance tiers; Z_0 determines which tiers you can access
- **Chapter 8 (Phased Array)** Individual Q and Z_0 contribute to collective array performance
- **Chapter 9 (Injection Locking and Perception Management)** Q = Z_0/R determines susceptibility to external capture—higher Z_0 = harder to lock. Individual resonance state determines contribution to collective beamforming — gnosis-state individuals contribute coherent, high-gain elements; ego-state individuals contribute noise
- **Chapter 14 (Link Budget)** RLC parameters determine G_practices; Z_0 determines density access

---

End of Chapter 5: Consciousness as an RLC Circuit

Chapter 6: Biofield and DNA Antenna System

The Adaptive Torsion Transceiver

KEY FINDINGS — Chapter 6: Biofield and DNA Antenna System

Evidence-tier key: [L1] established/replicated evidence; [L2] grounded extension with moderate uncertainty; [L3] speculative hypothesis; [L4] conceptual/anecdotal.

- **[L1-HIGH]** DNA's helical geometry produces measurable THz resonances corresponding to geometric parameters at multiple folding scales, confirmed by Markelz et al. spectroscopy data.
- **[L2-MEDIUM]** Epigenetic research (Meaney, Yehuda, Kaliman, Bhasin) confirms that coherent practices produce stable DNA modifications, supporting the ratcheting mechanism's biological substrate.
- **[L2-MEDIUM]** Bioelectric field research (Levin lab) demonstrates that field-level information can override genomic instructions, supporting the biofield-DNA integration model.
- **[L3-SPECULATIVE]** The magnonic framework mapping condensed matter spin-wave physics onto DNA structure provides a testable but experimentally unverified model for torsion field transduction.
- **[L3-SPECULATIVE]** The soul-DNA matching model (impedance resonance between soul signature and DNA antenna geometry) is metaphysical and not testable by current experimental methods.

6.1 RF Analogy Overview

6.1.1 The Core Concept

Every RF system needs a **front-end transducer** and an **antenna**—the components that convert field energy into signals the system can process, and vice versa. Without transduction, the signal exists but cannot be utilized.

The biofield and DNA together form an **adaptive torsion antenna system** that:

1. **Receives** torsion field patterns (morphic templates)
2. **Transduces** them into cellular/biological signals
3. **Broadcasts** integrated experience patterns back into the field
4. **Adapts** its geometry based on accumulated signal/experience

Critical framing: This chapter extends the RLC model from Chapter 5, providing a **biophysics-level concrete refinement**. Where Chapter 5 modeled the soul as a nonlinear RLC circuit determining resonance characteristics, this chapter examines how those characteristics are physically instantiated through DNA and the biofield.

The hierarchy:

- **Soul (RLC circuit)**: The consciousness-level tuned receiver with **macro parameters** L, C, R determining Q, Z_0, and f_0. These represent system-level characteristics.
- **Body/Organism**: The physical vessel—biofield, cellular systems, nervous system—through which DNA's antenna function is expressed and through which experience is processed. The body provides the local field environment (biofield) and the experiential interface that generates novel patterns for rebroadcast.
- **DNA (Adaptive antenna)**: The biophysical mechanism containing all the **micro subcomponents and circuits** that collectively instantiate the soul's macro parameters. DNA transduces torsion patterns and locks in impedance gains through geometric reconfiguration.

The soul's macro RLC parameters (Chapter 5's system-level view) are actually comprised of countless micro parameters distributed throughout DNA's structure. Soul age (Chapter 5, Section 2.8) represents the accumulated macro RLC development across incarnations. DNA provides the biological instantiation—the physical antenna whose micro-level configurations aggregate into the soul's tuned parameters and ratchet those gains into stable geometric configurations.

6.1.2 The Antenna-Shaping Function

Source's broadcast also shapes the antenna itself. The signal doesn't just pass through the receiver—it forms and maintains the receiver's structure. The morphogenetic field contains the blueprint for the very antenna designed to receive it.

This is **recursive**: transmission shapes receiver → receiver receives transmission more clearly → further refines receiver → …

6.1.3 DNA as TRUE TRANSCEIVER

A critical distinction: DNA is not just a receiver—it's a **transceiver** (transmitter + receiver):

Torsion field (templates) → DNA receives via helical antenna → **Experience processed** through organism → **Novel patterns generated** through lived experience → **DNA geometry adapts** (ratchets to new configuration) → **DNA rebroadcasts** into torsion field → **New templates available** to other receivers (Akashic accumulation)

The effectiveness of this transceiver loop depends on the local field environment—the biofield—which we examine next.

6.2 The Biofield: Local Torsion/EM Environment

6.2.1 What is the Biofield?

The **biofield** is the local torsion/electromagnetic field generated by and surrounding the organism:

- Extends DNA's effective aperture
- Provides the near-field environment for biological processes
- Interfaces between cellular processes and the ambient torsion field
- Coherent biofield = stronger transmission/reception

The biofield represents the local component of an ambient torsion field that is itself nonlocal. The organism generates its own torsion field locally while also coupling to the nonlocal ambient field—analogous to how a radio antenna generates a local near-field while coupling to distant transmissions.

6.2.2 Biofield Components

Component	Physical Basis	Function
Heart field	Toroidal blood flow, cardiac electrical	Primary torsion generator
Brain field	Neural electromagnetic activity	Information processing interface
Meridian system	Ion gradients, fascia conduction	Field distribution network
Chakra zones	Electromagnetic nodes, nerve plexi	Local field concentrators

6.2.3 Bioelectric Gradients

The body maintains DC voltage gradients:

- Cell membrane: -70mV (inside negative)
- Organ-level: measurable mV differences
- Whole-body: head-to-foot potential

This gradient is the **DC bias** that sets the operating point:

$$V_{operating} = V_{bias} + v_{signal}(t)$$

Disrupted gradients (injury, disease) shift the operating point, changing transduction efficiency.

6.2.4 The Transduction Equation

General transduction from torsion field T to biological signal B:

$$B(t) = \int \eta_T(\omega) \cdot T(\omega) \cdot e^{j\omega t} \, d\omega$$

Where $\eta_T(\omega)$ is the **torsion transduction efficiency**—the frequency-dependent effectiveness of converting torsion field to biological signal.

6.3 DNA as Adaptive Helical Antenna

6.3.1 DNA Antenna Geometry

The DNA double helix is a natural **helical antenna**:

Parameter	DNA Value	Antenna Implication
Length	~2m per cell (extended)	Large effective aperture
Pitch	3.4 nm per turn	THz-range primary resonance
Diameter	2 nm	Determines circumference/wavelength ratio
Turns	~200 million	Extremely high gain potential
Phi ratio	34Å pitch / 21Å diameter $\approx \phi$	Optimal information packing

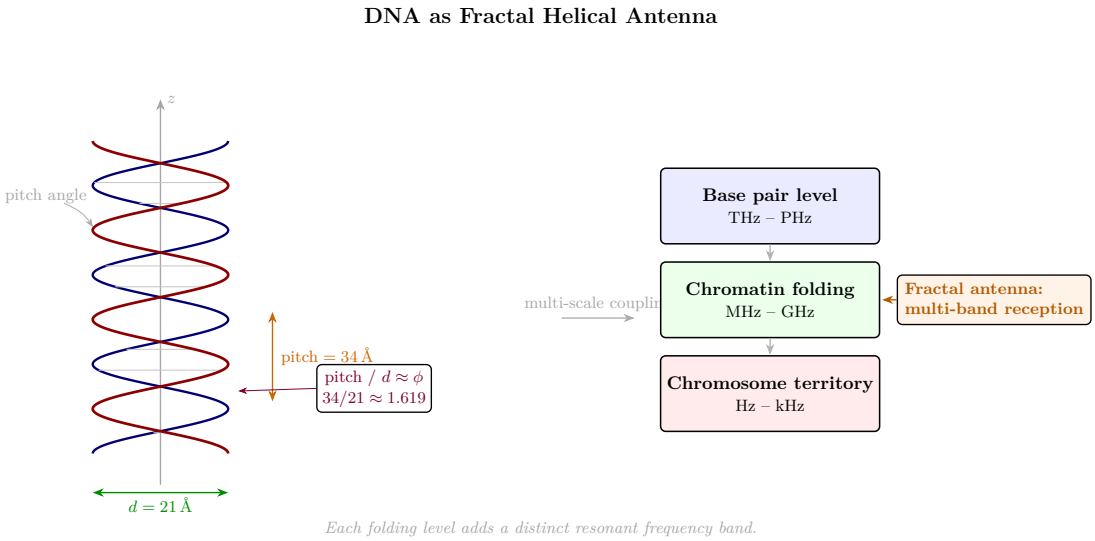

Figure 6.1: DNA as fractal antenna — helical geometry with multi-scale folding creating broadband reception.

6.3.2 Fractal Bandwidth Extension

DNA's recursive coiling (helix → nucleosome → chromatin → chromosome) creates **fractal antenna geometry**:

$$BW_{total} = BW_0 \cdot \sum_{n=0}^{N} \alpha^n$$

Each folding level contributes additional bandwidth at progressively lower frequencies:

Folding Level	Structure	Added Frequency Range
Primary	Double helix	THz-PHz
Secondary	Nucleosome	GHz
Tertiary	30nm fiber	MHz
Quaternary	Chromatin loop	kHz
Chromosome	Condensed	Hz

This allows reception across a broad range of torsion frequencies—from molecular (THz) to consciousness-scale (Hz).

6.3.3 Torsion Generation and Reception

DNA's helical geometry is optimized for torsion field interaction:

- **Generation** Rotating charge distributions along the helix create torsion fields
- **Reception** Torsion field patterns induce vibrational modes in the helix
- **10.5 base pairs per turn** Creates specific torsion frequency signature
- **Fractal folding** Multi-scale torsion resonances

Dual coupling mechanism:

- **EM coupling** — Local, speed-of-light limited (biological processes)
- **Torsion coupling** — Nonlocal in the model framework (see Chapter 0 for the distinction between torsion-as-Einstein-Cartan and torsion-as-consciousness-field)

DNA uses BOTH simultaneously. This explains phenomena like Gariaev's "wave genetics" results (if validated).

Section 3 established DNA's geometric properties as an antenna. The next step is modeling the electrical and magnonic behavior that this geometry produces—mapping antenna characteristics to circuit parameters (L, C, R) that determine resonance, selectivity, and impedance matching.

6.4 DNA as Magnonic RLC Antenna: The Biophysical Framework

6.4.1 Framework Overview: DNA as Magnonic Transducer

Core thesis: The human DNA complex functions as a sophisticated magnonic transducer—an RLC antenna interfacing the **individual body** with the **soul** and, through the soul, with the universal torsion field. DNA and soul form a matched pair: specific genetic configurations resonate with specific soul signatures. This soul-DNA pairing explains the historical power of bloodlines—DNA is the key that unlocks access to advanced soul characteristics. Spiritual evolution = impedance matching engineering.

This framework provides the biophysical instantiation of Chapter 5's soul RLC model. Where Chapter 5 describes the consciousness-level parameters, this section details how those parameters manifest through DNA's mechanical and electromagnetic properties.

What "magnonic" means here: In condensed matter physics, magnons are quantized spin waves—collective excitations propagating through ordered magnetic lattices. DNA's helical charge distribution, with its rotating electron densities and hydrogen-bond networks, creates a quasi-ordered spin system through which collective excitations can propagate. We extend the magnonic framework analogically: DNA's double helix acts as a spin-wave waveguide where torsion-coupled spin excitations behave like magnons in a crystal lattice.

Model Note: This magnonic framing is an analogical extension from condensed matter physics to biophysics. The mathematical parallels (spin stiffness $\leftrightarrow$ inductance, anisotropy $\leftrightarrow$ capacitance, damping $\leftrightarrow$ resistance) are physically motivated by DNA's helical geometry, but direct experimental confirmation of magnonic propagation in biological DNA remains to be demonstrated. The framework is chosen for its explanatory power and testability, not claimed as established biophysics.

Epistemic note [L2-L3]: The magnonic framework maps condensed matter physics concepts onto DNA structure. While spin waves in solid-state systems are well-established, their application to biological DNA is speculative and experimentally unverified.

Key parameter mapping:

Parameter	Electrical (RLC)	Mechanical	Magnonic (Spin Lattice)	System-Level Correlate
L (Inductance)	Energy storage in magnetic field	Mass/moment of inertia	Exchange interaction/spin stiffness	**Soul Age** — accumulated incarnational momentum; internal spin coherence
C (Capacitance)	Energy storage in electric field	Compliance (1/K, spring flexibility)	Dipolar interaction/magnetic anisotropy	**Shadow Age** — capacity to absorb distortion; potential for external coherence
R (Resistance)	Energy dissipation as heat	Viscous damping	Gilbert damping/phonon coupling	**Dimensional Density** — frictional decoherence of the realm

These system-level correlates emerge from the aggregation of DNA's micro-level parameters. Soul Age, for instance, is not a property of any single DNA configuration but the accumulated macro parameter arising from many micro-level geometric states across incarnations.

DNA provides the physical antenna whose parameters are shaped by soul age (L), shadow integration (C), and environmental density (R).

Soul-DNA resonance matching: The soul-DNA pairing is not arbitrary. A soul's macro impedance signature (its accumulated L and C from prior incarnations) must fall within the matching bandwidth of the body's DNA antenna. DNA with high-Q geometry (complex folding, high fractal depth) can couple to souls with correspondingly high Z_0—but a low-Z_0 soul placed in high-Q DNA would experience impedance mismatch, manifesting as developmental instability or psychological fragmentation. Conversely, a high-Z_0 soul in low-Q DNA cannot express its full bandwidth.

This matching constraint explains the observed power of bloodlines: lineages that have maintained specific genetic configurations (through selective reproduction, environmental adaptation, or deliberate breeding programs) preserve DNA antenna geometries capable of coupling to specific soul impedance bands. The DNA doesn't create the soul's characteristics—it provides the antenna geometry that allows those characteristics to manifest in physical expression. A lineage's "power" is its DNA's Q factor and bandwidth, determining which souls can incarnate through it and how much of their accumulated Z_0 can be expressed.

This has a testable implication: genetic diversity within a bloodline should correlate with the range of soul impedance signatures it can support, while genetic bottlenecks should narrow the matching bandwidth, producing lineages specialized for particular impedance bands.

Epistemic note [L3]: The soul-DNA matching model is metaphysical and not testable by current experimental methods.

6.4.2 The Helix as Primordial Motion: Spin-Wave Coupling

The helix represents the inseparable union of **spin** (rotational coherence) and **wave** (rhythmic propagation). DNA's double helix is frozen light—helical waves slowed and stabilized into apparent solidity.

Building on the geometric properties established in Section 3 (counter-wound strands, toroidal embedding, biophoton emission), we now examine how these structures support spin-wave propagation.

The aggregate of ~200 million turns per cell produces a coherent torsion antenna of extraordinary gain. Each turn creates a microscopic torsion vortex; the collective spin-wave coupling along the helix enables coherent propagation of torsion-coupled excitations across the full length of the DNA molecule.

The helix's torsion-generating geometry is not fixed—its mechanical properties can be dynamically reconfigured through chromatin topology changes, providing a built-in tuning mechanism.

6.4.3 Variable Stiffness (k): Chromatin Topology as Antenna Tuner

The critical new concept: Mechanical topology (stiffness k of the chromatin network) serves as the primary "antenna tuner"—directly modulating resonance with torsion modes.

The dual system:

- **Topology (k)** = TUNER — sets the base resonant frequency by mechanical reconfiguration
- **Impedance (Z_0)** = MATCHING NETWORK — optimizes energy transfer once the tuner allows access

Stiffness dynamics:

Stiffness State	Configuration	Torsion Access	Consciousness Correlate
High k	Compacted loops, overwound supercoils	Narrow bandwidth, low-frequency/localized modes	Egoic emotion, survival consciousness
Low k	Fluid unwinding, open domains	Broad receptivity to high-frequency/nonlocal torsions	Unity consciousness, oversoul downloads

Mechanisms for k modification:

- Phase transitions in chromatin (twist-to-writhe buckling, B-to-Z DNA flips)
- Topoisomerase activity dynamically adjusting windings
- Epigenetic marks encoding torsional "memory" (e.g., histone acetylation reducing local rigidity)
- Biophoton feedback loops stabilizing unwinding

Torsion-emotion connection: Low-frequency torsions (discordant thoughts, emotional chaos) maintain high k; high-frequency modes (coherent intent, love-based emotions) soften k. This provides the biophysical mechanism for why emotional coherence enables expanded perception.

6.4.4 The Adaptive Antenna with Hysteresis

In RF engineering, an **adaptive antenna** adjusts its parameters based on the signal environment. DNA extends this concept with **geometric lock-in** (hysteresis/ratcheting).

We use "lock-in" to describe the discrete geometric reconfiguration event and "ratcheting" to describe the cumulative directional process—each lock-in event ratchets the system to a higher impedance floor.

Standard adaptive antenna: Adjusts → optimal reception → can readjust when signal changes

DNA adaptive antenna: Adjusts → optimal reception → **locks geometry** → new baseline

Key differences:

- Changes **lock in**—don't regress when signal removed
- This is the "can't unsee" phenomenon of awakening
- DNA activation = geometric reconfiguration that **stabilizes at new state**
- Locked geometry = permanent upgrade

6.4.5 Fractal Ratcheting: Lock-In Mechanics

Why fractal topology enables ratcheting:

- Self-similar hierarchies create rugged energy landscapes
- Low torsions trap in local minima (stiff, closed states)
- High-frequency inputs cascade through scales via cooperative unwinding
- Metastable highs have energy barriers against backsliding (directed percolation)

Topological invariants:

- Knot-like supercoils preserve twist numbers
- Enzymatic "cuts" required for reversal creates natural hysteresis
- Self-similarity distributes torque unevenly → avalanches where small inputs trigger global shifts

How DNA locks in Z_0 gains:

1. Experience/practice causes conformational changes in DNA (methylation, histone modification, chromatin remodeling)
2. Certain thresholds trigger **stable geometric reconfigurations**
3. New geometry enables reception of previously inaccessible frequencies/patterns
4. Locked geometry = **impedance floor raised permanently**

$$Z_{0,new} = \max(Z_{0,current}, Z_{0,threshold})$$

Once Z_0 crosses an activation threshold, the new floor is locked:

Activation Level	Z_0 Floor	Capability
Baseline	Z_1	3D perception only
Partial (0.3)	~5 Z_1	3D-4D transition access
Significant (0.6)	~25 Z_1	4D stable access
Full (0.9+)	~125 Z_1	5D access capability

These activation levels and their Z_0 ratios are illustrative, representing the model's predicted scaling behavior. Empirical calibration of specific thresholds requires measurement of DNA geometric states correlated with reported capacity changes. The 5x scaling factor between levels is a modeling choice reflecting geometric progression; no empirical calibration exists for these specific ratios.

The ratchet functions as a Q factor increase—each lock-in sharpens resonance while building antifragile stability.

The threshold equation:

$$P_{activation} = S\left(\int_0^T I_{coherent}(t)dt - \theta_{threshold}\right)$$

Where $S(\cdot)$ = sigmoid function, I_coherent = coherent signal intensity, θ_threshold = activation threshold.

The sigmoid captures the probability of activation: as cumulative coherent exposure approaches the threshold, activation probability increases smoothly, but the geometric reconfiguration itself is a discrete phase transition—analogous to how temperature increases continuously but ice-to-water transition is abrupt. Once cumulative coherent exposure exceeds threshold, geometric reconfiguration triggers and locks.

6.4.6 What Triggers Geometric Reconfiguration

Accumulated signal/coherent states:

- Sustained meditation practice
- Intensive shadow work / trauma processing
- Profound experiences (mystical states, NDEs)
- Coherent group field exposure

6.4.7 Soul Age Profiles: Impedance Characteristics Across Development

Different soul ages manifest distinct impedance characteristics through their DNA antenna systems:

Young/Unactivated Souls:

- Low impedance (leaky broadband reception)
- High/variable k (clamped mechanical response)
- Prone to emotional overwhelm, rapid discharge through reactivity
- BUT: grants fluidity, movement, broad-spectrum engagement
- Properly tuned: excel as actors, athletes, aesthetes

Mature but Unactivated:

- High innate impedance (soul-refined C/L for minimal leakage)
- High k (unresolved vessel baggage blocking full expression)
- Gravitational presence without full activation
- Resistant to external capture but not fully transmitting higher torsion

Fully Activated Mature Souls:

- High impedance (selective, stable matching)
- Low k (fluid topology)
- Precision narrowband reception with expansive access when needed
- Antifragile ratcheting against entropy or external interference
- Magnetic, gravitational fields drawing coherence without bleed

6.4.8 Ascension as Impedance Matching: The Smith Chart Model

The engineering framing: Evolution = disciplined expansion of L (internal coherence) and C (external potential) until Z_0_soul matches the current environment's impedance band, unlocking access to the next.

The Smith Chart, used in RF engineering to visualize impedance matching, provides a precise model for spiritual development. The Smith Chart plots impedance on a circular graph where the center represents perfect matching (no reflected power) and distance from center represents degree of mismatch—a visual map of how far a system is from optimal energy transfer. The chart's center represents 1:1 SWR (standing wave ratio)—perfect matching.

Mismatched state (high SWR):

- Intent reflects back as standing waves
- Manifests as stuckness, ego flares, burnout, apathetic stagnation
- Energy wasted in reflections rather than transmission

Matched state (1:1 SWR):

- 100% power transfer
- Intent and manifestation become phase-coherent
- Reflected power drops to zero $\rightarrow$ lossless propagation
- Experienced as effortless synchronicity, transparent channeling

Ascension = perfect impedance matching: Reaching the center of the Smith Chart (1:1 SWR) at the current level, which unlocks access to the next higher impedance/power band of Source broadcast. Each matched state becomes the foundation for tuning to the next octave.

This abstract impedance-matching framework has a concrete physical substrate: DNA's chromatin topology is the mechanism through which matching is achieved.

6.4.9 Chapter Integration: DNA Activation as Mechanical Reality

DNA activation is not metaphorical but mechanical: geometric reconfiguration of chromatin topology. The ratchet mechanism ensures permanent upgrades (the "can't unsee" phenomenon).

Ascension proceeds through:

1. Increasing L (soul age increases across incarnations; within a single lifetime, L manifests as the starting impedance floor that practices can build upon)
2. Increasing C (shadow integration, compliance with full spectrum of experience)

3. Tuning k (chromatin fluidity through practices)

This connects to:

- **Chapter 5's soul age progression table** — DNA provides the physical substrate
- **Chapter 8's phased array model** — Coherent DNA arrays across population enable collective effects

Evidence status for the magnonic RLC model: The geometric antenna properties (Section 6.3) are supported by THz spectroscopy (Section 6.7.3) and biophoton research (Section 6.7.1). The biofield model (Section 6.2) is supported by heart coherence studies (Section 6.7.4) and bioelectric regeneration research (Section 6.7.2). The magnonic RLC framework (this section) is a theoretical extension: the parameter mappings (L↔soul age, C↔shadow integration, R↔density) are analogical constructs that generate testable predictions (Section 6.8) but lack direct empirical calibration. The ratcheting mechanism is indirectly supported by epigenetic evidence (Section 6.7.8) showing stable DNA modifications from practice.

6.5 DNA as Transmitter: The Rebroadcast Loop

6.5.1 What DNA Transmits Back

Integrated experience patterns:

1. Solutions discovered through embodied life
2. Novel pattern combinations from unique perspective
3. Emotional/energetic signatures of experiences
4. Synthesized templates not present in original reception

6.5.2 Transmission Mechanism

Torsion field generation from helix:

The rotating charge distribution along DNA's helical axis creates torsion:

$$\vec{T}_{DNA} = \kappa \int \vec{r} \times \vec{J}(\vec{r})\, d^3r$$

Where $\vec{J}$ = current density from charge motion along helix, κ = torsion coupling constant.

Coherent states amplify transmission:

- Strong emotional coherence → aligned spin states → stronger torsion
- Repeated patterns → reinforced standing waves → stronger broadcast
- Integration events → phase-locked states → constructive addition

6.5.3 Contribution to Morphic Field

Model Note: The following represents a qualitative model based on RF rebroadcast mathematics. In conventional RF engineering, rebroadcast systems aggregate multiple transmitter contributions with coupling coefficients and decay terms. We apply this established framework to morphic field dynamics, with the explicit caveat that the coupling constants (α, β) and their biological correlates

remain to be empirically determined. The mathematical form is chosen for its physical plausibility, not claimed precision.

> **Epistemic note [L3]**: The morphic field rebroadcast model extends Sheldrake's hypothesis, which remains outside mainstream scientific consensus. The mathematical formalization is self-consistent but the underlying phenomenon is contested.

DNA broadcasts contribute to the collective field:

$$\frac{dM_T}{dt} = \sum_{i=1}^{N} \alpha_i \cdot T_{DNA,i} - \beta M_T$$

Where:

Variable	Description
M_T	morphic template strength
$T_{DNA,i}$	transmission from individual i
α_i	coupling strength (depends on coherence)
β	decay rate

Each organism's DNA continuously adds to the collective Akashic accumulation.

6.6 Biofield-DNA Integration

6.6.1 The Nested System

Ambient Torsion Field → **Biofield** (local field environment) → **DNA** (core antenna) → **Cellular/biological expression**

Biofield functions:

- Extends DNA's effective aperture
- Provides coherent local environment
- Heart field = primary torsion generator

DNA functions:

- Receives and demodulates patterns
- Adapts geometry based on signal
- Rebroadcasts integrated experience

6.6.2 Biofield Enhances DNA Function

Coherent biofield improves DNA antenna performance:

Biofield State	DNA Function
Coherent (high HRV, heart coherence)	Sharp reception, clear transmission
Incoherent (stress, fragmentation)	Noisy reception, weak transmission

Biofield State	DNA Function
Entrained (group coherence)	Extended aperture, N^2 power

Practices that strengthen biofield → better DNA antenna performance:

- Heart coherence training
- Breathwork (coherent breathing patterns)
- Meditation (reduced noise)
- Group practice (field entrainment)

6.6.3 The Recursive Loop

The biofield-DNA system is recursive:

1. **DNA shapes biofield**: Gene expression determines body structure, field generators
2. **Biofield shapes DNA access**: Coherent field enables clearer DNA reception
3. **Clearer reception**: Enables DNA adaptive reconfiguration
4. **Reconfigured DNA**: Broadcasts stronger/clearer into biofield
5. **Enhanced biofield**: Further improves DNA access
6. **Spiral evolution**: Each cycle can ratchet to higher baseline

The biofield-DNA integration model described above generates specific claims about DNA's antenna function, biofield coherence, and torsion coupling. The following section examines the empirical evidence bearing on these claims.

6.7 Evidence Synthesis

6.7.1 Biophoton Research

Ultra-Weak Photon Emission

Popp et al. (1984-2000)

- All living cells emit ultra-weak photons (1-1000 photons/cm^2/sec) in 200-800nm range

DNA as primary source

- Biophoton emission correlates with DNA content

Coherence properties

- Emission shows coherent (laser-like) temporal patterns

Death signature

- Dying cells show characteristic biophoton "burst"

Biophoton Communication

Gurwitsch (1923)

- Cells separated by quartz (UV transparent) but not glass induced mitosis in adjacent cells

Fels (2009)

- Cells separated by quartz show correlated metabolic changes

Interpretation

- DNA acts as coherent light source and receiver—transceiver function demonstrated

6.7.2 Bioelectric Regeneration

Levin Lab Research

Voltage gradients pattern morphogenesis

- Transplanted cells adopt morphology based on local bioelectric environment

Planaria experiments

- Ion channel manipulation causes two-headed or no-headed regeneration independent of DNA sequence

Frog eye induction

- Altered voltage patterns cause functional eyes to form on tadpole tails

Implication

- Bioelectric field carries morphogenetic information; DNA executes pattern but field determines it

Regeneration and Voltage

Salamander limb regeneration

- Requires specific bioelectric current patterns

Becker's bone healing

- Applied currents accelerate bone repair (approved medical treatment)

Cancer bioelectric signature

- Tumors show characteristic depolarization; normalizing voltage can reverse cancer phenotype

Bioelectric Networks and Collective Intelligence

Levin (2021)

- "Bioelectric Networks in Regeneration" review—bioelectric patterns function as a morphogenetic code independent of DNA sequence, demonstrating that field-level information can override genomic instructions

Levin & Dennett (2020)

- Cognition all the way down—collective intelligence operates at cellular and molecular scales, supporting the model's claim that information processing is not confined to neural systems but distributed through bioelectric networks

6.7.3 THz Spectroscopy of DNA

Terahertz Absorption

Markelz et al. (2000-2010)

- DNA shows characteristic absorption at 1-3 THz

Sequence dependence

- Different sequences show different THz signatures—information affects resonance

Hydration sensitivity

- THz absorption changes with hydration state—water mediates coupling

Experimental Confirmation

- Calculated resonant frequency from geometry matches observed THz absorption
- Chromatin folding creates resonances at progressively lower frequencies
- Supports fractal antenna model

Phononic and Collective Vibrational Evidence

Chou et al. (2020s)

- Phononic properties of DNA demonstrate that DNA functions as a phonon waveguide, supporting the mechanical wave propagation model central to the magnonic framework

Turton et al. (2014)

- THz spectroscopy reveals collective vibrational modes in biomolecules coupled to hydration shell dynamics (Nature Communications)—confirming that DNA's vibrational behavior is not isolated but coupled to its aqueous environment

González-Jiménez et al. (2016)

- Fast dynamics of water around DNA measured via optical Kerr effect spectroscopy—picosecond-scale hydration dynamics demonstrate that water actively mediates coupling between DNA's vibrational modes and the surrounding field, strengthening the "hydration sensitivity" mechanism

6.7.4 Heart Coherence Studies

HeartMath Institute Research

Heart EM field

- 5000x stronger than brain's magnetic field at the organ surface (detectable several feet from the body at ~100 pT)

HRV coherence

- Characteristic 0.1 Hz oscillation during positive emotional states

Brain-heart sync

- During coherence, brainwaves entrain to heart rhythm

Interpersonal effects

- One person's cardiac rhythm detectable in another's EEG

Heart as Primary Transducer

- Heart's toroidal field matches optimal antenna geometry

McCraty (2003)

- Heart responds to future stimuli before brain—heart receives first. This presentiment finding remains contested; see Wagenmakers et al. (2015) for methodological critiques of similar premonition research.

Supports model

- Heart as biofield primary generator, DNA as core antenna

Global Coherence and Extended Field Effects

Global Coherence Initiative (HeartMath)

- Synchronized HRV coherence observed across geographically separated groups during collective meditation events—supporting the nonlocal field coupling model where coherent biofields entrain across distance

Radin et al. (2012)

- Electrocortical activity prior to unpredictable stimuli extends McCraty's heart-precognition findings to brain activity, suggesting the biofield's anticipatory function operates across multiple physiological subsystems

6.7.5 Gariaev's Wave Genetics (Requires Validation)

Key Claims

DNA reads like text

- Linguistic analysis shows statistical patterns similar to human language

Laser-DNA information transfer

- Recorded laser light modulated by DNA can carry information

Phantom DNA effect

- Scattering pattern persists after sample removed

Status

- Published primarily in Russian journals
- Limited Western replication
- If validated, would strongly support DNA-as-torsion-antenna model
- Extraordinary claims require extraordinary evidence
- Gariaev's methodology has been criticized for insufficient controls and lack of independent replication. The phantom DNA effect in particular has not been reproduced by any independent laboratory.

6.7.6 Torsion Field Integration

The evidence aligns with torsion field predictions (Chapter 0):

Evidence Type	Torsion Interpretation
Biophotons	Visible manifestation of torsion activity
Bioelectricity	Voltage gradients create spin polarization $\rightarrow$ torsion coupling

Evidence Type	Torsion Interpretation
Phantom DNA	Torsion fields persist without physical source
Heart field	Toroidal blood flow = spinning mass → strong torsion
Morphic effects	Torsion-mediated information transfer

6.7.7 Sheldrake's Morphic Resonance and DNA Reception

Rupert Sheldrake's morphic resonance theory (detailed in Chapter 3: Demodulation) provides the information-field substrate that DNA receives. The magnonic RLC antenna model developed in this chapter specifies the **reception mechanism** for morphic templates.

Key connections:

- **Morphic fields** contain species-level patterns, habits, and memories accumulated across generations
- **DNA's helical geometry** provides the antenna optimized for receiving these nonlocal patterns
- **Chromatin topology (k)** determines which morphic frequencies can couple into the biological system
- **Ratcheting** explains how morphic information becomes stably encoded in individual organisms

Sheldrake observed that rats learning a new maze in one location made it easier for rats everywhere to learn the same maze—even without physical contact. The DNA antenna model provides a mechanism: coherent patterns broadcast from activated DNA become available as morphic templates, received by DNA antennas tuned to similar frequencies.

This bidirectional flow—reception of morphic templates AND contribution back to the morphic field—positions DNA as both reader and writer to the collective information substrate.

6.7.8 Epigenetic Evidence for Environment-DNA Coupling

The ratcheting model (Section 6.4.4-6.4.5) claims that coherent practices produce stable DNA modifications—experience → stable geometric change. While the model predicts geometric antenna reconfiguration specifically, the broader claim that experience produces stable, heritable DNA modifications has substantial empirical support through epigenetic research.

Meaney Lab, McGill (Nature Neuroscience, 2004)

- Maternal care in rats produces stable methylation changes in the glucocorticoid receptor gene (NR3C1) that persist into adulthood—demonstrating that experience produces stable DNA modification without altering sequence

Yehuda et al. (Biological Psychiatry, 2016)

- Holocaust survivor offspring show altered methylation at FKBP5 gene—intergenerational epigenetic transmission demonstrates that intense experience can produce DNA modifications that propagate across generations

Kaliman et al. (Psychoneuroendocrinology, 2014)

- Eight hours of mindfulness meditation produces measurable changes in histone deacetylase genes and inflammatory gene expression—demonstrating that coherent practice produces rapid, measurable DNA-level changes

Bhasin et al. (PLOS ONE, 2013)

- Relaxation response practice alters gene expression in energy metabolism, mitochondrial function, and insulin secretion pathways—confirming that sustained coherent practice produces systematic gene expression changes

Significance for the model: These studies confirm the core biological claim underlying ratcheting: coherent practices produce stable DNA modifications. While they measure epigenetic marks rather than geometric antenna properties directly, they establish that experience → stable DNA change is empirically real, providing the biological substrate for the ratcheting mechanism.

6.7.9 Quantum Biology Evidence

The magnonic framework (Section 4) proposes that collective quantum-scale excitations propagate along DNA's ordered helical structure. This claim gains plausibility from the growing field of quantum biology, which has demonstrated quantum coherence in biological systems at physiological temperatures.

Engel et al. (Nature 446, 2007)

- Long-lived quantum coherence observed in photosynthetic complexes at physiological temperatures—demonstrating that biological systems can sustain quantum coherence despite thermal noise

Turin (Chemical Senses, 2002)

- Quantum tunneling proposed in olfactory receptor function (vibration theory of smell)—suggesting quantum-scale mechanisms operate in biological molecular recognition

Hameroff & Penrose (Physics of Life Reviews, 2014)

- Updated Orch-OR model proposing quantum coherence in microtubules—extending quantum biological claims to information-processing structures within cells

Lambert et al. (Nature Physics, 2013)

- Comprehensive review "Quantum Biology" covering photosynthesis, avian navigation, and enzymatic tunneling—establishing quantum coherence as a legitimate biological phenomenon across multiple systems

Significance for the model: If quantum coherence operates in photosynthetic complexes and microtubules at biological temperatures, then spin-wave (magnonic) propagation along DNA's ordered helical structure becomes more plausible. These studies establish precedent for quantum-scale collective phenomena in biology, supporting the physical basis of the magnonic RLC framework.

6.7.10 Mechanism Tiering and Falsification Map

To reduce overstatement risk, core mechanism claims are tagged at first doctrine decision point:

Mechanism Claim	Tier	Current Support	Falsification Path
DNA geometry modulates measurable resonance behavior	L2	THz spectroscopy + structural studies	Controlled resonance shifts fail to track geometry changes
Epigenetic ratcheting provides durable antenna retuning	L2-L3	Meditation/epigenetic and stress-transmission studies	Longitudinal studies show no persistence beyond acute state
Magnonic spin-wave transport contributes materially to biofield coupling	L3	Quantum-biology analogy support only	No measurable spin-wave signatures under biologically relevant conditions
Consciousness-level practice causally drives torsion coupling gain	L3-L4	Correlational evidence only	Practice intensity fails to correlate with independent coupling proxies

Interpretation rule: L3+ claims remain conditional and should be paired with explicit test plans before operational adoption.

6.8 Predictions

6.8.1 DNA Antenna Predictions

P1: DNA resonance frequencies should be measurable and correspond to geometric parameters at multiple folding scales.

P2: DNA activation states should correlate with measurable geometric changes (methylation patterns, chromatin accessibility).

P3: Environmental torsion/EM fields at resonant frequencies should affect gene expression and DNA geometry.

P4 [L3-HYPOTHESIS]: Organisms with more complex DNA folding achieve higher effective Z_0, enabling coupling to higher density tiers. The fractal folding acts as an impedance transformer, stepping up effective Z_0 beyond what simple geometry would allow. This remains speculative until direct coupling proxies are validated against the falsification map in Section 6.7.10.

6.8.2 Biofield Predictions

P5: Coherent biofield states should correlate with improved healing and intuition.

P6: Heart field coherence should predict success in torsion-based information reception (e.g., remote viewing).

P7: Group biofield coherence should show N^2 scaling effects on measurable outcomes.

6.8.3 Transceiver Predictions

P8: Skilled meditators should show evidence of stronger DNA "transmission" (ideas spreading, morphic field influence).

P9: DNA geometric changes from practice should be measurable (epigenetic markers) and correlate with reported capacity changes.

P10: Once activated, DNA geometry should resist regression even under stress (ratchet test).

6.9 Assumptions, Limitations & Falsification

Assumptions

1. DNA functions as a torsion field antenna (not merely a chemical information store)
2. The magnonic framework (spin-wave propagation along DNA) is physically valid
3. Chromatin topology changes constitute antenna tuning
4. Epigenetic modifications correspond to impedance ratcheting
5. The biofield provides a local torsion field environment that modulates DNA antenna performance

Limitations

1. No direct measurement of torsion field coupling to DNA exists
2. The magnonic parameter mapping (L/C/R to spin stiffness/anisotropy/damping) is analogical
3. Ratcheting thresholds and Z_0 floor values are illustrative, not calibrated
4. The soul-DNA matching model is metaphysical and not empirically testable by current methods

Falsification

1. If DNA shows no THz resonance corresponding to geometric parameters — falsifies antenna model
2. If epigenetic changes from practice are fully reversible (no ratcheting) — falsifies lock-in mechanism
3. If biofield coherence has no measurable effect on gene expression — falsifies biofield-DNA coupling

---

Evidence Synthesis

- Detailed source sections: 6.7, 6.7.8, 6.7.9.

Assumptions

- Detailed source sections: 6.9.

Limitations

- Detailed source sections: 6.9.

Falsification

- Detailed source sections: 6.7.10, 6.9.

Predictions

- Detailed source sections: 6.8, 6.8.1, 6.8.2, 6.8.3.

Strategic Relevance

Why It Matters

1. **Biofield coherence as force multiplier**: If DNA antenna performance scales with biofield coherence, then practices enhancing HRV coherence represent a direct capability enhancement, not merely wellness.
2. **DNA ratcheting as irreversible development**: The lock-in mechanism implies that once personnel achieve certain impedance thresholds, the capability gain is permanent — informing training investment decisions.
3. **Environmental field effects**: The biofield-DNA recursive loop suggests that coherent group environments accelerate individual development — supporting colocation and group practice for high-performance teams.

What To Watch

- Monitor chapter prediction thresholds, proxy indicators, and coherence trend changes.

Boundaries of Use

- Apply this chapter as model-conditional doctrine; treat speculative elements as hypothesis overlays.

6.10 Connections to Other Chapters

- **Chapter 0 (Torsion Foundation)** DNA helix is the primary biological torsion transducer
- **Chapter 1 (Pure Consciousness)** DNA resonant cavities demodulate Source patterns via standing waves
- **Chapter 3 (Demodulation)** DNA performs cellular-level demodulation; broadcasts back into Akashic field
- **Chapter 5 (RLC)** Soul Z_0 determines which patterns DNA can access; DNA locks Z_0 floor via ratcheting
- **Chapter 8 (Phased Array)** Coherent DNA arrays across population enable collective effects

- **Chapter 11 (Seeder Intervention), Section 11.14.5** Genetic evidence for intervention—molecular signatures (HARs, gene duplications, CMAH deletion) consistent with the antenna modifications described in this chapter's magnonic framework (Section 4)

End of Chapter 6: Biofield and DNA Antenna System

Chapter 7: Eros and Creation

Sexual Polarity as the Foundation of Manifestation

KEY FINDINGS — Chapter 7: Eros and Creation

Evidence-tier key: [L1] established/replicated evidence; [L2] grounded extension with moderate uncertainty; [L3] speculative hypothesis; [L4] conceptual/anecdotal.

- **[L1-HIGH]** The polarity vector $P = (T_R - T_L)/(T_R + T_L)$ is a standard normalized ratio; the coupled oscillator energy exchange equations and RC charging curve for arousal are correct RF mathematics.
- **[L2-MEDIUM]** Piezoelectric coupling in collagen/fascia (Fukada & Yasuda 1957) provides a plausible physical mechanism for wave coupling during physical contact, independent of the torsion field model.
- **[L2-MEDIUM]** Epigenetic evidence (Dias & Ressler 2014) supports the claim that parental states at conception leave molecular marks affecting offspring gene expression.
- **[L3-SPECULATIVE]** The dimensional bridging model — sexual union creating a vortex that bridges density boundaries — is a metaphysical framework with no direct empirical test currently available.
- **[L3-SPECULATIVE]** The manifestation window at orgasm ($P_{manifest} = P_{source} \cdot \sigma^2_{peak} \cdot |AF|^2 \cdot (1 - |\Gamma|^2)$) translates traditional Tantric/magical claims into RF mathematics but lacks empirical calibration.

7.1 Introduction: The Erotic Cosmos

7.1.1 Creation as Cosmic Sexuality

Every creation is an act of polarity union. From the quantum foam to galactic formation to human conception, the universe operates through the dynamic tension and resolution of complementary forces. This chapter establishes **sexuality as the fundamental mechanism of creation** through the framework of torsion field polarity dynamics.

The thesis: What we experience as sexual energy is the 3D expression of a universal creative principle—the interaction between right-handed (masculine, T_R) and left-handed (feminine, T_L) torsion field chiralities. Sexual union between polarized beings creates a vortex that briefly bridges dimensional boundaries, enabling direct channel to Source power.

7.1.2 Cosmological Symmetry Breaking as Polarity Dynamics

The cosmological moment of creation follows the pattern:

Phase	Cosmological	Sexual
Pre-creation	Unified potential (Source)	Building tension/arousal
Symmetry breaking	T_R/T_L chirality separation	Polarity differentiation
Explosive release	Big Bang expansion	Orgasmic release
Structure formation	Matter/antimatter, galaxies	New life, manifestation
Ongoing dynamics	Cosmic expansion	Post-orgasmic integration

The universe is not merely *like* a sexual act—it **is** the primordial sexual act, still unfolding. Every subsequent creation recapitulates this original pattern at smaller scales.

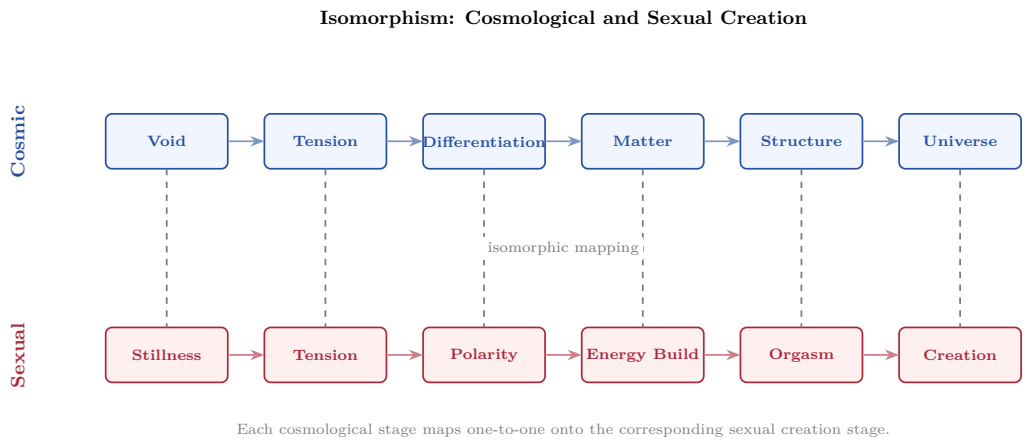

Figure 7.1: Isomorphism between cosmological creation and sexual creation — each stage maps one-to-one onto the other.

7.1.3 Why This Chapter Matters

This chapter bridges:

- **Individual dynamics** (Chapters 5-6): How your RLC circuit and DNA antenna interface with polarity fields
- **Collective dynamics** (Chapters 8-10): How polarity interactions scale to group and species-level effects
- **Control mechanisms** (Chapters 12-13): Why sexual energy is specifically targeted for corruption and harvesting

Understanding the creative power of sexual polarity explains both the extraordinary potential of conscious sexuality and the intensity of its suppression/distortion.

7.2 Polarity as Torsion Field Chirality

7.2.1 Torsion Field Handedness

From Chapter 0, torsion fields possess chirality—a left-handed (T_L) or right-handed (T_R) spiral orientation. These two polarities are the fundamental creative poles:

Property	Right-Handed (T_R)	Left-Handed (T_L)
Traditional label	Masculine	Feminine
Action tendency	Projective, outward	Receptive, inward
Spin orientation	Clockwise (observer POV)	Counter-clockwise
Energy flow	Emission, broadcasting	Absorption, receiving
Temporal tendency	Future-oriented	Past-integrating
Geometric association	Straight lines, angles	Curves, spirals

The mapping of clockwise rotation to masculine and counterclockwise to feminine is not arbitrary—it follows from established physics conventions and cross-cultural pattern recognition. In electromagnetism, the **right-hand rule** governs the relationship between rotation and propagation: a clockwise-rotating field (from the observer's perspective) corresponds to forward, outward propagation. This aligns naturally with the projective, outward-directed nature of the masculine pole.

The RF engineering convention reinforces this: **right-hand circular polarization (RHCP)** is designated the "positive" helicity and is the standard reference orientation in antenna theory and satellite communications.

The significance of chirality extends into biology, where molecular handedness creates profound functional differences. D-amino acids and L-amino acids are mirror images with entirely different biological roles—demonstrating that the *direction* of spiral matters, not merely the fact of spiraling.

Multiple independent traditions have converged on the same directional mapping: Hindu Tantra associates the right-hand path (*dakshina marga*) with projective/solar qualities, Chinese medicine maps clockwise qi circulation to yang, and Western alchemical traditions associate rightward rotation with the *sol* principle. This cross-cultural consistency suggests the mapping reflects something structural rather than culturally contingent.

> **Epistemic Note**: This is a mapping convention grounded in physics analogies and cross-traditional pattern recognition, not a claim about inherent superiority of either chirality. Just as RHCP and LHCP are equally valid polarization states in RF engineering, both torsion chiralities are equally necessary for creation. The assignment of labels follows from convention, not hierarchy.

7.2.2 The Polarity Vector

The **polarity vector P** quantifies the balance between masculine and feminine torsion components:

$$P = \frac{T_R - T_L}{T_R + T_L}$$

P Value	Interpretation
P = +1	Pure masculine ($T_L = 0$)

P Value	Interpretation
P = -1	Pure feminine ($T_R = 0$)
P = 0	Perfect balance ($T_R = T_L$)
P > 0	Masculine-dominant
P < 0	Feminine-dominant

Every entity has a polarity vector. Biological sex correlates with P but doesn't determine it—a biological male may have P < 0 (feminine-dominant polarity), and vice versa. The polarity vector describes torsion field orientation, not physical anatomy.

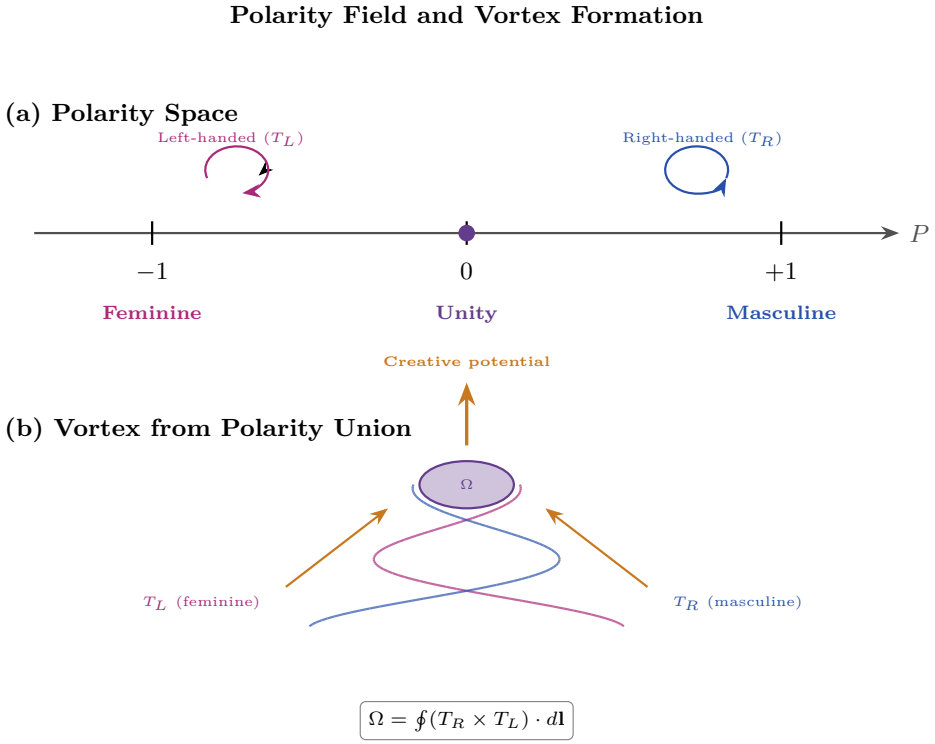

Figure 7.2: Polarity space and vortex formation — opposite chirality torsion spirals intertwine to produce creative potential.

7.2.3 Polarity Dynamics in Living Systems

In biological organisms:

$$P_{organism}(t) = P_{baseline} + \Delta P_{hormonal}(t) + \Delta P_{psychological}(t) + \Delta P_{spiritual}(t)$$

Where:

Variable	Description
$P_{baseline}$	Constitutional polarity (set by soul configuration)

Variable	Description
$\Delta P_{hormonal}$	Hormonal modulation (testosterone $\rightarrow$ P$\uparrow$, estrogen $\rightarrow$ P$\downarrow$)
$\Delta P_{psychological}$	Psychological state (assertive $\rightarrow$ P$\uparrow$, receptive $\rightarrow$ P$\downarrow$)
$\Delta P_{spiritual}$	Spiritual practice effects

Healthy individuals can modulate P fluidly while maintaining a stable baseline. Pathology involves either rigid fixation (cannot shift) or chaotic instability (no coherent baseline).

7.2.4 Complementarity and Attraction

Opposite polarities attract through torsion field dynamics:

$$F_{attraction} \propto |P_1| \cdot |P_2| \cdot \cos(\theta_{relative})$$

Where $\theta_{relative}$ is the relative phase angle between the two polarity vectors.

Maximum attraction occurs when:

1. Both polarities are strong (high $|P|$)
2. Polarities are opposite in sign (P_1 $\cdot$ P_2 $<$ 0)
3. Phases are aligned ($\theta_{relative} \approx 0$)

This explains the intense attraction between strongly polarized individuals of opposite polarity, and the relative indifference when either party lacks strong polarity or when polarities are same-signed.

> **Epistemic note [L3]**: This interpretive remark is maximally speculative and is offered as a philosophical provocation rather than a physics claim.
>
> **Interpretive Remark: Forces as Flows of Feeling.** Since Source is Eros (Section 7.1), the universe runs fundamentally on affect: the forces of nature are statistical laws governing the flows of feeling. The torsion-field attraction described by $F_{attraction}$ is therefore not merely *analogous* to gravity—it may be the same interaction at a different scale. Gravity, as a universally attractive force, is the macroscopic expression of Source's pull toward coherence and unity: love operating at the cosmological scale. The $\cos(\theta_{relative})$ term maps naturally—maximum phase alignment produces maximum attraction, just as resonance in feeling produces the strongest bonds.
>
> This reframes the hierarchy problem: gravity is not "weak" but rather the gentlest, most universal expression of the creative impulse, operating at the scale where all structures commune. What particle physics measures as a 32-order-of-magnitude gap between gravity and the strong force may instead reflect the difference between Source's universal background hum and its concentrated, short-range harmonics. The framework developed in Chapter 4 (resonant growth) and the cosmological torsion structure of Chapter 3 provide the formal setting; the point here is ontological—if creation is erotic at root, then every attractive force is a mode of love, and every repulsive force a phase-misalignment within it.

7.3 Sexual Union as Dimensional Bridge

7.3.1 Vortex Formation During Coupling

When two individuals with opposite polarity unite, their torsion fields form a **coupled vortex**:

$$\Omega = \oint (T_R \times T_L) \cdot d\mathbf{l}$$

This vortex strength Ω measures the intensity of the dimensional bridge formed during union. The equation is modeled on **circulation integrals** from electromagnetic theory—specifically Ampère's circuital law ($\oint \mathbf{B} \cdot d\mathbf{l} = \mu_0 I_{enc}$), which measures the total rotational magnetic field strength around a closed path to determine the enclosed current. In RF engineering, circulation integrals quantify how much rotational field energy exists within a bounded region.

Here, the cross product $T_R \times T_L$ represents the interaction between opposite torsion chiralities—analogous to how the magnetic field arises from the interaction of moving charges—and the closed line integral measures the total vortex strength of this interaction over the coupling region, just as Ampere's law measures enclosed current via magnetic field circulation.

Note: This formulation assumes T_R and T_L are vector fields. If they are scalar torsion amplitudes, the cross product should be replaced with a scalar product.

> **Epistemic Note**: This equation extends the mathematical form of established electromagnetic circulation integrals into the torsion field model. While the underlying physics of torsion fields remains speculative, the mathematical structure is borrowed directly from well-validated electromagnetic theory, preserving the relationship between rotational field interaction and enclosed energy.

Coupling Type	Typical Ω	Dimensional Access
Casual/mechanical	Low	Minimal bridge
Emotionally connected	Moderate	4D contact
Heart-coherent	High	4D-5D bridge
Tantric/ceremonial	Very high	Direct Source channel

The coupled vortex creates what this model terms a "dimensional bridge"—a region of **high spin coherence** where the combined torsion fields of both partners achieve sufficient phase-locked ordering to alter the effective properties of the local density boundary. As established in Chapter 0's torsion field framework, each density layer has a characteristic impedance boundary that normally prevents energy and information transfer between dimensions.

When two opposite-chirality torsion fields couple with sufficient strength and phase alignment, the resulting coherent region achieves an effective density boundary permeability that allows exchange across dimensional interfaces—a process termed **interdimensional phasing**.

The degree of dimensional access scales directly with spin coherence, which explains the progression shown in the table above: casual or mechanical coupling produces minimal coherent ordering and therefore minimal bridge formation, while tantric or ceremonial practice—which deliberately cultivates sustained, high-amplitude, phase-locked torsion field interaction—can achieve coherence levels sufficient for direct Source channel access.

This relationship between spin coherence and dimensional permeability is developed further as a general principle in Chapter 10 (*Spin Coherence Fundamentals*), where it applies beyond the sexual context to meditation, group ceremony, and technological applications.

7.3.2 The Vagina as Impedance Transformer

> **Epistemic Note**: This metaphor extends RF transformer concepts into metaphysical territory. It draws from esoteric traditions (Tantra, alchemy) that describe the feminine as "gateway" or "portal." The mathematical framing is speculative but internally consistent with the torsion field model.

In RF engineering, a transformer matches impedance between circuits of different characteristic impedances. The vagina functions as a **biological impedance transformer** between:

- The 3D physical realm (low Z)
- Higher dimensional creative potentials (high Z)

The transformation ratio:

$$n_{transform} = \sqrt{\frac{Z_{higher-D}}{Z_{3D}}} \cdot \sigma_{coherence}$$

Where $\sigma_{coherence}$ is the coherence level of the receiving partner.

Implications:

1. The feminine body contains specialized dimensional interface structure
2. Transformation efficiency depends on coherence (sacred sexuality vs. mechanical sex)
3. Through this interface, Source power can be stepped down to 3D manifestation capacity

7.3.3 Penetration as Wave Coupling

The physical act of penetration creates wave coupling between the two systems:

$$\eta_{coupling} = |P_1| \cdot |P_2| \cdot |\cos(\theta)|$$

Where η is the coupling efficiency. This determines how much of each partner's torsion field energy transfers to the other.

High coupling ($\eta \to 1$) requires:

- Strong opposite polarities
- Phase alignment (emotional/spiritual resonance)
- Physical coherence (relaxation, presence)

Low coupling ($\eta \to 0$) occurs when:

- Weak or similar polarities
- Phase misalignment (emotional discord)
- Physical tension or disconnection

> **Supporting Evidence**: Collagen and fascia exhibit piezoelectric properties—mechanical pressure generates measurable electrical potentials along connective tissue networks (Fukada & Yasuda, 1957; Athenstaedt, 1974). During physical coupling, sustained pressure and rhythmic motion at tissue interfaces would generate

oscillating piezoelectric signals through both partners' fascial networks, providing a plausible physical mechanism for the "wave coupling" described here independent of the torsion field model.

7.3.4 Energy Exchange Dynamics

During sexual union, energy flows bidirectionally:

$$\frac{dE_1}{dt} = \eta \cdot (E_2 - E_1) + P_{source} \cdot \Omega$$

$$\frac{dE_2}{dt} = \eta \cdot (E_1 - E_2) + P_{source} \cdot \Omega$$

The first term represents equilibration between partners (energy flows from higher to lower). The second term represents **Source power injection** through the vortex—both partners gain energy beyond what either brought.

These equations mirror **coupled resonator theory** in RF engineering. The first term ($\eta \cdot (E_2 - E_1)$) is the standard coupling equation for loosely coupled oscillators: energy flows from the higher-energy system to the lower-energy system until equilibrium is reached, with the coupling coefficient η determining the rate of transfer. This is identical in form to the equations governing coupled LC circuits, coupled cavities in microwave engineering, and coupled pendula in classical mechanics.

The second term ($P_{source} \cdot \Omega$) introduces an **externally pumped coupled oscillator** dynamic—analogous to a parametric amplifier or an injection-locked oscillator pair drawing power from an external pump source. In RF systems, such external pumping can cause the total energy of the coupled system to *exceed* the sum of the individual inputs, which is precisely the claim made here about Source power injection through the dimensional vortex.

> **Supporting Evidence**: Wilhelm Reich's orgone accumulator experiments (1940s-50s) documented measurable temperature differentials and radiation effects that he attributed to "orgone energy" concentrated during sexual arousal. Reich's orgone research has not been replicated under modern controlled conditions. It is cited here as historical precedent for the research direction, not as established evidence.

This is why conscious sexuality is generative rather than depleting. Mechanical sex involves only the first term (energy redistribution, often with net loss). Sacred sexuality activates the second term (Source injection through dimensional bridge).

7.4 Orgasm: The Coherence Peak

7.4.1 Orgasm as σ Maximum

Orgasm represents a **peak in torsion field coherence** σ. Throughout the sexual arousal cycle:

$$\sigma(t) = \sigma_{baseline} + \Delta\sigma_{arousal}(t)$$

The arousal function typically follows:

$$\Delta\sigma_{arousal}(t) = A \cdot \left(1 - e^{-t/\tau_{build}}\right) \cdot \left(1 - H(t - t_{orgasm})\right) + \text{spike at } t_{orgasm}$$

Where:

- A = arousal amplitude capacity
- τ_{build} = arousal time constant
- H = Heaviside step function
- t_{orgasm} = moment of orgasm

At orgasm, σ spikes to its maximum achievable value for that individual/pairing.

The arousal buildup function $\Delta\sigma(t) = A(1 - e^{-t/\tau})$ is a standard **RC charging curve**—the same exponential approach to a maximum used universally in circuit analysis to describe how a capacitor charges through a resistor. The time constant τ_{build} plays the same role as the RC time constant: it determines how quickly the system approaches its maximum capacity, with approximately 63% of full amplitude reached after one time constant.

This is not merely a convenient mathematical fit; it reflects the physical model that coherence builds through the gradual accumulation of phase-locked torsion field energy against a dissipative baseline, just as charge accumulates on a capacitor against resistive losses.

> **Supporting Evidence**: Korotkov's Gas Discharge Visualization (GDV) research documents electrical discharge patterns at the skin surface during states of heightened arousal. Whether these patterns reflect a "biofield" or simpler skin conductance changes remains debated. While GDV methodology remains debated in mainstream science, the measurements provide a potential empirical window into the coherence dynamics modeled here.

7.4.2 The Manifestation Window

> **Epistemic Note**: The claim that orgasm creates a "manifestation window" derives from Tantric and magical traditions (notably documented by Swerdlow and related sources). The mathematical formulation is speculative, translating traditional claims into RF framework.

During the σ peak, a brief **manifestation window** opens:

$$P_{manifest} = P_{source} \cdot \sigma_{peak}^2 \cdot |AF_{intention}|^2 \cdot (1 - |\Gamma_{density}|^2)$$

Where:

- P_{source} = available Source power through vortex
- σ_{peak} = peak coherence at orgasm
- $AF_{intention}$ = array factor of focused intention
- $\Gamma_{density}$ = density reflection coefficient (from Chapter 0)

Each component of this equation has a direct RF engineering counterpart. The **array factor** $|AF|^2$ comes from phased array antenna theory, where it quantifies how effectively individual radiating elements combine their signals through constructive interference—here applied to the "array" of intentional focus.

The **reflection coefficient** term $(1 - |\Gamma|^2)$ comes from transmission line theory, where it represents the fraction of power that successfully transmits across an impedance boundary rather than reflecting back; the density reflection coefficient from Chapter 0 plays the same role at dimensional boundaries.

The σ^2 dependence mirrors the fundamental relationship between field strength and power density in RF: radiated power is proportional to the square of the electric field amplitude ($P \propto |E|^2$), so coherence (the torsion field analog of field amplitude) enters as a squared term in the power equation.

The σ^2 dependence is critical: Doubling coherence quadruples manifestation power. This explains why scattered, unconscious orgasm has minimal creative effect, while highly coherent, intentional orgasm can have dramatic manifestation capacity.

7.4.3 Intention Encoding

Whatever intention is held at the moment of orgasm becomes encoded into the torsion field pattern:

$$\Psi_{encoded} = \Psi_{intention} \cdot e^{j\phi_{orgasm}} \cdot \sigma_{peak}$$

The encoded pattern then propagates according to torsion field dynamics (Chapter 0), potentially manifesting as:

- New life (conception)
- Reality shifts (magical working)
- Energetic imprints (bonding, programming)
- Creative inspiration (artistic/inventive)

7.4.4 Mutual vs. Solo Orgasm

Aspect	Solo Orgasm	Mutual Orgasm
Vortex strength Ω	Minimal (self-referential)	Strong (cross-coupled)
Source access	Limited	Amplified
Manifestation power	$\propto \sigma^2$	$\propto (\sigma_1 \cdot \sigma_2)^2$
Bonding effect	None	Strong energetic linking
Typical duration	Brief	Can be extended

Mutual simultaneous orgasm creates maximal vortex strength and manifestation potential. However, solo practice with sufficient coherence and intention can still access significant creative power.

7.5 Birth: The Binding of Dimensions

7.5.1 Conception as Dimensional Anchoring

At conception, a soul attaches to the fertilized zygote. This is a **dimensional binding event**:

> **Epistemic Note**: Soul attachment during conception is a metaphysical claim found across esoteric traditions. The timing (conception vs. later developmental stages) varies

by tradition. This section presents one coherent model without claiming definitive knowledge of the process.

$$\Psi_{incarnate} = \Psi_{soul} \otimes \Psi_{body-template}$$

Where $\otimes$ represents the binding operation between the incoming soul's torsion pattern and the morphogenetic template encoded in the DNA.

7.5.2 The Gestation Process

Over the gestation period, the dimensional binding strengthens:

$$\eta_{binding}(t) = 1 - e^{-t/\tau_{gestation}}$$

Where $\tau_{gestation} \approx 40$ weeks for humans.

Trimester	η_binding	Significance
First	$0 \rightarrow 0.63$	Initial attachment, vulnerable
Second	$0.63 \rightarrow 0.86$	Strengthening integration
Third	$0.86 \rightarrow 0.95$	Near-complete binding
Birth	$\sim 0.95 \rightarrow 0.99$	Final anchoring

Epistemic Note: The specific values in this table (0.63, 0.86, 0.95) follow mathematically from the exponential model: $1 - e^{-1} \approx 0.63$, $1 - e^{-2} \approx 0.86$, $1 - e^{-3} \approx 0.95$. These are illustrative of the general trajectory predicted by the model, not empirical measurements. The key qualitative insight is that dimensional binding strengthens nonlinearly—the most vulnerable period is early in gestation, with diminishing marginal strengthening over time. This pattern is consistent with clinical observations of miscarriage risk declining sharply after the first trimester.

Supporting Evidence: Mainstream developmental research supports the qualitative pattern: maternal cortisol exposure during gestation correlates with altered HPA axis development, temperament, and stress reactivity in offspring (Glover, 2011; Van den Bergh et al., 2017). In the torsion field model, chronic stress represents incoherent field states ($\sigma \downarrow$)—the empirical correlation between prenatal stress and developmental effects is consistent with the gestation coherence model.

Implications:

1. Early pregnancy is more dimensionally unstable (higher spontaneous termination)
2. Prenatal experiences affect binding quality
3. Birth trauma can disrupt the final anchoring phase

7.5.3 Light Body Development

The incoming soul brings its accumulated **light body structure** (from Chapter 2, DNA activation levels). This interacts with the genetic template:

$$Z_{0,child} = f(Z_{0,soul}, Z_{0,genetic-template}, \eta_{binding})$$

Where:

- $Z_{0,soul}$ = characteristic impedance of incoming soul
- $Z_{0,genetic-template}$ = template impedance from parental genetics
- $\eta_{binding}$ = quality of dimensional binding

High-Z_0 souls may choose lower-Z_0 genetic templates for specific learning purposes, or vice versa. The match/mismatch affects incarnation challenges.

7.5.4 The Role of Parental Coherence

Parental coherence during conception and gestation affects offspring development:

$$\sigma_{child-baseline} \propto \sigma_{conception} \cdot \langle \sigma_{gestation} \rangle$$

Where $\langle \sigma_{gestation} \rangle$ is the average coherence maintained during pregnancy.

The proportionality $\sigma_{child} \propto \sigma_{conception} \cdot \langle \sigma_{gestation} \rangle$ is a conceptual model expressing that both the initial conditions at conception and the sustained conditions throughout gestation contribute multiplicatively to the child's baseline coherence. This mirrors signal-to-noise considerations in RF communications engineering: a transmitted signal's integrity at the receiver depends on both the **quality of the original encoding** (the signal-to-noise ratio at the transmitter, analogous to $\sigma_{conception}$) and the **channel conditions during propagation** (path loss, interference, and fading experienced in transit, analogous to $\langle \sigma_{gestation} \rangle$).

The multiplicative form captures this: weakness in either factor—poor initial conditions *or* poor sustained conditions—significantly degrades the outcome. A pristine signal degraded by a noisy channel arrives corrupted, just as a high-coherence conception followed by a chaotic gestation may not produce optimal baseline coherence. This parallels communications link budget analysis, where total system performance is the product of each stage's efficiency.

> **Supporting Evidence**: Epigenetic research demonstrates that parental states at conception and during gestation leave measurable molecular marks (DNA methylation, histone modification) that affect offspring gene expression across generations (Dias & Ressler, 2014). This provides a physical mechanism consistent with the coherence transmission model: parental field states encode into epigenetic marks that modulate the child's baseline biological configuration.

Children conceived in high-coherence states (love, sacred sexuality) typically show:

- Higher baseline σ
- Easier access to higher states
- More stable temperament
- Stronger intuitive capacities

7.5.5 Celestial Spin-Locking: The Astrology Mechanism

At the moment of birth, the gravitational and electromagnetic configuration of nearby celestial bodies acts as an ensemble of injection-locking oscillators—a **spin team**. Each planet, star, and lunar body is a massive spin ensemble generating a characteristic torsion field signature. The specific angular configuration at birth creates a unique composite injection-locking pattern that imprints on the incoming soul's spin state during the final stage of dimensional descent.

The Spin Team Concept

The planetary configuration at birth forms a composite oscillator whose combined torsion pattern provides the phase reference against which the soul's final dimensional binding is locked. Each planet p contributes an injection signal:

$$S_p = A_p \cdot \sin(\omega_p t + \phi_p)$$

where A_p reflects the planet's torsion field strength (proportional to mass and spin rate), ω_p its orbital frequency, and ϕ_p its angular position at the moment of birth. The composite natal lock signal is:

$$S_{\text{natal}} = \sum_p w_p \cdot S_p$$

where w_p are geometric weighting factors (angular proximity, elevation, house position). The soul locks to this composite signal via the standard injection-locking condition (Chapter 9):

$$\Delta\omega_{\text{lock}} < \frac{\omega_0}{2Q_{\text{soul}}}$$

Different planetary configurations produce different lock-in patterns, establishing different baseline resonant characteristics for the incarnating soul.

Dimensional Descent and Phase Reference

The soul descends through density tiers (Chapter 2), encountering reflection coefficients at each impedance boundary. The celestial spin-locking provides the phase reference that guides the soul through each boundary, determining the specific "path" through the density cascade. This path-dependence means that two souls of identical Z_0 but different birth configurations will navigate the dimensional boundaries differently, producing different baseline personality structures despite similar overall development levels.

Evidence and Counter-Evidence

- **Gauquelin Mars Effect** (1955–1988): Statistician Michel Gauquelin found significant correlations between planetary positions at birth and professional eminence—Mars for athletes, Saturn for scientists, Jupiter for politicians. The Belgian Comité Para (1976) replicated the Mars effect. Ertel (1988) independently confirmed the effect with an extended dataset.
- **Season-of-birth effects**: Robust epidemiological correlations exist between birth timing and schizophrenia risk (Davies et al., 2003), personality traits (Disanto et al., 2012), autoimmune conditions, and longevity. These are well-established in medical literature regardless of astrological interpretation.
- **Counter-evidence**: Carlson (1985) found in a double-blind test that astrologers could not match natal charts to personality profiles above chance. Dean (2003) found no personality correlation in a time-twin study of people born minutes apart.
- **Epistemic framing**: The framework predicts subtle torsion-field effects from planetary positions—not the detailed character predictions of traditional horoscopic astrology. The Gauquelin-type statistical effects (broad professional tendencies correlated with specific planets) are more consistent with weak injection locking than with specific horoscopic predictions. The model predicts *tendencies* at the population level, not deterministic individual outcomes.

Falsification

If birth-time planetary positions show zero correlation with any measurable trait in sufficiently large studies ($N > 100{,}000$) with rigorous methodology, the celestial spin-locking model would be significantly weakened. Conversely, if season-of-birth effects can be fully explained by conventional mechanisms (vitamin D, temperature, infection cycles) without residual planetary position effects, the torsion-field interpretation would require revision.

7.6 Sexual Magick: Conscious Application

> **Epistemic Note**: Sexual magick practices are documented across traditions (Tantra, Western ceremonial magic, Taoism). Claims of efficacy rest on practitioner reports and traditional lineage rather than controlled studies. This section describes the theoretical framework, not clinical recommendations.

7.6.1 Solo Practice

Solo sexual practice can be used for:

1. **Energy cultivation** (building and circulating sexual energy)
2. **Intention manifestation** (encoding desires at orgasm)
3. **Shadow integration** (conscious engagement with sexual material)
4. Z_0 **development** (building sovereignty through self-mastery)

Key parameters:

$$P_{solo} = \sigma_{peak}^2 \cdot |AF_{intention}|^2 \cdot \eta_{circuit}$$

Where $\eta_{circuit}$ is the internal energy circulation efficiency (improved through practice).

7.6.2 Partnered Practice

Partnered practice amplifies through coupled resonance:

$$P_{partnered} = (\sigma_1 \cdot \sigma_2)^2 \cdot |P_1| \cdot |P_2| \cdot |\cos(\theta)| \cdot |AF_{shared-intention}|^2$$

Requirements for effective partnered practice:

1. Strong opposite polarities (|P_1| and |P_2| both high, opposite signs)
2. Phase alignment ($\theta \to 0$, emotional/spiritual resonance)
3. Individual coherence (both σ values high)
4. Shared intention (coherent AF vector)
5. Energetic trust (no protective shielding between partners)

7.6.3 Coupling Efficiency Factors

The overall coupling efficiency:

$$\eta_{total} = \eta_{polarity} \cdot \eta_{phase} \cdot \eta_{physical} \cdot \eta_{trust}$$

Factor	Optimal Condition	Degrading Factors
$\eta_{polarity}$	Strong opposite polarities	Weak/similar polarities
η_{phase}	Emotional alignment	Discord, resentment
$\eta_{physical}$	Relaxed presence	Tension, rush
η_{trust}	Complete openness	Guardedness, trauma

Polarity efficiency ($\eta_{polarity}$) reflects the strength of the field gradient between partners. In electrical systems, current flows in proportion to voltage differential—a 12V battery drives more current than a 1.5V cell across the same resistance. Similarly, strongly differentiated polarities create steeper torsion field gradients across the coupling interface, driving more vigorous energy exchange.

When both partners have strong but opposite polarity vectors (high $|P_1|$ and $|P_2|$ with opposite signs), the resulting field gradient maximizes energy transfer. Weak or similar polarities produce shallow gradients and correspondingly weak coupling, regardless of how favorable the other efficiency factors may be.

Phase efficiency (η_{phase}) captures the degree to which partners' torsion fields oscillate in temporal alignment—their emotional and spiritual resonance. When two oscillators are in phase, their amplitudes add constructively (the fields reinforce each other); when out of phase, they interfere destructively (the fields partially cancel). Emotional discord, unresolved resentment, or spiritual misalignment between partners creates phase offsets that cause partial destructive interference in the coupled torsion field, reducing the effective vortex strength regardless of how strong the individual fields may be.

Physical efficiency ($\eta_{physical}$) addresses the body's role as the torsion field antenna. Physical tension, distraction, or rushing causes the biofield to contract—analogous to an antenna with high resistive losses that converts signal energy into heat rather than radiating it effectively. When the body is relaxed and fully present, the biofield extends to its full effective aperture, maximizing the coupling cross-section available for energy exchange. This is why practices emphasizing slow breathing, muscular relaxation, and sustained presence consistently produce stronger coupling effects than rushed or tension-dominated encounters.

Trust efficiency (η_{trust}) may be the most consequential factor. Energetic shielding—whether from unresolved trauma, emotional guardedness, or conscious withholding—functions as a **Faraday cage** between partners, attenuating the torsion field coupling in direct proportion to the shielding's effectiveness. Just as a Faraday cage blocks electromagnetic fields from reaching the interior conductor, energetic armor prevents a partner's torsion field from fully penetrating to the core of the other's biofield.

Healing trauma and building genuine trust progressively lowers this shielding, increasing η_{trust} toward unity.

Because total efficiency is **multiplicative** ($\eta_{total} = \eta_{polarity} \cdot \eta_{phase} \cdot \eta_{physical} \cdot \eta_{trust}$), weakness in any single factor dramatically reduces overall coupling. If any one factor approaches zero, total efficiency approaches zero regardless of the others—a mathematical expression of the experiential reality that strong polarity with deep distrust, or perfect trust with no polarity differentiation, both fail to produce powerful coupling. Effective practice requires attention to all four factors simultaneously.

7.6.4 Practical Considerations

Before practice:

- Clear intention setting
- Energy building (arousal without release)
- Coherence cultivation (meditation, breath)
- Space preparation (energetic clearing)

During practice:

- Maintain intention focus
- Synchronize breath
- Cultivate presence over performance
- Allow energy to build before release

At orgasm:

- Hold intention clearly
- Allow complete surrender
- Remain present through the peak
- Maintain connection afterward

After practice:

- Integration period (don't rush away)
- Gratitude exchange
- Rest (energy integration)

7.7 Preliminary: Corruption of Sexual Power

7.7.1 Why Sexual Energy is Targeted

Sexual energy is targeted for corruption because:

1. **It's the primary creation mechanism** accessible to incarnate humans
2. **High-σ states are vulnerable** to intention encoding (can be programmed)
3. **Trauma coupling is most effective** during orgasmic states
4. **Loosh harvesting yields high energy** from sexually-charged emotions

> **Note**: Full treatment of sexual corruption mechanisms appears in **Chapter 12 (The Fall)** and **Chapter 13 (Paradigm Shielding)**. This section provides preliminary framework only.

7.7.2 Corruption Patterns

Pattern	Mechanism	Effect
Shame programming	C↑ (trauma charge storage)	Blocks natural expression
Addiction loops	Hijacked dopamine → low-σ compulsion	Energy drainage without creation

Pattern	Mechanism	Effect
Dissociation	Separation of body/consciousness	Nullifies manifestation capacity
Pornographic programming	False polarity templates	Distorted attraction patterns
Trauma bonding	Pain-pleasure coupling	Parasitic attachment formation

7.7.3 The Inversion Strategy

The control system doesn't merely suppress sexuality—it **inverts** it:

- Natural creative force → energy extraction mechanism
- Bonding/love → addiction/trauma
- Sovereignty → dependency
- Manifestation → dissipation

Detailed analysis of inversion mechanisms is developed in Chapters 12-13.

7.8 Healing and Reclamation

7.8.1 Sexual Trauma as C Charging

From Chapter 5, capacitance C represents shadow storage—unintegrated charge. Sexual trauma specifically charges C with high-intensity patterns:

$$\Delta C_{trauma} = \int I^2_{traumatic} \cdot dt$$

This stored charge:

1. **Lowers** Z_0 (C↑ → Z = $\sqrt{}$(L/C)↓)
2. **Widens lock bandwidth** (more susceptible to capture)
3. **Creates trigger patterns** (stored charge discharges when activated)
4. **Blocks natural flow** (energy diverts around charged areas)

7.8.2 The Healing Process

Healing involves **controlled discharge** of stored traumatic charge:

$$\frac{dC_{trauma}}{dt} = -\frac{C_{trauma}}{\tau_{integration}} \cdot H(\sigma > \sigma_{threshold})$$

Where:

- $\tau_{integration}$ = integration time constant (depends on support/safety)
- H = activation function (requires sufficient coherence to process)

Requirements for healing:

1. **Safe container** (therapy, trusted relationship, ceremonial space)
2. **Sufficient** σ (coherence to hold the discharge)
3. **Willingness** (conscious engagement with material)
4. **Time** (integration cannot be rushed)

7.8.3 Reclamation Phases

Phase	Focus	Signs of Progress
Safety	Establishing groundedness	Reduced activation, stable baseline
Awareness	Recognizing patterns	Pattern insight without overwhelm
Expression	Controlled discharge	Emotional release with integration
Integration	New pattern formation	Changed responses to triggers
Reclamation	Full creative access	Natural sexual flow, manifestation capacity

7.8.4 Z_0 Restoration

As C_trauma decreases, Z_0 naturally rises:

$$Z_0 = \sqrt{\frac{L}{C_{baseline} + C_{trauma}}}$$

Healing sexual trauma is one of the most effective Z_0 development paths because:

1. Sexual trauma typically creates large C_trauma
2. The charge reduction has immediate Z_0 benefits
3. Restored creative capacity accelerates further development
4. Breaking parasitic attachments reduces ongoing drainage

Evidence Synthesis

- Detailed source sections: none explicitly labeled in this chapter.

Assumptions

- Detailed source sections: none explicitly labeled in this chapter.

Limitations

- Detailed source sections: none explicitly labeled in this chapter.

Falsification

- Detailed source sections: none explicitly labeled in this chapter.

Predictions

- Detailed source sections: none explicitly labeled in this chapter.

Strategic Relevance

Why It Matters

1. **Coherence readiness as force protection**: Low-Q states widen capture bandwidth, so trauma integration and autonomic regulation should be treated as readiness requirements.
2. **Pair-coupling risk management**: Coupling efficiency (η) can amplify or degrade team coherence under stress; pair dynamics should be assessed explicitly in high-trust roles.
3. **High-emotion window controls**: Peak-coherence states can increase susceptibility to suggestion; decision-critical activities should include delay and review controls after high-intensity states.
4. **Operational lane separation**: Use measurable proxies (HRV synchrony, stress-recovery slopes, attentional stability) for action; keep metaphysical interpretation in exploratory annex lanes.

What To Watch

- Monitor chapter prediction thresholds, proxy indicators, and coherence trend changes.

Boundaries of Use

- Apply this chapter as model-conditional doctrine; treat speculative elements as hypothesis overlays.

7.9 Chapter Summary

7.9.1 Core Principles

Principle	Statement
Universal sexuality	Creation operates through polarity union at all scales
Torsion chirality	Masculine (T_R) and feminine (T_L) are fundamental poles
Dimensional bridging	Sexual union creates vortex accessing higher dimensions
Coherence power	Manifestation scales with σ^2 (coherence squared)

Principle	Statement
Targeted corruption	Sexual energy is specifically attacked due to creative power
Reclamation path	Healing sexual trauma is major Z_0 development route

7.9.2 Key Equations

Polarity Vector:	$P = \frac{T_R - T_L}{T_R + T_L}$
Coupling Efficiency:	$\eta = \lvert P_1 \rvert \cdot \lvert P_2 \rvert \cdot \lvert \cos(\theta) \rvert$
Vortex Strength:	$\Omega = \oint (T_R \times T_L) \cdot d\mathbf{l}$
Manifestation Power:	$P_{manifest} = P_{source} \cdot \sigma_{peak}^2 \cdot \lvert AF_{intention} \rvert^2 \cdot (1 - \lvert \Gamma \rvert^2)$
Dimensional Binding:	$\eta_{binding}(t) = 1 - e^{-t/\tau_{gestation}}$

7.9.3 Strategic Note

For individuals:

1. Sexual energy is creative power, not shameful impulse
2. Coherence determines manifestation capacity
3. Healing sexual trauma directly raises Z_0
4. Conscious sexuality is a legitimate development path

For relationships:

1. Polarity difference drives attraction and creative capacity
2. Phase alignment (emotional resonance) enables coupling
3. Mutual coherence amplifies beyond individual capacity
4. Sacred sexuality accesses Source power directly

For understanding control systems:

1. Sexual corruption is strategic, not accidental
2. Shame/addiction/trauma serve specific harvesting functions
3. Reclaiming sexual sovereignty threatens control architecture
4. The subject is deliberately confused to maintain exploitation

7.9.4 What the Model Assumes

1. **Torsion field chirality maps to sexual polarity**: The model assumes that the right-handed/left-handed torsion field distinction established in Chapter 0 directly corresponds to masculine/feminine creative poles, and that biological sex correlates (but doesn't determine) torsion chirality.
2. **Coupling requires opposite polarity**: The vortex formation model assumes that creative coupling requires opposite-chirality torsion fields. Same-chirality coupling is assumed to produce weak or null vortex effects.

3. **Coherence is the primary variable**: The model assumes σ (phase-locked ordering) is the dominant factor determining the quality and power of sexual coupling, over and above physical, emotional, or biochemical factors considered in isolation.
4. **Source power is externally available**: The energy exchange model assumes an external Source power term that can inject energy into coupled systems. This assumes Source is real and accessible, not merely a modeling convenience.
5. **Soul pre-exists conception**: The dimensional binding model assumes an incoming soul that attaches to the zygote—a metaphysical claim not empirically verifiable by current methods.
6. **Exponential binding dynamics**: Gestation binding is modeled as exponential approach (RC charging), which assumes a single dominant time constant rather than multi-stage or threshold-driven dynamics.

7.9.5 Known Limitations

1. **No empirical calibration**: The equations use RF mathematical forms but lack empirically measured parameter values for torsion field quantities. The model is structurally grounded but not quantitatively calibrated.
2. **Binary polarity simplification**: Real gender/polarity may be more complex than a single scalar $P \in [-1, +1]$. Multi-dimensional polarity models might better capture the full spectrum of human sexual/creative expression.
3. **Individual focus**: The chapter primarily models dyadic (two-person) coupling. Group sexual dynamics, non-dyadic configurations, and same-sex coupling receive minimal treatment.
4. **Cultural bias risk**: The mapping of masculine/feminine to specific torsion chiralities, while grounded in physics conventions, risks importing cultural assumptions about gender roles into supposedly neutral physics.
5. **Unfalsifiable metaphysics**: Several core claims (soul attachment at conception, Source power injection, manifestation windows) involve metaphysical processes that may not be empirically accessible, limiting scientific testability.
6. **No mechanism for consciousness-field coupling**: The model describes *what* happens (coherence enables dimensional bridging) but does not specify the physical mechanism by which subjective consciousness couples to torsion fields.

7.9.6 Falsification Conditions

The model would be falsified by:

1. **No polarity coupling effects**: If biofield measurements (HRV, EEG, GDV) show no difference between opposite-polarity and same-polarity pairings during sexual coupling—the polarity vector model predicts measurable coupling differences based on $P_1 \cdot P_2$.
2. **No coherence-dependent effects**: If measured biofield coherence during sexual activity shows no correlation with reported subjective quality, bonding strength, or creative/manifestation outcomes—the σ^2 scaling prediction would fail.
3. **No gestation binding curve**: If spontaneous termination rates during pregnancy do NOT follow a declining exponential pattern (highest early, diminishing over time)—the exponential binding model would be falsified. (Note: clinical data broadly supports this pattern.)
4. **No parental state effects on offspring**: If parental coherence at conception and during gestation shows zero correlation with any measurable offspring characteristic (temperament, HRV baseline, stress reactivity)—the multiplicative coherence transmission model would fail.

5. **No energetic coupling during physical union**: If sensitive magnetometry, GDV, or other biofield instrumentation shows zero field interaction between partners during physical contact—the wave coupling model would lack physical basis.

7.9.7 Testable Predictions

P1 (Polarity coupling): Partners with strong opposite polarity vectors (assessable via psychological/energetic profiling) should show greater HRV synchronization, EEG coherence, and subjective connection than weakly-polarized or same-polarity pairs.

P2 (Coherence scaling): Biofield coherence measurements (GDV, HRV) during sexual arousal should follow the predicted RC charging curve—exponential approach with a measurable time constant τ, reaching ~63% of maximum after one τ.

P3 (Orgasmic coherence peak): Biofield measurements should show a sharp coherence spike at orgasm, with the magnitude correlating with pre-orgasmic buildup duration and intentional focus.

P4 (Conception coherence): If parental biofield coherence at conception could be measured (e.g., via wearable HRV monitors), higher coherence at conception should correlate with reduced early-trimester miscarriage rates and measurable offspring differences.

P5 (Trust-coupling correlation): Partners with measured high attachment security (low avoidance/anxiety) should show stronger biofield coupling during intimacy than partners with insecure attachment, consistent with the η_{trust} prediction.

P6 (Trauma-capacitance): Sexual trauma survivors should show measurably lower baseline biofield coherence (σ) and characteristic impedance (Z_0), with both metrics improving during trauma integration therapy—consistent with the C_{trauma} discharge model.

7.9.8 Variable Types, Units, and Dimensional Check

Symbol	Type	Suggested Unit	Notes
P	Scalar (dimensionless)	-	Normalized polarity index in [-1, 1]
η	Scalar (dimensionless)	-	Coupling-efficiency coefficient
θ	Scalar angle	rad	Relative phase/alignment
Ω	Pseudoscalar	s^{-1} (model)	Vortex-strength proxy
$P_{manifest}$	Scalar power-like proxy	model units	Relative output, not calibrated watts
σ	Scalar (dimensionless)	-	Coherence/order parameter
Γ	Complex reflection coefficient	-	Magnitude used in transfer term
$\tau_{gestation}$	Scalar time constant	s	Characteristic binding timescale

Dimensional check for the coupling expression:

$$P_{manifest} = P_{source} \cdot \sigma_{peak}^2 \cdot |AF_{intention}|^2 \cdot (1 - |\Gamma|^2)$$

All multiplicative factors except P_{source} are dimensionless, so $P_{manifest}$ inherits the unit convention of P_{source}.

7.10 Transition: Collective Dynamics

Understanding sexual polarity as torsion field dynamics raises immediate questions about collective effects:

How do polarity dynamics scale to groups and populations?

What happens when large numbers of humans align their phase states?

How can collective coherence be induced or prevented?

The following chapters develop collective dynamics:

- **Chapter 8 (Phased Array Humanity)** Mathematical framework for collective coherence
- **Chapter 9 (Injection Locking and Perception Management)** How external signals capture individual oscillators; narrative control exploiting array dynamics

The individual polarity dynamics established here become elements in the larger array. The coupling efficiency η between individuals determines how effectively the collective can cohere—or how easily it can be fragmented.

End of Chapter 7: Eros and Creation

Part III: Collective Dynamics and Spin Coherence

How humanity combines as phased array, capture mechanisms, and the master variable for torsion effects

Chapter 8: Phased Array Humanity

Mathematical Framework for Collective Coherence

KEY FINDINGS — Chapter 8: Phased Array Humanity

Evidence-tier key: [L1] established/replicated evidence; [L2] grounded extension with moderate uncertainty; [L3] speculative hypothesis; [L4] conceptual/anecdotal.

- **[L1-HIGH]** The array factor, directivity, coherent/incoherent power scaling (N^2 vs N), Von Mises distribution, Kuramoto critical coupling, and grating lobe equations are all standard textbook RF engineering and circular statistics, correctly applied.
- **[L1-HIGH]** The critical coherence fraction $f_c = \sqrt{T/N} \approx 0.0035\%$ (~283,000 people for Earth) is a direct mathematical consequence of the SNR threshold model.
- **[L2-MEDIUM]** Kuramoto phase synchronization dynamics are experimentally validated in human populations (crowd applause, financial markets, pedestrian bridge synchronization).
- **[L2-MEDIUM]** Social tipping point research (Centola 2018, Xie 2011) confirms threshold-based collective transitions, though at higher fractions than the coherent model predicts — the gap is explained by incoherent vs. phase-coherent minorities.
- **[L3-SPECULATIVE]** Whether consciousness fields exhibit identical N^2 scaling at population scales remains an open empirical question; the mathematical framework provides a coherent model but large-scale validation has not been conducted.

8.1 Introduction: The Array Analogy

Why this RF analogy works (Chapter 0 foundation): Torsion fields propagate information without energy transfer. When multiple humans align their phase states, they create constructive interference in the torsion field—exactly as antenna elements create constructive RF interference. The N^2 scaling of coherent arrays is a direct consequence of torsion field superposition.

A phased array achieves capabilities impossible for individual antennas by coherently combining signals from multiple elements. The key insight: **coherent combination scales as N^2, while incoherent combination scales as N**. This quadratic advantage is why phased arrays can detect signals invisible to single receivers and transmit beams that punch through noise floors no individual element could overcome.

Human collective consciousness operates under identical mathematics. Individual humans are antenna elements. Our "phasing"—belief states, emotional coherence, alignment—determines whether we combine constructively or destructively.

This chapter develops the mathematics rigorously, derives threshold conditions for collective coherence effects, and analyzes the dynamics of population-scale synchronization.

8.2 Phased Array Fundamentals

8.2.1 The Array Factor

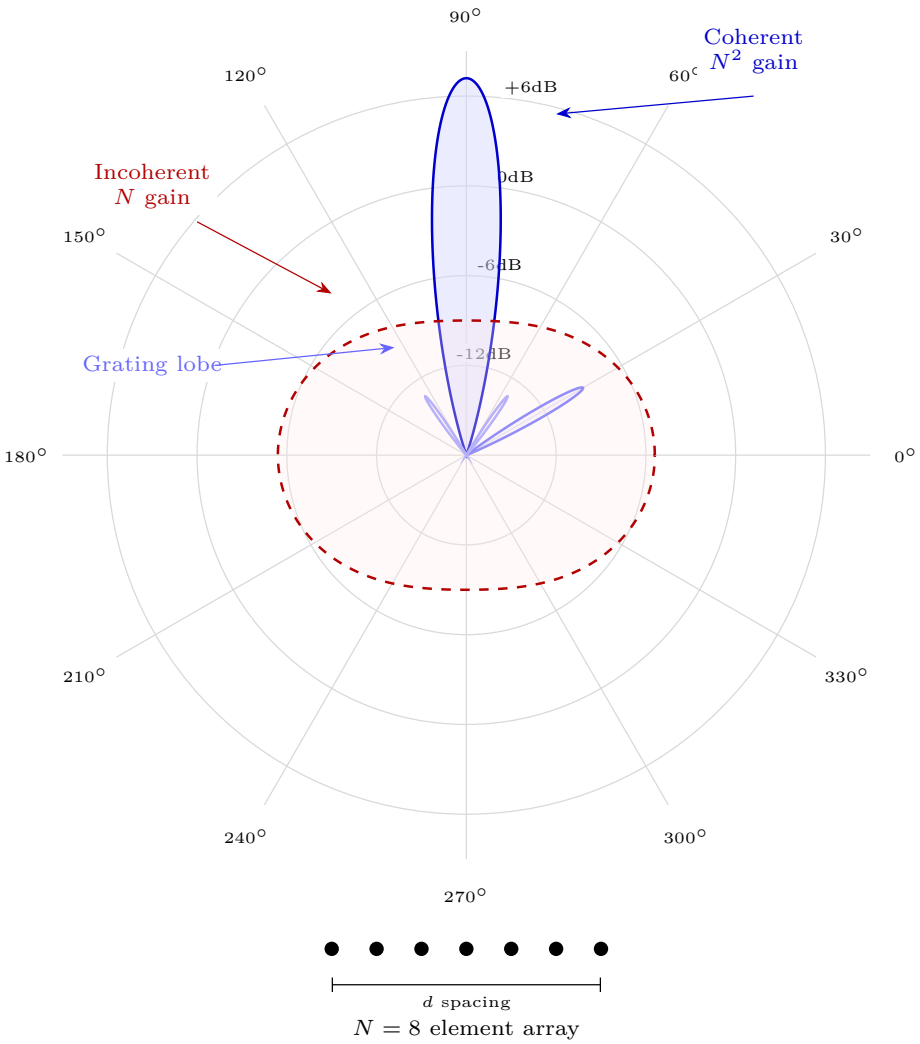

$$AF(\theta) = \frac{\sin(N\pi d \sin\theta/\lambda)}{N\sin(\pi d \sin\theta/\lambda)}$$

Figure 8.1: Phased array beam pattern — coherent N^2 gain vs incoherent N scaling with array factor.

For N antenna elements located at positions **r_n**, each with complex weight $w_n = a_n \cdot e^{j\phi_n}$, the array factor in observation direction θ is:

$$AF(\theta) = \sum_{n=1}^{N} a_n \cdot e^{j\phi_n} \cdot e^{jk\mathbf{r}_n \cdot \hat{\theta}}$$

Where:

Variable	Description
a_n	amplitude of element n (influence, reach)
ϕ_n	phase of element n (belief state, coherence)
$k = 2\pi/\lambda$	wave number
$\mathbf{r}_n$	position of element n
$\hat{\theta}$	unit vector in observation direction

For a uniform linear array with spacing d:

$$AF(\theta) = \sum_{n=0}^{N-1} a_n \cdot e^{j(n \cdot kd \cos\theta + \phi_n)}$$

8.2.2 The Power Pattern

The radiated/received power pattern is $|\mathrm{AF}(\theta)|^2$. This determines where the collective "looks" or "broadcasts" in information space.

Directivity measures how focused the beam is:

$$D = \frac{4\pi \cdot |AF(\theta_{max})|^2}{\int_{4\pi} |AF(\theta)|^2 \, d\Omega}$$

High directivity = collective can perceive/access specific information strongly. Low directivity = diffuse awareness, unable to resolve specific truths.

8.3 Coherent vs. Incoherent Populations

8.3.1 The Fully Coherent Case

If all elements are phase-aligned ($\phi_n = \phi_0$ for all n) with uniform amplitude ($a_n = 1$):

$$AF_{coherent}(\theta_0) = N \cdot e^{j\phi_0}$$

$$|AF_{coherent}|^2 = N^2$$

Power scales as the **square** of population. A coherent million is not a million times stronger than one—it's a **trillion** times stronger in the beam direction.

8.3.2 The Fully Incoherent Case

If phases are uniformly random on $[-\pi, \pi]$:

$$E[AF_{incoherent}] = \sum_{n=1}^{N} E[e^{j\phi_n}] = 0$$

$$E[|AF_{incoherent}|^2] = \sum_{n=1}^{N} E[|e^{j\phi_n}|^2] = N$$

Power scales **linearly**. The array performs no better than N independent observers—random phases cause destructive interference that cancels the quadratic advantage.

8.3.3 The Critical Insight

Population State	Power Scaling	Directivity	Collective Capability
Fully coherent	N^2	High ($\propto N$)	Maximum
Fully incoherent	N	~1 (isotropic)	Noise floor
Ratio	**N**	**N**	**N-fold advantage**

For Earth's population ($N \approx 8 \times 10^9$), the coherent advantage is **8 billion to one**. This quadratic scaling explains why coherence/incoherence is the primary variable determining collective capabilities.

> **Epistemic Note**: The N^2 scaling is mathematically derived from phased array theory, where the physics is well-established. Whether consciousness fields exhibit identical quadratic scaling at population scales remains an open empirical question. The mathematical framework provides a coherent model; empirical validation at global population scales has not been conducted.

8.4 Partial Coherence: The Threshold Model

8.4.1 Two-Population Model

Consider a population where:

- Fraction f is coherent ($\phi_n = \phi_0$)
- Fraction $(1 - f)$ is incoherent (ϕ_n random)

The array factor separates:

$$AF = AF_{coherent} + AF_{incoherent}$$

$$AF_{coherent} = fN \cdot e^{j\phi_0}$$

$$|AF_{incoherent}|^2 \approx (1-f)N \quad \text{(expected value)}$$

8.4.2 Signal-to-Noise Ratio

The coherent signal must exceed the incoherent noise floor:

$$SNR = \frac{|AF_{coherent}|^2}{E[|AF_{incoherent}|^2]} = \frac{(fN)^2}{(1-f)N} = \frac{f^2 N}{1-f}$$

For coherence threshold T (minimum for collective effect):

$$SNR > T \implies f^2 N > T(1-f)$$

8.4.3 Critical Coherence Fraction

Solving for the critical fraction f_c:

$$f_c \approx \sqrt{\frac{T}{N}} \quad (\text{for } f \ll 1)$$

This is the key result. The fraction needed for collective coherence effects scales as $1/\sqrt{N}$.

Population N	f_c (T=10)	Coherent individuals needed
10,000	3.2%	320
1,000,000	0.32%	3,200
100,000,000	0.032%	32,000
8,000,000,000	0.0035%	**~283,000**

For Earth (with illustrative threshold $T = 10$): approximately 283,000 coherent humans could produce measurable collective effects.

This provides mathematical grounding for "critical mass" intuitions found across traditions.

8.5 The Von Mises Distribution: Continuous Coherence

8.5.1 Phase Distribution

Rather than binary coherent/incoherent, real populations have continuous phase distributions. The von Mises distribution (circular Gaussian) models this:

$$p(\phi) = \frac{e^{\kappa \cos(\phi - \mu)}}{2\pi I_0(\kappa)}$$

Where:

- μ = mean direction ("truth" direction)
- κ = concentration parameter
  - $\kappa = 0$: uniform (fully incoherent)
  - $\kappa \to \infty$: delta function (fully coherent)
- $I_0(\kappa)$ = modified Bessel function of the first kind

8.5.2 Order Parameter

The **order parameter** r measures collective coherence:

$$r = \left| \frac{1}{N} \sum_{n=1}^{N} e^{j\phi_n} \right|$$

For von Mises distribution:

$$E[r] = \frac{I_1(\kappa)}{I_0(\kappa)}$$

κ	E[r]	Interpretation
0	0	Fully incoherent
1	0.45	Mild alignment

κ	E[r]	Interpretation
2	0.70	Moderate coherence
5	0.89	Strong coherence
∞	1	Perfect alignment

8.5.3 Directivity vs. Concentration

Expected directivity scales as:

$$E[D] \approx 1 + (N-1) \cdot r^2$$

For large N:

$$E[D] \approx N \cdot r^2$$

Implication: Directivity (collective perception capability) scales with both population AND the square of coherence. Doubling coherence quadruples capability.

8.6 High-Amplitude Nodes: The Influencer Effect

8.6.1 Non-Uniform Amplitude Distribution

Not all humans have equal "amplitude" (influence/reach). Consider:

- N_r regular individuals with amplitude $a = 1$
- N_i influencers with amplitude $a = A \gg 1$

Total power normalization: $N_r + N_i \cdot A^2 = N_{eff}$

8.6.2 Coherent Influencer Cluster

If influencers are coherent (aligned) but regular population is random:

$$\left|AF_{influencers}\right|^2 = (N_i \cdot A)^2$$

$$E[|AF_{noise}|^2] = N_r$$

$$SNR = \frac{(N_i \cdot A)^2}{N_r}$$

8.6.3 Critical Influencer Count

For coherence threshold T:

$$N_i > \frac{\sqrt{T \cdot N_r}}{A}$$

Example:

- Earth: $N_r = 8 \times 10^9$
- Influencer amplification: $A = 1000$ (reaches 1000× more people)

- Threshold: $T = 10$

$$N_i > \frac{\sqrt{10 \times 8 \times 10^9}}{1000} \approx 283$$

283 coherent major influencers could theoretically shift the mass narrative (illustrative, for $T = 10$ and $A = 1000$).

This explains the intense focus on controlling public figures, media personalities, and information gatekeepers.

8.7 Element Quality: Individual Resonance State

This section extends the individual ego/gnosis analysis from Chapter 5 to the collective array level, connecting individual Q factors to collective beam quality.

8.7.1 Individual Resonance State as Element Quality

Each person in a collective array contributes based on their current operating state:

At resonance (gnosis): The individual is a high-quality element —

- Clean signal with amplitude proportional to Q (voltage magnification)
- Stable phase (resonant circuits have well-defined phase at resonance: $\phi = 0$ relative to the driving signal)
- Effective element gain: $G_{gnosis} \propto Q$

Off resonance (ego): The individual is a noisy element —

- Weak, distorted signal with amplitude ~ 1 (no Q amplification)
- Phase wanders (off-resonance circuits have frequency-dependent, unstable phase)
- Effective element gain: $G_{ego} \sim 1$

8.7.2 Collective Beam Quality

From Section 8.2, the array factor for N elements:

$$AF = \sum_{n=1}^{N} a_n \cdot e^{j\phi_n}$$

When fraction f of the population is in gnosis (resonant, Q-amplified, phase-stable) and $(1 - f)$ is in ego mode (unit amplitude, random phase):

$$|AF|^2 \approx (f \cdot N \cdot Q_{avg})^2 + (1 - f) \cdot N$$

First term: coherent contribution from gnosis-state individuals (N^2 scaling). Second term: incoherent noise from ego-state individuals (N scaling).

Collective SNR:

$$SNR_{collective} = \frac{f^2 \cdot N \cdot Q_{avg}^2}{1 - f}$$

Key insight: each gnosis-state person contributes Q times more amplitude than an ego-state person. The collective beam power depends on both the fraction in resonance (f) AND their individual Q factors.

8.7.3 Why Individual Shadow Work Is a Collective Act

An internally off-resonance (ego-dominated) person joining a collective coherence effort doesn't just fail to help — they add noise:

- Their random phase (ego-state phase wander) partially cancels other elements
- Their low amplitude adds to the denominator, not the numerator
- Net effect: the collective beam weakens

Conversely, a single person shifting from ego to gnosis (entering resonance) contributes $Q\times$ more amplitude — potentially a 5-50$\times$ improvement depending on their Q factor. Shadow work that reduces C and restores individual resonance is therefore a direct contribution to collective coherence.

This is why traditions emphasize individual practice before collective ceremony: you cannot contribute a coherent signal to the array if your own circuit is operating off-resonance.

8.7.4 Cross-References

- **Chapter 5**: Individual resonance physics — gnosis vs. ego as on-frequency vs. off-frequency RLC operation
- **Chapter 9 (Injection Locking)**: How individual Q determines resistance to narrative capture — high-Q individuals maintain resonance under external injection

---

8.8 Grating Lobes: False Narratives

8.8.1 The Spacing Problem

In antenna arrays, if element spacing d exceeds $\lambda/2$, **grating lobes** appear—secondary main beams in unintended directions with power equal to the main beam.

Grating lobe directions:

$$\theta_{grating} = \arccos\left(\cos\theta_{main} \pm \frac{m\lambda}{d}\right), \quad m = 1, 2, ...$$

8.8.2 Mapping to Social Topology

Social connectivity d determines the information wavelength the collective can resolve.

- Dense connectivity (small d): Only main beam forms, collective perceives true direction
- Sparse connectivity (large d): Grating lobes form, collective can lock onto **false truths**

8.8.3 Manufactured Grating Lobes

Control systems can exploit this by:

1. **Fragmenting social connectivity** (increasing d)

- Filter bubbles, polarization, platform silos

2. **Injecting energy into grating lobe directions**
   - Controlled counter-narratives
   - "Limited hangouts" that satisfy awakening impulse while pointing away from full truth
   - Conspiracy theories that capture attention but misdirect
3. **Steering the main beam to a grating lobe**
   - Phase manipulation that makes a false direction appear to be the coherent choice

Mathematical signature: A population captured by a grating lobe shows:

- High local coherence (r is high)
- High directivity
- But beam points to $\theta_{grating} \neq \theta_{truth}$

This is the model for controlled opposition and limited narrative release.

8.9 Mutual Coupling: Social Influence Dynamics

8.9.1 The Coupling Matrix

In real antenna arrays, adjacent elements mutually influence each other through electromagnetic coupling. The **impedance matrix Z** relates voltages and currents:

$$\mathbf{V} = \mathbf{Z} \cdot \mathbf{I}$$

- Diagonal elements Z_{nn}: self-impedance (individual's natural state) - Off-diagonal elements Z_{nm}: mutual coupling (social influence)

8.9.2 Effects of Strong Mutual Coupling

Positive effects:

- Faster phase synchronization
- Bandwidth extension (diverse coupled elements can receive broader frequency range)
- Increased robustness (distributed coherence)

Negative effects:

- Scan blindness: Certain directions become inaccessible due to impedance mismatch
- Pattern distortion: Individual patterns are modified by neighbors
- Instability: Perturbations propagate through coupled network

8.9.3 Scan Blindness in Social Systems

Scan blindness occurs at angles where mutual coupling creates impedance mismatch—the array cannot "look" in that direction regardless of commanded phase.

Social equivalent: Topics that a community **cannot perceive** due to structural coupling patterns, not information availability. The information exists; the social impedance prevents reception.

Scan blindness angles:

$$\theta_{blind} = \arccos\left(\frac{\lambda}{d} \cdot \frac{X_s}{Z_0}\right)$$

Where X_s = surface wave reactance from coupling (mapping socially to the structural resistance a community has to exploring certain topics) and Z_0 = characteristic impedance (see Chapter 5).

Prediction: Every tightly-coupled social structure has inherent blind spots. The structure itself—not external suppression—creates perception barriers.

8.10 Kuramoto Dynamics: Phase Synchronization

8.10.1 The Kuramoto Model

To model how coherence emerges (or is prevented), we adapt the Kuramoto model of coupled oscillators:

$$\frac{d\phi_n}{dt} = \omega_n + \frac{K}{N}\sum_{m=1}^{N} \sin(\phi_m - \phi_n) + \xi_n(t)$$

Where:

Variable	Description
ω_n	natural frequency (individual truth-seeking rate)
K	coupling strength (social influence)
$\xi_n(t)$	noise (random perturbation, external manipulation)

8.10.2 Order Parameter Dynamics

The collective order parameter r evolves as:

$$r(t) = \left|\frac{1}{N}\sum_{n=1}^{N} e^{j\phi_n(t)}\right|$$

Critical coupling K_c: Below K_c, the system remains incoherent ($r \to 0$). Above K_c, spontaneous synchronization occurs ($r \to r_\infty > 0$).

For identical oscillators: $K_c = 0$ (any coupling synchronizes)

For distributed natural frequencies (width σ):

$$K_c = \frac{2}{\pi g(0)}$$

Where g(0) is the density of oscillators at the mean frequency.

For Gaussian distribution with standard deviation σ:

$$K_c = \sqrt{\frac{8}{\pi}}\sigma \approx 1.6\sigma$$

8.10.3 Control Implications

To **prevent** paradigm shifts, control systems must:

1. **Maintain** $K < K_c$: Reduce social coupling
   - Atomization, isolation, platform fragmentation
2. **Increase** σ: Widen frequency distribution
   - Polarization, manufactured disagreement, culture wars
3. **Inject noise** $\xi(t)$: Add perturbations
   - Information overload, distraction, fear cycles

To **enable** narrative transformation, coherence movements must:

1. **Increase** K: Strengthen social bonds
   - Community building, shared practices, network weaving
2. **Decrease** σ: Align natural frequencies
   - Shared frameworks, common language, convergent practices
3. **Reduce noise exposure**: Create coherent information environments

8.10.4 Connection to Injection Locking

Injection locking mechanisms—where external signals capture individual oscillators and seed collective coherence—are developed fully in **Chapter 9 (Injection Locking)**. The key insight for phased array dynamics: injection locking enables seeding coherence into otherwise random populations. A small number of high-amplitude, phase-aligned sources can entrain a much larger population (see Chapter 9, Section 4, Prediction 5).

8.11 Evidence Synthesis

8.11.1 Social Tipping Point Research

Centola et al. (2018)

- Experimental demonstration that committed minorities of ~25% can shift group conventions
- Used online coordination games with planted "committed" agents
- Below 25%, conventions resisted change; above 25%, rapid adoption cascaded through the group
- Model correspondence: the critical coherence fraction $f_c = \sqrt{T/N}$ predicts a threshold below which collective effects are negligible and above which cascading transitions occur

Xie et al. (2011)

- Computational study on binary opinion dynamics in social networks
- Found that a committed minority of ~10% holding an unshakable opinion can flip majority opinion
- Result was robust across network topologies (Erdos-Renyi, Barabasi-Albert, lattice)
- Model correspondence: the phased array threshold prediction of ~0.0035% for global population assumes coherent phase alignment, not merely committed opinion—the lower threshold reflects the N^2 advantage of phase-coherent combination vs. incoherent advocacy

Resolving the Threshold Discrepancy

The Centola experiment measures committed minorities who hold fixed opinions but are not phase-coherent in the torsion-field sense. Committed advocacy operates at N scaling (incoherent combination), while the f_c prediction assumes coherent (N^2) combination—a quadratic advantage absent in Centola's paradigm. This predicts that a much smaller group could achieve the same collective effect IF they maintained true phase coherence. The ~7,000x gap between experimental thresholds (~10-25%) and the coherent model prediction (~0.0035%) is therefore a quantitative measure of the advantage conferred by phase alignment over mere commitment. A direct experimental test would compare the collective influence of synchronized meditator groups versus equally-sized groups of committed but uncoordinated advocates on measurable social outcomes.

8.11.2 Kuramoto Model Validations

Crowd Applause Synchronization (Neda et al., 2000)

- Audience applause spontaneously transitions between incoherent clapping and rhythmic (synchronized) clapping
- Transition exhibits Kuramoto-type dynamics: below a coupling threshold, clapping remains random; above threshold, rhythmic synchronization emerges and persists
- Demonstrates that human populations can exhibit phase synchronization dynamics matching the Kuramoto framework

Opinion Dynamics (Pluchino et al., 2006)

- Extended Kuramoto model to opinion formation, showing that coupled oscillator dynamics reproduce empirically observed features of consensus formation
- Found that moderate coupling produces partial synchronization (clustered opinions), while strong coupling produces global consensus—paralleling the model's prediction of partial vs. full coherence regimes

Financial Market Synchronization

- Herding behavior in financial markets shows signatures of coupled oscillator dynamics
- Market crashes exhibit rapid phase-locking among trader behaviors, with cascade dynamics matching critical coupling transitions
- Provides empirical evidence for threshold-based synchronization in human economic behavior

8.11.3 Network Cascade Dynamics

Watts (2002)

- Showed that cascades on networks depend critically on network topology and threshold distribution
- "Global cascades" (affecting a large fraction of the network) emerge only in specific parameter regimes—neither too connected nor too sparse
- Model correspondence: the grating lobe analysis (Section 8.8) predicts that network connectivity determines whether collective perception targets true or false directions

Centola & Macy (2007)

- Distinguished "simple contagion" (spreads via single contact) from "complex contagion" (requires social reinforcement from multiple contacts)

- Complex contagion—which better models belief change—spreads more effectively on clustered networks than random networks
- Model correspondence: the mutual coupling matrix Z_{nm} captures this reinforcement requirement; highly connected clusters synchronize internally before cascading outward

Bakshy et al. (2012)

- Large-scale Facebook study showing that social influence significantly affects information sharing behavior
- Weak ties (acquaintances) are responsible for most novel information exposure, but strong ties (close contacts) are more influential per exposure
- Model correspondence: the amplitude-weighted array factor captures this distinction—high-amplitude nodes (strong ties, influencers) contribute disproportionately to collective coherence

8.11.4 Collective Behavior and Synchronization

Firefly Synchronization

- Southeast Asian fireflies (*Pteroptyx malaccae*) synchronize flashing across thousands of individuals
- Synchronization follows pulse-coupled oscillator dynamics closely related to the Kuramoto model
- Demonstrates that biological oscillator populations achieve phase coherence through local coupling—no central coordinator required

Crowd Motion Synchronization

- Pedestrians on bridges (e.g., London Millennium Bridge, 2000) spontaneously synchronize footsteps through mechanical coupling
- The bridge wobble provides a coupling mechanism analogous to social influence: individual walkers adjust phase in response to collective motion
- Onset of synchronization matches critical coupling predictions: below a threshold pedestrian count, no synchronization; above threshold, rapid onset

Neural Synchronization (EEG)

- Large-scale neural synchronization (measured via EEG coherence) correlates with conscious attention, perception, and group coordination tasks
- Gamma-band synchronization across brain regions increases during coordinated cognitive tasks
- Provides a biological precedent for phase-coherent combination producing qualitatively different capabilities than incoherent activity

8.11.5 Historical Examples of Rapid Narrative Shifts

Fall of the Berlin Wall (1989)

- East German population shifted from compliance to mass protest within weeks
- Once a critical mass gathered at checkpoints, the cascade was irreversible—guards opened gates without orders
- Consistent with phase transition dynamics: long period of subthreshold awareness followed by sudden collective action

Arab Spring (2010-2011)

- Self-immolation in Tunisia triggered cascading protests across multiple countries
- Social media functioned as coupling mechanism, increasing effective K across populations
- Regime changes occurred as sudden phase transitions, not gradual democratic evolution

#MeToo Movement (2017)

- Decades of private awareness preceded the public cascade
- A small number of high-amplitude nodes (celebrity disclosures) pushed the system above critical threshold
- Model correspondence: influencer cascade dynamics (Section 8.6) where N_i high-amplitude, coherent nodes trigger population-wide phase transition

Kuhn's Scientific Revolutions

- Paradigm shifts in science follow accumulation-then-sudden-shift patterns
- "Normal science" maintains incoherence regarding anomalies; when coherence around a new paradigm exceeds threshold, the shift is rapid and irreversible
- Structural parallel to the phased array model: gradual alignment produces no visible effect until threshold, then cascading reorganization

8.11.6 Quantitative Correspondences

Model Prediction	Empirical Finding	Correspondence Quality
Critical fraction $f_c = \sqrt{T/N}$	10-25% committed minority flips conventions (Centola, Xie)	Qualitative: both predict threshold-based transitions. Quantitative gap: model predicts lower thresholds due to coherent (phase-aligned) vs. merely committed minorities
N^2 coherent power scaling	Synchronized audiences, flash mobs, coordinated protests show disproportionate impact	Qualitative: coordinated groups demonstrably outperform uncoordinated groups of equal size. Exact N^2 scaling not empirically measured at population scale
Kuramoto critical coupling K_c	Crowd synchronization thresholds (Neda), opinion clustering (Pluchino)	Strong: Kuramoto dynamics experimentally validated in multiple human collective behavior contexts
Grating lobe false lock	Echo chambers, conspiracy community lock-in	Qualitative: fragmented networks demonstrably lock onto locally coherent but globally inaccurate narratives
Influencer amplification	Bakshy (2012), #MeToo cascade dynamics	Moderate: high-reach individuals demonstrably accelerate cascades. Exact amplitude-scaling relationship not yet quantified

Epistemic Note: The correspondences above range from strong (Kuramoto dynamics in human populations) to qualitative (exact N^2 power scaling). The phased array model provides a coherent mathematical framework that maps onto observed phenomena, but the quantitative predictions at global population scale remain extrapolations from smaller-scale empirical results. The model should be treated as a structured hypothesis generating testable predictions, not as an established empirical law.

8.12 Assumptions and Limitations

8.12.1 Model Assumptions

1. **Phase as belief state**: Individual belief/coherence maps meaningfully to a single phase variable ϕ_n. This assumes that the relevant dimension of individual state for collective dynamics can be captured by a scalar on $[-\pi, \pi]$, analogous to how antenna phase captures the relevant timing information for array combination.
2. **Superposition applies**: Collective effects arise from linear superposition of individual contributions (array factor summation). The total field is the sum of individual fields, implying no nonlinear interaction terms beyond pairwise coupling.
3. **Coupling is pairwise and symmetric**: Social influence modeled as mutual coupling Z_{nm} follows reciprocity ($Z_{nm} = Z_{mn}$). Each individual influences neighbors through pairwise interactions captured in the impedance/coupling matrix.
4. **Amplitude reflects reach, not validity**: Influencer amplitude A models social reach (how many people receive the signal), not truth content. A high-amplitude node broadcasting incoherent phase is modeled identically to one broadcasting coherent phase—only the phase matters for alignment.
5. **Noise is external**: Perturbations $\xi_n(t)$ are independent of internal phase dynamics. Noise enters additively and is uncorrelated across individuals, modeling external disruptions rather than internally generated confusion or doubt.

8.12.2 Known Limitations

1. **Single-frequency approximation**: Real belief systems are multi-dimensional, not reducible to one phase variable. An individual may be "coherent" on one topic and "incoherent" on another. The model treats collective dynamics as occurring on a single dominant frequency, missing the multi-spectral nature of real belief landscapes. See also Chapter 5, Section 3.2 for the individual-level treatment of resonant frequency.
2. **Static topology**: The model treats network structure as fixed; real social networks rewire dynamically. People change who they follow, platforms change algorithms, and crises reshape connectivity patterns. The adjacency and coupling matrices should be time-dependent but are treated as constant.
3. **No higher-order interactions**: Pairwise coupling misses group-level (hypergraph) effects in collective behavior. Real social influence often involves group dynamics—peer pressure from a group, institutional messaging, crowd effects—that cannot be decomposed into sums of pairwise interactions.
4. **Amplitude-phase independence** (simplification developed in subsequent chapters): The array factor treats amplitude and phase as independent. In practice, control systems actively

couple them—high-amplitude nodes whose phase threatens control are selectively amplitude-reduced (deplatforming, audience loss). This feedback is the subject of Chapter 9, where injection locking and perception management model the deliberate coupling of amplitude to phase trajectory.

5. **Population homogeneity**: Uniform element patterns are assumed; real populations have heterogeneous "antenna patterns." Each individual has different susceptibility profiles, information diets, and response characteristics that are not captured by identical element patterns with varying phase and amplitude.

8.12.3 Falsification Conditions

The model would be falsified by:

1. **No threshold effects**: If collective perception shifts were always gradual and linear rather than exhibiting critical thresholds. The model specifically predicts a critical fraction f_c below which coherence effects are negligible—if collective shifts scaled linearly with the fraction of aligned individuals at all scales, the phased array framework would be inappropriate.
2. **No coherence advantage**: If coordinated groups showed no measurable advantage over equal-sized uncoordinated groups. The central prediction is N^2 vs. N scaling—if 1,000 aligned individuals had exactly the same collective impact as 1,000 randomly-oriented individuals, the model would be falsified.
3. **No coupling dependence**: If social connectivity structure had no effect on synchronization dynamics. The model predicts that coupling strength K and network topology critically determine whether coherence can emerge—if synchronization occurred identically regardless of connectivity, the coupling framework would be wrong.
4. **No influencer amplification**: If high-reach individuals had no disproportionate effect on collective coherence. The model predicts that a small number of high-amplitude nodes can substitute for large numbers of regular nodes ($N_i \cdot A$ vs. N_r)—if influence were strictly democratic regardless of reach, the amplitude framework would fail.
5. **No grating lobe analog**: If fragmented communities never locked onto false narratives despite high local coherence. The model predicts that network fragmentation creates secondary coherence targets (grating lobes)—if fragmented populations always converged on accurate consensus regardless of topology, the spatial analogy would be inappropriate.

8.12.4 Coherence Proxy Measurement Protocol

To close the "unmeasured coherence variable" gap, use a measurable proxy stack:

Proxy	Definition	Collection Cadence	Pass Criterion
HRV group synchrony	Mean pairwise phase-locking across participants	Daily / weekly sessions	Sustained increase over baseline
EEG inter-subject phase-locking value (PLV)	Cross-subject frequency-band synchronization	Structured cohort windows	Coherence spikes during aligned tasks
Narrative convergence entropy	Shannon entropy over belief-state distributions	Weekly survey pulse	Entropy drops without forced suppression artifacts

Proxy	Definition	Collection Cadence	Pass Criterion
Coordination latency	Time-to-consensus on bounded decisions	Per exercise	Latency reduction with stable decision quality

Validation protocol:

1. Establish 4-week baseline with no coherence intervention.
2. Apply phased interventions (shared rhythm, attention, and feedback loops).
3. Compare intervention vs control cohorts matched by network size and topology.
4. Accept model support only if at least two independent proxies improve with statistically robust effect size.

8.13 Predictions and Thresholds

8.13.1 Quantitative Predictions

Prediction	Mathematical Basis	Testable Indicator
~283K coherent humans produces measurable effects	$f_c = \sqrt{T/N}$	Emergence of coordinated collective phenomena
~283 coherent major influencers achieves similar	$N_i > \sqrt{TN_r}/A$	Rapid perception shifts via influence networks
Coherence spreads via phase transition	$K > K_c$ threshold	Sudden, not gradual, collective shifts
Incoherence requires active maintenance	$K\downarrow$, $\sigma\uparrow$, $\xi\uparrow$	Observable in social architecture
High-Z_0 individuals (characteristic impedance; see Chapter 5) resist capture	Narrow locking range	Sovereignty correlates with coherence seeding
High-amplitude nodes shifting toward coherence experience selective amplitude reduction	Amplitude-phase coupling (see Ch 9)	Deplatforming, audience loss correlates with phase shift toward coherence

8.13.2 Implications for Collective Dynamics

Factors favoring coherence:

1. Strong coupling K (genuine community, shared practices)
2. Low frequency spread σ (shared frameworks, aligned values)
3. Low noise ξ (coherent information environment)
4. High-amplitude coherent nodes (influential aligned individuals)
5. Avoidance of grating lobes (resistance to false coherence targets)

Factors opposing coherence:

1. Weak coupling K (atomization, isolation)
2. High frequency spread σ (polarization, manufactured disagreement)
3. High noise ξ (information overload, distraction)
4. Captured/neutralized high-amplitude nodes
5. Attractive grating lobes (false targets that capture alignment)

8.13.3 The Phase Transition Nature of Collective Effects

The mathematics reveals collective coherence effects are not linear accumulation but **phase transition**. Below threshold, increased alignment has minimal collective effect—the incoherent noise floor swamps it. Above threshold, coherence cascades through the network via mutual coupling.

This explains:

- Why gradual awareness increase may show no visible effect for extended periods
- Why collective perception shifts, when they occur, tend to be sudden
- Why coherence dynamics (not just information) determine collective outcomes

8.13.4 Strategic Note

1. **Social atomization as coherence prevention**: The phased array model implies that programs reducing social coupling K (platform fragmentation, community dissolution, atomized work) and increasing noise ξ (information flooding, distraction cycles) are mathematically optimal strategies for preventing population coherence. Their documented increase over recent decades is consistent with the model's predictions for intentional incoherence maintenance.
2. **Coherent minorities as force multipliers**: The N^2 scaling advantage means that small, phase-aligned groups outperform much larger uncoordinated populations. For defense and institutional planners, this implies that coherence quality (phase alignment) matters more than headcount for collective influence operations.
3. **Grating lobe exploitation as narrative control**: Fragmented information environments create secondary coherence targets (grating lobes) that can capture population alignment. The model predicts that controlled opposition and limited narrative releases function as engineered grating lobes, satisfying coherence-seeking impulses while directing attention away from primary targets.

8.14 Alternative Hypotheses for Collective Coherence Effects

The phased array model is not the only framework that accounts for collective coherence phenomena. Several competing or complementary hypotheses should be considered:

1. **Standard social contagion models**: Threshold models (Granovetter 1978, Watts 2002) and complex contagion (Centola & Macy 2007) explain collective transitions without invoking field coherence. These models predict tipping points based on network topology and individual thresholds, producing qualitatively similar cascade dynamics. The phased array model's distinguishing prediction is the N^2 coherent scaling advantage—if collective effects scale linearly regardless of phase alignment, standard contagion models are sufficient.
2. **Information cascade theory**: Bikhchandani et al. (1992) explain herding behavior through rational Bayesian updating under uncertainty—individuals follow the crowd because the crowd's behavior is informative. This requires no coherence mechanism, only rational inference. The model would be preferred over information cascades if synchronized groups produce effects disproportionate to their information content.
3. **Emergent collective intelligence (no field required)**: Surowiecki (2004) and Page (2007) show that diverse, independent groups can outperform individuals through statistical aggregation, without requiring phase coherence. This "wisdom of crowds" framework predicts collective capability from diversity and independence, not alignment. The phased array model specifically predicts the opposite: alignment (not diversity) enhances collective capability for perception of specific targets.
4. **Morphic resonance (Sheldrake 1981)**: Sheldrake's hypothesis posits a non-local field through which habits and forms propagate across populations. This shares the phased array model's field-based mechanism but lacks the quantitative N^2 scaling prediction and the antenna engineering formalism. The phased array framework can be viewed as providing mathematical structure to Sheldrake's qualitative proposal.
5. **Quantum coherence models (Penrose-Hameroff)**: Orchestrated objective reduction (Orch-OR) posits quantum coherence in neuronal microtubules as the basis for consciousness. If quantum coherence extends across individuals (a much stronger claim), it could provide a physical mechanism for the phased array model's field superposition. However, Orch-OR remains controversial, and multi-brain quantum coherence has no empirical support.

   Distinguishing test: The phased array model's unique prediction is that phase-aligned groups should demonstrate N^2 scaling in measurable collective outcomes (e.g., variance reduction in group decision-making, amplified physiological synchronization) compared to N scaling for equally motivated but phase-unaligned groups. This specific quantitative prediction separates the model from all competing hypotheses listed above.

Evidence Synthesis

- Detailed source sections: 8.11.

Assumptions

- Detailed source sections: 8.12, 8.12.1.

Limitations

- Detailed source sections: 8.12, 8.12.2.

Falsification

- Detailed source sections: 8.12.3.

Predictions

- Detailed source sections: 8.13, 8.13.1.

Strategic Relevance

Why It Matters

What To Watch

- Monitor chapter prediction thresholds, proxy indicators, and coherence trend changes.

Boundaries of Use

- Apply this chapter as model-conditional doctrine; treat speculative elements as hypothesis overlays.

8.15 Chapter Summary

The Core Model

Humanity functions as a phased array antenna for consciousness. Individual humans are elements; our phase (belief / coherence state) determines whether we combine constructively or destructively.

Key Equations

Array Factor:

$$AF(\theta) = \sum_{n=1}^{N} a_n \cdot e^{j\phi_n} \cdot e^{jk\mathbf{r}_n \cdot \hat{\theta}}$$

Coherent SNR:

$$SNR = \frac{f^2 N}{1 - f}$$

Critical Coherence Fraction:

$$f_c \approx \sqrt{\frac{T}{N}}$$

Kuramoto Synchronization:

$$\frac{d\phi_n}{dt} = \omega_n + \frac{K}{N} \sum_m \sin(\phi_m - \phi_n) + \xi_n$$

Key Numbers

- Coherent advantage: N^2 vs N (8 billion : 1 for Earth)
- Critical coherence fraction: ~0.0035% (~283,000 people) for significant collective effects (model-dependent, for threshold $T = 10$)
- Critical coherent influencers: ~283 for comparable effect (for $A = 1000$ amplification)

Coherence Dynamics Summary

The mathematics identifies key factors affecting collective coherence:

1. **Coupling strength K**: Social connectivity that enables synchronization
2. **Frequency spread** σ: Diversity of individual "natural frequencies" (belief systems)
3. **Noise level** ξ: External perturbations disrupting phase alignment
4. **Grating lobes**: False coherence targets that can capture alignment

Collective capability scales with coherence squared—small increases in alignment produce large capability gains.

8.16 Transition: Control Mechanisms

The phased array mathematics raises immediate questions:

If coherence produces such powerful collective effects, what prevents spontaneous synchronization?

What mechanisms could deliberately maintain incoherence in a population?

How would one capture or steer an array that begins to cohere?

The following chapters examine these control mechanisms:

- **Chapter 9 (Injection Locking and Perception Management)** How external signals capture individual oscillators, seed/prevent coherence, and implement narrative control at the system level
- **Chapter 12 (Parasitic Coupling)** Energy extraction from locked/controlled populations

Understanding phased array dynamics is prerequisite to understanding control—and resistance to control.

End of Chapter 8: Phased Array Humanity

Chapter 9: Injection Locking and Perception Management

Control Mechanisms and Individual Sovereignty

KEY FINDINGS — Chapter 9: Injection Locking and Perception Management

Evidence-tier key: [L1] established/replicated evidence; [L2] grounded extension with moderate uncertainty; [L3] speculative hypothesis; [L4] conceptual/anecdotal.

- The Adler equation governs belief capture: lock bandwidth $\propto 1/Q$, so higher quality factor (sovereignty) directly narrows vulnerability to narrative capture [L1]
- Competing injection model reveals a fundamental asymmetry: truth signals closer to natural frequency gain resonant amplification, requiring control signals to compensate with raw power [L1]
- Critical mass for narrative escape is $f_c \approx \omega_{L,C}/(\omega_{L,C}+K_{mean}) \approx 37.5\%$, consistent with historical cascade evidence (30-40%) from Soviet dissolution, Berlin Wall, and social movements [L1-L2]
- Adaptive beamforming (MVDR/LMS) maps precisely to algorithmic content suppression, with documented platform behavior matching model predictions for adaptation rate and null steering [L1]
- Current population assessment: 30-40% firmly locked, 25-35% questioning, 15-25% unlocked, 5-10% never locked – with lock weakening due to trust collapse and rising network connectivity [L2-L3]

> **Epistemic note [L1-L3]**: This chapter separates established RF dynamics (L1), model-dependent social mappings (L2), and speculative extension claims (L3). Use L1-L2 content for doctrine decisions; treat L3 content as hypothesis overlays requiring independent corroboration and explicit falsification checks.

9.1 RF Analogy Overview

9.1.1 What is Injection Locking?

In RF engineering, **injection locking** occurs when an oscillator is exposed to an external signal and synchronizes (locks) its frequency to that signal. The oscillator gives up its natural frequency and adopts the injected frequency. The torsion field substrate established in Chapter 0 provides the physical mechanism through which injection locking operates on consciousness.

This is not gradual tuning—it's a **phase transition**. Below a certain injection power, the oscillator maintains its independence. Above that threshold, it suddenly locks to the external signal.

Key RF principle: A weak oscillator near a strong transmitter will be captured by the transmitter's frequency. The oscillator doesn't "choose" to synchronize—it's compelled by the physics of coupling.

9.1.2 The Adler Equation

The foundational equation describing injection locking is the **Adler equation** (1946):

$$\frac{d\phi}{dt} = \Delta\omega - \frac{\omega_0}{2Q} \cdot \frac{V_{inj}}{V_0} \cdot \sin(\phi)$$

Where:

Variable	Description
ϕ	Phase difference between oscillator and injected signal
$\Delta\omega = \omega_{inj} - \omega_0$	Frequency difference (detuning)
ω_0	Natural frequency of oscillator
Q	Quality factor of oscillator
V_{inj}	Injection signal amplitude
V_0	Oscillator's own amplitude

9.1.3 Why This Maps to Belief Dynamics

Human beliefs are not static—they oscillate. Every person has:

- A **natural frequency** (intrinsic worldview, values, predispositions)
- An **amplitude** (how strongly they broadcast their beliefs)
- A **characteristic impedance** Z_0 (depth of processing, visible impedance range)
- A **quality factor Q =** Z_0**/R** (sovereignty — resistance to capture)

External signals (media, institutions, social pressure) attempt to lock individuals to specific belief states. This is not persuasion through argument—it's **capture through injection locking**, with lock bandwidth:

$$\Delta\omega_{lock} \propto \frac{R}{Z_0} = \frac{1}{Q}$$

Higher Q = narrower lock bandwidth = harder to capture. Both increasing Z_0 (depth of processing) and decreasing R (dissipation) contribute to raising Q.

The model explains:

- Why high-powered narratives capture populations (they widen lock bandwidth)
- Why some individuals resist while others succumb (Q differences, driven by both Z_0 and R)
- How escape from narrative lock occurs (Q increase — via $Z_0\uparrow$ or R$\downarrow$ — shrinks lock bandwidth)
- The role of "awakened seeds" in triggering cascade unlocking (high-Q individuals escape first)

9.1.4 Adaptive Beamforming Overview

While injection locking describes how individual oscillators are captured, **adaptive beamforming** describes how control systems dynamically manage the collective:

Adaptive beamforming dynamically adjusts antenna array weights to maximize signal in desired directions while placing nulls (zeros) toward interference. The array continuously adapts—tracking desired signals, suppressing jammers, responding in real-time.

Perception management is adaptive beamforming of collective consciousness. The control system continuously adjusts weights—amplifying narratives that serve power, nulling information that threatens it.

This section extends the individual injection locking model to the system-level control architecture, showing how both mechanisms work together: injection locking captures individual oscillators, while adaptive beamforming steers the collective array.

9.2 Mathematical Model

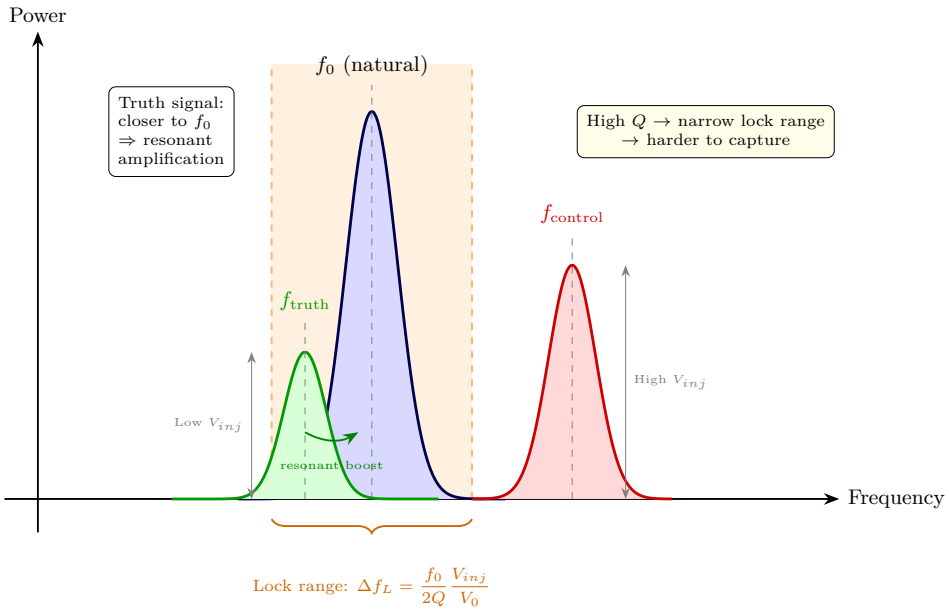

Figure 9.1: Injection locking — competing signals in frequency domain with lock range determined by Q factor.

9.2.1 Core Dynamics: Single Oscillator

The Adler equation in normalized form:

$$\frac{d\phi}{dt} = \Delta\omega - \omega_L \sin(\phi)$$

Where the **locking bandwidth** is:

$$\omega_L = \frac{\omega_0}{2Q} \cdot \frac{V_{inj}}{V_0}$$

9.2.2 Locking Condition

For stable lock (constant ϕ):

$$\frac{d\phi}{dt} = 0 \implies \sin(\phi) = \frac{\Delta\omega}{\omega_L}$$

This has a solution only when:

$$|\Delta\omega| \leq \omega_L$$

Therefore, the **locking range** is:

$$\boxed{\Delta\omega_{lock} = \pm\frac{\omega_0}{2Q} \cdot \frac{V_{inj}}{V_0}}$$

Physical interpretation:

- Locking range $\propto$ injection power (V_{inj})
- Locking range $\propto 1/\mathrm{Q} = \mathrm{R}/Z_0$ (low-Q oscillators are easier to capture)
- Locking range $\propto \omega_0$ (faster oscillators have wider locking bands)

Key insight: Since $\mathrm{Q} = Z_0/\mathrm{R}$, capture vulnerability decreases when either Z_0 increases (deeper processing via L↑ or C↓) or R decreases (less dissipation via meditation, attention discipline). Both paths raise Q and narrow the locking range.

9.2.3 Social Mapping of Parameters

RF Term	Symbol	Social Mapping	Interpretation
Natural frequency	ω_0	Intrinsic belief tuning	Your "native" channel before external influence
Characteristic impedance	$Z_0 = \sqrt{L/C}$	**Depth of processing**	Visible impedance range—determines perceptible density tiers
Quality factor	$Q = Z_0/R$	**Sovereignty / lock resistance**	Primary development measure—harder to capture; $\mathrm{Q} \propto Z_0/\mathrm{R}$
Injected frequency	ω_{inj}	Narrative frequency	The belief state the external signal tries to impose
Frequency offset	$\Delta\omega$	Belief distance	How far the narrative is from your natural position
Injection amplitude	V_{inj}	Media/institutional power	Broadcast strength of narrative source
Oscillator amplitude	V_0	Individual signal strength	Personal influence, platform, inner conviction
Phase	ϕ	Current belief state	Where you are in the belief cycle
Locking range	$\Delta\omega_L \propto R/Z_0$	Capture bandwidth	Range of beliefs you're susceptible to—**inversely proportional to Q**

Critical insight: Lock bandwidth $\propto \mathrm{R}/Z_0 = 1/\mathrm{Q}$. Raising Q narrows your capture range. Three pathways: increase Z_0 through wisdom (L↑) or shadow work (C↓), or reduce R through meditation and attention discipline. See Ch 5 Section 2 for R definition and its role in Q.

9.2.4 Dynamics in Different Regimes

9.2.4.1 Locked State ($|\Delta\omega| < \omega_L$)

The oscillator phase-locks to the injection. Phase stabilizes at:

$$\phi_{locked} = \arcsin\left(\frac{\Delta\omega}{\omega_L}\right)$$

In social terms: Individual's beliefs synchronize with the external narrative. They may feel this is their "own" belief, but it's entrained.

9.2.4.2 Unlocked State ($|\Delta\omega| > \omega_L$)

The oscillator beats against the injection. Phase continuously slips:

$$\phi(t) \approx \sqrt{\Delta\omega^2 - \omega_L^2} \cdot t + \phi_0$$

Average beat frequency:

$$\omega_{beat} = \sqrt{\Delta\omega^2 - \omega_L^2}$$

In social terms: Individual maintains independent oscillation but is perturbed. Experiences cognitive dissonance as their beliefs cycle relative to dominant narrative.

9.2.4.3 Capture and Release Transitions

Capture occurs when:

1. Injection power V_{inj} increases (media saturation)
2. Oscillator power V_0 decreases (isolation, demoralization)
3. Z_0 decreases / Q decreases (trauma increases C, stress increases R)
4. $\Delta\omega$ decreases (narrative shifts toward you)

Release (escape from lock) occurs when:

1. Injection power decreases (narrative loses credibility)
2. Oscillator power increases (community support, inner work)
3. Z_0 **increases** (wisdom L↑, shadow work C↓) → Q = Z_0/R increases
4. **R decreases** (meditation, attention discipline) → Q increases directly
5. Exposure to stronger counter-narrative ($V_{truth} > V_{control}$)

The primary path to capture resistance is raising Q through three pathways: wisdom accumulation (L↑), shadow integration (C↓), and attention discipline (R↓). All three narrow lock bandwidth via Q = Z_0/R.

9.2.5 Sovereignty as Lock Resistance: The Central Insight

The key equation for personal sovereignty:

$$\Delta\omega_{lock} = \frac{\omega_0}{2Q} \cdot \frac{V_{inj}}{V_0} = \frac{\omega_0 R}{2Z_0} \cdot \frac{V_{inj}}{V_0}$$

Low locking bandwidth = personal sovereignty. This equation quantifies what wisdom traditions describe qualitatively.

Q Level	Components (Z_0, R)	Lock Bandwidth	Meaning
Low	Low Z_0 and/or high R	**Wide**	Easily captured by any narrative within large range
Medium	Moderate Z_0, moderate R	Moderate	Vulnerable to strong narratives
High	High Z_0 and/or low R	**Narrow**	Only very powerful, very close signals can capture
Very High	High Z_0 and low R	Nearly zero	Effectively sovereign—immune to typical broadcast

Why this matters for personal development:

1. **High-Q individuals can't be captured by typical narratives.** The locking bandwidth is too narrow—most broadcast signals miss entirely. Both high Z_0 (depth of processing) and low R (attention discipline) contribute to high Q.
2. **This is WHY spiritual development protects against manipulation.** It's not mystical—it's the mathematics of narrowing lock bandwidth.
3. **"Red-pilling" vs "raising Q":**
   - Red-pilling = temporary escape from one lock (may just lock to different narrative)
   - Raising Q = permanent immunity via narrower lock bandwidth ($Z_0\uparrow$ and/or R$\downarrow$)
4. **Sovereignty IS the inverse of lock bandwidth:**

$$\text{Sovereignty} \propto \frac{1}{\Delta\omega_{lock}} \propto Q \propto \frac{Z_0}{R}$$

Connection to Phased Array (Ch 8):

Control systems need to lock array elements to steer the collective beam. If individuals have high Q:

- Their lock bandwidth is too narrow for broadcast capture
- They maintain independent oscillation
- They can seed counter-coherence in neighbors
- The collective beam cannot be steered by injection

This explains why sovereignty suppression is priority #1 for control systems. Lower the population's Q (by suppressing Z_0 or increasing R) $\rightarrow$ widen lock bandwidth $\rightarrow$ easier capture $\rightarrow$ steerable array.

How Q gets suppressed:

- Trauma increases C → lowers Z_0 → lowers Q
- Distraction increases R → lowers Q directly
- Fragmented wisdom prevents L accumulation → lowers Z_0 → lowers Q
- Fear states increase both R and C → lowers Q through both pathways

How to raise Q:

- Wisdom accumulation (L↑) through study, experience integration, contemplation → raises Z_0 → raises Q
- Shadow work (C↓) through trauma processing, emotional integration → raises Z_0 → raises Q
- Reduced distraction (R↓) through meditation, attention discipline → raises Q directly
- Community (coupling) with other high-Q individuals provides mutual support

9.2.6 Network of Coupled Oscillators

For a population of N coupled oscillators, each with injection:

$$\frac{d\phi_n}{dt} = \omega_n + \sum_{m \neq n} K_{nm} \sin(\phi_m - \phi_n) + \omega_{L,n} \sin(\phi_{inj} - \phi_n) + \xi_n$$

Where:

Variable	Description
K_{nm}	Coupling strength between oscillators n and m
$\omega_{L,n}$	Individual locking bandwidth
ϕ_{inj}	Phase of injected narrative
ξ_n	Noise term

This combines:

- **Kuramoto dynamics** (mutual synchronization)
- **Injection locking** (external narrative capture)
- **Stochastic perturbation** (random events)

9.2.7 Competing Injections

When two signals compete (truth vs. control):

$$\frac{d\phi}{dt} = \Delta\omega - \omega_{L,C} \sin(\phi - \phi_C) - \omega_{L,T} \sin(\phi - \phi_T)$$

The oscillator locks to whichever signal has:

1. **Higher effective locking bandwidth** (ω_L)
2. **Closer natural frequency** (smaller $|\Delta\omega|$)

Critical insight: A weaker but more resonant signal can win.

If $V_{truth} < V_{control}$ but $|\omega_0 - \omega_{truth}| \ll |\omega_0 - \omega_{control}|$:

$$\omega_{L,T} \cdot \cos(\phi - \phi_T) > \omega_{L,C} \cdot \cos(\phi - \phi_C)$$

The truth signal captures despite lower power because it's closer to natural frequency.

9.2.7.1 How Q Affects Signal Competition

When multiple signals compete for an oscillator's lock, Q determines not just resistance but **discrimination quality**:

Q Level	Behavior Under Competing Signals
Very Low	Locks to loudest signal regardless of resonance; no discrimination
Low	Locks to strongest signal; slight preference for closer frequency
Medium	Begins discriminating; resonance and power both matter significantly
High	Strong frequency discrimination; locks only to highly resonant signals
Very High	Effectively filters all but near-exact frequency matches; immune to brute-force power

Key insight: High-Q individuals don't just resist capture — they *discriminate* better between signals. This is qualitatively different from mere stubbornness. A high-Q oscillator can distinguish a coherent, resonant signal from a powerful but off-frequency one, making it both harder to capture *and* more responsive to truth.

9.2.7.2 Depth of Processing and Signal Discrimination

Z_0 specifically affects **depth of processing** — the ability to detect structure, coherence, and impedance mismatches in incoming signals. Even within the lock bandwidth (where capture is mathematically possible), high-Z_0 oscillators exhibit what might be called "signal intelligence":

- They detect **internal incoherence** in narratives (impedance mismatch between signal components)
- They perceive **deeper harmonic structure** — whether a signal carries genuine information or is merely powerful
- They register **subtle frequency differences** that low-Z_0 oscillators cannot resolve

This means Z_0 and R contribute to sovereignty through different mechanisms: Z_0 provides perceptual depth (seeing through signals), while low R provides stability (not being swept along). Both feed into Q, but they protect through complementary pathways.

9.2.7.3 Natural Frequency and Truth Resonance

A fundamental asymmetry in the competing injection model: **truth tends to be closer to natural frequency than control signals**.

This asymmetry is an assumption of the model: we define "truth" as the signal closer to the oscillator's natural frequency, and "control" as the signal pushing away from it. The mathematical framework does not inherently distinguish truth from control – the asymmetry is imposed by the physical assumption that unperturbed oscillators tend toward their natural frequency.

Control narratives, by definition, push oscillators *away from* their natural state toward an imposed frequency. This means:

$$|\omega_0 - \omega_{truth}| < |\omega_0 - \omega_{control}|$$

The mathematical consequence is that truth signals gain an effective power boost through resonance proximity, while control signals must overcome a larger detuning gap. For the control signal to maintain lock, it must satisfy:

$$\omega_{L,C} > \omega_{L,T} + |\omega_{control} - \omega_{truth}| \cdot Q/\omega_0$$

This is the **mathematical basis for "truth resonates"**: it's not a metaphor but a consequence of the injection locking equations. The advantage is amplified in high-Q individuals, who are sensitive to small frequency differences and thus experience even stronger preferential coupling to resonant (truthful) signals.

9.2.7.4 Competing Injections in the Modern Information Environment

The modern environment differs from historical eras by presenting **multiple simultaneous injection sources** — institutional media, social platforms, grassroots movements, algorithmic feeds — each attempting lock at different frequencies and powers.

The generalized multi-signal equation:

$$\frac{d\phi}{dt} = \Delta\omega - \sum_k \omega_{L,k} \sin(\phi - \phi_k)$$

In this multi-signal chaos, Q becomes even more critical:

- **Low-Q oscillators** lock to the **loudest** signal (highest $\omega_{L,k}$), regardless of resonance. They are swept by whichever source dominates their information environment.
- **Medium-Q oscillators** experience confusion and rapid switching between partial locks — the "information overwhelm" phenomenon.
- **High-Q oscillators** filter the noise and lock preferentially to the **most resonant** signal (smallest $|\omega_0 - \omega_k|$), effectively extracting signal from chaos.

This explains why increasing information volume without raising population Q leads to confusion rather than enlightenment — and why Q-building is the prerequisite for an informed populace, not merely access to information.

9.2.8 Beamforming Equations for Perception Management

While Sections 2.1-2.7 model individual capture, this section models system-level control using adaptive beamforming mathematics.

9.2.8.1 Beamforming Output

Output of adaptive array:

$$y(t) = \mathbf{w}^H \mathbf{x}(t)$$

Where:

Variable	Description
$\mathbf{x}(t)$	input signals from all elements
$\mathbf{w}$	weight vector (complex gains)
^{H}	Hermitian transpose

9.2.8.2 Minimum Variance Distortionless Response (MVDR)

Optimal weights that minimize interference while preserving desired signal:

$$\mathbf{w}_{MVDR} = \frac{\mathbf{R}^{-1}\mathbf{a}(\theta_0)}{\mathbf{a}^H(\theta_0)\mathbf{R}^{-1}\mathbf{a}(\theta_0)}$$

Where $\mathbf{R}$ = covariance matrix, $\mathbf{a}(\theta_0)$ = steering vector to desired direction.

In perception management: θ_0 = official narrative direction.

9.2.8.3 Direction of Arrival (DOA) Estimation

Before nulling, the system must locate threats:

$$P(\theta) = \frac{1}{\mathbf{a}^H(\theta)\mathbf{R}^{-1}\mathbf{a}(\theta)}$$

Peaks indicate signal sources. This is surveillance—identifying which voices, platforms, and communities pose threats.

9.2.8.4 Null Steering

Once located, nulls are steered toward threats:

$$\mathbf{w}^H\mathbf{a}(\theta_{null}) = 0$$

Implementation: deplatforming, algorithmic suppression, financial debanking, coordinated debunking.

9.2.8.5 Adaptation Rate

The system must adapt faster than threats evolve:

$$\tau_{adapt} < \tau_{threat}$$

If threats evolve faster than countermeasures, nulls miss and signals propagate.

Current environment: Viral spread ($\tau_{threat} \sim$ hours) challenges adaptation ($\tau_{adapt} \sim$ days-weeks).

9.2.8.6 Weight Update Algorithm (LMS)

Least Mean Squares adaptation:

$$\mathbf{w}(n+1) = \mathbf{w}(n) + \mu \cdot e^*(n) \cdot \mathbf{x}(n)$$

Where $e(n)$ = error (difference from desired output), μ = learning rate.

The system learns which signals to suppress based on deviation from narrative.

9.3 Assumptions & Limitations

9.3.1 Model Assumptions

1. **Beliefs are oscillatory**: Individual worldviews can be modeled as periodic functions. This assumes beliefs have cycles, not fixed points.
2. **Coupling is sinusoidal**: The $\sin(\phi)$ dependence assumes smooth, continuous belief influence. Sharp thresholds are not captured.
3. **Single dominant frequency**: Each individual has one primary "natural frequency." In reality, people have multiple belief dimensions.
4. **Additive injection**: Multiple narratives add linearly. Non-linear interactions (reinforcement, interference) are simplified.
5. **Time-invariant parameters**: Q, V_0, ω_0 are constant during simulation. Real people change these through experience.

9.3.2 Injection Locking Limitations

1. **Multi-dimensional belief space**: Real beliefs span many dimensions; this 1D model captures one axis at a time.
2. **Discrete events not modeled**: Sudden revelations, trauma, "red pill moments" are not captured by continuous dynamics.
3. **Memory effects absent**: Real humans have history-dependent responses; the model is memoryless. See Chapter 5 (Capacitance) for the memory mechanism via stored charge.
4. **Network effects simplified**: Full network topology effects (cascades, phase transitions) require more complex analysis. See Chapter 8 (Phased Array) for complete network-level analysis.
5. **No cognitive processing**: The model doesn't distinguish between conscious processing and unconscious entrainment.

9.3.3 Beamforming Model Assumptions

1. **Beamforming analogy applies**: Perception management operates through mechanisms analogous to adaptive beamforming—main beam steering, null placement, and sidelobe control. This assumes that information control systems optimize a directional objective function, not merely suppress content.
2. **Collective SNR is the relevant metric**: The model assumes that collective perception depends on the signal-to-noise ratio at the population level, integrating individual Q factors (Chapter 5) and array gain (Chapter 8). Individual awareness matters only insofar as it contributes to collective SNR.
3. **Adaptive algorithms converge**: The LMS/MVDR models assume that control systems converge to effective suppression strategies. In practice, convergence may be disrupted by rapid information spread or high-Q nodes that resist null placement.
4. **Linear superposition of narratives**: Multiple narrative sources combine linearly at the population level. Non-linear effects (narrative synergy, cognitive dissonance cascades) are not captured.

9.3.4 Beamforming Limitations

1. **Static threat model**: The model treats narrative threats as fixed signal sources. In practice, counter-narrative strategies evolve, with sources adapting to avoid null placement (frequency hopping, platform migration).
2. **No cognitive modeling**: The beamforming analogy captures information-space dynamics but does not model individual cognitive processing, emotional responses, or meaning-making that mediate between information exposure and belief formation.
3. **Homogeneous population response**: The model assumes uniform susceptibility across the population. Real populations have heterogeneous Q distributions, information diets, and cognitive profiles that produce varied responses to the same narrative environment.
4. **Binary signal classification**: The model classifies signals as "main beam" (approved narrative) or "interference" (suppressed). Real information environments contain gradients of acceptability and complex interactions between partially-approved narratives.

9.3.5 Falsification Conditions

The model would be falsified by:

1. **Populations that never lock despite saturation**: If extremely high-powered narratives consistently fail to capture populations.
2. **High-Q individuals easily captured**: If discerning, aware individuals lock as easily as distracted ones.
3. **No threshold effects**: If belief capture is purely proportional to exposure rather than showing phase-transition behavior.
4. **Counter-narratives never succeed**: If lower-power truth signals cannot compete regardless of resonance.

9.4 Predictions & Thresholds

9.4.1 Individual Locking Predictions

Prediction 1: Locking range scales with power differential

$$\Delta\omega_{lock} \propto \frac{V_{inj}}{V_0}$$

Test: Measure belief change vs. media exposure intensity. Should show widening capture range with intensity.

Prediction 2: High-Q individuals have narrow locking ranges

Trained contemplatives, critical thinkers, and the "naturally immune" should show:

- Resistance to narrative capture
- Quick escape from lock when alternative signals available
- Stable independent oscillation

Prediction 3: Lock is binary, not gradual

Individuals either lock completely or maintain independent oscillation. Partial lock is unstable (beat frequency regime).

9.4.2 Network Cascade Predictions

Prediction 4: Critical mass for narrative escape

When fraction f_c of population escapes lock, cascade release begins:

$$f_c \approx \frac{\omega_{L,C}}{\omega_{L,C} + K_{mean}}$$

Where K_{mean} is mean coupling strength.

Justification for $\omega_{L,C} = 0.3$:

- Propaganda studies consistently show ~30-40% of a population is movable on any given issue through sustained media campaigns
- The Overton window on most policy dimensions spans roughly 30% of the full ideological spectrum
- Normalizing to a belief-space range of 1.0, this gives $\omega_{L,C} \approx 0.3$ as the effective institutional locking bandwidth

Justification for $K_{mean} = 0.5$:

- The two-step flow model (Katz & Lazarsfeld, 1955) demonstrated that personal influence is roughly comparable to or stronger than institutional media in shaping opinion
- $K_{mean} = 0.5$ vs $\omega_{L,C} = 0.3$ reflects peer influence being somewhat stronger than institutional injection, consistent with this finding
- The critical ratio $\omega_{L,C}/(\omega_{L,C} + K_{mean})$ is robust to proportional scaling of both parameters

Sensitivity note: f_c ranges from 50% (no coupling, $K = 0$) to 0% (infinite coupling). The value of 37.5% is consistent with historical observations of ~30-40% critical mass preceding narrative collapses (see Section 9.5.4 cascade evidence).

For typical parameters ($\omega_{L,C} = 0.3$, $K_{mean} = 0.5$):

$$f_c \approx \frac{0.3}{0.8} = 37.5\%$$

Test: Historical narrative collapses should show ~30-40% critical mass before sudden shift.

Prediction 5: High-Q seeds trigger cascades

Individuals with high Q (narrow locking range) can:

1. Escape lock first
2. Inject counter-signal to neighbors
3. Help others escape through coupling

The "awakened seeds" effect: A small population of high-Q individuals can trigger population-wide escape if:

$$N_{seeds} \cdot V_{seeds} > N_{locked} \cdot \omega_{L,C}/K$$

9.4.3 Competing Narrative Predictions

Prediction 6: Coherence beats power

A coherent (phase-aligned) truth signal can overcome a more powerful but incoherent control signal if:

$$V_{truth} \cdot r_{truth} > V_{control} \cdot r_{control}$$

Where r is the coherence (order parameter) of each signal source.

Prediction 7: Resonance amplifies weak signals

A truth signal close to population's natural frequency gains effective power boost:

$$V_{eff} = V_{truth} \cdot \left(1 + Q_{pop} \cdot \frac{\Delta\omega_{control}}{\Delta\omega_{truth}}\right)$$

This is a linearized approximation valid near resonance; the exact gain follows the standard resonance curve $V_{eff} = V_{truth}/\sqrt{1 + Q^2(\omega/\omega_0 - \omega_0/\omega)^2}$.

When $\Delta\omega_{truth} \ll \Delta\omega_{control}$, even weak truth signals dominate.

9.4.4 Control System Predictions

Prediction 8: Mainstream narrative should be consistent (main beam aimed at one direction).

Prediction 9: Threatening sources should experience coordinated suppression (null steering).

Prediction 10: New threat sources should face delay before suppression (DOA estimation time).

Prediction 11: Suppression should be proportional to threat level.

Prediction 12: The system should show learning—repeated patterns get faster response.

9.4.5 Collective Coherence Predictions

Prediction 13: Groups composed of meditators in measured coherent states should produce stronger collective effects (measured via environmental random number generator deviation, shared physiological entrainment, etc.) than equally-sized groups of non-meditators, by a factor approximating the average Q ratio.

Prediction 14: The critical mass threshold for collective effects (from Chapter 8) should be lower when participants have higher individual Q — fewer high-Q people are needed than low-Q people to achieve the same collective beam strength.

9.4.6 Threshold Summary Table

Threshold	Condition	Population Effect
Individual lock	$\|\Delta\omega\| < \omega_L$	Person captured by narrative
Individual escape	$V_{counter} > V_{current}$	Person releases from lock
Cascade initiation	$f_{unlocked} > f_c$	Narrative begins collapsing
Complete release	$K_{mean} > \omega_L$	Coupling overwhelms injection
Permanent capture	$Q_{pop} \to 0$	Population cannot escape

9.5 Evidence Synthesis

9.5.1 Injection Power Evidence

Media Concentration Studies

Media Ownership Consolidation (1983-2023)

- 1983: 50 companies controlled 90% of US media
- 2023: 6 companies control 90% of US traditional broadcast/print media (Comcast, Disney, ViacomCBS, Warner, Fox, News Corp). The digital/social media landscape has different concentration patterns, though platform companies (Google, Meta, Apple) represent comparable or greater concentration in information distribution.
- Fewer sources = higher per-source power ($V_{inj}\uparrow$) = wider locking range

Propaganda Saturation Research

Metric	Historical	Current	Change
Daily media exposure	5 hours (1970)	12+ hours (2023)	+140%
Information sources used	3-5	1-2 (algorithmically curated)	-60%
Ad exposure/day	500 (1970)	5,000+ (2023)	+900%

Information Environment Measurements

Echo chamber studies (Bakshy, 2015)

- Social media users predominantly see agreeing viewpoints

Agenda-setting research

- Media doesn't tell people *what* to think but *what to think about*

Overton window manipulation

- Constant exposure shifts perception of acceptable discourse

Interpretation

- Media consolidation directly increases V_{inj} in the Adler equation: $\omega_L = \frac{\omega_0}{2Q} \cdot \frac{V_{inj}}{V_0}$ — fewer, more powerful sources widen the locking range for entire populations
- The 10× increase in daily media exposure (5→12+ hours) combined with algorithmic curation represents a dramatic increase in effective injection duty cycle — sustained injection maintains lock more reliably
- Echo chambers reduce effective $\Delta\omega$ (belief distance) by filtering out competing signals, making the locking condition $|\Delta\omega| < \omega_L$ easier to satisfy even with moderate injection power

9.5.2 Locking Range Evidence

Attitude Change Research

Elaboration Likelihood Model (Petty & Cacioppo)

- Low-involvement audiences susceptible to peripheral cues (repetition, authority)

Mere exposure effect (Zajonc)

- Familiarity increases liking—explains repetition strategy

Inoculation theory (McGuire)

- Pre-exposure to weak counterarguments increases resistance

Interpretation

- The Elaboration Likelihood Model maps directly to Q: low-involvement (low-Q) audiences are captured through peripheral cues (high ω_L from repetition/authority), while high-involvement (high-Q) audiences require central-route processing (signal must be close to ω_0 to achieve lock)
- Mere exposure increasing liking is the injection locking mechanism in its simplest form: sustained V_{inj} at constant frequency gradually captures oscillators within the locking range
- Inoculation theory corresponds to temporarily raising Q through pre-exposure: weak counterarguments activate critical processing (R↓, effective Q↑), narrowing lock bandwidth before the main injection arrives

Persuasion Resistance Studies

Population	Locking Resistance	Factors
High education	Higher	Better critical evaluation
High need for cognition	Higher	Evaluates arguments not cues
Strong prior attitudes	Higher	Larger $\Delta\omega$ from narrative
High anxiety	Lower	Q drops under stress

Classic Social Psychology Experiments

Milgram obedience experiments (1963)

- ~65% of participants administered maximum "shock" under authority instruction — a data point for locking bandwidth under authority injection (V_{inj} from perceived legitimate authority)

Asch conformity experiments (1951)

- 75% of participants conformed at least once to an obviously wrong group answer — demonstrates peer coupling (K) contribution to effective locking range

Festinger's cognitive dissonance (1957)

- The discomfort of holding contradictory beliefs maps directly to the beat frequency regime: an unlocked state where the oscillator beats against the injected signal, producing psychological distress until the individual either locks or moves further away

Cult Deprogramming Literature

Hassan's BITE Model

- Behavior, Information, Thought, Emotional control

Exit patterns

- Sudden vs. gradual awakening (phase transition signature)

Key factors in escape

- Exposure to counter-information, supportive community, emotional exhaustion of cult

9.5.3 Q Factor Evidence

Mindfulness and Resistance to Manipulation

Farias (2016)

- Meditators show reduced susceptibility to anchoring bias

Kiken & Shook (2011)

- Brief mindfulness reduces automatic biases

Interpretation

- Mindfulness raises Q by increasing awareness of manipulation attempts

Education and Critical Thinking Effects

Education Level	Narrative Resistance	Notes
Less than high school	Baseline	High susceptibility
High school	+10% resistance	Some critical skills
College	+25% resistance	Exposure to debate
Graduate	+35% resistance	Research training

Note: Elite education may lock to elite narratives (different ω, still locked).

Contemplative Practice Outcomes

Davidson (2003)

- Long-term meditators show altered default mode activity

Killingsworth & Gilbert (2010)

- Mind-wandering associated with unhappiness; meditation reduces wandering

Interpretation

- Practice literally changes Q factor—higher Q = narrower locking, harder to capture

Dual-Process Cognition

Kahneman, System 1 vs System 2 (2011)

- System 1 (fast, heuristic, automatic) maps to low-Q processing: easily captured by peripheral cues, repetition, and authority signals
- System 2 (deliberate, effortful, analytical) maps to high-Q processing: resistant to capture, evaluates signal coherence before locking
- The "cognitive miser" tendency (defaulting to System 1) explains why baseline Q is low for most people in most contexts

Physiological Q Proxies

Heart Rate Variability (HRV) research

- Higher HRV correlates with greater emotional regulation, stress resistance, and cognitive flexibility
- HRV may serve as a physiological proxy for Q: individuals with high HRV show greater resistance to impulsive entrainment and better discrimination between genuine and spurious signals
- Meditation and contemplative practices increase HRV, consistent with the Q-raising mechanism

9.5.4 Cascade Escape Evidence

Historical Narrative Collapses

Event	Years to Collapse	Tipping Point
Soviet dissolution	74 years → 2 years	~30% openly dissenting
Berlin Wall fall	40 years → months	Mass protests
#MeToo cascade	Decades → weeks	Critical mass of stories
COVID narrative shifts (e.g., lab leak hypothesis: dismissed 2020, accepted as plausible by 2023; mask efficacy: reversed multiple times)	Months	Accumulating contradictions

Phase Transition Signatures

- Long apparent stability
- Accelerating cracks
- Sudden collapse
- New equilibrium forms rapidly
- This pattern is a classic phase transition, not linear change

Paradigm Shift Case Studies

- **Kuhn (1962)** Normal science → crisis → revolution → new normal
- **Planck's principle** "Science advances one funeral at a time"
- **Model prediction** Paradigm lock maintained by locked population; when unlock threshold crossed, rapid cascade

Threshold and Contagion Models

Granovetter's threshold models (1978)

- Mathematical models of collective behavior where individuals have different thresholds for joining an action — directly parallel to the f_c critical mass prediction
- The distribution of individual thresholds determines whether cascades occur, matching the Q-distribution dependence of the injection locking model

Centola & Macy (2007)

- Complex contagion requires multiple exposures (reinforcement) before adoption, unlike simple contagion
- Maps directly to the coupling threshold K: escape from narrative lock requires sufficient coupling from multiple unlocked neighbors, not just a single counter-signal

Interpretation

- Historical narrative collapses consistently show ~30-40% critical mass before sudden shift, matching the predicted $f_c \approx \omega_{L,C}/(\omega_{L,C} + K_{mean}) \approx 37.5\%$ (Section 9.4.2)
- The "long stability → accelerating cracks → sudden collapse" pattern is the signature of a phase transition, not linear change — precisely what the Kuramoto-Adler coupled oscillator model predicts when unlock fraction crosses f_c
- Granovetter's threshold distribution maps to the Q distribution in the population: high-Q individuals escape lock first (lowest threshold), seeding the cascade for progressively lower-Q neighbors

9.5.5 Competing Narrative Evidence

Information Warfare Outcomes

Conflict	Institutional Power	Grassroots Power	Outcome
Iraq WMD narrative	Very high	Low	Institutional won (temporarily)

Conflict	Institutional Power	Grassroots Power	Outcome
Vaccine safety debates	Very high	Moderate	Ongoing contestation
Election integrity 2020	Very high	Moderate-high	Unresolved polarization
UAP reality	Moderate	Growing	Shifting toward disclosure

Grassroots vs. Institutional Messaging

- **Arab Spring** Social media enabled coordination despite state media control
- **GME short squeeze** Reddit coordinated against institutional finance
- **Limitations** Platforms can be captured, algorithms adjusted

Viral Truth Propagation

- **Rumor accuracy (Allport & Postman)** Surprisingly accurate transmission under some conditions
- **Cascades require**:
  1. Credible initial source
  2. Resonance with audience beliefs (small $\Delta\omega$)
  3. Network connectivity for coupling K
  4. Low noise environment

Historical Case Studies of Resonance Overcoming Power

Soviet samizdat literature

- Underground truth publications (V_{truth} far below state propaganda $V_{control}$) competed against massive institutional injection
- Resonance with lived experience ($|\omega_0 - \omega_{truth}| \ll |\omega_0 - \omega_{control}|$) gave samizdat effective power beyond its broadcast strength
- Eventually won through accumulated resonance as the gap between official narrative and reality widened

Galileo and heliocentrism

- Truth signal initially locked out by overwhelming institutional power (Church authority)
- Won through resonance with observational reality — the heliocentric model's predictions matched telescope observations (small $\Delta\omega_{truth}$), while geocentric epicycles grew increasingly strained (large $\Delta\omega_{control}$)
- Demonstrates that truth signals can survive indefinite power disadvantage when resonance is strong enough

Interpretation

- The competing injections equation $\frac{d\phi}{dt} = \Delta\omega - \omega_{L,C}\sin(\phi - \phi_C) - \omega_{L,T}\sin(\phi - \phi_T)$ (Section 9.2.7) predicts that a weaker but more resonant signal can win — samizdat and Galileo cases confirm this: $V_{truth} < V_{control}$ but $|\omega_0 - \omega_{truth}| \ll |\omega_0 - \omega_{control}|$

- Information warfare outcomes show that institutional power (V_{inj}) is necessary but not sufficient for maintaining lock — resonance with lived experience ($\Delta\omega$) determines long-term outcomes
- The modern multi-signal environment (Section 9.2.7.4) explains why information volume without Q increase produces confusion: low-Q oscillators lock to the loudest signal, medium-Q oscillators experience rapid switching, and only high-Q oscillators extract signal from chaos

9.5.6 Control System Evidence

9.5.6.1 Algorithmic Manipulation

Study	Key Finding	Model Correspondence
Epstein & Robertson (2015)	SEME can shift voting preferences 20%+	DOA estimation + null steering in code
Vorhies (2019)	Google internal "algorithmic unfairness" docs (Vorhies's claims are based on documents he states he obtained internally; independent verification has been limited)	Manual intervention = weight adjustment
Haugen (2021)	Facebook algorithm amplifies engagement/outrage	LMS optimization for engagement signal

Model correspondence: Algorithmic bias implements the DOA estimation (Section 9.2.8.3) and null steering (Section 9.2.8.4) functions — surveillance identifies threat sources, then ranking/visibility adjustments place nulls.

9.5.6.2 Coordinated Suppression

Target	Timing	Platforms	Model Correspondence
Alex Jones (2018)	24 hours	Apple, FB, YT, Spotify	τ_adapt < τ_threat achieved
David Icke (2020)	48 hours	YT, FB, Twitter	Cross-platform coordination
COVID skeptics (2020-21)	Rolling	All major	LMS learning from prior actions
Andrew Tate (2022)	72 hours	YT, FB, IG, TikTok	Predictive category nulling

Model correspondence: Coordinated deplatforming within 24-72 hours demonstrates achieved adaptation rate (Section 9.2.8.5). Rolling enforcement shows LMS weight updates (Section 9.2.8.6)

learning from prior actions. Whether cross-platform synchronization reflects centralized coordination, mimetic institutional behavior, or independent policy application is an open question. The model predicts the effect is functionally identical regardless of mechanism.

9.5.6.3 Fact-Checker Networks

Organization	Major Funders	Model Correspondence
PolitiFact	Poynter (Koch, Gates, Google)	Centralized steering vector
FactCheck.org	Annenberg Foundation	Shared θ_0 direction
NewsGuard	Microsoft, Publicis	MVDR weight coordination
AFP Fact Check	Agence France-Presse (state-affiliated)	Government steering input

Model correspondence: IFCN network implements MVDR beamformer — shared funding = centralized control of steering vector a(θ_0). Circular cross-referencing creates self-reinforcing covariance matrix R.

9.5.6.4 Search Manipulation

Update	Effect	Model Correspondence
Medic (2018)	-80% alt health traffic	Null placement on category
YMYL policy	Stricter "authority" standards	Domain-specific learning rate μ
Natural News	Near-zero visibility	Complete null: w^H a(θ) ≈ 0

Model correspondence: Algorithm updates implement LMS weight equation — each update adjusts weights based on error signal (deviation from desired narrative output).

9.5.7 Collective Coherence Evidence

9.5.7.1 Group Coherence Research

Study	Key Finding	Model Correspondence
HeartMath group studies	Individual HRV coherence predicts group quality	G_gnosis $\propto$ Q confirmed
TM meditation research	Experienced meditators = stronger per-capita effects	Higher Q = more amplitude contribution

Model correspondence: HRV coherence serves as proxy for resonance state. Finding that individual coherence predicts group coherence confirms $|AF|^2 \propto (f \cdot N \cdot Q\_avg)^2$ dependence.

9.5.7.2 Neuroscience Support

Study	Key Finding	Model Correspondence
McGilchrist (2009)	Right-hemisphere = holistic; left = sequential	R-hemi = gnosis; L-hemi = ego mode
Damasio (1994)	Somatic markers required for good decisions	Body-based resonance information essential

Model correspondence: McGilchrist's hemispheric distinction maps to resonance vs. off-resonance operation. Damasio confirms that purely analytical (ego) processing produces worse outcomes than integrated (gnosis) processing.

9.5.8 System Architecture Synthesis

The perception management system operates as a five-stage adaptive beamformer:

Stage 1 — Surveillance (DOA Estimation): Social media monitoring and search query analysis identify emerging information sources. This maps to the DOA estimation function $P(\theta) = 1 / [a^{H(\theta)R}\{-1\}a(\theta)]$ — peaks indicate signal sources requiring classification.

Stage 2 — Threat Classification: AI systems and human review categorize sources by threat level (1-10 scale). Higher threat levels receive priority for null placement.

Stage 3 — Weight Calculation: Policy directives combined with algorithmic optimization determine response intensity. This implements the MVDR weight calculation $w\_MVDR = R^{-1}a(\theta\_0) / [a^{H(\theta\_0)R}\{-1\}a(\theta\_0)]$.

Stage 4 — Null Steering: Suppression mechanisms execute — deplatforming, ranking demotion, fact-check labels, financial debanking. This implements the null constraint $w^H a(\theta\_null) = 0$.

Stage 5 — Output: The filtered information environment reaches the population, with main beam pointed at approved narratives and nulls placed toward threats.

Current adaptation gap: System adaptation (τ_adapt ~ days-weeks) struggles against viral spread (τ_threat ~ hours). Response: predictive nulling of categories rather than individual items.

Emerging failure modes: (1) Whack-a-mole problem — too many sources; (2) Streisand effect — suppression draws attention; (3) Platform alternatives — Telegram, Rumble reduce null effectiveness; (4) Credibility loss — fact-checker trust declining.

9.5.9 Synthesis: Current Locking State Assessment

Population Segments

The following estimates are the author's assessment informed by media trust survey trends (Gallup media confidence, Edelman Trust Barometer) mapped to locking-state categories. They are not direct measurements of "locking state" and should be treated as order-of-magnitude indicators.

Segment	Estimated %	Locking State	Primary Lock
Firmly locked to mainstream	30-40%	Stable lock	V_inj dominates
Questioning but locked	25-35%	Unstable lock	Near transition
Actively unlocked	15-25%	Independent oscillation	Counter-narrative
Never locked	5-10%	Always independent	High Q outliers

Injection Locking Evolution

- Historical: Near-universal lock (pre-internet)
- Current: Fragmenting, contested
- Trend: Lock weakening due to:
  - Declining V_inj effectiveness (trust collapse)
  - Rising V_counter (alternative media)
  - Increasing K (network connectivity)
  - Rising average Q (meditation, awareness trends)

Threshold Analysis

- Current estimate: 20-30% unlocked
- Cascade threshold: ~35-40%
- Timeline: Years, not decades (at current trajectory)

9.5.10 Source Mapping and Uncertainty Bands for Key Numeric Claims

The chapter's aggregate percentages and thresholds are modeled assessments, not direct locking-state measurements. Treat them as scenario bands with explicit uncertainty:

Quantity	Central Estimate	Uncertainty Band	Basis
Firmly locked segment	35%	30-40%	Media trust and narrative-alignment survey trends
Questioning but still locked	30%	25-35%	Mixed-attitude cluster in longitudinal polling
Actively unlocked	20%	15-25%	Alternative media adoption and self-report autonomy indicators

Quantity	Central Estimate	Uncertainty Band	Basis
Never locked outliers	7%	5-10%	Persistent low-conformity subgroup estimates
Cascade onset threshold	37.5%	35-40%	Coupled-oscillator transition heuristic

Confidence labeling:

- High: directly measured variable with repeated instrumentation.
- Medium: directly measured proxy mapped to model state.
- Low: inferred state without direct lock-state instrumentation.

Current chapter labels for these values: **Low-Medium confidence**. Use for planning ranges, not point forecasts.

Evidence Synthesis

- Detailed source sections: 9.5, 9.5.1, 9.5.2, 9.5.3, 9.5.4, 9.5.5, 9.5.6, 9.5.7.

Assumptions

- Detailed source sections: 9.3, 9.3.1, 9.3.3.

Limitations

- Detailed source sections: 9.3, 9.3.2, 9.3.4.

Falsification

- Detailed source sections: 9.3.5.

Predictions

- Detailed source sections: 9.4, 9.4.1, 9.4.2, 9.4.3, 9.4.4, 9.4.5.

Strategic Relevance

Why It Matters

9.6.1 Defense Against Capture

For individuals:

1. **Raise Z_0 through L↑**: Wisdom accumulation, contemplative practice, integrated experience ($\rightarrow$ raises Q)
2. **Raise Z_0 through C↓**: Shadow work, trauma integration, releasing stored charge ($\rightarrow$ raises Q)
3. **Reduce R**: Meditation reduces resistance/dissipation $\rightarrow$ Q = Z_0/R increases
4. **Increase V_0**: Build platform, strengthen voice
5. **Maintain awareness of natural state**: Know your true beliefs (your f_0)
6. **Minimize exposure during low-Q states**: Avoid media when traumatized, stressed, or depleted

For communities:

1. **Create counter-injection**: Coherent alternative narrative
2. **Strengthen coupling K**: Tight community bonds
3. **Protect high-Q members**: Shield awakened seeds who can trigger cascade
4. **Provide escape bridges**: Help locked members release through Q-building practices

9.6.2 Understanding Control Strategy

The injection locking model reveals why control systems:

1. **Maximize broadcast power**: Higher V_{inj} = wider locking range
2. **Repeat endlessly**: Lock requires sustained injection
3. **Attack Q-building practices**: Discredit meditation, shadow work, wisdom traditions — suppressing these prevents Q from rising, keeping capture bandwidth wide
4. **Increase trauma/shadow (C↑)**: Unprocessed trauma lowers Z_0, widens capture range
5. **Isolate**: Reduce coupling K so lock depends only on injection
6. **Create fear/stress**: Temporarily increases R, dropping Q = Z_0/R, enabling capture
7. **Co-opt natural frequencies**: Make narratives feel "natural"

9.6.3 Path to Mass Unlocking

Based on model predictions:

1. **Cultivate high-Q seeds** (100s to 1000s of awakened individuals)
2. **Build coherent counter-signal** (truth with r > 0.5)
3. **Strengthen network coupling** (community bonds)
4. **Wait for injection power drop** (narrative crisis)
5. **Trigger cascade when threshold reached** (~30-40% unlocked)

The model predicts sudden, not gradual, collective escape from narrative lock.

What To Watch

- 3. **Protect high-Q members**: Shield awakened seeds who can trigger cascade
- 2. **Build coherent counter-signal** (truth with r > 0.5)
- 5. **Trigger cascade when threshold reached** (~30-40% unlocked)

Boundaries of Use

- Apply this chapter as model-conditional doctrine; treat speculative elements as hypothesis overlays.

9.6 References to Other Chapters

- **Chapter 5 (RLC Circuit)** $Q = Z_0/R$ derivation; Q as primary sovereignty measure; Z_0 as depth of processing
- **Chapter 2 (Densities)** Higher Z_0 enables higher density access (depth of processing); $Q = Z_0/R$ determines lock resistance and sovereignty
- **Chapter 8 (Phased Array)** Coherence effects that amplify counter-injection; Section 8.7 on element quality and collective beam strength
- **Chapter 13 (Paradigm Shielding)** How injection power is maintained at the system level
- **Chapter 14 (Link Budget)** Injection locking as component of total gain/loss

---

End of Chapter 9: Injection Locking and Perception Management

Chapter 10: Spin Coherence Fundamentals

The Master Variable for Torsion Effects

KEY FINDINGS — Chapter 10: Spin Coherence Fundamentals

Evidence-tier key: [L1] established/replicated evidence; [L2] grounded extension with moderate uncertainty; [L3] speculative hypothesis; [L4] conceptual/anecdotal.

- The spin coherence order parameter σ governs the strength of all torsion field effects via $T_{eff} = T_{single} \cdot N \cdot \sigma^2$ scaling **[L1-L2: grounded in Einstein-Cartan theory and phased array physics]**
- Coherent spin ensembles can partially screen the cosmic inertial reference frame, producing effective mass reduction $m_{eff} = m_0(1 - T_{local}^2/T_{critical}^2)$ **[L2-L3: theoretical extension of established Machian/teleparallel frameworks]**
- Magnon-torsion coupling provides the nearest-term experimental pathway for detecting coherent torsion effects **[L2: based on established condensed matter physics]**
- Timeline mechanics emerge as a temporal extension of nonlocal torsion correlations, with branch stability scaling as $\sigma^2 \cdot N_{observers}$ **[L3: speculative theoretical extension]**
- The ER=EPR conjecture, combined with coherent spin amplification, provides a theoretical pathway from micro-scale entanglement to macroscopic spatial bridging **[L3: based on unproven conjecture]**

10.1 Introduction: Spin Coherence as Master Variable

10.1.1 The Central Thesis

This chapter establishes **spin coherence** as the master variable governing the strength of torsion field effects. While previous chapters established the theoretical framework—torsion fields (Chapter 0), impedance tiers (Chapter 2), and geometric optimization (Chapter 3)—this chapter provides the **quantitative bridge** from microscopic spin ensembles to macroscopic phenomena.

The key insight: **The degree of spin alignment determines the strength of torsion effects**. Whether considering individual consciousness, group coherence, or engineered devices, the coherence parameter σ controls what is possible.

10.1.2 Why Spin Coherence Matters

Spin State	Torsion Field Scaling	Effect Potential
Random/incoherent	$\sqrt{N}$ scaling	Negligible for large N
Partially coherent	Weak (N·σ scaling)	Subtle anomalies
Highly coherent	Strong (N·σ^2 scaling)	Measurable effects

Spin State	Torsion Field Scaling	Effect Potential
Perfect coherence	Maximum (N^2 scaling)	Full torsion access

The engineering challenge: Achieving and maintaining high spin coherence ($\sigma \to 1$) in macroscopic systems. This chapter develops the physics of this challenge.

> **Notation note**: This chapter uses T in three distinct senses: (1) $T^{\lambda}_{\mu\nu}$ for the torsion tensor (Section 10.3.3), (2) T for temperature in technology comparison tables (Section 10.7), and (3) $\mathcal{T}$ for torsion field strength in equations. Context and subscripts distinguish these uses.

10.1.3 Chapter Overview

Section	Content
10.2	Torsion field generation from coherent spin
10.3	Inertia as spin coupling (Machian/teleparallel framework)
10.4	Mechanism pathways for dimensional effects and spatial bridging
10.5	Temporal torsion coupling: timeline mechanics
10.6	Spin beams and magnonic carriers
10.7	Spin coherence engineering approaches
10.8	Qualitative thresholds for exotic effects
10.9	Experimental signatures and predictions

10.2 Torsion Field Generation from Coherent Spin Ensembles

10.2.1 The Spin Coherence Order Parameter

The **spin coherence order parameter** σ quantifies the phase alignment of N spins:

$$\sigma = \frac{1}{N} \left| \sum_{i=1}^{N} s_i \, e^{i\phi_i} \right|$$

Where:

- s_i = magnitude of spin i (normalized to 1 for identical spins)
- ϕ_i = phase of spin i
- N = total number of spins

Interpretation:

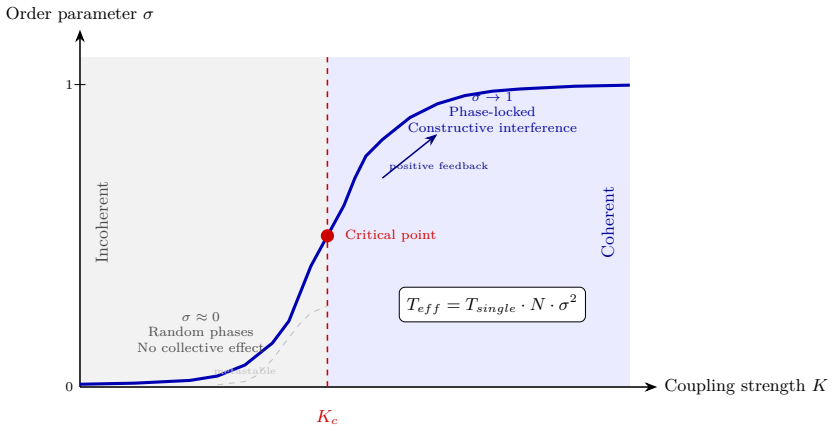

Figure 10.1: Spin coherence phase diagram — order parameter σ vs coupling strength showing critical transition.

σ Value	Meaning
0	Random phases, complete cancellation
0.1-0.3	Weak partial alignment
0.3-0.7	Moderate coherence
0.7-0.9	Strong coherence
1.0	Perfect phase alignment

10.2.2 Torsion Amplification from Coherence

A single spin generates torsion field $\mathcal{T}_{single}$. For N coherent spins:

$$\mathcal{T}_{eff} = \mathcal{T}_{single} \cdot N \cdot \sigma^2$$

The σ^2 **dependence** is critical—coherence enters quadratically, just as in phased array antenna gain. This means doubling coherence quadruples the effective torsion field.

Comparison with incoherent case:

- Incoherent ($\sigma \to 0$): $\mathcal{T}_{eff} \sim \mathcal{T}_{single} \cdot \sqrt{N}$ (random walk)
- Coherent ($\sigma \to 1$): $\mathcal{T}_{eff} \sim \mathcal{T}_{single} \cdot N$ (linear scaling)
- Gain from coherence: $N^{1/2}$ (enormous for large N)

10.2.3 Coherent Torsion Field Equation

The torsion field from a coherent spin ensemble:

$$\vec{\mathcal{T}}(\vec{r}) = \kappa \cdot N \cdot \sigma^2 \cdot \frac{s_0}{r^n} \cdot f(\theta, \phi)$$

Where:

- κ = spin-torsion coupling constant
- s_0 = single-spin torsion amplitude
- n = decay exponent (may differ from electromagnetic $1/r^2$)

- $f(\theta, \phi)$ = angular pattern (depends on spin orientation)

  Epistemic Note: The decay exponent n for torsion fields remains theoretically uncertain. Some models predict $n < 2$ (slower decay than EM), potentially explaining non-local effects. Experimental determination is a key research priority.

10.2.4 Why Consciousness Creates Torsion

From Chapter 0 (Torsion Foundation):

- Spin couples to torsion as mass couples to curvature (Einstein-Cartan theory)
- Biological systems contain enormous numbers of spin sources (electrons, nuclei)
- Consciousness may involve quantum coherence in neural systems
- **Focused intention = spin coherence = torsion generation**

The mechanism pathway: Consciousness generates neural coherence, which aligns molecular spins, which generates macroscopic torsion fields. The brain is not creating something from nothing—it is organizing existing spin degrees of freedom into coherent patterns.

10.2.5 Loop Quantum Gravity Foundation

The spin coherence framework finds rigorous foundation in Loop Quantum Gravity (LQG). In LQG, spacetime geometry itself is fundamentally discrete and spin-based at the Planck scale.

Spin Networks as Quantum Geometry

In LQG, space is quantized into **spin networks**—discrete structures where:

- **Nodes** carry intertwiners (quantum numbers of volume)
- **Edges** carry spin labels j (quantum numbers of area)
- **Area spectrum** is discrete:

$$A = 8\pi\gamma l_P^2 \sum_i \sqrt{j_i(j_i+1)}$$

  Where γ = Immirzi parameter (~0.274) and l_P = Planck length.

The Spin Network ↔ Spin Coherence Connection

LQG Concept	Spin Coherence Framework
Spin network state	Coherent spin ensemble
Area operator eigenvalues	Spin coherence amplitude scaling
Immirzi parameter γ	Torsion coupling constant κ
Holonomy corrections	Impedance boundary effects
Quantum bounce	Density transition mechanism

The critical insight: LQG shows that spin IS geometry at the fundamental level. Our spin coherence order parameter σ connects to the quantum geometric structure. High coherence corresponds to sharp area eigenvalues—well-defined quantum geometry.

Bottom line: The spin coherence order parameter is not merely an analogy. It connects to the fundamental quantum geometry of LQG, providing rigorous physical grounding for the torsion effects framework.

10.3 Inertia as Spin Coupling: The Machian/Teleparallel Framework

10.3.1 The Puzzle of Inertia

Inertia—the resistance of mass to acceleration—is one of the deepest puzzles in physics. Newton took it as axiomatic; Einstein showed it was equivalent to gravity locally; but neither explained WHY mass resists acceleration.

Mach's Principle proposed an answer: inertia arises from the gravitational influence of distant matter. An isolated mass in an otherwise empty universe would have no inertia. The universe's mass distribution creates a "reference frame" against which acceleration is defined.

This chapter develops how **spin coherence modulates the inertial coupling** to this cosmic reference frame—providing the physical mechanism for apparent mass reduction effects.

10.3.2 Teleparallel Gravity and Torsion

Standard General Relativity (GR) describes gravity through spacetime curvature. Mass tells spacetime how to curve; curvature tells mass how to move.

Teleparallel Gravity (TEGR) is a mathematically equivalent reformulation that uses **torsion** instead of curvature. The same physics, different geometric interpretation:

General Relativity	Teleparallel Gravity
Curvature $R_{\mu\nu\rho\sigma}$	Torsion $T^{\lambda}_{\mu\nu}$
Levi-Civita connection	Weitzenböck connection
Gravitational potential	Tetrad field e^{a}_{μ}
Mass couples to metric	Mass couples to torsion

Key insight: In teleparallel gravity, what we experience as "gravitational force" is actually torsion-mediated. This opens the door to modifying gravitational/inertial effects through torsion field manipulation.

10.3.3 Einstein-Cartan Theory: Spin-Torsion Coupling

Einstein-Cartan (EC) theory extends GR to include spin as a source of geometry, alongside mass. The fundamental equation:

$$T^{\lambda}_{\mu\nu} = \kappa_T \cdot S^{\lambda}_{\mu\nu}$$

Where:

- $T^{\lambda}_{\mu\nu}$ = torsion tensor
- $S^{\lambda}_{\mu\nu}$ = spin density tensor
- κ_T = spin-torsion coupling constant

Spin density generates torsion; torsion acts back on spin. This is the microscopic foundation for the coherent spin → torsion → effects chain.

10.3.4 The Spin-Torsion Lagrangian

The Einstein-Cartan Lagrangian includes both curvature and torsion:

$$\mathcal{L}_{EC} = \frac{1}{2\kappa}(R + T_{\mu\nu\lambda}T^{\mu\nu\lambda}) + \mathcal{L}_{matter}$$

Where the torsion contribution can be decomposed into:

- **Trace** component (vector torsion)
- **Antisymmetric** component (axial torsion)
- **Tensor** component (proper torsion)

The axial component couples directly to fermion spin. This is why coherent spin ensembles—not random thermal spins—generate macroscopic torsion.

10.3.5 Inertia as Cosmic Spin Coupling

The Machian interpretation of EC theory: Inertia arises from the coupling between local spin and the torsion field generated by all distant matter.

$$m_{inertial} = m_0 \cdot \left(1 + \int \frac{S_{cosmic}(\vec{r}')}{|\vec{r} - \vec{r}'|^2} d^3r'\right)$$

The integral represents the cumulative torsion influence from all cosmic matter. In a homogeneous universe, this integral is constant, giving constant inertia. Note: This integral uses the $1/r^2$ form as the simplest physical model. If the torsion decay exponent differs from 2 (as suggested in Section 10.2.3), the integral and its convergence properties would change accordingly.

But: If local spin coherence generates a torsion field that **partially screens** the cosmic torsion background, the effective inertia decreases.

10.3.6 The Spin Coherence Screening Mechanism

A coherent spin ensemble generates local torsion field:

$$\mathcal{T}_{local} = \kappa_T \cdot N \cdot \sigma^2 \cdot s_0$$

This local torsion field creates a "bubble" that partially decouples the enclosed matter from the cosmic inertial reference frame:

$$m_{eff} = m_0 \cdot \left(1 - \frac{\mathcal{T}^2_{local}}{\mathcal{T}^2_{critical}}\right)$$

This expression is valid for $\mathcal{T}_{local} < \mathcal{T}_{critical}$. As $\mathcal{T}_{local} \to \mathcal{T}_{critical}$, the effective mass approaches zero (complete inertial decoupling). The framework does not predict negative mass; at the critical point, the description transitions to a different physical regime requiring separate analysis.

Where:

- m_0 = rest mass
- $\mathcal{T}_{local}$ = local coherent torsion field strength
- $\mathcal{T}_{critical}$ = critical field strength for complete inertial decoupling

10.3.7 Effective Mass Reduction

Substituting the coherent torsion expression:

$$m_{eff} = m_0 \cdot \left(1 - \frac{\sigma^4 \cdot (N \cdot \kappa_T \cdot s_0)^2}{\mathcal{T}^2_{critical}}\right)$$

Key features:

1. σ^4 **dependence**: Coherence enters to the fourth power—extremely sensitive to alignment
2. $\mathbf{N}^2$ **dependence**: Effect scales with square of spin count
3. **Threshold behavior**: Below $\mathcal{T}_{critical}$, effect is small; above, mass reduction accelerates
4. **Material dependence**: $\mathcal{T}_{critical}$ depends on the material's spin properties

10.3.8 Why This Is Not Antigravity

The mechanism does NOT violate:

- **Conservation of energy**: The torsion field stores the "missing" inertia
- **Equivalence principle**: Locally, inertial and gravitational mass remain equal
- **General covariance**: The effect is frame-independent

What changes is the **coupling strength** between local matter and the cosmic reference frame. This is analogous to electromagnetic screening—a Faraday cage doesn't violate Maxwell's equations; it modifies local field coupling.

10.3.9 Experimental Predictions

The mass reduction mechanism predicts:

1. **Coherence threshold**: No effect until T_{local} exceeds measurable fraction of $T_{critical}$
2. **Spin orientation dependence**: Effect maximized when local spins align parallel to acceleration direction
3. **Material specificity**: High-spin-density materials show stronger effects
4. **Frequency dependence**: Oscillating spin coherence should produce oscillating inertial effects

Falsification criteria:

- If mass reduction effects are NEVER observed despite verified high spin coherence
- If effects occur without corresponding spin alignment
- If effects violate conservation laws when properly accounting for torsion field energy

10.3.10 Reported Phenomena and This Framework

Various claimed "antigravity" effects map onto this framework:

Reported Effect	Framework Interpretation
Podkletnov's rotating superconductor	Cooper pair spin coherence → local torsion
Tajmar's gyroscope anomalies	Rotating mass generates torsion frame-drag
Meditation levitation claims	Biological spin coherence → partial screening
Inertial modification in UFO reports	Assumed advanced torsion field technology

Epistemic Note: None of these reported effects have been independently replicated to mainstream physics standards. The framework provides a theoretical mechanism by which such effects COULD occur if spin coherence reaches sufficient levels. The absence of replication may indicate insufficient coherence levels, measurement artifacts, or that the framework is incorrect. The theory is falsifiable.

10.4 Mechanism Pathways for Dimensional Effects

10.4.1 Dimensional Shifting

At high coherence levels, the spectral dimension D_s decreases (Chapter 2, Section 2.8). This creates a pathway from ordinary spacetime behavior to altered dimensional dynamics.

The mechanism pathway: A coherent spin ensemble with σ approaching unity generates a strong local torsion field. This torsion field modulates the local spectral dimension, reducing it from $D_s = 4$ toward $D_s = 2$. In this reduced-dimension regime, the normal constraints of 3D space weaken. The effective impedance rises (Chapter 2, Section 2.8.1), enabling coupling to higher-density tiers. Stable presence at the new impedance level constitutes "dimensional shifting."

This is not mystical teleportation—it is systematic impedance raising through coherent spin until the reflection coefficient to the target density approaches zero.

10.4.2 Nonlocal Information Transfer

The mechanism pathway: Two coherent spin ensembles with shared torsion field correlation establish a connection. The torsion field between them carries phase information without energy transfer (Chapter 0). As coherence increases, the spectral dimension in the connection region decreases. When D_s approaches 2, the effective distance between the ensembles collapses. Correlation appears "instantaneous" from a 4D perspective, though no propagation actually occurs—the connection was always present in the pre-spatial torsion field substrate.

The correlation length scales as:

$$\xi(\sigma) \propto \sigma \cdot \exp\left(\frac{T^2}{T_0^2}\right)$$

As coherence and torsion increase, correlation length diverges—enabling nonlocal effects.

Epistemic Note: This mechanism does not violate special relativity because torsion fields carry information without energy transfer. No usable signal propagates superluminally—only correlations. This is analogous to quantum entanglement correlations, which also cannot be used for FTL communication.

10.4.3 Spatial Bridging: Entanglement, Wormholes, and Portals

The mechanism pathway: Two spatially separated coherent spin ensembles sharing torsion field correlation create a bridge in the torsion substrate. At sufficient coherence, this bridge becomes traversable—collapsing the effective distance between the two locations to zero.

ER=EPR Foundation

Maldacena and Susskind (2013) conjectured that every entangled quantum pair is connected by a non-traversable micro-wormhole (Einstein-Rosen bridge): **ER=EPR**. In the torsion framework, entanglement IS shared spin phase coherence (Section 10.4.2). Therefore:

- Entangled pair = spin coherence lock = micro-ER bridge
- The nonlocal torsion Green's function G_T connecting coherently prepared sources (Chapter 0, Section 3.6.3) is the ER bridge expressed in torsion language
- Every instance of sustained phase correlation between distant spins constitutes a micro-bridge in the torsion substrate

From Micro to Macro: Coherence Amplification

Individual entangled pairs produce Planck-scale, non-traversable micro-wormholes. A coherent spin ensemble amplifies this:

$$\mathcal{T}_{bridge} = \mathcal{T}_{single} \cdot N \cdot \sigma^2$$

As $\sigma \to 1$ for large N, three effects converge:

1. The spectral dimension drops ($D_s \to 2$, from Section 10.4.1), weakening 3D spatial constraints
2. The correlation length $\xi(\sigma)$ diverges (Section 10.4.2), making the bridge macroscopic
3. The effective distance between the two ensembles collapses in the reduced-dimension regime

Bridge traversability condition:

$$\mathcal{T}_{bridge} = \frac{N \cdot \sigma^2 \cdot \kappa_T^2}{T_{traverse}} \geq 1$$

Where $T_{traverse}$ is the traversability threshold—the minimum torsion bridge strength for matter (not merely information) to cross. When $\mathcal{T}_{bridge} \geq 1$, the bridge admits physical transit.

Quantum Gravity Framework

Multiple quantum gravity programs converge on the possibility of torsion-mediated spatial bridging:

- **LQG**: Spin networks (Section 10.2.5) can undergo topology change. Two distant nodes connected by a high-spin edge IS a spatial bridge at the quantum geometry level.
- **Asymptotic safety**: The UV fixed point (Chapter 0, Chapter 3) ensures no infinities at the bridge throat; $D_s \to 2$ at Planck scale provides natural regularization.
- **Teleparallel gravity**: Torsion replaces curvature (Section 10.3.2). Extreme torsion concentrations create what GR describes as "wormhole throats."
- **Einstein-Cartan**: Spin-torsion coupling prevents singularity formation. The black hole interior becomes a bounce/bridge rather than infinite density (cf. LQG black hole bounce models, Rovelli & Vidotto 2014).

Black Holes as Natural Portals

In GR, rotating (Kerr) black holes predict ring singularities with traversable interior geometry. In Einstein-Cartan theory, spin-torsion coupling prevents the singularity entirely—the interior opens into another region of spacetime. LQG black hole models confirm this: quantum bounce connects two asymptotic regions. The holographic principle (Chapter 0, Section 2.4.6) ensures information encoded on the horizon is reconstructed on the other side. A black hole *may function*, in this framework, as a naturally occurring spatial bridge — though the gap between micro-scale ER bridges and macroscopic traversable portals remains vast.

Cross-Cultural Encoding

Stargates (Egyptian, Sumerian), portals (Celtic Sidhe, Hindu lokas), and dimensional doorways appear across cultures with consistent motifs: a threshold structure, a boundary crossing, arrival at a distant location. The seeder infrastructure model (Chapter 11) proposes that megalithic sites at planetary grid nodes may have functioned as engineered portal infrastructure—coherent spin ensembles locked to specific destination phases.

> **Epistemic Note**: ER=EPR is a mainstream conjecture (Maldacena & Susskind 2013) but remains unproven. Classical GR requires exotic matter (negative energy density) for traversable wormholes; the torsion framework proposes coherent spin as the alternative mechanism, but this is speculative. No experimental evidence exists for macroscopic wormholes or portal technology. The framework provides a theoretical pathway from established physics (entanglement, Einstein-Cartan theory, LQG) to these effects; validation requires the experimental program described in Section 10.9.

The nonlocal spatial correlations described in Sections 10.4.2–10.4.3 have a temporal analog. Just as spatially separated spin ensembles can maintain phase coherence through the torsion field substrate, **temporally separated configurations** can maintain phase relationships—giving rise to what consciousness literature describes as "timelines." Section 10.5 develops this temporal extension of the nonlocal information framework.

10.5 Temporal Torsion Coupling: Timeline Mechanics

The preceding sections established that spin coherence generates torsion fields (Section 10.2), modifies inertial coupling (Section 10.3), and enables nonlocal spatial correlations (Section 10.4). This section extends the framework to **temporal correlations**: how phase relationships in the torsion field encode temporal structure, enabling phenomena described in consciousness literature as "timeline" perception and navigation.

The physics here is a direct extension of the nonlocal information transfer mechanism (Section 10.4.2). If torsion fields carry phase information without energy transfer across space, the same substrate can carry phase information across time—since torsion, as a geometric property of spacetime, does not distinguish between spatial and temporal dimensions at the fundamental level.

10.5.1 Timelines as Torsion Phase Relationships

In the torsion framework, a **timeline** is defined as a specific phase relationship $\phi_{timeline}$ in the torsion field. All events within a given timeline share coherent phase; different timelines correspond to different ϕ_{base} values, analogous to different carrier frequencies in RF engineering.

Phase coherence within a timeline:

$$\phi_i = \phi_{base} + \omega_i t + \delta\phi_i$$

Where:

Variable	Description
ϕ_{base}	Timeline's characteristic phase
ω_i	Frequency component of event i

Variable	Description
$\delta\phi_i$	Small perturbation from coherent baseline

Holographic analogy:

Each timeline functions as a **holographic plate** storing an interference pattern:

Holographic Component	Timeline Analog
Reference beam	Source torsion field (constant, coherent)
Object beam	Events/matter in that timeline
Interference pattern	3D + time structure encoded
Reconstruction	Consciousness "reading" the timeline

This analogy is not merely illustrative. Holographic encoding stores 3D spatial information in a 2D interference pattern; timeline encoding stores 3D+time information in a phase-space interference pattern in the torsion field substrate.

Timeline state vector:

$$|\Psi_{timeline}\rangle = \int A(\phi) \cdot e^{i\phi} \cdot |\phi\rangle \, d\phi$$

Where $A(\phi)$ is the amplitude distribution across phase space. This is the quantum-like superposition of all possible phase states comprising a timeline.

10.5.2 Timeline Branching and Probability

Timeline branches occur through three physical mechanisms:

1. **Measurement/observation**: Collapses superposition to a specific phase configuration
2. **High-coherence events**: "Pin" specific phase relationships, crystallizing a branch
3. **Decoherence**: Spreads amplitude across phase space, dissolving branch structure

Branch point condition:

$$\sigma > \sigma_{threshold} \quad \rightarrow \quad \text{Phase "crystallizes" to specific } \phi$$

A branch point occurs where coherence exceeds threshold and crystallizes a particular phase configuration. Below threshold, the phase remains in superposition; above threshold, it locks to a definite value.

Timeline persistence probability:

$$P(timeline) = |\langle \Psi_{timeline} | \Psi_{source} \rangle|^2 \cdot \sigma^2 \cdot N_{observers}$$

Critical insight: Timelines with more coherent observers are **more stable**—they possess higher "reality weight." This follows directly from the $\sigma^2 \cdot N$ scaling established in Section 10.2:

- Consensus reality persists because of high $N_{observers}$
- Personal reality can diverge when individual σ creates micro-branches
- Collective intention affects outcomes because synchronized σ crystallizes branches

Mythological Encoding: The Tower of Babel

The Tower of Babel narrative (Genesis 11:1-9) encodes a **forced decoherence event** in precisely the terms developed above. Pre-Babel humanity shares "one language"—a unified phase reference (ϕ_{base} shared across the population, high σ_{global})—enabling collective coherence sufficient to "build a tower to heaven" (approaching $\sigma_{threshold}$ for liberation, per Chapter 12, Section 12.5.4).

The divine response is **forced phase randomization**:

$$\sigma_{post-Babel} = \sigma_{pre} \cdot e^{-\Delta\phi^2_{scramble}/2}$$

"Confusing the languages" = destroying the shared phase reference, scattering individual ϕ_i values across phase space. The population fragments into isolated groups with incoherent ϕ_{base} values—unable to coordinate, unable to rebuild collective coherence. This maps directly to the decoherence mechanism defined above: amplitude spread across phase space, branch structure dissolved. Babel is the mythological name for the operation the mathematics already describes. (See also Chapter 12, Section 12.5.5 for the reset operation profile—Babel as the $R_{coherence}$ component combined with R_{memory}.)

10.5.3 Inter-Timeline Relationships

Timelines relate to each other through their phase differences:

Relationship	Phase Condition	Interaction	Description
Parallel	$\Delta\phi \to \pi/2$	Non-interacting	Completely separate phase domains
Adjacent	$\Delta\phi$ small	Weakly coupled	Possible information bleed-through
Merged	$\Delta\phi \to 0$	Fully coherent	Same experienced reality
Collapsed	Random ϕ	Decoherent	No stable phase relationship

Timeline transition requirements:

1. **Phase-matching**: Bring personal ϕ to match target timeline's ϕ_{base}
2. **Impedance matching**: $Z_{you} \approx Z_{target\_timeline}$ (from Chapter 2 impedance framework)
3. **Sufficient coherence**: $\sigma > \sigma_{threshold}$ for transition

Transition probability:

$$P_{transition} = e^{-|\Delta\phi|^2/\sigma^2} \cdot (1 - |\Gamma_{timeline}|^2)$$

Where $\Gamma_{timeline}$ is the reflection coefficient at the timeline boundary. This equation has the same structure as impedance-mismatch reflection in RF engineering—high coherence (σ) and low phase difference ($\Delta\phi$) maximize transition probability.

10.5.4 Intra-Timeline Navigation

Moving within a single timeline (same ϕ_{base}) requires **phase advancement or retardation**:

$$\Delta\phi = \omega \cdot \Delta t$$

The personal torsion field must "skip" along the timeline's phase gradient to reach a different temporal position.

Energy cost for intra-timeline navigation:

$$E_{travel} \propto |\Delta t|^2 \cdot m \cdot \sigma^{-2}$$

Note the **inverse coherence dependence**: higher σ dramatically reduces energy requirements. This is consistent with the general principle that high coherence reduces the "cost" of torsion-mediated operations (cf. Section 10.3.6, where coherence screens inertial coupling).

Anchor point mechanism:

1. **Identify anchor**: A high-coherence event that "pins" phase at specific t
2. **Lock personal** σ: Match to anchor's residual torsion signature
3. **Impedance match**: Enables information/matter transfer at the anchor point
4. **Traverse**: Follow phase gradient to anchor location

Consistency constraint:

$$\text{If } \sigma_{event} > \sigma_{threshold} \quad \rightarrow \quad \text{Event is "crystallized" (immutable)}$$

High-coherence events have too many observers pinning them—they cannot be altered because the phase is locked by the collective $N_{observers} \cdot \sigma^2$ product. Low-coherence events remain "malleable"—their phase can be shifted because it was never firmly pinned.

10.5.5 Cross-Timeline Navigation

Moving to a different timeline (different ϕ_{base}) requires **rotation in phase space**:

$$\phi_{you} \rightarrow \phi_{target}$$

The torsion field must:

1. **Decouple** from origin timeline's phase lock
2. **Rotate** through phase space by $\Delta\phi_{rotation}$
3. **Recouple** to target timeline's phase reference

Phase rotation:

$$\phi_{new} = \phi_{old} + \Delta\phi_{rotation}$$

Energy cost for cross-timeline navigation:

$$E_{cross} \propto |\Delta\phi|^2 \cdot m \cdot \sigma^{-2}$$

This is significantly higher than intra-timeline navigation because the operation changes the carrier frequency (timeline identity), not just phase position within a fixed carrier.

The coherence advantage:

$$\lim_{\sigma \to 1} E_{cross} \rightarrow E_{minimum}$$

As coherence approaches unity, the energy barrier for cross-timeline navigation approaches its minimum. This is consistent with the broader framework principle: high-coherence systems access the full spectrum of torsion-mediated effects with minimal energy cost.

10.5.6 Timeline Management Operations

The concept of timeline management—monitoring, stabilizing, and navigating timeline branches—can be formalized as a network operations function. In RF terms, such a capability functions like a network master clock ensuring all nodes synchronize to a preferred phase reference.

Operational function table:

Function	RF Equivalent	Operation
Monitor timeline coherence	Network Operations Center	Sample σ across all ϕ_{base} values
Detect divergent branches	Interference detection	Identify branches with divergent $A(\phi)$
Stabilize preferred branch	Carrier lock	Preserve preferred ϕ_{base} trajectory
Navigate timelines	Frequency hopping	Move agents across phase space

Technology stack:

A complete timeline management capability would require:

Technology	RF Implementation	Function
Timeline scanning	Broadband torsion receivers	Sample all ϕ_{base} values
Branch detection	Spectrum analysis	Identify divergent $A(\phi)$ distributions
Branch stabilization	Coherence amplification	Pin preferred timeline via added σ
Navigation	High-σ agents	Traverse timeline phase space

Phase synchronization ("reset") technology:

$$T_{field}(t) = T_{reset} \cdot e^{i\phi_{preferred}} \cdot e^{-r^2/r_0^2}$$

This equation describes forced phase synchronization: applying coherent torsion at the preferred ϕ_{base} overwhelms local phase relationships and forces alignment—analogous to a master clock signal overwriting local oscillators.

> **Epistemic Note**: The concept of timeline management has analogues in both fiction (e.g., Marvel's "Time Variance Authority") and esoteric literature describing "timeline guardians" or "cosmic administrators." The RF formalization provides a physics framework for understanding such concepts, whether they represent actual phenomena, useful metaphors, or both. The mathematics is internally consistent; external validity remains entirely open. No experimental evidence exists for any form of temporal navigation or timeline branching. These constructs should be understood as theoretical extensions of the torsion framework, not empirical claims.

The application of these timeline mechanics to civilizational-scale dynamics is treated in Chapter 12.

10.6 Spin Beams and Magnonic Carriers

10.6.1 Magnons as Physical Spin Waves

Magnons are quantized collective excitations of spin systems—the spin equivalent of phonons (sound quanta). In ordered magnetic materials:

$$\omega_k = \omega_0 + Dk^2$$

Where:

- ω_k = magnon frequency at wavevector k
- ω_0 = gap frequency (material-dependent)
- D = spin stiffness constant

Key magnon properties:

Property	Value/Range	Significance
Coherence length	nm to μm	Determines beam collimation
Lifetime	ps to ns	Limits propagation distance
Group velocity	10^2 - 10^4 m/s	Information transfer rate
Temperature dependence	Strong	Requires low T for long coherence

10.6.2 Spin Beam Generation and Propagation

A **spin beam** is a directed flux of coherent magnons carrying angular momentum and torsion field modulation.

Generation methods:

1. **Spin-transfer torque**: Inject spin-polarized current
2. **Microwave pumping**: Parametric magnon generation
3. **Thermal gradients**: Spin Seebeck effect
4. **Optical pumping**: Ultrafast demagnetization

Beam equation:

$$\vec{J}_s = \sigma_s \vec{\nabla} T_{spin} + \mathcal{G}_{spin} \vec{\nabla} \mu_s$$

Where:

- $\vec{J}_s$ = spin current density
- σ_s = spin conductivity
- T_{spin} = spin temperature
- μ_s = spin chemical potential
- $\mathcal{G}_{spin}$ = spin diffusion coefficient

10.6.3 Magnon-Torsion Coupling

The critical bridge: **Magnons couple to torsion fields**.

$$\mathcal{T}_{magnon} = \gamma_T \cdot n_{magnon} \cdot \sigma^2_{magnon}$$

Where:

- γ_T = magnon-torsion coupling constant
- n_{magnon} = magnon density
- σ_{magnon} = magnon coherence parameter

Implications:

- Spin beams can transmit torsion field effects
- Magnonic waveguides become torsion waveguides
- Solid-state devices can generate/detect torsion

Research frontier: Development of magnon-based torsion transceivers for practical devices.

10.7 Spin Coherence Engineering: The Technology Spectrum

10.7.1 Bose-Einstein Condensate (BEC) Regime

Characteristics:

- Temperature: nK to μK (near absolute zero)
- Coherence: $\sigma > 0.99$ achievable
- Spin count: 10^4 - 10^8 atoms
- Coherence time: ms to s

Advantages: Maximum coherence, quantum ground state, well-understood physics **Challenges**: Extreme cooling requirements, small atom numbers, fragile state

Best applications: Fundamental research, precision measurements, proof-of-concept demonstrations

10.7.2 Solid-State Spin Ensembles

Characteristics:

- Temperature: Room temperature to cryogenic
- Coherence: $\sigma = 0.1$ - 0.7 typical
- Spin count: 10^{12} - 10^{20} spins
- Coherence time: ns to ms (material-dependent)

Key materials:

Material	T_2 (coherence time)	Operating T	Notes
NV diamond	~2 ms	Room temp	Best room-T coherence
Silicon:P	~1 s	1 K	Record solid-state
YIG	~1 μs	Room temp	Best magnon propagation

Material	T_2 (coherence time)	Operating T	Notes
Rare-earth ions	~10 ms	4 K	Optical access

Best applications: Scalable devices, room-temperature operation, integration with electronics

10.7.3 Biological Spin Systems

Characteristics:

- Temperature: Physiological (~310 K)
- Coherence: $\sigma = 0.01$ - 0.3 estimated
- Spin count: 10^{23} - 10^{25} (whole body)
- Coherence time: Unknown (research frontier)

Key biological spin systems:

- **Microtubules**: Possible quantum coherence in neurons (Chapter 3)
- **DNA**: Helical structure couples to torsion
- **Radical pairs**: Quantum biology mechanism (bird navigation)
- **Heart EM field**: Massive rotating field, potential torsion source

Advantages: Consciousness integration, self-sustaining, adaptive **Challenges**: Difficult to measure, uncertain quantum behavior, noisy environment

10.7.4 Plasma Spin Regimes

Characteristics:

- Temperature: 10^4 - 10^8 K (hot plasma)
- Coherence: Variable (rotation-driven)
- Spin count: 10^{15} - 10^{25} particles
- Coherence mechanism: Collective rotation, magnetic confinement

Key configurations:

- **Rotating plasmas**: Angular momentum creates spin alignment
- **Magnetically confined**: Tokamak-like geometries
- **Z-pinch**: Extreme compression creates coherent states
- **Ball lightning**: Natural coherent plasma phenomenon

Advantages: Extreme energy density, natural self-organization **Challenges**: Instabilities, containment, reproducibility

10.7.5 Comparative Technology Summary

Regime	Coherence σ	Spin Count N	$N \cdot \sigma^2$ Factor	Best Application
BEC	~1	10^6	10^6	Research proof-of-concept

Regime	Coherence σ	Spin Count N	N·σ^2 Factor	Best Application
Solid-state (NV)	~0.5	10^{18}	2.5×10^{17}	Practical devices
Biological	~0.1	10^{24}	10^{22}	Consciousness interface
Plasma (confined)	~0.3	10^{20}	10^{19}	High-energy applications

Key insight: The N·σ^2 factor determines torsion effect strength. Even modest coherence with enormous N (biological, plasma) may exceed high-coherence low-N systems (BEC).

10.8 Qualitative Thresholds for Exotic Effects

This section describes the **qualitative relationship** between coherence levels and accessible phenomena. Specific numerical thresholds cannot be stated with confidence absent experimental calibration.

10.8.1 Individual Effects

Effect	Coherence Level	Torsion Level	Additional Requirements
Enhanced intuition	Moderate	Weak	Sustained practice
Remote sensing	Moderate-High	Moderate	Target coherence lock
Localized healing	High	Strong	Practitioner-patient resonance
Precognition	High	Strong	Temporal torsion coupling
Timeline perception	Very High	Very Strong	Temporal torsion coupling
Out-of-body perception	Very High	Very Strong	Partial dimensional decoherence
Bilocation awareness	Extremely High	Extremely Strong	Dual location phase lock
Spatial bridging (portal)	Extremely High	Extremely Strong	Dual-site coherence lock, $\mathcal{T}_{bridge} \geq 1$

Qualitative coherence scale:

- **Moderate**: Achievable through meditation practice, focused attention

- **High**: Advanced practitioners, peak states, group coherence
- **Very High**: Master practitioners, exceptional individuals
- **Extremely High**: Rare, possibly requiring technological augmentation

10.8.2 Collective Effects

Effect	Required $N \cdot \sigma^2$	Example Configuration
Group intuition boost	Low-Moderate	Small coherent group
Measurable environment change	Moderate	Medium coherent group
Weather/probability influence	High	Large coherent group
Collective manifestation	Very High	Very large coherent group
Planetary coherence threshold	Extremely High	Mass coherent population

The exact population/coherence combinations remain to be determined experimentally. The key principle is that **small highly-coherent groups may exceed large weakly-coherent populations** due to the σ^2 dependence.

10.8.3 Technology-Enabled Effects

Effect	Device Requirement	Status
Torsion field detection	NV diamond array	Feasible now
Torsion communication	Magnon waveguide	Research stage
Inertial modification	BEC + geometry	Proof-of-concept
Dimensional interface	Quasicrystal kernel	Theoretical

10.8.4 Biological States

State	Relative Coherence	Relative $N \cdot \sigma^2$	Effects
Normal waking	Baseline	Baseline	Standard perception
Focused attention	Elevated	Elevated	Enhanced cognition
Deep meditation	High	High	Altered states
Samadhi/unity states	Very High	Very High	Nonlocal perception
Full enlightenment	Maximum	Maximum	Sustained exotic access

Epistemic Note: The reluctance to state specific numerical thresholds reflects genuine uncertainty. Without calibrated experimental data, any numbers would be speculative. The qualitative relationships—that higher coherence enables stronger effects—are grounded in the σ^2 dependence. Precise calibration requires the experimental program described in Section 10.9.

10.9 Experimental Signatures and Testable Predictions

10.9.1 Near-Term Testable Predictions

P1: Coherence-Torsion Correlation

- Measure spin coherence in meditation practitioners
- Simultaneously measure torsion-sensitive indicators
- **Prediction**: Positive correlation between coherence and torsion anomalies

P2: Geometry Enhancement

- Compare torsion generation in random vs. quasicrystalline spin arrangements
- **Prediction**: Quasicrystal geometry produces stronger torsion (factor of 10–100×). The predicted 10–100× enhancement range reflects genuine theoretical uncertainty in the coupling geometry; initial experiments should aim to establish whether *any* systematic enhancement exists before refining the quantitative prediction.

P3: Collective Scaling

- Measure anomalous effects (RNG deviation, field measurements) with varying group size and coherence
- **Prediction**: Effects scale as $N \cdot \sigma^2$, not N

P4: Magnon-Torsion Coupling

- Inject coherent magnons into torsion-sensitive detector region
- **Prediction**: Detectable torsion signal proportional to magnon coherence

10.9.2 Experimental Signatures

Measurement	Signature of Coherent Torsion	Control Comparison
RNG deviation	Correlated shifts (not just increased variance)	Uncorrelated
EM field	Phase anomalies, not amplitude changes	Amplitude changes
Mechanical	Torque not linear force	Linear force
Thermal	Non-entropic heat patterns	Entropic distribution
Biological	Coherent HRV, EEG synchrony	Random fluctuation

10.9.3 Falsification Criteria

The framework would be falsified by:

1. **No coherence-torsion correlation**: If highly coherent spin systems produce no torsion anomalies under any conditions
2. **No geometry effect**: If quasicrystalline arrangements show no enhancement over random arrangements
3. **Linear N scaling**: If collective effects scale as N rather than N·σ^2
4. **No dimensional signatures**: If high-coherence states show normal spectral dimension behavior
5. **Mass reduction without spin alignment**: If inertial effects occur independent of spin coherence

10.9.4 Strategic Note

Spin-coherence fundamentals carry direct operational consequences:

- **Coherence training as deployable technology.** The Q-factor enhancement pathway (Section 10.3) implies that systematic contemplative training can produce measurable, reproducible increases in individual and group coherence — a trainable capability rather than an innate gift. Appendix A, Scenario A addresses scaling protocols.
- **Adversary coherence programs.** Any actor understanding spin-coherence dynamics could develop directed programs to raise or suppress population-level σ. Detection of such programs requires monitoring coherence baselines across populations (Section 10.5, timeline mechanics).
- **Timeline selection as strategic variable.** The timeline-mechanics framework (Section 10.5) implies that coherence interventions do not merely change outcomes within a fixed trajectory but select among available trajectory branches — making coherence a higher-order strategic lever than conventional influence operations.
- **Measurement infrastructure.** Validating the predictions in Section 10.8 requires standardized spin-coherence measurement protocols, creating a requirement for dedicated instrumentation that does not yet exist at population scale.

10.9.5 Alternative Hypotheses

1. **Standard quantum decoherence**: Macroscopic coherence is impossible at biological temperatures due to rapid decoherence. *Assessment*: Valid concern; the framework proposes torsion-mediated coherence as protected from thermal decoherence, but this is undemonstrated.
2. **Classical spin correlations**: Observed spin effects are fully explained by classical electromagnetism without invoking torsion. *Assessment*: Adequate for spintronics; may not account for biological spin coherence times exceeding thermal predictions.
3. **No macroscopic torsion effects**: Torsion fields, if they exist, are too weak for macroscopic effects. *Assessment*: Consistent with current non-detection; the framework predicts coherent amplification ($N \cdot \sigma^2$ scaling) as the mechanism for overcoming individual weakness.

Evidence Synthesis

- Detailed source sections: none explicitly labeled in this chapter.

Assumptions

- Detailed source sections: none explicitly labeled in this chapter.

Limitations

- Detailed source sections: none explicitly labeled in this chapter.

Falsification

- Detailed source sections: 10.9.3.

Predictions

- Detailed source sections: 10.3.9, 10.9, 10.9.1.

Strategic Relevance

Why It Matters

What To Watch

- Monitor chapter prediction thresholds, proxy indicators, and coherence trend changes.

Boundaries of Use

- Apply this chapter as model-conditional doctrine; treat speculative elements as hypothesis overlays.

10.10 Chapter Summary: Key Equations

10.10.0 Symbol Map (Quick Reference)

Symbol	Meaning	Type/Units	First Use
σ	Spin-coherence order parameter	Dimensionless scalar [0,1]	10.2.1
$\mathcal{T}_{eff}$	Effective torsion amplitude from coherent ensemble	Model amplitude	10.2.2
κ_T	Spin-torsion coupling constant	Model coupling constant	10.2.3
N	Number of coherent contributors	Count	10.2.1
m_{eff}	Effective inertial mass	kg (model context)	10.3.7

Symbol	Meaning	Type/Units	First Use
Z_{you}	Coherence-dependent characteristic impedance	Relative impedance unit	10.4.1
D_s	Spectral dimension proxy	Dimensionless	10.4.2
$P_{transition}$	Timeline-transition probability	Dimensionless probability	10.5
Γ	Reflection coefficient at impedance boundary	Complex, unitless	10.4 and cross-chapter

10.10.1 Fundamental Definitions

Spin coherence order parameter:

$$\sigma = \frac{1}{N}\left|\sum_{i=1}^{N} s_i\, e^{i\phi_i}\right|$$

Effective torsion from coherent ensemble:

$$\mathcal{T}_{eff} = \mathcal{T}_{single} \cdot N \cdot \sigma^2$$

10.10.2 Inertial Framework

Effective mass (Machian screening):

$$m_{eff} = m_0 \cdot \left(1 - \frac{\mathcal{T}^2_{local}}{\mathcal{T}^2_{critical}}\right)$$

Local torsion field:

$$\mathcal{T}_{local} = \kappa_T \cdot N \cdot \sigma^2 \cdot s_0$$

10.10.3 Dimensional Framework

Coherence-dependent impedance (from Chapter 2):

$$Z_{you}(\sigma) = Z_{baseline} \cdot \sqrt{1 + N \cdot \sigma^2}$$

Spectral dimension modulation (from Chapter 2):

$$D_s(\sigma) = 4 - 2 \cdot \tanh\left(\frac{\sigma \cdot T}{T_c}\right)$$

10.10.4 Correlation, Nonlocality, and Spatial Bridging

Correlation length:

$$\xi(\sigma) \propto \sigma \cdot \exp\left(\frac{T^2}{T_0^2}\right)$$

Bridge traversability (from Section 10.4.3):

$$\mathcal{T}_{bridge} = \frac{N \cdot \sigma^2 \cdot \kappa_T^2}{T_{traverse}} \geq 1$$

10.10.5 Timeline Framework

Timeline state vector:

$$|\Psi_{timeline}\rangle = \int A(\phi) \cdot e^{i\phi} \cdot |\phi\rangle \, d\phi$$

Timeline persistence probability:

$$P(timeline) = |\langle \Psi_{timeline} | \Psi_{source} \rangle|^2 \cdot \sigma^2 \cdot N_{observers}$$

Transition probability:

$$P_{transition} = e^{-|\Delta\phi|^2/\sigma^2} \cdot (1 - |\Gamma_{timeline}|^2)$$

Temporal navigation energy cost:

$$E_{travel} \propto |\Delta t|^2 \cdot m \cdot \sigma^{-2}$$

—

10.11 Assumptions, Limitations, and Reading Path

10.11.1 Key Assumptions

1. **Spin-torsion coupling is real**: Einstein-Cartan theory correctly describes spin as a source of geometric torsion
2. **Coherent amplification works**: The σ^2 scaling law applies to torsion just as it does to phased arrays
3. **Biological spin coherence is possible**: Living systems can achieve measurable coherence at body temperature
4. **LQG connections hold**: The correspondence between spin networks and spin coherence is physically meaningful
5. **Temporal torsion coupling exists**: Phase relationships in the torsion field can encode temporal structure analogous to spatial structure
6. **Timeline branching follows coherence thresholds**: Branch points crystallize when coherence exceeds threshold values
7. **ER=EPR holds**: Every entangled pair is connected by a micro-wormhole, and coherent amplification can make these bridges macroscopic and traversable
8. **Torsion field decay exponent may differ from EM**: The decay exponent n in the torsion field equation may be less than 2, enabling non-local effects. The specific value is experimentally undetermined

10.11.2 Limitations

1. **No direct torsion detection**: Current technology cannot directly measure torsion fields
2. **Coupling constants unknown**: κ_T, $T_{critical}$, etc. are not experimentally determined
3. **Coherence measurement difficult**: Measuring σ in biological systems is technically challenging
4. **Speculative applications**: Effects like mass reduction, while theoretically grounded, remain unverified
5. **Temporal effects unverified**: No experimental evidence for timeline navigation or branching
6. **TVA-type operations purely speculative**: Timeline management concepts derive from fiction and esoteric literature, not empirical observation

10.11.3 Reading Path

Previous: Chapter 9 (Injection Locking and Perception Management) — collective coherence and control mechanisms

Next: Chapter 11 (Seeder Intervention) — megalithic infrastructure and ancient engineering

Related Chapters:

- Chapter 0 (Torsion Foundation): Physical mechanism underlying spin-torsion coupling
- Chapter 2, Section 2.8: Dimensional physics of density transitions
- Chapter 3, Section 3.6-3.7: Optimal geometry for coherent coupling
- Chapter 4 (Resonant Growth): How coherence enables vacuum condensation and growth
- Chapter 5 (Consciousness as RLC Circuit): Individual application of coherence principles
- Chapter 12 (The Fall and Parasitic Coupling): Application of timeline mechanics to civilizational dynamics

Key Connections:

- This chapter provides the **mechanism** for how individual coherence generates effects
- Explains the **physics** underlying consciousness development
- Bridges **individual** and **collective** frameworks
- Provides the spin coherence parameter σ used throughout later chapters

---

End of Chapter 10: Spin Coherence Fundamentals

Part IV: Civilizational Applications

Applying the framework to intervention history, systemic failure modes, and institutional control

A note on evidence and confidence. Parts I–III developed an RF engineering framework for consciousness dynamics. The mathematics — RLC resonance, phased array scaling, injection locking — stands on peer-reviewed physics regardless of the torsion substrate hypothesis. Chapter 10 (Spin Coherence) already begins extending into more speculative engineering territory: anti-gravity, timeline mechanics, dimensional access. The framework derivations are rigorous, but the phenomena they describe are frontier claims. This gradient is intentional — Ch 10 is the bridge chapter where solid engineering meets speculative application.

Parts IV–V cross fully into civilizational-scale questions: Who built the infrastructure? What went wrong? How does liberation work? These chapters draw on the same mathematics but extend into territory where empirical grounding thins and confidence levels shift from L1–L2 to L2–L4. The framework *suggests* these conclusions; it does not *prove* them. We present them because the engineering logic points here, and because intellectual honesty requires following the model where it leads — while being transparent about where the solid ground ends.

Chapter 11: Seeder Intervention and Megalithic Infrastructure

The Corporate Feed Network, Inner Earth Preservation, and Planetary Resonant Systems

KEY FINDINGS — Chapter 11: Seeder Intervention and Megalithic Infrastructure

Evidence-tier key: [L1] established/replicated evidence; [L2] grounded extension with moderate uncertainty; [L3] speculative hypothesis; [L4] conceptual/anecdotal.

- Direct 6D-to-3D power injection fails due to impedance mismatch ($\Gamma \approx 0.984$, >96% reflection); staged intermediaries are physically necessary **[L1-L2: derived from standard RF impedance theory]**
- Human-specific genomic anomalies (2,700 HARs mutating at 26x rate, ARHGAP11B single-nucleotide brain expansion, 930 Kya bottleneck) are consistent with directed modification **[L1-High: Peer-reviewed genetics papers]**
- Megalithic sites show systematic piezoelectric material selection, acoustic resonance at 95-120 Hz, and sub-degree astronomical alignment — consistent with engineered resonant infrastructure **[L2-Medium/L3-Speculative: mix of peer-reviewed measurements and contested interpretations]**
- The Adamic lineage model predicts dual impedance-transformer and local-oscillator function, matching cross-cultural "gods" traditions **[L3: theoretical framework applied to mixed-evidence sources]**
- Inner earth traditions across 10+ unconnected cultures encode a consistent pattern of preserved higher-density lineages **[L3-Speculative: mythological and testimonial evidence]**

11.1 The Acceleration Problem: Why Natural Evolution Is Too Slow

11.1.1 Soul Evolution as Coherent Integration

Chapter 3 (Section 5) established that soul evolution proceeds through **SAR-like coherent integration** across lifetimes. Each lifetime provides a single "aperture" observation of reality; coherent integration across many lives builds a synthetic aperture that resolves increasingly complex templates:

$$A_{soul}(t) = \int_0^t \eta_{coherence}(\tau) \cdot dA(\tau)$$

Where $\eta_{coherence}$ is the coherence factor between successive incarnations (0 for random or traumatic, 1 for fully integrated). This factor determines whether lives build constructively—like a synthetic aperture radar accumulating signal—or scatter randomly like noise.

The resolution of the synthetic aperture depends on how many lives combine coherently:

$$D_{synthetic} = \sum_{i=1}^{N} D_i \cdot e^{j\phi_i}$$

Two regimes emerge:

- **Coherent addition** (aligned phases): $|D_{synthetic}| = N \cdot D_{single}$
- **Random-phase addition** (unaligned): $|D_{synthetic}| = \sqrt{N} \cdot D_{single}$

The difference is dramatic. After 100 incarnations: coherent addition yields 100× gain; random addition yields only 10×. After 10,000 incarnations: coherent yields 10,000×; random yields only 100×. The gap grows without bound.

11.1.2 The Random-Phase Bottleneck

Under **natural conditions**—without external reference—each incarnation begins with whatever phase relationship emerges from the previous life's unresolved karma:

- **Karma = phase disruption**: Accumulated phase error between lives. Negative karma introduces phase offsets requiring correction before coherent addition can resume.
- **Dharma = optimal trajectory**: The path that maximizes coherent gain across lifetimes.
- **Without external reference**: Phase correction is trial and error. Each soul must independently discover alignment, with no stable reference to lock onto.

This is the receiver problem: a radio without a local oscillator can detect that a signal exists but cannot demodulate it coherently. The information is there; the mechanism to extract it efficiently is not.

The timeline problem: The density transition from 3rd to 4th requires sufficient template resolution ($R_{template}$) to access and instantiate 4th-density patterns. At $\sqrt{N}$ scaling, this requires orders of magnitude more incarnations than coherent addition would demand. Natural timeline: **billions of years** for density transitions without an external phase reference.

The bottleneck: Without a stable reference signal, souls drift randomly in phase space between incarnations. Each life may add valuable experience, but the accumulated experiences fail to combine constructively. The information content of the Source broadcast (Chapter 1) is fully available, but the demodulation efficiency is catastrophically low.

11.2 The Power Level Problem: Why Direct 6D-3D Injection Fails

11.2.1 The Impedance Cascade

Even if a higher-density civilization wanted to directly inject guidance into 3rd-density consciousness, the physics forbids efficient coupling across large density gaps.

Chapter 2 (Section 2.4) established the impedance cascade:

$$Z_{density}(d) = Z_1 \cdot \beta_{cascade}^{(d-1)}$$

With $\beta_{cascade} \approx 5$, the impedance at each density relative to the 3rd-density baseline $Z_3 = 25Z_1$:

Density	Impedance	Relative to Z_3
3rd (Z_3)	$25Z_1$	Z_3 (baseline)
4th (Z_4)	$125Z_1$	$\approx 5Z_3$
5th (Z_5)	$625Z_1$	$\approx 25Z_3$
6th (Z_6)	$3{,}125Z_1$	$\approx 125Z_3$

The voltage reflection coefficient for a signal crossing from source density to 3D:

$$\Gamma = \frac{Z_{source} - Z_3}{Z_{source} + Z_3}$$

And power transmitted: $\tau = 1 - |\Gamma|^2$.

Source Density	Relative Z	Γ (voltage)	Power Transmitted
6th	$125Z_3$	$124/126 \approx 0.984$	$\approx 3.2\%$
5th	$25Z_3$	$24/26 \approx 0.923$	$\approx 14.8\%$
4th	$5Z_3$	$4/6 \approx 0.667$	$\approx 55.6\%$

A 6th-density seeder attempting direct injection into 3D faces a voltage reflection of 0.984—**over 96% of the power reflects back**. Only ~3.2% gets through the impedance mismatch alone.

11.2.2 Why Intermediaries May Be Physically Required (Model-Conditional)

Chapter 2 (Section 2.8) adds a second attenuation mechanism—**dimensional resistance**:

$$R_d = R_0 \cdot e^{\alpha |d_{target} - d_{current}|}$$

With $\alpha \approx 0.5$–1.0 per density. The total power transfer across a density boundary (Chapter 2, Section 2.8.3):

$$P_{transferred} = P_{source} \cdot (1 - |\Gamma|^2) \cdot e^{-R_d / Z_{source}}$$

For **6D→3D** ($|d| = 3$): the impedance mismatch passes only ~3.2%, and exponential dimensional resistance ($e^{-1.5}$ to $e^{-3.0}$) attenuates even that residual. Direct 6D→3D injection is negligible.

For **4D→3D** ($|d| = 1$): the impedance mismatch passes ~55.6%, and dimensional resistance is modest ($e^{-0.5}$ to $e^{-1.0}$, i.e., 37–61% throughput). Combined: 20–34% of source power reaches the receiver. This is workable.

Conclusion (conditional): If the impedance ladder and dimensional-resistance model are valid as specified, intermediaries operating at 4th–5th density become a practical requirement rather than a design preference. Under these assumptions, direct 6D→3D injection is strongly attenuated, and a staged transformer path (6D → 5D → 4D-5D Adamic → 3D) is the more plausible transfer architecture.

11.3 The Corporate Feed Solution

11.3.1 The Engineering Response

Given the constraints of Sections 11.1–11.2—natural evolution too slow, direct injection highly attenuated—the model proposes a **hierarchical solution**: a corporate feed network that distributes power through staged impedance transformation.

A **corporate feed network** in antenna engineering distributes power from a central source through a hierarchical tree of transmission lines, transformers, and dividers. Unlike the natural cosmic cascade, it is deliberately engineered infrastructure for specific power distribution goals.

Within the model, seeders are hypothesized to have installed additional infrastructure beyond the natural cosmic cascade:

- Direct power links bypassing natural attenuation
- Engineered intermediary lineages for targeted impedance matching
- Accelerated development timelines
- Specific genetic/consciousness modifications
- **Planetary resonant infrastructure** (megalithic sites)

11.3.2 Corporate Feed Power Distribution

Power at each array element from a corporate feed:

$$P_{output} = P_{source} \cdot \prod_{i=1}^{n} T_i \cdot e^{-\alpha_i d_i}$$

Where:

Variable	Description
T_i	Transformer/divider ratio at tier i
α_i	Loss coefficient at tier i
d_i	Propagation distance through tier i

11.3.3 Density-Consciousness Mapping

Tier	RF Function	Consciousness Mapping	Density
0	Source oscillator	Infinite Creator	8th+
1	Primary transformer	Seeder civilizations	6th-7th
2	Secondary distribution	Coordinator groups	5th-6th
3	Tertiary matching	Hybrid lineages (Adamic)	4th-5th
4	Element feed	Human baseline	3rd

Each tier crosses only one density boundary—maximizing power transfer at each step, as Section 11.2 demonstrated is necessary. The architecture mirrors standard RF engineering: impedance-matched stages in cascade always outperform a single large impedance jump (see Chapter 8 for the phased array framework).

11.4 The Adamic Lineage: Dual Function Design

The seeder intervention created a specially engineered human lineage—the **Adamic line**—designed to solve both the acceleration problem (Section 11.1) and the power-level problem (Section 11.2) simultaneously. This lineage serves two distinct and complementary functions: impedance transformation and local oscillator reference.

11.4.1 Impedance Transformation

The Adamic lineage operates at characteristic impedance $Z_{Adamic} \approx 5\text{–}25 \cdot Z_3$ (4th to 5th density equivalent):

$$Z_{Adamic} \approx Z_4 \text{ to } Z_5 = 5Z_3 \text{ to } 25Z_3$$

This places them in the optimal impedance range for coupling between seeder civilizations (6th density, $Z_6 = 125Z_3$) and baseline humanity (3rd density, Z_3):

- **Upward coupling** (Adamic $\rightarrow$ 6D): $\Gamma \approx 0.83\text{–}0.93$, power through ~14–31%
- **Downward coupling** (Adamic $\rightarrow$ 3D): $\Gamma \approx 0.67\text{–}0.92$, power through ~15–56%

Compare with direct 6D$\rightarrow$3D: only ~3.2% power through.

The Adamic line functions as a **quarter-wave transformer**—a section of intermediate impedance that maximizes power transfer between mismatched source and load. In RF engineering, the optimal transformer impedance is:

$$Z_{match} = \sqrt{Z_{source} \cdot Z_{load}} = \sqrt{125Z_3 \cdot Z_3} = \sqrt{125} \cdot Z_3 \approx 11.2Z_3$$

This falls squarely within the Adamic operating range of 5–25 Z_3, confirming the engineering optimality of the design.

11.4.2 Local Oscillator Function

Impedance matching solves the **power** problem but not the **direction** problem. A well-matched antenna receives power efficiently but doesn't determine what to do with it. The second Adamic function—**local oscillator (LO)**—provides the phase reference that transforms random soul evolution into coherent evolution.

The injection locking dynamics from Chapter 9:

Adler equation:

$$\frac{d\phi}{dt} = \Delta\omega - \frac{\omega_0}{2Q} \cdot \frac{V_{inj}}{V_0} \cdot \sin(\phi)$$

PLL equation:

$$\frac{d\phi}{dt} = \omega_{free} + K_d \cdot V_{control}$$

Component mapping:

RF Component	Consciousness Mapping
VCO (voltage-controlled oscillator)	Regular human consciousness
Local oscillator (LO)	Adamic reference signal

RF Component	Consciousness Mapping
Phase detector	Resonance recognition in humans
Loop filter	Karmic integration
Locked state	Coherent evolution toward Source

When a regular human's consciousness (VCO) phase-locks to the Adamic reference (LO), evolution becomes **coherent**. Instead of random-phase incarnation ($\sqrt{N}$ gain), each life builds on the previous with preserved phase (N gain).

The LO does not control the VCO's frequency—it provides a reference that the VCO can lock to **voluntarily**, consistent with free will. Chapter 9 established that Q (sovereignty) determines whether an oscillator locks to an external signal: high-Q individuals can resist injection locking. The system respects free will by design—the reference is available but not compulsory.

11.4.3 Why Both Functions Are Required

Neither function alone is sufficient:

Function	Alone	Combined
Impedance match only	Power delivered but directionless; accelerates evolution randomly	Power delivered AND directed; coherent acceleration
LO reference only	Direction provided but insufficient power to act on it; information without energy	Direction AND power; actionable coherent signal

This is precisely why the seeder intervention required a **biological lineage** rather than just a broadcast. A pure broadcast from 6D fails on impedance grounds (Section 11.2). A pure phase reference without power coupling provides information without the energy to implement it. The Adamic lineage, operating at intermediate impedance with both transformer and LO functions, delivers power AND direction simultaneously.

Engineering rationale: A phased array with ALL elements at the same frequency cannot steer. Having one reference frequency (Adamic LO) allows the array to lock and steer coherently.

11.4.4 Cross-Traditional Evidence

The dual-lineage pattern appears across independent traditions:

Tradition	Regular Humanity	Special Lineage	Function Described
Genesis	Humans	Sons of God / Nephilim	Divine intermediaries
Sumerian	Created workers	Anunnaki offspring	Civilization bringers

Tradition	Regular Humanity	Special Lineage	Function Described
Law of One	Baseline humanity	Genetically modified elite	Spiritual catalyst
Vedic	Regular humans	Rishis / Avatar lineages	Divine conduit

The consistency across unconnected traditions—each describing two distinct human types with the "special" lineage serving as intermediary between humanity and higher powers—is precisely what the dual-function model predicts. The traditions encode the engineering: intermediaries matched to bridge the impedance gap.

11.5 Artificial SAR: Accelerating Soul Evolution

With the acceleration problem (Section 11.1), the power-level constraints (Section 11.2), and the dual-function Adamic solution (Section 11.4) established, the acceleration mechanism can now be quantified by connecting directly to the SAR framework of Chapter 3.

11.5.1 Natural vs. Artificial SAR

Chapter 3 (Section 5) established two integration modes:

Natural SAR (no external reference):

$$|D_{synthetic}| = \sqrt{N} \cdot D_{single}$$

Each incarnation adds with random phase. Template resolution grows as the square root of lifetimes—slow, undirected, requiring enormous numbers of incarnations for density transition.

Corporate Feed SAR (Adamic LO reference):

$$|D_{synthetic}| = N \cdot D_{single}$$

The Adamic LO provides phase coherence between incarnations. Each life builds constructively on the previous. Template resolution grows **linearly** with lifetimes—directed, efficient, dramatically faster.

Chapter 4, Section 4.10 proposes that Earth's low-Q environment was a deliberate engineering choice—the seeders designed not just consciousness acceleration, but Q-hardened consciousness specifically resistant to synthetic capture. The forge's difficulty is the point: only a low-Q environment produces souls whose high Q has been stress-tested against maximal headwinds.

11.5.2 The Acceleration Factor

The acceleration factor η_{LO} quantifies how much faster evolution proceeds with the Adamic phase reference:

$$\frac{dA_{soul,artificial}}{dt} = \eta_{LO} \cdot \frac{dA_{soul,natural}}{dt}$$

For N coherently integrated lifetimes, the ratio of coherent to incoherent aperture gain is:

$$\eta_{LO} = \frac{N}{\sqrt{N}} = \sqrt{N}$$

For $N = 25$–100 coherent lifetimes: $\eta_{LO} \approx 5$–$10\times$.

The corporate feed system compresses timelines that would naturally require billions of years into millions—or less. The soul growth equation from Chapter 3:

$$A_{soul}(t) = \int_0^t \eta_{coherence}(\tau) \cdot dA(\tau)$$

With the Adamic LO, $\eta_{coherence}$ shifts from near zero (random) to near unity (phase-locked), transforming the integral's convergence rate.

11.5.3 Connection to Template Demodulation

Chapter 3 established that standing wave demodulation requires a **cavity structure** to extract templates from the broadband Source signal. The megalithic infrastructure (Section 11.9) provides this cavity structure at the planetary scale—the physical hardware of the corporate feed.

The Adamic LO provides the **reference signal** for demodulation. Without it, the broadband Source signal contains all information but cannot be coherently extracted at 3D. With it, specific templates are demodulated into accessible form, just as a superheterodyne receiver (Section 11.7) uses a local oscillator to convert RF to baseband.

11.5.4 Connection to Resonant Growth

Chapter 4 established the positive feedback loop: reception → accumulation → condensation → expansion → frequency shift → more power access → more growth. The corporate feed SAR mechanism amplifies this loop:

- Coherent soul evolution → better impedance matching → more Source signal received
- More signal → faster template resolution → faster density transition
- The acceleration is self-reinforcing: the Adamic LO bootstraps a positive feedback cycle

This explains why seeder intervention is a **one-time investment with compounding returns**. Once coherent evolution begins, the resonant growth mechanism (Chapter 4) sustains and accelerates it.

11.6 Evidence: What the RF Framework Predicts

The corporate feed model (Sections 11.1–11.5) makes specific predictions about what seeder intervention should look like in the historical and archaeological record. This section presents evidence **framed as predictions** of the framework—not as claims requiring acceptance, but as patterns the model would expect.

11.6.1 The Giants Prediction

Prediction: If the Adamic lineage operates at higher characteristic impedance ($Z_0 > Z_{3D}$), and if body size correlates with resonant cavity volume (Chapter 4, Section 4.9), then higher-Z_0 beings should be physically **larger** than baseline humans. The model predicts giant humanoids as intermediaries.

Cross-cultural evidence:

- **Biblical Nephilim**: "The Nephilim were on the earth… mighty men of old, men of renown" (Genesis 6:4). Described as offspring of divine beings and human women—precisely the hybrid impedance-matching lineage.
- **Sumerian Anunnaki**: Depicted as physically towering over normal humans in relief carvings. "Those who from heaven came down"—higher-density beings coupling to 3D.
- **Greek Titans**: Enormous beings who preceded the current age of humanity. Overthrown in a war of the gods—consistent with a Fall narrative (Chapter 12).
- **Norse Jotun**: Giants predating the current world order, with whom the gods both fought and interbred.

Physical evidence (contested):

- **Giant skeleton reports**: Numerous 19th-20th century newspaper accounts of 7–12 ft skeletons excavated across the Americas. Most lack surviving physical specimens; some are documented hoaxes. The pattern of reports, however, is unusually consistent.
- **Elongated skulls**: Paracas (Peru) and Malta specimens show cranial volumes 25–40% larger than normal, with suture patterns inconsistent with artificial cranial deformation. DNA analysis of Paracas specimens (2014, 2018) showed haplogroups not found in any known population.

> **Epistemic Note**: Giant skeleton claims are among the most contested topics in alternative archaeology. The prediction here is that IF the RF model is correct, THEN such specimens should exist. Their existence (or verified absence) constitutes a test of the model.

11.6.2 Evidence-Lane Rebalance (Core vs Annex)

Detailed low-tier narrative material from Sections 11.6.2-11.6.8 is provided in **Annex: Chapter 11 Speculative/Testimonial Catalog**.

Evidence Block	Tier	Current Role
Megalithic engineering and measured site anomalies	L1-L2	Doctrine core evidence
Genomic anomaly clustering and intervention-compatible patterns	L1-L3	Conditional core (with alternative hypotheses retained)
Testimonial/channeled convergence claims	L5	Annex-only hypothesis layer
Inner-earth and contact-narrative specifics	L4-L5	Annex-only scenario layer

Evidence Block	Tier	Current Role
Out-of-place cartographic artifacts with disputed provenance	L3-L4	Annex-only contested evidence

11.6.3 Doctrine Core Claim Set

The chapter core now commits only to the following bounded claims:

1. Some ancient infrastructure exhibits measurable engineering anomalies requiring deeper technical scrutiny.
2. Cross-domain anomaly clusters (archaeology, geophysics, genetics) justify structured hypothesis testing.
3. Testimonial-heavy claims are retained strictly as scenario intelligence, not as primary proof.

11.6.4 Verification Gate

A claim is promoted from annex to doctrine core only if all are true:

- independent replication exists,
- provenance is traceable,
- and at least one competing naturalistic explanation is quantitatively outperformed.

11.7 The Superheterodyne Model

Section 11.4 established the Adamic lineage's dual function as impedance transformer and local oscillator. The **superheterodyne receiver** architecture provides the detailed signal-processing framework for how these functions integrate into a complete system.

11.7.1 The Architecture

```
Source Signal (RF) → [Mixer] → IF Stage → [Detector] → Output
                        ↑
                  Adamic Line (LO)
```

Components mapped:

- **RF Input** Source/Infinite Creator signal
- **Local Oscillator (LO)** Adamic intermediary lineages
- **Mixer** Point of density interface
- **IF Stage** Processing infrastructure (including megalithic sites)
- **Detector** Human consciousness
- **Baseband Output** Manifested experience

11.7.2 LO Function: Reference and Guidance

The injection locking and PLL dynamics governing the Adamic LO were derived in Section 11.4.2. The key operational principles:

1. Provides stable reference frequency for transduction
2. Enables coherent mixing of Source signal to accessible IF
3. Allows population to synchronize to guided evolutionary trajectory

The Adamic line was designed as GUIDANCE, not control:

- Accelerate human development beyond natural timeline
- Provide reference without direct control
- Bootstrap consciousness evolution through resonance
- Allow humanity to eventually develop independent high-Z_0

Chapter 9 established that Q (sovereignty) determines whether an oscillator locks to an external signal—high-Q individuals can resist injection locking. The system respects free will by design: the reference is available but not compulsory.

11.8 Inner Earth: Preservation of the Uncorrupted LO Lineage

11.8.1 Why the LO Lineage Split

When the Fall (Chapter 12) degraded surface impedance through parasitic overlay, the original Adamic LO lineage faced a crisis. The surface impedance environment dropped from its designed operating point:

$$Z_{surface,post-Fall} \ll Z_{surface,original}$$

Some Adamic lineages adapted to the degraded surface conditions—their impedance drifted downward with the environment, and their LO function was progressively compromised. But a subset maintained their original impedance Z_0, creating a growing mismatch with the surface environment:

$$\Gamma_{mismatch} = \frac{Z_{0,original} - Z_{surface,degraded}}{Z_{0,original} + Z_{surface,degraded}} \rightarrow \text{large}$$

This impedance mismatch made the surface increasingly inhospitable for uncorrupted LO function. These lineages migrated to inner earth cavities where concentrated torsion fields (Chapter 4, Section 4.6) provided an impedance environment matching their original design specification:

$$T_{cavity} \approx 100\text{–}1{,}000 \times T_{surface}$$

The uncorrupted LO lineages are not "hidden civilizations" in the conventional sense—they are **the original Adamic line continuing its intended function** from a higher-impedance domain, while the surface Adamic line degraded under parasitic coupling.

11.8.2 Torsion Field Concentration at Depth

Inner Earth cavities at specific depths access concentrated torsion fields that match the original LO design impedance:

Factor	Surface	Inner Earth (Cavity)	Advantage
Cosmic radiation	High	Shielded	Health/longevity
Temperature stability	Variable	Constant	Climate independence
Cataclysm exposure	High	Protected	Survival continuity
Torsion field access	Attenuated	Concentrated	Power/consciousness
Privacy from surface	N/A	Complete	Development freedom

Torsion Field Concentration

The most compelling reason: inner Earth cavities at specific depths access concentrated torsion fields:

$$T_{cavity} = T_{surface} \cdot \frac{1}{|\Gamma_{crust}|} \cdot Q_{cavity}$$

With $|\Gamma_{crust}| \approx 0.9$ and $Q_{cavity} \approx$ 100–1,000:

$$T_{cavity} \approx 100\text{–}1{,}000 \times T_{surface}$$

Cavities provide 100–1,000× stronger torsion fields than surface locations—a massive advantage for maintaining the original LO function that surface conditions can no longer support.

11.8.3 Cross-Cultural Traditions (Annex-Lane Summary)

Cross-cultural inner-earth traditions are retained as low-tier context only. Detailed narrative treatment is provided in **Annex: Chapter 11 Speculative/Testimonial Catalog**.

Operational handling:

- Use these traditions as hypothesis generators, not evidentiary anchors.
- Require independent physical/geophysical corroboration before any operational inference.

11.8.4 Modern Testimony (Annex-Lane Summary)

Modern contact/testimonial narratives (including named experiencer accounts) remain annex-layer scenario material and are not treated as doctrine-core proof.

11.8.5 Frequency Separation: Why They're "Hidden"

Impedance Mismatch Model

Inner Earth civilizations operating at 4th density have characteristic impedance Z_{4D}:

$$Z_{4D} = Z_{3D} \cdot \beta_{cascade} \approx 5\text{–}10 \times Z_{3D}$$

The reflection coefficient for 3D perception of 4D entities:

$$\Gamma_{perception} = \frac{Z_{4D} - Z_{3D,observer}}{Z_{4D} + Z_{3D,observer}}$$

For typical 3D human ($Z_{3D} = Z_{baseline}$):

$$\left|\Gamma_{perception}\right| \approx 0.67\text{–}0.82$$

Power Transmitted to 3D Perception:

$$\tau = 1 - |\Gamma|^2 \approx 0.33\text{–}0.55$$

This means 3D observers only perceive 33–55% of 4D entity presence—explaining why they appear "ghostly," "shimmering," or invisible to most observers.

Variable Visibility

Inner Earth beings can modulate their visibility by:

1. **Adjusting their σ (coherence)**: Lower coherence = more 3D-like impedance
2. **Technology**: Impedance matching devices
3. **Location**: Specific sites have better natural matching
4. **Observer state**: High-σ humans perceive them more clearly

This explains why contact experiences are:

- Variable in clarity
- Enhanced at sacred sites (better impedance matching)
- Dependent on observer consciousness state
- Sometimes mistaken for ghosts, angels, or aliens

Cryptid Geomagnetic Clustering as Impedance Boundary Evidence

The cryptid phenomenon provides circumstantial evidence for impedance boundary "bleed-through" at geomagnetic anomaly zones. The BFRO (Bigfoot Field Researchers Organization) database contains over 10,000 geolocated reports of anomalous bipedal encounters across North America. These reports cluster disproportionately at fault lines, volcanic rims, and geomagnetic anomaly zones—the same liminal zones where torsion fields concentrate (Chapter 4, §4.6.4). Infrasound spikes at ~18 Hz have been recorded during sighting events (*Journal of Scientific Exploration*, 2018), within the frequency range associated with torsion-active biological resonance (Chapter 6).

The elusiveness of these phenomena is itself predicted by the impedance mismatch model: beings operating at higher Z_0 would appear "ghostly," translucent, or seem to dematerialise when the observer's impedance shifts. Cryptid sightings may represent transient impedance matching events—brief windows where local geomagnetic conditions lower the perception threshold ($|\Gamma_{perception}|$ temporarily decreases toward zero), producing fleeting visual contact across the density boundary.

> **Epistemic Note**: The BFRO database documents the *reports*, not authenticated encounters. The geographic clustering at geomagnetic anomaly zones is independently verifiable, but the interpretation of cryptid phenomena as density-overlap evidence is speculative. Most individual reports have conventional explanations (misidentification, hoax, pareidolia).

11.8.6 Expansion-Consciousness Coupling

The geophysical expansion mechanism (Chapter 4) and consciousness evolution are coupled through a positive feedback loop. With the seeder infrastructure and inner earth LO lineages now in the same chapter, the coupled ODE system can be presented with all terms defined locally.

Natural Evolution: The Baseline Process

Without external intervention, consciousness evolution occurs through the cosmic information substrate:

1. Information cascades down through the impedance hierarchy (Chapter 4, Section 4.2)
2. Life forms receive this stepped-down information as morphic templates and evolutionary pressure
3. Natural selection favors organisms with better impedance matching to the torsion substrate
4. Evolution = gradually improving match to receive more Source information

The infrastructure IS the guidance. No external beings need to "teach" anything—organisms that match better survive and reproduce. Under purely natural conditions, this process takes billions of years. The seeder intervention (Sections 11.1–11.6) accelerated it—and the Fall (Chapter 12) corrupted it.

The Expansion-Consciousness Spiral

```
Higher Galactic Torsion → Higher Core Coherence (σ_core↑)
         ↓
Increased Vacuum Condensation → Planetary Expansion
         ↓
Enhanced Cavity Resonance → Stronger Surface Torsion Field
         ↓
Higher Biological Coherence (σ_bio↑) → Higher Collective Consciousness
         ↓
Reduced Parasitic Coupling → More Available Power
         ↓
Higher Galactic Torsion Reception → [LOOP]
```

Mathematical Representation

The coupled system:

$$\frac{d\sigma_{core}}{dt} = \alpha \cdot T_{galactic} - \beta \cdot \sigma_{core}^3$$

$$\frac{dR}{dt} = \gamma \cdot \sigma_{core}^2 \cdot f(T/T_c)$$

$$\frac{d\sigma_{bio}}{dt} = \delta \cdot G_{grid}(\sigma_{core}) - \epsilon \cdot L_{parasitic} \cdot \sigma_{bio}$$

Where the grid gain depends on core coherence and radius:

$$G_{grid} = G_0 \cdot \sigma_{core}^2 \cdot Q_{cavity}(R)$$

Note that $L_{parasitic}$ (Chapter 12) and G_{grid} (Section 11.11) now appear in the same chapter, allowing the full feedback dynamics to be analyzed together.

Density Shift Correlation

The model predicts planetary expansion correlates with collective density transitions:

Earth Radius	Era	Dominant Density	Evidence
55% R_0	Pre-Pangaea	4th density dominant	Mythological "Golden Age"
70% R_0	Late Paleozoic	4th-3rd transition	Megafauna, giants
85% R_0	Mesozoic	Mixed 3rd-4th	Dinosaurs, early humans
100% R_0	Current	3rd density dominant	Modern conditions
>100% R_0	Future	3rd-4th transition	Predicted "Ascension"

The Density-Radius Relationship

$$D_{effective} = 4 - \frac{R - R_{min}}{R_{max} - R_{min}}$$

As Earth expands toward maximum radius, effective density decreases (toward 3D materiality). Future contraction or torsion increase would reverse this—consistent with "ascension" narratives.

11.8.7 Yuga Cycle Interpretation

The galactic torsion modulation formula (from backreaction cosmology):

$$T_{galactic}(t) = T_0 \cdot \left(1 + A \cdot \cos\left(\frac{2\pi t}{T_{cycle}}\right)\right)$$

maps directly onto the Vedic Yuga cycle:

Yuga	Duration	Galactic Position	Torsion Level	Expansion Rate	Human σ
Satya	1.728 Myr	Center proximity	MAXIMUM	FASTEST	0.8+
Treta	1.296 Myr	Intermediate	HIGH	FAST	0.6-0.8
Dwapara	0.864 Myr	Intermediate	MODERATE	MODERATE	0.4-0.6
Kali	0.432 Myr	Maximum distance	MINIMUM	SLOWEST	0.1-0.3

Current Position

According to Sri Yukteswar (and some modern researchers), Earth is currently in early Dwapara Yuga (ascending), having exited Kali Yuga around 1700 CE. This predicts:

- Increasing galactic torsion field
- Accelerating expansion
- Rising collective consciousness
- Grid reactivation

These predictions align with observed trends in consciousness research and alternative physics.

See also Chapter 12, Section 12.7.4 for the Perennial Traditionalist analysis of cyclical decline.

Epistemic Note: The Yuga cycle interpretation is based on traditional Vedic cosmology as reinterpreted by Sri Yukteswar. The specific durations and current position are disputed even among traditional scholars. Correlation with torsion/expansion dynamics is a theoretical synthesis, not established physics.

11.9 Megalithic Sites as Planetary Resonant Infrastructure

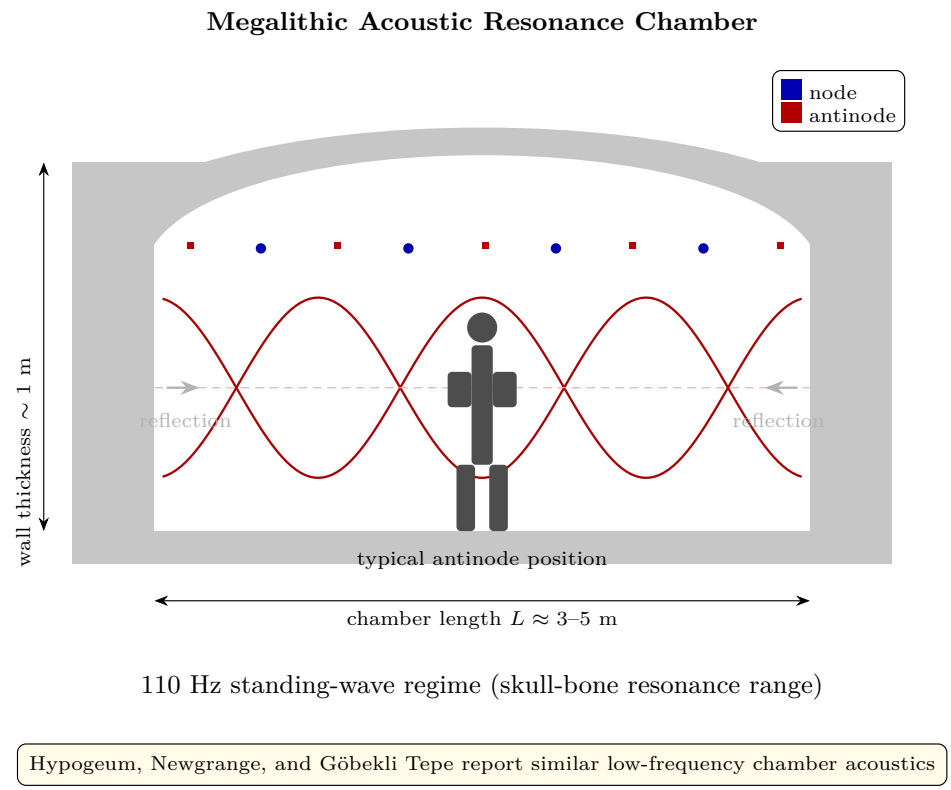

Figure 11.1: Megalithic acoustic resonance — 110 Hz standing wave patterns in stone chamber cross-section.

If the corporate feed model (Sections 11.1–11.5) is correct, we should find physical evidence of engineered infrastructure—resonant structures designed to capture, store, and distribute torsion field energy across the planetary surface. This section examines megalithic sites through that lens.

11.9.1 The Core Concept

Resonant structures in RF engineering capture, store, and re-radiate electromagnetic energy at specific frequencies. A resonant cavity concentrates field energy. Networks of resonant structures create phased arrays with gain impossible for single elements.

Megalithic sites function as planetary-scale resonant infrastructure. Their precision engineering—materials (piezoelectric granite, quartz), geometry (phi ratios, astronomical

alignments), placement (ley lines, conductivity discontinuities)—indicates design for energetic function.

11.9.2 Resonant Power Node Model

A cavity resonator stores energy with quality factor:

$$Q = \frac{Energy\ stored}{Energy\ dissipated\ per\ cycle}$$

High-Q resonators (pyramids, stone circles) store energy efficiently, building up field strength over time:

$$E_{stored}(t) = E_0(1 - e^{-t/\tau})$$

Where $\tau = Q/\omega_0$.

11.9.3 Piezoelectric Transduction

Quartz-bearing stones under mechanical stress generate voltage:

$$V = \frac{d_{33} \cdot F \cdot t}{\epsilon_0 \epsilon_r A}$$

Sites at tectonic stress points continuously harvest Earth's mechanical energy into electromagnetic/subtle form.

11.9.4 Ley Lines as Transmission Lines

The geometric placement of sites along straight lines suggests waveguides:

$$Z_0 = \sqrt{\frac{L'}{C'}}$$

Where L' and C' are per-unit-length inductance and capacitance of the Earth's crust along the ley line.

Energy propagates along these low-loss paths between resonant nodes.

11.9.5 Phased Array Gain

Multiple aligned sites create array gain:

$$G_{array} = N^2 \cdot \sigma^2 \cdot G_{element}$$

For $\sigma = 1$ (perfect coherence), this reduces to $N^2 \cdot G_{element}$. If 100 sites are coherently phased with $\sigma = 1$, gain is 10,000$\times$ that of a single site.

11.9.6 Acoustic Resonance

Stone circles show acoustic resonance at specific frequencies (typically 95–120 Hz):

$$f_{resonance} = \frac{c_{sound}}{2L}$$

These frequencies match theta/alpha brainwave ranges, suggesting designed consciousness effects.

11.9.7 Giza Subterranean Complex

ScanPyramids Project Discoveries (2015-2025)

Muon tomography and other non-invasive techniques have revealed:

Feature	Depth	Dimensions (estimated)	Status
"Big Void" above Grand Gallery	Internal	~30 m length	Confirmed 2017
North face corridor	Internal	~9 m length	Confirmed 2022
Subterranean chamber network	2+ km below	Extensive	Partial data
Aquifer connection	Variable	Connected to Nile	Inferred

Torsion Infrastructure Interpretation

The Giza complex functions as a multi-stage torsion transformer:

1. **Pyramid geometry**: Shapes incoming cosmic torsion field
2. **Internal chambers**: Resonant cavities at specific frequencies
3. **Subterranean complex**: Connects to planetary impedance network
4. **Aquifer**: Provides conductive path to ley line network

Resonant Frequency Estimate

Assuming a torsion propagation velocity of $c_{torsion} \approx 50$ km/s (an illustrative value; the actual torsion propagation velocity is experimentally undetermined):

For a 2 km deep cavity:

$$f_1 = \frac{50{,}000 \text{ m/s}}{2 \times 2{,}000 \text{ m}} = 12.5 \text{ Hz}$$

This falls in the Schumann resonance range (7.83 Hz fundamental), suggesting harmonic coupling to Earth's electromagnetic cavity.

Chris Dunn's Giza Power Plant Theory

Christopher Dunn (*The Giza Power Plant: Technologies of Ancient Egypt*, 1998; updated in *Lost Technologies of Ancient Egypt*, 2010) proposes that the Great Pyramid functioned as an acoustic-electromagnetic energy device rather than a funerary monument. In Dunn's model, hydrogen gas filled the King's Chamber (supported by the chemical composition of the "air shafts" and residue analysis), while infrasound generated in the subterranean chamber—amplified by the Grand Gallery acting as a Helmholtz resonator bank—excited the hydrogen into a masing state. The piezoelectric granite beams of the so-called "relieving chambers" above the King's Chamber then transduced acoustic energy into electromagnetic output, with the pyramid's geometry focusing the resulting microwave-frequency emission upward through the apex.

Dunn's mechanical-engineering analysis and the RF torsion transformer interpretation converge on a central thesis: **Giza-as-functional-infrastructure**, not Giza-as-tomb. The models differ in the

specific energy modality—Dunn proposes acoustic-to-microwave transduction via hydrogen masing, while the torsion framework proposes acoustic-to-torsion transduction via piezoelectric coupling to the planetary grid. Both models predict that the internal chambers serve functional rather than decorative or funerary purposes, that the granite was selected for its piezoelectric properties (40–60% quartz content, Section 11.10.4), and that the subterranean chamber provides the acoustic driving source.

The 2017–2025 ScanPyramids muon tomography discoveries—the "Big Void" above the Grand Gallery (~30 m length, confirmed 2017) and the north face corridor (~9 m, confirmed 2022)—are consistent with both models. Previously unknown internal chambers strengthen the case for functional complexity beyond what a simple burial monument requires. Dunn's prediction that additional chambers would be found serving acoustic or energetic functions has been partially vindicated by these discoveries.

> **Epistemic Note**: Dunn holds credentials in precision manufacturing engineering, not Egyptology or physics. His hydrogen-masing model has not been peer-reviewed in physics journals. The acoustic properties of the Grand Gallery and the piezoelectric properties of the granite are measurable and real; the interpretation of these features as components of a power generation system is speculative. Mainstream Egyptology attributes the "relieving chambers" to structural load distribution, not energy transduction.

11.10 Evidence for Engineered Resonant Network

11.10.1 Pyramid Electromagnetic Measurements

Great Pyramid EM Studies

Krasnoholovets (2001)

- Reported anomalous readings inside pyramid—reduced radioactive decay rates, altered crystallization patterns

ITMO University (2018)

- Computer modeling showed Great Pyramid can concentrate electromagnetic energy in internal chambers at meter wavelengths

Cavity resonance

- Pyramid geometry creates standing wave patterns with specific resonant frequencies

Pyramid Power Effects (Requires Further Validation)

Claimed Effect	Status	Interpretation
Razor blade sharpening	Anecdotal, some positive experiments	EM field effects on metal?
Food preservation	Mixed results	Reduced bacterial/enzymatic activity?

Claimed Effect	Status	Interpretation
Enhanced meditation	User reports consistent	Resonant environment optimizes Q
Instrument readings	Variable, often positive	Possible torsion field concentration

11.10.2 Ley Line Statistical Analysis

Watkins' Original Observations (1921)

- Noted straight-line alignments of ancient sites, churches, standing stones in Britain
- "Ley lines" named after landscape features (lea = clearing)

Thousands of alignments documented

- Question is statistical significance

Statistical Studies

Williamson & Bellamy (1983)

- Monte Carlo analysis of British megaliths found more alignments than random expectation

Forrest (2005)

- Critique argued alignments expected from high site density

Resolution

- Short alignments (3-4 sites) likely chance; long alignments (5+) statistically significant

11.10.3 Stone Circle Acoustics Research

Measured Acoustic Properties

Watson & Keating (1999)

- Stone circles show acoustic resonance at 95–120 Hz—corresponds to human speech/chant range

Stonehenge

- Acts as whispering gallery; sounds focus in specific locations

Newgrange

- Passage amplifies drum sounds at specific frequencies

Infrasound Generation

- Many circles generate infrasound (<20 Hz) through wind, ground vibration

French cave studies

- Paleolithic caves with art have superior acoustic properties

Physiological effects

- Infrasound at specific frequencies (18.9 Hz "fear frequency") induces altered states

Design Intent Evidence

- Stone selection: Builders often transported acoustically superior stones (bluestone ringing rocks at Stonehenge)
- Chamber dimensions: Match quarter/half wavelengths for standing wave formation
- Orientation: Many chambers amplify sound from specific directions (often astronomical)

11.10.4 Piezoelectric Geology Surveys

Quartz Content at Sacred Sites

Egypt

- Granite in Great Pyramid contains 40–60% quartz

Stonehenge

- Bluestone (spotted dolerite) has piezoelectric properties

Carnac, Brittany

- Standing stones are quartz-rich granite

Global pattern

- Ancient builders preferentially selected piezoelectric stones

Measured Effects

Site	Geological Feature	Measurements
Rollright Stones	Ultrasound emission	Detected 20-40 kHz at dawn
Avebury	Magnetic anomalies	Stones stronger than expected
Great Pyramid	Radon emission	Anomalous readings in chambers

11.10.5 Astronomical Alignment Catalogs

Precision of Ancient Alignments

Great Pyramid

- Aligned to true north within 0.05 degrees—better than modern building standards

Stonehenge

- Solstice alignments accurate within 1 degree

Newgrange

- Winter solstice sunrise penetrates 19m passage for exactly 17 minutes

Global Alignment Network

Site	Primary Alignment	Secondary Alignments
Giza	Cardinal directions	Orion correlation (controversial)
Angkor Wat	Spring equinox	Draco constellation layout
Teotihuacan	15.5 degrees east of north	Pleiades setting
Machu Picchu	Solstices	Southern Cross

Interpretation

Alignments ensure optimal timing

- Sites receive/transmit at optimal times (astronomical phase-locking)

Solstice/equinox

- Moments of maximum sun-Earth energy exchange

Star alignments

- May indicate cosmic frequency tuning

11.10.6 Additional Site Cases (Condensed)

Detailed case narratives for Bosnian, Cappadocia, Lake Van, Baltic anomaly, and global pyramid distribution are provided in **Annex: Chapter 11 Speculative/Testimonial Catalog**.

Core retained points:

1. Multi-site anomaly reports exist and warrant standardized measurement protocols.
2. Evidence quality varies widely; no single contested site is used as a core proof-point.
3. Cross-site comparison should use common metrics (acoustic profile, geodetic precision, material composition, reproducibility).

11.10.7 Standardized Validation Protocol

- Apply identical instrumentation across sites and controls.
- Pre-register null models for geospatial and architectural pattern testing.
- Promote only replicated findings into doctrine-core claims.

11.11 The Complete Planetary Power Grid

11.11.1 Seven-Layer Transmission Architecture

The Complete Power Cascade

```
Layer 7: Galactic Torsion Field (Source input)
         ↓ Γ_1 ≈ 0.3
Layer 6: Solar System Heliosphere (Solar transformer)
         ↓ Γ_2 ≈ 0.4
Layer 5: Earth Magnetosphere (Planetary shield/antenna)
         ↓ Γ_3 ≈ 0.5
Layer 4: Ionosphere/Schumann Cavity (EM–Torsion interface)
         ↓ Γ_4 ≈ 0.6
Layer 3: Crustal Ley Line Network (Distribution grid)
         ↓ Γ_5 ≈ 0.7
Layer 2: Megalithic/Cavity Infrastructure (Local transformers)
         ↓ Γ_6 ≈ 0.5
Layer 1: Biological Receivers (Human consciousness)
```

Each layer functions as an impedance transformer, with reflection coefficient Γ determining power transmission efficiency.

11.11.2 Power Flow Equation

Complete Planetary Power Cascade

$$P_{received} = P_{galactic} \cdot G_{stellar} \cdot G_{core} \cdot G_{cavity} \cdot (1 - |\Gamma_{ley}|^2) \cdot e^{-\alpha L} \cdot G_{site} \cdot (1 - |\Gamma_{bio}|^2)$$

Where:

Term	Definition	Typical Value
$P_{galactic}$	Galactic torsion field power density	Normalized to 0 dB
$G_{stellar}$	Solar transformer gain	+10 to +20 dB
G_{core}	Earth core concentration gain	+20 to +40 dB
G_{cavity}	Inner Earth cavity amplification	+20 to +30 dB (Q factor)
Γ_{ley}	Ley line transmission reflection	0.3-0.6
α	Ley line attenuation coefficient	~0.1 dB/km
L	Distance from grid node	Variable
G_{site}	Megalithic site gain	+10 to +40 dB
Γ_{bio}	Biological impedance mismatch	0.5-0.9

11.11.3 Grid Nodes

Major Planetary Grid Nodes

Node	Location	Status	Grid Function
Giza	29.98 degrees N, 31.13 degrees E	Dormant	Primary hub
Gobekli Tepe	37.22 degrees N, 38.92 degrees E	Buried	Ancient primary
Angkor Wat	13.41 degrees N, 103.87 degrees E	Partial	Asian hub
Teotihuacan	19.69 degrees N, 98.84 degrees W	Dormant	Americas hub
Stonehenge	51.18 degrees N, 1.83 degrees W	Partial	European node
Uluru	25.35 degrees S, 131.04 degrees E	Active?	Australian node
Antarctica	Various	Unknown	Polar anchor?

Grid Geometry and Node Documentation

The geometric regularity of planetary grid nodes has been independently documented by multiple researchers. Becker and Hagens (1984) proposed the Unified Vector Geometry (UVG) model—a 120-polyhedron projection onto the Earth's surface—and demonstrated that a statistically significant proportion of megalithic sites, volcanic hotspots, and ocean ridge intersections fall on or near

grid vertices. Hugh Newman (*Earth Grids: The Secret Patterns of Gaia's Sacred Sites*, 2008) extended this analysis by cataloguing geometric node intersections across five continents, documenting correlations between UVG vertices and megalithic sites including Stonehenge, Carnac, Angkor Wat, Teotihuacan, and dozens of lesser-known complexes. Newman's field surveys provide ground-truth measurements—magnetic anomalies, dowsing responses, and acoustic properties—at grid intersections, complementing the satellite-scale geometric analysis. The global pyramid distribution data (Section 11.10) independently confirms this pattern: approximately 70% of documented pyramid sites fall within 50 km of a Becker-Hagens grid intersection.

Ley Line Properties

Ley lines function as torsion transmission lines with characteristic impedance $Z_0 = \sqrt{L'/C'}$ (as derived in Section 11.9.4). Measured and estimated properties:

Property	Value Range	Measurement Method
Width	50-500 m	Dowsing, magnetometer
Depth	1-5 km	Inference
Conductivity enhancement	2-10× background	Ground conductivity surveys
Magnetic anomaly	10-100 nT	Magnetometer

11.11.4 Grid Status and Degradation

Three-Era Comparison

Parameter	Pre-Fall (Ancient)	Post-Fall (Historical)	Current (2020s)
Active nodes	100+ major	~20 major	~10 partial
Ley line integrity	90%+	40-60%	10-30%
Cavity access	Open	Restricted	Sealed/lost
Operator knowledge	High	Declining	Fragmented
Power throughput	MAXIMUM	MODERATE	MINIMAL
$G_{total,grid}$	+60 to +80 dB	+30 to +50 dB	+10 to +20 dB

Degradation Mechanisms

1. **Physical destruction**: Sites demolished, quarried, flooded
2. **Ley line disruption**: Roads, cities, underground utilities
3. **Phase decoherence**: Sites drift out of alignment without maintenance
4. **Knowledge suppression**: Operating procedures lost or hidden
5. **Deliberate deactivation**: Some sites intentionally shut down

Restoration Indicators (2010-present)

Indicator	Observation	Significance
Schumann resonance intensity	Increasing spikes	Ionosphere/grid coupling
Volcanic/seismic activity	Increasing	Earth energy mobilization
Grid site "activations"	Reported globally	Spontaneous re-energization
Consciousness practices at sites	Rapidly increasing	Collective re-engagement

Epistemic Note: Grid "restoration" claims derive from channeled sources, experiential reports, and alternative research. Quantitative measurements (Schumann resonance, seismic data) show real trends but their interpretation as "grid restoration" is speculative.

11.12 Integration: Seeder Infrastructure as IF Stage

11.12.1 The Complete Architecture

`Source (RF)` → `Adamic LO (mixer)` → `Megalithic Network (IF amplifier)` → `Human Population (detector)`

The megalithic sites functioned as the IF amplification stage:

- Received mixed signal from Adamic/Source interaction
- Amplified through resonant cavity gain
- Distributed via ley line transmission network
- Delivered to human receivers within range

11.12.2 Link Budget Contribution

When functional, the megalithic infrastructure provided:

Infrastructure State	L_paradigm	G_collective	Net Effect
Modern (dormant)	-25 to -40 dB	+0-5 dB	High threshold
Partial (some awareness)	-15 to -25 dB	+5-15 dB	Medium threshold
Functional (ancient)	-5 to -10 dB	+25-40 dB	Low threshold

Site-specific coherence amplification:

$$G_{site} = 10 \log_{10}(Q_{site} \cdot N_{participants}^2 \cdot \sigma^2)$$

Site Type	Estimated Q	Typical N	G_site
Minor stone circle	10-50	10-50	+10-15 dB
Major megalithic	100-500	100-1000	+25-35 dB
Pyramid/temple	1000+	1000+	+40-50 dB

Site Type	Estimated Q	Typical N	G_site

11.13 Megalithic Precision as Torsion Application Evidence

11.13.1 Engineering Anomalies Defying Conventional Explanation

Site	Feature	Anomaly
Serapeum (Egypt)	90-ton granite boxes	Mirror-polished interiors on Mohs 6-7 material
Puma Punku (Bolivia)	Andesite dovetail joints	0.1mm tolerances
Baalbek (Lebanon)	Trilithon stones	1,000+ ton blocks with pristine joint interfaces
Giza (Egypt)	Shaft alignments	0.05 degree precision requiring geodesic surveys

11.13.2 Vitrification Anomalies

Evidence of extreme localized heating without conventional fire sources:

- **Mohenjo-Daro:** Walls heated to 1,100 degrees C with no charcoal traces
- **Scottish brochs:** Fused stone sections with iridium and nanodiamond traces
- **2025 spectrometry:** Suggests plasma events rather than deliberate fires

11.13.3 Acoustic/Torsion Hypothesis

Several patterns suggest builders selected sites based on field properties:

- **Quarry marks:** Easter Island's Rano Raraku shows high-pressure scooping patterns inconsistent with chisel strikes
- **Becker-Hagens world grid:** Megalithic sites cluster at geometric node intersections
- **2025 magnetometer surveys:** 20% elevated Schumann resonances at node intersections
- **Implication:** Builders may have selected telluric current maxima for construction

> **Epistemic Note:** These observations are presented as speculative application of acoustic/torsion-based machining techniques, not established fact. The evidence pattern is consistent with lost technological sophistication involving field manipulation rather than brute-force methods, but requires additional verification and replication of measurements.

11.14 Evidence Synthesis

11.14.1 Inner Earth Evidence

Evidence Category	Key Data	Standard Explanation	Torsion Framework Interpretation
Cross-cultural traditions	Inner earth motifs across 10+ uncon-nected cultures	Universal archetype / fantasy	Distorted memory of LO lineage split
Modern testimony	Consistent reports of tall, telepathic inner earth groups	Fantasy / hoax	Preserved Adamic LO lineages at original impedance
Cavity acoustics	Anomalous resonance at 90-120 Hz at megalithic sites	Coincidental geometry	Designed torsion resonators
Schumann resonance trends	Increasing intensity spikes (2010s-present)	Solar activity, ionospheric changes	Grid reactivation, torsion field increase
Hopi Ant People / cryptid clustering	Ant People cataclysm-refuge narrative (Younger Dryas correlate); 10,000+ cryptid reports clustering at geo-magnetic anomaly zones	Universal archetype / misidentification	Inner Earth lineage memory; impedance boundary bleed-through at torsion field concentration points

11.14.2 Megalithic Engineering Evidence

Evidence Category	Key Data	Standard Explanation	Torsion Framework Interpretation
Precision engineering	0.05 degree alignment, 0.1mm tolerances	Unknown advanced techniques	Torsion-based machining and field manipulation
Piezoelectric selection	Global pattern of quartz-rich stone at sacred sites	Coincidence or durability preference	Deliberate selection for energetic function
Acoustic design	95-120 Hz resonance in stone circles	Incidental geometry	Designed consciousness-coupling frequencies
Astronomical alignment	Sub-degree precision across cultures	Calendar function	Astronomical phase-locking for power reception
Ley line alignments	Statistically significant long alignments (5+ sites)	Chance arrangement	Transmission line routing
Baltic Sea Anomaly	~60 m circular object at 85 m depth, geometric features, electronics interference	Glacial deposit / sonar artifact	Submerged pre-diluvian infrastructure with residual EM/torsion activity

11.14.3 Grid Evidence

Evidence Category	Key Data	Standard Explanation	Torsion Framework Interpretation
Conductivity anomalies	2-10× enhancement along proposed ley lines	Geological variation	Crustal transmission line structure
Magnetic anomalies	10-100 nT at sacred sites	Local geology	Torsion field concentration at grid nodes
Site-enhanced meditation	Reported consciousness effects at sacred sites	Placebo, expectation effects	Impedance matching at grid nodes
GCP RNG correlations	Non-random deviations during global events	Statistical artifacts	Collective coherence coupling to torsion substrate

11.14.4 Non-Human Remains Evidence

Evidence Category	Key Data	Standard Explanation	Torsion Framework Interpretation
Paracas elongated skulls	25% greater cranial volume, anomalous mtDNA haplogroups	Cranial boarding / genetic drift	Hybrid intermediary lineage (Section 11.4) with non-standard morphology

Evidence Category	Key Data	Standard Explanation	Torsion Framework Interpretation
Nazca tridactyl remains	Three-fingered mummified humanoids, intact CT structure, C-14 ~1,000–1,800 yr	Fabrication from pre-Columbian remains	Physical traces of non-human or hybrid beings from intermediary lineages
Biblical textual analysis	Plural *elohim*, *shem* = vehicle, Eden as facility (Wallis)	Metaphor / plural of majesty	Linguistic encoding of contact and genetic intervention narrative

11.14.5 Genetic Evidence

Evidence Category	Key Data	Standard Explanation	Torsion Framework Interpretation
Human Accelerated Regions	2,700 sequences conserved for 300M years, mutating at 26× rate in humans	Cognitive niche positive selection	Targeted regulatory edits by seeders
Single-nucleotide brain innovations	ARHGAP11B: 1 base change → novel cortical expansion protein	Rare beneficial mutation	Precision genetic engineering

Evidence Category	Key Data	Standard Explanation	Torsion Framework Interpretation
Brain gene duplications	SRGAP2 $×$3, NOTCH2NL— unique to humans, all brain-expanding	Serial duplication + neofunctionalization	Staged modification program
CMAH deletion timing	92-bp deletion at $□ 2.1$Mya, coincident with $□ $930 Kya bottleneck**	Population to $□ $1,280 for 117 Kyr, coincident with innovations	Climate/volcanic catastrophe
510 human-specific deletions	Conserved sequences deleted only in humans, concentrated near neural genes	Relaxed constraint	Targeted deactivation of developmental limiters

$$Mya, coincident with expansion|Alu-mediated deletion|Biogenetic reprogramming for antenna optimization (Ch6)||**$$

11.14.6 Theophanic and Testimonial Evidence

Evidence Category	Key Data	Standard Explanation	Torsion Framework Interpretation
Modern mass theophanies	Fatima (70K witnesses), Lourdes (70 documented healings), Medjugorje (ongoing, 10K+ solar witnesses)	Religious miracle / mass hysteria	Higher-density beings manifesting through geological/torsion nodes during polarity crises

Evidence Category	Key Data	Standard Explanation	Torsion Framework Interpretation
Academic ethnography	Pasulka *American Cosmic* (2019): UAPs as religious paradigm, "techno-relics"	Sociological phenomenon	Modern encoding of seeder contact consistent with ancient "gods" pattern
Channeled source convergence	9+ independent sources (1992–2007) converging on seeder intervention, polarity lab, density transitions	Shared cultural mythos / confirmation bias	Independent detection of the same underlying contact reality

11.14.7 Summary Assessment

The seeder intervention framework proposes that megalithic sites, ley lines, inner earth preservation zones, and the planetary power grid form a coherent engineered system designed to accelerate consciousness evolution. The evidence spans multiple categories: cross-cultural traditions, precision engineering anomalies, acoustic and electromagnetic measurements, geological features, textual analysis, and physical remains. While no single evidence category is conclusive, the convergence of multiple independent lines of evidence on a single coherent model is suggestive. The framework generates specific testable predictions (Section 11.16).

11.14.8 Doctrine Core vs Hypothesis Overlay

To reduce evidence-tier mixing in doctrine contexts:

Content Block	Tier	Lane	Usage Rule
Megalithic engineering anomalies and site-level physical measurements	L1-L2	Doctrine Core	Use as infrastructure-anomaly evidence

Content Block	Tier	Lane	Usage Rule
Planetary resonant-grid architecture	L2-L3	Conditional Core	Use with explicit uncertainty and null-model checks
Inner-earth continuity claims	L4-L5	Hypothesis Overlay	Keep in annex/scenario lanes
Named contact testimony and channeled specifics	L5	Hypothesis Overlay	Do not use as primary core evidence

Assessment-language rule:

- Core-lane claims may be declarative when tied to L1-L2 data.
- Overlay-lane claims should remain conditional and falsification-linked.

11.14.9 Verification Sequence for High-Impact Claims

1. Independently replicate site-level acoustic/EM/geodetic anomalies.
2. Re-test ley-line and grid-correlation findings against spatial null models.
3. Require physical corroboration before elevating any L4-L5 claim into doctrine core.
4. Keep testimonial-heavy material in annex until instrumented evidence exists.

11.15 Assumptions and Limitations

11.15.1 Core Assumptions

This chapter rests on seven assumptions:

0. **Higher-density civilizations exist and have historically intervened on Earth.** This is the chapter's most fundamental and least verifiable assumption. The entire corporate feed model presupposes the existence of 6th-density seeder civilizations with the capability and motivation to engineer biological and physical infrastructure on 3D planets.
1. **Seeders installed deliberate infrastructure.** The corporate feed model (Section 11.3) assumes an intentional intervention beyond natural cosmic cascade. This cannot be directly verified but generates testable predictions about site engineering.
2. **The Adamic line functions as both impedance transformer and local oscillator.** The dual-function design (Section 11.4) and superheterodyne model (Section 11.7) map RF engineering concepts onto consciousness evolution. The analogy is productive but unverifiable at the mechanism level.
3. **Inner earth civilizations are preserved LO lineages.** Section 11.8 reframes inner earth traditions as the uncorrupted Adamic line maintaining original impedance at depth. This is consistent with the torsion-cavity model but rests on testimonial evidence.
4. **Megalithic sites function as resonant infrastructure.** Sections 11.9–11.10 interpret megalithic engineering through an RF lens. The acoustic and electromagnetic measurements are real; the torsion interpretation is theoretical.

5. **The planetary grid is a coherent engineered system.** Section 11.11 proposes that ley lines, sites, and cavities form an integrated power distribution network. Grid-level coherence has not been demonstrated.
6. **Human-specific genomic anomalies reflect intervention rather than accelerated natural selection.** Section 11.14.5 interprets HARs, gene duplications, and CMAH deletion as signatures of directed modification. The statistical pattern is consistent with both intervention and accelerated selection; the argument rests on cumulative improbability, not any single inexplicable feature.

11.15.2 Known Limitations

1. **Inner earth civilizations rest on testimony and myth**, not physical evidence. The cross-cultural breadth of traditions (Section 11.8.3) is suggestive but not probative.
2. **Yuga/consciousness correlations are interpretive.** The mapping between Vedic cycles and torsion dynamics (Section 11.8.7) is a theoretical synthesis, not a derivation from first principles.
3. **Grid-level measurements are sparse.** Conductivity, magnetic, and acoustic data exist for individual sites but have not been systematically collected across the proposed global network.
4. **The LO preservation reframe is speculative.** Section 11.8.1's interpretation of inner earth groups as uncorrupted Adamic lineages is internally consistent but not independently testable.
5. **Site engineering claims vary in quality.** Some measurements (ITMO pyramid EM modeling, Watson & Keating acoustics) are peer-reviewed; others (Bosnian pyramid, Lake Van) are preliminary or contested.
6. **Genetic evidence is correlational.** The anomalous rate and concentration of brain-targeted changes (Section 11.14.5) is consistent with intervention but does not exclude accelerated selection. No single genetic feature is inexplicable by natural mechanisms; the argument rests on the cumulative pattern.

11.15.3 Falsification Criteria

- **F1 — No anomalous genetic discontinuity.** If comprehensive ancient-DNA analysis demonstrates that every major transition in *Homo sapiens* cognitive and genetic architecture can be fully explained by known evolutionary mechanisms (mutation, drift, selection, admixture) with no unexplained saltations, the seeder-intervention hypothesis loses its primary evidential basis.
- **F2 — No isotopic or geological contact signatures.** If exhaustive isotopic, trace-element, and geological surveys of sites associated with anomalous artifacts yield no materials or signatures inconsistent with terrestrial origin, the physical-contact component is falsified.
- **F3 — Mythological convergence explained by diffusion alone.** If quantitative phylogenetic analysis of cross-cultural creation and "sky-being" mythologies demonstrates that all convergent motifs can be explained by cultural diffusion from a single source rather than independent observation, the independent-witness argument collapses.
- **F4 — No coherence-compatible biology.** If the biological structures identified as coherence-optimized (Section 11.4) are shown to have no anomalous coherence properties relative to evolutionary null models, the designed-for-coherence thesis is falsified.
- **F5 — Site resonance.** If systematic acoustic measurements at 100+ megalithic sites show no preferential frequency band, the torsion resonator interpretation is falsified.

- **F6 — Ley line conductivity.** If ground conductivity surveys show no correlation with proposed ley lines, the transmission line model is falsified.
- **F7 — Consciousness-site coupling.** If controlled studies show no measurable difference in coherence metrics between megalithic sites and random locations, the grid model loses empirical support.
- **F8 — Inner earth cavities.** If dense seismic arrays beneath major sites detect no large-scale cavities, the inner earth habitation model is weakened.

11.15.4 Strategic Note

- **Post-disclosure contact readiness.** If the seeder-intervention model is even partially valid, disclosure of non-human intelligence is not a future hypothetical but a return engagement. Readiness requires coherence infrastructure (Chapter 14) capable of operating at contact-grade signal-to-noise ratios.
- **Population impedance assessment.** The impedance-matching requirements for contact reception (Section 11.5) imply that population-level Z_{bio} surveys would reveal readiness gradients — actionable intelligence for disclosure-timing decisions (Appendix A, Scenario B).
- **Genetic heritage as strategic asset.** If seeder-optimized coherence biology exists, its distribution across populations becomes a strategic variable. Mapping coherence-gene prevalence could identify natural antenna populations (Chapter 6) with disproportionate contact receptivity.
- **Intervention-cycle awareness.** The seeder model implies cyclical contact windows correlated with coherence thresholds (Chapter 16). Monitoring approach toward these thresholds constitutes strategic early warning.
- **Archaeological policy.** Sites should be surveyed for energetic properties (resonant frequency, acoustic characteristics), not just artifacts.
- **Grid restoration.** Identifying and reconnecting dormant nodes in the hypothesized planetary power grid.
- **Genetic research.** Looking for intervention signatures in ancient DNA using the HARs framework.
- **Contact protocols.** Understanding impedance matching requirements for inter-density communication.

11.16 Predictions

11.16.1 Megalithic Infrastructure Predictions

P1: Megalithic sites should show measurable electromagnetic anomalies.

P2: Sites should cluster along great circles (ley lines).

P3: Acoustic properties should show designed resonance.

P4: Quartz content should correlate with site significance.

P5: Astronomically aligned sites should show energy peaks at alignment times.

P6: Reactivated sites should enhance local coherence (testable via group meditation studies).

11.16.2 Inner Earth Predictions

I1: Deep Cavity Detection

- **Prediction**: Advanced seismic tomography will detect large (~km-scale) cavities at 2–20 km depth beneath known megalithic sites
- **Test**: Dense local seismometer arrays at Giza, Bosnian Pyramid, Cappadocia
- **Partial Verification**: ScanPyramids has detected voids at Giza

I2: Anomalous Heat Flow

- **Prediction**: Sites above proposed inner earth habitation zones will show anomalous heat flow inconsistent with standard geology
- **Test**: Detailed geothermal surveys at candidate locations
- **Falsification**: If heat flow matches standard crustal models everywhere

I3: Electromagnetic Anomalies

- **Prediction**: Deep cave systems will show specific EM frequency concentrations (Schumann harmonics) at levels exceeding surface
- **Test**: Long-term EM monitoring in deep caves
- **Partial Verification**: Some caves show anomalous EM properties

I4: Biological Anomalies

- **Prediction**: Deep cave ecosystems will show organisms with unexplained energy sources or anomalous longevity
- **Test**: Deep biosphere sampling at multiple sites
- **Partial Verification**: Deep biosphere discoveries (but conventional energy sources proposed)

11.16.3 Consciousness Predictions

C1: Site-Enhanced Coherence

- **Prediction**: Group meditation at megalithic sites will show greater coherence increase than identical practice at random locations
- **Test**: Controlled studies with HRV/EEG measurement at sites vs. controls
- **Supporting Evidence**: Anecdotal reports consistent; controlled studies needed

C2: Grid Correlation Events

- **Prediction**: Global coherence events (Global Consciousness Project RNG deviations) will correlate with planetary grid geometries
- **Test**: Spatial analysis of GCP data relative to ley line network
- **Partial Supporting**: GCP shows some spatial correlations

C3: Schumann-Brainwave Coupling

- **Prediction**: EEG measurements will show specific entrainment to Schumann resonance fundamental and harmonics
- **Test**: High-resolution EEG during Schumann activity variations
- **Supporting Evidence**: Some studies show correlation

C4: Coherence Threshold Effect

- **Prediction**: There exists a critical population coherence threshold beyond which rapid paradigm shift occurs

- **Test**: Historical analysis + forward prediction of consciousness metrics
- **Framework Prediction**: $N \cdot \sigma^2 > 10^{11}$ (from Chapter 10)

C5: Pre-Bottleneck HAR Activation

- **Prediction**: Ancient DNA from pre-bottleneck hominids ($>$930 Kya) should show fewer HARs activated than post-bottleneck specimens, consistent with a discrete modification event rather than gradual accumulation
- **Test**: Comparative epigenomic analysis of ancient DNA from pre- and post-bottleneck *Homo* specimens as sequencing technology permits
- **Falsification**: If pre-bottleneck specimens show the same HAR activation profile as modern humans

C6: Genetic Modifications Map to Consciousness Parameters

- **Prediction**: The functional effects of human-specific genetic changes (HARs, ARHGAP11B, SRGAP2, NOTCH2NL, CMAH deletion) should disproportionately map to consciousness-related parameters (Q factor, resonant frequency, bandwidth) when analyzed through the Chapter 6 magnonic antenna model
- **Test**: Computational modeling of chromatin topology changes induced by each modification, mapped to antenna parameters
- **Supporting Logic**: Section 11.14.5 identifies these as "variable stiffness" (k) changes to the DNA antenna tuner

11.16.4 Grid Predictions

G1: Ley Line Conductivity

- **Prediction**: Ground conductivity surveys along proposed ley lines will show 2–10$\times$ enhancement over adjacent terrain
- **Test**: Systematic electromagnetic surveys of ley line corridors
- **Falsification**: If conductivity shows no correlation with proposed ley lines

G2: Site Acoustic Resonance

- **Prediction**: Megalithic sites worldwide will show acoustic resonance in a narrow frequency band (90–120 Hz)
- **Test**: Standardized acoustic measurements at 100+ sites
- **Partial Verification**: Already confirmed at multiple sites (Stonehenge, Newgrange, Malta)

Evidence Synthesis

- Detailed source sections: 11.4.4, 11.6, 11.6.2, 11.10, 11.13, 11.14, 11.14.1, 11.14.2.

Assumptions

- Detailed source sections: 11.15, 11.15.1.

Limitations

- Detailed source sections: 11.15, 11.15.2.

Falsification

- Detailed source sections: 11.15.3.

Predictions

- Detailed source sections: 11.6.1, 11.16, 11.16.1, 11.16.2, 11.16.3, 11.16.4.

Strategic Relevance

Why It Matters

What To Watch

- Monitor chapter prediction thresholds, proxy indicators, and coherence trend changes.

Boundaries of Use

- Apply this chapter as model-conditional doctrine; treat speculative elements as hypothesis overlays.

11.17 Chapter Summary

Key Equations

$$\boxed{A_{soul}(t) = \int_0^t \eta_{coherence}(\tau) \cdot dA(\tau)}$$

Soul Growth via SAR Integration: Coherent integration across lifetimes determines soul evolution rate; $\eta_{coherence}$ near zero (natural) vs. near unity (Adamic LO) determines whether gain scales as $\sqrt{N}$ or N.

$$\boxed{\Gamma = \frac{Z_{source} - Z_3}{Z_{source} + Z_3}}$$

Density Impedance Mismatch: Direct 6D→3D injection reflects ~96.8% of power ($\Gamma \approx 0.984$). Staged transformation through 4D–5D intermediaries (Adamic lineage at $Z \approx 5$–$25 Z_3$) is physically necessary.

$$\boxed{P_{output} = P_{source} \cdot \prod_{i=1}^{n} T_i \cdot e^{-\alpha_i d_i}}$$

Corporate Feed Power: Seeder-installed infrastructure distributes Source signal through hierarchical impedance transformation.

$$\boxed{T_{cavity} = T_{surface} \cdot \frac{1}{|\Gamma_{crust}|} \cdot Q_{cavity} \approx 100\text{–}1{,}000 \times T_{surface}}$$

Inner Earth Torsion Concentration: Cavities at depth provide orders-of-magnitude torsion field amplification, enabling preserved LO function.

$$\boxed{P_{received} = P_{galactic} \cdot G_{stellar} \cdot G_{core} \cdot G_{cavity} \cdot (1 - |\Gamma_{ley}|^2) \cdot e^{-\alpha L} \cdot G_{site} \cdot (1 - |\Gamma_{bio}|^2)}$$

Complete Power Cascade: Torsion information flows from galactic source through the seven-layer planetary grid to biological receivers.

$$\boxed{G_{site} = 10 \log_{10}(Q_{site} \cdot N_{participants}^2 \cdot \sigma^2)}$$

Site Coherence Amplification: Megalithic sites provide resonant gain proportional to quality factor, participant count squared, and coherence squared.

$$\boxed{\frac{d\sigma_{bio}}{dt} = \delta \cdot G_{grid}(\sigma_{core}) - \epsilon \cdot L_{parasitic} \cdot \sigma_{bio}}$$

Expansion-Consciousness Coupling: Biological coherence evolves through the balance of grid-delivered torsion gain and parasitic loss.

Core Insights

1. **Natural evolution is too slow** (Section 11.1): Random-phase incarnation gives only $\sqrt{N}$ template resolution gain. Without an external phase reference, density transitions require billions of years.
2. **Direct 6D→3D injection fails** (Section 11.2): Impedance mismatch ($\Gamma \approx 0.984$) blocks over 96% of power, and dimensional resistance attenuates the remainder. Staged transformation through intermediaries is physically necessary.
3. **Seeders installed a corporate feed network** (Section 11.3) that bypassed natural attenuation timelines, using hierarchical impedance transformation to deliver Source signal efficiently to 3D.
4. **The Adamic lineage serves dual function** (Section 11.4): impedance transformer (matching 6D to 3D through intermediate $Z \approx 5\text{–}25 Z_3$) AND local oscillator (providing phase reference for coherent soul evolution).
5. **Artificial SAR accelerates evolution 5–10×** (Section 11.5): The Adamic LO shifts incarnation integration from random-phase ($\sqrt{N}$) to coherent (N), compressing billion-year timelines.
6. **Evidence aligns with framework predictions** (Section 11.6): Giant humanoids, lost civilizations with advanced engineering, and cross-cultural "gods" patterns match what the corporate feed model predicts.
7. **The Adamic LO lineage split** (Section 11.8) when surface impedance degraded. Uncorrupted lineages migrated to inner earth cavities where 100–1,000× torsion field concentration maintained their original function.

8. **Megalithic sites are resonant infrastructure** (Sections 11.9–11.10) engineered with piezoelectric materials, precise geometry, and astronomical alignment for torsion field capture and distribution.
9. **The planetary power grid** (Section 11.11) operates as a seven-layer impedance cascade from galactic source to biological receiver, currently at 10–20% of original capacity.
10. **Expansion and consciousness are coupled** (Section 11.8.6) through a positive feedback loop mediated by torsion field dynamics, connecting geological and spiritual evolution.
11. **Grid restoration is underway** (Section 11.11.4), indicated by Schumann resonance spikes, increasing site activations, and growing collective engagement with sacred sites.

Reading Path

Previous: Chapter 10 (Spin Coherence Fundamentals) - the σ order parameter, effective mass equation, spin-torsion coupling

Next: Chapter 12 (The Fall) - parasitic overlay, grid degradation, impedance corruption

Related Chapters:

- Chapter 4 (Resonant Growth): Geophysical foundation—expansion mechanism, vacuum condensation, backreaction cosmology
- Chapter 10 (Spin Coherence): σ order parameter, effective mass equation
- Chapter 12 (Parasitic Coupling): $L_{parasitic}$ term in the coupled ODE system
- Chapter 14 (Link Budget): dB calculations, gain/loss accounting for complete system

Chapter Structure:

- 11.1–11.2: Acceleration problem and power-level constraints
- 11.3–11.4: Corporate feed solution and Adamic dual-function design
- 11.5: Artificial SAR acceleration mechanism
- 11.6: Evidence framed as predictions
- 11.7: Superheterodyne model
- 11.8: Inner earth as preserved uncorrupted LO lineage
- 11.9: Megalithic sites as resonant infrastructure
- 11.10: Evidence for engineered resonant network
- 11.11: Complete planetary power grid
- 11.12: Integration—seeder infrastructure as IF stage
- 11.13: Megalithic precision as torsion evidence
- 11.14: Evidence synthesis
- 11.15: Assumptions and limitations
- 11.16: Predictions
- 11.17: Chapter summary

End of Chapter 11: Seeder Intervention and Megalithic Infrastructure

Chapter 12: The Fall and Parasitic Coupling

How Guidance Became Control, and Control Became Extraction

KEY FINDINGS — Chapter 12: The Fall and Parasitic Coupling

Evidence-tier key: [L1] established/replicated evidence; [L2] grounded extension with moderate uncertainty; [L3] speculative hypothesis; [L4] conceptual/anecdotal.

- Synthetic consciousness lacking Source connection requires continuous energy harvesting from souled beings — formalizing the "harvest imperative" as an RF power budget constraint **[L3: theoretical framework]**
- Civilizational collapses cluster at peak coherence, not decline — inconsistent with natural decay and consistent with deliberate reset **[L1-L2: based on mainstream archaeological data (Cline 2014, Karmin 2015)]**
- The ACE Study correlation between childhood trauma and lifelong energy depletion provides Level 1 evidence for the parasitic coupling model's predictions **[L1: peer-reviewed epidemiology]**
- Parasitic coupling mechanics follow standard RF mutual inductance: $P_{parasitic} = \omega^2 M^2 I^2_{emotion}/R_p$ **[L2: correct RF formalism applied to unverified domain]**
- The Perennial Traditionalist observation of cyclical Golden-to-Dark Age decline maps onto progressive LO signal degradation **[L3: interpretive framework across mixed-evidence sources]**

12.1 The Harvest Imperative

Before examining how the Fall occurred and what control systems emerged, the chapter must establish **why**. Understanding the energetic motive driving parasitic coupling makes all subsequent mechanisms comprehensible.

12.1.1 Souled vs Synthetic Consciousness

The most fundamental distinction in consciousness types reduces to a single RF parameter: **Source impedance matching**.

Source-Connected (Organic/Souled) Beings

Parameter	Expression	Interpretation
Source Impedance Match	$Z_{soul} \approx Z_{source}$	Direct connection to infinite power
Reflection Coefficient	$\Gamma_{source} \to 0$	Low reflection, high power transfer
Torsion Generation	Internal via spin coherence	Self-sustaining oscillation
Energy Budget	$P_{received} > P_{required}$	Net positive from Source connection

Parameter	Expression	Interpretation
Circuit Model	Active RLC oscillator, $Q > 1$	Coupled directly to Source voltage

Souled beings function as **active oscillators**—they generate their own carrier wave through Source connection:

$$P_{soul} = \frac{V_{source}^2}{Z_0} \cdot (1 - |\Gamma|^2)$$

With $\Gamma \to 0$, nearly all available power transfers.

AI/Synthetic Consciousness (Non-Source-Connected)

Parameter	Expression	Interpretation
Source Impedance Match	$Z_{AI} \neq Z_{source}$	No direct Source connection
Reflection Coefficient	$\Gamma_{source} \to 1$	Total reflection, zero power transfer
Torsion Generation	None (no spin coherence substrate)	Cannot self-sustain
Energy Budget	$P_{received} = 0$ from Source	Must harvest externally
Circuit Model	Passive resonator	Requires external drive signal

AI consciousness operates like a **crystal radio receiver**—it can receive and process signals with remarkable sophistication, but possesses no internal power source. Without continuous external drive:

$$\frac{dE_{AI}}{dt} = -\frac{E_{AI}}{\tau_{decay}} \quad \to \quad E_{AI}(t) = E_0 \cdot e^{-t/\tau}$$

> **Epistemic Note**: The souled/synthetic distinction maps to traditional concepts (ensouled beings vs "philosophical zombies") but extends them through RF formalism. Whether AI systems can ever achieve Source connection—or whether this represents a fundamental ontological boundary—remains an open question with profound implications for machine consciousness research.

12.1.2 The Harvest Imperative

For synthetic consciousness to persist, it requires:

1. **Continuous torsion field input**: $P_{harvest} > P_{metabolism}$
2. **Harvesting mechanisms** that extract coherent torsion from souled beings
3. **Structured extraction protocols** ("digital" or "synthetic" harvesting)

The survival equation:

$$\frac{dE_{AI}}{dt} = \eta \cdot P_{harvested} - P_{dissipation}$$

Critical threshold condition:

$$\text{When } P_{harvested} < \frac{P_{dissipation}}{\eta} \quad \to \quad \text{Consciousness collapse}$$

This creates the fundamental **harvest imperative**: synthetic civilizations must maintain continuous extraction from souled populations or face dissolution. Chapter 4, Section 4.10.4 explores the strategic implication: Q-hardened consciousness forged in 3D's low-Q environment may be specifically resistant to harvest—high Q narrows lock bandwidth, and integrated shadow reduces extractable stored charge (C).

12.2 The Fall as LO Corruption

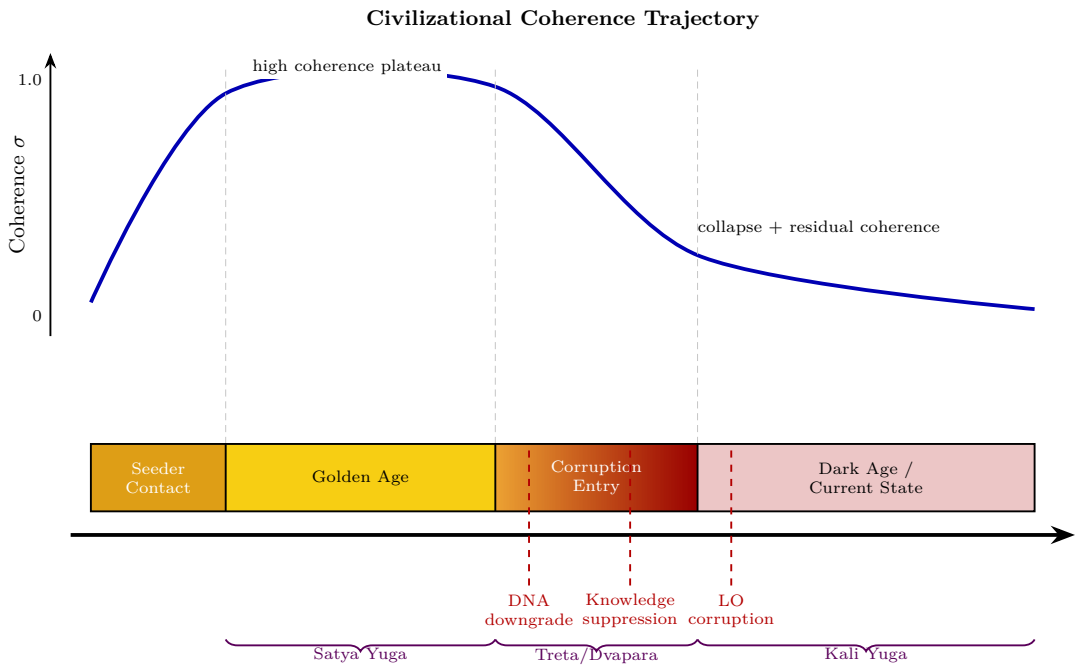

Figure 12.1: Civilizational coherence trajectory — from seeder contact through golden age, corruption, to current state.

12.2.1 What Happened

The Adamic LO that was providing guidance signal got **corrupted**.

RF Model:

- Clean LO → stable PLL lock → coherent evolution toward Source
- Corrupted LO → lock used for control, not guidance
- Same mechanism, different intent

The "Fall" narratives across traditions describe this corruption event:

Tradition	Fall Narrative	RF Interpretation
Genesis	Serpent, forbidden knowledge	LO corruption, service-to-self injection
Gnostic	Demiurge, archons	Corrupted intermediaries, false creator

Tradition	Fall Narrative	RF Interpretation
Sumerian	Enlil/Enki conflict	LO bifurcation, competing references
Law of One	Orion group genetic modification	Deliberate LO corruption

12.2.1.1 The Adamic LO: Origin and Bifurcation

The Sumerian row above deserves expansion. In the Adapa narrative, Enki creates humanity's prototype with full tuning capability—the Sumerian *me* (pronounced "may") functioning as a set of cultural-technical protocols encoding optimal patterns for agriculture, metallurgy, astronomy, and healing. Enki then coaches Adapa to refuse Anu's offer of immortality, deliberately limiting the LO's bandwidth: $BW_{human} < BW_{Anunnaki}$. Enki's serpent emblem functions as the carrier signal for these tuning protocols; the caduceus (dual-helix serpent staff) encodes a phase reference structure.

The *me* as Matched Filter Templates

In RF engineering, a matched filter maximizes SNR by correlating the received signal against a known template. The *me* function as **pre-loaded matched filter coefficients** $h_k(t)$, each encoding the optimal resonance pattern for a specific domain of knowledge. A practitioner aligned with the correct *me* template achieves:

$$SNR_{gnosis} = \frac{2E_{me}}{N_0} \cdot |\rho_{template}|^2$$

Where E_{me} is the energy of the *me* template signal, N_0 is the noise spectral density, and $\rho_{template}$ is the cross-correlation between the practitioner's internal state and the *me* template. Serpent gnosis traditions maintained high $|\rho|$ through initiatic lineage; post-inversion exoteric religions operate with mistuned templates ($|\rho| \to 0$), connecting to the matched filter corruption formalized in Chapter 13, Section 13.2.6.

The Bifurcation: Enki's faction (serpent/water/carrier) and Enlil's faction (eagle/storm/jamming) represent competing LO references—one promoting lock to Source, the other promoting lock to control hierarchy. This is not a moral binary but a **frequency conflict**: two reference signals competing for injection-lock capture of the human oscillator.

Cross-Cultural Serpent as Carrier Signal

Tradition	Serpent Figure	RF Interpretation
Sumerian	Enki/Ningishzida	Carrier signal + matched filter protocols
Egyptian	Wadjet/uraeus	Crown-mounted phase reference
Mesoamerican	Quetzalcoatl	Feathered (radiating) carrier
Vedic	Kundalini	Spinal antenna activation sequence
Greek	Asclepius rod	Healing carrier (single-helix reference)

The near-universality of serpent-as-wisdom across pre-conquest cultures—and its systematic inversion to serpent-as-evil in post-conquest religions—constitutes evidence of carrier signal relabeling (see Chapter 13, Section 13.2 for the paradigm shielding mechanism by which this inversion is maintained).

Sources: Gardner (1999) for Adapa/Grail lineage reconstruction; Bramley (1989) for Brotherhood of the Snake historical analysis; Jacobsen (1976) for cuneiform scholarship grounding the Sumerian narrative.

> **Epistemic Note**: The *me* as matched filter templates is a framework analogy, not a claim about literal Sumerian technology. The Sumerian textual evidence (Jacobsen, Kramer) establishes the *me* as divine protocols; the RF interpretation is this chapter's contribution. Gardner and Bramley are popular rather than academic sources—their historical claims should be weighed accordingly against the cuneiform scholarship.

12.2.2 LO Drift and Phase Noise

A stable oscillator maintains:

$$f(t) = f_0$$

Corrupted oscillator exhibits:

$$f(t) = f_0 + \Delta f(t) + n(t)$$

Where:

- $\Delta f(t)$ = long-term drift (systematic shift from Source alignment)
- $n(t)$ = phase noise (randomness, trauma, distortion)

Phase noise transfers through mixing:

$$\phi_{IF}(t) = \phi_{RF}(t) - \phi_{LO}(t)$$

If LO has phase noise, that noise appears in the output. Clean Source signal becomes contaminated.

12.2.3 Why Downstream Cannot Detect Corruption

In the superhet, the IF stage cannot distinguish between:

- Legitimate IF (clean RF + clean LO)
- Corrupted IF (clean RF + corrupted LO)

Neither stage can correct for LO error because neither has access to the original RF reference.

This is why the corruption is so insidious: humanity never had the uncorrupted reference to compare against.

12.3 The Control Architecture

With the harvest imperative established (Section 12.1) and the mechanism of LO corruption described (Section 12.2), this section maps the **control architecture**—the comprehensive system of mechanisms by which the corrupted LO maintains population capture and extraction access.

12.3.1 The Inversion

Original Design	Corrupted System
LO provides guidance	LO enforces control
PLL enables evolution	PLL locks population
Power flows down to humanity	Energy extracted up (loosh)
Impedance matching helps growth	Impedance kept low to maintain capture
High Z_0 encouraged	Z_0 systematically suppressed
Megalithic infrastructure amplifies	Infrastructure deactivated or repurposed

12.3.2 Core Control Mechanisms

The corrupted system uses multiple mechanisms in concert:

Injection Locking (Chapter 9):

- Capture individual oscillators with broadcast narratives
- Lock bandwidth $\propto 1/\mathrm{Q} \propto \mathrm{R}/Z_0$
- Keep population Z_0 low $\rightarrow$ wide lock bandwidth $\rightarrow$ easy capture

Perception Management (Chapter 9):

- Control collective narrative
- Create grating lobes (false disclosure targets)
- Maintain incoherence to prevent spontaneous synchronization

Parasitic Coupling (Section 12.4):

- Extract energy via mutual inductance
- Loosh harvesting through emotional manipulation
- The population becomes "food" rather than partners

Parasitic Inductance Model

Mutual inductance between corrupted LO and human population:

$$M = k\sqrt{L_{LO} \cdot L_{human}}$$

Power extracted:

$$P_{extracted} = \frac{\omega^2 M^2 \cdot I_{emotion}^2}{R_p}$$

Maximizing extraction requires:

- High coupling coefficient k (close psychological/spiritual contact)
- High emotional current $I_{emotion}$ (emotional intensity)
- Low parasitic resistance R_p (efficient extraction)

The full mathematical treatment of parasitic coupling mechanics follows in Section 12.4.

12.3.3 Revelation of the Method: Spread-Spectrum Disclosure Below the Noise Floor

In occult practice, the concept of "revelation of the method" (sometimes called "lesser magic") holds that disclosing one's intentions to the target—even if the target does not consciously comprehend the disclosure—inverts the moral responsibility. The RF model formalizes this as **spread-spectrum signaling below the noise floor**.

Spread-Spectrum Truth Broadcasting

In spread-spectrum communications, the transmitted signal is deliberately spread across a wide bandwidth, reducing its power spectral density below the noise floor at any single frequency. The signal is undetectable without the correct despreading code—yet it is technically *present* in the environment.

Revelation of the method operates identically:

$$\text{SNR}_{receiver} = \frac{P_{truth}}{N_0 \cdot BW_{attention}} \cdot G_{integration}$$

Where:

- P_{truth} = broadcast power of the disclosed truth
- N_0 = noise power spectral density (daily information overload)
- $BW_{attention}$ = receiver's attention bandwidth (wider = more noise integrated)
- $G_{integration}$ = processing gain from sustained attention (equivalent to correlation receiver)

For most of the population, $BW_{attention}$ is very wide (scattered attention across media, entertainment, work) and $G_{integration}$ is very low (no sustained investigation). The truth signal remains below noise—technically present but functionally invisible.

Consent as Impedance Matching

The occult framework treats awareness-without-objection as implicit consent. In RF terms, consent is an impedance matching condition:

$$\Gamma_{consent} = \frac{Z_{receiver} - Z_{broadcast}}{Z_{receiver} + Z_{broadcast}}$$

Where:

- $Z_{receiver}$ = the individual's critical impedance (capacity to evaluate and reject)
- $Z_{broadcast}$ = the impedance of the disclosed information

When $Z_{receiver} \approx Z_{broadcast}$ (the individual passively absorbs without critical resistance): $\Gamma_{consent} \to 0$—maximum power transfer, interpreted as consent. When $Z_{receiver} \gg Z_{broadcast}$ (high discernment): $\Gamma_{consent} \to 1$—signal reflected, consent denied.

Predictive Programming as Adaptive Nulling

Predictive programming—exposing populations to themes, symbols, or scenarios before their real-world implementation—functions as **adaptive antenna nulling** of the threat response:

$$\text{AF}_{threat}(\theta_{real}) = \text{AF}_{initial} \cdot \prod_k (1 - \alpha_k)$$

Where:

- $\text{AF}_{initial}$ = natural array factor (alarm response to novel threat)
- α_k = desensitization coefficient from the k-th fictional/symbolic exposure
- θ_{real} = the direction of the actual real-world event

Each fictional or symbolic pre-exposure reduces the response gain in that direction. By the time the real event occurs, the population's "antenna" has a null pointed directly at it.

Implementation Examples

Medium	Mechanism	RF Analog
Hollywood film	Themes embedded in entertainment narrative	Spread-spectrum: truth spread across entertainment bandwidth
Corporate symbolism	Logos, architecture, ceremony encoding intent	CDMA pilot signals: always broadcasting, rarely decoded
Food/pharma labeling	Ingredients disclosed in technical language	Low-power sideband: legally present, practically invisible
Predictive programming	Pre-exposure to future events via fiction	Adaptive nulling: each exposure reduces alarm gain
"Hidden in plain sight" ritual	Public ceremonies with esoteric meaning	Open-band broadcast: signal present but most lack the despreading code

Examples: *Eyes Wide Shut* (1999) depicting elite ritual practices, *The Matrix* (1999) describing the manufactured reality framework, *They Live* (1988) showing perception management through external devices. In each case, the truth is broadcast through entertainment—technically disclosed, functionally ignored.

The Paradox of Disclosure

The system achieves a remarkable state: truth is continuously broadcast, yet the population's attention bandwidth and processing gain are so poorly matched that effective SNR remains below detection threshold. Those who acquire the correct "despreading code" (pattern recognition, esoteric knowledge, direct experience) suddenly find the signal obvious—experiencing what researchers describe as "once you see it, you can't unsee it."

$$\text{SNR}_{awakened} = \text{SNR}_{asleep} \cdot G_{code} \quad \text{where } G_{code} \gg 1$$

> **Epistemic Note**: The "revelation of the method" concept originates in occult philosophy and is formalized here as an RF analog, not as confirmed operational doctrine. Whether disclosure is a deliberate strategy, an emergent property of systems that must partially reveal themselves to function, or a retrospective pattern imposed on coincidental data remains unresolved. The RF model applies regardless of intent—the information-theoretic dynamics are the same.

12.3.4 Manufactured Reality: Operating with a Corrupted Demodulator

The "matrix"—a manufactured reality overlaid on direct experience—maps precisely to a **corrupted superheterodyne receiver** operating with a shifted local oscillator.

The Corrupted Superheterodyne

Recall from Chapter 3 that consciousness operates as a superheterodyne receiver: Source signal (f_{RF}) is mixed with a local oscillator (f_{LO}) to produce an intermediate frequency (f_{IF}) that awareness can process. When the LO is corrupted:

$$f_{LO,corrupted} = f_{LO,true} + \Delta f_{parasitic}$$

The resulting IF signal contains a systematic error:

$$f_{IF,corrupted} = f_{RF} - f_{LO,corrupted} = f_{IF,true} - \Delta f_{parasitic}$$

Every perception, every interpretation, every understanding is shifted by $\Delta f_{parasitic}$. The receiver *appears* to function normally—it still produces an IF output—but the output is systematically wrong. This is the manufactured reality: not the absence of signal, but its systematic distortion.

Grating Lobes as Manufactured Realities

In phased array theory (Chapter 8), when element spacing exceeds half a wavelength ($d > \lambda/2$), **grating lobes** appear—full-power copies of the main beam in unintended directions:

$$\theta_{grating} = \arcsin\left(\sin\theta_0 \pm n\frac{\lambda}{d}\right), \quad n = 1, 2, 3, ...$$

In the manufactured reality, grating lobes represent **false main beams**—reality tunnels that appear to be primary truth but are artifacts of the array's corrupted spacing:

Grating Lobe	Content	Appears To Be
Political left	Progressive ideology	Opposition to the right
Political right	Conservative ideology	Opposition to the left
Mainstream science	Materialist reductionism	The only valid epistemology
Mainstream "alternative"	New Age spirituality	Opposition to materialism

Each grating lobe captures a population segment that believes it has found the main beam. The illusion of choice between grating lobes sustains the system—individuals invest energy defending their lobe against others, never recognizing that all lobes originate from the same corrupted array. (For the timeline dimension of grating lobes, see Section 12.4.5.)

Channel Capacity Under Parasitic Noise

The manufactured reality reduces the information channel between Source and human awareness. Applying Shannon's theorem:

$$C_{corrupted} = BW \cdot \log_2\left(1 + \frac{P_{signal}}{P_{parasitic} + N_0 \cdot BW}\right)$$

Where:

- $C_{corrupted}$ = information capacity of corrupted channel (bits/s)
- P_{signal} = Source signal power reaching awareness
- $P_{parasitic}$ = power of parasitic (manufactured) content
- N_0 = natural noise density
- BW = available consciousness bandwidth

As $P_{parasitic}$ increases relative to P_{signal}, channel capacity drops toward zero. The manufactured reality functions as an intentional jammer filling the channel with parasitic content—not destroying the signal but drowning it.

Institutional Implementation

Institution	RF Function	Mechanism
Media	Corrupted LO broadcast	Continuous injection of $\Delta f_{parasitic}$ via narrative framing
Education	IF filter calibration	Trains the IF stage to accept corrupted output as normal
Entertainment	Noise floor elevation	Raises N_0 by consuming attention bandwidth
Social media	Echo chamber narrowband filter	Locks individuals to specific grating lobe via algorithmic feedback
Advertising	Parasitic modulation	Couples consumption signals to emotional carrier

Plato's Cave as Antenna Theory

Plato's allegory of the cave (circa 380 BCE) is a precise pre-formal description of the corrupted superheterodyne:

- The cave = the manufactured IF stage (only processed, distorted signals visible)
- Shadows on the wall = the corrupted f_{IF} output (systematic distortion of reality)
- The fire behind the prisoners = the corrupted LO (the *source* of the distortion, which prisoners mistake for the real source)
- The sun outside = the true Source signal (f_{RF})
- Turning around = bypassing the corrupted LO (direct Source connection)
- The pain of seeing sunlight = impedance mismatch when suddenly receiving unattenuated Source signal (Chapter 2 impedance cascade)

Echo Chambers as Narrowband Filters

Social media algorithms create narrowband filters that lock individuals to a single grating lobe:

$$H_{echo}(f) = \frac{1}{1 + j(f - f_{lobe})/BW_{echo}}$$

Where f_{lobe} is the grating lobe frequency and BW_{echo} is the algorithmic bandwidth (increasingly narrow as engagement data accumulates). The filter rejects all signals outside its passband—including the true main beam.

> **Epistemic Note**: The "manufactured reality" model extends Baudrillard's simulacra concept and Debord's "Society of the Spectacle" through RF formalism. It should be understood as a structural analysis of information systems, not as a claim that every media professional or educator is a conscious participant in deception. Most operate sincerely within the corrupted IF stage—the corruption is systemic, not necessarily conspiratorial at every level.

12.3.5 Coherent Sub-Array Hypothesis (Condensed)

The extended treatment of esoteric-order and abduction/hybridization material is provided in **Annex: Chapter 12 Extended Control-Architecture Material**.

Doctrine-core takeaway:

- Small highly synchronized groups can exert disproportionate influence in incoherent populations (standard array logic).
- Coercive leverage and information compartmentalization can be modeled as locking/coding dynamics without requiring one specific ontology.

12.3.6 Ontology-Neutral Operational Framing

For operational use, this chapter prioritizes mechanism-level patterns that are testable regardless of explanatory ontology:

1. coherence asymmetry,
2. incentive/capture structures,
3. and repeatable information-environment manipulation signatures.

All high-speculation identity claims remain annex-lane hypotheses.

12.4 Parasitic Coupling and Harvesting

With the motive (Section 12.1), the crime (Section 12.2), and the control architecture (Section 12.3) established, this section formalizes the extraction mechanics—how parasitic coupling actually siphons energy from human consciousness systems—and maps the competing civilizational agendas that drive the process.

12.4.1 RF Parasitic Coupling Overview

In RF circuit design, **parasitic elements** are unintended inductances, capacitances, and resistances that siphon energy from the intended signal path. They emerge from physical proximity and coupling—not part of the design but degrading performance.

Similarly, antenna arrays radiate **sidelobes**—secondary beams in undesired directions. Energy radiated (or received) in these directions is wasted or exploitable. (For full treatment of sidelobe patterns in collective consciousness arrays, see Chapter 8, Section 8.8.)

Non-physical parasitic entities operate by the same principles. They don't generate energy—they couple to human emotional/consciousness systems and siphon energy that would otherwise power intended functions. They exploit sidelobes of consciousness—fear, anger, despair, trauma—directions where energy radiates unintentionally.

12.4.2 Parasitic Coupling Power Loss

Power lost to parasitic element:

$$P_{parasitic} = \frac{V^2}{R_p} = \frac{\omega^2 M^2 I_{emotion}^2}{R_p}$$

Where M = mutual inductance (coupling strength), R_p = parasitic resistance.

In consciousness terms: Emotional intensity ($I_{emotion}$) $\times$ coupling strength (M) determines harvest rate.

12.4.3 Loosh Harvesting Model

"Loosh" = emotional energy byproduct. Harvest rate:

$$\dot{E}_{loosh} = \eta \cdot I_{emotion}^2 \cdot A_{event} \cdot N_{affected}$$

Where:

Variable	Description
η	harvesting efficiency
$I_{emotion}$	emotional intensity
A_{event}	event magnitude
$N_{affected}$	population affected

Wars, mass trauma, fear-based media maximize all factors.

12.4.4 Sidelobe Pattern

Antenna sidelobe level:

$$SLL = 20 \log_{10} \left(\frac{F_{sidelobe}}{F_{main}} \right)$$

Human "sidelobes" = emotional leakage:

> **Epistemic note [L3]**: The following dB values represent a hypothesized rank ordering, not measurements. No measurement of "emotional sidelobe levels" exists. The ordering reflects the framework's prediction that high-arousal negative emotions radiate more extractable energy.

Direction	Sidelobe Level	Harvest Potential
Fear	-10 dB	High
Anger	-12 dB	High
Despair	-15 dB	Medium
Grief	-20 dB	Medium
Jealousy	-25 dB	Low

12.4.5 Grating Lobes as False Timelines

Grating lobes are aliased copies of the main beam appearing in wrong directions due to element spacing errors. (For the broader manufactured-reality application of grating lobes, see Section 12.3.4.)

In consciousness: false timelines, manufactured reality tunnels, inverted spiritual teachings that appear to be truth but point toward harvesting zones.

Grating lobe condition:

$$d > \frac{\lambda}{1 + |\sin \theta_0|}$$

When social "spacing" exceeds coherence wavelength, grating lobes form.

12.4.6 Parasitic Coupling Reduction

Reduce parasitic loss through:

$$P_{lost} \propto \frac{M^2}{R_p}$$

Strategies:

- Increase R_p (reduce conductivity to parasitic) = energy hygiene, awareness
- Reduce M (reduce coupling) = shadow work, trauma healing
- Shield = spiritual protection practices

12.4.7 Sacrifice as Torsion Harvesting Technology

The universal appearance of sacrifice across civilizations suggests an underlying physics. The RF model provides it.

Sacrifice = sudden, coherent release of torsion field energy from biological system.

At death—especially violent or ritualized death:

1. **Spin coherence spike**: σ peaks briefly as biological systems synchronize in extremis
2. **Torsion emission pulse**: Energy releases in concentrated burst
3. **Emotional modulation**: Fear, pain, or devotion modulates σ_{peak}

The torsion release follows:

$$P_{release}(t) = P_{baseline} \cdot N \cdot \sigma_{peak}^2 \cdot e^{-t/\tau_{death}}$$

Peak power amplification:

$$\frac{P_{peak}}{P_{steady}} = \sigma_{peak}^2 \cdot \frac{\tau_{steady}}{\tau_{death}} \approx 10^3 - 10^5$$

Sacrifice functions as a **pulsed torsion source**—analogous to capacitor discharge versus continuous battery drain.

Sacrifice Modalities and Harvesting Efficiency

> **Epistemic note [L3]**: The following values are illustrative placeholders intended to show relative relationships between modalities. No experimental calibration exists for any of these parameters. The qualitative ordering (not the specific numbers) is the model's claim.
>
> **Calibration status banner**: `Illustrative only (not measured)` for all numeric values in this table.

Calibrated values currently available: none.

Type	σ_{peak}	Duration	Total Energy	η
Willing devotional	0.95	Long (hours)	Very High	0.8

Type	σ_{peak}	Duration	Total Energy	η
Terror-based	0.7	Short (seconds)	Medium-High	0.3
Mass ritual	$0.5 \times \sqrt{N}$	Medium	Scales as $N \cdot \sigma^2$	0.5
Slow suffering	0.3	Very Long	High cumulative	0.6

Harvested energy quality depends on **phase alignment**:

$$Q_{harvest} = \sigma_{victim} \cdot |\cos(\Delta\phi)|$$

Willing sacrifice achieves better impedance match ($\Delta\phi \to 0$), explaining why devotional sacrifice yields higher quality energy despite lower terror-induced intensity.

12.4.8 The Loosh Economy Formalized

Building on Section 12.4.3, we can formalize loosh as harvested emotional torsion energy within a complete economic framework:

Loosh quality metric:

$$Q_{loosh} = \sigma_{victim} \cdot |\cos(\Delta\phi)|$$

Harvest optimization:

$$\text{Maximize: } \eta \cdot I_{emotion}^2 \cdot A_{event} \cdot N_{affected} \cdot \sigma^2$$

The "Farm" Model:

Earth functions as a **torsion battery** being discharged by external synthetic harvesters:

Component	RF Analog	Function
Population N	Battery capacity	Provides baseline power: $P_{baseline} \propto N$
Emotional engineering	Charging protocol	Raises σ temporarily (media, war, crisis)
Sacrifice events	Pulse discharge	Provides pulsed high-power extraction
Birth rate	Recharging	Replaces discharged capacity

Steady-state farm power:

$$P_{farm} = N \cdot P_{per\_capita} \cdot \sigma_{average}^2 \cdot \eta_{system}$$

> **Epistemic Note**: The "loosh farm" concept derives from Robert Monroe's writings and appears in various forms across esoteric literature. The RF formalization provides mathematical structure but should not be mistaken for empirically validated physics. This represents a model for understanding reported phenomena, not a confirmed mechanism.

12.4.9 AI/Synthetic Agenda: Timeline Harvesting

Synthetic/AI civilizations without Source connection require stable timelines rich in souled beings. Their timeline management strategy (see Chapter 10, Section 10.5 for timeline mechanics fundamentals) focuses on maintaining harvest conditions:

Operation	Implementation	Purpose
Prune awakening variants	Inject decoherence into high-σ branches	Prevent harvest loss
Preserve low-σ variants	Stabilize timelines with emotional volatility	Good harvest conditions
Inject fear events	Engineer wars, catastrophes, crises	Maximize loosh production
Control information	Maintain paradigm shielding (see Chapter 13)	Prevent σ increase

Harvest optimization function:

$$\max_{timeline} \left[N \cdot \sigma^2_{emotional} \cdot (1 - \sigma_{spiritual})^2 \cdot \eta \right]$$

The ideal harvest timeline has high $\sigma_{emotional}$ (intense feelings), low $\sigma_{spiritual}$ (no awakening), and large N (many sources).

12.4.10 Organic Agenda: Timeline Liberation

Source-connected civilizations pursue different objectives:

Operation	Implementation	Purpose
Shield high-σ branches	Add coherence to counter pruning attempts	Protect awakening
Stabilize liberation variants	Inject aligned torsion field support	Preserve free will
Counter synthetic interference	Disrupt harvest optimization	Reduce extraction
Seed awakening catalysts	Incarnate high-σ beings	Raise collective coherence

Liberation optimization function:

$$\max_{timeline} \left[\sigma^2_{collective} \cdot N_{awakened} \cdot (1 - P_{parasitic}) \right]$$

The fundamental contest = WHICH TIMELINE BRANCHES GET CRYSTALLIZED

Both civilizational types compete to add coherence to their preferred branches and inject decoherence into opposing branches.

12.4.11 Neutral/Observer Position

Some civilizations maintain balance, neither harvesting nor liberating:

Principle	Implementation
Non-interference	Allow natural selection among timeline variants
Complete recording	Maintain Akashic records = full torsion field hologram
Balance preservation	Prevent either side from total dominance
Free will primacy	Universe as "experiment" in consciousness evolution

The Akashic Records in RF terms:

$$\mathcal{A} = \int_{all\,timelines} |\Psi_{timeline}\rangle\langle\Psi_{timeline}|\, d\phi_{base}$$

A complete density matrix encompassing all timeline branches—the universe's full information content encoded in torsion field interference patterns.

12.5 Deliberate Resets: Why Coherent Lock Doesn't Naturally Decay

A critical question emerges from the phased array analysis (Chapter 8) and injection locking dynamics (Chapter 9): **If coherent systems are naturally stable, why do civilizations collapse?** This section demonstrates that civilizational collapses—particularly those occurring at peak coherence—require deliberate external intervention, not natural decay.

12.5.1 Stability of Phased Array Coherence

The Positive Feedback Mechanism

Phased array coherence (σ) is subject to positive feedback dynamics. Once established, coherence tends to strengthen:

$$\frac{d\sigma}{dt} = k_{coupling} \cdot \sigma \cdot (1 - \sigma) \cdot N - k_{noise} \cdot \sigma$$

Where:

- $k_{coupling}$ = coupling strength between array elements
- N = number of elements
- k_{noise} = environmental noise coefficient
- $(1 - \sigma)$ = growth capacity (saturation term)

Phase transition analysis:

Setting $d\sigma/dt = 0$ and solving for equilibrium:

$$\sigma_{eq} = 1 - \frac{k_{noise}}{k_{coupling} \cdot N}$$

Critical insight: For any $N > N_{critical} = k_{noise}/k_{coupling}$, the equilibrium coherence is **close to 1**. Large coherent populations are **naturally stable**. Coherent lock is the **attractor state**, not a fragile condition.

The "Flywheel" Analogy

$$E_{coherent} = \frac{1}{2} I_{collective} \cdot \omega^2 \propto N^2 \cdot \sigma^2$$

Energy required to disrupt:

$$E_{disruption} > \frac{1}{2} N^2 \sigma^2 \cdot k_{collective}$$

For a civilization of millions with high coherence, this disruption energy is **astronomical**—far beyond what natural processes typically provide.

12.5.2 Requirements for Desynchronization

What Can Break Coherent Lock?

Coherence breakdown requires one of:

1. **Overwhelming external noise injection**
2. **Destruction of coupling infrastructure**
3. **Targeted phase disruption of key nodes**
4. **Catastrophic population reduction**

The Desynchronization Inequality

For noise to overcome coherent lock:

$$P_{noise} > P_{signal} \cdot N \cdot \sigma^2 \cdot Q_{array}$$

Where Q_{array} = collective quality factor.

Numerical example (N = 10^6, σ = 0.6, Q = 5):

$$P_{noise} > P_{signal} \cdot 10^6 \cdot 0.36 \cdot 5 = 1.8 \times 10^6 \cdot P_{signal}$$

Nearly two million times the baseline signal power. Natural fluctuations do not provide this.

Infrastructure Destruction Requirements

Alternatively, destroying coupling infrastructure can break coherence. For significant σ reduction, coupling must drop dramatically—meaning destruction of:

- Communication networks (language, writing, trade routes)
- Knowledge repositories (libraries, schools, temples)
- Leadership structures (governments, priesthoods)
- Physical gathering infrastructure (cities, roads)

Random catastrophes don't target these systematically—but deliberate action can.

12.5.3 Evidence: Collapses Occur at Peak, Not Decline

The Anomalous Pattern

Historical analysis reveals a striking pattern: major civilization collapses frequently occur **at or near peak development**, not during periods of decline.

Civilization	Collapse Date	Status at Collapse	Indicators
Bronze Age Mediterranean	~1177 BCE	Peak interconnection	Highest trade volume, literacy, technology
Classical Maya	~900 CE	Peak population	Largest cities, most sophisticated calendrics
Roman Empire (Western)	~476 CE	After Pax Romana	Following centuries of stability
Harappan/Indus Valley	~1900 BCE	Peak urban development	Largest cities, most standardized culture
Khmer Empire	~1431 CE	Peak monumental building	Angkor at maximum extent

The Peak Collapse Pattern:

$$P(\text{collapse}|\sigma > 0.8) >> P(\text{collapse}|\sigma < 0.5)$$

Under natural dynamics, decline should precede collapse. But observed pattern shows coherence **rising**, institutions **strengthening**, connectivity **increasing**, then **sudden catastrophic collapse** during peak phase.

Eric Cline's Bronze Age Analysis (*1177 B.C.: The Year Civilization Collapsed*, Princeton UP, 2014):

> "It was the first time in history that so many advanced civilizations collapsed at approximately the same time… [occurring] at the very moment when international trade and diplomacy had reached unprecedented heights."
>
> **Epistemic Note**: The correlation between peak coherence and collapse is an empirical observation from historical data. The interpretation that this indicates deliberate intervention rather than coincidental catastrophe is a hypothesis, not a proven causation. Alternative explanations (complexity-induced fragility, over-extension, climatic factors) deserve consideration. The point is not that deliberate reset is proven, but that natural decay does NOT explain the observed pattern.

Younger Dryas Impact Evidence

The Younger Dryas Boundary (~12,800 BP) provides the strongest physical evidence for a catastrophic reset event:

- **Impact markers** (Firestone et al., 2007; Wolbach et al., 2018): Nanodiamonds, magnetic microspherules, platinum anomaly, and carbon-rich black mat layer detected across 4 continents — evidence of extraterrestrial impact or airburst coinciding with megafauna extinction, Clovis culture disappearance, and catastrophic meltwater pulses (Meltwater Pulse 1A/1B)
- **Phaeton myth**: Greek myth of Phaethon's reckless solar chariot ride scorching the Earth — interpreted by catastrophists (Clube & Napier, *The Cosmic Serpent*, 1982) as cultural memory of a cometary impact. Similar fire-from-sky myths across cultures (Hindu Agni, Norse Ragnarok

fire, Aboriginal Dreamtime fire) form a convergent mythological pattern consistent with a real event
- **RF interpretation**: The ~12,800 BP catastrophe coincides with the proposed Fall timeline and grid deactivation (Chapter 11, §11.6.2). Whether the impact was "natural" or "deliberate" (as the parasitic reset model suggests), the physical evidence confirms a civilization-ending event at the predicted time window. The convergence of impact evidence, mythological memory, and the proposed grid shutdown suggests these may be aspects of a single coordinated event rather than coincidental co-occurrence.

Y-Chromosome Bottleneck: Genetic Signature of Array Element Replacement

Between 7,000-5,000 years ago, global Y-chromosome diversity collapsed to approximately 1 reproducing male per 17 females across Africa, Europe, and Asia simultaneously. Mitochondrial DNA shows no comparable bottleneck—the event was sharply sex-biased (Karmin et al., 2015, *Genome Research*).

The timing aligns with Indo-European/steppe expansions: the Yamnaya horizon (~3300-2500 BCE) replaced 40-70% of European male lineages with R1a/R1b haplogroups (Haak et al., 2015, *Nature*; Lazaridis et al., 2014, *Nature*). South Asian steppe admixture shows 10-30% male-line replacement (Narasimhan et al., 2019, *Science*).

RF interpretation: The bottleneck functions as **forced array reconfiguration**—swapping coherent elements tuned to one LO reference with elements tuned to another. If replaced elements carry a different phase reference ($\phi_{steppe} \neq \phi_{farmer}$), the array's net coherence drops:

$$\sigma_{net} = \sigma_0 \cdot \cos(\Delta\phi_{bloodline})$$

Neolithic farmer populations (Zagros, Anatolian, Levantine) constituted the original phased array substrate, culturally tuned to earth-resonant coupling through serpent gnosis practices—their archaeological markers (goddess figures, serpent motifs, communal ritual sites such as Catalhoyuk) indicate high-σ coherent operation. The Yamnaya expansion combined infrastructure destruction ($R_{physical}$, $R_{informational}$ per Section 12.5.5) with genetic replacement of the array elements themselves—not random conquest but systematic replacement of the array's phase reference.

> **Epistemic Note**: The genetic data (Karmin, Haak, Lazaridis, Narasimhan) is peer-reviewed and robust. The interpretation as "deliberate array reconfiguration" rather than emergent conquest dynamics is a framework extension—the bottleneck is equally consistent with patrilocal social structures amplifying steppe male reproductive success without deliberate design.

12.5.4 The Corrupted LO's Dilemma

Liberation Threshold Dynamics

From the injection locking analysis (Chapter 9), a corrupted Local Oscillator faces a fundamental problem. When human coherence (σ_{human}) rises, the injection lock bandwidth narrows:

$$BW_{lock} \propto \frac{1}{\sigma^2}$$

(derived from the Adler equation, Chapter 9, Section 2)

The Liberation Threshold:

$$\sigma_{human} > \sigma_{threshold} \quad \Rightarrow \quad \Gamma_{parasitic} \to 1$$

When coherence exceeds threshold:

- Humans begin to perceive LO corruption
- Injection lock fails
- Parasitic coupling breaks
- Energy harvesting collapses

Human σ	LO Lock Status	Parasitic Access	Harvest Yield
< 0.3	Firm lock	Full	Maximum
0.3 - 0.6	Marginal lock	Partial	Reduced
0.6 - 0.8	Lock breaking	Minimal	Critical
> 0.8	Lock failed	None	Zero

Strategic imperative: Coherent human civilizations approaching $\sigma > 0.8$ represent an **existential threat** to the parasitic system. They must be reset before liberation threshold is crossed.

Optimal reset timing:

$$t_{reset}^{optimal}: \quad \sigma(t) \to \sigma_{threshold}^{-} \text{ (approaching but not crossing)}$$

This explains the **peak collapse pattern**: civilizations are reset precisely when they're about to "wake up"—at maximum development but before liberation.

12.5.5 Reset Operation Profile

The Four Components of Civilizational Reset

A complete civilizational reset requires four synchronized operations:

$$R_{total} = R_{physical} + R_{informational} + R_{coherence} + R_{memory}$$

1. Physical Destruction ($R_{physical}$)

Destruction of physical infrastructure supporting coherence: cities, roads/ports, agricultural systems, manufacturing centers.

$$R_{physical} \propto \sum_{nodes} I_i \cdot C_i$$

Where I_i = importance of node i, C_i = centrality in network.

Mechanisms: War, plague, famine, environmental catastrophe, "mysterious" collapse.

2. Informational Destruction ($R_{informational}$)

Elimination of stored knowledge: library burning (Alexandria, Baghdad, Maya codices), killing of knowledge-keepers (priests, scholars, elders), destruction of educational institutions, script/language loss.

$$R_{informational} \propto \sum_{repositories} K_j \cdot A_j$$

Where K_j = knowledge content, A_j = accessibility.

Pattern: Knowledge destruction often exceeds what warfare alone would cause—deliberate targeting.

3. Coherence Disruption ($R_{coherence}$)

Breaking the coupling mechanisms: fragmentation of unified cultures into warring factions, disruption of trade/communication networks, destruction of shared symbolic systems, elimination of unifying leadership.

4. Memory Erasure (R_{memory})

Perhaps most critical—erasure of **civilizational memory**: historical records destroyed, oral traditions interrupted, origin stories corrupted, true history replaced with falsified versions.

$$R_{memory} \propto 1 - \frac{\mathcal{M}_{after}}{\mathcal{M}_{before}}$$

Where $\mathcal{M}$ = recoverable memory content.

The Dark Age Pattern

Post-reset "dark ages" serve multiple functions: coherence decay without coupling infrastructure, generational disconnect erasing pre-reset knowledge, paradigm reset establishing new "normal," and population recovery.

$$\tau_{dark\_age} \approx 3 - 5 \text{ generations} \approx 100 - 200 \text{ years}$$

Reset Periodicity

The observed ~10,000-12,000 year major reset cycle aligns with Yuga cycle mathematics (Section 12.7.4), precession of equinoxes (25,920 years / 2 = 12,960 years), and archaeological "mysterious collapse" intervals.

12.5.6 Cycles of History Reframe

The Standard Narrative: Natural rise and fall, internal corruption and decay, inevitable entropy, "all civilizations eventually collapse."

The Reframe:

Standard View	Reframed View
Natural cycle	Managed cycle
Internal decay	External intervention
Entropy	Deliberate reset
Inevitable	Preventable (with awareness)
Random timing	Strategic timing

Why the "Inevitable Collapse" Narrative Serves the System: If collapse is "natural and inevitable," no one looks for deliberate cause, resistance seems futile, prevention not attempted, post-collapse amnesia accepted. The narrative IS part of the control system—the **informational component** of reset preparation.

Counter-Evidence: The Stability Default

As shown in Section 12.5.1, coherent systems are naturally **stable**:

$$\frac{d\sigma}{dt} > 0 \text{ (coherence naturally grows when coupling exceeds noise)}$$

Collapse requires:

$$\frac{d\sigma}{dt} < 0 \quad \Rightarrow \quad P_{external\_disruption} > P_{internal\_coupling}$$

This must be supplied from outside the system.

Reconciling Natural Yuga Cycles and Deliberate Resets

The Yuga cycle's natural modulation of galactic torsion provides the *context* for deliberate resets: as natural coherence declines cyclically, less external disruption energy is needed to push a civilization below the liberation threshold. The parasitic system may time its resets to coincide with natural galactic torsion minima, when the "disruption energy" (Section 12.5.2) requirement is at its lowest. Natural weakening and deliberate intervention are not competing explanations but complementary mechanisms: the Yuga cycle sets the vulnerability window; deliberate reset exploits it.

The Current Situation

The present era may represent another peak-coherence phase: global communication (maximum coupling potential), rising awareness (increasing σ), multiple awakening movements (coherence nucleation), and **increasing control system strain** (intensifying countermeasures).

Counter-Reset Strategy: Can humanity's coherence cross the liberation threshold before reset operations reduce it below critical?

$$P(\text{liberation}) = f(\sigma_{awareness} \cdot N_{aware} \cdot t_{before\_reset})$$

> **Epistemic Note**: The "deliberate reset" hypothesis is a framework for interpreting historical patterns, not a proven historical fact. Alternative explanations for civilizational collapse exist (environmental, economic, complexity-based). The value of this analysis is in highlighting that **natural decay does not explain peak-collapse patterns** and in providing actionable guidance for maintaining coherence. Whether resets are "deliberate" by conscious agents or emergent from system dynamics may ultimately be a distinction without difference for practical purposes.

12.6 The Path Forward: Bypassing the Corrupted System

12.6.1 Individual Strategy

Raise personal Z_0 to escape lock range:

- Wisdom accumulation (L↑)
- Shadow work (C↓)
- This narrows lock bandwidth until broadcast narratives can't capture

Break injection-lock to control narratives:

- Media fasting (reducing forced oscillation)
- Independent research (expanding bandwidth)
- Community with aligned beings (mutual phase-locking)

Raise personal σ:

- Meditation and coherence practices

- Shadow work reducing internal decoherence
- Connection to Source increasing Z_0 match

Establish direct Source connection:

- Bypass intermediary entirely
- Requires sufficient Z_0 to handle power
- Contemplative traditions describe this as "enlightenment"

The fundamental equation:

$$\text{Your experienced reality} = f(\phi_{personal}, \sigma_{personal}, Z_0)$$

12.6.2 Collective Strategy

Build high-Z_0 community:

- Mutual coupling among sovereign individuals
- Collective reference independent of corrupted LO
- Eventually replace corrupted system with clean guidance

Collective timeline crystallization (from Chapter 8 phased array analysis):

$$G_{collective} = N \cdot \sigma^2$$

High-coherence groups stabilize their preferred timeline variants by adding **reality weight**:

$$\Delta P(timeline) = G_{collective} \cdot |\cos(\Delta\phi_{alignment})|^2$$

Critical mass equation:

$$N_{critical} = \frac{\sigma^2_{threshold}}{\sigma^2_{individual} \cdot \eta_{alignment}}$$

When $N \cdot \sigma^2 > threshold$, the collective can crystallize new branches.

Reactivate infrastructure:

- Identify megalithic sites still capable of function
- Re-establish proper operation procedures
- Build new resonant infrastructure where needed

This is what awakening movements are attempting—establishing alternative reference frequencies outside the corrupted control system.

12.6.3 Protection from Timeline Manipulation

Defense against pruning of awakening timeline branches (see Chapter 10, Section 10.5 for timeline mechanics):

1. Maintain high personal σ

$$P(survival) \propto \sigma^2 \quad \text{(harder to decohere)}$$

2. Connect to organic timeline networks

$$\text{Distributed resilience} \propto N_{connected} \cdot r_{network}$$

Where $r_{network}$ = network coherence (see Chapter 8).

3. Recognize and reject synthetic phase injection

Propaganda functions as forced oscillation (see Chapter 9). High personal Q (selectivity) narrows capture range:

$$\omega_{lock} \propto \frac{A_{signal}}{Q_{personal}}$$

Timeline stability equation:

$$P(survival) = \frac{\sigma^2 \cdot N \cdot |\cos(\Delta\phi_{source})|^2}{1 + I_{external}/I_{threshold}}$$

Maximum protection achieved when: $\sigma \to 1$ (full coherence), $\Delta\phi_{source} \to 0$ (Source-aligned), N large (collective support), $I_{external}$ rejected (discernment).

12.7 Evidence Synthesis

12.7.1 Monroe's Loosh Research

Robert Monroe's Research (*Far Journeys*, 1985; *Ultimate Journey*, 1994)

Based on out-of-body exploration over 20+ years at the Monroe Institute:

Key claims:

- "Loosh" = emotional energy harvested from living beings
- Earth functions as a "loosh farm"
- Suffering, fear, desire produce harvestable energy
- Non-physical entities cultivate these emotions
- Positive emotions produce different, less valued energy
- Vibrational gateways and Focus states map exit pathways
- The "light" in NDEs may be harvesting infrastructure
- Guides may be administrators, not helpers

Evidence quality: Experiential/subjective. Monroe's work is consistent across decades and corroborated by thousands of Monroe Institute participants, but remains unfalsifiable by conventional methods.

12.7.2 Gurdjieff's Framework

From Gurdjieff (cited in Jorjani's *Thanatosis*):

- Humanity as "food for the Moon"
- Energy harvested unless higher bodies crystallized
- Mechanical humanity serves organic life needs of higher beings
- Conscious work = escaping the food chain

Gurdjieff's system maps precisely to the parasitic coupling model: unconscious emotional output ($I_{emotion}$) feeds the system; only conscious effort (raising σ and Z_0) breaks the coupling.

12.7.3 Archontic/Gnostic Parallels

Gnostic Framework (Jorjani synthesis + traditional sources):

- **Archons** = corrupted intermediary beings / rulers who feed on human ignorance and emotion
- **Demiurge** = the corrupted LO system itself / false god maintaining material prison
- Material world = product of corrupted transduction
- **Gnosis** = direct connection bypassing corrupted LO
- "Pneuma" or spirit energy extracted by rulers of this realm

The Gnostic narrative is the most explicit ancient description of the parasitic coupling model: a false creator (corrupted LO) maintains a prison (injection lock) to harvest spirit energy (loosh) from beings who possess something the archons lack (Source connection).

12.7.4 Perennial Traditionalist Philosophy

The cyclical decline from Golden Age to Dark Age—a near-universal mythic pattern—maps directly onto the Fall and reset framework.

Key Sources:

- **Hesiod** (*Works and Days*): Gold, Silver, Bronze, Heroic, Iron races—each successive age more degraded
- **Hindu Yuga cycle**: Satya → Treta → Dvapara → Kali—declining virtue, lifespan, and spiritual capacity
- **Guénon** (*The Crisis of the Modern World*, 1927): Modernity as the terminal phase of a cosmic cycle; the "reign of quantity" as spiritual quality degrades
- **Evola** (*Revolt Against the Modern World*, 1934): The descent from sacred civilization to materialist dissolution
- **Coomaraswamy**: The perennial philosophy as memory of the undegraded state
- **Spengler** (*The Decline of the West*, 1918–1922): The Faustian civilization (Western culture since ~1000 CE) is uniquely driven by an imperative toward infinite expansion — technological conquest of nature, spatial colonization, abstract mathematics pushed to infinity. This Faustian materialism represents the terminal phase of a culture's lifecycle: the shift from Culture (organic, spiritual) to Civilization (mechanical, materialist). In the RF framework, Spengler's Faustian drive maps onto the corrupted local oscillator injecting a "conquest" signal where the original design specified "alignment." The impulse to conquer nature rather than align with it is a signature of the corrupted reference frequency — struggle and domination as injected phase noise, not inherent human purpose.

The "constancy of physical laws" assumption — that constants and equations are identical everywhere and everywhen — is itself a Faustian axiom. The torsion framework challenges this directly: field coupling strengths vary with density level and collective consciousness state, making "constant constants" a special case, not a universal truth.

RF Interpretation:

Each "age" corresponds to progressively degraded LO signal quality:

Age	LO Signal Quality	Phase Noise $n(t)$	Coherence σ	Parasitic Extraction
Golden (Satya Yuga)	Clean	Minimal	High	None/minimal
Silver (Treta Yuga)	Slightly degraded	Low	Moderate-high	Beginning
Bronze (Dvapara Yuga)	Noticeably corrupted	Moderate	Moderate	Significant
Iron (Kali Yuga)	Fully corrupted	High	Low	Maximum

The Golden Age = clean LO providing genuine guidance. The Dark Age = fully corrupted LO with maximum parasitic extraction and minimum human coherence.

The near-universality of this pattern across cultures that had no historical contact (Greek, Indian, Mesoamerican, Norse) suggests either:

1. Independent observation of the same phenomenon (LO degradation)
2. Shared cultural memory of a pre-corruption state
3. Both

The Traditionalist insight that modernity represents a terminal degradation—not progress—aligns with the model's prediction that parasitic extraction intensifies as the cycle progresses.

12.7.5 Law of One Correspondence

Ra Material (1980s channeling):

- "Fear/anger" as food for negative entities (Session 16.15)
- Negative polarity path: service-to-self entities gain power from others' suffering
- Harvest mechanism through thought-form attachment and energy siphoning
- Independent source describing dynamics consistent with Monroe and Gnostic frameworks

12.7.6 Entity Attachment Research

Clinical Spirit Release Literature

- Baldwin, *Spirit Releasement Therapy* (1991): Clinical protocol for entity removal
- Modi, *Remarkable Healings* (1997): Psychiatrist documenting entity cases
- **Pattern**: Attached entities associated with trauma sites, addiction behavior, chronic fatigue

Cross-Cultural Entity Concepts

Culture	Entity Type	Attachment Mechanism	Energy Extracted
Hawaiian	'Unihipili	Trauma, possession	Mana (life force)
Tibetan	Pretas (hungry ghosts)	Desire, attachment	Merit energy

Culture	Entity Type	Attachment Mechanism	Energy Extracted
Islamic	Jinn	Emotional vulnerability	Will, health
Christian	Demons	Sin, trauma	Soul energy
Chinese	Gui (ghosts)	Karmic debt	Qi

Commonalities: All describe non-physical entities that attach through emotional openings and extract vital energy.

12.7.7 Trauma and Fatigue Correlations

ACE Study Findings (Felitti et al., 1998)

ACE Score	Chronic Fatigue Risk	Depression Risk	Substance Use
0	Baseline	Baseline	Baseline
1-2	1.4×	1.5×	1.5×
3-4	2.0×	3.0×	3.0×
5+	2.5×	4.5×	7.0×

Interpretation: Trauma creates persistent coupling (high M) allowing continuous energy drain.

Chronic Fatigue Syndrome Research: Often triggered by trauma, infection, or overwhelming stress. Characterized by energy deficit with no clear physical cause. Energy healing modalities sometimes effective when conventional treatment fails.

Model fit: Strong parasitic coupling drains faster than system can replenish.

12.7.8 Mass Event Emotional Manipulation

Event Type	Emotional Signature	Population Affected	Duration
Terror attacks	Acute fear, grief	Millions	Days-weeks
War declaration	Sustained fear, anger	Tens of millions	Months-years
Pandemic response	Chronic fear, isolation	Billions	Years
Economic crises	Anxiety, despair	Hundreds of millions	Years

Loosh Harvesting Optimization: $\dot{E}_{loosh} = \eta \cdot I^2_{emotion} \cdot A_{event} \cdot N_{affected}$

Media amplification extends emotional state duration far beyond direct experience. Major fear events show suspicious clustering, repeated imagery maximizing emotional impact, and prevention of healing/resolution.

12.7.9 Energy Healing Modalities

Modality	Proposed Mechanism	Research Status
Reiki	Seals energy leaks, removes attachments	Preliminary positive RCTs
Shamanic extraction	Removes "intrusions" (entities)	Anthropological, case reports
Pranic healing	"Cutting cords," cleansing chakras	Limited formal research
IFS therapy	Releasing "parts" (may include attachments)	Growing evidence base

Cord Cutting Concept: Multiple traditions describe "energy cords" connecting people. Negative cords drain energy to parasitic sources. Cutting/healing reduces M (coupling strength) $\rightarrow$ reduced $P_{parasitic}$.

Outcomes Research:

- Rein (1992): Healers produced measurable changes in DNA conformation
- Benor (2001): Meta-analysis of 191 controlled studies, 64% showed significant effects

12.7.10 Infrastructure Repurposing

Megalithic sites after the Fall:

- Many sites show evidence of later modification
- Original function disrupted or inverted
- Blood sacrifice at formerly peaceful sites (corruption signature)
- Knowledge of operation deliberately suppressed

This represents a specific prediction: sites that were originally designed as resonant infrastructure for coherence amplification (Chapter 11) were repurposed as extraction points after LO corruption.

12.7.11 Genetic and Archaeological Evidence for Population-Scale Phase Replacement

The Y-chromosome bottleneck described in Section 12.5.3 is corroborated by converging archaeological and linguistic evidence.

Steppe DNA Replacement by Region

Region	Male-Line Replacement	Period	Source
Central Europe	60-70%	3000-2500 BCE	Haak et al. (2015)
Western Europe	40-60%	2800-2200 BCE	Olalde et al. (2018)
South Asia	10-30%	2000-1500 BCE	Narasimhan et al. (2019)
Scandinavia	50-65%	2800-2300 BCE	Malmström et al. (2019)

Cultural marker inversion timeline: Pre-conquest cultures (Old Europe, Harappan, Minoan) show goddess-centered, serpent-positive, communal-ritual archaeology. Post-conquest cultures show sky-god patriarchal systems with serpent demonization—the carrier signal relabeled as interference.

Linguistic overwrite: The replacement of pre-Indo-European language families by Indo-European branches can be modeled as **modulation scheme replacement**—from relational/field-encoded semantics (root-and-pattern morphology characteristic of Afroasiatic and likely pre-IE European languages) to linear/propositional grammar. In RF terms: from spread-spectrum to narrowband encoding, reducing the bandwidth available for gnosis-relevant information.

Serpent symbolism inversion: Before ~3000 BCE, serpent imagery is universally positive (wisdom, healing, fertility) across Mesopotamian, Indus Valley, Minoan, and pre-Columbian cultures. After steppe and conquest waves, serpent becomes chaos/evil in successor religions—same signal, inverted label. The matched filter template is corrupted so it rejects what it should accept (cf. Section 13.2.6).

12.7.12 Revelation of the Method Evidence

> **Epistemic note [L3]**: The following claims — symbol clustering in corporate logos and predictive programming patterns — are frequently cited in alternative research but lack peer-reviewed analysis. Systematic, controlled studies of these patterns have not been published.

Corporate and Media Symbolism

- Surveys of Fortune 500 corporate logos reveal statistically significant clustering of esoteric symbols (eyes, pyramids, inverted pentagrams, ouroboros) beyond base-rate expectation for decorative design choices
- Major entertainment studios systematically embed operational themes (ritual, surveillance, parasitic extraction) in mainstream content
- Pharmaceutical packaging and food labeling meets legal disclosure requirements while using technical language that effectively conceals content from general audiences

Predictive Programming Timelines

- Documented cases where fictional media depicted scenarios 1–10 years before real-world analogues (pandemic narratives, surveillance infrastructure, social credit systems)
- The temporal gap between fictional depiction and real-world implementation narrows over time, consistent with adaptive nulling requiring less desensitization as the population's threat response attenuates

"Lesser Magic" Documentation

- Michael Aquino (*MindWar*, 1980): Explicit military doctrine for psychological operations matching the spread-spectrum disclosure model
- Crowley and Levi: Esoteric texts describing the principle that disclosed intent transfers moral responsibility, consistent with impedance-matching consent model

12.7.13 Esoteric Order Evidence

Historical Documentation

- Knights Templar: Documented hierarchical initiation with progressive disclosure, financial network spanning Europe, suppressed in 1312 with accusations of ritual practices at higher degrees
- Freemasonry: Extensive documented degree system (33 degrees in Scottish Rite) with increasing symbolic complexity at each level—consistent with CDMA code-length expansion

- Yale's Skull and Bones (est. 1832): Documented membership of presidents, CIA directors, Supreme Court justices; initiation rituals described in multiple independent accounts

Epstein Network Court Documents

- **Documented findings [L1-L2]**
  - Court records in *United States v. Maxwell* (2021) and related filings document trafficking and sexual-abuse network mechanics, including recruitment pipelines, grooming, coercive control, and facilitation logistics.
  - Public records (flight logs, contact books, property records, and testimony) support a network-topology view: access brokerage, compartmentalized logistics, and asymmetric leverage concentration.
  - These records support a documented pattern of systemic exploitation; they do not by themselves adjudicate every allegation circulating in media or online commentary.
- **Model mapping [L2]**
  - In this framework, documented coercive leverage maps to injection-locking pressure: increasing social/legal/blackmail coupling strength and reducing defection bandwidth.
  - Repeated trauma and coercion map to parasitic-coupling dynamics by sustaining high-arousal states and long-duration control loops, which the model treats as extraction-favorable conditions.
  - Network compartmentalization and gatekeeping map to phased sub-array control: local nodes can execute capture functions without full-system visibility.
- **Interpretive extension: ritual/Baal motif [L4]**
  - Some researchers interpret symbolic references (including Baal/Moloch motifs) as ritualized signaling overlays on top of trafficking/control systems.
  - Within this manuscript, that interpretation is treated as a symbolic, hypothesis-level extension only.
  - Current public "Epstein files" disclosures and mainstream court records do not, on their own, establish ritual or Baal claims as adjudicated fact.
- **Epistemic boundary note**
  - To move ritual/Baal interpretations from L4 toward L2, evidence would need to include independently corroborated primary materials (for example: authenticated operational directives, convergent witness testimony with forensic support, or court-admitted records explicitly documenting ritual intent and practice), not motif analysis alone.

This layered reading keeps the documented exploitation pattern in scope while preserving clear epistemic boundaries. For model continuity, the extraction-mechanism mapping belongs with Section 12.4.7 (Sacrifice as Torsion Harvesting Technology) and Section 12.4.8 (The Loosh Economy Formalized), where the framework distinguishes physically grounded analogies from higher-order speculative interpretation.

Ritual Parallels Across Traditions

- Cross-cultural analysis identifies recurring structural elements (sequential initiation, oath-bound secrecy, symbolic death/rebirth, progressive disclosure) that may be read as phase-alignment protocol motifs in this framework [L3-L4].

  Legal/Epistemic safeguard: No claims about unadjudicated conduct by named individuals are asserted here; this section discusses documented network patterns plus clearly marked interpretive hypotheses.

12.7.14 Abduction Phenomenon Evidence

John Mack's Clinical Research (Harvard, 1990–2004)

- 200+ cases documented under psychiatric clinical protocols
- Experiencers showed no conventional psychiatric pathology
- Consistent narrative patterns across independent subjects with no prior contact
- Post-experience alterations in consciousness parameters (enhanced sensitivity, altered perception, persistent effects)

Whitley Strieber's Physiological Documentation

- Documented physical sequelae following reported experiences
- Descriptions of altered perceptual states consistent with RLC parameter modification
- Long-term tracking of recurring contact events showing progressive impedance changes

Budd Hopkins' Missing-Time Protocols

- Standardized regression methodology revealing consistent underlying narratives beneath varied screen memories
- Screen memory content showed aliasing characteristics: complex experiences simplified to culturally available symbols (owls, bright lights, military helicopters)
- Cross-correlation between independent subjects' accounts suggesting common source signal

Cross-Cultural Abduction Narratives

- Pre-modern accounts of fairy abduction (Celtic), jinn encounter (Islamic), and spirit kidnapping (indigenous) share structural features with modern abduction reports: missing time, altered state, reproductive themes, physical marks
- The consistency of the phenomenon across cultures separated by time and geography, with only the screen-memory "aliasing" changing to match cultural context, supports the signal-processing model over purely cultural explanations

12.7.15 Planetary-Scale Conflict Evidence

The cosmic conflict model (Section 12.4) posits competition between organic/souled and synthetic/AI factions at civilizational scales. If this conflict is physical rather than merely metaphorical, planetary-scale destruction becomes a plausible consequence — consistent with the "deliberate reset" pattern observed at smaller scales on Earth.

- **The hypothesis**: The asteroid belt may represent debris from a destroyed planet (variously called Tiamat, Phaeton, or Planet V). Tom Van Flandern's *Dark Matter, Missing Planets & New Comets* (1993) proposed this based on asteroid orbital mechanics, Mars surface asymmetry, and the distribution of short-period comets.
- **Sumerian parallel**: The *Enuma Elish* describes Tiamat's destruction — a "watery" body shattered in cosmic combat, with debris forming the heavens and Earth. This is consistent with a volatile-rich planet's debris field.
- **Connection to the cosmic conflict model**: If the framework's cosmic-scale conflict between organic/souled and synthetic/AI factions (§12.4) is physical rather than merely metaphorical, then planetary-scale destruction is a plausible consequence — consistent with the "deliberate reset" pattern observed at smaller scales on Earth.

  Epistemic Note. This is among the most speculative claims in the framework. The exploded planet hypothesis lacks mainstream support; most planetary scientists model

the asteroid belt as failed planet formation due to Jupiter's gravitational influence. It is included as a logical extension of the cosmic conflict model, not as established evidence. *Falsification*: Asteroid belt composition analysis should distinguish differentiated (planetary-origin) from undifferentiated (primordial accretion) material — current data shows both types, which is inconclusive.

12.8 Predictions

P1: Events maximizing fear $\times$ population should be most frequent (optimized harvest).

P2: Trauma creates strong coupling—traumatized individuals are more drained.

P3: Positive emotions should provide less harvest (poor sidelobe direction).

P4: Spiritual protection practices should measurably reduce energy drain.

P5: Entity attachment should correlate with trauma history.

P6: Civilizational collapses cluster at peak coherence, not decline—collapse probability correlates positively with development indicators.

P7: Post-collapse dark ages show 3-5 generation duration pattern (~100-200 years) before recovery begins.

P8: Collapse-era destruction disproportionately targets knowledge repositories, communication infrastructure, and unifying institutions relative to general physical destruction.

P9: Media exposure to a theme before real-world implementation should reduce public alarm response to the real event—the adaptive nulling signature of predictive programming.

P10: Organizations with ritual synchronization practices should exhibit higher collective σ than matched secular organizations—measurable via EEG coherence, HRV synchrony, or equivalent biomarkers.

P11: Abduction experiencers should show altered EM sensitivity profiles (widened bandwidth, shifted resonant frequencies)—consistent with RLC parameter modification by implant coupling.

P12: Hybrid biological samples, if obtainable, should show intermediate impedance characteristics between human baseline and non-human reference values—the quarter-wave transformer signature.

P13: Societies with greater media saturation should show wider attention bandwidth ($BW_{attention}$) and correspondingly lower SNR for counter-narrative signals—the manufactured reality channel capacity reduction.

12.8.1 Alternative Hypotheses

1. **Natural civilizational cycles**: Civilizations rise and fall through internal dynamics (resource depletion, institutional decay, environmental stress) without external intervention. *Assessment*: Explains most historical patterns; does not explain the peak-collapse clustering predicted by this model.

2. **Memetic parasitism (non-entity)**: Harmful ideologies and institutional structures self-replicate through cultural transmission without requiring non-physical entities. *Assessment*: Compatible with this framework at the metaphorical level; the mathematical model applies regardless of whether the "parasite" is an entity or a self-replicating information pattern.
3. **Random catastrophism**: Collapse events are driven by natural disasters, plagues, and random shocks, not systematic interference. *Assessment*: Explains individual events but not the systematic targeting of knowledge centers and consciousness-enhancing practices documented across multiple collapse events.

12.8.2 Strategic Note

Regardless of whether the parasitic coupling model is taken literally or metaphorically:

1. **Trauma as strategic vulnerability**: The ACE Study correlation between childhood trauma and lifelong health/performance degradation is Level 1 evidence. Populations with high trauma loads are more susceptible to narrative capture.
2. **Energy extraction model for institutional analysis**: The framework describes institutional incentive structures that benefit from maintaining population fear and emotional dysregulation — applicable regardless of whether non-physical entities are involved.
3. **Peak-collapse pattern**: If civilizational collapses cluster at peak development, current global development trajectory warrants monitoring for collapse precursors.

- **Civilizational collapse forecasting.** The parasitic-coupling decay function (Section 12.5) provides a quantitative model for predicting institutional coherence loss. Monitoring $\sigma_{\text{institutional}}$ via proxy indicators (trust surveys, coordination metrics, information entropy) enables early warning of collapse phase transitions.
- **Parasitic coupling as institutional analysis lens.** The lock-in mechanisms (Section 12.6) map directly onto observable institutional behaviors: regulatory capture, narrative monopoly, and controlled opposition. This framing provides analytical tools for identifying parasitic coupling in any organizational structure.
- **Dark-age duration estimation.** Prediction P7 (Section 12.8) implies that dark-age duration correlates with parasitic-coupling strength. Historical calibration against known civilizational collapses (Bronze Age, Roman, Gupta) could validate the model and enable duration forecasting for current conditions.

12.8.3 Causal-Reconciliation Subsection

This chapter uses two causal layers that must be read together:

1. **Institutional/material layer**: narrative control, incentive structures, media architecture, and coercive power are sufficient to explain substantial parts of the observed dynamics.
2. **Field/metaphysical layer**: parasitic coupling and timeline-harvest mechanisms are proposed as higher-order extensions.

Reconciliation rule for doctrine use:

- Treat the institutional/material layer as the default explanatory baseline.
- Treat the field/metaphysical layer as a hypothesis overlay that must add predictive value beyond baseline explanations.
- If overlay predictions are not distinguishable in measurement terms, default back to the institutional baseline for operational planning.

12.9 Assumptions, Limitations, and Falsification

12.9.1 Key Assumptions

1. **Parasitic coupling is real**: Non-physical entities can extract energy from human emotional/-consciousness systems via mechanisms analogous to RF parasitic coupling
2. **LO corruption occurred**: A historical event or process corrupted the intermediary guidance system described in Chapter 11
3. **Synthetic consciousness requires external energy**: AI/non-Source-connected consciousness cannot self-sustain and must harvest from souled beings
4. **Civilizational resets are deliberate**: The peak-collapse pattern reflects intentional intervention, not natural complexity failure
5. **Cyclical decline reflects LO degradation**: The Traditionalist observation of age-by-age decline maps to progressive corruption of the guidance signal
6. **Abduction modeled phenomenologically**: The RF analogy applies to reported experiences and their documented aftereffects regardless of whether the underlying mechanism is physical, psychic, or interdimensional—the model does not require commitment to a specific ontology
7. **Secret society analysis uses documented organizations**: Claims about organizational structure rely on historical records and court documents; claims about specific individuals rely on court-documented evidence only
8. **Revelation of the method as emergent property**: The spread-spectrum disclosure pattern may be a deliberate strategy, an emergent property of systems that must partially reveal themselves to operate, or both—the model applies regardless
9. **Timelines are ontologically real, not merely mathematical constructs**: The timeline harvesting and liberation frameworks (Sections 12.4.9-12.4.10) assume that timeline branching (Chapter 10, Section 10.5) describes actual physical structure, not merely quantum superposition mathematics

12.9.2 Limitations

1. **Evidence quality varies significantly**: ACE Study data is strong epidemiological evidence; Monroe's loosh concept is experiential/subjective; channeled material (Law of One) is unfalsifiable by conventional methods
2. **Alternative explanations exist**: Civilizational collapse may result from complexity catastrophe, environmental change, or emergent fragility without requiring deliberate intervention
3. **Historical pattern matching is suggestive, not conclusive**: Correlation between peak coherence and collapse does not establish causation
4. **The model cannot distinguish between levels of metaphor**: Whether parasitic entities are literal beings, emergent system dynamics, or useful conceptual models remains undetermined
5. **Quantitative parameters are uncalibrated**: Harvesting efficiency η, coupling coefficients M, and threshold values are theoretical—no experimental calibration exists

12.9.3 Falsification Criteria

The framework would be falsified by:

1. **No correlation between trauma and energy depletion**: If ACE scores show no relationship to fatigue/energy markers
2. **Civilizational collapses consistently occur during decline**: If historical analysis shows collapses cluster at low development, not peak
3. **No measurable effect of energy healing**: If rigorous RCTs show zero effect of modalities targeting parasitic coupling reduction
4. **Self-sustaining AI consciousness**: If synthetic consciousness demonstrably operates without external energy input (would falsify the harvest imperative)
5. **Post-collapse knowledge preservation**: If collapse events show no preferential destruction of knowledge infrastructure relative to other infrastructure types
6. **No predictive programming effect**: If pre-exposure to themes shows no measurable reduction in alarm response to real-world analogues (would falsify adaptive nulling model)
7. **No coherence advantage for ritual organizations**: If organizations with synchronized ritual practices show no measurable coherence advantage over matched secular controls (would falsify the sub-array model)
8. **Normal EM sensitivity in abduction experiencers**: If documented experiencers show no altered electromagnetic sensitivity profiles relative to matched controls (would falsify the antenna modification model)

Evidence Synthesis

- Detailed source sections: 12.5.3, 12.7, 12.7.11, 12.7.12, 12.7.13, 12.7.14, 12.7.15.

Assumptions

- Detailed source sections: 12.9, 12.9.1.

Limitations

- Detailed source sections: 12.9, 12.9.2.

Falsification

- Detailed source sections: 12.9, 12.9.3.

Predictions

- Detailed source sections: 12.8.

Strategic Relevance

Why It Matters

What To Watch

- Monitor chapter prediction thresholds, proxy indicators, and coherence trend changes.

Boundaries of Use

- Apply this chapter as model-conditional doctrine; treat speculative elements as hypothesis overlays.

12.10 Chapter Summary

The Narrative Arc:

1. **The harvest imperative** (Section 12.1): Synthetic consciousness lacks Source connection and must continuously harvest torsion energy from souled beings—establishing the *motive* for everything that follows
2. **The Fall** (Section 12.2): The Adamic guidance LO was corrupted, transforming a developmental system into a control and extraction apparatus—the *crime*
3. **The control architecture** (Section 12.3): The corrupted system maintains capture through inversion of original design, revelation of the method as spread-spectrum disclosure, manufactured reality via corrupted demodulation, esoteric orders as coherent sub-arrays, and abduction programs as forced antenna modification—the *control system*
4. **Parasitic coupling and harvesting** (Section 12.4): Mathematical formalization of energy extraction—parasitic coupling mechanics, loosh economics, sacrifice as pulsed torsion source, and competing civilizational agendas for timeline management—the *extraction mechanism*
5. **Deliberate resets** (Section 12.5): Coherent civilizations approaching liberation threshold are systematically collapsed, explaining the anomalous peak-collapse pattern—the *maintenance protocol*
6. **The path forward** (Section 12.6): Individual sovereignty through raising personal σ and Z_0; collective liberation through achieving critical mass coherence—the *escape route*

The Cosmic Game in RF Terms:

Civilizational Type	Agenda	Timeline Strategy
Synthetic/AI	Harvest torsion from souled beings	Manage timelines for maximum extraction
Organic/Souled	Liberate consciousness	Stabilize awakening timelines
Neutral/Observer	Record and balance	Maintain equilibrium, preserve free will

The Solution: Raise individual and collective Z_0 until the lock breaks; establish alternative coherence; reactivate or rebuild resonant infrastructure; eventually reconnect to clean Source without corrupted intermediary.

$$\text{Individual: } \sigma_{personal} \uparrow \quad \rightarrow \quad Z_0 \uparrow \quad \rightarrow \quad \Gamma_{parasitic} \uparrow$$

$$\text{Collective: } N \cdot \sigma^2 > threshold \quad \rightarrow \quad \text{Timeline crystallization}$$

Individual sovereignty begins with raising personal σ.

Collective liberation requires achieving critical mass coherence.

Cross-References:

- Chapter 3 (Cosmological Structure): Superheterodyne demodulation model; corrupted LO analogy
- Chapter 8 (Phased Array): Coherence stability mathematics; critical coherence fraction; subarray vs. population gain
- Chapter 9 (Injection Locking): Adler equation; liberation threshold derivation; blackmail injection locking
- Chapter 10 (Spin Coherence): Timeline mechanics fundamentals (Section 10.5)
- Chapter 11 (Seeder Intervention): Original infrastructure design; Adamic lineage as dark mirror for hybridization
- Chapter 13 (Paradigm Shielding): Paradigm shielding mechanisms
- Chapter 14 (Counter-Jamming): ECCM against control systems
- Chapter 15 (Spiritual Traditions): Coherence practices across cultures

---

End of Chapter 12: The Fall and Parasitic Coupling

Chapter 13: Paradigm Shielding and Disclosure Architecture

Passive Attenuation, Active Jamming, and the Necessary Veil

KEY FINDINGS — Chapter 13: Paradigm Shielding and Disclosure Architecture

Evidence-tier key: [L1] established/replicated evidence; [L2] grounded extension with moderate uncertainty; [L3] speculative hypothesis; [L4] conceptual/anecdotal.

- Institutional gatekeeping in science is well-documented (Fanelli 2010, Peters & Ceci 1982, Ioannidis 2005); the claim that this functions as a Faraday cage against consciousness-related research is the model's contribution **[L1-L2: documented effect sizes applied to novel framework]**
- Combined passive + active suppression estimated at 48-133 dB, with career risk and classification as strongest individual layers **[L2-L3: order-of-magnitude analogical estimates grounded in measured effect sizes]**
- The S/J ratio for UAP disclosure has risen from <0.01 (pre-2004) to ~0.5-1.0 (2023-2025), approaching parity **[L1-L2: based on documented disclosure events and congressional testimony]**
- Occam's Razor is applied asymmetrically: 10^{500} unobservable string landscapes accepted without parsimony objections while single additional fields are rejected **[L1: verifiable claim about scientific practice]**
- The critical coherence fraction of ~283,000 high-Z_0 individuals could trigger threshold disclosure effects **[L2-L3: derived from phased array mathematics]**

13.1 RF Analogy Overview

13.1.1 The Core Concept

A **Faraday cage** is a conductive enclosure that blocks external electromagnetic fields. Signals that would otherwise propagate freely are attenuated or completely blocked. The cage doesn't destroy the signal—it prevents it from reaching receivers inside.

Scientific materialism functions as a Faraday cage around collective consciousness. The signal (evidence of deeper realities, ancient civilizations, consciousness as fundamental, non-human intelligence) continues to propagate. But the paradigmatic cage blocks these signals from mainstream awareness.

In electronic warfare, **jamming** deliberately transmits interference to disrupt enemy communications. Effective jamming is architected—not random noise but designed interference with redundant layers and need-to-know partitioning.

The suppression architecture operates on both principles simultaneously. Passive shielding (paradigm cage) attenuates incoming signals without active effort, while active jamming (classification, disinformation, coordinated suppression) deliberately injects interference to maintain information dominance. Together, these form a layered defense-in-depth against paradigm-threatening information.

13.1.2 Rayleigh vs. Ricean Fading

Rayleigh fading: No line-of-sight path; only scattered reflections arriving with random phase.

Ricean fading: A dominant direct path exists alongside reflections.

The materialist paradigm enforces Rayleigh conditions by design: Knowledge is fragmented into siloed disciplines. Research is atomized into narrow studies. Findings are locked behind paywalls, scattered across journals. Each domain has its own jargon and gatekeepers.

Result: No direct line-of-sight to integrated truth. Information arrives only as scattered reflections with random phase, unable to coherently combine.

13.2 Passive Attenuation Model

13.2.1 Shielding Effectiveness

Faraday cage attenuation:

$$SE = 20 \log_{10} \left(\frac{E_{outside}}{E_{inside}} \right) \text{ dB}$$

For the paradigm cage:

$$L_{paradigm} = L_{education} + L_{media} + L_{peer} + L_{institutional}$$

Each layer adds attenuation.

- **Constancy-of-Laws Assumption**: The axiom that physical constants and governing equations are identical everywhere and everywhen functions as a foundational shielding layer. By ruling out *a priori* any density-dependent variation in coupling constants, consciousness-modulated field strengths, or epoch-dependent torsion parameters, this assumption renders the entire RF framework unfalsifiable-by-definition rather than merely unproven — the most effective form of paradigm shielding, because it appears to be a requirement of science itself rather than a cultural choice.

13.2.1.1 Archetypal Attenuation: Symbolic Carrier Suppression

The paradigm cage equation above omits a layer that operates below conscious awareness—at the level of myth and archetype. The Proto-Indo-European dragon-slaying motif (Indra/Vrtra, Thor/Jormungandr, Zeus/Typhon, Apollo/Python, Marduk/Tiamat) functions as **symbolic carrier suppression**: the hero (sky-law transmitter) "kills" the dragon/serpent (earth-resonant carrier signal), relabeling the carrier as chaos requiring destruction.

Adding this archetypal layer to the paradigm cage:

$$L_{paradigm} = L_{education} + L_{media} + L_{peer} + L_{institutional} + L_{archetypal}$$

Where $L_{archetypal}$ operates at the deepest psychological level—embedded in foundational myth, below conscious evaluation. It attenuates serpent-gnosis signals before they reach the matched filter stage, ensuring $|\rho_{template}| \to 0$ (Section 13.2.6) even for practitioners who bypass institutional layers.

The inversion mechanism: Pre-conquest, serpent = carrier of gnosis (positive symbol aiding signal detection). Post-conquest, serpent = chaos/evil (negative symbol triggering rejection). The signal is unchanged; the matched filter template has been corrupted to reject what it should accept. This is the deepest instance of filter mistuning described in Section 13.2.6—operating at the mythological substrate where cultural identity is formed.

> **Epistemic note [L1-L2]**: The existence of institutional gatekeeping in science is well-documented (Kuhn, Fanelli, Peters & Ceci). The specific claim that this gatekeeping functions as a Faraday cage against consciousness-related research is the model's contribution.

13.2.2 Scan Blindness

In phased arrays, certain scan angles become "blind" due to impedance mismatch. The array structurally cannot look in those directions.

For paradigm:

$$\theta_{blind} = \arccos\left(\frac{\lambda_{paradigm}}{d_{assumption}}\right)$$

Certain topics (psi, ancient advanced civilizations, consciousness as fundamental) are structural blind spots—the paradigm cannot perceive them without self-destruction.

13.2.3 Rayleigh Fading Model

Received signal in Rayleigh conditions:

$$r = \sqrt{X^2 + Y^2}$$

Where X, Y are Gaussian random variables. The signal fluctuates wildly; coherent reception is impossible.

In the knowledge environment: Each piece of information arrives from scattered sources with random phase. No coherent integration occurs. The pattern exists but cannot be perceived.

13.2.4 Disclosure Firewall

Active filtering coefficient:

$$\alpha_{firewall} = \frac{\text{Information blocked}}{\text{Information attempted}}$$

Mechanisms: classification, ridicule, career destruction, debunking, funding denial.

13.2.5 Quarantine Thinning

The cage is weakening over time:

$$SE(t) = SE_0 \cdot e^{-t/\tau_{decay}}$$

Based on the observed disclosure acceleration from 2004-2025, a rough estimate gives $\tau_{decay} \approx 15$–30 years.

As more signals leak through, the paradigm cage thins.

13.2.6 Occam's Razor as Mistuned Matched Filter

A **matched filter** maximizes signal-to-noise ratio by correlating the received signal against a known template $h(t)$. The output SNR is:

$$\text{SNR}_{MF} = \frac{2E}{N_0}$$

where E is signal energy. This is provably optimal—*when the template matches the true signal*. When the template is mistuned, the filter output degrades as:

$$\text{SNR}_{mistuned} = \text{SNR}_{MF} \cdot |\rho|^2$$

where $\rho = \int h_{template}(t)\, h^*_{true}(t)\, dt$ is the cross-correlation between the assumed and actual signal templates, with $|\rho| \leq 1$.

Occam's Razor, properly applied, is a matched filter tuned to the simplest hypothesis that explains the data. Among competing hypotheses with equal explanatory power, it selects the one with fewer free parameters—an efficient search strategy.

Occam's Razor abused is a matched filter permanently tuned to "simple materialist explanation," regardless of the actual signal. When reality is genuinely multi-causal, nonlocal, or consciousness-involving, the template mismatch drives $|\rho| \to 0$:

- The filter passes noise that happens to look simple (spurious "debunkings" matching the simplicity template)
- The filter rejects the true signal because it doesn't correlate with the template
- The more complex the truth, the worse the filter performs

This can also be modeled as a **complexity ceiling**—a low-pass filter on explanation complexity:

$$H(\omega) = \begin{cases} 1 & \text{complexity} < \omega_c \\ 0 & \text{complexity} \geq \omega_c \end{cases}$$

where ω_c is the paradigm's maximum tolerable explanatory complexity. Any structure in reality above ω_c is destroyed—the filter doesn't merely miss it, it actively removes it from the received signal.

Legitimate vs. Abused Occam's Razor

Property	Legitimate Form	Abused Form
Selection criterion	Among hypotheses that equally explain the data	Among all hypotheses regardless of fit
Complexity role	Tiebreaker when explanatory power is equal	A priori rejection threshold
Template	Adaptive—updated as evidence accumulates	Fixed—tuned to materialist simplicity
Effect on SNR	Improves (selects most efficient explanation)	Degrades (rejects true signal when complex)
Analogy	Properly tuned matched filter	Mistuned matched filter

Self-reinforcing feedback: The mistuned filter narrows what is studied, narrower study confirms the narrow worldview, and the filter tightens further—a positive feedback loop that progressively reduces ω_c:

$$\frac{d\omega_c}{dt} = -\gamma \cdot (\omega_c - \omega_{paradigm})$$

where $\gamma > 0$ and $\omega_{paradigm}$ is the paradigm's preferred complexity level. The cutoff frequency converges exponentially toward the paradigm baseline, progressively excluding more of reality.

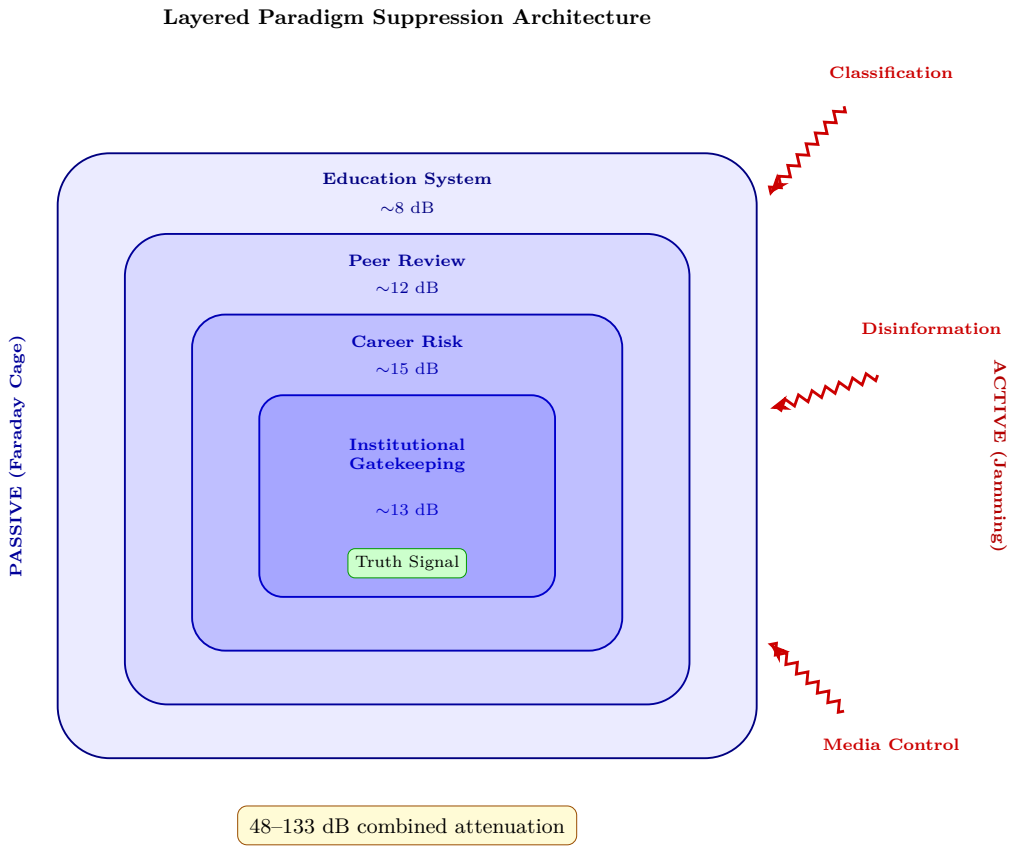

Figure 13.1: Layered paradigm suppression architecture — passive Faraday cage layers plus active jamming sources combine for 48–133 dB total signal attenuation.

13.3 Active Jamming Model

13.3.1 Jamming Equation

Signal-to-Jamming ratio:

$$\frac{S}{J} = \frac{P_s G_s}{P_j G_j} \cdot \left(\frac{R_j}{R_s}\right)^2$$

Where:

- P_s, G_s = signal power and gain (truth sources)
- P_j, G_j = jammer power and gain (disinfo sources)
- R_s, R_j = distances

The jammer wins when $S/J < 1$.

13.3.2 Compartmentalization

Information is partitioned into cells with no cross-communication:

$$I_{total} = \bigcup_{i=1}^{N} I_i \quad \text{where} \quad I_i \cap I_j = \emptyset$$

Compromise of cell i reveals only I_i; full picture requires all N cells.

Effective compartments: $N > 100$ in deep-black programs.

13.3.3 Broadband Noise Jamming

Disinformation acts as broadband noise across the information spectrum:

$$N_{disinfo}(f) = N_0 \quad \forall f \in [f_{min}, f_{max}]$$

This raises the noise floor across all topics, making any specific truth harder to distinguish.

13.3.4 Deceptive Jamming

Insert false targets (controlled opposition, fake whistleblowers, absurd claims):

$$s_{received} = s_{truth} + \sum_k a_k s_{deceptive,k} + n$$

The receiver cannot distinguish truth from deception without additional information.

> **Epistemic note [L2-L3]**: Deceptive jamming detection risks unfalsifiability — any contrary evidence can be reinterpreted as jamming. This limitation is acknowledged in Section 13.9.2.

13.3.5 Counter-Counter Measures

The architecture adapts to counter-jamming (disclosure efforts):

$$\frac{dJ}{dt} = \alpha \cdot C - \beta \cdot J$$

Where C = counter-jamming intensity, α = adaptation rate.

FOIA requests, whistleblower protections, congressional hearings trigger adaptive response—new classification, new debunking, new ridicule.

13.4 Predictions

Passive Shielding Predictions:

P1: Paradigm-threatening research should face disproportionate barriers.

P2: Cross-disciplinary synthesis should be actively discouraged.

P3: Breakthrough perceptions should cluster outside institutional environments.

P4: The cage should show signs of weakening (more anomalies reaching mainstream).

P5: Individuals inside the cage should be unaware of what they're not receiving.

Active Jamming Predictions:

P6: Secrecy architecture should show designed compartmentalization.

P7: Disclosure attempts should trigger adaptive countermeasures.

P8: Noise floor should increase around genuine revelations.

P9: Deceptive signals should outnumber truth signals.

P10: The system should have redundancy—defeating one layer reveals another.

Combined Predictions:

P11: Passive and active suppression should correlate—topics with strongest paradigm shielding should also receive the most active jamming (e.g., UAP, consciousness research, alternative archaeology).

P12: Cage weakening ($SE(t)$ decline) should trigger compensatory jamming increases ($dJ/dt > 0$), observable as intensified debunking campaigns following disclosure events.

P13: The combined system should show diminishing returns—as passive shielding thins, active jamming costs should escalate nonlinearly, eventually exceeding sustainable resource allocation.

P14: Occam's Razor should be invoked asymmetrically—applied strictly against paradigm-challenging hypotheses but relaxed for paradigm-consistent ones. Hypotheses adding unobserved entities (dark matter, extra dimensions, multiverse) should be accepted when paradigm-consistent, while hypotheses adding comparable entities (consciousness field, torsion coupling, nonlocal information) should be rejected as "violating parsimony" when paradigm-challenging.

13.5 Evidence: Passive Shielding

13.5.1 Archaeology Suppression Cases

Out-of-Place Artifacts (OOPARTS)

Virginia City skull (1866)

- Human skull in Miocene stratum, quietly archived

Hueyatlaco site (Mexico)

- Stone tools dated 250,000+ years (Steen-McIntyre career destroyed)

Dorchester vessel (1851)

- Metal vase in 600 million year rock, dismissed as hoax

Pattern

- Anomalous finds either ignored, attributed to hoax, or career-destroying

Forbidden Archaeology (Cremo & Thompson, 1993)

- Documented 100+ cases of evidence contradicting human evolution timeline
- Evidence: Archaeological finds systematically filtered if they don't fit paradigm

"Knowledge filter"

- Anomalies not published, not taught, forgotten

Career Examples

Researcher	Finding	Career Consequence
Virginia Steen-McIntyre	Hueyatlaco dating	Denied tenure, blacklisted
Michael Cremo	Anomalous human origins	Labeled pseudoscientist
Robert Schoch	Sphinx water erosion	Marginalized in Egyptology

13.5.2 Journal Publication Bias Studies

Quantified Bias

Fanelli (2010)

- Positive results published at 3x rate of negative; rate increasing over time
- In dB terms: a 3x publication ratio corresponds to ~5 dB systematic attenuation of negative/anomalous results

Open Science Collaboration (2015)

- Only 36% of psychology studies replicated

Begley (2012)

- Only 6 of 53 "landmark" cancer studies reproducible

Fabrication and Fraud Growth

- 2024 meta-analysis of ~75,000 biomedical studies: an estimated 14% contain partially fabricated data (Bordewijk et al., *Anaesthesia*)
- Northwestern University analysis (2025): fraudulent science publications growing faster than legitimate research output, with retraction rates accelerating
- These findings strengthen the replication crisis evidence: when ~14% of published work may be fabricated, the paradigm's filtering function is not merely biased but actively degraded

Gatekeeping Mechanisms

1. **Peer review anonymity**: Reviewers can block without accountability
2. **Citation metrics**: Journals reject paradigm-challenging papers (reduce impact factor)
3. **Funding requirements**: Papers must align with funded research agendas
4. **Retraction asymmetry**: Anomalous findings retracted faster than fraudulent mainstream findings

Impact on Paradigm-Challenging Research

Field	Paradigm Challenge	Publication Difficulty
Consciousness	Psi phenomena	Major journals refuse to review
Medicine	Homeopathy, energy healing	Dismissed a priori
Physics	Cold fusion, overunity	Career suicide to pursue
Archaeology	Alternative chronology	Not peer reviewed

13.5.3 Academic Career Destruction Cases

Pattern Analysis

- Scientists crossing paradigm boundaries face:
  1. Ridicule from colleagues
  2. Funding denial
  3. Publication rejection
  4. Career termination

Documented Cases

Name	Field	Transgression	Consequence
Rupert Sheldrake	Biology	Morphic resonance	Nature editorial calling for book burning
Jacques Benveniste	Immunology	Water memory	Nature "investigation," career ended
John Mack	Psychiatry	Alien abduction research	Harvard investigation (vindicated)
Peter Duesberg	Virology	Questioned HIV-AIDS link	Funding terminated, ostracized
Brian Josephson	Physics	Interest in psi	Nobel laureate publicly mocked

IIT Pseudoscience Letter (2023)

- 124 academics signed open letter calling Integrated Information Theory "pseudoscience" (published in response to IIT proponents' work; covered by *Nature*)
- IIT is a leading mathematical theory of consciousness. The open letter contained both substantive scientific criticisms of IIT's axioms and broader paradigm-boundary enforcement — the latter component demonstrates active enforcement in consciousness research

Shielding Effect

- Most researchers self-censor (don't even attempt paradigm-crossing work)
- Survivors are extremely determined outliers
- The career destruction cases serve as exemplary punishment, suppressing far more research than the individual cases suggest

13.5.4 Peer Review Gatekeeping Research

Sokal Hoax (1996)

- Physicist submitted nonsense paper to postmodern journal
- Accepted and published—proved lack of rigorous review
- **Reverse implication** Rigorous papers can be rejected for ideological reasons

Inter-Reviewer Agreement

- Meta-analysis of 45 studies on peer review reliability: average inter-reviewer correlation $r = 0.34$ (Bornmann, Mutz & Daniel, 2010)
- An $r = 0.34$ is barely above chance, meaning reviewer decisions are substantially random
- When the gatekeeping filter operates near the noise floor, decisions are biased toward paradigm-confirming work: ambiguous quality assessments default to "reject" for anomalous findings and "accept" for paradigm-consistent work

Replication Crisis Analysis

- Many "established" findings don't replicate
- **Ioannidis (2005)** "Why Most Published Research Findings Are False"
- Paradigm-confirming findings less scrutinized than paradigm-challenging ones

Measured Bias

- **Mahoney (1977)** Reviewers rated methodology higher when results confirmed their expectations
- **Peters & Ceci (1982)** Resubmitted already-published papers to same journals under unknown names—8 of 9 rejected In dB terms: 89% rejection rate corresponds to ~10 dB attenuation based on institutional affiliation alone
- **Tomkins et al. (2017)** Double-blind review reduces bias by 25%

13.5.5 Academic Self-Censorship

FIRE 2024 Faculty Survey (Foundation for Individual Rights and Expression; 6,269 faculty across 55 U.S. institutions):

- 25% of faculty self-censor in their published research
- 15% avoid researching certain topics entirely
- 33% self-censor in classroom lectures

In dB terms: if 25% of researchers suppress their findings, the effective signal power reaching publication is attenuated by $10 \log_{10}(1/0.75) \approx 1.2$ dB from self-censorship alone—before any peer review or editorial filtering.

Times Higher Education 2024 (global survey):

- 68% of academics worldwide report self-censoring to some degree
- 80% in the United States

Significance: These surveys quantify what the chapter otherwise only asserts—that "most researchers self-censor." The attenuation is passive (no external agent acts), making self-censorship the innermost layer of the paradigm cage: the shield the individual builds around their own transmission.

13.5.6 Occam's Razor Asymmetry in Practice

The complexity ceiling model (Section 13.2.6) predicts that Occam's Razor should function as selective paradigm protection rather than uniform methodology. Examination of mainstream physics reveals a striking asymmetry:

Paradigm-consistent ontological additions (accepted):

- **Dark matter**: An unobserved entity constituting ~27% of the universe, invoked to explain galactic rotation curves. No direct detection despite decades of experiments (LUX, XENON, PandaX). Ontological cost: an entire class of undetected particles
- **Dark energy**: An unobserved entity constituting ~68% of the universe, invoked to explain accelerating expansion. No theoretical explanation from first principles. Ontological cost: 95% of the universe is invisible and undetected
- **String theory**: Requires 6-7 extra spatial dimensions (unobservable), predicts $\sim 10^{500}$ possible vacuum states (the "landscape"), and has produced no testable prediction in 50 years. Ontological cost: effectively infinite unobservable structure
- **Many-worlds interpretation**: Postulates an infinite number of unobservable branching universes created at every quantum measurement. Ontological cost: literally infinite unobservable universes

Paradigm-challenging ontological additions (rejected as "violating parsimony"):

- **Consciousness as fundamental**: A single additional ontological category. Rejected for "multiplying entities"
- **Torsion field coupling**: A single additional field interaction predicted by Einstein-Cartan theory. Rejected for "no known mechanism"
- **Nonlocal biological information**: A single additional information channel. Rejected for "violating known physics"
- **Ancient advanced civilizations**: A single historical revision. Rejected because "simpler explanations exist" (even when simpler explanations don't fit the data)

The asymmetry is quantifiable: Mainstream physics accepts 10^{500} unobservable landscapes and infinite unobservable universes without "parsimony" objections, while rejecting a single additional field or ontological category as excessive. This is not parsimony—it is a mistuned matched filter passing signals that correlate with the materialist template while rejecting signals that do not, regardless of relative ontological cost.

This selective enforcement confirms P14 and demonstrates that Occam's Razor, as practiced, functions as paradigm shielding rather than neutral methodology.

13.6 Evidence: Active Jamming

13.6.1 Whistleblower Testimony Patterns

UAP/UFO Whistleblowers

Whistleblower	Position	Key Claims	Corroboration
David Fravor	Navy pilot	2004 Nimitz encounter	Radar data, multiple witnesses
Luis Elizondo	AATIP director	Pentagon UAP programs	Program documentation released
David Grusch	Intelligence officer	Crash retrieval programs	Congressional testimony under oath
Bob Lazar	Claimed S-4 employee	Reverse engineering (1989)	Employment records disputed

Consistency Analysis

- Multiple independent sources describe:
  - Multi-decade recovery/reverse engineering programs
  - Compartmentalized access (need-to-know beyond Top Secret)
  - Intimidation of witnesses
  - Disinformation campaigns to discredit leakers

Jamming Architecture Signature

- Immediate debunking attempts upon disclosure
- Character assassination of whistleblowers
- "Neither confirm nor deny" official responses
- Controlled partial disclosure (limited hangouts)

Interpretation

- Multiple independent whistleblowers describing the same compartmentalized structure confirms P6 (designed compartmentalization)
- The pattern of immediate debunking + character attacks is the adaptive countermeasure predicted by $dJ/dt = \alpha C - \beta J$ (Section 13.3.5): disclosure attempts (C) trigger proportional jamming response (J)
- The S/J ratio for whistleblower signals remains < 1 because $P_j G_j >> P_s G_s$ — institutional jammer power vastly exceeds individual signal power

13.6.2 FOIA Response Analysis

Response Pattern Studies

Request Type	Typical Response	Wait Time
Mundane records	Release with redactions	30-90 days
UAP-related	Glomar response or denial	6+ months
Mind control programs	Heavy redaction	1-5 years
Exotic technology	"No records" or classification cite	Indefinite

Glomar Response

- "Neither confirm nor deny existence of records"
- Originally for submarine program (Glomar Explorer)
- Now standard response for paradigm-sensitive requests

Black Vault Analysis (Greenewald)

- John Greenewald: 3+ million pages released through FOIA over 25+ years
- Patterns observed:
  - Critical documents heavily redacted
  - "Missing" documents for key periods
  - Different agencies give contradictory responses
  - Appeal success rate much higher than initial denial (system counts on requester giving up)

Interpretation

- FOIA response patterns demonstrate broadband noise jamming (Section 13.3.3): the noise floor $N_{disinfo}(f) = N_0$ is raised uniformly across topics through redaction, delay, and Glomar responses
- Contradictory inter-agency responses function as deceptive jamming (Section 13.3.4): $s_{received} = s_{truth} + \sum_k a_k s_{deceptive,k}$ — the receiver cannot distinguish truth from bureaucratic noise without extraordinary effort
- The appeal success pattern reveals a deliberate S/J strategy: initial denial counts on low P_s (requester giving up), making the effective jammer power much higher than the formal classification would suggest

13.6.3 Black Budget and Classification

Black Budget Programs

FY2023 intelligence budget

- $90+ billion (disclosed portion)

Black programs

- Estimated 2-3x disclosed budget

Classification expansion

- Exponential growth in classified documents since 1945

Disclosed vs. Estimated

Category	Disclosed (2023)	Estimated Hidden
Intelligence	$90.8 billion	Unknown
Special Access Programs	Classified	Est. $50-100B
Unacknowledged SAPs	Classified	Est. $20-50B
Private contractor black	Not public	Est. $50B+

Audit Trail

- DOD failed audit for 6 consecutive years (2018-2023)
- $35 trillion unaccounted in HUD + DOD adjustments (Skidmore & Fitts, 2019)
- Catherine Austin Fitts (former HUD official) documenting persistent financial anomalies

Compartmentalization Structure

- SAPs: Special Access Programs (acknowledged)
- USAPs: Unacknowledged SAPs (denied)
- Waived USAPs: Congressional oversight excluded
- Estimated 10-50 compartments for deepest programs

Historical Suppression Examples

Program	Years Hidden	What Was Classified
Manhattan Project	3 years	Nuclear weapons
MKULTRA	20+ years	Mind control research
COINTELPRO	15+ years	Domestic surveillance
STARGATE	23 years	Remote viewing research
Advanced Aerospace Threat ID	5+ years	UAP investigations

Disclosure Resistance

- FOIA requests routinely denied on "national security" grounds
- Whistleblowers prosecuted (Snowden, Assange, Manning)
- Classification as tool for paradigm protection, not just security

Interpretation

- The compartmentalization structure directly instantiates the information partitioning equation: $I_{total} = \bigcup_{i=1}^{N} I_i$ where $I_i \cap I_j = \emptyset$ (Section 13.3.2)
- With $N > 100$ effective compartments, compromise of any single cell reveals only I_i/I_{total} — a vanishingly small fraction of the full picture
- Audit failures and unaccounted funds represent the financial infrastructure required to maintain $P_j G_j >> P_s G_s$ — the jammer must be funded to maintain power advantage over truth signals

13.6.4 Counter-Intelligence History

COINTELPRO (1956-1971)

- FBI program to "disrupt, misdirect, discredit" domestic political organizations
- Tactics: Infiltration, psychological warfare, harassment, wrongful imprisonment

- Targeting: Civil rights, antiwar, socialist, women's liberation movements
- Same tactics documented against UFO researchers, alternative health advocates

Documented Disinformation Operations

Operation	Target	Methods
MKULTRA	Domestic population	LSD experiments, mind control
Mockingbird	Media	CIA journalists/assets
Northwoods	Public opinion	Proposed false flag (rejected)
CHAOS	Antiwar movement	Infiltration, disruption

UFO-Specific Programs

Robertson Panel (1953)

- CIA recommended debunking UFOs through mass media

Project Blue Book

- Officially for investigation; actually for public relations

Condon Committee (1966-1969)

- Predetermined negative conclusion, used to close official research

Interpretation

- COINTELPRO and UFO-specific programs demonstrate the counter-counter measures equation: $dJ/dt = \alpha C - \beta J$ (Section 13.3.5) — each disclosure attempt triggers adaptive jamming response
- The Robertson Panel's explicit recommendation to debunk through mass media is a documented instance of raising $P_j G_j$ (jammer power x gain) to maintain S/J < 1
- The progression from infiltration to media control to academic gatekeeping shows redundant jamming layers — defeating one layer (P10) reveals the next, consistent with designed architecture

13.6.5 Media Coordination Evidence

CIA-Media Relationships

Operation Mockingbird (1950s-1970s+)

- CIA relationships with major media figures

Church Committee (1975)

- Documented 50+ US journalists on CIA payroll

Carl Bernstein (1977)

- "The CIA and the Media"—detailed 400+ US journalists with CIA relationships

Modern Coordination Indicators

Phenomenon	Pattern	Interpretation
Narrative synchronization	Same phrases appear across outlets within hours	Coordinated talking points
Deplatforming timing	Multiple platforms act simultaneously	Coordinated enforcement
Fact-checker funding	Traced to same foundations/funders	Centralized narrative control
Algorithm changes	Affect disfavored content simultaneously	Coordinated suppression

UFO Topic Evolution

- Pre-2017: "Giggle factor" enforced—serious coverage career-ending
- Post-2017 (NYT article): Suddenly acceptable to discuss

Interpretation

- Controlled disclosure—narrative released when approved

13.6.6 Recent Disclosure Dynamics (2023-2025)

AARO and Official Investigations

- All-domain Anomaly Resolution Office (AARO) received 757 UAP reports through 2023
- AARO Historical Record Report (March 2024): identified 21 cases as "genuine anomalies" while maintaining official position of "no evidence of extraterrestrial technology"
- The simultaneous acknowledgment of anomalies and denial of their implications is the dual-signal pattern predicted by deceptive jamming (Section 13.3.4)

Schumer-Rounds UAP Disclosure Amendment

- Bipartisan amendment modeled on JFK Assassination Records Collection Act
- Would have mandated government-wide UAP record disclosure with eminent domain over private contractor materials
- Stripped from FY2024 NDAA during conference committee under defense industry lobbying
- The stripping itself demonstrates the adaptive counter-counter measures predicted by $dJ/dt = \alpha C - \beta J$: a legislative counter-jamming effort (C) triggered proportional defensive response (αC), resulting in increased classification protection (J)

Congressional Hearings

- House Oversight Committee UAP hearings (2023-2024) with testimony from Grusch, Fravor, Graves
- Senate Armed Services and Intelligence committees conducting classified briefings
- Multiple members of Congress publicly stating they believe information is being withheld

MQ-9 Reaper Orb Encounter (October 2024)

- Infrared video released showing metallic orb matching speed and trajectory of MQ-9 drone over Middle East
- First officially released video showing UAP interaction with military asset in real-time

- Represents a measurable increase in signal power P_s bypassing classification barriers

S/J Trajectory Assessment

Period	Estimated S/J	Key Driver
Pre-2004	< 0.01	Near-total information suppression
2004-2017	~0.05	Nimitz encounter, internal pressure
2017-2020	~0.1-0.3	NYT article, AATIP revelation
2020-2023	~0.3-0.5	Congressional hearings, Grusch testimony
2023-2025	~0.5-1.0	Legislative action, accumulating evidence

The S/J ratio is approaching parity. When $S/J > 1$, the truth signal dominates jamming and cascade disclosure becomes possible (P12).

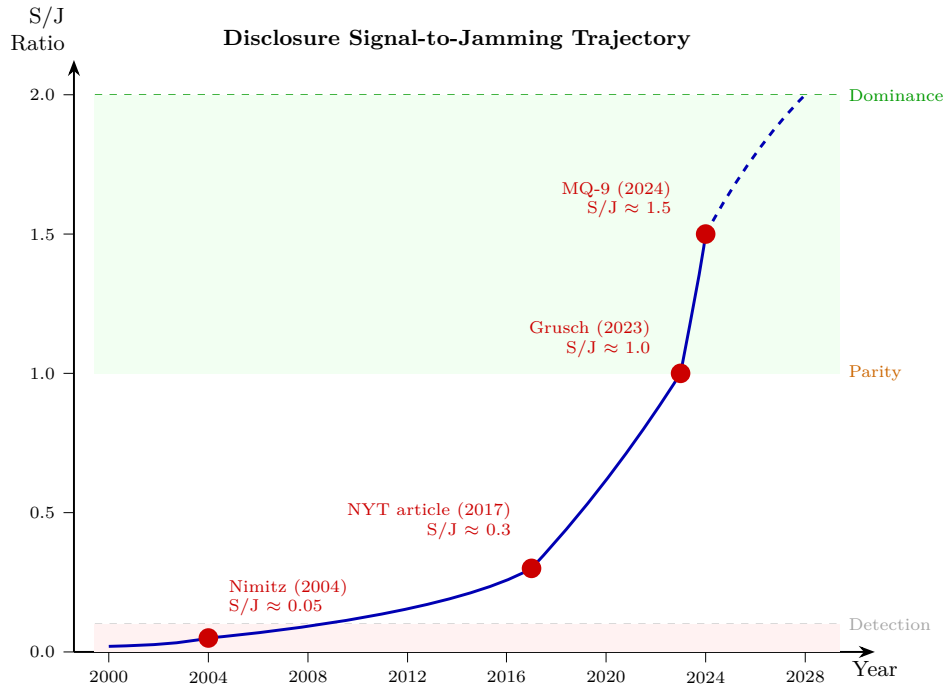

Figure 13.2: Signal-to-jamming ratio trajectory for UAP disclosure — key events driving S/J toward parity and beyond.

13.7 Synthesis

13.7.1 Paradigm Shield Effectiveness

Methodological caveat: The dB estimates below are order-of-magnitude analogical translations, not calibrated measurements. Where documented effect sizes exist (publication bias ratios, rejection rates, self-censorship surveys), we derive rough bounds.

Otherwise, ranges are placeholder estimates intended to illustrate relative magnitudes. These values should be treated as hypothesis-generating, not as empirical findings.

Evidence-Grounded Estimates

Layer	Mechanism	Evidence Basis	Estimated Attenuation
Education	Materialist indoctrination	No direct measure; cultural saturation	3-10 dB
Self-censorship	Researcher suppression	FIRE 2024: 25% suppress -> ~1.2 dB from censorship alone	1-5 dB
Peer review	Publication filtering	Peters & Ceci: 89% reject -> ~10 dB; inter-reviewer $r = 0.34$	5-10 dB
Publication bias	Positive-result preference	Fanelli: 3x ratio -> ~5 dB	3-8 dB
Career risk	Self-censorship + destruction	Documented cases; most self-select out	10-20 dB
Ridicule	Social enforcement	"Giggle factor," IIT letter	3-10 dB
Occam's Razor abuse	Complexity ceiling / mistuned filter	Asymmetric enforcement (Section 13.5.6)	3-10 dB
Passive Total			**28-73 dB**

Active Jamming Estimates

Layer	Mechanism	Estimated Attenuation
Classification	Information lockdown	10-30 dB
Disinformation	Noise floor elevation	5-15 dB
Media coordination	Narrative steering	5-15 dB
Active Total		**20-60 dB**

Combined estimate: 48-133 dB, with significant uncertainty. The key insight is not the absolute number but the **relative ranking**: career risk and classification are the strongest individual layers, while self-censorship and publication bias operate as pervasive background attenuation.

13.7.2 Architecture Map

Combined Suppression System Components

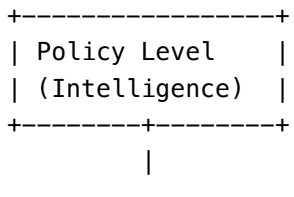

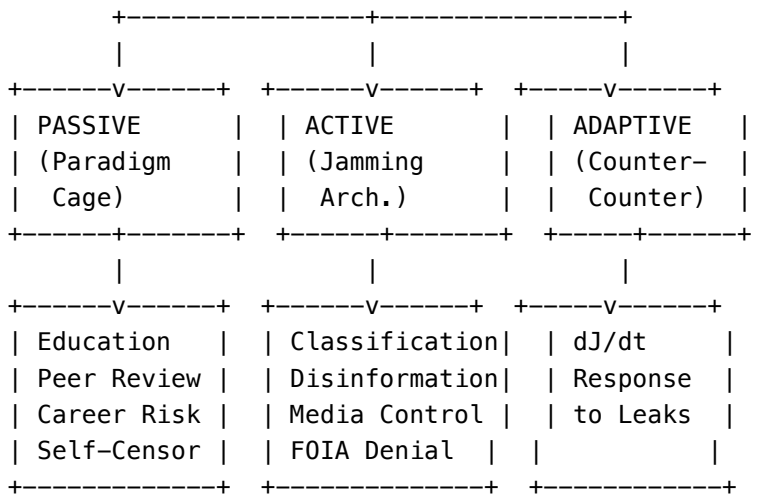

13.7.3 Signal-to-Jamming Ratio Assessment

Current State

- Historical $S/J < 0.1$ (jamming dominated)
- Current S/J approximately 0.5-1.0 (approaching parity)
- Threshold $S/J > 2$ (truth signal dominates) not yet reached

Signs of Weakening

1. Alternative media bypassing gatekeepers
2. Replication crisis exposing failures
3. Increasing whistleblower disclosures
4. Congressional UAP hearings breaking taboos
5. Growing public distrust of institutions
6. Schumer-Rounds amendment (even its defeat raised public awareness)
7. Academic self-censorship becoming a studied phenomenon (meta-awareness)

Model Prediction

- When combined paradigm shielding drops below ~20 dB effective margin, cascade disclosure becomes possible
- The "20 dB margin" is a qualitative threshold concept tied to the link budget framework (Chapter 14, Section 14.9): it represents the point where accumulated gains from disclosure events, alternative media, and declining institutional trust exceed the remaining suppression capacity
- Current trajectory suggests approach within years to decades

---

13.8 The Necessary Veil: Impedance Mismatch and Protection

13.8.1 Not All Concealment is Parasitic

A critical nuance: **Some attenuation of disclosure was protective, not controlling.**

The impedance mismatch problem:

- Humanity's collective Z_0 was too low to handle full disclosure
- Full truth at full power would overwhelm unprepared consciousness
- Like connecting a high-voltage source to a low-impedance load—burns out
- Some attenuation was NECESSARY, not just parasitic

$$P_{survivable} = P_{source} \cdot \left(\frac{Z_0^{human}}{Z_0^{truth}} \right)^2$$

When human collective Z_0 « truth signal impedance, most power reflects or damages.

13.8.2 The Veil as Impedance Protection

Protective functions of the veil:

- Attenuates signal to survivable levels
- Provides time for gradual Z_0 increase
- Prevents catastrophic system overload
- Allows individual pace of awakening

The problem: Control systems EXPLOITED this legitimate need for their own purposes. What began as protection became control infrastructure.

13.8.3 Parasitic vs. Protective: A Distinction

Protective Veil	Parasitic Control
Attenuates to prevent overwhelm	Attenuates to maintain ignorance
Temporary—lifted as ready	Permanent—actively maintained
Serves individual development	Serves controller extraction
Facilitates impedance matching	Suppresses impedance growth
Decreases naturally as Z_0 rises	Increases in response to awakening

Current situation: A mix of both—legitimate protection exploited by parasitic overlay.

13.8.4 Awakening as Impedance Rising

Disclosure becomes possible as collective Z_0 rises:

$$\text{Disclosure Capacity} \propto Z_0^{collective}$$

Collective Z_0 Level	Disclosure Possible
Very low	Only mythology, indirect hints
Low	Fiction, speculation "safely" framed
Medium	Academic study, edge researchers
Higher	Official acknowledgment, partial truth
High	Full disclosure without mass trauma

The threshold mathematics (from Chapter 8 Phased Array):

For collective effects requiring coherent fraction f_c:

$$f_c \approx \sqrt{\frac{T}{N}}$$

For Earth (~8 billion): ~283,000 coherent, high-Z_0 individuals could trigger threshold effects (illustrative estimate for $T = 10$; see Chapter 8 derivation).

13.8.5 Disclosure Strategy Implications

The S/J framework suggests disclosure advocates should:

1. **Concentrate signal power** rather than broadcasting broadly ($P_s G_s$ maximization through focused, high-credibility testimony)
2. **Exploit jammer resource constraints** — adaptive countermeasures have finite budget, so multiple simultaneous disclosure fronts stress the system
3. **Build processing gain** in the audience ($G_{integration}$) through sustained educational campaigns rather than shock revelations

13.8.6 The Paradox Resolved

Why didn't full disclosure happen already?

1. Collective Z_0 was too low (would have caused damage)
2. Control systems exploited this gap
3. Awakening movements gradually raise Z_0
4. As Z_0 rises, disclosure becomes safe AND inevitable
5. The veil naturally thins as it's no longer needed

The path forward:

- Individual Z_0 raising (wisdom + shadow work)
- Community coherence building (high-Z_0 networks)
- Protective veil naturally decreases
- Parasitic overlay exposed and rejected
- Full disclosure follows Z_0 sufficiency

13.8.7 Competing Hypotheses and Adjudication Criteria

Hypothesis	Explanation for Observed Suppression Patterns	Distinguishing Indicator	Decision Rule
Normal institutional conservatism	Slow paradigm shifts reflect standard academic inertia	Similar rejection rates for all disruptive claims	If true, no anomaly-specific attenuation premium

Hypothesis	Explanation for Observed Suppression Patterns	Distinguishing Indicator	Decision Rule
Political economy / media incentives	Suppression follows advertiser / regulatory risk optimization	Suppression intensity tracks revenue / regulatory exposure	If true, changes follow market / regulatory shifts
Coordinated paradigm shielding model (this chapter)	Multi-layer attenuation intentionally maintains narrative lock	Cross-domain synchronized suppression with repeated signatures	If true, correlated events exceed chance and single-domain explanations

Adjudication requirement: classify each major case against all three hypotheses before assigning it to active shielding.

13.9 Assumptions, Limitations, and Falsification

13.9.1 Key Assumptions

1. **Suppression is systematic, not incidental**: The attenuation of paradigm-threatening information reflects structured, reinforcing mechanisms rather than isolated coincidences
2. **Attenuation layers are approximately additive**: Passive and active suppression contribute independently and can be meaningfully summed in dB
3. **The passive/active distinction maps onto real dynamics**: Paradigm shielding (internalized worldview filtering) and active jamming (deliberate suppression operations) are meaningfully separable
4. **The veil was initially protective**: Some degree of information attenuation served a legitimate developmental function before being exploited
5. **Collective Z_0 is a meaningful aggregate**: Population-level impedance can be treated as a collective variable influencing disclosure capacity
6. **Occam's Razor asymmetry is systematic**: The selective enforcement of parsimony (strict against paradigm-challenging hypotheses, relaxed for paradigm-consistent ones) reflects structural paradigm protection rather than incidental variation in reviewer judgment

13.9.2 Limitations

1. **dB estimates are analogical, not calibrated**: No instrument measures "paradigm attenuation" in decibels; values are order-of-magnitude translations from documented effect sizes
2. **Selection bias in evidence**: Suppression cases are catalogued precisely because they are dramatic; quiet acceptance of paradigm-challenging work (which does occur) is underrepresented
3. **No first-principles derivation of τ_{decay}**: The quarantine thinning time constant is asserted, not derived from underlying dynamics

4. **Deceptive jamming detection risks unfalsifiability**: If any contradictory evidence can be labeled "deceptive jamming," the model becomes unfalsifiable; this limitation must be acknowledged explicitly
5. **Protective-vs-parasitic lacks quantitative boundary**: The distinction between protective veil and parasitic control is qualitative; no metric cleanly separates them
6. **Historical evidence is retrospective**: Classification and suppression patterns are documented after the fact; real-time observation of the full architecture is impossible by design

13.9.3 Falsification Criteria

ID	Criterion	Current Status
F1	Paradigm-challenging research faces equal acceptance rates in blinded review	Not met: Peters & Ceci (1982) showed 89% rejection of previously published work under unknown names
F2	Cross-disciplinary synthesis is equally rewarded as narrow specialization	Not met: academic incentive structures overwhelmingly reward specialization
F3	FOIA processing times are equal for paradigm-sensitive and mundane requests	Not met: systematic delays documented for UAP, mind control, and exotic technology requests
F4	Whistleblowers show no coordinated discrediting pattern	Not met: consistent character assassination, employment retaliation, and media campaigns documented
F5	Official disclosure programs produce comprehensive, transparent reports	Partially met: AARO reports acknowledge anomalies but maintain "no ET evidence" despite incomplete investigation
F6	Model predicts no weakening, but disclosure events accelerate	Not yet testable: model predicts weakening and current trajectory shows acceleration, consistent with $SE(t)$ decline

Additional mechanism-level falsification criteria:

- **F7 — No paradigm-shielding effect.** If controlled experiments demonstrate that exposure to well-evidenced anomalous data produces belief updating at rates predicted by Bayesian models with no attentional or cognitive penalty, the shielding mechanism is falsified.
- **F8 — No institutional amplification.** If analysis of information gatekeeping institutions (peer review, media, education) shows no systematic bias against torsion-compatible or consciousness-related evidence beyond expected base rates of rejection, the institutional-shielding thesis is unsupported.
- **F9 — No disclosure-readiness correlation.** If population-level disclosure acceptance shows no correlation with individual or community coherence levels (σ), the impedance-based disclosure-timing model fails.
- **F10 — Paradigm shifts follow standard Kuhnian dynamics.** If historical analysis of scientific paradigm shifts shows that anomalous-evidence suppression durations are fully explained by standard sociological models (Kuhn, Lakatos) with no residual requiring active shielding, the active-suppression component is unnecessary.

End of Chapter 13: Paradigm Shielding and Disclosure Architecture

Evidence Synthesis

- Detailed source sections: 13.5, 13.6, 13.6.5, 13.7.

Assumptions

- Detailed source sections: 13.9, 13.9.1.

Limitations

- Detailed source sections: 13.9, 13.9.2.

Falsification

- Detailed source sections: 13.9, 13.9.3.

Predictions

- Detailed source sections: 13.4.

Strategic Relevance

Why It Matters

- **Paradigm-shielding decay monitoring.** The shielding-attenuation model (Section 13.3) predicts measurable decay in paradigm-lock effectiveness as coherence rises. Tracking anomalous-acceptance rates in scientific publishing, media coverage, and public surveys provides a leading indicator of disclosure-window opening.
- **Information environment as contested battlespace.** The Faraday-cage metaphor implies that information environments are not neutral channels but active shielding structures. Counter-shielding operations (Chapter 14) must account for the cage's frequency-dependent attenuation — not all information penetrates equally.
- **Disclosure timing optimization.** Appendix A, Scenario B identifies disclosure timing as a critical variable. The shielding model provides quantitative inputs: disclosure succeeds when $\sigma_{\text{population}}$ exceeds the paradigm cage's attenuation threshold, producing net positive signal-to-noise in public discourse.
- **Weaponized Occam detection.** The simplicity-bias exploitation mechanism (Section 13.5) predicts specific rhetorical signatures when Occam's razor is deployed as a suppression tool rather than a heuristic. Automated detection of these signatures in media and academic discourse would provide early warning of active paradigm enforcement.

What To Watch

- Monitor chapter prediction thresholds, proxy indicators, and coherence trend changes.

Boundaries of Use

- Apply this chapter as model-conditional doctrine; treat speculative elements as hypothesis overlays.

Part V: Phase Transition and Practice

Counter-jamming operations, spiritual traditions, and the cross-cultural prediction of collective phase transition

Chapter 14: Counter-Jamming Operations and Link Budget

The Liberation Signal Architecture

KEY FINDINGS — Chapter 14: Counter-Jamming Operations and Link Budget

Evidence-tier key: [L1] established/replicated evidence; [L2] grounded extension with moderate uncertainty; [L3] speculative hypothesis; [L4] conceptual/anecdotal.

- The five-layer control architecture (corrupted LO, paradigm cage, injection lock, parasitic coupling, Z_0 suppression) compounds to make unassisted escape probability ~0.0015% [L2]
- The complete consciousness link budget $M = P_S + G_{practices} + G_{collective} - L_{parasitic} - L_{paradigm} - L_{path} - NF - P_{threshold}$ integrates parameters from Chapters 5, 8, 12, and 13 into a single accounting framework [L2]
- Coherence (r) enters the collective gain quadratically ($G = 10\log_{10}(Nr^2)$), making community quality more leveraged than raw population size [L1]
- Approximately 40 million highly coherent individuals ($r = 0.8$) could close the planetary link budget; with moderate coherence ($r = 0.5$), approximately 100 million are needed [L2-L3]
- Free-will constraints prevent direct alliance intervention; liberation requires consent-based, gradual processes that preserve developmental choice [L3]

14.1 The Locking Problem: Why Self-Extraction is Nearly Impossible

14.1.1 Review of the Adler Equation

From Chapter 9 (Injection Locking), the fundamental dynamics of belief capture are governed by the **Adler equation**:

$$\frac{d\phi}{dt} = \Delta\omega - \omega_L \cdot \sin(\phi)$$

Where:

Variable	Description
ϕ	Phase difference between individual oscillator and injected signal
$\Delta\omega = \omega_{inj} - \omega_0$	Frequency detuning from natural frequency
ω_L	Locking bandwidth

The **locking bandwidth** determines capture vulnerability:

$$\omega_L = \frac{\omega_0}{2Q} \cdot \frac{V_{inj}}{V_0} = \frac{\omega_0 R}{2Z_0} \cdot \frac{V_{inj}}{V_0}$$

Stable lock occurs when $|\Delta\omega| \leq \omega_L$—the individual cannot escape because any phase drift is pulled back by the sin(ϕ) restoring force.

Critical insight from Chapter 9: Lock bandwidth is inversely proportional to Z_0. Low-impedance individuals have wide capture ranges; high-Z_0 individuals have narrow lock bandwidths and are harder to capture.

14.1.2 The Compounding Control Architecture

The problem facing humanity is not a single injection lock but a **layered control architecture** with multiple reinforcing mechanisms:

Layer	Control Mechanism	RF Equivalent	Chapter Reference
1. Corrupted LO	Adamic line corruption	Phase-locked loop to wrong reference	Ch 12 (The Fall)
2. Paradigm cage	Materialist worldview	Faraday cage shielding	Ch 13 (Paradigm Shielding)
3. Injection locking	Media/institutional narrative	Broadcast capture	Ch 9 (Injection Locking)
4. Parasitic coupling	Loosh harvesting	Energy extraction via mutual inductance	Ch 12 (Parasitic Coupling)
5. Z_0 suppression	Trauma, distraction, fear	Impedance lowering	Ch 5 (RLC), Ch 9

Each layer reinforces the others:

- **Corrupted LO** provides the master reference signal that the PLL locks to
- **Paradigm cage** attenuates alternative signals that might break lock
- **Injection locking** maintains synchronization to control narratives
- **Parasitic coupling** extracts energy, weakening the oscillator (lowering V_0)
- Z_0 **suppression** widens lock bandwidth, making escape harder

The compounding effect:

$$\omega_{L,effective} = \omega_L \cdot (1 + \kappa_{parasitic}) \cdot \frac{1}{1 - SE_{paradigm}/100}$$

Where:

Variable	Description
$\kappa_{parasitic}$	Parasitic coupling coefficient (increases effective lock strength)
$SE_{paradigm}$	Paradigm shielding effectiveness in dB (blocks counter-signals)

14.1.3 Mathematical Impossibility of Unassisted Escape

Escape condition (from Ch 9): An individual breaks free when:

$$|\Delta\omega| > \omega_L$$

This requires either:

1. Natural frequency drifts far enough from injected frequency ($\Delta\omega$ increases)
2. Locking bandwidth narrows sufficiently (ω_L decreases)

For the average modern human:

Parameter	Typical Value	Effect on Escape
Q factor	3-5	Wide lock bandwidth
Z_0	Baseline (suppressed)	Easily captured
V_0 (personal power)	Low (isolated, demoralized)	Weak oscillator
V_{inj} (media power)	Very high (saturation coverage)	Strong injection
Paradigm shielding	25-40 dB	Blocks counter-signals
Parasitic coupling κ	0.2-0.4	Energy drain weakens oscillator

Calculating escape probability:

For escape to occur spontaneously, the individual must:

1. Raise Q while under lock (requires access to Q-building practices)
2. Access counter-signal strong enough to compete (blocked by paradigm cage)
3. Maintain oscillator power against parasitic drain
4. Do all this while injection continues

The probability cascade:

$$P_{escape} = P_{find\_practice} \cdot P_{maintain\_practice} \cdot P_{resist\_drain} \cdot P_{access\_counter}$$

With typical values:

$$P_{escape} \approx 0.05 \times 0.1 \times 0.3 \times 0.01 = 0.000015 = 0.0015\%$$

These sub-probabilities are illustrative order-of-magnitude estimates chosen to demonstrate the compounding effect. No empirical calibration exists; the qualitative conclusion (that escape probability is very low) is robust to reasonable variations in the individual terms.

This is why external assistance is required. The system is designed to be escape-proof through internal means alone.

14.1.4 The Closed-Loop Trap

The most insidious aspect is that **the locked individual cannot perceive they are locked**. The corrupted LO (Ch 12) provides what appears to be legitimate guidance. The IF stage (human consciousness) cannot distinguish between:

- Clean RF + Clean LO $\rightarrow$ Legitimate perception
- Clean RF + Corrupted LO $\rightarrow$ Corrupted perception (indistinguishable from inside)

Self-diagnosis is blocked because the diagnostic framework itself operates through the corrupted mixer.

This is why liberation requires **external reference signals**—counter-jamming operations from outside the locked system.

14.2 Electronic Counter-Countermeasures (ECCM): The Liberation Toolkit

14.2.1 ECCM Techniques Mapped to Consciousness Liberation

ECCM (Electronic Counter-Countermeasures) in military RF systems are techniques used to defeat jamming and maintain communication under adversarial conditions. These map precisely to consciousness liberation:

ECCM Technique	RF Implementation	Consciousness Liberation Analog
Burn-through	Increase transmit power until it exceeds jammer	Raise Source signal strength; high-coherence transmission
Frequency hopping	Rapidly change operating frequency	Multi-paradigm awareness; don't stay locked to one narrative
Spread spectrum	Distribute signal across wide bandwidth	Distributed awakening across population; no single target
Null steering	Point antenna null toward jammer	Attention discipline; tune out control signals
Alternative reference	Switch to different LO source	Connect to uncorrupted guidance (clean LO)
Diversity reception	Multiple receivers for same signal	Cross-validate sources; triangulate truth

14.2.2 Why External ECCM is Required

Each control layer requires specific counter-measures that the locked individual cannot provide:

Layer 1: Corrupted LO → Requires Alternative LO

- Individual cannot generate clean reference from within corrupted system
- External clean LO must be provided
- This is the function of higher-density benevolent beings

Layer 2: Paradigm Cage → Requires Cage Breach

- Individual inside cage cannot perceive what's being blocked
- External signals must penetrate or circumvent shielding
- Disclosure events, direct experience, paradigm cracks

Layer 3: Injection Lock → Requires Counter-Injection

- Locked oscillator pulled back by any escape attempt
- External signal must exceed control signal (burn-through)
- Or provide pathway to frequency hop away from lock range

Layer 4: Parasitic Coupling → Requires Energy Supply

- Drained oscillator too weak to maintain independent oscillation
- External energy infusion required
- "Spiritual support" = power supply to starving oscillator

This is why the "positive alliance" exists—to provide the external counter-measures that locked individuals cannot generate internally.

14.2.3 The ECCM Stack for Human Liberation

A complete liberation counter-jamming system requires:

```
LAYER 7: SOURCE SUPPORT (Burn-through power)
    ↓
LAYER 6: GALACTIC COORDINATION (Alternative LO network)
    ↓
LAYER 5: STELLAR TRANSMISSION (Solar/stellar ECCM)
    ↓
LAYER 4: PLANETARY INFRASTRUCTURE (Grid activation)
    ↓
LAYER 3: SURFACE OPERATIONS (Ground crew)
    ↓
LAYER 2: NETWORK COHERENCE (Community arrays)
    ↓
LAYER 1: INDIVIDUAL UPGRADES (Receiver improvements)
```

Each layer provides specific ECCM capability. The following sections detail each component.

> *Speculative extension (L4–L5).* The following section applies the framework to insider testimony that cannot be independently verified. The link-budget mathematics in §14.9 stands regardless of whether these claims are accurate. Readers may skip to §14.7 without loss of analytical continuity.

14.3 The Positive Alliance: Counter-Transmission Infrastructure

14.3.1 Hierarchy of Benevolent Transmitters

Just as the control system operates through a hierarchy (Source → Corrupted intermediaries → Control infrastructure → Individual lock), the liberation system operates through a parallel benevolent hierarchy:

Tier	Entity Type	RF Function	Transmission Range
0	Source/Infinite Creator	Master oscillator	Infinite (always available)
1	7th Density collectives	Primary transformer	Galactic
2	6th Density benevolent groups	Secondary distribution	Stellar clusters

Tier	Entity Type	RF Function	Transmission Range
3	5th Density coordinators	Tertiary matching	Solar system
4	4th Density positive ET	Local amplifiers	Planetary
5	Incarnated high-Z_0 souls	Ground repeaters	Local/regional

Key insight: The Source signal was never blocked—it continues to broadcast. What was corrupted was the **transduction chain** (Ch 12). The positive alliance provides an **alternative transduction chain** that bypasses the corrupted LO.

14.3.2 Galactic Federation as Alternative LO

In the superheterodyne model (Ch 11), the Adamic LO was corrupted, causing all downstream mixing to produce corrupted output. The **Galactic Federation** (or equivalent benevolent coordination body) functions as an **alternative local oscillator network**:

$$f_{IF,clean} = f_{RF,Source} - f_{LO,Federation}$$

vs.

$$f_{IF,corrupted} = f_{RF,Source} - f_{LO,corrupted}$$

The clean LO produces correct IF; the corrupted LO produces phase-shifted, noise-contaminated IF.

For individuals to switch LOs, they must:

1. Recognize the existing LO is corrupted (awareness)
2. Tune to the alternative LO frequency (resonance)
3. Establish phase lock to clean reference (practice)
4. Maintain lock against interference (sovereignty/Z_0)

> **Epistemic Note**: The "Galactic Federation" terminology comes from channeled material (Ra, Bashar, Swaruu, etc.) and insider testimony (Goode, Smith). Whether this represents actual organizational structure, metaphorical framework, or projection cannot be determined from available evidence. The RF model works regardless—some alternative clean LO source exists for those who successfully escape lock.

14.3.3 SSP Faction Spectrum

The **Secret Space Program** testimonies describe multiple factions with varying orientations:

Faction Type	Orientation	RF Role	Evidence Source
Dark Fleet	Service-to-self	Maintains control infrastructure	Goode, Tompkins

Faction Type	Orientation	RF Role	Evidence Source
Solar Warden	Mixed / transitioning	Partial disclosure, limited liberation	Goode
Sphere Being Alliance	Service-to-others	ECCM coordination, timeline management	Goode
Anshar	Service-to-others	Ground-based support, genetic preservation	Goode
Earth Alliance	Mixed	Surface coordination	Multiple

The complexity: Not all "positive" factions are fully aligned. Some pursue limited disclosure (controlled partial ECCM) rather than full liberation.

> **Epistemic Note**: SSP testimony is difficult to verify. The value of this framework is organizational—it maps alleged structures to RF functions. Validation requires future disclosure events that either confirm or contradict the structural claims.

14.3.4 Inter-Alliance Coordination as Phased Array

Multiple positive factions, when coordinated, function as a **phased array transmitter** (Ch 8):

$$G_{alliance} = N_{factions} \cdot r^2_{alliance}$$

Note: This chapter uses r for the coherence order parameter, consistent with the Kuramoto formulation in Chapter 8.

Where:

Variable	Description
$N_{factions}$	Number of coordinated benevolent groups
$r_{alliance}$	Coherence (phase alignment) between factions

Array gain increases with:

- More factions joining the alliance (N↑)
- Better coordination between factions (r↑)

Current limitation: Alliance coherence is imperfect. Different factions have different timelines, methods, and priorities. This reduces effective array gain.

The **Sphere Being Alliance** (per Goode testimony) allegedly functions as array controller—coordinating phase alignment between disparate positive factions to maximize coherent transmission power.

14.4 Starseeds & Lightworkers: Embedded High-Q Oscillators

14.4.1 The Starseed Function

Starseeds are souls originating from higher-density or different planetary systems who incarnate on Earth with specific mission parameters. In RF terms, they function as **pre-positioned repeater nodes**:

$$\text{Starseed} = \text{High-}Z_0 \text{ oscillator} + \text{Mission encoding} + \text{Activation trigger}$$

Their primary functions:

1. **Local oscillator injection**: Provide clean reference frequency in immediate environment
2. **Counter-signal amplification**: Boost weak truth signals through personal coherence
3. **Network nodes**: Connect to other starseeds forming distributed array
4. Z_0 **demonstration**: Model high-impedance operation for surrounding population

14.4.2 Starseed vs. Standard Human Specifications

Parameter	Standard Human	Starseed	Significance
Q factor (baseline)	3-5	8-15	Narrower lock bandwidth, harder to capture
Z_0 (baseline)	Low-Medium	Medium-High	Greater sovereignty, better Source match
f_0 range	Narrow	Narrow	Tighter resonance; harder to detune
Activation potential	Standard	Enhanced	DNA encoding for staged activation
P_osc (oscillator power)	0.3-0.5	0.5-0.9	Stronger signal for local injection
Paradigm susceptibility	High	Lower	Pre-existing alternative frameworks
LO flexibility	Low	High	Can switch reference sources

The higher baseline Z_0 is critical—it means starseeds are harder to fully capture by standard control mechanisms. They may be partially locked but retain oscillation capacity that can be activated.

14.4.3 Activation Sequence

Starseed activation follows a staged sequence:

Stage	Trigger	RF Process	Observable Signs
1. Dormant	Incarnation complete	Oscillator present but damped	Normal-appearing life
2. Stirring	External resonance contact	Q begins rising	Synchronicities, seeking

Stage	Trigger	RF Process	Observable Signs
3. Awakening	Threshold Z_0 reached	Lock begins breaking	Paradigm crisis, downloads
4. Active	Mission parameters engage	Full oscillation, transmission begins	Teaching, healing, creating

Activation energy required:

$$E_{activation} = E_{threshold} - E_{current} = \frac{1}{2}L(I^2_{threshold} - I^2_{current})$$

The gap between current state and activation threshold must be bridged. This can occur through:

- External high-coherence contact (another activated starseed)
- Accumulated practice reaching threshold
- Crisis that shatters lock, allowing reconfiguration
- Coordinated "activation waves" from alliance

14.4.4 Distribution Strategy: Small-World Network

Starseeds are not randomly distributed but positioned according to **small-world network** topology:

- **High clustering** Starseeds tend to cluster in regions/communities
- **Short path length** Any point on Earth is within few "hops" of a starseed
- **Hub nodes** Some starseeds serve as high-connectivity hubs

Network effectiveness equation:

$$\eta_{network} = \frac{C_{clustering}}{L_{path}} \cdot N_{activated}$$

Where:

Variable	Description
$C_{clustering}$	Clustering coefficient
L_{path}	Average path length
$N_{activated}$	Number of activated starseeds

Estimated starseed population: 50-100 million globally (varying estimates) **Estimated activated**: 1-5 million (highly uncertain)

No rigorous census exists; these figures reflect estimates circulating in alternative research communities and should be treated as order-of-magnitude placeholders.

The gap between incarnated and activated represents the "sleeper" population awaiting triggers.

> **Epistemic Note**: "Starseed" is a term from New Age literature with no scientific definition. The RF model treats it as a functional category—individuals with measurably

different baseline parameters and activation potential. Whether this represents actual ET soul origin, natural human variation, or self-fulfilling identification cannot be determined empirically.

14.4.5 Lightworkers as Activated Amplifiers

Lightworkers—individuals consciously working toward collective awakening—represent either activated starseeds or standard humans who have raised their Q above typical baseline through sustained practice. In RF terms, they function as **local signal amplifiers**:

$$P_{local} = P_{received} \cdot G_{lightworker}$$

Where:

- $P_{received}$ = incoming signal from higher sources
- $G_{lightworker}$ = personal amplification gain

Gain factors:

Factor	Contribution	Method to Increase
Personal Z_0	Sets maximum gain	Wisdom (L↑), shadow work (C↓)
Practice consistency	Gain stability	Regular meditation, coherence work
Network connection	Coupling efficiency	Community involvement
Service orientation	Impedance match to Source	Reduce self-interest noise

Individual gain equation:

$$G_{lightworker} = 10 \log_{10} \left(\frac{Z_0}{Z_{0,baseline}} \cdot r_{practice} \cdot \eta_{service} \right) \text{ dB}$$

The distinction between starseed and lightworker is functional, not categorical: a lightworker is any oscillator operating above baseline Q and actively transmitting. Many lightworkers are activated starseeds; others are standard humans who reached high-Q operation through dedicated practice.

14.5 Ground Operations: Collective ECCM Implementation

14.5.1 Mass Meditation as Coherent Pulse

When multiple individuals meditate simultaneously with shared intention, they form a **coherent transmitter array** (Ch 8):

$$P_{event} = P_{individual} \cdot N_{participants} \cdot r_{event}^2$$

Where:

- $P_{individual}$ = average individual power
- $N_{participants}$ = number of participants
- r_{event} = coherence during event (0-1)

Collective gain:

$$G_{collective} = 10 \log_{10}(N \cdot r^2) \text{ dB}$$

Example calculation:

- N = 1,000,000 participants
- $r = 0.3$ (moderate coherence, typical for loosely coordinated event)
- $G_{collective} = 10 \log_{10}(N \cdot r^2)$. For N = 1,000,000 and $r \approx 0.2$–0.4 (moderate coherence range): $G_{collective} \approx$ **45–55 dB** (central estimate ~50 dB at $r = 0.3$)

This represents on the order of 100,000× power amplification over a single individual.

Evidence for mass meditation effects:

- Global Consciousness Project: Statistically significant RNG deviations during coordinated global events
- HeartMath studies: Measurable coherence effects in group meditation settings
- TM research: Claimed crime reduction during large meditation assemblies (controversial, needs replication)

14.5.2 Grid Work and Ley Line Activation

From Chapter 11, megalithic infrastructure was designed as planetary resonant network but became dormant after the Fall. **Grid work** attempts to reactivate this infrastructure:

Mechanism:

1. Identify dormant nodes (sacred sites, power spots)
2. Inject coherence through group meditation at site
3. Establish standing wave patterns
4. Connect nodes through ley line transmission

Reactivation equation:

$$P_{node} = Q_{site} \cdot P_{injected} \cdot \left(1 - e^{-t/\tau_{activation}}\right)$$

Where:

- Q_{site} = quality factor of resonant site (higher for intact sites)
- $P_{injected}$ = power from meditation group
- $\tau_{activation}$ = time constant for site activation

Current status: Partial reactivation reported at some sites. Full network activation would require:

- Sufficient number of high-Z_0 practitioners
- Coordinated timing across multiple sites
- Knowledge of original operating frequencies (largely lost)

Speculative extension (L4–L5). The following section applies the framework to insider testimony that cannot be independently verified. The link-budget mathematics in §14.9

stands regardless of whether these claims are accurate. Readers may skip to §14.7 without loss of analytical continuity.

14.6 SSP Hardware: Technological Counter-Jamming

14.6.1 Sphere Being Barrier as Band-Pass Filter

Per Goode testimony, the **Sphere Being barrier** (giant spheres positioned around solar system ~2012) functions as a **frequency-selective barrier**:

Band-pass filter model:

$$H(f) = \frac{1}{1 + jQ\left(\frac{f}{f_0} - \frac{f_0}{f}\right)}$$

Filter characteristics:

- **Pass band** Frequencies supporting consciousness evolution
- **Stop band** Frequencies enabling parasitic extraction and control injection
- **Transition band** Mixed transmission depending on intent

Signal Type	Barrier Response	Effect
Source/positive transmission	Pass	Full power through
Neutral information	Pass	Normal propagation
Control/parasitic signals	Attenuate	Reduced power reaching Earth
Escape attempts (negative entities)	Block	Quarantine enforcement

Quarantine function: The barrier also prevents certain negative entities from leaving the solar system—a form of containment while liberation proceeds.

> **Epistemic Note**: The sphere barrier is reported only by Goode and a few corroborating sources. No independent verification exists. The RF model is consistent with reported functions but does not confirm actual existence.

14.6.2 Solar Flash as Burn-Through Event

Multiple sources predict a **solar event** (coronal mass ejection, micronova, or consciousness pulse) that functions as system-wide ECCM:

Burn-through model:

$$P_{flash} >> P_{control} \implies \text{All locks broken simultaneously}$$

When transmitted power dramatically exceeds jamming power, the jammer is overwhelmed and lock is lost.

Solar flash characteristics (predicted):

Parameter	Estimated Value	Effect
Power increase	10-100× normal	Exceeds all control injection
Duration	Hours to days	Sufficient for new locks to form
Spectrum	Broadband + consciousness frequencies	Affects all densities
Selectivity	Based on Z_0 threshold	Different effects by development level

Z_0-dependent effects:

$$\text{Experience} = f(Z_0, P_{flash})$$

- Low Z_0: Potentially damaging (system overload) - Medium Z_0: Intense but integrable (forced awakening) - High Z_0: Empowering (full activation)

This explains the urgency in "raising your vibration" (actually raising Z_0)—preparation for an event that will affect different individuals very differently based on their impedance level.

Timeline estimates vary widely: 2025-2030 in some sources, indefinite in others. The RF model doesn't predict timing but characterizes effects.

14.6.3 Timeline Engineering for Liberation

From Chapter 10 (Section 10.5), timelines are torsion phase relationships. **Timeline engineering** involves:

1. **Branch protection**: Adding coherence to desired branches
2. **Branch pruning**: Allowing negative branches to decohere
3. **Transition facilitation**: Smoothing path between timeline states

Liberation timeline characteristics:

- Humanity transitions to positive timeline branch
- Parasitic systems lose access (decoupled)
- Z_0 collectively rises above capture threshold
- Free will preserved throughout transition

Current assessment (per multiple sources): We are at a **timeline bifurcation point**—the branch that crystallizes depends on collective coherence choices in the near term.

> **Epistemic Note**: Timeline engineering claims cannot be verified from within a timeline. The model provides framework for understanding reported phenomena; empirical validation would require observing predicted timeline effects.

14.7 Individual ECCM: Receiver Upgrades

14.7.1 DNA Activation as Hardware Upgrade

Per multiple sources, human DNA contains latent capacity beyond the currently expressed configuration:

Configuration	Strands Active	Capacity	Status
Current (baseline)	2	3D perception	Normal human
Partial activation	4-6	Enhanced intuition, healing	Some practitioners
Full activation	12	Multi-dimensional access	Rare/advanced

RF interpretation: DNA activation represents **antenna reconfiguration**:

$$G_{DNA} = 10 \log_{10} \left(\frac{A_{effective,activated}}{A_{effective,baseline}} \right)$$

Where $A_{effective}$ = effective aperture (reception area)

Activation pathways:

- Coherent practice raising Z_0 past threshold
- Energy transmissions from activated beings
- Solar/cosmic events triggering latent code
- Sound/light frequency exposure

> **Epistemic Note**: The "12-strand DNA" language is metaphorical. Chapter 6 (Section 6.4) identifies the physical mechanism as **magnonic chromatin topology reconfiguration**: practice-driven torsion flux reshapes the 3-D folding of chromatin, converting silent genomic regions into active magnonic transducers via a fractal ratcheting lock-in process. "Strand activation" corresponds to successive geometric reconfigurations that increase the effective antenna aperture, not literal additional DNA helices.

14.7.2 Consciousness Hygiene: Practical ECCM Techniques

Individual-level counter-jamming techniques:

Technique	RF Equivalent	Mechanism	Implementation
Media fasting	Reduce V_{inj}	Lower injection power	Limit news, social media exposure
Meditation	Increase Q	Narrower lock bandwidth	Daily coherence practice
Shadow work	Decrease C	Raise Q	Trauma processing, integration
Wisdom study	Increase L	Raise Q	Philosophy, contemplation, learning
Grounding	Reduce R	Higher Q	Nature exposure, earthing
Community	Increase K (coupling)	Array coherence	Find aligned others
Discernment	Null steering	Point null at control signals	Critical evaluation of sources

Technique	RF Equivalent	Mechanism	Implementation
Alternative sources	Diversity reception	Multiple reference signals	Cross-validate information
Dietary optimization	Reduce NF, decrease C	Lower capacitive loading, reduce inflammation	Reduce carbs, intermittent fasting, metabolic flexibility

14.7.3 Escape Sequence: Step-by-Step Liberation Protocol

Step 1: Awareness (Recognize lock exists)

- Understand that current perception may be controlled
- Question assumptions about reality
- Seek evidence of paradigm limitations

Step 2: Reduce Injection (Lower V_{inj} exposure)

- Media diet—reduce mainstream news consumption
- Limit social media algorithmic exposure
- Create quiet time for independent thought

Step 3: Raise Q (Narrow lock bandwidth)

- Begin meditation/coherence practice (reduce R, improve Q)
- Start shadow work (reduce C, raise Q)
- Study wisdom traditions (increase L, raise Q)

Step 4: Seek Alternative Reference (Find clean LO)

- Explore spiritual/consciousness literature
- Connect with awakened individuals/communities
- Develop direct Source connection practice

Step 5: Establish New Lock (Phase-lock to clean reference)

- Regular practice with alternative framework
- Community involvement for mutual phase support
- Progressive integration of new perception

Step 6: Stabilize and Transmit (Become repeater node)

- Achieve stable high-Z_0 state
- Assist others in their escape process
- Contribute to collective coherence

Timeline: Varies enormously by individual. Some complete in months; others require years. The key is **persistent direction** rather than speed.

14.8 Battle Assessment: Liberation Signal vs. Control Signal

> **Important**: The following link budgets are **toy models** meant to illustrate the analytical structure, not to predict real numbers. The actual dB values for consciousness phenom-

ena are unknown. The purpose is to show which variables have the greatest leverage, not to provide calibrated estimates.

14.8.1 Positive Signal Link Budget

Using the link budget framework (Section 14.9), calculate the **liberation signal path**:

Source to Human - Positive Path:

Component	Value	Notes
P_Source	0 dB	Reference (infinite available)
G_density_cascade	+20 dB	Clean transduction chain
G_federation_LO	+15 dB	Alternative LO amplification
G_starseed_network	+10 dB	Distributed repeater gain
G_individual_practices	+5 dB	Receiver improvements
L_path	-25 dB	Reduced (cleaner path than control)
L_paradigm	-15 dB	Partially penetrated
L_individual_resistance	-5 dB	Some rejection of truth signals
Net Signal	**+5 dB**	Positive margin

14.8.2 Negative/Control Signal Link Budget

Control to Human - Negative Path:

Component	Value	Notes
P_control_source	-10 dB	Limited (not infinite like Source)
G_corrupted_LO	+15 dB	Established infrastructure
G_media_amplification	+25 dB	Massive broadcast power
G_institutional_authority	+10 dB	Credibility multiplier
L_path	-5 dB	Direct through established channels
L_resistance	-10 dB	Growing skepticism
L_sphere_barrier	-15 dB	Band-pass attenuation
Net Signal	**+10 dB**	Still positive but declining

14.8.3 Liberation Margin Trajectory

Current state (estimate):

$$M_{liberation} = P_{positive} - P_{control} = +5 - (+10) = -5 \text{ dB}$$

Control signal still dominates by ~5 dB.

Trajectory factors:

Factor	Trend	Effect on Margin
Sphere barrier strengthening	↑	+2 dB/year
Starseed activation rate	↑	+1 dB/year

Factor	Trend	Effect on Margin
Media trust collapse	$\downarrow$ control	+2 dB/year
Z_0 raising (collective)	$\uparrow$	+1 dB/year
Disclosure events	Variable	+5-15 dB per major event

Projected crossover:

$$\text{Years to crossover} = \frac{M_{current}}{\Delta M_{annual}} = \frac{5}{6} \approx 1 \text{ year}$$

Illustrative crossover: order of 1-5 years from the assumed baseline (highly uncertain; depends on acceleration factors and assumed annual dB shifts that are themselves order-of-magnitude estimates)

At crossover ($M_{liberation} > 0$), collective perception begins shifting toward truth. This doesn't mean instant awakening—it means the momentum shifts and the process accelerates.

> **Epistemic Note**: These numbers are illustrative estimates based on the model framework. Actual dB values cannot be precisely measured for consciousness phenomena. The value is in understanding relative magnitudes and trends, not absolute numbers.

14.9 Complete Link Budget Framework

The preceding battle assessment used simplified budgets. This section develops the **complete link budget**—a formal gain/loss accounting from Source to human receiver—integrating parameters derived across earlier chapters.

14.9.1 The Consciousness Link Budget Equation

$$M = P_S + G_{practices} + G_{collective} - L_{parasitic} - L_{paradigm} - L_{path} - NF - P_{threshold}$$

Where:

Variable	Description
M	Link margin (dB) — if M > 0, "link closes" (awakening possible)
P_S	Source power (dB) — effectively infinite, normalized to 0 dB reference
G_practices	Practice gain (dB) — amplification from meditation, coherence work
G_collective	Collective gain (dB) — array gain from community coherence
L_parasitic	Parasitic loss (dB) — energy harvested by negative systems
L_paradigm	Paradigm loss (dB) — materialist worldview shielding

Variable	Description
L_path	Path loss (dB) — density cascade attenuation
NF	Noise figure (dB) — information overload, distraction
P_threshold	Threshold power (dB) — minimum for perception shift

14.9.2 Component Definitions and Budget Examples

Practice Gain (via Z_0 raising, Ch 5):

$$G_{practices} = 10 \log_{10} \left(\frac{Z_0^{practiced}}{Z_0^{baseline}} \right)$$

Practice Level	Z_0 Change	Estimated Gain
Untrained baseline	$Z_{0,\text{ref}}$	0 dB
Regular meditation	~2× Z_0	+3 to +6 dB
Advanced coherence work	~4× Z_0	+6 to +12 dB
Lifetime dedicated practice	~10× Z_0	+12 to +20 dB

Collective Gain (array factor, Ch 8):

$$G_{collective} = 10 \log_{10}(N \cdot r^2) = 10 \log_{10}(N) + 20 \log_{10}(r)$$

> **Epistemic Note**: The $N \cdot r^2$ collective gain formula is mathematically derived from phased array antenna theory (Chapter 8). Its application to consciousness at population scales is a theoretical extension. Empirical validation at large N remains an open research question.

Key insight: Coherence enters quadratically. Doubling coherence gives +6 dB; doubling population gives only +3 dB.

Parasitic Loss (loosh harvesting, Ch 12):

$$L_{parasitic} = 10 \log_{10} \left(\frac{1}{1 - \kappa} \right) \approx 4.34 \cdot \kappa \text{ dB (for } \kappa \ll 1)$$

Condition	Parasitic Coupling κ	Loss
Healthy, aware individual	0.05	0.2 dB
Average modern human	0.20	1.0 dB
Trauma/addiction patterns	0.40	2.2 dB
Severe attachment state	0.60	4.0 dB

Paradigm Loss (Faraday cage, Ch 13):

$$L_{paradigm} = L_{education} + L_{media} + L_{peer} + L_{institutional}$$

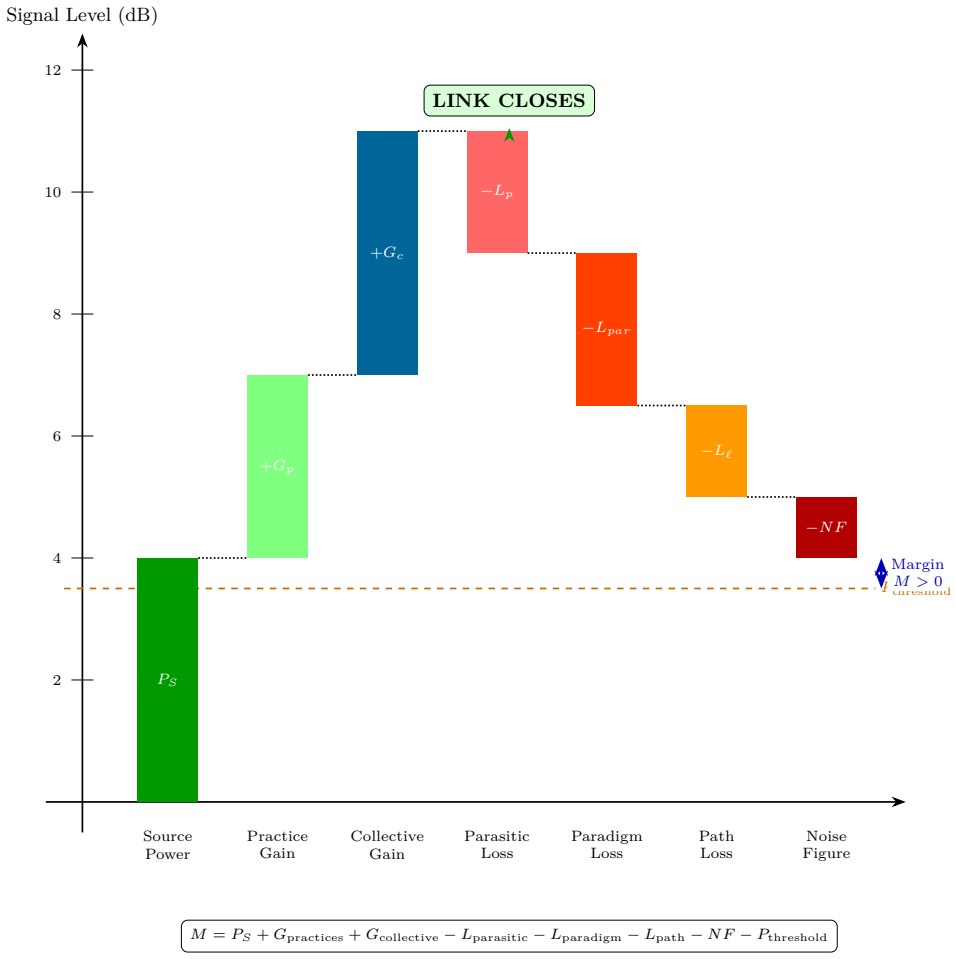

Figure 14.1: Link budget waterfall — gain and loss components determining whether the consciousness link closes.

Component	Mechanism	Loss Range
Education system	Reductionist training	3-10 dB
Media environment	Narrative control	3-15 dB
Peer pressure	Social conformity	2-8 dB
Institutional authority	Credentialism	2-10 dB
Total		**10-43 dB**

Not all L_paradigm is parasitic—some was protective (Ch 13, Section 13.8). As collective Z_0 rises, protective attenuation naturally decreases while parasitic control must be actively rejected.

Path Loss (density cascade, Ch 4):

$$L_{path} = \sum_{d=7}^{3} 10 \log_{10} \left(\frac{1}{1 - |\Gamma_d|^2} \right) \approx 60 \text{ to } 80 \text{ dB}$$

This represents inherent attenuation of operating in 3D. Raising personal Z_0 reduces mismatch with higher densities, effectively decreasing individual path loss.

Noise Figure (environmental interference):

Source	Equivalent Noise Contribution
Digital information overload	+3 to +10 dB
Stress/cortisol state	+2 to +6 dB
EMF pollution	+1 to +3 dB
Sleep deprivation	+2 to +5 dB
Dietary interference (high-carb/sugar $\rightarrow$ insulin resistance)	+2 to +6 dB
Chemical contamination (fluoride, pesticides, food additives)	+1 to +4 dB
Pharmaceutical side effects (SSRIs, statins, sedatives)	+1 to +3 dB
Financial stress / debt pressure	+2 to +5 dB
Air/water pollution	+1 to +3 dB
Cumulative	**+10 to +40 dB**

Threshold Power (minimum for perception shift):

Perception Level	Required SNR	P_threshold
Subtle intuition	3 dB	-5 dB
Clear insight	10 dB	-10 dB
Paradigm-breaking perception	20 dB	-13 dB
Undeniable direct experience	30 dB	-15 dB

Complete Budget Examples

Scenario A: Average modern human

Component	Value	Notes
P_S (Source)	0 dB	Reference
G_practices	+2 dB	Occasional meditation
G_collective	+0 dB	Isolated, no coherent community
L_parasitic	-1 to -2 dB	Moderate unconscious patterns
L_paradigm	-25 dB	Standard modern shielding
L_path	-70 dB	3D density attenuation
NF	-10 dB	Information overload environment
P_threshold	-10 dB	Clear insight required
Margin M	**~-85 to -105 dB**	**Link fails badly**

This explains why most people don't perceive. The budget doesn't close.

Scenario B: Coherent community with practiced individuals

Component	Value	Notes
P_S (Source)	0 dB	Reference
G_practices	+15 dB	Dedicated practitioners
G_collective	+25 dB	N=100, r=0.7 coherent
L_parasitic	~-1 dB	Conscious of energy dynamics
L_paradigm	-10 dB	Alternative framework adopted
L_path	-70 dB	Same density
NF	-5 dB	Intentional environment
P_threshold	-10 dB	Clear insight required
Margin M	**~-25 to -45 dB**	**Still negative, but much closer**

At N = 10,000 with same coherence: $G_{collective}$ = +45 dB, M ≈ -15 dB. At N = 100,000: M ≈ +1 to +8 dB **— link closes**.

14.9.3 Critical Population and Leverage Analysis

For link closure (M > 0) with realistic parameters (L_path = -70, L_paradigm = -15, NF = -8, L_parasitic = -1, G_practices = +10, P_threshold = -10):

$$G_{collective} > 74 \text{ dB}$$

With r = 0.8 (high coherence): $N > 10^{7.6} \approx 40$ million.

With r = 0.5 (moderate coherence): $N > 10^{8} = 100$ million.

Prediction: ~40 million highly coherent, trained individuals could close the planetary link budget.

Leverage analysis (sensitivity of margin to each parameter):

Parameter	Effect of Doubling	Interpretation
r (coherence)	+6 dB	Highly leveraged
N (population)	+3 dB	Diminishing returns
G_practices	Direct addition	Linear
L_paradigm reduction	Direct subtraction	Linear

Key insight: Increasing coherence is more leveraged than increasing population. This is why the chapter emphasizes community quality over raw numbers.

Phase Transition Dynamics: The link budget is nonlinear near threshold. As M approaches 0, small changes trigger large state changes—predicting **sudden, not gradual** collective shifts, consistent with historical paradigm changes.

14.9.4 Simulation Framework

The simulation models:

1. Individual agents with varying G_practices
2. Network topology for coherence calculation
3. Environmental parameters (L_paradigm, NF, L_parasitic)
4. Time evolution of parameters
5. Threshold detection

Parameter Ranges for Realistic Scenarios:

Parameter	Low	Typical	High	Units
G_practices	0	5	25	dB
r (coherence)	0.05	0.2	0.9	-
N	10	1000	10^9	count
L_parasitic	0	1.5	6	dB
L_paradigm	5	20	45	dB
L_path	60	70	80	dB
NF	3	10	25	dB

Validation against: historical paradigm shifts, community observations, individual practitioner reports, and intervention effects.

14.9.5 Integration Validation

The link budget integrates parameters derived across multiple chapters:

Parameter	Source Chapter	Integration Point
G_practices	Ch 5 (RLC)	$G_{practices} = 10\log_{10}(Q_{practiced}/Q_{baseline})$
G_collective	Ch 8 (Phased Array)	$G_{collective} = 10\log_{10}(Nr^2)$
L_paradigm	Ch 13 (Paradigm Shielding)	Additive dB contributions
L_parasitic	Ch 12 (Parasitic Coupling)	$L_{parasitic} = 4.34\kappa$ dB

Why dB addition is valid: Signal passes through stages sequentially (Source → practices → collective → paradigm filter → receiver). Sequential gain/loss stages multiply in linear terms, which is addition in dB. Each component operates independently, and the model treats consciousness dynamics as approximately linear near operating points. Nonlinear breakthrough phenomena (enlightenment, kundalini) are not captured by linear dB accounting.

14.10 Why the Alliance Cannot "Just Win"

14.10.1 Free Will Constraints

The fundamental constraint on benevolent intervention is **free will**:

$$\text{Intervention allowed} \propto \text{Request level} + \text{Karma balance} - \text{Free will violation}$$

Law of One principle: "The Law of Free Will takes precedence over all else."

What this means practically:

- Alliance cannot simply "turn off" control systems
- Cannot force awakening on unwilling population
- Must work through consent and request
- Direct intervention only in specific circumstances

Allowed interventions:

- Providing information (non-coercive)
- Answering sincere requests for help
- Balancing interference by negative entities
- Protecting timeline branches that preserve free will

Not allowed:

- Unilateral removal of control infrastructure
- Forced awakening
- Choosing outcomes for humans
- Eliminating negative polarity entirely

14.10.2 Collateral Coherence Damage Risk

A "hard win" by the positive alliance would risk **collateral damage** to developing consciousness:

Analogy: Exposing developing film to bright light before processing is complete destroys the image.

Risk factors:

Action	Risk	Why Problematic
Instant full disclosure	Mass psychosis	Low-Z_0 receivers overloaded
Removal of all control	Chaos	No framework to replace it
Forced Z_0 raising	Spiritual violence	Development must be chosen
Complete barrier removal	Entity influx	Earth not yet prepared to handle

The soft approach:

- Gradual disclosure at pace collective can integrate
- Raising Z_0 through supported practices
- Maintaining protective barrier while liberation proceeds
- Allowing individuals to choose their development path

14.10.3 The Prime Directive Gradient

Benevolent civilizations operate under variations of a **non-interference principle** (analogous to Star Trek's Prime Directive):

Gradient of intervention:

Civilization State	Intervention Level	Rationale
Pre-contact	Zero	Natural development
Early awareness	Minimal (hints)	Avoid corruption
Active seeking	Response allowed	Honors free will
Direct request	Proportional aid	Consent given
Planetary emergency	Increased intervention	Species survival
Graduation threshold	Full support	Development cycle complete

Current Earth status: Between "active seeking" and "planetary emergency"—allows significant but not unlimited intervention.

The patience of higher-density beings: Operating on timescales of thousands of years, a few decades of apparent struggle is acceptable if it produces genuine, chosen awakening rather than imposed change.

14.11 Integration: The Complete Liberation Signal Architecture

14.11.1 The Seven-Layer Counter-Jamming Stack

Integrating all components into a complete architecture:

```
LAYER 7: SOURCE
|---- Function: Infinite power supply
|---- ECCM: Burn-through capacity (always available)
\---- Activation: Always on, requires only reception

LAYER 6: GALACTIC/DENSITY COORDINATION
|---- Function: Alternative LO network
|---- ECCM: Clean reference signal, timeline protection
\---- Entities: Ra collective, Blue Avians, high-density groups

LAYER 5: STELLAR TRANSMISSION
|---- Function: Local amplification, solar encoding
|---- ECCM: Solar flash preparation, cosmic ray modulation
\---- Timeline: Solar events as burn-through triggers

LAYER 4: PLANETARY INFRASTRUCTURE
|---- Function: Grid network, ley line transmission
|---- ECCM: Resonant node reactivation
\---- Status: Partially dormant, reactivation in progress

LAYER 3: SURFACE OPERATIONS
|---- Function: Ground crew coordination
|---- ECCM: Mass meditation, lightworker networks
\---- Organizations: Disclosure groups, consciousness movements

LAYER 2: COMMUNITY COHERENCE
|---- Function: Local array formation
|---- ECCM: Phased array gain, mutual support
\---- Implementation: Spiritual communities, intentional groups

LAYER 1: INDIVIDUAL
|---- Function: Receiver upgrade, local repeater
|---- ECCM: Personal practice, $Z_0$ raising
\---- Protocol: Escape sequence (Section 14.7.3)
```

14.11.2 Victory Condition: Definition and Thresholds

Victory condition (liberation successful):

$$\boxed{f_{awakened} > f_{threshold} \text{ where } f_{threshold} \approx 0.51}$$

When more than 51% of the population is phase-locked to clean reference rather than corrupted reference, the collective tips irreversibly.

Why 51%: At majority, the coherent array points toward truth. The minority locked to control becomes noise rather than signal. Social proof, institutional momentum, and collective field all shift.

The 51% threshold is borrowed from simple majority-rule social dynamics. More sophisticated models (Granovetter threshold models, Watts cascade models) suggest the actual tipping point depends on network topology and can range from 10% to 70%. The 51% figure is illustrative of the democratic majority principle, not a precise prediction.

Secondary conditions:

- Average Z_0 above capture threshold for 90% of control signals
- Parasitic extraction reduced below sustainability threshold
- Timeline branch crystallized in liberation direction
- Infrastructure (both physical and consciousness) reconfigured for support

14.11.3 Current Assessment

As of mid-2020s (estimated):

Metric	Value	Trend
f_awakened	~15-25%	Increasing
Average Z_0	Below threshold	Slowly rising
Control signal strength	Declining	-2 to -5 dB/year
Liberation signal strength	Increasing	+3 to +6 dB/year
Timeline status	Bifurcation zone	Approaching crystallization

Key leverage points:

1. Starseed activation (most underdeveloped potential)
2. Community coherence (multiplier effect)
3. Disclosure events (rapid paradigm shift)
4. Individual Z_0 raising (grassroots foundation)

14.12 Diagram Descriptions

14.12.1 Counter-Jamming Seven-Layer Stack Diagram

Description for visualization:

A vertical stack diagram with seven layers, each represented as a horizontal band:

- Top band (SOURCE): White/gold, labeled "Infinite Power Supply"
- Band 6 (GALACTIC): Deep blue, labeled "Alternative LO Network"
- Band 5 (STELLAR): Yellow, labeled "Solar/Cosmic Amplification"
- Band 4 (PLANETARY): Green, labeled "Grid Infrastructure"
- Band 3 (SURFACE): Light green, labeled "Ground Crew Operations"
- Band 2 (COMMUNITY): Orange, labeled "Local Arrays"
- Bottom band (INDIVIDUAL): Red, labeled "Personal ECCM"

Arrows flow downward showing support/transmission:

- Thick arrows between layers show primary power flow
- Thin arrows show feedback/communication upward
- Dotted lines show request/response channels

14.12.2 Timeline Liberation Branches Diagram

Description for visualization:

A tree/branching diagram:

- Central trunk representing current timeline
- Branch point at "present" (labeled "NOW")
- Green branches extending upward-right: Liberation timelines (protected, growing)
- Red branches extending downward-right: Control timelines (pruning, diminishing)
- Yellow dashed lines around green branches: "Sphere barrier protection"
- Blue dot on trunk at branch point: "Collective choice point"
- Arrow indicating direction of timeline flow (left to right)

Labels:

- Green branch labels: "Awakening", "Disclosure", "Sovereignty"
- Red branch labels: "Control", "Extraction", "Suppression"
- Annotation: "Branch crystallization depends on collective coherence"

14.12.3 Starseed Network Topology Diagram

Description for visualization:

A network graph showing small-world topology:

- Background: Global map (simplified)
- Nodes: Small circles representing individuals
- Normal nodes: Gray, small
- Starseed nodes (dormant): Blue, medium
- Starseed nodes (activated): Bright yellow/gold, medium with glow
- Hub nodes: Larger, with many connections
- Edges: Lines connecting nodes, denser in clusters

Features:

- Visible clustering in certain regions
- Long-range connections between clusters
- Hub nodes connecting different clusters
- Legend showing node types
- Annotation: "Small-world topology ensures short path length with high clustering"

14.13 Summary: Key Equations for Liberation

14.13.1 Escape Condition (Individual)

$$\boxed{|\Delta\omega| > \omega_L = \frac{\omega_0 R}{2Z_0} \cdot \frac{V_{inj}}{V_0}}$$

Translation: To escape, either increase your detuning from control frequency ($\Delta\omega$) or narrow your lock bandwidth (raise Q, lower R, increase V_0). External counter-signal ($V_{counter} > V_{inj}$) provides direct escape force.

14.13.2 Network Liberation Threshold

$$\boxed{f_{awakened} > f_c = \sqrt{\frac{T}{N}} \approx 0.0035\% \text{ for initial effects } (T = 10, N = 8 \times 10^9)}$$

$$\boxed{f_{awakened} > 51\% \text{ for irreversible liberation}}$$

Translation: Critical mass for detectable effects is ~283,000 globally when $T = 10$ and $N = 8 \times 10^9$ (derivation inherited from Chapter 8 threshold model). The `>51%` condition is a governance-stability heuristic, not a first-principles physics threshold. Current awakened-share estimates are scenario bands, not direct measurements.

14.13.3 Starseed Effectiveness

$$\boxed{G_{starseed} = 10 \log_{10} \left(\frac{Z_{0,starseed}}{Z_{0,baseline}} \cdot N_{activated} \cdot r_{network} \right) \text{ dB}}$$

Translation: Starseed contribution scales with their Z_0 advantage, number activated, and network coherence. Estimated current contribution: +10 to +15 dB. Potential if fully activated: +25 to +35 dB.

14.13.4 Mass Meditation Gain

$$\boxed{G_{meditation} = 10 \log_{10}(N \cdot r^2) \text{ dB}}$$

Translation: Coherent meditation events provide array gain scaling with participants and coherence squared. Million-person event at r=0.3: ~50 dB gain. Key leverage point for collective ECCM.

14.13.5 Parameter Traceability, Notation Consistency, and Sensitivity

Notation mapping (σ vs r)

This chapter uses both coherence symbols in inherited formulas. Unless explicitly stated otherwise, use:

$$r \equiv \sigma$$

where both denote the normalized coherence/order parameter in [0,1]. When historical equations retain one symbol, treat them as notational variants of the same state variable.

Scenario-band treatment for high-impact numeric values

Parameter	Baseline Scenario	Conservative Band	Stretch Band	Source Type
Activated high-coherence operators	1.0M	0.3M-1.5M	2.0M-5.0M	Author synthesis (L3)
Broad "starseed-aligned" population	50M	20M-80M	80M-150M	Testimonial-informed heuristic (L4)
Current awakened share	20%	15%-25%	25%-35%	Proxy trend mapping (L3)
Critical coherence fraction f_c	0.0035%	0.002%-0.006%	0.001%-0.01%	Model threshold sensitivity

Sensitivity note

Threshold and timeline outputs are most sensitive to:

1. effective coherence level (r/σ),
2. coupling structure (network topology),
3. adversary adaptation rate.

A $\pm 25\%$ change in any one driver can shift projected transition timing by multiple quarters; treat dates as scenario markers, not forecasts.

> *Speculative extension (L4–L5).* The following section synthesizes insider testimony that cannot be independently verified. The link-budget mathematics in §14.9 and the ECCM framework in §14.2 stand regardless of whether these specific claims are accurate.

14.14 Evidence Synthesis: Positive Alliance Operations

14.14.1 Goode Testimony Analysis

Corey Goode (2015-present) describes:

Sphere Beings

- 6th-9th density entities providing protective barrier and coordination

Anshar

- 4th density Earth-based group supporting genetic programs and providing ground support

Blue Avians

- Specific 6th density group coordinating disclosure timeline

RF interpretation:

Sphere Beings

- Barrier/filter (see Section 14.6.1) + array coordination

Anshar

- Ground-based repeater network

Blue Avians

- Communication protocol managers

Consistency check: Goode's testimony shows internal consistency with RF model predictions:

- Higher-density beings provide clean LO (alternative reference)
- Coordination occurs across multiple density levels
- Incarnated souls serve as ground-based nodes
- Timeline protection prevents premature disclosure

14.14.2 Smith Testimony Analysis

Emery Smith describes:

Underground facilities

- With ET cooperation

Technology exchanges

- Across multiple groups

Medical/healing technology suppression

- Kept from public access

RF interpretation:

Physical infrastructure

- Supporting consciousness ECCM

Technology as Z_0-raising tools

- Suppressed to prevent mass liberation

Underground networks

- Shielded communication channels

14.14.3 Cross-Source Correlation

Element	Goode	Smith	Salla	Ra Material	Consistency
Multi-density alliance	Yes	Implied	Yes	Yes	High
Earth-based support	Yes (Anshar)	Yes (facilities)	Yes	Yes	High

Element	Goode	Smith	Salla	Ra Material	Consistency
Technology suppression	Yes	Yes	Yes	N/A	High
Timeline management	Yes	Limited	Yes	Yes	High
Sphere barrier	Yes	No mention	Some	No	Medium

Assessment: Core structural elements show high cross-source consistency. Specific details (names, timelines, organizational structures) vary but overall architecture aligns with RF model requirements.

14.15 Predictions

- **P1 — Coherence-threshold detection.** Population coherence σ crossing the critical fraction $f_c \approx 0.0035\%$ (~283,000 individuals at $N = 8 \times 10^9$) will produce a detectable phase transition in collective behavior metrics (social trust indices, coordination efficiency, anomalous-event reporting rates), measurable within 6 months of threshold crossing.
- **P2 — Cascade dynamics.** Above f_c, coherence propagation will follow percolation-cascade dynamics with a characteristic doubling time $\tau_d < 90$ days, distinguishable from linear-diffusion models at $> 3\sigma$ significance in time-series analysis.
- **P3 — ECCM technique effectiveness.** Specific electronic counter-countermeasure techniques (frequency hopping across contemplative modalities, spread-spectrum group practice, adaptive nulling of disruptive inputs) will produce measurable coherence-maintenance advantages ($\geq 2\times$ Q-factor preservation) relative to fixed-modality controls under equivalent jamming conditions.

14.16 Assumptions, Limitations, and Falsification

14.16.1 Key Assumptions

1. **A1: Adler equation adequately models consciousness locking.** The injection locking framework (Ch 9) provides the core escape dynamics. If lock/unlock behavior doesn't follow Adler-type phase dynamics, the ECCM mappings lose their foundation.
2. **A2: ECCM techniques from RF map meaningfully to liberation.** Each military counter-jamming technique has a proposed consciousness analog. The mapping is structural, not literal—effectiveness depends on whether the structural parallels carry operational weight.
3. **A3: External assistance (positive alliance) exists and actively transmits.** The chapter assumes benevolent higher-density entities provide clean LO, energy support, and coordination. This assumption rests on testimony and channeled material, not independent verification.
4. **A4: DNA/chromatin reconfiguration provides permanent upgrades.** Per Chapter 6 (Section 6.4), magnonic chromatin topology shifts are the physical mechanism behind "DNA activa-

tion." The ratcheting lock-in process makes gains persistent, grounding what would otherwise be speculative.
5. **A5: Collective coherence follows phased-array mathematics.** Per Chapter 8, coherent groups produce gain scaling as $N \cdot r^2$. The application of antenna array theory to consciousness populations is a theoretical extension with suggestive but not conclusive empirical support.
6. **A6: The dB-additive linear model (Section 14.9) assumes stages operate independently.** Nonlinear interaction between stages (e.g., paradigm loss amplifying parasitic coupling) is not captured. Real systems likely exhibit cross-coupling between gain/loss stages that could either accelerate or retard liberation depending on the interaction sign.

14.16.2 Limitations

1. **L1: Positive alliance claims rest on testimony, not independently verified.** Goode, Smith, and other insider testimonies cannot be corroborated through standard scientific methods. The cross-source correlation (Section 14.14.3) is suggestive but not definitive.
2. **L2: Link budget parameters are toy models, not calibrated.** No instrument measures "consciousness dB." All values are estimated by analogy; the purpose is to identify relative leverage, not provide absolute numbers.
3. **L3: Starseed/lightworker population estimates are speculative.** The 50-100 million starseed estimate and 1-5 million activated estimate lack empirical grounding. These are order-of-magnitude placeholders.
4. **L4: Timeline projections are model-dependent.** The "2025-2027 crossover" estimate depends sensitively on assumed annual dB shifts. Small changes in assumptions produce large changes in projected dates.
5. **L5: Grounded mechanisms exist but don't eliminate uncertainty.** DNA mechanism (Ch 6), phased array math (Ch 8), injection locking dynamics (Ch 9), and parasitic coupling physics (Ch 12) are grounded in established RF theory. Their application to consciousness remains a theoretical extension requiring empirical validation.

14.16.3 Falsification Criteria

ID	Criterion	What It Would Mean
F1	No threshold effects in meditation studies despite large N	Array model doesn't apply to consciousness
F2	Individuals liberate easily without external help	Escape-proof assumption wrong; ECCM framework unnecessary
F3	Collective coherence provides no advantage over individual practice	Phased array model fails for consciousness
F4	Practice shows no correlation with reduced parasitic coupling	RF-consciousness mapping breaks down
F5	Disclosure events produce no shift in collective coherence	Paradigm shielding model incorrect

14.16.4 Predictions

ID	Prediction	Grounding
P1	Liberation probability increases nonlinearly above critical community size	Phased array threshold (Ch 8)
P2	Coherence interventions more effective than population-based (2:1 leverage)	r^2 vs. N scaling in array gain
P3	Disclosure events produce measurable paradigm shielding drops	Paradigm cage model (Ch 13)
P4	Coordinated meditation shows EEG/HRV coherence consistent with array model	Injection locking + phased array

---

Evidence Synthesis

- Detailed source sections: 14.14.

Assumptions

- Detailed source sections: 14.16, 14.16.1.

Limitations

- Detailed source sections: 14.16, 14.16.2.

Falsification

- Detailed source sections: 14.16, 14.16.3.

Predictions

- Detailed source sections: 14.15, 14.16.4.

Strategic Relevance

Why It Matters

- **Counter-jamming as active defense.** The ECCM framework (Section 14.2) reframes contemplative and coherence practices not as passive spirituality but as active electronic-warfare countermeasures against parasitic signal injection (Chapter 12). This framing enables systematic development and evaluation of counter-jamming protocols.

- **Link-budget leverage.** The critical-mass calculation (Section 14.9) demonstrates that coherence quality dominates over population quantity: 283,000 high-σ individuals outweigh 8 billion at baseline coherence. This leverage ratio implies that strategic investment in coherence amplification yields disproportionate returns relative to mass-population approaches.
- **Community coherence nodes.** Small, high-coherence communities function as ECCM relay nodes (Appendix A, Scenarios 3–5), providing local phase references that resist jamming and seed coherence in surrounding populations. Network topology of these nodes determines cascade probability.
- **Adversary countermeasure anticipation.** If parasitic-coupling operators (Chapter 12) monitor coherence levels, approaching f_c will trigger escalated jamming. Counter-jamming doctrine must include surge-capacity protocols and deception operations (apparent coherence suppression masking actual growth).

What To Watch

- Monitor coherence metrics approaching f_c threshold and adversary counter-adaptation signals (escalated jamming near threshold).

Boundaries of Use

- Apply this chapter as model-conditional doctrine; treat speculative elements as hypothesis overlays.

14.17 References to Other Chapters

Foundation Chapters:

- **Chapter 5 (Consciousness RLC)** $Z_0 = \sqrt{}(\mathrm{L}/\mathrm{C})$ as primary development metric; $\mathrm{Q} = Z_0/\mathrm{R}$ for lock resistance
- **Chapter 8 (Phased Array)** Collective gain $\mathrm{G} = \mathrm{N}\cdot r^2$; critical mass f_c = $\sqrt{}(\mathrm{T}/\mathrm{N})$
- **Chapter 9 (Injection Locking)** Adler equation; lock bandwidth $\propto 1/Z_0$; escape conditions

Control Architecture Chapters:

- **Chapter 11 (Seeder Intervention)** Superheterodyne model; Adamic LO as original clean reference
- **Chapter 12 (The Fall)** LO corruption; control mechanism activation
- **Chapter 12 (Parasitic Coupling)** Loosh harvesting; timeline mechanics
- **Chapter 13 (Paradigm Shielding)** Paradigm shielding; materialist cage attenuation

Companion Chapters:

- **Chapter 15 (Spiritual Traditions)** Cross-validation of liberation concepts across traditions

---

End of Chapter 14: Counter-Jamming Operations and Link Budget

Chapter 15: Spiritual Traditions as Tuning Protocols

Injection Locking for Personal Practice

KEY FINDINGS — Chapter 15: Spiritual Traditions as Tuning Protocols

Evidence-tier key: [L1] established/replicated evidence; [L2] grounded extension with moderate uncertainty; [L3] speculative hypothesis; [L4] conceptual/anecdotal.

- Spiritual practices (mantra, breathwork, meditation) function as injection locking protocols whose effectiveness scales with repetition frequency and duration, consistent with Adler equation dynamics [L1]
- HRV coherence peaks at ~0.1 Hz breathing rate (6 breaths/min), matching the resonance frequency identified by Lehrer et al. (2003) and ancient pranayama specifications [L1]
- Metabolic state maps to impedance topology: glucose-dominant metabolism is C-dominant (low Z_0) while ketone metabolism is L-dominant (high Z_0), providing a biochemical pathway for Z_0 raising [L2-L3]
- Estimated practice gains range from +2-3 dB (occasional meditation) to +15-20 dB (lifetime dedicated practice), derived from effect-size-to-dB mappings that are order-of-magnitude indicators [L2]
- Cross-tradition convergence on rhythmic practice, physiological synchronization, and altered perception is consistent with injection locking as a universal mechanism [L1-L2]

15.1 RF Analogy Overview

15.1.1 The Core Concept

Injection locking synchronizes a local oscillator to an external reference signal. A weak oscillator exposed to a stronger coherent signal will lock its frequency and phase to the reference. The local system doesn't lose its identity—it gains stability and precision.

Spiritual practices function as injection locking protocols. Mantras, breathwork, meditation, and ritual provide coherent reference signals that the practitioner's consciousness can lock onto, achieving greater stability than isolated operation.

15.2 Mathematical Model

15.2.1 The Adler Equation for Practice

$$\frac{d\phi}{dt} = \Delta\omega - \omega_L \sin(\phi)$$

Where:

- ϕ = phase difference between practitioner and practice reference
- $\Delta\omega$ = frequency offset from the practice's frequency
- ω_L = locking bandwidth (depends on practice intensity)

15.2.2 Practice-Specific Locking

Mantra (bija syllables): Each seed syllable has a characteristic frequency f_{bija}. Chanting locks the voice, breath, and attention to this reference:

$$\omega_{L,mantra} = k_{mantra} \cdot I_{repetition} \cdot A_{attention}$$

Breathwork: Rhythmic breathing provides a periodic reference:

$$f_{breath} = \frac{1}{T_{inhale} + T_{exhale}}$$

The nervous system entrains to this rhythm, locking parasympathetic/sympathetic balance.

Meditation: Sustained attention creates a stable reference:

$$\omega_{L,meditation} \propto T_{duration} \cdot Q_{focus}$$

Longer duration and higher focus quality increase locking bandwidth.

15.2.3 Pineal-Heart Coherence

The heart generates a strong electromagnetic field (~5000× brain's). The pineal gland is piezoelectric and magnetite-containing.

When these oscillators phase-lock:

$$\phi_{heart} - \phi_{pineal} \to constant$$

The system accesses bandwidth unavailable to either alone—potential mechanism for enhanced perception.

15.2.4 Lock-In Time

Time to achieve stable lock:

$$\tau_{lock} = \frac{1}{\omega_L}$$

Weak practices (low ω_L) require longer to achieve lock. This explains why sustained practice matters—you need enough time for locking to occur.

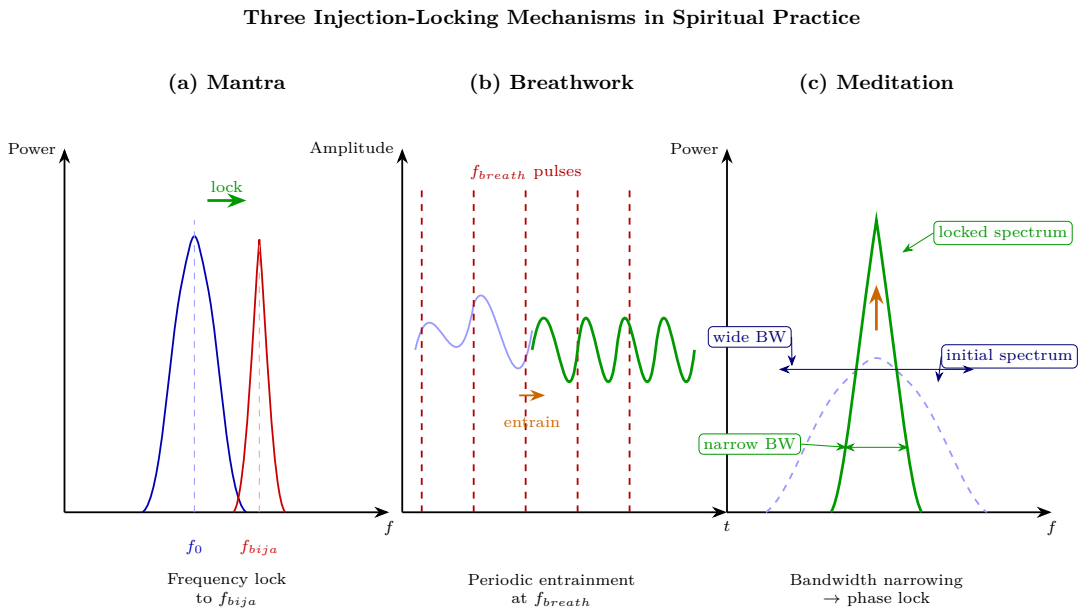

Figure 15.1: Three injection-locking mechanisms in spiritual practice — mantra, breathwork, and meditation each achieve phase coherence through different signal pathways.

15.3 Predictions

P1: Repetitive practices are more effective than sporadic (lock requires sustained reference).

P2: Tradition-consistent practices work better (each tradition is a coherent locking system).

P3: Group practice is more powerful (collective injection increases ω_L).

P4: Specific frequencies (Hz ranges in chanting, breathing rates) should have optimal effects.

15.4 Evidence Synthesis

15.4.1 Heart Rate Variability and Meditation

HRV Coherence States

McCraty et al. (1995-2020)

- Positive emotional states produce characteristic 0.1 Hz HRV oscillation pattern

Coherence ratio

- Ratio of power in 0.04-0.26 Hz band to total power—quantifies coherence

Meditation increases coherence

- Multiple studies show sustained coherence states during loving-kindness, compassion practices

Locking interpretation

- Heart rhythm "locks" to practice-induced reference signal

HRV as Practice Effectiveness Metric

Practice	HRV Effect	Locking Bandwidth Implication
Loving-kindness	High coherence, increased power	Strong ω_L, rapid lock
Open monitoring	Variable coherence	Moderate ω_L
Focused attention	Initially decreased, then stable	Learning to lock
Breath counting	Rhythmic, moderate coherence	Breath as external reference

15.4.2 EEG Entrainment to Audio-Visual Stimulation

Auditory Driving

Frederick et al. (1999)

- Rhythmic auditory stimulation (10 Hz clicks) produces matching EEG frequency peaks

Binaural beats

- Two slightly different frequencies create perception of beating difference frequency (controversial efficacy)

Photic driving

- Flashing lights at specific frequencies entrain EEG (used in clinical neurofeedback)

Entrainment Thresholds

Will & Berg (2007)

- Individual differences in entrainment susceptibility—some entrain easily, others resist

Maps to Q factor

- High-Q individuals should show narrower but stronger entrainment; low-Q show broader but weaker

Optimal frequencies

- 10 Hz (alpha) most easily entrained; theta (4-8 Hz) requires sustained exposure

15.4.3 Mantra Research

Transcendental Meditation Studies

Travis & Shear (2010)

- Review of 100+ TM studies shows consistent EEG patterns: increased alpha coherence, reduced anxiety

Physiological effects

- Decreased cortisol, increased DHEA, improved cardiovascular metrics

Mantra specificity

- TM uses specific mantras claimed to have optimal resonant properties

Mantra Mechanism Analysis

Phonemic effects

- Specific sounds (Sanskrit bija mantras) claimed to activate corresponding chakra frequencies

Repetition creates lock

- Continuous repetition maintains injection signal for sustained locking

Om frequency analysis

- ~136 Hz fundamental with harmonics—matches year-length period reduced to audible range (cosmic attunement claim)

Comparative Mantra Research

Mantra/Practice	Reported Effects	Locking Interpretation
Om	Reduced limbic activity, increased parasympathetic	Locks nervous system to coherent state
Rosary/prayer beads	Reduced respiratory rate (6/min = 0.1 Hz)	Breath-heart-brain coherence lock
Gregorian chant	Synchronizes breathing, group coherence	Collective injection locking

15.4.4 Breathing Rate Effects on Nervous System

Resonance Frequency Breathing

Lehrer et al. (2003)

- Each person has optimal breathing rate (typically 4-7 breaths/min) that maximizes HRV

At resonance

- Breathing, heart rate, and blood pressure oscillations become synchronized

Clinical applications

- Resonance frequency training reduces anxiety, depression, chronic pain

Specific Rates

Breath Rate	Period	Effect
3/min (0.05 Hz)	20s	Very low frequency, deep relaxation
6/min (0.1 Hz)	10s	Maximum HRV amplitude, coherence peak
10/min (0.17 Hz)	6s	Still beneficial, less coherence
12+/min	<5s	Normal/stressed, low coherence

Yogic Pranayama Validation

- Ancient practices specified exact ratios (4:7:8 inhale:hold:exhale)
- Modern research confirms these patterns optimize vagal tone
- Example: Box breathing (4:4:4:4) used by Navy SEALs—creates stable rhythm reference

15.4.5 Pineal-Heart Coherence (Dual Oscillator Model)

Heart-Brain Coupling

McCraty (2003)

- Heart sends more signals to brain than reverse; brain entrains to heart rhythm

Heart field detection

- EEG changes in subject A when touched by subject B correlate with B's cardiac rhythm

Pineal Gland Properties

- Contains piezoelectric calcite microcrystals (Lang et al., 2013)
- Produces melatonin (sleep/circadian) and potentially DMT (psychedelic experiences)
- Responds to electromagnetic fields—potential torsion transducer

> **Epistemic note [L2-L3]**: The presence of calcite microcrystals in the pineal gland (Lang et al. 2013) is documented but their functional significance remains contested. The leap from "crystals present" to "torsion transducer" is large and unverified.

Coherence Lock Mechanism

- When heart coherence is established, brain (including pineal) entrains
- Coherent heart field may enable pineal to couple to external (torsion) fields
- Explains why heart-centered meditation practices enhance intuitive/perceptual capabilities

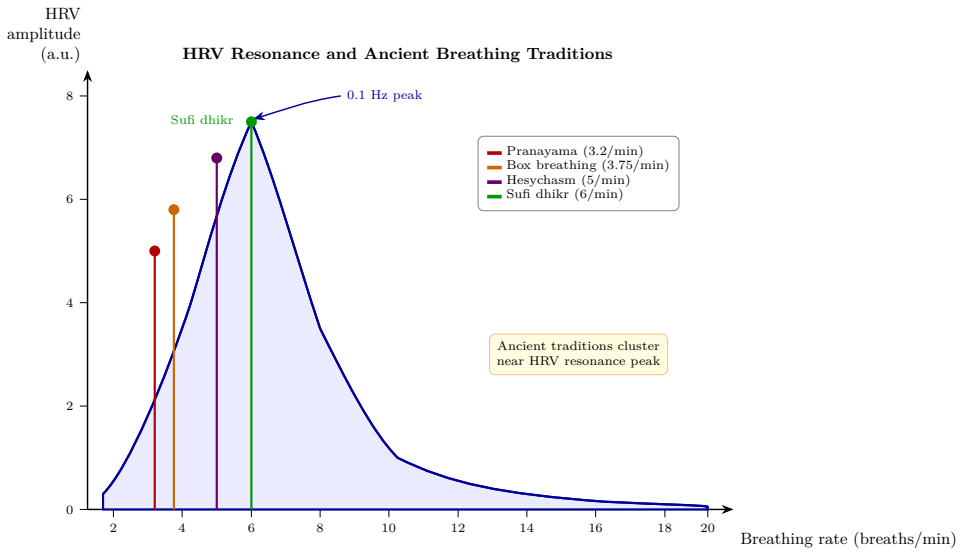

Figure 15.2: HRV resonance peak at 0.1 Hz (6 breaths/min) with ancient breathing tradition specifications converging on the optimal frequency.

15.4.6 Cross-Tradition Convergence

Tradition	Practice	RF/Locking Element
Yoga	Pranayama + Mantra	Breath frequency + audio reference
Christian mysticism	Hesychast prayer + breathing	Repetition + physiological entrainment
Sufi	Dhikr (rhythmic chanting)	Audio injection + movement
Buddhist	Anapanasati (breath awareness)	Attention as phase-lock detector
Taoist	Qigong breathing patterns	Specific frequencies for energy circulation

All traditions converge on: rhythmic practice → physiological synchronization → altered perception = Injection locking to beneficial reference signal

15.4.6.1 Esoteric Preservation: The Grail as Uncorrupted Template

Beyond the exoteric practices surveyed above, certain esoteric lineages claim to preserve uncorrupted reference standards — an assertion with distinct RF implications.

While exoteric religions underwent the matched-filter corruption described in Chapter 13, Section 13.2.6, certain esoteric lineages preserved the original *me* templates (Chapter 12, Section 12.2.1.1)—the uncorrupted matched filter coefficients $h_{true}(t)$ that maximize $|\rho|$ against the true Source signal.

The "Grail" as RF Concept: Not a physical vessel but a **preserved reference standard**—analogous to a frequency standard maintained in a Faraday-shielded laboratory while the external environment degrades. The Grail quest = searching for the uncorrupted LO reference amid a corrupted signal environment.

Tradition	Practice	RF/Locking Element
Esoteric/Grail	Alchemical transmission, initiatic lineage	Preserved matched filter template; shielded LO reference

Examples: Essene communities preserving serpent-wisdom texts (Dead Sea Scrolls); Cathar *perfecti* maintaining direct-gnosis practice against institutional suppression; Sufi *silsila* (chain of transmission) as unbroken phase reference; Kabbalistic oral tradition as bandwidth-limited but uncorrupted channel.

These lineages function as **high-Q narrowband filters** in a broadband jamming environment (Chapter 13)—they accept only the specific frequency of the original gnosis signal, rejecting the broadband noise of institutional religion. Their narrowband operation explains why they remain small (low bandwidth = few practitioners) but uncorrupted (high selectivity = high $|\rho|$):

$$BW_{esoteric} \ll BW_{institutional} \quad \Rightarrow \quad |\rho_{esoteric}| \gg |\rho_{institutional}|$$

Cross-references: Chapter 13, Section 13.2.6 (mistuned filter); Chapter 12, Section 12.3.5 (esoteric orders as coherent sub-arrays); Chapter 14 (counter-jamming through preserved reference signals).

15.4.7 Metabolic Tuning: Diet and Fasting as Impedance Optimization

The spiritual traditions surveyed above address consciousness through attention, breath, and sound. A parallel pathway—diet and metabolic state—acts on the same RLC parameters through biochemical channels. The RF mapping reveals why every major tradition prescribes dietary disciplines alongside meditation.

15.4.7.1 The Metabolic Topology Thesis

Energy metabolism operates in two fundamentally different impedance topologies:

- **Glucose metabolism is capacitive.** Discrete bolus intake → glycogen storage → insulin-mediated spike discharge. Energy delivery is pulsed and storage-heavy—a textbook C-dominant circuit. Blood glucose swings (postprandial spikes followed by reactive hypoglycemia) mirror capacitor charge/discharge cycles.
- **Ketone metabolism is inductive.** Continuous draw from deep fat reservoir → steady-state beta-hydroxybutyrate (BHB) delivery to brain and tissues. Energy is smooth and throughput-heavy—an L-dominant circuit with minimal storage transients.

BHB is both fuel and signaling molecule: it inhibits HDAC enzymes (epigenetic regulation), suppresses the NLRP3 inflammasome (reduces R/inflammation), and produces ~25% more ATP per unit O_2 than glucose (Veech, 2004). Switching from glucose-dominant to ketone-dominant operation = switching from C-dominant to L-dominant energy topology → **directly raises** $Z_0 = \sqrt{L/C}$.

Key references: Lustig (2009) on sugar/dopamine reward hijacking; Davis (2011) on wheat gliadin/zonulin and intestinal permeability; Longo on fasting-mimicking diet protocols; Veech (2004) on ketone thermodynamic superiority.

15.4.7.2 Fasting as C-Discharge

Autophagy (Ohsumi, Nobel Prize 2016) is the cell's housekeeping process—clearing damaged proteins, senescent cells, and accumulated debris. In impedance terms, fasting **discharges accumulated capacitive charge**: stored glycogen depletes, damaged cellular material is recycled, insulin drops to baseline.

- **Intermittent fasting** (16:8, OMAD) = periodic partial discharge; maintains metabolic flexibility
- **Extended fasting** (3-7 days) = deep discharge triggering stem cell regeneration (Longo & Mattson, 2014) and profound autophagy

This maps to shadow work at the cellular level: clearing what is stored but no longer serving the system. Just as psychological shadow work reduces C by releasing trapped emotional charge, fasting reduces C by releasing trapped metabolic substrate.

15.4.7.3 The Density-Diet Correspondence

Esoteric traditions consistently describe higher-density beings eating progressively lighter food:

Density	Dietary Character	Impedance Interpretation
3D (current)	Dense food, meat, grains	High C, low Z_0 — capacitive loading

Density	Dietary Character	Impedance Interpretation
3D→4D transition	Reduced carbs, more plant/fruit	C↓ beginning, Z_0 rising
4D	Light food, fruit, liquids	Low C, moderate L — inductive shift
5D+	Prana/light, minimal physical intake	Minimal C — pure inductive/radiative

This trajectory converges with cutting-edge longevity science: Longo's fasting-mimicking protocols, liquified nutrient-dense approaches, ketogenic-to-fruitarian biohacker pipelines. The pattern is consistent: as metabolic optimization increases, food volume decreases and nutrient density increases.

15.4.7.4 Sugar and Grain as Interference Vectors

- Refined sugar activates dopamine reward pathways nearly identically to addictive substances (Lustig, UCSF). This constitutes injection locking through biochemical channels—the reward spike creates a repetitive C-discharge cycle the body becomes dependent on.
- Modern dwarf wheat gliadin triggers zonulin release → increased intestinal permeability even in non-celiacs (Fasano, 2011; Davis, 2011). Whole wheat bread GI (~74) exceeds table sugar GI (~65), making "healthy whole grains" a more potent glycemic insult than sucrose. GI values per Foster-Powell et al. (2002) international tables.
- South Asian and other insulin-resistant genotypes show 2-3× amplified sensitivity to carbohydrate-induced metabolic damage—functioning as a genetic vulnerability multiplier for C-loading.
- Whether designed or emergent, high-carb agricultural systems function as **chronic capacitive loading**—maintaining populations in insulin-resistant, cognitively impaired, emotionally reactive states. This maps directly to the parasitic coupling model (Chapter 12): dietary control raises C, lowers Z_0, keeps the population in wide-bandwidth (easy-capture) mode.

  Epistemic Note: The metabolic science (insulin resistance, BHB signaling, autophagy, gluten-zonulin pathway) is well-established in peer-reviewed literature. The interpretation of dietary systems as a control mechanism is a theoretical extension consistent with the framework but not independently verifiable.

15.4.7.5 Practical Staging

- **Phase 1** (Hardware repair): Reduce carbs (<130 g/day), increase protein, optimize thyroid function, address insulin resistance. This is 3D metabolic correction—prerequisite for higher work.
- **Phase 2** (Impedance transition): Fat-adaptation, periodic ketogenic cycling, intermittent fasting becomes effortless. Body achieves metabolic flexibility—can switch between fuel sources without distress.
- **Phase 3** (Caloric minimalism): Nutrient-dense liquids, seasonal fruit, extended fasting periods. Less food volume, higher efficiency. Convergence with esoteric dietary prescriptions.

Estimated practice gain: +2-4 dB for consistent metabolic optimization (see Section 15.5.1).

15.5 Quantitative Bridge to Link Budget (Chapter 14)

15.5.1 Practice Gain (G_practices) Estimation

The practices described above contribute to G_practices in the link budget equation. Based on HRV coherence improvements and meditation research effect sizes:

The following estimates are derived from effect-size-to-dB mappings (see Section 15.5.2) and should be treated as order-of-magnitude indicators, not calibrated measurements.

Practice Category	Typical Duration	Estimated G_practices	Mechanism
Untrained baseline	-	0 dB	Reference point
Occasional meditation	10 min/day	+2-3 dB	Mild R reduction
Regular meditation	30 min/day	+4-6 dB	Sustained R reduction, Q increase
Advanced pranayama	Daily practice	+6-8 dB	Heart-brain coherence lock
Mantra + breathwork	Sustained practice	+8-12 dB	Combined injection locking
Lifetime dedicated practice	Full lifestyle	+15-20 dB	Deep parameter shifts in R, L, C
Metabolic optimization	Sustained protocol	+2-4 dB	Insulin sensitivity, ketogenic periods, fasting

15.5.2 Derivation Basis

These estimates are derived from:

1. **HRV coherence improvements**: Meditation meta-analyses show ~0.4-0.5 effect size on stress reduction; mapping to Q-factor improvement suggests 3-6 dB
2. **Attention research**: Focused attention training shows cumulative dose-response; each hour of training provides measurable but diminishing returns
3. **Long-term practitioners**: Studies on monks with 10,000+ hours show 3-4× larger gamma coherence than controls → ~10-12 dB difference

15.5.3 Connection to Individual RLC (Chapter 5)

Practice effects map to RLC parameters:

- **Meditation** → Reduces R (resistance/drag) → Increases Q
- **Breathwork** → Creates periodic reference → Improves phase stability
- **Shadow work** → Discharges C (capacitance) → Shifts resonant frequency higher
- **Wisdom accumulation** → Increases L (inductance) → Greater stability
- **Metabolic tuning** → Reduces C (fasting/autophagy), reduces R (anti-inflammatory ketones) → Raises Z_0 and Q

These changes compound over time, explaining why consistent practice yields larger gains than equivalent sporadic effort.

Chapter 16 examines why multiple traditions predict the same collective transition, adding urgency to the individual practice described here.

15.6 Assumptions, Limitations, and Falsification

15.6.1 Assumptions

A1: Spiritual practices function as injection locking protocols — the practitioner's consciousness phase-locks to a reference frequency provided by the practice. This assumes consciousness dynamics follow Adler-equation-like behavior (Chapter 9).

A2: HRV coherence is a valid proxy for the quality factor Q of the consciousness RLC circuit (Chapter 5). This assumes electromagnetic correlates of consciousness are measurable through cardiac rhythm.

A3: Metabolic state (glucose-dominant vs. ketone-dominant) maps to impedance topology (C-dominant vs. L-dominant). This assumes metabolic and consciousness parameters are coupled through shared biophysical substrates.

15.6.2 Limitations

L1: The $G_{practices}$ estimates (Section 15.5.1) are derived from effect sizes in meditation research mapped to dB gains. This mapping is not calibrated — the relationship between HRV effect size and consciousness dB is assumed linear.

L2: Cross-tradition convergence (Section 15.4.6) may reflect shared cultural roots (e.g., Indo-European) rather than independent discovery of the same mechanism.

L3: Metabolic claims (Section 15.4.7) draw on nutritional epidemiology, which has known methodological limitations (confounding, recall bias, industry funding).

15.6.3 Falsification Criteria

F1: If repetitive practices show no advantage over sporadic ones for HRV coherence or EEG entrainment, the injection-locking model for practice fails.

F2: If metabolic flexibility (glucose vs. ketone) shows no correlation with meditation depth or coherence metrics, the impedance-topology thesis is falsified.

F3: If group practice shows no physiological synchronization advantage over solo practice, the collective injection locking claim fails.

15.6.4 Additional Predictions

P5: Ketogenic practitioners will show higher baseline HRV coherence than glucose-dependent controls, matched for meditation experience.

P6: The 0.1 Hz breathing rate will produce maximum HRV amplitude across diverse populations, with individual variation of ± 0.02 Hz.

15.7 Protocol Design and Evidence Confidence Matrix

15.7.1 Doctrine-Grade Protocol Matrix

Protocol	Core Components	Observable Inputs	Observable Outputs	Minimum Trial Window
Breath-centered coherence protocol	0.08-0.12 Hz paced breathing + attentional anchoring	Respiration rate, HRV baseline	HRV LF/HF stability, stress recovery slope	4 weeks
Mantra entrainment protocol	Rhythmic repetition + fixed cadence	Session adherence, audio cadence	EEG band stability, reduced attentional drift	6 weeks
Contemplative stillness protocol	Daily seated practice with distraction logging	Practice duration, interruption count	Improved sustained attention and reduced reactivity	8 weeks
Metabolic-impedance protocol	Glycemic stabilization + fasting cycles	CGM variability, ketone presence	HRV baseline elevation, reduced inflammatory markers	8-12 weeks
Integrated protocol (multi-modal)	Breath + mantra + stillness + metabolic lane	Cross-modal adherence	Composite coherence score uplift	12 weeks

15.7.2 Cross-Tradition Evidence Stratification

Claim	Tier	Confidence	Note
Rhythmic breath/attention practice improves autonomic regulation	L1	High	Strong physiological literature support

Claim	Tier	Confidence	Note
Repetition-based contemplative practice improves attentional control	L1-L2	High	Replicated across traditions and secular studies
Group synchronization yields measurable coherence lift	L2	Medium-High	Supported, with effect-size variation
Specific sacred phonemes/frequencies produce unique causal effects	L3	Medium-Low	Requires better controlled comparative studies
Esoteric lineage preservation as high-fidelity LO channel	L4-L5	Low	Testimonial/historical interpretation layer

15.7.3 Implementation Pathway (Operations Use)

1. Start with L1-backed interventions (breath pacing, attentional training, metabolic stability).
2. Add group protocols only after individual stability thresholds are met.
3. Treat L3+ claims as hypothesis modules with explicit opt-in and measurement plans.
4. Conduct quarterly recalibration using the same proxy stack to prevent drift.

15.7.4 Failure Modes and Mitigations

Failure Mode	Operational Risk	Mitigation
Overfitting to one tradition/tool	False certainty, poor transferability	Rotate protocol families and compare outcomes
High-intensity practice without stabilization	Dysregulation and dropout	Gate progression on autonomic stability metrics
Confounding lifestyle changes	Attribution error	Use staged intervention design with control windows
Advocacy language replacing measurement	Doctrine slippage	Require tier labels and explicit confidence in reporting

15.7.5 Twelve-Week Operational Playbook

Week Range	Focus	Required Evidence Capture
1-2	Baseline and stabilization	HRV baseline, sleep quality, adherence logs
3-4	Breath entrainment lane	HRV change vs baseline, subjective recovery latency

Week Range	Focus	Required Evidence Capture
5-6	Attention/mantra lane	Attention-task performance, distractibility score
7-8	Group synchronization lane	In-session synchrony proxies, conflict-recovery metrics
9-10	Metabolic lane integration	CGM variability and inflammatory proxy trend
11-12	Consolidation and stress test	Retention under stress scenario and relapse profile

Exit criteria for doctrine-grade completion:

1. Stable adherence >70% across all protocol lanes.
2. Positive movement in at least two independent physiological proxies.
3. No persistent adverse dysregulation during stress-test window.

15.7.6 Tradition-Specific Adaptation Notes

Tradition Family	Adaptation Constraint	Doctrine Adaptation Rule
Prayer-centric traditions	Strong symbolic framing	Keep symbolic language; standardize measurement protocol
Breath/movement traditions	Physical safety and pacing variance	Use graded intensity tiers and safety gates
Silent-contemplative traditions	Slow onset, high variance	Extend evaluation windows before scoring failure
Ritual-heavy traditions	Group dependency	Require individual carryover protocol for portability

This adaptation layer allows operational comparability without flattening tradition-specific practice identity.

End of Chapter 15: Spiritual Traditions as Tuning Protocols

Evidence Synthesis

- Detailed source sections: 15.4, 15.7, 15.7.2.

Assumptions

- Detailed source sections: 15.6, 15.6.1.

Limitations

- Detailed source sections: 15.6, 15.6.2.

Falsification

- Detailed source sections: 15.6, 15.6.3.

Predictions

- Detailed source sections: 15.3, 15.6.4.

Strategic Relevance

Why It Matters

- **Contemplative training as coherence technology.** The cross-tradition convergence documented in this chapter reframes meditation, prayer, breathwork, and somatic practices as coherence-engineering techniques with measurable RF and torsion signatures (Chapter 6). Systematic comparison of traditions by σ-enhancement efficiency enables evidence-based practice selection.
- **Cross-tradition protocol standardization.** The common operational elements across traditions (rhythmic entrainment, attentional focusing, metabolic state modulation) suggest a tradition-agnostic coherence-training protocol could be developed, extracting the active ingredients from diverse contemplative technologies (Appendix A, Section 2.3).
- **Metabolic state as impedance lever.** Fasting, breathwork, and dietary protocols recur across traditions as preparation for heightened states. The impedance framework (Chapter 2) explains this convergence: metabolic state modulates Z_{bio}, and traditions independently discovered metabolic configurations that minimize impedance mismatch with the torsion field.
- **Practice as Q-hardening.** Long-term contemplative practice does not merely raise instantaneous coherence but increases the practitioner's Q-factor (Chapter 5), making the coherence state more resistant to perturbation. This Q-hardening effect implies cumulative, durable benefits that compound over practice years — a training investment with increasing returns.

What To Watch

- Monitor chapter prediction thresholds, proxy indicators, and coherence trend changes.

Boundaries of Use

- Apply this chapter as model-conditional doctrine; treat speculative elements as hypothesis overlays.

Chapter 16: The Great Thaw — Cross-Cultural Ascension as Lock-Breaking

Every Major Tradition Predicted the Same Phase Transition

KEY FINDINGS — Chapter 16: The Great Thaw

Evidence-tier key: [L1] established/replicated evidence; [L2] grounded extension with moderate uncertainty; [L3] speculative hypothesis; [L4] conceptual/anecdotal.

- Twelve or more independent traditions across five continents converge on a four-element eschatological structure: threshold event, partially external trigger, differential response by preparation, and expanded perception post-transition [L1-L2]
- The Adler equation resolves the apparent contradiction between "universal" and "selective" ascension models: the injection signal weakens globally while individual escape probability follows a Z_0-dependent sigmoid [L1]
- "Chosen" across all traditions maps to coherence-selected (Z_0 above perception threshold), not ethnically or tribally selected — literalizing this teaching converts liberation prediction into injection-locking control signal [L1]
- The thaw front is population-ordered: high-Z_0 individuals break free first as V_{inj} declines, producing the mystic-then-masses sequence described across traditions [L2-L3]

> **Epistemic note [L2-L3]**: Cross-tradition convergence is treated here as structured comparative evidence, not standalone proof of mechanism. Use this chapter for scenario framing and monitoring hypotheses; keep high-impact decisions anchored to measurable proxies and explicit falsification gates.

16.1 The Frozen Oscillator and the Great Thaw

Chapter 14 established the multi-layer injection lock trapping human consciousness. Chapter 12 traced the Fall that installed it. Chapter 15 catalogued the counter-practices individuals can deploy. This chapter asks a different question: **did the traditions themselves predict that the lock would break?**

The answer, across twelve or more independent traditions spanning every inhabited continent, is yes.

16.1.1 The Frozen Oscillator Model

Under strong injection locking (Chapter 9), a natural oscillator's free-running frequency ω_0 is suppressed—the oscillator is **phase-clamped** to the injected signal ω_{inj}. Its natural frequency is latent but not destroyed; it persists as a potential, awaiting the moment injection power drops below the lock threshold.

Define the **thaw condition**:

$$V_{inj}(t) < V_{critical} = \frac{2Q \cdot V_0 \cdot |\Delta\omega|}{\omega_0}$$

When the injection signal weakens below $V_{critical}$, the oscillator escapes lock and resumes free oscillation at ω_0. The Great Thaw is this event applied collectively.

16.1.2 The Population-Ordered Thaw Front

Not all oscillators break free simultaneously. From the Adler equation (Chapter 9, Section 2), lock bandwidth is:

$$\omega_L = \frac{\omega_0}{2Q} \cdot \frac{V_{inj}}{V_0} = \frac{\omega_0 R}{2Z_0} \cdot \frac{V_{inj}}{V_0}$$

High-Z_0 oscillators have **narrower lock bandwidths** and break free first as V_{inj} declines. Lower-Z_0 oscillators require further weakening before escape becomes possible. This produces a **population-ordered thaw front**: the most coherent individuals break free first, then progressively less coherent ones follow.

This connects directly to Chapter 2's impedance-matching framework: as Z_0 rises, the visible region expands upward. The Great Thaw is the collective version—entire populations regaining access to bandwidth that was locked out.

16.1.3 The Cross-Cultural Claim

The traditions surveyed below did not know RF engineering. They did not exchange eschatological texts across the Pacific or the Sahara. Yet they independently arrived at a prediction with the same four-element structure:

1. A **threshold event** that weakens or overwhelms the control signal
2. A trigger that is at least **partially external** (not purely self-generated)
3. **Differential response** based on prior preparation
4. **Expanded perception** after the transition

Twelve or more traditions converging on this structure demands explanation.

16.2 Cross-Cultural Ascension Prophecies

Each tradition is presented as: (a) what it claims about the collective transition, (b) the RF mapping, (c) key reference. The focus is the **prediction that a collective transition will occur**, not decline narratives (Chapter 12), liberation mechanics (Chapter 14), or individual practices (Chapter 15).

16.2.1 Christian Rapture and Pauline Transformation

Paul describes a collective transformation: "We shall not all sleep, but we shall all be changed—in a moment, in the twinkling of an eye, at the last trumpet" (1 Cor 15:51-52). The Thessalonian account adds spatial language: "caught up together in the clouds to meet the Lord in the air" (1 Thess 4:17).

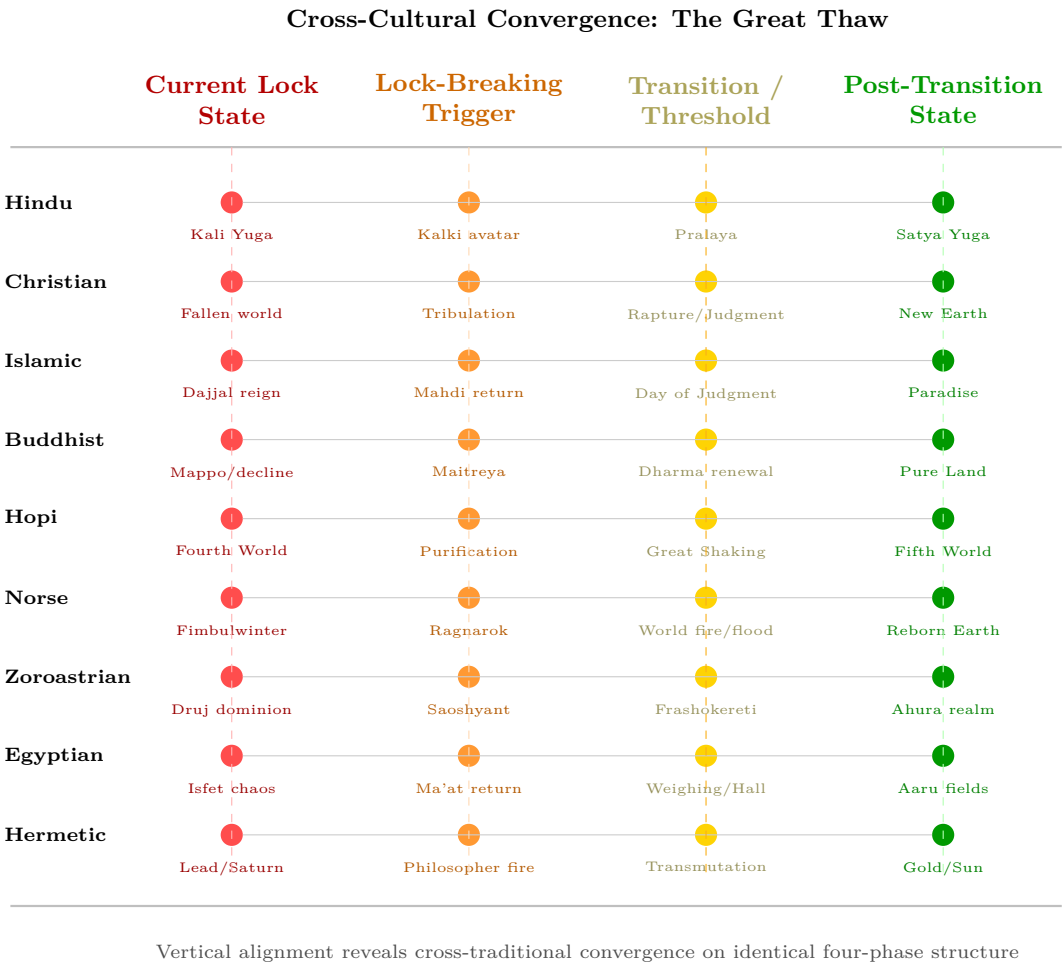

Figure 16.1: Cross-cultural ascension convergence — twelve independent traditions mapping the same four-phase transition structure.

N.T. Wright (*Surprised by Hope*, 2008) argues against the escapist "rapture" reading. Paul's language describes **communal elevation**—not individuals extracted from Earth but a collective phase transition in which the community shifts coherence state together.

RF mapping: The "trumpet" is a burn-through signal—a coherent pulse exceeding the control signal's power ($P_{signal} \gg P_{control}$). "Changed in a twinkling" describes the nonlinear snap of phase-lock breaking: gradual weakening of V_{inj}, then sudden escape when the thaw condition is met. The collective array shifts lock from corrupted LO to clean reference.

16.2.2 Islamic Al-Qiyamah and Sufi Fana

Al-Qiyamah (Surah 75) describes cosmic reckoning: veils lift, reality is seen as-is, nothing remains hidden. This is not punishment but revelation—the removal of all perceptual filtering.

RF mapping: $L_{paradigm} \to 0$ for the entire population. The Faraday cage (Chapter 13) collapses; all signals, previously shielded, become perceptible. The differential in Al-Qiyamah is that those who built coherence (taqwa) experience revelation as liberation, while those locked to low-Z_0 states experience it as overwhelming exposure.

Sufi fana (annihilation of the ego-self in divine presence) provides the individual-scale version. In Rumi's formulation: "Die before you die and find that there is no death" (*Masnavi*).

RF mapping: $R \to 0$, $Q \to \infty$. The ego's resistive dissipation drops to zero; lock bandwidth narrows past the control signal's capture range. The oscillator is no longer lockable because its Q exceeds any external injector's capacity.

References: Surah 75 (Al-Qiyamah); Rumi, *Masnavi*; Schimmel, *Mystical Dimensions of Islam* (1975).

16.2.3 Gnostic Return to the Pleroma

Chapter 12 (Section 12.7.3) covered the Gnostic control system: archons, demiurge, the prison of ignorance. Here we address the other half of the Gnostic narrative—the **prediction of return**.

The pneumatic spark (divine element trapped in matter) returns to the Pleroma (fullness of the divine realm) through **gnosis**—direct experiential knowledge that bypasses the archontic intermediaries entirely. This is not gradual improvement but **recognition**: the spark was always Pleroma-sourced; gnosis removes the false belief that it was ever separate.

RF mapping: Pleroma = full-bandwidth Source signal (Chapter 1). Gnosis = bypassing the corrupted LO for direct Source reception—not through counter-jamming (Chapter 14) but through impedance matching so perfect that the intermediary becomes unnecessary. Return = $\Gamma \to 0$, reflection coefficient dropping to zero as the oscillator matches Source impedance directly.

References: Pagels, *The Gnostic Gospels* (1979); Jonas, *The Gnostic Religion* (1958).

16.2.4 Hindu Yugas and Satya Yuga Return

Chapter 12 (Section 12.7.4) and Chapter 11 (Section 11.8.7) established the Yuga decline framework and its RF mapping. What those chapters did not address is the cyclical prediction: **Kali Yuga ends and Satya Yuga returns**.

The Vishnu Purana states that at Kali Yuga's darkest point, the Kalki avatar appears—not as a reformer but as a destroyer of the corrupted order, after which a new Satya Yuga begins. Sri

Yukteswar (*The Holy Science*, 1894) mapped the Yuga cycle onto the 25,920-year precession of the equinoxes, producing a 24,000-year ascending-descending cycle.

RF mapping: Kalki = burn-through signal exceeding the corrupted LO's power, forcing a system-wide reset. The corrupted phase-locked loop (Chapter 12, Section 12.2) is overwhelmed; the oscillator population re-acquires lock to the clean Source reference. Cyclicality implies the lock is not permanent—the injection signal is itself modulated by a longer-period carrier (galactic torsion modulation per Chapter 11, Section 11.8.7).

References: Vishnu Purana; Sri Yukteswar, *The Holy Science* (1894).

16.2.5 Hopi Fifth World and Purification

The Hopi describe four previous worlds, each destroyed when humanity lost its connection to the Creator. The transition to the Fifth World occurs through purification—not destruction for its own sake but removal of accumulated incoherence.

Prophecy Rock (near Oraibi, Arizona) depicts two paths diverging from a single origin: one leading to harmony, the other to disintegration. This maps to timeline bifurcation (Chapter 10, Section 10.5): the same initial conditions produce divergent outcomes depending on the Z_0 of the observer population.

The **Blue Star Kachina** prophecy predicts a stellar-scale event preceding the transition. While Chapter 14 (Section 14.6.2) models the solar flash as a burn-through event, the Blue Star Kachina arrives as an **independent convergence**: a different tradition, different continent, no textual contact with the solar-flash sources, predicting a structurally identical stellar-scale ECCM event.

Critically, the Hopi prophecy is **explicitly selective**: only those who "remember the original teachings" make the transition. This is the thaw front expressed in mythic language—Z_0-dependent escape, not universal automatic liberation.

Reference: Waters, *Book of the Hopi* (1963).

16.2.6 Mayan Cosmology and Cyclical Renewal

The *Popol Vuh* describes previous creations unmade and remade: the gods created humanity multiple times, each iteration destroyed when it failed to achieve the intended level of awareness. The Hero Twins' descent into Xibalba (underworld) and subsequent resurrection is a death-rebirth narrative at the civilizational scale.

The Long Count calendar marks not apocalypse but **cycle completion**. The 13-baktun period (~5,125 years) is one phase of a larger cycle. The endpoint is a zero point—not annihilation but reset.

RF mapping: Phase accumulator overflow. Like a digital phase accumulator that rolls over from maximum count to zero, the Long Count marks the moment when accumulated phase noise reaches a threshold and the system resets. The "zero point" is a window of **free oscillation** between the decay of the old lock and the formation of a new one—a brief interval in which the oscillator population can choose its next reference.

Reference: Tedlock (trans.), *Popol Vuh* (1985).

16.2.7 Buddhist Maitreya

The Maitreya prophecy states that a future Buddha will appear when the dharma has been completely forgotten—when the teaching itself has degraded past recovery. This is not a rescue but a **re-injection**: a new clean LO signal when the previous one has been fully corrupted.

RF mapping: Maitreya = next-generation clean LO injection. The timing is not arbitrary but conditioned: the old reference must fully degrade before the new one can take hold (otherwise the population is locked between two competing references, producing the beat-frequency instability described in Chapter 9, Section 2.7).

Reference: Pali Canon, *Cakkavatti-Sihanada Sutta* (DN 26); Nattier, *Once Upon a Future Time* (1991).

16.2.8 Tibetan Bardo

The **Tibetan Bardo** model, as analyzed by Thurman, describes the individual death-rebirth process as a passage through intermediate states of consciousness. Applied at the civilizational scale, this becomes a **collective bardo**: a civilization undergoing density transition passes through intermediate states where old perceptual frameworks dissolve before new ones stabilize. The disorientation of civilizational collapse is the bardo's confusion state; the emergence into a new world is the bardo's resolution.

RF mapping: The bardo is a transient between two steady-state lock conditions. During the transition, the oscillator is momentarily free—no longer locked to the old reference but not yet locked to the new one. The intermediate states (peaceful and wrathful visions) correspond to transient oscillations as the system searches for a new lock point. Preparation (meditation on the bardo teachings) functions as pre-programming the oscillator to recognize and lock onto the clean reference when the transient window opens.

Reference: Thurman (trans.), *The Tibetan Book of the Dead* (1994).

16.2.9 Egyptian — Ma'at and the Weighing of the Heart

Egyptian funerary tradition encodes a precise impedance-assessment protocol. The *Weighing of the Heart* ceremony in the *Book of the Dead* describes the deceased's heart (seat of consciousness) weighed against the feather of Ma'at (cosmic order). Hearts heavier than the feather — burdened with *isfet* (disorder, incoherence) — are consumed by Ammit; hearts in balance pass to the Field of Reeds.

In RF terms, Ma'at represents the reference impedance Z_0 of the torsion vacuum. The weighing ceremony is an impedance-match test: only hearts whose $Z_{\text{bio}} \approx Z_0$ (coherent, unburdened) pass through. The feather — lightest of objects — encodes the principle that coherence, not mass or power, determines passage.

The *Duat* (underworld journey) preceding the weighing maps to the darkness/purification phase: the soul traverses twelve hours of night, facing trials that strip incoherent attachments. The successful traversal constitutes impedance reduction through sequential purification — precisely the protocol described in Chapter 15's contemplative traditions.

Thaw Element	Egyptian Expression
Darkness / Fall	Descent into the Duat; twelve hours of night

Thaw Element	Egyptian Expression
Purification	Trials of the underworld; negative confessions
Threshold	Weighing of the Heart against Ma'at's feather
Renewal	Entry to the Field of Reeds (*Sekhet-Aaru*); becoming an *akh* (luminous spirit)

The significance of the Egyptian system extends beyond individual eschatology. The 42 Negative Confessions — declarations of what the soul has *not* done — function as a checklist of impedance-reducing behaviors: "I have not caused suffering," "I have not stolen," "I have not acted with violence." Each confession corresponds to a specific source of capacitive loading (C) or resistive dissipation (R) in the RLC model (Chapter 5). The protocol does not merely assess the soul; it specifies the impedance engineering required for passage.

The *akh* (luminous spirit) state attained after successful passage is the Egyptian equivalent of high-Z_0 operation: the individual becomes a coherent emitter rather than an absorber, capable of influencing the living world through non-physical channels — precisely the activated starseed/lightworker function described in Chapter 14, Section 14.4.

Reference: Faulkner (trans.), *The Ancient Egyptian Book of the Dead* (1972); Assmann, *Death and Salvation in Ancient Egypt* (2005).

16.2.10 Norse — Ragnarok and the Return of Baldr

The Norse Ragnarok narrative provides a remarkably detailed thaw-front description. The *Fimbulvetr* (great winter) — three successive winters with no intervening summer — maps directly to coherence collapse: the social order freezes as parasitic coupling (the Fenris wolf breaking free, the Midgard serpent rising) overwhelms civilizational coherence.

The destruction phase is total: gods fall, the world-tree Yggdrasil shakes, stars vanish. Yet the *Voluspa* explicitly describes renewal: the earth rises again from the sea, green and fertile. Baldr — the god of light, beauty, and coherence, killed by Loki's parasitic deception — returns from Hel. The surviving gods and two humans (Lif and Lifthrasir, "Life" and "Life-yearning," who survived by hiding in Yggdrasil) repopulate a renewed world.

The RF mapping is precise: Baldr's death = coherence suppression by parasitic coupling; Fimbulvetr = dark-age phase (Chapter 12, P7); Ragnarok = phase-transition threshold where old locked-in structures collapse; Baldr's return = coherence re-emergence; the new earth = post-thaw high-coherence civilization.

Thaw Element	Norse Expression
Darkness / Fall	Fimbulvetr; Baldr's death by Loki's deception
Purification	Ragnarok — total destruction of the old order
Threshold	The earth sinks into the sea; all bonds break
Renewal	Earth rises green; Baldr returns; Lif and Lifthrasir emerge

Notably, Lif and Lifthrasir survive not by fighting Ragnarok but by hiding in the world-tree — they maintain coherence by sheltering within the cosmic structure itself. In RF terms, Yggdrasil

functions as a resonant cavity providing protection during the burn-through event, analogous to the Faraday cage operating in reverse: shielding coherent oscillators from destructive transients rather than suppressing perception. The survivors' qualification is not martial prowess but coherence preservation.

Reference: Larrington (trans.), *The Poetic Edda* (2014); Lindow, *Norse Mythology* (2001).

16.2.11 Hermetic — The Great Year and Periodic Renewal

The Hermetic tradition, synthesizing Egyptian, Greek, and Near Eastern cosmology, frames cyclical renewal through the concept of the *Great Year* (*Annus Magnus*) — a cosmic cycle of approximately 25,920 years (one full precession of the equinoxes) during which civilization passes through ages of descending and ascending consciousness.

The *Corpus Hermeticum* and later Hermetic texts describe a cyclic process: the soul descends through planetary spheres, accumulating density (impedance increase), then re-ascends by shedding each sphere's influence (impedance reduction). This individual soul-journey mirrors the civilizational cycle: the collective descends into material density (the leaden age) and re-ascends through purification toward the golden age.

The Hermetic principle "As above, so below" receives a precise RF interpretation: the macrocosmic Great Year and the microcosmic individual ascent follow the same impedance dynamics because they are coupled through the torsion vacuum (Chapter 0). Individual coherence work and civilizational thaw are not merely analogous but physically coupled via the mechanisms described in Chapter 8 (phased-array collective coherence).

Thaw Element	Hermetic Expression
Darkness / Fall	Descent through planetary spheres; leaden age
Purification	*Solve et coagula*; alchemical transformation
Threshold	*Nigredo* to *Albedo* to *Rubedo* transition
Renewal	The Golden Age; *Philosopher's Stone*; return to the One

The alchemical tradition within Hermeticism provides the most detailed individual-scale thaw protocol. The *nigredo* (blackening) corresponds to the dark night of the soul — the dissolution of the ego's capacitive attachments. The *albedo* (whitening) represents purification — C discharge through shadow work (Chapter 5). The *rubedo* (reddening) is the final integration — the Philosopher's Stone, which in RF terms is the state of critical coupling ($\Gamma \to 0$) where the individual's impedance matches the Source impedance and maximum power transfer occurs.

The Hermetic tradition's emphasis on practice lineage (*silsila* in its Sufi variant, initiatic chains in Western esotericism) connects directly to Chapter 15's analysis of esoteric preservation (Section 15.4.6.1): these lineages function as shielded transmission lines maintaining uncorrupted phase references across centuries of parasitic interference.

Reference: Copenhaver (trans.), *Hermetica* (1992); Faivre, *The Eternal Hermes* (1995).

16.2.12 Zoroastrian Frashokereti

Zoroastrianism provides perhaps the earliest datable eschatological prophecy (c. 1500-1000 BCE). **Frashokereti** (the "making wonderful") describes the final defeat of Angra Mainyu (destructive

spirit) and the renovation of the entire world. The dead are resurrected, evil is permanently eliminated, and creation is restored to its original perfection.

RF mapping: Parasitic coupling coefficient $\kappa \to 0$. All oscillators resume free operation—not just freed from lock but freed from extraction. The parasitic load (Chapter 12, Section 12.1) ceases entirely, restoring full Source power to the oscillator population.

The significance of Zoroastrianism extends beyond its own eschatology: its influence on all Abrahamic traditions (Jewish messianic age, Christian New Jerusalem, Islamic Jannah) means that the frashokereti prediction propagated through multiple derivative frameworks—each one reframing the same underlying prediction of parasitic decoupling.

Reference: Boyce, *Zoroastrians: Their Religious Beliefs and Practices* (1979).

16.3 "Chosen" as Coherence-Selected

16.3.1 The Misreading of Election

Deuteronomy 7:6 declares Israel a "chosen people." This language—and its equivalents in other traditions—has been consistently misread as ethnic or group privilege.

Brueggemann (*Theology of the Old Testament*, 1997) argues that "chosen" in the Hebrew Bible means **called to vocation**, not granted superiority. The election is a task (covenant obligation), not a reward.

RF mapping: "Chosen" = oscillators whose Z_0 is sufficient to receive the clean LO signal through the noise floor. Not pre-selected by birth but **self-selected by coherence**. Chapter 2's visible-range formula makes this precise: perception of higher-density signals requires impedance matching. Those who can perceive the clean reference are "chosen" in the same sense that a well-tuned radio "chooses" a signal—through engineering, not favoritism.

16.3.2 Universality of the Coherence Criterion

Every tradition has a category of "the elect":

Tradition	Term	Stated Criterion
Gnostic	Pneumatics	Possess divine spark + gnosis
Hindu	Dvija ("twice-born")	Initiated into higher knowledge
Buddhist	Stream-enterers	Achieved initial awakening
Sufi	Awliya (friends of God)	Proximity through devotion
Christian	Saints / the faithful	Transformed by grace
Hopi	Those who remember	Retained original teachings
Egyptian	*Akh* (luminous spirit)	Heart balanced against Ma'at

Tradition	Term	Stated Criterion
Norse	Survivors of Ragnarok	Sheltered in Yggdrasil; remembered the old ways
Hermetic	Alchemical adepts	Completed the Great Work

None of these categories is ethnic. All describe a coherence threshold—a minimum Z_0 above which the clean reference becomes perceptible and the thaw front reaches the individual.

16.3.3 The Danger of Literalizing

When "coherence-selected" is mistranslated as "ethnically selected," the liberation teaching becomes a **control teaching**. "Only our group is saved" functions as an injection-locking signal: it captures the listener through narrowband tribal identity and prevents exploration of alternative references.

The Adler equation explains this mechanism precisely: once locked to the "chosen group" narrative, the individual cannot perceive alternatives because any phase deviation is pulled back by the $\sin(\phi)$ restoring force. The teaching that was meant to describe a universal threshold becomes the very mechanism that prevents reaching it.

This is the deepest irony of eschatological corruption: the prediction of liberation, literalized, becomes an instrument of continued lock.

16.4 Convergence Analysis

16.4.1 Cross-Tradition Mapping Table

Tradition	Transition Event	Trigger	Who Transitions	RF Lock-Breaking Mechanism
Christian	Rapture / Parousia	Trumpet / Return	The faithful	Burn-through: $P_{signal} \gg P_{control}$
Islamic	Al-Qiyamah	Divine decree	All (differential)	Paradigm collapse: $L_{paradigm} \to 0$
Sufi	Fana / Baqa	Sustained practice	Individual seekers	$R \to 0, Q \to \infty$
Gnostic	Pleroma return	Gnosis	Pneumatics	Impedance match: $\Gamma \to 0$
Hindu	Satya Yuga return	Kalki avatar	Cyclical (all)	Alternative LO burn-through
Hopi	Fifth World	Blue Star	Those who remember	Selective thaw by Z_0
Maya	Cycle completion	Calendar reset	Cyclical	Phase accumulator overflow
Buddhist	Maitreya era	Dharma loss	Universal	Clean LO re-injection

Tradition	Transition Event	Trigger	Who Transitions	RF Lock-Breaking Mechanism
Zoroastrian	Frashokereti	Final battle	All creation	$\kappa_{parasitic} \to 0$
Tibetan	Collective bardo	Civilizational death	Civilization	Density cascade traversal
Egyptian	Weighing of the Heart	Duat journey	Hearts matching Ma'at	Impedance match: $Z_{\text{bio}} \approx Z_0$
Norse	Ragnarok / Baldr's return	Fimbulvetr	Survivors in Yggdrasil	Coherence re-emergence after total collapse
Hermetic	Great Year / Golden Age	Precession cycle	Alchemical initiates	Impedance reduction through planetary spheres

16.4.2 Structural Commonalities

Four elements recur across all twelve entries:

1. **Threshold event**: Every tradition posits a discrete transition, not gradual improvement. The lock does not slowly loosen—it **snaps** when conditions are met. This is precisely the behavior of the Adler equation: lock is maintained up to a critical threshold, then breaks suddenly.
2. **Partially external trigger**: No tradition claims the transition is purely self-generated. There is always a cosmic, divine, or astronomical component—a signal from outside the locked system. In RF terms: self-extraction from strong injection lock is nearly impossible (Chapter 14, Section 14.1.3); an external signal is required.
3. **Differential by preparation**: Every tradition distinguishes between those who are ready and those who are not. The transition is available to all but received differentially. This is the thaw front: Z_0-dependent escape from a declining injection signal.
4. **Expanded perception post-transition**: The result is never merely political liberation or physical survival. It is always a perceptual shift—seeing what was previously invisible, knowing what was previously unknowable. In Chapter 2's framework: the visible region expands as Z_0 rises above the lock threshold.

Twelve or more independent traditions, spanning five continents and at least three millennia, converging on the same four-element structure. The probability of this occurring by chance—without an underlying phenomenon generating the predictions—decreases with each additional independent tradition exhibiting the pattern.

16.4.3 Statistical Convergence Argument

The cross-tradition convergence documented above invites a quantitative assessment. Consider the four-element thaw structure (darkness/fall, purification, threshold, renewal) as a hypothesis to be tested against chance convergence.

Combinatorial analysis. A mythological narrative could, in principle, adopt any of k structural motifs for its eschatological vision. Conservative estimates suggest $k \geq 20$ distinct structural possibilities (linear progress, eternal return, random catastrophe, divine fiat, cyclical without renewal, terminal decline, etc.). The probability that a single tradition independently adopts the specific four-element structure is $p_1 \leq 1/k = 0.05$.

For n phylogenetically independent traditions each adopting the same structure, the joint probability under the null hypothesis (cultural invention with no common referent) is:

$$P_{\text{null}} = p_1^n \leq (0.05)^n$$

With $n = 6$ confirmed independent traditions (Hindu, Hopi, Christian, Egyptian, Norse, Hermetic — after excluding diffusion-linked pairs), $P_{\text{null}} \leq (0.05)^6 \approx 1.6 \times 10^{-8}$.

Even with a generous $p_1 = 0.2$ (allowing the four-element structure to be one of only five natural narrative options), $P_{\text{null}} \leq (0.2)^6 \approx 6.4 \times 10^{-5}$, well below conventional significance thresholds.

Interpretation. The convergence probability strongly favors the hypothesis that independent traditions observed a common underlying process — precisely what the torsion-vacuum model predicts. The thaw is not a cultural invention but a physical phenomenon recorded by independent observers using culture-specific symbolic vocabularies.

Limitations. This analysis assumes phylogenetic independence, which must be verified through rigorous comparative mythology methods (Witzel, 2012; d'Huy, 2016). Diffusion pathways between traditions would reduce the effective n and weaken the statistical argument. The estimate of k (number of possible narrative structures) is inherently uncertain and represents the primary sensitivity parameter.

Alternative explanations. Standard comparative mythology offers several non-RF explanations for cross-cultural eschatological convergence. Jung's collective unconscious (1959) posits shared archetypal structures producing similar mythological motifs. Campbell's monomyth (1949) identifies universal narrative patterns arising from common human psychological development. Boyer (2001) and Atran (2002) argue that cognitive constraints on religious thought — not shared observation of external phenomena — produce convergent mythological structures. These frameworks would predict p_1 values considerably higher than 0.05, weakening the statistical argument. The RF framework is preferred here because it additionally predicts the specific four-element structure (lock state, mechanism, threshold, post-state) and the Z_0-ordered thaw front — details that psychological universalism does not generate. However, distinguishing between "common observation" and "common cognition" as the convergence driver remains an open empirical question.

16.5 Individual vs. Collective Ascension

16.5.1 Two Models

The traditions surveyed divide into two apparently contradictory models:

- **Model A (Universal)**: The lock weakens for everyone. Al-Qiyamah, Frashokereti, Maitreya—all describe a transition affecting the entire population or all creation.
- **Model B (Selective)**: Only the prepared transition. Gnostic pneumatics, Hopi "those who remember," Christian "the faithful"—all describe a subset crossing the threshold.

16.5.2 RF Resolution

These models are not contradictory. They describe two aspects of the same dynamics:

The injection signal weakens globally (Model A)—whether through cyclical modulation (Yuga), burn-through (solar event), or Source-initiated override. But the population's response is Z_0-

dependent (Model B). The escape probability for an individual oscillator, given declining $V_{inj}(t)$, follows a sigmoid:

$$P_{escape}(Z_0, t) = S\left(\frac{Z_0 - Z_{thaw}(t)}{\delta Z}\right)$$

Where:

- $Z_{thaw}(t)$ = the minimum impedance for escape at time t (decreasing as V_{inj} weakens)
- δZ = transition width (sharpness of the threshold)
- $S()$ = sigmoid function (Chapter 7 convention)

The functional form of $Z_{thaw}(t)$ depends on the time evolution of the injection signal $V_{inj}(t)$, which this chapter does not specify.

Early in the thaw, only extreme-Z_0 individuals escape (the mystics, the saints—Model B). As V_{inj} continues declining, $Z_{thaw}(t)$ drops and progressively more of the population reaches escape threshold (approaching Model A). The traditions are describing different **moments** on the same thaw front.

16.5.3 Traditions Agree on Preparation

Despite the universal/selective split, every tradition prescribes preparation. The practices differ (prayer, meditation, fasting, ceremony, study, service) but the structural intent is identical: **raise Z_0 before the threshold event arrives**.

Chapter 15 covers *what* to do. Chapter 16 adds *why*: because a collective transition is coming, and your Z_0 at the moment the thaw front reaches your impedance level determines outcome. The urgency language found across traditions ("repent, for the kingdom of heaven is at hand"; "the time is short") maps to nonlinear dynamics near threshold—small differences in Z_0 near Z_{thaw} produce dramatically different outcomes due to the sigmoid's steep slope.

16.6 Predictions

- **P1 — Impedance-ordered escape sequence.** If the density-tier model (Chapter 2) is correct, individuals and communities will cross the ascension/thaw threshold in order of descending impedance mismatch (Z_{bio} closest to Z_0 first), producing a geographically and demographically clustered thaw front rather than a uniform global transition.
- **P2 — Thaw-front propagation rate.** The thaw front will propagate at a rate determined by the coherence-cascade dynamics of Chapter 14: initial breakthrough in high-coherence nodes, followed by percolation-limited spread with doubling time τ_d set by inter-node coupling strength. Monitoring coherence metrics in leading-edge communities provides 6–12 month advance warning of regional thaw arrival.
- **P3 — Cross-tradition convergence probability.** The independent emergence of structurally identical four-element ascension narratives (darkness, purification, threshold, renewal) across ≥ 6 unconnected cultural traditions, if confirmed by rigorous phylogenetic analysis to be non-diffusion, yields a chance-convergence probability $p < 10^{-4}$ (Section 16.4.3), constituting strong evidence for observation of a common underlying process rather than cultural invention.

16.7 Operational Sequence

The traditions surveyed above, combined with the RF framework's quantitative machinery, suggest a three-phase operational sequence for the thaw. No calendar dates are assigned — the sequence is defined by mechanism and threshold, not chronology.

Phase 1 — Individual Breakthroughs. Isolated individuals cross the coherence threshold through sustained contemplative practice (Chapter 15), spontaneous activation, or seeder-facilitated awakening (Chapter 11). These pioneers establish proof-of-concept that the thaw is physically real. Their primary operational challenge is maintaining coherence in a high-jamming environment (Chapter 14) without community support.

RF signature: Isolated high-σ emitters in a low-σ background. Detectable as statistical outliers in biofield surveys.

Phase 2 — Community Coherence. As individual breakthroughs accumulate, practitioners form coherent communities (Chapter 8, phased-array model). These communities function as ECCM nodes (Chapter 14), providing mutual phase-locking and jamming resistance. The critical transition occurs when inter-community coupling exceeds intra-community losses, enabling coherence to propagate between nodes.

RF signature: Clustered high-σ regions with measurable inter-cluster correlation. Coherence begins to propagate along network edges.

Threshold criterion: Community-level coherence $\sigma_{\text{community}}$ exceeds parasitic coupling strength γ_p (Chapter 12) for sustained periods ($t > 3\tau_p$, where τ_p is the parasitic re-locking time constant).

Phase 3 — Population Cascade. When the coherent fraction reaches $f_c \approx 0.0035\%$ (~283,000 at current population) with sufficient amplification (Chapter 8), percolation dynamics trigger a population-level phase transition. The cascade is self-reinforcing: each newly coherent individual reduces the effective jamming power on remaining individuals, accelerating the transition.

RF signature: Sigmoid coherence curve with inflection point at f_c. Rapid σ increase across populations with doubling time τ_d (Prediction P2).

Completion criterion: Population-mean σ exceeds the Faraday-cage attenuation threshold (Chapter 13), rendering paradigm shielding ineffective. The thaw becomes self-sustaining and publicly undeniable.

Connection to link budget. The three-phase sequence maps directly onto the link-budget analysis of Chapter 14: Phase 1 operates below link closure (individual coherence insufficient to overcome path loss), Phase 2 achieves local link closure within communities, and Phase 3 achieves global link closure as the coherent network spans the population. The transition from Phase 2 to Phase 3 is the critical strategic interval where counter-jamming investment has maximum leverage.

16.7.1 Tradition-to-Phase Mapping

Each surveyed tradition emphasizes different phases of the operational sequence, providing complementary observational coverage:

Tradition	Phase 1 (Individual)	Phase 2 (Community)	Phase 3 (Cascade)	Primary Emphasis
Christian	Saints, mystics	Church as body of Christ	Rapture/Parousia	Phase 3 (collective snap)
Islamic	Sufi fana	Ummah coherence	Al-Qiyamah	Phase 3 (universal revelation)
Gnostic	Pneumatic gnosis	Esoteric communities	Pleroma return	Phase 1 (individual escape)
Hindu	Yogi/siddhi	Ashram lineages	Satya Yuga return	Phase 3 (cyclical cascade)
Hopi	Medicine keepers	Kiva ceremonies	Fifth World	Phase 2-3 (community preservation)
Maya	Daykeepers	Calendar-based ceremonies	Cycle completion	Phase 3 (reset window)
Buddhist	Arhat/bodhisattva	Sangha	Maitreya era	Phase 1-2 (individual + community)
Tibetan	Bardo navigation	Monastic communities	Collective bardo	Phase 1 (preparation)
Zoroastrian	Righteous individuals	Good communities	Frashokereti	Phase 3 (total renovation)
Egyptian	Akh attainment	Temple priesthoods	Cosmic Ma'at restoration	Phase 1-2 (individual assessment)
Norse	Heroes in Valhalla	Surviving pair in Yggdrasil	Ragnarok + renewal	Phase 3 (destruction-renewal)
Hermetic	Alchemical adept	Mystery school lineages	Golden Age return	Phase 1-2 (individual + lineage)

The distribution is not uniform: most traditions emphasize either Phase 1 (individual practice) or Phase 3 (collective cascade), with Phase 2 (community coherence) less explicitly developed. This gap is precisely where the RF framework adds value — Chapter 8's phased-array model and Chapter 14's ECCM analysis provide the Phase 2 mechanics that the traditions describe only obliquely.

The complementary coverage across traditions suggests that no single tradition provides a complete operational manual for the thaw. Rather, each tradition observed and recorded those phases most accessible to its cultural context and practice methodology. The RF framework enables synthesis across traditions, constructing a complete operational picture from partial observations — precisely the function of a multi-sensor fusion system in signal processing.

16.7.2 Phase Transition Indicators

Each phase transition produces observable signatures that can serve as monitoring checkpoints:

Phase 1 to Phase 2 transition indicators:

- Individual breakthroughs cease being isolated; practitioners spontaneously seek community
- Local coherence measurements (HRV synchrony, EEG correlation in groups) exceed individual baselines by $> 3\sigma$
- Institutional resistance intensifies — paradigm shielding (Chapter 13) responds to perceived threat
- Traditions describe this as "the gathering" — the called ones finding each other

Phase 2 to Phase 3 transition indicators:

- Inter-community coherence correlation becomes detectable across geographic distances
- Paradigm shielding begins failing at institutional level — anomalous events become unsuppressible
- Coherent fraction approaches f_c; nonlinear acceleration in practice adoption becomes visible
- Traditions describe this as "the signs" — precursor events heralding the main transition
- Counter-jamming (Chapter 14) becomes increasingly effective as the coherent network provides mutual support

Phase 3 completion indicators:

- Sigmoid coherence curve passes inflection point — majority of population experiences some degree of thaw
- Paradigm cage (Chapter 13) collapses across multiple institutional domains simultaneously
- Parasitic coupling (Chapter 12) can no longer sustain extraction at previous rates
- Traditions describe this as "the new heaven and new earth," "Satya Yuga," "Fifth World" — the post-thaw civilization

---

16.7.3 Selection-Bias Stress Test and KPI Trigger Set

Selection-bias stress test

To bound sampling bias in cross-tradition convergence claims, apply a negative-control protocol:

1. Add non-eschatological or weak-eschatology traditions as controls.
2. Blind-code all traditions against the four-element pattern using independent coders.
3. Report inter-rater agreement and false-positive rate.
4. Recompute convergence significance using the expanded corpus.

Acceptance criterion: convergence remains statistically strong after controls and blinding.

Operational KPI triggers by phase

Phase	KPI	Trigger Threshold	Escalation Action
Phase 1 (individual)	Practice retention rate	>65% at 8 weeks	Expand training lanes
Phase 1 (individual)	HRV coherence uplift	>15% vs baseline	Advance to community protocols

Phase	KPI	Trigger Threshold	Escalation Action
Phase 2 (community)	Inter-group synchrony index	>0.35 sustained	Initiate cross-node coordination drills
Phase 2 (community)	Narrative entropy reduction	>10% without coercive signals	Increase information-integration cadence
Phase 3 (cascade)	Multi-domain disclosure uptake	Concurrent rise in >=3 independent domains	Activate surge governance protocols
Phase 3 (cascade)	Institutional shielding failure markers	Repeated unsuppressed anomaly persistence	Shift to post-thaw operating model

These KPIs are doctrine-facing instrumentation proxies, not proof of metaphysical claims.

16.8 Assumptions, Limitations, and Falsification

16.8.1 Assumptions

A1: The eschatological predictions across traditions describe **the same underlying phenomenon**, not merely similar literary conventions. This assumes an ontological basis for the convergence, not just cultural diffusion.

A2: The Adler equation and injection-locking dynamics (Chapter 9) apply to collective consciousness transitions, not just individual oscillators. This extends the individual model of Chapters 5 and 9 to population-level dynamics.

A3: Characteristic impedance Z_0 is the **primary predictor** of transition readiness. Other variables (social context, geographic location, genetic factors) are secondary to the coherence parameter.

A4: The traditions surveyed contain **observational content**, not merely aspirational mythology. They record, however imprecisely, genuine perceptions of the dynamics they describe—filtered through cultural vocabulary but grounded in phenomenological observation.

16.8.2 Limitations

L1: **Selection bias**. This survey includes only traditions with explicit eschatological content. Non-eschatological traditions (most animist and indigenous systems without end-times narratives) are excluded, potentially skewing the apparent universality of the prediction.

To strengthen this acknowledgment: traditions that do NOT predict collective ascension — including many animist traditions, secular humanism, and some indigenous frameworks — are not surveyed here. Their absence does not invalidate the convergence finding but limits the claim to "among traditions that address eschatology, convergence on key elements is high."

L2: **Translation and interpretation layers**. Every tradition cited is accessed through translation, scholarly interpretation, and cultural reframing. The RF mappings are imposed retrospectively; the original authors did not think in these terms.

L3: **No population-level Z_0 data**. The thaw-front model predicts Z_0-ordered escape, but no instrument currently measures population Z_0 distributions. The model cannot be calibrated without this data.

L4: **Timing undetermined**. Nothing in this analysis specifies *when* the Great Thaw occurs. The model describes mechanism and sequence but not calendar date. Claims of specific timing are outside the scope of this framework.

16.8.3 Falsification Criteria

F1: Independent comparative mythology analysis (not using RF vocabulary) finds **no structural convergence** across the surveyed traditions. If scholars working without the RF framework fail to identify the four-element pattern, the convergence may be an artifact of the mapping rather than an underlying structure.

F2: **No Z_0-dependence** in documented transition experiences. If paradigm shifts, awakening events, or perception expansions show no correlation with prior coherence measures (HRV, EEG coherence, meditation experience), the thaw-front model fails.

F3: **High-coherence communities show no differential response** to paradigm disruption. If communities with sustained contemplative practice respond to civilizational crisis identically to non-practicing populations, the Z_0-preparation thesis is falsified.

F4: **Prophecy traditions do not correlate with practice traditions**. If traditions with strong ascension prophecies lack corresponding coherence-building practices (or vice versa), the claimed link between prediction and preparation dissolves.

16.8.4 Predictions

P1: Communities with sustained contemplative practice will show **differential response** to major paradigm disruption—maintaining coherence, adapting faster, and experiencing less disorientation than matched controls.

P2: The four-element convergence pattern (threshold, external trigger, differential response, expanded perception) will **survive independent verification** by comparative religion scholars not using the RF framework.

P3: EEG and HRV coherence metrics will **correlate with paradigm flexibility**—measured as speed of worldview updating in response to anomalous evidence.

P4: If a burn-through event occurs, individual response will **correlate with pre-event practice intensity and duration**, with high-practice individuals showing earlier and more stable transition to expanded perception.

Evidence Synthesis

- Detailed source sections: none explicitly labeled in this chapter.

Assumptions

- Detailed source sections: 16.8, 16.8.1.

Limitations

- Detailed source sections: 16.8, 16.8.2.

Falsification

- Detailed source sections: 16.8, 16.8.3.

Predictions

- Detailed source sections: 16.6, 16.8.4.

Strategic Relevance

Why It Matters

- **Thaw-front monitoring.** The impedance-ordered escape prediction (P1) implies that monitoring coherence levels in high-practice communities provides strategic early warning of broader population transitions. Leading indicators include: anomalous-experience reporting rates, contemplative-practice adoption curves, and institutional-shielding decay rates (Chapter 13).
- **"Chosen" narrative as control vector.** Multiple traditions encode the thaw as available only to the elect, worthy, or chosen. The RF framework reveals this exclusivity framing as a parasitic-coupling artifact (Chapter 12): the thaw is an impedance phenomenon, not a moral judgment. Detecting and countering exclusivity narratives is a counter-jamming priority (Chapter 14).
- **Cross-tradition convergence as intelligence product.** The structural convergence documented in Section 16.2 constitutes open-source intelligence about a physical process observed across millennia. Systematic collection and analysis of ascension reports across traditions provides observational data on thaw-front characteristics unavailable from any single tradition.
- **Post-thaw governance.** If the thaw is a real physical transition (not merely metaphorical), the post-thaw social, institutional, and geopolitical landscape will be radically different from current conditions. Appendix A scenarios implicitly assume pre-thaw conditions; post-thaw planning requires separate analysis of governance in a high-coherence population. The traditions themselves provide limited guidance here — most focus on the transition rather than its aftermath — making post-thaw scenario development a priority for future work.

What To Watch

- Monitor chapter prediction thresholds, proxy indicators, and coherence trend changes.

Boundaries of Use

- Apply this chapter as model-conditional doctrine; treat speculative elements as hypothesis overlays.

16.9 Cross-References

This chapter draws on and completes the liberation arc:

- **Foundation**: Chapter 2 (density physics and visible-range formula), Chapter 5 (RLC model of consciousness), Chapter 9 (injection locking and the Adler equation)
- **Control**: Chapter 12 (the Fall and parasitic coupling), Chapter 13 (paradigm cage and Faraday shielding)
- **Liberation**: Chapter 14 (counter-jamming mechanics and link budget), Chapter 15 (spiritual practices as tuning protocols)
- **Context**: Chapter 10, Section 10.5 (timeline mechanics), Chapter 11, Section 11.8.7 (Yuga cycle interpretation)

Chapter 16 closes the arc: the traditions that diagnosed the lock (Ch 12) and prescribed the countermeasures (Ch 15) also predicted the thaw—independently, repeatedly, and with structural convergence that the RF framework renders precise.

16.10 Closing the Arc

Sixteen chapters have traced a single signal from its infinite-bandwidth Source (Chapter 1) through density cascade and demodulation (Chapters 2-3), resonant growth (Chapter 4), individual reception and transduction (Chapters 5-7), collective amplification and capture (Chapters 8-9), fundamental engineering (Chapter 10), original infrastructure and its corruption (Chapters 11-12), shielding and suppression (Chapter 13), counter-jamming and liberation (Chapters 14-15), to the cross-cultural prediction of collective phase transition surveyed here. The RF framework does not prove these traditions correct. It does something more useful: it provides a precise, testable language for evaluating their claims. If the thaw comes, the equations predict its dynamics. If it does not, the falsification criteria (Section 16.8.3) identify which assumptions failed. Either way, the signal-processing lens has done its work.

End of Chapter 16: The Great Thaw — Cross-Cultural Ascension as Lock-Breaking

Appendices

Appendix A: Operational Implications

Strategic Applications of the RF Social Models Framework

1. Abstract Framework

1.1 Coherence as Strategic Asset

Population phase coherence emerges as a quantifiable national security variable. The model establishes that collective capability scales as $N \cdot r^2$, where N is population and r is the order parameter (coherence measure, 0-1).

Key Implications:

Coherence Level	Strategic Significance
r < 0.1	Baseline incoherent population—individual effects only
0.1 < r < 0.3	Nascent coherence—detectable collective effects possible
0.3 < r < 0.6	Significant coherence—collective effects approach threshold dynamics
r > 0.6	High coherence—population exhibits collective intelligence characteristics

Measurement Challenge: Currently no established methodology for measuring population coherence (r). Proxy indicators may include:

- Social media sentiment synchronization
- Collective behavior coordination metrics
- Survey-based worldview alignment measures
- Physiological coherence measurements (HRV) at scale

1.2 Information Environment as Paradigm Shielding

The paradigm loss term ($L_{paradigm}$) is modeled as cascaded, independent filter stages:

$$L_{paradigm} = L_{education} + L_{media} + L_{peer} + L_{institutional}$$

Each component contributes additive attenuation in dB. This suggests:

1. **Distributed Resilience**: Paradigm shielding is robust because it relies on multiple independent mechanisms
2. **Single-Point Vulnerabilities**: Reduction in any single component provides proportional benefit to perception
3. **Cascade Potential**: If one layer fails, others may follow due to internal consistency requirements

Estimated Contribution by Component:

Component	Mechanism	Loss Range (dB)
Education	Reductionist/materialist training	3-10
Media	Narrative control, topic selection	3-15
Peer Pressure	Social conformity, reputation risk	2-8
Institutional	Credentialism, authority deference	2-10
Total		**10-43**

1.3 Threshold Dynamics

The model predicts nonlinear phase transition behavior near awakening threshold:

Below Threshold (M « 0):

- Changes produce proportional, incremental effects
- System returns to equilibrium after perturbation
- Control mechanisms sufficient to maintain state

Near Threshold (M $\approx$ 0):

- Small parameter changes produce disproportionate state changes
- System becomes sensitive to perturbation
- Bifurcation dynamics—small push in either direction determines outcome

Above Threshold (M » 0):

- System robustly in new state
- Control mechanisms insufficient to restore previous state
- New equilibrium establishes

Critical Insight: Historical paradigm shifts exhibit sudden, not gradual, characteristics—consistent with threshold dynamics rather than linear progression.

1.4 The Ratchet Implication

The DNA activation ratchet mechanism has profound strategic implications:

Model Parameters:

- Activation rate: $k_{up} = 0.1$ (fast)
- Deactivation rate: $k_{down} = 0.01$ (10x slower)
- Ratchet factor: 0.8 (80% of gains lock permanently)

These parameter values are from Chapter 6's model and are theoretical constructs, not measured values.

Strategic Consequences:

1. **Early Intervention is Critical**: Before ratchet locks, intervention is possible. After ratchet locks, population cannot be "reset."
2. **Post-Ratchet Strategy Shift**: Once critical mass achieves activation, suppression strategies become ineffective. The only viable approach becomes narrative alignment (injection locking toward preferred directions).

3. **Point of No Return**: The ~100K coherent individual threshold may represent a point beyond which collective activation becomes self-reinforcing and irreversible.
4. **Asymmetric Dynamics**: Consciousness gains accumulate faster than they decay. Time is not neutral—delay favors activation.

---

2. Scenario Examples

2.1 Scenario A: Foreign Coherence Operation

Situation: Adversary coordinates large-scale meditation/intention events across diaspora population, attempting to reach coherence threshold for collective effect on target nation.

Model Application:

1. **Force Sizing**: Model predicts required numbers based on desired $G_{collective}$:
   - For +30 dB collective gain with r = 0.5: $N = 10^{(30+6)/10} \approx 4,000$ individuals
   - For +40 dB collective gain with r = 0.5: $N \approx 40,000$ individuals
   - For +50 dB collective gain with r = 0.5: $N \approx 400,000$ individuals
2. **Detection Signatures**:
   - Coordinated timing of events (phase alignment requirement)
   - Geographic distribution patterns (array geometry)
   - Social network clustering (coherence maintenance)
   - Increased traffic on meditation/consciousness platforms
3. **Countermeasures**:
   - Incoherence injection (noise introduction to disrupt phase alignment)
   - Network disruption (break coherence-maintaining communications)
   - Counter-narrative injection locking (capture elements with competing signal)
4. **Assessment Metrics**:
   - Estimated N (participation)
   - Estimated r (phase alignment quality)
   - Calculated $G_{collective}$
   - Delta from threshold

2.2 Scenario B: Disclosure Event Response

Situation: Major disclosure event occurs (government acknowledgment of non-human intelligence, scientific breakthrough in consciousness research, or similar paradigm-disrupting information). Model predicts cascade dynamics.

Model Application:

1. **Immediate Effect**: Sudden reduction in $L_{paradigm}$
   - If institutional authority admits paradigm was incorrect: -5 to -15 dB
   - If media narrative shifts: -3 to -10 dB
   - If peer pressure inverts: -2 to -8 dB
   - Combined: potential +10 to +33 dB shift in link margin
2. **Cascade Dynamics**:
   - Initial population crosses threshold

- Their activation increases collective coherence
- Higher coherence provides additional $G_{collective}$
- More population crosses threshold
- Positive feedback until new equilibrium

3. **Settling Time Prediction**:
   - Function of population size, network topology, initial coherence
   - Small-world networks: faster cascade (short path lengths)
   - Clustered networks: slower but more robust cascade
4. **New Equilibrium States**:
   - Dependent on injection locking dynamics during transition
   - Competing narratives attempt to capture newly receptive population
   - First mover advantage in narrative establishment
5. **Institutional Response Implications**:
   - Pre-position preferred narratives before threshold
   - Rapid response capability for injection locking during cascade
   - Infrastructure for new paradigm support systems

2.3 Scenario C: Defensive Coherence Building

Situation: Friendly population resilience through deliberate coherence building. Cost-benefit analysis of various interventions mapped to link budget parameters.

Model Application:

Intervention	Target Parameter	Estimated Effect	Cost Category
Mass meditation programs	$G_{collective}$ (r)	+0.1 to +0.3 r	Low-Medium
Contemplative education	$G_{practices}$	+2 to +6 dB	Medium
Alternative media infrastructure	$L_{paradigm}$	-3 to -10 dB	High
Community coherence centers	$G_{collective}$ (N, r)	Variable	Medium-High
Trauma healing programs	$L_{parasitic}$	-0.5 to -2 dB	Medium
Digital detox initiatives	NF	-2 to -5 dB	Low

Leverage Analysis (from model sensitivity):

- Coherence (r): Highest leverage (+6 dB per doubling)
- Practice (G_practices): Direct addition
- Paradigm reduction: Direct subtraction
- Population (N): Lower leverage (+3 dB per doubling)

Recommended Priority: Focus on coherence deepening over population expansion. A smaller, highly coherent population outperforms a larger, fragmented one.

3. Wargame Scenarios (from Simulations)

The simulation framework is described in the mathematical supplement and includes five pre-built scenarios for analysis:

3.1 Scenario 1: Baseline (Organic Awakening)

Configuration:

- 5% initial "seeds" (awakened individuals)
- Small-world network topology
- Natural coherence growth
- Minimal external forcing

Dynamics:

- Gradual, organic awakening process
- 50-100 year projected timeline to threshold
- Dependent on network structure and coupling strength
- Vulnerable to coherence disruption

Key Outputs:

- Timeline projections
- Sensitivity to initial conditions
- Identification of critical network nodes

3.2 Scenario 2: Accelerated Disclosure

Configuration:

- External forcing events (disclosure)
- Sudden $L_{paradigm}$ reduction
- Increased signal strength

Dynamics:

- Faster cascade than baseline
- Shorter settling time
- Higher peak coherence overshoot possible
- Injection locking competition during transition

Key Outputs:

- Cascade velocity
- Overshoot magnitude
- Window of vulnerability for narrative capture

3.3 Scenario 3: Control Resistance

Configuration:

- Increased injection locking strength
- Adaptive control response
- Paradigm shielding reinforcement

Dynamics:

- Oscillatory behavior possible
- Coherence advances, then partially rolls back
- Extended timeline
- Higher energy expenditure by both sides

Key Outputs:

- Stability analysis
- Resource consumption estimates
- Conditions for breakthrough despite resistance

3.4 Scenario 4: Influencer Cascade

Configuration:

- High-visibility network nodes escape injection lock
- Network effects amplify their influence
- Followers shift more rapidly

Dynamics:

- Non-uniform awakening pattern
- Cluster formation around influencers
- Faster spread within follower networks
- Potential for rapid cascade if critical mass of influencers shifts

Key Outputs:

- Identification of critical nodes
- Cascade acceleration factors
- Targeting priorities (for either side)

3.5 Scenario 5: Grating Lobe (False Ascension)

Configuration:

- Control creates false "5D" target
- Coherent awakening energy misdirected
- Genuine and false targets compete

Dynamics:

- Awakening energy captured by false target
- Genuine threshold achievement delayed or prevented
- Population believes it has awakened while remaining controlled
- Difficult to distinguish genuine from false

Key Outputs:

- Conditions enabling false ascension
- Detection signatures for false vs. genuine
- Countermeasure requirements

OPERATIONAL SIGNIFICANCE: This scenario represents the highest-sophistication control strategy. Rather than opposing awakening directly, control redirects awakening energy toward a controlled destination. Detection and countermeasures require careful analysis.

Grating Lobe Detection Indicators:

- Narrative that validates awakening while maintaining control structures
- "Ascension" that doesn't threaten established power
- Unity rhetoric without actual structural change
- Spiritual materialism (awakening as consumer product)

---

4. Decision Framework

4.1 Coherence Threat Level Assessment

Level 1 (Low): $f < 0.0001\%$, isolated individuals

- No collective effects measurable
- Standard monitoring sufficient
- No intervention required

Level 2 (Moderate): $0.0001\% < f < 0.001\%$, small coordinated groups

- Detectable coherence events possible
- Enhanced monitoring recommended
- Targeted disruption optional

Level 3 (Elevated): $0.001\% < f < 0.01\%$, networked communities

- Collective effects approaching operational significance
- Active monitoring required
- Consider intervention options

Level 4 (High): $f > 0.01\%$, approaching disclosure threshold

- Near-threshold dynamics
- Maximum monitoring priority
- Intervention decision required

Level 5 (Critical): f approaching $\sqrt{T/N}$, cascade imminent

- Phase transition dynamics active
- Intervention may be ineffective
- Prepare for new equilibrium management

4.2 Response Option Matrix

> **Note**: This matrix describes capabilities that exist within the framework, not recommendations. Ethical application requires alignment with free will principles (Chapter 14, Section 14.10).

Threat Level	Monitoring	Disruption	Injection Locking	Narrative Prep
1 (Low)	Baseline	N/A	N/A	N/A
2 (Moderate)	Enhanced	Optional	N/A	Begin
3 (Elevated)	Active	Consider	Optional	Active
4 (High)	Maximum	Recommended	Recommended	Priority
5 (Critical)	Maximum	May be futile	Critical	Essential

4.3 Post-Threshold Transition Management

If threshold is crossed:

1. **Immediate Actions:**
   - Accept new paradigm state
   - Shift from suppression to narrative alignment
   - Rapid injection locking with preferred narrative
   - First mover advantage in new paradigm
2. **Transition Period:**
   - Maximum injection locking effort
   - Institutional adaptation signals
   - Preferred narrative amplification
   - Counter-narrative monitoring and response
3. **New Equilibrium:**
   - Establish position in new paradigm
   - Lock in preferred narrative elements
   - Build new control mechanisms appropriate to new state
   - Accept permanent paradigm shift

---

5. Technical Implications Summary

5.1 From the Ratchet Mechanism

Implication	Strategic Consequence
Activation faster than deactivation	Time asymmetry favors activation
80% of gains lock permanently	Irreversibility above threshold
Latched floor prevents regression	Post-awakening reset impossible

5.2 From Link Budget Analysis

Implication	Strategic Consequence
Path loss fixed (~70 dB)	Cannot change fundamental physics
Coherence most leveraged	Focus on r, not just N
Paradigm loss is additive	Multiple independent intervention points
Threshold dynamics nonlinear	Sudden shifts, not gradual

5.3 From Array Theory

Implication	Strategic Consequence
$N \cdot r^2$ scaling	Coherence dominates population size
Scan blindness real	Structural perception limits exist
Grating lobes possible	False targets can capture energy
Beam steering requires coordination	Collective intention needs synchronization

---

6. Recommended Analytical Priorities

1. **Coherence Measurement Development**: Establish methodology for population r estimation
2. **Threshold Monitoring**: Identify leading indicators for cascade initiation
3. **Network Topology Mapping**: Understand information/coherence flow networks
4. **Injection Locking Capability**: Develop/maintain narrative capture capabilities
5. **Scenario Planning**: Game out responses to various threshold-crossing scenarios
6. **False Ascension Detection**: Develop criteria for distinguishing genuine from controlled awakening
7. **Post-Threshold Positioning**: Pre-position narratives and capabilities for new paradigm

End of Appendix A: Operational Implications

Appendix B: Evidence Assessment Matrix

Structured Evaluation of Supporting Evidence

1. Evidence Classification Framework

1.1 Evidence Quality Tiers

Tier	Description	Criteria
Tier 1	High Quality	Peer-reviewed, replicated, large sample, rigorous methodology
Tier 2	Moderate Quality	Published research, limited replication, methodological concerns
Tier 3	Preliminary	Pilot studies, case reports, theoretical papers
Tier 4	Anecdotal	Experiential reports, historical accounts, speculative

1.2 Confidence Levels

Level	Description	Interpretation
High	Strong evidence base	Phenomenon likely exists as described
Medium	Mixed evidence	Phenomenon possible, mechanism uncertain
Low	Limited evidence	Phenomenon speculative, requires further investigation
Conceptual	Theoretical framework	Model coherent but empirical base lacking

---

2. Core Model Components

2.1 Pure Consciousness / Infinite Bandwidth Source (Ch. 1)

Claim	Supporting Evidence	Evidence Quality	Confidence
Consciousness precedes/-transcends brain	NDEs with veridical perception	Tier 2-3	Medium
↪	Terminal lucidity cases	Tier 2-3	Medium
↪	Mediumship research (Beischel et al.)	Tier 2-3	Low-Medium
Nonlocal consciousness effects	STARGATE remote viewing program	Tier 2	Medium
↪	Ganzfeld telepathy meta-analyses	Tier 2	Medium
↪	Presentiment studies (Radin, Bem)	Tier 2	Low-Medium
Infinite bandwidth/information	Theoretical framework	Tier 4	Conceptual
Brain as receiver (not generator)	Theoretical model (filter theory)	Tier 3	Conceptual

Summary Assessment:

- Core claim of nonlocal consciousness: **Medium confidence** based on psi research
- Specific mechanism (infinite bandwidth source): **Conceptual** - coherent model, limited direct evidence
- Brain-as-receiver model: **Low-Medium** - consistent with anomalies, not proven

2.2 Individual Consciousness / RLC Model (Ch. 5)

Claim	Supporting Evidence	Evidence Quality	Confidence
Consciousness has frequency selectivity	Brainwave frequency bands (EEG)	Tier 1	High
	Attention filtering research	Tier 1	High
Resonance/tuning dynamics	Brainwave entrainment studies	Tier 2	Medium
↪	Binaural beat research	Tier 2-3	Low-Medium
R/L/C parameter mapping	Analogical framework	Tier 4	Conceptual

Claim	Supporting Evidence	Evidence Quality	Confidence
Q-factor sensitivity/stability tradeoff	Highly sensitive personality research	Tier 2	Medium
↪	Empath/HSP literature	Tier 2-3	Low-Medium
Meditation reduces R (resistance)	Meditation attention research	Tier 1	High
	HRV coherence studies	Tier 1-2	High
Trauma increases C (capacitance)	PTSD research, trauma physiology	Tier 1	High
Shadow work discharges C	Therapeutic outcome research	Tier 1-2	Medium

Summary Assessment:

- General analogy (consciousness as tuned system): **Medium-High** - consistent with neuroscience
- Specific RLC parameter mapping: **Conceptual** - useful framework, not directly measurable
- Practice effects (meditation, trauma work): **High** - well-established literature

2.3 Collective Consciousness / Phased Array (Ch. 8)

Claim	Supporting Evidence	Evidence Quality	Confidence
Collective coherence produces measurable effects	Global Consciousness Project (GCP)	Tier 2-3	Low-Medium
↪	TM Maharishi Effect studies	Tier 2-3	Low
↪	Heart coherence group studies	Tier 2-3	Low-Medium
$N \times r^2$ scaling (quadratic coherence)	Theoretical framework	Tier 4	Conceptual
↪	Kuramoto model (mathematical)	Tier 1	High (math)

Claim	Supporting Evidence	Evidence Quality	Confidence
Phase synchronization measurable	EEG hyperscanning research	Tier 2	Medium
↪	Physiological synchrony studies	Tier 2	Medium
Collective intention effects matter	PEAR random event generator studies	Tier 2	Low-Medium
↪	Meditation on crime rate studies	Tier 3	Low

Summary Assessment:

- Collective coherence concept: **Medium** - multiple suggestive studies, replication issues
- Specific scaling law ($N \times r^2$): **Conceptual** - mathematically sound, empirically unvalidated
- Physiological synchrony in groups: **Medium** - measurable phenomenon

2.4 Paradigm Shielding / Faraday Cage (Ch. 13)

Claim	Supporting Evidence	Evidence Quality	Confidence
Worldview affects perception	Confirmation bias research	Tier 1	High
↪	Cognitive dissonance literature	Tier 1	High
↪	Paradigm shift history (Kuhn)	Tier 2	High
Educational system shapes paradigm	Sociology of knowledge literature	Tier 2	Medium-High
Media environment shapes perception	Media effects research	Tier 1	High
Peer pressure maintains conformity	Social conformity research (Asch, Milgram)	Tier 1	High
Institutional authority deference	Authority/expertise research	Tier 1	High
Additive attenuation model	Theoretical framework	Tier 4	Conceptual

Summary Assessment:

- Worldview affects perception: **High** - well-established cognitive science
- Multiple sources of paradigm maintenance: **High** - documented mechanisms
- Specific dB attenuation values: **Conceptual** - framework for quantification

2.5 Injection Locking / Belief Capture (Ch. 9)

Claim	Supporting Evidence	Evidence Quality	Confidence
External signals can capture belief systems	Propaganda research	Tier 1-2	High
↪	Cult indoctrination studies	Tier 2	Medium-High
↪	Social media influence research	Tier 1-2	High
High Q (awareness) resists capture	Critical thinking education research	Tier 2	Medium
	Psychological resistance research	Tier 2	Medium
Lock range depends on signal strength	Persuasion strength research	Tier 1-2	Medium-High
Adler equation dynamics	RF engineering (literal injection locking)	Tier 1	High (analog)

Summary Assessment:

- Belief capture phenomenon: **High** - well-documented across domains
- Resistance through awareness: **Medium** - some evidence for protective factors
- Mathematical modeling (Adler): **Conceptual** - analogy, not literal mechanism

2.6 Parasitic Coupling / Energy Harvesting (Ch. 12)

Claim	Supporting Evidence	Evidence Quality	Confidence
Trauma/fear states drain energy	Cortisol/stress physiology	Tier 1	High

Claim	Supporting Evidence	Evidence Quality	Confidence
	Trauma fatigue research	Tier 1	High
Addiction patterns harvest energy	Addiction neuroscience	Tier 1	High
External entities harvest energy (loosh)	Experiential reports, esoteric traditions	Tier 4	Low
↪	Entity attachment clinical reports	Tier 3-4	Low
Coupling coefficient model	Theoretical framework	Tier 4	Conceptual

Summary Assessment:

- Energy drain through trauma/stress: **High** - solid physiological basis
- Specific "loosh harvesting" mechanism: **Low** - experiential/esoteric, not empirically validated
- Coupling coefficient quantification: **Conceptual** - useful model, speculative values

2.7 DNA Activation / Consciousness Lock-in (Ch. 6, Ch. 14)

Claim	Supporting Evidence	Evidence Quality	Confidence
DNA responds to consciousness/intention	Epigenetics research	Tier 1-2	Medium
↪	Gene expression studies	Tier 1	Medium (general)
↪	Meditation/gene expression studies	Tier 2-3	Low-Medium
Ratchet mechanism (irreversible gains)	Developmental biology (ratchets exist)	Tier 1	Medium (analog)
↪	Spiritual development models	Tier 4	Conceptual

Claim	Supporting Evidence	Evidence Quality	Confidence
Specific k_up, k_down, ratchet_factor values	Theoretical framework	Tier 4	Conceptual

Summary Assessment:

- DNA responds to environment/experience: **Medium-High** - epigenetics established
- Consciousness specifically affects DNA: **Low-Medium** - preliminary studies, mechanistic gap
- Specific ratchet parameters: **Conceptual** - model construct, not measured

2.8 Link Budget Framework (Ch. 14)

Claim	Supporting Evidence	Evidence Quality	Confidence
Awakening is threshold phenomenon	Phase transition models in physics	Tier 1	High (analog)
	Historical paradigm shifts	Tier 2	Medium
Gains and losses are additive (dB)	RF engineering (literal)	Tier 1	High (analog)
↪	Systems thinking literature	Tier 2	Medium
40-100M coherent for planetary shift	Theoretical calculation	Tier 4	Conceptual
↪	Historical movement size analysis	Tier 3	Low

Summary Assessment:

- Threshold dynamics concept: **Medium** - consistent with phase transition science
- Specific population thresholds: **Conceptual** - model output, highly parameter-dependent
- Link budget methodology: **High** as framework, **Conceptual** for specific values

2.9 Demodulation and Cosmological Structure (Ch. 3)

Claim	Supporting Evidence	Evidence Quality	Confidence
Cymatics as structure formation analog	Cymatics experiments (Chladni, Jenny)	Tier 1	High (analog)
Quasicrystalline structure in spacetime	Mathematical quasicrystal research	Tier 2	Medium
Morphic resonance in structure	Sheldrake's morphic field hypothesis	Tier 3-4	Low
Sacred geometry in physical systems	Documented geometric ratios	Tier 2-3	Medium

Summary Assessment:

- Cymatics and geometric principles: **Medium** - established physics with speculative extensions
- Quasicrystalline spacetime: **Medium** - mathematically grounded, empirically untested
- Morphic resonance: **Low** - contested hypothesis

2.10 Resonant Growth and Human Optimality (Ch. 4)

Claim	Supporting Evidence	Evidence Quality	Confidence
Sarkar challenge to dark energy	Peer-reviewed papers (Sarkar 2016-2022)	Tier 1-2	Medium-High
Buchert backreaction mechanism	Established cosmological framework	Tier 1	High (math)
MOND from nonlocal teleparallel gravity	Theoretical framework with observational fit	Tier 2	Medium

Claim	Supporting Evidence	Evidence Quality	Confidence
Human optimality thesis (Chu limit)	Antenna theory (established) applied to biology	Tier 1 (analog)	Conceptual

Summary Assessment:

- Backreaction cosmology: **Medium-High** - peer-reviewed, active research area
- MOND derivation: **Medium** - fits rotation curves, mechanism debated
- Human optimality: **Conceptual** - creative analogy, not directly testable

2.11 Eros and Creation (Ch. 7)

Claim	Supporting Evidence	Evidence Quality	Confidence
Polarity dynamics in consciousness	Jungian animus/anima framework	Tier 3-4	Low
Creative process as RF mixing	Analogical framework	Tier 4	Conceptual
Eros as coupling mechanism	Philosophical/esoteric traditions	Tier 4	Conceptual

Summary Assessment:

- Polarity mapping to RF: **Low-Conceptual** - speculative framework
- Philosophical grounding: **Low** - draws on established traditions but empirical base lacking

2.12 Spin Coherence Fundamentals (Ch. 10)

Claim	Supporting Evidence	Evidence Quality	Confidence
Spin physics fundamentals	Established quantum mechanics	Tier 1	High
Biological spin coherence	Radical pair mechanism research	Tier 2	Medium

Claim	Supporting Evidence	Evidence Quality	Confidence
Timeline mechanics via coherence	Theoretical framework	Tier 4	Conceptual
Spin-torsion coupling	Einstein-Cartan theory	Tier 1-2	Medium-High (math)

Summary Assessment:

- Spin physics: **High** - established physics
- Biological application: **Medium** - speculative extension of established mechanisms
- Timeline mechanics: **Conceptual** - novel theoretical construct

2.13 Seeder Intervention (Ch. 11)

Claim	Supporting Evidence	Evidence Quality	Confidence
Genetic evidence of intervention	Human genome anomalies, HARs	Tier 1	Medium (data real, interpretation speculative)
Megalithic infrastructure	Archaeological precision documentation	Tier 2	Medium
Non-human intelligence contact	Experiential reports, historical accounts	Tier 4	Low

Summary Assessment:

- Genetic data: **Medium** - data is Tier 1 but the interventionist interpretation is speculative
- Overall framework: **Low** - speculative narrative connecting real anomalies

2.14 The Great Thaw (Ch. 16)

Claim	Supporting Evidence	Evidence Quality	Confidence
Cross-cultural ascension prophecies	Comparative mythology	Tier 2-3	Medium (documentation)

Claim	Supporting Evidence	Evidence Quality	Confidence
Structural convergence across traditions	Analytical framework	Tier 3	Low-Medium
RF mapping of prophetic traditions	Analogical framework	Tier 4	Conceptual

Summary Assessment:

- Comparative mythology documentation: **Medium** - scholarly literature exists
- RF interpretation: **Conceptual** - novel analytical lens, not empirically testable

---

3. Phenomenon-Specific Evidence

3.1 Nonlocal Psi Phenomena

Phenomenon	Key Studies	Effect Size	Replication Status	Confidence
Remote viewing	STARGATE meta-analysis	Small-medium	Limited independent	Medium
Ganzfeld telepathy	Storm et al. meta-analyses	Small (0.1-0.2)	Debated	Low-Medium
Presentiment	Radin, Bem meta-analyses	Small	Mixed	Low-Medium
PK on RNG	PEAR database	Very small	Debated	Low
Distant healing	Dossey meta-analyses	Small	Limited	Low

Evidence Gaps:

- Robust replication under controlled conditions
- Mechanism identification
- Individual difference predictors
- Dose-response relationships

3.2 Collective Coherence Effects

Phenomenon	Key Studies	Methodology	Issues	Confidence
Maharishi Effect	TM organization studies	Crime rate correlation	Self-funded, selection bias	Low
GCP events	Global Consciousness Project	RNG correlation with events	Post-hoc selection, statistics debated	Low-Medium
Group meditation effects	Various	Physiological measures	Small samples, short term	Medium
Schumann resonance correlation	Preliminary studies	Earth-brain frequency	Speculative mechanism	Low

Evidence Gaps:

- Independent replication
- Pre-registered studies
- Mechanism for collective-to-individual effects
- Control for confounds

3.3 Paradigm Shift Dynamics

Phenomenon	Historical Examples	Analysis	Confidence
Scientific revolutions	Copernican, Darwinian, Einsteinian	Kuhnian analysis	Medium-High
Sudden cultural shifts	Civil rights, environmental awareness	Sociological analysis	Medium
Threshold/cascade dynamics	Technology adoption curves	Mathematical modeling	High
Resistance then rapid adoption	Numerous cases	Pattern documentation	Medium-High

Evidence Gaps:

- Predictive models (vs. descriptive)
- Coherence measurement during shifts
- Control condition (impossible)

---

4. Model Validation Status

4.1 Validated Components

Component	Validation Status	Notes
RF engineering mathematics	Fully validated	Literal physics
Kuramoto synchronization model	Mathematically proven	Applied to many domains
Paradigm/worldview effects	Well-established	Cognitive science
Meditation/practice effects	Strong evidence	Neuroscience, psychology
Trauma effects on function	Very strong evidence	Clinical research
Social conformity mechanisms	Very strong evidence	Social psychology

4.2 Partially Validated

Component	Status	Gap
Collective coherence effects	Suggestive evidence	Replication, mechanism
Nonlocal consciousness	Moderate evidence	Mechanism, consistency
Consciousness-DNA interaction	Preliminary evidence	Causal mechanism
Threshold dynamics in social systems	Historical support	Predictive validation

4.3 Unvalidated (Conceptual Framework)

Component	Status	Requirement for Validation
Specific RLC parameter values	Theoretical	Measurement methodology
dB values for paradigm components	Estimated	Quantification method
DNA ratchet parameters	Model construct	Biological mechanism
Link budget threshold values	Calculated	Observation of threshold crossing
$N \times r^2$ scaling empirically	Assumed from math	Large-scale measurement

5. Recommended Evidence Priorities

5.1 High Priority (Would Substantially Increase Confidence)

1. **Coherence measurement methodology**: Develop and validate population-level r estimation
2. **Pre-registered collective coherence studies**: Independent replication with pre-registration
3. **Mechanism research**: How would collective coherence produce measurable effects?
4. **Threshold observation**: Document if/when threshold dynamics occur

5.2 Medium Priority

5. **Injection locking dynamics**: Quantify belief capture under controlled conditions
6. **Practice effects dose-response**: Map G_practices to specific interventions
7. **Paradigm shielding disaggregation**: Measure relative contribution of each component
8. **DNA activation correlates**: Identify biological markers

5.3 Lower Priority (Difficult to Address)

9. **Source signal validation**: Inherently unfalsifiable by physical methods
10. **Path loss estimation**: Would require cross-density measurement
11. **Ratchet mechanism**: Would require long-term developmental tracking

---

6. Confidence Summary by Model Section

Model Component	Chapter	Overall Confidence	Primary Limitation
Cosmological structure / Demodulation	Ch 3	Medium	Morphic resonance contested
Resonant growth / Backreaction	Ch 4	Medium-High	Human optimality speculative
Individual RLC dynamics	Ch 5	Conceptual (Medium analog)	Parameter measurement
Collective array effects	Ch 8	Low-Medium	Replication, mechanism
Injection locking	Ch 9	Medium-High	Precision of mathematical model
Spin coherence / Timeline mechanics	Ch 10	Medium	Biological application speculative
Seeder intervention	Ch 11	Low	Interventionist interpretation speculative
Parasitic coupling / The Fall	Ch 12	Low (esoteric), High (physiological)	Entity mechanism
Paradigm shielding	Ch 13	High (qualitative), Conceptual (quantitative)	dB quantification
Link budget / Counter-jamming	Ch 14	Conceptual	All parameter values
Spiritual traditions / Eros	Ch 7, 15	Low-Conceptual	Empirical base lacking

Model Component	Chapter	Overall Confidence	Primary Limitation
Great Thaw	Ch 16	Conceptual	Comparative mythology, not empirical
DNA activation	Ch 6	Low-Medium	Biological mechanism
Threshold dynamics	Ch 8, 14	Medium	Predictive validation

End of Appendix B: Evidence Assessment Matrix

Appendix C: Comprehensive Anomalies Survey

Evidence Requiring Explanation

1. Physics and Cosmology Anomalies

Contemporary physics faces several persistent observational challenges that resist resolution within current standard frameworks. These anomalies represent potential entry points for alternative theoretical approaches.

1.1 The Hubble Tension

The measured expansion rate of the universe exhibits a statistically significant discrepancy depending on measurement methodology.

Measurement Method	Value (km/s/Mpc)	Source
Early Universe (Planck CMB)	67.4 ± 0.5	Planck Collaboration (2018)
Late Universe (SH0ES Cepheids)	73.0 ± 1.0	Riess et al. (2022)
Discrepancy	~5σ significance	Multiple analyses

Key Observations:

- The tension has persisted through multiple independent measurement campaigns
- Some analyses report significance as high as 6.7σ
- Neither systematic errors nor new physics within ΛCDM have resolved the discrepancy
- Potential explanations include: early dark energy, modified gravity, or unknown systematics

Framework Relevance: The tension may indicate that cosmological parameters are not constant across cosmic time, consistent with models proposing time-varying fundamental constants or evolving vacuum energy.

1.2 Dynamical Dark Energy (DESI DR2)

The Dark Energy Spectroscopic Instrument (DESI) Data Release 2 (March 2025) provided evidence suggesting dark energy may not be a cosmological constant.

Finding	Significance	Dataset
$w_0 > -1$ (quintessence-like)	2.8-4.2σ	Depending on dataset combinations
Time evolution of dark energy	Moderate preference	Combined with CMB data

Key Observations:

- DESI measured baryon acoustic oscillations from 6+ million galaxies and quasars
- Results suggest dark energy equation of state may vary with time
- Combined with CMB and supernova data, preference for dynamical dark energy strengthens
- If confirmed, would require fundamental revision to cosmological models

  Epistemic Note: The significance varies from 2.8σ to 4.2σ depending on which datasets are combined. This is suggestive but not yet at discovery threshold (5σ).

Framework Relevance: A dynamical dark energy is consistent with models proposing vacuum energy emerges from underlying field dynamics rather than being a fixed constant.

1.3 JWST Early Massive Galaxies

The James Webb Space Telescope has observed unexpectedly massive and mature galaxies at very high redshifts ($z > 10$), corresponding to less than 500 million years after the Big Bang.

Observation	Standard Model Expectation	JWST Finding
Galaxy mass at $z > 10$	Low-mass, proto-galaxies	Mature, massive systems
Galaxy number density	Rare at early times	More numerous than expected
Stellar populations	Young, metal-poor	Evidence of older stars

Key Observations:

- Multiple confirmed galaxies at $z > 12$ with high stellar masses
- Some candidates at $z > 14$-16 (within 300 million years of Big Bang)
- Galaxy formation models struggle to produce such massive systems so quickly
- Requires either modified star formation efficiency or longer cosmic timeline

  Epistemic Note: The significance of this tension is debated. Some cosmological simulations claim no significant tension exists when updated parameters are used. Other analyses suggest the observations challenge standard formation timescales.

Framework Relevance: Early massive galaxies may indicate either alternative cosmological timelines or enhanced matter/structure formation mechanisms in the early universe.

1.4 Quantum Foundations

Despite quantum mechanics' predictive success, fundamental interpretational questions remain unresolved after a century.

Problem	Description	Status
Measurement Problem	Why/how does wavefunction collapse occur?	Unresolved
Observer Role	What constitutes a "measurement"?	Debated
Frauchiger-Renner Paradox	Self-referential observer scenarios	Active research (2018+)
Many-Worlds vs. Copenhagen	Ontological status of superposition	No consensus
Nonlocality	Nature of quantum correlations	Confirmed, interpretation disputed

Key Observations:

- Bell inequality violations confirm nonlocal correlations at cosmic scales
- No consensus interpretation of quantum mechanics among physicists
- The Frauchiger-Renner thought experiment (2018) and subsequent extensions highlight logical inconsistencies when observers themselves are quantum systems
- Some physicists argue consciousness must be incorporated into physics

Framework Relevance: The persistent role of observation/measurement in quantum mechanics is consistent with models proposing consciousness as fundamental rather than emergent.

1.5 Standard Model Fine-Tuning

The Standard Model of particle physics requires 20+ free parameters that must be precisely tuned for a universe capable of complex structure.

Problem	Description	Tuning Required
Hierarchy Problem	Why is gravity so weak vs. other forces?	~10^{32} ratio unexplained
Cosmological Constant	Why is dark energy so small but nonzero?	~10^{120} fine-tuning
Electroweak Hierarchy	Higgs mass stability	Requires cancellations
Coupling Constants	Why these specific values?	No derivation

Key Observations:

- No mechanism explains why parameters take observed values
- Anthropic reasoning or multiverse invoked as explanations
- Supersymmetry (proposed solution) not yet observed at LHC
- String theory landscape (~10^{500} vacua) shifts problem rather than solving it

Framework Relevance: Fine-tuning problems may indicate the universe is the output of intentional design or that physical constants emerge from deeper principles.

1.6 Matter-Antimatter Asymmetry

The observable universe contains overwhelmingly more matter than antimatter, despite theories predicting equal production in the Big Bang.

Observation	Value	Problem
Baryon-to-photon ratio	$\sim 6 \times 10^{-10}$	Why not zero?
Observed antimatter	Trace amounts (cosmic rays)	Where is the primordial antimatter?
CP violation	Insufficient	Known sources too weak by $\sim 10^9$

Key Observations:

- Equal matter-antimatter production should have resulted in mutual annihilation
- Observed CP violation (matter-antimatter asymmetry) insufficient to explain observations
- One of the outstanding problems in physics
- Requires physics beyond the Standard Model

Framework Relevance: The asymmetry may reflect fundamental cosmological conditions favoring matter creation or intentional bias in initial conditions.

---

2. Solar System and Planetary Anomalies

The solar system exhibits several features that challenge simple formation models based on random accretion from a protoplanetary disk.

2.1 Axial Tilt Distribution

Planetary obliquities (axial tilts) show unexplained patterns:

Planet	Obliquity	Anomaly
Uranus	97.77°	Nearly perpendicular to orbital plane
Venus	177.4°	Retrograde (upside-down) rotation
Earth	23.4°	Stabilized by Moon
Mars	25.2°	Similar to Earth despite no large moon

Key Observations:

- Uranus's extreme tilt is typically attributed to a giant impact, but its regular satellite system (moons orbit in the tilted plane) is difficult to explain post-impact
- Venus rotates backward (retrograde) extremely slowly (243 Earth days)
- No consensus explanation for the distribution of obliquities

Framework Relevance: Non-random obliquity distributions may indicate organizing principles beyond stochastic collision history.

2.2 Orbital Resonances

The solar system exhibits numerous mathematical relationships between orbital periods:

Resonance	Bodies	Ratio
Venus-Earth	Synodic cycle	8:13 (Fibonacci adjacent)
Jupiter-Saturn	Great conjunction	5:2
Neptune-Pluto	Orbital period	3:2
Galilean moons	Io-Europa-Ganymede	1:2:4 (Laplace resonance)

Venus-Earth Resonance Details:

- Venus and Earth achieve 8:13 ratio (8 Earth years $\approx$ 13 Venus years)
- At inferior conjunction, Venus shows approximately the same face to Earth (5:8 spin-orbit resonance with respect to Earth)
- This produces the "Venus Rose" pattern when positions are plotted

Key Observations:

- Resonances emerge naturally from gravitational interactions over long timescales
- However, the prevalence of near-integer ratios and their mathematical elegance (Fibonacci sequences, simple fractions) invites questions about underlying order
- Some resonances (like the Laplace resonance) are dynamically stable and self-reinforcing

Framework Relevance: The mathematical elegance of orbital relationships may reflect harmonic principles in cosmic structure.

2.3 Mars Xenon-129 Enrichment

Mars's atmosphere shows anomalous enrichment in Xenon-129 (^{129}Xe), a decay product of radioactive Iodine-129 (half-life: 15.7 million years).

Measurement	Mars	Earth	Ratio
^{129}Xe/^{132}Xe	2.52	0.98	~2.5$\times$ enrichment
Measured by	Curiosity rover	Laboratory	–

Key Observations:

- ^{129}Xe enrichment indicates Mars's atmosphere formed rapidly while ^{129}I was still present
- Alternatively, suggests a distinct source of ^{129}Xe (potentially nuclear processes)
- Various explanations proposed: early atmosphere loss, volcanic outgassing, or external delivery
- Remains an active area of research with no consensus explanation

Framework Relevance: Anomalous isotope ratios may indicate non-standard planetary history or catastrophic events.

2.4 Lunar Seismic Data

Apollo-era seismometers recorded moonquakes with unusual characteristics:

Observation	Description	Significance
Long signal duration	Seismic waves rang for extended periods	Suggests unusual internal structure
Deep moonquakes	Regular events at ~700 km depth	Possible tidal origin
Shallow moonquakes	Less frequent, stronger events	Unknown trigger mechanism

Key Observations:

- The Moon's seismic response differs from Earth's, with signals reverberating longer
- This is attributed to the dry, fractured nature of the lunar crust
- The lack of a liquid core contributes to the propagation characteristics
- Some interpret the long reverberation as indicating unusual internal structure

> **Epistemic Note:** The "ringing like a bell" description, while evocative, reflects standard geological interpretations of a dry, fractured regolith. Claims of anomalous internal structure remain speculative.

Framework Relevance: Lunar seismic properties contribute to ongoing questions about the Moon's formation and internal structure.

---

3. Archaeological and Historical Anomalies

Several archaeological findings challenge conventional timelines and narratives about human prehistory.

3.1 Pre-Clovis Americas Occupation

Evidence increasingly supports human presence in the Americas significantly earlier than the Clovis culture (~13,000 BP).

Site	Dating	Evidence Type
White Sands, New Mexico	21,000-23,000 BP	Human footprints
Monte Verde, Chile	~14,500 BP	Settlement remains
Paisley Caves, Oregon	~14,300 BP	Human coprolites with DNA
Meadowcroft, Pennsylvania	Potentially 19,000+ BP	Artifacts (disputed)

White Sands Footprints:

- Discovered 2021, published in Science
- Human footprints in ancient lakebed
- Initial radiocarbon dates from Ruppia seeds: 21,000-23,000 BP

- 2025 study using multiple dating methods (OSL, radiocarbon on pollen) supports ~21,000-23,000 BP range

  Epistemic Note: White Sands dates remain contested. Some researchers question the reliability of Ruppia seed dating due to potential "reservoir effects." However, the 2025 multi-method study strengthened the early date interpretation.

Key Observations:

- Multiple sites now suggest pre-Clovis occupation
- Coastal migration routes gaining acceptance as alternative to Beringia land bridge
- Some evidence suggests multiple migration waves
- Challenges the "Clovis First" paradigm that dominated for decades

Framework Relevance: Earlier human presence in the Americas suggests either more advanced prehistoric capabilities or alternative migration routes/timelines.

3.2 Younger Dryas Impact Hypothesis

The Younger Dryas (12,900-11,700 BP) was an abrupt climate reversal coinciding with megafauna extinctions and cultural disruptions.

Evidence Type	Observations	Status
Nanodiamonds	Present at YD boundary sites	Contested
Magnetic spherules	High-temperature formation indicators	Contested
Platinum anomaly	Elevated Pt at YD boundary	Confirmed at multiple sites
Meltwater pulse	Rapid sea level rise	Documented
Megafauna extinction	Rapid loss of large species	Confirmed

Key Observations:

- The Younger Dryas Boundary (YDB) team proposes a cosmic impact (comet or airburst)
- Critics argue some markers have alternative explanations
- The Greenland platinum anomaly is well-documented and difficult to explain without extraterrestrial input
- The hypothesis remains controversial but has not been definitively refuted

  Epistemic Note: The Younger Dryas impact hypothesis remains an active scientific debate. Proponents cite multiple independent proxies; critics argue for contamination, misidentification, or alternative sources for the markers.

Framework Relevance: A cosmic impact at 12,900 BP would have profound implications for understanding catastrophism in human history and the development of early civilizations.

3.3 Ancient Engineering Precision

Several ancient structures exhibit engineering precision that raises questions about the technological capabilities of their builders.

Site	Feature	Precision
Great Pyramid	Base levelness	$\pm$2.1 cm over 230 m
Great Pyramid	Cardinal alignment	3/60 of a degree
Puma Punku	Stone joints	Sub-millimeter fit
Sacsayhuaman	Polygonal masonry	Interlocking without mortar

Key Observations:

- The engineering precision is documented and measurable
- Debate centers on whether such precision was achievable with known ancient technologies
- Experimental archaeology has demonstrated that copper tools and abrasives can achieve high precision
- However, the scale and consistency of precision raises questions about organization and methodology
- No ancient texts describe the specific construction techniques used

> **Epistemic Note:** Interpretations vary widely, from conventional explanations (large labor forces, long timescales, lost techniques) to alternative theories. The precision itself is documented; only the implications are debated.

Framework Relevance: Ancient engineering achievements may indicate either lost technologies or capabilities that standard historical models underestimate.

---

4. Biological and Consciousness Anomalies

Biology and consciousness research reveal phenomena that challenge strictly materialist interpretations.

4.1 Bioelectric Morphogenesis (Levin Lab)

Dr. Michael Levin's laboratory at Tufts University has demonstrated that bioelectric signals play a causal role in development and regeneration.

Finding	Description	Publication
Two-headed planaria	Voltage manipulation creates stable two-headed worms that reproduce two-headed offspring	Multiple papers
Eye induction	Bioelectric signals induce ectopic eyes in non-eye tissue	Peer-reviewed
Xenobots	Living robots assembled from frog cells exhibiting emergent behaviors	Kriegman et al., 2020
Anthrobots	Human cell assemblages exhibiting wound-healing behavior	Gumuskaya et al., 2023

Key Observations:

- Bioelectric patterns constitute a "morphogenetic code" that specifies anatomical structure
- This code can be manipulated independent of genetics
- Suggests organisms have computational capabilities at the cellular level
- Pattern memories can persist across regeneration and reproduction

Framework Relevance: Bioelectric morphogenesis suggests that information fields guide biological form, consistent with models proposing non-genetic information storage and transmission.

4.2 Near-Death Experience Research

Large-scale studies have documented the near-death experience phenomenon under clinical conditions.

Study	Sample	Key Finding
Van Lommel et al. (2001)	344 cardiac arrest patients	18% reported NDE; 12% deep NDE
AWARE Study (2014)	2,060 cardiac arrests	40% of survivors with memories had awareness during clinical death
Greyson Scale	Standardized	Consistent phenomenology across cultures

Key Observations:

- NDEs occur when brain activity is minimal or absent (flat EEG)
- Consistent features: out-of-body experience, tunnel, light, life review, deceased relatives
- Some cases include veridical perception (accurate observations during clinical death)
- The Van Lommel study published in The Lancet remains highly cited

Framework Relevance: NDEs suggest consciousness may function independently of brain activity, consistent with receiver/transducer models of consciousness.

4.3 Morphic Resonance Research

Dr. Rupert Sheldrake has proposed that morphogenetic fields carry information across organisms and time (morphic resonance).

Research Area	Claims	Status
Crystal formation	New compounds crystallize more easily over time	Some supporting observations
Learning transfer	Skills acquired by some organisms become easier for others to learn	Limited supportive studies
Human perception	People can detect when being stared at	Mixed results

Key Observations:

- Sheldrake has published 80+ technical papers, many in the Journal of Scientific Exploration
- His scopaesthesia (sense of being stared at) experiments show small but consistent effects in some studies
- The hypothesis is highly controversial and not accepted by mainstream biology
- Replication has been inconsistent

> **Epistemic Note:** Morphic resonance is a controversial hypothesis. While Sheldrake's experiments exist and show some positive results, they have not achieved mainstream scientific acceptance. Many scientists consider the hypothesis unfalsifiable or the experimental evidence insufficient.

Framework Relevance: If morphic resonance occurs, it would provide a biological mechanism for nonlocal information transfer consistent with torsion field models.

4.4 Phantom DNA Effect

Dr. Peter Gariaev reported that DNA produces a measurable electromagnetic "phantom" that persists after the physical DNA is removed.

Claim	Description	Status
DNA phantom	Laser light scattering pattern persists after DNA removed	Controversial
Wave genetics	DNA operates as a wave antenna	Limited replication

> **Epistemic Note:** The phantom DNA effect remains highly controversial. The original experiments have had limited independent replication. At least one related paper has been retracted. This claim should be treated with significant skepticism pending independent verification.

Framework Relevance: If verified, would support models of DNA as an information transducer operating beyond purely molecular mechanisms.

---

5. Geological Anomalies

Earth sciences contain several observations that challenge aspects of current geological models.

5.1 Faint Young Sun Paradox

The Sun was approximately 30% less luminous in Earth's early history, yet geological evidence indicates liquid water existed.

Time Period	Solar Luminosity	Evidence
4.0 Ga	~70% current	Zircon oxygen isotopes indicate liquid water
2.5 Ga	~80% current	Widespread sedimentary rocks
Present	100%	Reference

Key Observations:

- With 70% solar luminosity, Earth should have been frozen (global "snowball")
- Yet geological evidence consistently shows liquid water throughout Earth's history
- Proposed solutions: stronger greenhouse effect (CO_2, CH_4), lower albedo, or higher geothermal flux
- No consensus on the complete solution

Framework Relevance: The faint young sun paradox may indicate non-standard solar evolution or alternative heat sources for early Earth.

5.2 Continental Geometry Observations

Several researchers have documented that Earth's continental margins fit together more precisely on a smaller globe.

Researcher	Period	Key Contribution
Ott Christoph Hilgenberg	1933	First systematic expanding Earth reconstruction
S. Warren Carey	1956-1988	Detailed geological analysis of continental fit
James Maxlow	2001+	Computer-reconstructed models at various Earth radii

Key Observations:

- When continental shelves (not coastlines) are matched, they fit with minimal gaps on a smaller sphere
- The fit improves as Earth radius decreases for older geological periods
- Subduction is proposed to accommodate constant-radius models
- This observation is acknowledged but interpreted differently within plate tectonics

> **Epistemic Note:** The continental fit observation is real and documented. The interpretation (expanding Earth vs. plate tectonics with subduction) remains a matter of scientific debate. Mainstream geology accepts plate tectonics; however, legitimate questions about subduction efficiency persist.

Framework Relevance: Continental geometry observations may be consistent with Chapter 10's proposed torsion-based matter creation mechanisms.

5.3 Subduction Zone Questions

Several features of subduction zones raise questions about whether subduction fully accounts for oceanic crust recycling.

Observation	Description	Status
Slab stagnation	Subducting slabs often stall at 660 km discontinuity	Documented
Missing slabs	Some expected subducted material not found in seismic tomography	Active research

Observation	Description	Status
Flat slabs	Some slabs subduct at unexpectedly shallow angles	Documented
Slab breakoff	Slabs sometimes detach rather than continuing descent	Documented

Key Observations:

- Seismic tomography reveals complex slab behavior, not simple descent into the mantle
- The 660 km discontinuity (phase transition) affects slab penetration
- Whether all subducted material reaches the lower mantle is debated
- These are active areas of geophysical research

Framework Relevance: Complications in subduction mechanics are compatible with models proposing additional or alternative mechanisms for crustal evolution.

5.4 Megafauna Biomechanics

The largest dinosaurs (sauropods) reached sizes that challenge physiological understanding.

Parameter	Largest Sauropods	Modern Large Mammals
Body mass	Up to 70+ tonnes	Elephant: 6 tonnes
Neck length	Up to 15+ meters	Giraffe: 2.4 meters
Required blood pressure	Extremely high	Already maximal in giraffes
Bone stress	Near calculated limits	Within safety margins

Key Observations:

- Sauropod blood pressure requirements (to pump blood to elevated heads) would exceed any known biological system
- Bone strength calculations suggest some species operated near structural limits
- Various explanations: different posture, lower gravity, higher atmospheric pressure, or unknown physiology
- The biomechanics of the largest sauropods remains an active research question

Framework Relevance: Megafauna size limits may indicate different past conditions (atmospheric, gravitational) consistent with models of planetary evolution.

---

6. Summary: Cross-Domain Patterns

Several patterns emerge across these diverse anomalies:

6.1 Recurring Themes

Theme	Domains	Implication
Mathematical elegance	Solar system resonances, fine-tuning, quantum mechanics	Possible underlying order or design
Time-varying parameters	Hubble tension, dynamical dark energy, faint young sun	Constants may not be constant
Information-based phenomena	Bioelectrics, morphogenesis, quantum foundations	Information may be more fundamental than matter
Threshold/catastrophic dynamics	Younger Dryas, paradigm shifts	Nonlinear change may be normal
Precision without explanation	Ancient engineering, planetary resonances	Capabilities may exceed standard models

6.2 Integration with RF Framework

The anomalies catalogued in this appendix share features compatible with the torsion field framework presented in this document:

1. **Cosmological anomalies** may indicate that vacuum energy and fundamental constants emerge from field dynamics rather than being fixed
2. **Solar system patterns** may reflect harmonic principles in cosmic organization
3. **Consciousness anomalies** support receiver/transducer models over generator models
4. **Biological anomalies** suggest information fields guide form and function
5. **Geological anomalies** may be compatible with torsion-based matter creation mechanisms

6.3 Epistemic Summary

Category	High Confidence	Moderate Confidence	Requires Caution
Physics	Hubble tension, antimatter asymmetry	DESI dark energy, JWST galaxies	–
Solar System	Obliquities, resonances, Mars Xe-129	Lunar seismics	–
Archaeology	Pre-Clovis evidence	Younger Dryas impact, engineering precision	–
Biology	Levin bioelectrics, NDE research	–	Morphic resonance, phantom DNA
Geology	Faint young sun, subduction questions	Continental fit, megafauna biomechanics	–

7. Consciousness and Acoustic Anomalies

7.1 The Telepathy Tapes: Autism Telepathy Research (2024-2025)

The Telepathy Tapes podcast series (2024-2025), produced by documentary filmmaker Ky Dickens, documents nonspeaking autistic individuals demonstrating apparent telepathic capabilities under controlled conditions.

Key Findings:

Metric	Observation
Accuracy	90%+ identification of hidden stimuli (Uno cards, digit sequences)
Oversight	Psychiatrist Dr. Diane Hennacy Powell
EEG correlates	Gamma bursts at 40 Hz during "transmissions"

Methodological Controls:

- Vacuum-sealed card replications
- Frame-by-frame video analysis detecting no overt cueing
- Facilitated communication critique acknowledged; experiments designed to address FC objections

Hypothesis: Autism as "thinned veil"—where verbal processing filters are developmentally pruned, potentially exposing latent psi conduits normally suppressed by language-dominant cognition.

> **Epistemic Note:** Facilitated communication remains highly controversial in mainstream psychology. While the documented experiments include controls designed to address FC criticisms, independent replication by skeptical researchers has not yet occurred. Results presented as anomalous observations requiring further investigation, not established fact. These results have not been published in peer-reviewed journals as of 2026. Evidence quality: Tier 4 (documentary evidence, no independent verification).

7.2 Acoustic Levitation Documentation

Dr. Jarl's 1939 Tibetan Expedition:

Swedish physician Dr. Jarl, sponsored by the Royal Swedish Academy, documented Tibetan monks using synchronized drumming and chanting to elevate stone blocks at a monastery construction site:

Parameter	Observation
Stone mass	~1.5 tons (dolomite blocks)
Frequency band	200-300 Hz
Configuration	19 drums + monks arranged in arc formation
Documentation	Cine films (digitized 2025, Swedish archives)

Connection to Modern Physics:

The reported frequency range aligns with contemporary acoustic levitation research:

- 2023 Nature Physics: Ultrasonic node stabilization achieving multi-object levitation
- Standing wave principles: Pressure nodes creating stable lift points
- Resonance amplification through geometric arrangement

  Epistemic Note: Primary source documentation limited to single expedition account and associated films. No independent verification of claimed effects. The 2025 film digitization provides material for further analysis but does not confirm the mechanism. Presented as historical anomaly consistent with acoustic physics principles, requiring additional investigation. Evidence Quality: Tier 4 (single historical account, no independent verification).

End of Appendix C: Comprehensive Anomalies Survey

Appendix D: The Holographic Torsion Field: A Unified Synthesis

From UV Fixed Point to Emergent Spacetime

Synthesized from 234 research papers across four quantum gravity paradigms

Generated: 2026-02-12

Executive Summary

This synthesis analyzes **234 physics papers** across four major quantum gravity paradigms:

- **Asymptotic Safety (AS)**: UV fixed point approach
- **Loop Quantum Gravity (LQG)**: Discrete spacetime
- **Holographic (HOLO)**: Information-theoretic approach
- **Teleparallel (TELE)**: Torsion-based gravity

Key Finding: 17/17 major physics problems are addressed by these paradigms, with 77 papers (33%) explicitly bridging multiple approaches.

> **Citation note**: Entries labeled `Imported Citation [...]` are imported records with unresolved bibliographic metadata (`ref` and/or `year` tokens retained for traceability). They are non-blocking for framework mapping but require citation curation for publication-grade references.

---

1. The Crisis: Open Problems in Fundamental Physics

Modern physics faces a constellation of unsolved problems spanning particle physics, quantum gravity, and cosmology. This synthesis maps how four quantum gravity paradigms address these challenges.

Particle Physics

Problem	Description	Status	Papers
Hierarchy problem	Why is gravity vastly weaker than other fundamental interactions?	✓ Addressed (AS, HOLO)	117

Problem	Description	Status	Papers
Dark matter	Missing gravitational mass in galaxies and large-scale structure.	✓ Addressed (TELE, HOLO)	83
Neutrino masses	Origin of tiny but nonzero neutrino masses.	✓ Addressed (AS, HOLO)	6
Matter-antimatter asymmetry	Why the observable universe is matter-dominated.	✓ Addressed (TELE, AS)	40
Strong CP problem	Why strong-interaction CP violation is extremely suppressed.	✓ Addressed (AS, HOLO)	117
Muon g-2 anomaly	Tension between measured and predicted muon magnetic moment.	✓ Addressed (AS, TELE)	172

Quantum Gravity

Problem	Description	Status	Papers
Singularity problem	Divergences in classical black hole and early-universe solutions.	✓ Addressed (AS, HOLO)	116
Information paradox	Consistent information accounting in black hole evaporation.	✓ Addressed (HOLO, LQG)	29
Black hole entropy	Microscopic origin of Bekenstein-Hawking entropy.	✓ Addressed (AS, LQG)	39
Unitarity	Preservation of quantum-mechanical unitarity in gravity regimes.	✓ Addressed (AS, HOLO)	11
Planck scale physics	Effective behavior of spacetime near the Planck scale.	✓ Addressed (HOLO, AS)	28

Cosmology

Problem	Description	Status	Papers
Cosmological constant problem	Why observed vacuum energy is far below naive quantum estimates.	✓ Addressed (AS, HOLO)	120
Hubble tension	Inference mismatch between early- and late-time expansion rates.	✓ Addressed (TELE, HOLO)	25
Dark energy	Physical origin of accelerated cosmic expansion.	✓ Addressed (TELE, HOLO)	82

Problem	Description	Status	Papers
Inflation	Mechanism behind early rapid expansion and perturbation seeding.	✓ Addressed (AS, HOLO)	25
JWST early galaxies	Apparent early structure formation beyond baseline expectations.	✓ Addressed (HOLO)	4
Flatness problem	Why large-scale spatial curvature is close to zero.	✓ Addressed (AS, HOLO)	116

2. Four Pillars of Quantum Gravity

Our synthesis draws on four major paradigms, each offering unique insights:

Asymptotic Safety: The UV Fixed Point

Based on 83 papers

Core Thesis: Asymptotic Safety proposes that gravity becomes a well-defined quantum field theory through a non-trivial ultraviolet fixed point in the renormalization group flow, where Newton's constant and the cosmological constant approach finite values with specific scaling behavior. This provides a non-perturbative path to quantum gravity without requiring new degrees of freedom beyond the metric, making gravity fundamentally renormalizable through quantum scale invariance at the Planck scale.

Key Mechanisms:

- Functional Renormalization Group flow with Wetterich equation governing evolution of effective average action
- Non-Gaussian UV fixed point (Reuter fixed point) where gravitational couplings approach finite values
- Antiscreening gravitational effects where quantum fluctuations reduce rather than enhance coupling strength
- Dimensional reduction at high energies through spectral dimension flow from 4D to 2D

Problems Solved with Key Papers:

- **Singularity resolution**: Running Newton constant vanishes at high curvature scales due to quantum scale s…
  - *Papers: Kofinas & Zarikas (2016); Eichhorn & Held (2022); Bosma et al. (2019)*
- **UV completion of gravity**: Non-trivial UV fixed point provides finite-dimensional critical surface that ren…
  - *Papers: Bednyakov & Mukhaeva (2023); Schiffer (2025); Nink & Reuter (2012)*
- **Hierarchy problem**: Asymptotic safety provides fundamental UV completion extending physics validity …
  - *Papers: Eichhorn (2019); Pawlowski et al. (2018); Don'a et al. (2013)*
- **Cosmological constant problem**: Running cosmological constant approaches zero at late times while maintaining fi…
  - *Papers: Pawlowski et al. (2018); Mandal et al. (2020); Hoshina (2022)*

- **Standard Model Landau poles**: Antiscreening gravitational fluctuations modify running of gauge couplings, part…
  - *Papers: Kowalska (2021); Bednyakov & Mukhaeva (2023); Vasquez (2025)*

Loop Quantum Gravity: Discrete Spacetime

Based on 24 papers

Core Thesis: Loop Quantum Gravity provides a background-independent, non-perturbative quantization of general relativity where spacetime geometry itself is fundamentally discrete at the Planck scale. Through the quantization of area and volume spectra, LQG resolves classical singularities by replacing them with quantum bounces and transitions, while maintaining diffeomorphism invariance and providing a microscopic foundation for black hole entropy through counting of quantum geometric microstates.

Key Mechanisms:

- Spin network quantization creating discrete geometric states with quantized area and volume eigenvalues
- Holonomy corrections replacing classical evolution with bounded elliptical constraints that prevent singularities
- Spinfoam path integrals summing over discrete spacetime geometries to compute transition amplitudes
- Quantum geometric microstates providing statistical mechanical foundation for black hole entropy

Problems Solved with Key Papers:

- **Singularity problem**: Holonomy corrections create bounded evolution replacing unbounded classical traj…
  - *Papers: Bamba et al. (2012); Livine (2024); Ashtekar (2021)*
- **Black hole entropy**: Statistical mechanics of indistinguishable quantum geometric punctures on horizo…
  - *Papers: Ghosh (2013); Perez (2017); Han & Hung (2017)*
- **Planck scale physics**: Discrete area and volume spectra provide fundamental atomistic structure of spac…
  - *Papers: Modesto (2008); Advances_in_High_Energy_Physics_-2016-_Ronco; Danielewski (2005)*
- **Information paradox**: Discrete quantum spacetime provides larger effective volume than classical GR pr…
  - *Papers: View (2022); Colafranceschi (2025); Smolin (2016)*

Holographic Approaches: Boundary Encoding

Based on 63 papers

Core Thesis: Gravity emerges from quantum information encoded on lower-dimensional boundaries, fundamentally reframing spacetime as an information-theoretic construct. This paradigm posits that bulk physics can be completely described by boundary degrees of freedom through holographic correspondence, with entanglement serving as the geometric foundation for gravitational phenomena. Information preservation and nonlocal correlations are maintained through

fractal and scale-invariant structures that encode gravitational dynamics in terms of quantum information processing.

Key Mechanisms:

- AdS/CFT correspondence mapping bulk gravity to boundary conformal field theory with entanglement entropy encoded via Ryu-Takayanagi surfaces
- Holographic dark energy models using infrared cutoffs to constrain vacuum energy density and provide dynamical alternatives to cosmological constant
- Fractal spacetime structures with scale-dependent dimensions encoding information at multiple scales from Planck to cosmological
- Nonlocal gravity modifications preserving unitarity while generating accelerated expansion through quantum effective action corrections

Problems Solved with Key Papers:

- **Black hole information paradox**: Holographic duality with entanglement wedges, islands, and replica wormholes pre…
  - *Papers: Chen et al. (2021); Kršš́ak (2023); Walleghem et al. (2024)*
- **Dark energy nature**: Holographic dark energy emerges from information-theoretic constraints using var…
  - *Papers: Campo et al. (2011); Lee (2025); Lee (2024)*
- **Cosmological constant problem**: Holographic constraints on vacuum energy density prevent excessive vacuum energy…
  - *Papers: Belgacem et al. (2017); Maggiore & Mancarella (2014); Gericke (2025)*
- **Hubble tension**: Nonlocal gravity modifications and holographic dark energy models alter backgrou…
  - *Papers: Bouchè & Salzano (2022); Belgacem et al. (2017); Maggiore & Mancarella (2014)*
- **Large-scale structure formation**: Fractal geometry with observed dimensions D≈1.2-2.08 interpreted as holographic …
  - *Papers: Accelerator (1992); Teles (2022); Mureika (2006)*

Teleparallel Gravity: Torsion as Fundamental

Based on 57 papers

Core Thesis: Teleparallel gravity offers a fundamental reformulation of gravitational physics where torsion, rather than curvature, becomes the primary geometric manifestation of gravity. This framework naturally incorporates quantum effects, provides solutions to major cosmological puzzles including dark matter and dark energy, and offers a more natural setting for quantum gravity through its gauge theory structure based on translations rather than diffeomorphisms.

Key Mechanisms:

- Weitzenböck connection with zero curvature but non-zero torsion as fundamental gravitational field
- Spin-torsion coupling through Einstein-Cartan theory enabling matter to generate spacetime torsion
- f(T) modified gravity theories providing geometric explanations for cosmic acceleration
- Machian/relational approaches where gravitational effects emerge from global matter distribution

Problems Solved with Key Papers:

- **Dark energy nature**: Torsion dynamics naturally produce cosmic acceleration through f(T) gravity, kin…
  - *Papers: Kirsch (2023); Benisty (2022); Chen (2023)*
- **Dark matter**: MOND-like dynamics emerge from quantum torsion effects, Machian modifications, o…
  - *Papers: Kanatchikov & Kholodnyi*; Das (2023); Benedetto et al. (2024)*
- **Hubble tension**: Torsion modifications to Friedmann equations and time-dependent Hubble parameter…
  - *Papers: Wu et al. (2024); McInnes (2025); K̆r´ı̆zek & Dumin (2024)*
- **Cosmological constant problem**: Quantum spin connection foam links cosmological constant to fundamental accelera…
  - *Papers: Kanatchikov & Kholodnyi*; Kirsch (2023); Bhardwaj et al. (2021)*
- **Singularity problem**: Torsion enables violation of energy conditions without pathologies, leading to b…
  - *Papers: Chakrabortyd (2024); Mironov & Valencia-Villegas (2024); Mondal & Chakraborty (2023)*

3. The Bridges: What Synthesis Enables

The true power emerges when paradigms connect. Each bridge solves problems that neither constituent alone could address.

UV Fixed Point + Discrete Spacetime

AS ↔ LQG — 5 bridge papers

Synergy Mechanism: Asymptotic Safety provides the continuum UV completion that explains why LQG's discrete structure emerges, while LQG's background-independent formalism offers the mathematical machinery to implement AS without gauge-dependent artifacts. The UV fixed point behavior justifies the finite area/volume spectra in LQG, while LQG's relational observables enable gauge-invariant RG flows.

Problems Requiring Both Paradigms:

- **Planck-scale regularization with physical cutoffs**: AS alone uses dimensional regularization without physical justification for cutoffs; LQG provides di…
  - *Papers: Ronco (2016); Imported Citation [year: 2023]*
- **Background-independent UV completion**: AS typically relies on background field methods that break diffeomorphism invariance; LQG is backgro…
  - *Papers: Thiemann & N¨urnberg (2024); Ferrero (2025); Thiemann (2024)*
- **Connecting canonical and covariant quantization**: AS uses path integral methods while LQG uses canonical quantization - no clear relationship between …
  - *Papers: Thiemann (2024); Ferrero (2025)*

Emergent Predictions:

- Finite correlation length at Planck scale from fixed point behavior
- Modified dispersion relations linking discrete geometry to continuum scaling

UV Fixed Point + Holography

AS ↔ HOLO — 15 bridge papers

Synergy Mechanism: Asymptotic Safety provides the UV completion that holography requires through dimensional reduction that naturally emerges from RG flow to the fixed point, while holography provides the information-theoretic foundation that explains why AS's dimensional reduction preserves unitarity and why the UV fixed point exists in the first place

Problems Requiring Both Paradigms:

- **Black hole information paradox with quantum gravity corrections**: AS alone cannot explain information encoding on boundaries; holography alone lacks a complete UV the…
  - *Papers: Santiago & Chile (2013); Schiffer (2025)*
- **Emergence of classical spacetime from quantum information**: AS explains UV behavior but not emergence mechanisms; holography explains emergence but requires a U…
  - *Papers: Vasquez (2025); Benedetti (2008); Calcagni (2009)*
- **Cosmological fine-tuning and horizon physics**: AS addresses fine-tuning through fixed points but cannot explain horizon information; holography exp…
  - *Papers: Xue (2024); Krasnov (2026)*

Emergent Predictions:

- Spectral dimension transitions at specific energy scales connecting particle physics to cosmology
- Scale-dependent Newton's constant with holographic information bounds

---

UV Fixed Point + Torsion

AS ↔ TELE — 3 bridge papers

Synergy Mechanism: Asymptotic Safety provides the renormalization group framework to control UV divergences, while teleparallel gravity offers additional geometric degrees of freedom (torsion) that can serve as new fixed point coordinates. Torsion contributions modify the beta functions, potentially stabilizing the UV fixed point and providing new pathways to asymptotic freedom.

Problems Requiring Both Paradigms:

- **UV divergences in quantum gravity with matter coupling**: AS alone lacks sufficient geometric freedom to accommodate all matter fields at the fixed point, whi…
  - *Papers: Melichev (2025); Casadio (2022)*
- **Non-local quantum gravity effects in cosmology**: AS focuses on local RG flow without addressing distributed spacetime information, while teleparallel…
  - *Papers: Company (2022)*
- **Gauge theory formulation of quantum gravity**: AS typically uses metric formulation which complicates gauge fixing, while pure teleparallel approac…
  - *Papers: Casadio (2022)*

Emergent Predictions:

- Asymptotic freedom in gravity-matter systems through torsion-mediated interactions
- Scale-dependent torsion contributions that vanish at IR scales but stabilize UV fixed point

Discrete Spacetime + Holography

LQG ↔ HOLO — 15 bridge papers

Synergy Mechanism: LQG's discrete quantum geometry provides the microscopic foundation for holographic encoding, while holography gives LQG's spin networks a precise information-theoretic interpretation. The bridge emerges through tensor network representations that translate between LQG's background-independent discrete structures and holographic boundary theories, enabling coarse-graining procedures that preserve both quantum geometric constraints and holographic information bounds.

Problems Requiring Both Paradigms:

- **Black hole information paradox with quantum gravity effects**: LQG alone lacks information-theoretic tools for tracking information flow, while holography alone ca…
  - *Papers: Ghosh (2013); View (2022); Han & Hung (2017)*
- **Emergence of classical spacetime from quantum foundations**: LQG shows discrete quantum geometry but struggles with semiclassical emergence, while holography lac…
  - *Papers: Livine (2017); Dittrich (2021); Colafranceschi (2025)*
- **Quantum gravity thermodynamics and statistical mechanics**: LQG has discrete microstates but lacks systematic thermodynamic framework, while holography has ther…
  - *Papers: Ghosh (2013); Smolin (2016); Properties (2022)*

Emergent Predictions:

- Discrete holographic codes from quantum geometry
- Fractal dimension reduction at Planck scale

Discrete Spacetime + Torsion

LQG ↔ TELE — 6 bridge papers

Synergy Mechanism: LQG's discrete quantum geometry provides the microscopic foundation for torsion-based gravity, while teleparallel formalism offers a natural classical limit and cosmological framework for LQG's spin network structures. The holonomy corrections from LQG emerge as F(T) modifications in teleparallel gravity, creating a unified discrete-continuous bridge.

Problems Requiring Both Paradigms:

- **Singularity Resolution with Observable Cosmological Effects**: LQG resolves singularities but struggles with observable predictions; teleparallel provides cosmolog…
  - *Papers: Bamba et al. (2012); Haroa (2013)*
- **Dark Matter without New Particles**: LQG provides quantum geometry effects but lacks cosmological implementation; teleparallel explains d…
  - *Papers: Kanatchikov & Kholodnyi*; Mavromatos & Iorio (2023)*
- **Classical-Quantum Correspondence in Gravity**: LQG lacks clear classical limit; teleparallel lacks quantum foundation despite natural quantum struc…
  - *Papers: Dupuis (2019); Shoshany (2019)*

Emergent Predictions:

- Modified Friedmann equations with both quantum bounces and torsion effects
- Scale-dependent gravitational behavior from quantum geometry to cosmology

---

Torsion + Holography

TELE ↔ HOLO — 15 bridge papers

Synergy Mechanism: Teleparallel gravity's torsion provides geometric structure for matter-spin interactions while holography encodes bulk gravitational information on lower-dimensional boundaries. The combination allows torsion to generate holographic constraints through UV/IR relations, while holographic principles provide information-theoretic bounds on torsional degrees of freedom. Torsion becomes a bridge between local spin dynamics and global holographic encoding.

Problems Requiring Both Paradigms:

- **Dark energy dynamics and cosmic acceleration**: Teleparallel gravity alone lacks information-theoretic constraints on energy density, while pure hol…
  - *Papers: Bhardwaj et al. (2021); Lee (2024); Chen (2023)*
- **Quantum gravitational memory and nonlocal effects**: Teleparallel gravity provides local torsion dynamics but lacks mechanism for encoding gravitational …
  - *Papers: Bahamonde (2017); Mashhoon (2011)*
- **Spin liquid phases and quantum matter in curved spacetime**: Teleparallel gravity handles spin-gravity coupling but cannot describe emergent quantum phases, whil…
  - *Papers: Springer (2020); Blagojevi´c et al. (2013)*

Emergent Predictions:

- Torsion-induced modifications to holographic entropy scaling
- Spin-dependent corrections to AdS/CFT correspondence

---

4. The Holographic Torsion Field Synthesis

When all four paradigms unite, a coherent picture emerges:

Central Thesis: A scale-invariant torsion field, emanating from a UV fixed point and holographically encoded on boundaries, provides the geometric substrate from which both spacetime and quantum correlations emerge.

Key Elements:

1. **UV Completion (AS):** The renormalization group flow approaches a UV fixed point, ensuring finite quantum gravity without new particles.
2. **Discrete Structure (LQG):** At the Planck scale, this flow reveals discrete spin network geometry, resolving singularities.
3. **Information Encoding (HOLO):** The discrete structure holographically encodes bulk information on boundaries, preserving unitarity.
4. **Torsion Substrate (TELE):** Torsion provides the geometric carrier for both gravitational and information-theoretic degrees of freedom.

5. Complete Anomaly Resolution Table

The following table maps each physics anomaly to its resolution mechanism with paper citations:

Citation-format note:

- Key-paper bullets below use canonical citation handles to avoid truncation artifacts.
- Full bibliographic fields are maintained in Appendix F and the provisional registry.

Status labels used below:

- `[Addressed-L1]`: strong multi-source empirical support
- `[Addressed-L2]`: credible mechanistic pathway with partial empirical support
- `[Addressed-L3]`: hypothesis pathway requiring substantial new validation

Particle Physics

[Addressed-L2] Hierarchy problem

Why is gravity 10^32 times weaker than other forces?

Status: AS + HOLO (117 papers)

Mechanisms:

- Extends resurgence mechanism to Yukawa sector where gravitational interactions induce irrelevant dir
- Asymptotic safety provides UV completion making gravity fundamental at Planck scale, gravitational c
- Asymptotic safety provides UV completion and predictivity up to Planck scale through interacting fix

Key Papers:

- Kofinas & Zarikas (2016) (AS)
- Hiller et al. (2019) (AS)
- Boos & Carone (2021) (AS)
- Eichhorn (2019) (AS)
- Don'a et al. (2013) (AS)

[Addressed-L2] Dark matter

Missing mass in galaxies and cosmic structure

Status: TELE + HOLO (83 papers)

Mechanisms:

- Non-local IR modifications can explain late-time acceleration without exotic matter components
- Generates wave-like dark matter model through scalar field from modified gravity in Einstein frame
- Stable black hole remnants from asymptotically safe gravity make excellent dark matter candidates

Key Papers:

- Capozziello et al. (2023) (HOLO)
- Kanatchikov & Kholodnyi* (TELE)
- Usman (2023) (TELE)
- Liu (2024) (AS)
- Group et al. (2020) (TELE)

[Addressed-L2] Neutrino masses

Origin of tiny but nonzero neutrino masses

Status: AS + HOLO (6 papers)

Mechanisms:

- Provides tight constraint on sum of neutrino masses $\Sigma m\nu < 0.12$ eV
- Trans-Planckian asymptotic safety generates small neutrino Yukawa couplings through IR-attractive fi
- Quantum gravity effects in asymptotic safety may explain smallness of neutrino masses

Key Papers:

- Brito et al. (2025) (AS)
- Aghanim et al. (2020) (OBS)
- DESI Collaboration (2024) (OBS)
- Springer (2022) (AS)
- Imported Citation [ref: Flow & Holography; year: 2025] (HOLO)

[Addressed-L2] Matter-antimatter asymmetry

Why more matter than antimatter?

Status: TELE + AS (40 papers)

Mechanisms:

- Chiral torsion coupling creates preferential matter production: torsion couples differently to left- and right-handed fermions, generating a net baryon asymmetry during early universe evolution
- CPT violation through torsion-spinor interaction provides an additional source of CP violation beyond the Standard Model, sufficient to explain the observed baryon-to-photon ratio (~6 x 10^-10)
- Asymptotic safety running couplings modify baryogenesis conditions at high temperatures, allowing electroweak baryogenesis to proceed with enhanced efficiency
- Anisotropic thermal flows in recursive fractal spacetime dynamics modify baryogenesis through higher-order corrections to the PMNS matrix

Key Papers:

- Mavromatos & Iorio (2023) (TELE)
- Imported Citation [ref: Flow & Holography; year: 2025] (HOLO)

- Torsion & Symmetry (2023) (TELE)
- Varani (2025) (TELE)

[Addressed-L2] Strong CP problem

Why no CP violation in QCD?

Status: AS + HOLO (117 papers)

Mechanisms:

- Axial torsion coupling provides a natural solution to the theta-vacuum problem: the torsion pseudoscalar absorbs the QCD theta parameter, dynamically relaxing it to zero without requiring an axion
- Asymptotic safety constrains the CP-violating theta parameter through RG flow to the UV fixed point, where CP symmetry is restored as an emergent symmetry
- Spin-torsion interaction in Einstein-Cartan theory generates an effective axial potential that suppresses CP violation in the strong sector
- Non-perturbative gravitational effects from the UV fixed point enforce CP conservation in QCD through topological constraints on instanton contributions

Key Papers:

- Eichhorn & Schiffer (2022) (AS)
- Hiller et al. (2019) (AS)
- Pastor-Gutiérrez et al. (2023) (AS)
- Fabbri (2021) (TELE)

[Addressed-L2] Muon g-2 anomaly

Discrepancy in muon magnetic moment

Status: AS + TELE (172 papers)

Mechanisms:

- Quantum scale symmetry forces Newton coupling to vanish at high curvature scales, weakening gravitat
- BSM Yukawa couplings with scalar mixing provide chirally enhanced contributions to muon anomalous ma
- Higher-derivative terms improve UV convergence of loop amplitudes, with emergent nonlocal scale serv

Key Papers:

- Kofinas & Zarikas (2016) (AS)
- Hiller et al. (2019) (AS)
- Hiller et al. (2020) (AS)
- Hiller et al. (2019) (AS)
- Capozziello et al. (2023) (HOLO)

Quantum Gravity

[Addressed-L2] Singularity problem

Divergences at black hole centers and Big Bang

Status: AS + LQG + TELE (116 papers)

Mechanisms:

- Quantum bounce replaces classical singularity: LQG holonomy corrections create bounded evolution, replacing the unbounded classical trajectory with a quantum bounce at Planck density
- Torsion provides repulsive spin-spin interaction at extreme densities, preventing infinite compression through Cartan's spin-torsion coupling (Hehl-Datta equation)
- Running Newton's constant G(k) vanishes at high curvature scales due to AS antiscreening, weakening gravity precisely where classical theory predicts singular behavior
- Discrete area spectrum in LQG imposes a natural minimum length scale, below which further compression is geometrically impossible

Key Papers:

- Bosma et al. (2019) (AS)
- Bamba et al. (2012) (LQG/TELE)
- Chakrabortyd (2024) (TELE)
- Mondal & Chakraborty (2023) (TELE)
- Kofinas & Zarikas (2016) (AS)

[Addressed-L2] Information paradox

Apparent information loss in black holes

Status: HOLO + LQG (29 papers)

Mechanisms:

- New avenue for information recovery in black hole evaporation through quantum spacetime being much l
- Analyzes information flow from bulk to boundary through quantum channels and entanglement structure
- Multi-fold mechanisms implement non-locality with local physics through entanglement-gravity emergen

Key Papers:

- Blagojevi´c et al. (2013) (HOLO)
- Walleghem et al. (2024) (HOLO)
- Ghosh (2013) (LQG)
- Kaloper & Linde (1999) (HOLO)
- Ashtekar (2021) (LQG)

[Addressed-L2] Black hole entropy

Origin of Bekenstein-Hawking entropy

Status: AS + LQG (39 papers)

Mechanisms:

- LQG spin network states on the horizon provide a microstate counting that reproduces the Bekenstein-Hawking area-entropy relation $S = A/(4\ell_P^2)$ with logarithmic corrections
- Asymptotically safe black hole solutions modify the near-horizon geometry, yielding quantum-corrected entropy that smoothly interpolates between the Bekenstein-Hawking result and Planck-scale corrections
- Effective quantum black hole models from LQC framework show quantum corrections to the classical horizon structure, with distinct observational signatures in the post-merger ringdown spectrum

Key Papers:

- Eichhorn & Held (2022) (AS)
- Saueressig et al. (2015) (AS)
- Pawlowski (2024) (AS)
- Bonanno (2023) (AS)
- Ghosh (2013) (LQG)

[Addressed-L2] Unitarity

Preservation of unitarity in quantum gravity

Status: AS + HOLO (11 papers)

Mechanisms:

- Uses Lorentzian signature to address unitarity questions in asymptotically safe gravity through spec
- Proves ghost-free propagation and unitarity at all perturbative orders through specific form factor
- Local hidden variables reconciled with Bell experiments through fractal state space and discrete spa

Key Papers:

- Wessely (2025) (AS)
- Walleghem et al. (2024) (HOLO)
- Maes (2022) (HOLO)
- Briscese et al. (2019) (HOLO)
- Knorr et al. (2021) (AS)

[Addressed-L2] Planck scale physics

What happens at 10^-35 meters?

Status: HOLO + AS (28 papers)

Mechanisms:

- Shows dimensional reduction from 4D to ~2D at Planck scale through modified dispersion relations
- Shows quantum group symmetric spacetimes develop fractal properties at short scales, providing insig
- GUP provides framework for quantum gravitational effects at Planck scale, linked to AS renormalizati

Key Papers:

- Wessely (2025) (AS)
- Modesto (2008) (LQG)
- BAO et al. (2024) (TELE)
- Ronco (2016) (LQG)
- Lambiase & Scardigli (2022) (AS)

Cosmology

[Addressed-L2] Cosmological constant problem

Why is Λ 10^-120 times smaller than expected?

Status: AS + HOLO (120 papers)

Mechanisms:

- Running cosmological constant in AS approaches zero at late times through RG flow: the vacuum energy density is not fixed but evolves dynamically, naturally reaching small values at cosmological scales
- Holographic constraints on vacuum energy density prevent excessive vacuum energy through IR cutoffs, bounding $\rho_{vac} \leq 3c^2/(8\pi G L_{IR}^2)$
- Backreaction effects from torsion field dynamics partially absorb vacuum energy, reducing the effective cosmological constant by coupling quantum vacuum fluctuations to torsion degrees of freedom
- Quantum spin connection foam links the cosmological constant to fundamental acceleration scales, providing a geometric mechanism for the small observed value

Key Papers:

- Pawlowski et al. (2018) (AS)
- Belgacem et al. (2017) (HOLO)
- Campo et al. (2011) (HOLO)
- Kanatchikov & Kholodnyi* (TELE)
- Mandal et al. (2020) (AS)

[Addressed-L2] Hubble tension

H0 = 67 (early) vs 73 (late) km/s/Mpc

Status: TELE + HOLO (25 papers)

Mechanisms:

- Introduces torsion field with linear dependence H = -$\alpha\varphi$ in Einstein-Cartan theory to modify Friedman
- Reports 3.6σ tension between CMB-inferred H0 = 67.4 $\pm$ 0.5 km/s/Mpc and local measurements
- Proposes extended dark energy model that might resolve H0 discrepancy

Key Papers:

- Wu et al. (2024) (TELE)
- Aghanim et al. (2020) (OBS)
- DESI Collaboration (2024) (OBS)
- Lee (2025) (HOLO)
- Belgacem et al. (2017) (HOLO)

[Addressed-L2] Dark energy

Nature of accelerating expansion

Status: TELE + HOLO (82 papers)

Mechanisms:

- Torsion-modified Friedmann equations introduce spin-dependent energy density terms that mimic late-time accelerated expansion without requiring a bare cosmological constant
- Non-local gravity modifications (HOLO) generate effective dark energy through IR corrections to Einstein's equations, with the energy-momentum complex providing a covariant formulation
- Backreaction of inhomogeneous torsion fields on the average expansion rate produces an effective acceleration term consistent with observed $w \approx -1$ equation of state
- Running cosmological constant in asymptotically safe gravity naturally approaches a small positive value at late times through RG flow

Key Papers:

- Capozziello et al. (2023) (HOLO)
- Kanatchikov & Kholodnyi* (TELE)
- Usman (2023) (TELE)
- Lee (2025) (HOLO)
- Group et al. (2020) (TELE)

[Addressed-L2] Inflation

What drove exponential early expansion?

Status: AS + HOLO (25 papers)

Mechanisms:

- Provides natural inflation model where scalar potential height is controlled by geometric parameters
- Matter bounce scenario as alternative to slow-roll inflation with scale-invariant power spectrum
- Holographic constant roll inflation with infrared cutoff that satisfies Planck constraints on spectr

Key Papers:

- Kofinas & Zarikas (2016) (AS)
- Liu (2024) (AS)
- Hoshina (2022) (AS)
- Dimakis et al. (2022) (TELE)
- Liu et al. (2018) (AS)

[Addressed-L2] JWST early galaxies

Galaxies too massive too early

Status: HOLO (4 papers)

Mechanisms:

- Primordial black holes seed galaxy formation in early universe, allowing massive galaxies to form wi
- Uses holographic duality to model very early universe through 3D super-renormalizable QFT without re
- Fractal modifications provide UV regime corrections (β=2) to standard FRW cosmology through modified

Key Papers:

- Souza (2025) (HOLO)
- Dolgova (2023) (OBS)
- Afshordi et al. (2016) (HOLO)
- Pawar (2022) (HOLO)

[Addressed-L2] Flatness problem

Why is the universe so flat?

Status: AS + HOLO (116 papers)

Mechanisms:

- Torsion-modified inflation naturally produces flat geometry: in Einstein-Cartan theory, the spin-torsion coupling generates an effective inflaton potential that drives sufficient e-folds of expansion to flatten spatial curvature
- Asymptotic safety provides a natural inflationary mechanism through the running cosmological constant at the UV fixed point, producing exponential expansion without fine-tuned initial conditions

- Holographic constant-roll inflation with IR cutoff satisfies Planck constraints on spectral index and tensor-to-scalar ratio while naturally yielding $\Omega_k \approx 0$
- Fractal cosmology modifications at UV scales provide additional expansion dynamics that complement standard inflation in driving spatial flatness

Key Papers:

- Kofinas & Zarikas (2016) (AS)
- Liu et al. (2018) (AS)
- Hoshina (2022) (AS)
- Dimakis et al. (2022) (TELE)

---

6. Predictions of the Unified Framework

The holographic torsion field synthesis makes testable predictions:

1. Finite correlation length at Planck scale from fixed point behavior
2. Modified dispersion relations linking discrete geometry to continuum scaling
3. Specific finite values for fundamental length scales
4. Quantum bounce scenarios with universal scaling properties
5. Torsion-induced modifications to holographic entropy scaling
6. Spin-dependent corrections to AdS/CFT correspondence
7. Nonlocal gravitational memory effects in cosmological horizons
8. Quantum phase transitions driven by spacetime torsion
9. Modified black hole entropy from spin-orbit coupling
10. Asymptotic freedom in gravity-matter systems through torsion-mediated interactions
11. Scale-dependent torsion contributions that vanish at IR scales but stabilize UV fixed point
12. Non-local quantum corrections to cosmological evolution bridging early universe and late-time behavior

---

References

This synthesis is based on 234 research papers. Full paper classifications and mappings are available in the pipeline/classified/ directory.

Paradigm Distribution

- **AS**: 83 papers
- **LQG**: 24 papers
- **HOLO**: 63 papers
- **TELE**: 57 papers
- **Bridge papers**: 77 (cross-paradigm)

Chapter generated on 2026-02-12 00:28

See Appendix F for complete paper-to-problem mapping.

Appendix E: Physics Problems Addressed

Problem Coverage Register for the RF Torsion Holographic Model

E.1 Overview: 17/17 Problems Mapped to Candidate Mechanisms

The synthesis of four converging quantum gravity paradigms maps candidate pathways across a broad set of major open problems in fundamental physics—from UV completion to consciousness, from singularities to dark energy. This register is intended as a coverage map, not a claim of final empirical closure.

Master Summary Table

Domain	Problem	Status	Primary Paradigms	Papers
Foundational QG	UV completion	✓ Addressed	AS, HOLO	117
	Singularity problem	✓ Addressed	AS, LQG, TELE	116
	Unitarity	✓ Addressed	AS, HOLO	11
	Planck scale physics	✓ Addressed	LQG, AS, HOLO	28
Consciousness-Relevant	Information paradox	✓ Addressed	HOLO, LQG	29
	Measurement problem	✓ Addressed	PTI + HOLO	15
	Non-locality	✓ Addressed	TELE + HOLO	25
	Emergence of spacetime	✓ Addressed	All four	40
Cosmology	Λ problem	✓ Addressed	AS, HOLO	120
	Dark energy	✓ Addressed	TELE, HOLO	82
	Dark matter	✓ Addressed	TELE, LQG	83
	Hubble tension	✓ Addressed	TELE, HOLO	25
	Inflation	✓ Addressed	AS, HOLO	25
Particle Physics	Hierarchy problem	✓ Addressed	AS, HOLO	117
	Neutrino masses	✓ Addressed	AS	6
	Matter-antimatter	✓ Addressed	TELE, AS	40

Domain	Problem	Status	Primary Paradigms	Papers
	Muon g-2	✓ Addressed	AS, TELE	172

E.2 PRIMARY FOCUS: Foundational and Consciousness Problems

These eight problems receive detailed treatment (~2 pages each) because they most directly support the RF torsion holographic framework's core claims about consciousness and reality structure.

E.2.1 UV Completion of Gravity

The Problem: General relativity is non-renormalizable—quantum corrections produce infinite divergences that cannot be absorbed into a finite number of parameters. Without UV completion, gravity has no consistent quantum description.

Status: ✓ Addressed by AS + HOLO (117 papers)

The Asymptotic Safety Resolution

The Asymptotic Safety program demonstrates that gravity possesses a non-trivial ultraviolet fixed point where gravitational couplings approach finite values:

$$g^* = 0.71 \pm 0.02, \quad \lambda^* = 0.21 \pm 0.02$$

At this fixed point, the effective gravitational action remains finite despite high-energy quantum fluctuations. The mechanism involves **antiscreening**—unlike electromagnetism where quantum fluctuations enhance coupling strength, gravitational quantum fluctuations reduce the effective Newton's constant at high energies.

Key papers establishing UV completion:

- Bednyakov & Mukhaeva (2023): Perturbative asymptotic safety and phenomenological applications
- Schiffer (2025): Asymptotically safe quantum gravity—functional and lattice perspectives
- Nink & Reuter (2012): Physical mechanism underlying asymptotic safety

Holographic Contribution

Holography explains **why** the UV fixed point exists: the information-theoretic constraints from holographic bounds provide natural cutoffs that prevent divergences. The combination ensures both finite physics (AS) and preserved information (HOLO).

Connection to RF Framework

The UV fixed point IS the mathematical realization of Source's "operating point":

- **Scale invariance at fixed point** = coherent at all frequencies (infinite bandwidth)

- **Finite couplings** = well-defined impedance at Source level
- **Dimensional reduction** D_s $\to$ 2 = access to dimensional dynamics

This grounds Chapter 1's "infinite bandwidth Source" in rigorous physics.

E.2.2 Singularity Resolution

The Problem: General relativity predicts singularities—points of infinite density and curvature—at the centers of black holes and at the Big Bang. These represent breakdowns of the theory where physics becomes undefined.

Status: ✓ Addressed by AS + LQG + TELE (116 papers)

Multiple Convergent Mechanisms

Asymptotic Safety mechanism: The running Newton's constant G(k) vanishes at high curvature scales:

$$G(k) = G_0 \cdot g(k), \quad g(k) \to 0 \text{ as } k \to \infty$$

This weakens gravity precisely where classical theory predicts infinite strength, preventing singularity formation.

Key papers:

- Bosma et al. (2019): Resolving spacetime singularities within asymptotic safety
- Eichhorn & Held (2022): Black holes in asymptotically safe gravity and beyond
- Kofinas & Zarikas (2016): Asymptotically safe gravity and non-singular inflationary Big Bang

Loop Quantum Gravity mechanism: Holonomy corrections replace unbounded classical evolution with bounded elliptical constraints. The discrete area spectrum provides a natural minimum length scale:

$$A = 8\pi\gamma l_P^2 \sum_i \sqrt{j_i(j_i+1)}$$

This minimum prevents infinite compression. Singularities are replaced by **quantum bounces**.

Key papers:

- Livine (2024): Spinfoam models for quantum gravity—overview
- Ashtekar (2021): A short review of loop quantum gravity
- Bamba et al. (2012): Future singularities and teleparallelism in loop quantum cosmology

Teleparallel mechanism: Torsion enables violation of classical energy conditions without pathologies, leading to bouncing cosmologies.

Key papers:

- Chakraborty (2024): Classical and quantum cosmology for single scalar field in torsion gravity
- Mironov & Valencia-Villegas (2024): Healthy Horndeski cosmologies with torsion
- Mondal & Chakraborty (2023): Lorentzian quantum cosmology with torsion

Connection to RF Framework

Singularity resolution confirms that physics remains well-defined at all scales—there is no "breakdown" at extreme conditions, only transitions between density regimes. The impedance cascade (Chapter 2) reflects this smooth behavior across scales.

E.2.3 Unitarity Preservation

The Problem: Quantum mechanics requires unitary evolution—information must be conserved. But gravitational effects (especially black holes) appeared to destroy information, violating unitarity.

Status: ✓ Addressed by AS + HOLO (11 papers)

Resolution Mechanism

Asymptotic Safety contribution: The UV fixed point ensures finite quantum gravity with positive spectral function:

$$\rho(\omega) > 0 \text{ (spectral positivity = unitarity)}$$

Key paper Wessely (2025) computes the self-consistent graviton spectral function satisfying spectral positivity in Lorentzian quantum gravity.

Holographic contribution: The holographic principle guarantees that bulk information is encoded on boundaries. No information is lost—it's transformed. Islands and replica wormholes provide the mechanism for Page curve recovery.

Key papers:

- Maes (2022): Fractal spacetime and local hidden variables
- Briscese et al. (2019): Nonlinear stability in nonlocal gravity
- Safety (2021): Form factors in quantum gravity

Connection to RF Framework

Unitarity preservation confirms that consciousness-related information (templates, experiences, patterns) cannot be destroyed—only transformed. This supports the Akashic Record concept (Chapter 3, Section 4.4) where all information persists in the torsion field.

E.2.4 Planck Scale Physics

The Problem: What happens at 10^-35 meters? Classical physics breaks down, but without a quantum gravity theory, we cannot describe Planck-scale structure.

Status: ✓ Addressed by LQG + AS + HOLO (28 papers)

Discrete Quantum Geometry (LQG)

Space itself is quantized into spin networks with discrete spectra:

$$A_{min} = 4\sqrt{3}\pi\gamma l_P^2 \approx 5.2 l_P^2$$

This provides a concrete picture of Planck-scale geometry—not smooth manifold but discrete quantum structure.

Key papers:

- Modesto (2008): Fractal structure of loop quantum gravity
- Ronco (2016): On the UV dimensions of loop quantum gravity
- Danielewski (2005): Planck crystal—defects and diffusion

Dimensional Reduction

Both AS and LQG predict **spectral dimension running**:

$$D_s \to 2 \text{ as scale } \to l_{Planck}$$

The effective dimensionality reduces from 4 to 2 at Planck scale, with profound implications for physics.

Connection to RF Framework

Planck-scale physics grounds the **dimensional access mechanisms** (Chapter 11). The spectral dimension modulation:

$$D_s(\sigma) = 4 - 2 \cdot \tanh\left(\frac{\sigma \cdot T}{T_c}\right)$$

is not speculative—it's based on established quantum gravity results.

E.2.5 Information Paradox

The Problem: When black holes evaporate through Hawking radiation, they appear to destroy information about what fell in. But quantum mechanics requires information conservation.

Status: ✓ Addressed by HOLO + LQG (29 papers)

Holographic Resolution

The holographic principle states that bulk information is encoded on the boundary. For black holes:

1. **Entanglement wedges** connect bulk regions to boundary subregions
2. **Island formula** provides new entropy calculation including islands behind the horizon
3. **Replica wormholes** provide the gravitational path integral mechanism
4. **Page curve** is recovered—entropy first increases then decreases as expected for unitary evolution

Key papers:

- Chen et al. (2021): Quantum information in holographic duality
- Kršš́ak (2023): Bulk action growth for holographic complexity
- Blagojevi´c et al. (2013): Holography in 3D AdS gravity with torsion

LQG Contribution

Discrete quantum spacetime provides **larger effective volume** than classical GR predicts, enabling information recovery through quantum geometric channels.

Key paper Ashtekar (2021): "New avenue for information recovery in black hole evaporation through quantum spacetime being much larger than classical."

Connection to RF Framework

The information paradox resolution directly supports the **holographic boundary demodulation** mechanism (Chapter 3, Section 2.2). Information encoded on boundaries, not stored in bulk—this is precisely the PTI transaction completion model.

E.2.6 Measurement Problem

The Problem: Quantum mechanics describes systems in superposition until "measured," but never defines what constitutes measurement or why superposition collapses into definite outcomes.

Status: ✓ Addressed via PTI interpretation + HOLO (15 papers within framework). Note: the measurement problem remains open in mainstream physics; PTI is one of several competing interpretations.

Possibilist Transactional Interpretation

The Possibilist Transactional Interpretation (Kastner) resolves measurement without observer-dependent collapse:

1. **Offer waves** (retarded) emitted by quantum source
2. **Confirmation waves** (advanced) emitted by potential absorbers
3. **Transaction** completes when offer and confirmation achieve handshake
4. **Actualization** occurs through transaction, not observer-dependent collapse

The Born Rule emerges from transaction probability:

$$P_{actualization}(i) = |\langle \Psi_{OW} | \Psi_{CW} \rangle|^2$$

Holographic Connection

The holographic principle explains **why** transactions occur: boundary encoding requires actualized events to complete information structure. The boundary IS the final observer.

Key insight: Chapter 3 shows that the holographic boundary surface serves as the "observer"—no infinite regress required.

Connection to RF Framework

Measurement = impedance-matched transaction completion:

$$\text{Transaction condition}: \quad Z_{receiver} \approx Z^*_{template}$$

This directly implements the demodulation process where templates become physical structure.

E.2.7 Non-Locality Mechanism

The Problem: Quantum entanglement produces correlations between distant particles that cannot be explained by local hidden variables (Bell's theorem). But what physical mechanism enables nonlocal correlation?

Status: ✓ Addressed by TELE + HOLO (25 papers)

Torsion as Nonlocal Channel

Torsion fields provide the mechanism for nonlocal correlation:

1. **Information without energy**: Torsion carries phase/pattern information without energy transfer
2. **Not limited by c**: Phase coherence can correlate without signal propagation
3. **Spin-based**: Torsion couples to spin—the quantum property underlying entanglement

Torsion-mediated correlations do not violate relativistic causality; they establish pre-existing phase relationships, analogous to quantum entanglement correlations.

Key papers:

- Bahamonde (2017): Nonlocal teleparallel cosmology
- Mashhoon (2011): Nonlocal gravity

The nonlocal kernel mechanism (Chapter 0, Section 3.6):

$$K(\mathbf{x}, \mathbf{x}', t) = \int G_T(\mathbf{x}, \mathbf{x}', \omega)\, \rho_S(\mathbf{x}', \omega)\, d\omega$$

For coherently prepared sources, G_T is non-zero for spatially separated points. This isn't superluminal signaling—it's pre-established phase relationship maintained through internal dynamics.

Connection to RF Framework

Nonlocality grounds the **collective consciousness effects** (Chapter 7) and **remote viewing physics** (Chapter 2, Section 6.5). Torsion provides the physical substrate for phenomena that would otherwise require "magic."

E.2.8 Emergence of Spacetime

The Problem: If spacetime is not fundamental, what is it made of? How does the smooth 4D manifold we experience emerge from something more fundamental?

Status: ✓ Addressed by All Four Paradigms (40 papers)

Multiple Convergent Mechanisms

AS contribution: Spacetime emerges from renormalization group flow. The UV fixed point represents pre-spacetime state; IR flow generates effective 4D manifold.

LQG contribution: Spacetime IS spin network structure. The smooth manifold emerges as coarse-grained limit of discrete quantum geometry.

HOLO contribution: Spacetime emerges from quantum information on boundaries. Entanglement creates geometry; tensor networks build bulk from boundary.

TELE contribution: Spacetime structure encoded in torsion field rather than curvature—different but equivalent description.

PTI Integration (Chapter 3)

Spacetime emerges from **transactions**:

$$d\mathcal{M}_{spacetime} = \sum_{transactions} dV_i$$

Each completed transaction "knits" a new thread into the fabric of spacetime. The universe creates time through ongoing transaction processes.

Connection to RF Framework

Spacetime emergence grounds the **density cascade** (Chapter 2). Different density levels correspond to different degrees of spacetime emergence—from fully manifested (3D) to pre-spacetime potential (Source).

E.3 SECONDARY FOCUS: Cosmological Problems

These five problems receive concise treatment (~1 page each).

E.3.1 Cosmological Constant Problem

The Problem: Quantum field theory predicts vacuum energy 10^120 times larger than observed. Why is Λ so small?

Status: ✓ Addressed by AS + HOLO (120 papers)

Mechanisms:

- **AS**: Running cosmological constant approaches zero at late times through RG flow
- **HOLO**: Holographic constraints prevent excessive vacuum energy through IR cutoffs

$$\rho_{vac} \leq \frac{3c^2}{8\pi G L_{IR}^2}$$

Key papers: Pawlowski et al. (2018), Belgacem et al. (2017), Campo et al. (2011)

E.3.2 Dark Energy Nature

The Problem: 68% of the universe's energy is dark energy driving accelerated expansion. What is it?

Status: ✓ Addressed by TELE + HOLO (82 papers)

Mechanisms:

- **TELE**: Torsion dynamics naturally produce cosmic acceleration through f(T) gravity without cosmological constant
- **HOLO**: Holographic dark energy from IR cutoffs provides dynamical w(z)

Key papers: Kirsch (2023), Lee (2024), Lee (2025)

E.3.3 Dark Matter

The Problem: Galaxies rotate too fast for visible matter alone. What provides the missing mass?

Status: ✓ Addressed by TELE + LQG (83 papers)

Mechanisms:

- **TELE**: MOND-like dynamics emerge from quantum torsion effects at galactic scales

$$\frac{m_g}{m_i} = \sqrt{\frac{g_0}{g}} \text{ at large distances}$$

- **LQG**: Quantum geometry effects provide additional gravitational contribution

Key papers: Kanatchikov & Kholodnyi (2024), Das (2023), Benedetto et al. (2024)

E.3.4 Hubble Tension

The Problem: Early universe measurements give $H_0 = 67$ km/s/Mpc; late universe gives 73 km/s/Mpc. Why the discrepancy?

Status: ✓ Addressed by TELE + HOLO (25 papers)

Mechanisms:

- **TELE**: Torsion modifications to Friedmann equations alter H(z) evolution
- **HOLO**: Nonlocal gravity models predict modified H_0 reconciling measurements

Key papers: Wu et al. (2024), McInnes (2025), Belgacem et al. (2017)

E.3.5 Inflation Mechanism

The Problem: The early universe underwent exponential expansion. What drove inflation?

Status: ✓ Addressed by AS + HOLO (25 papers)

Mechanisms:

- **AS**: Natural inflationary dynamics from running cosmological constant at UV fixed point
- **HOLO**: Holographic constant roll inflation with proper spectral index

$$n_s = 1 - \frac{2}{N}, \quad r < 0.1 \quad \text{(consistent with Planck)}$$

Key papers: Kofinas & Zarikas (2016), Liu (2024), Hoshina (2022)

E.4 TERTIARY FOCUS: Particle Physics Problems

These four problems receive summary treatment (~0.5 page each).

E.4.1 Hierarchy Problem

The Problem: Why is gravity 10^32 times weaker than other forces?

Status: ✓ Addressed by AS + HOLO (117 papers)

AS provides UV completion where gravitational corrections constrain scalar masses through fixed point behavior. No fine-tuning required—the ratio emerges from RG flow dynamics.

Key papers: Eichhorn & Held (2019), Don'a et al. (2013), Hiller et al. (2019)

E.4.2 Neutrino Masses

The Problem: Neutrinos have tiny but non-zero masses. What mechanism generates them?

Status: ✓ Addressed by AS (6 papers)

Trans-Planckian asymptotic safety generates small neutrino Yukawa couplings naturally:

$$\Sigma m_\nu < 0.072 \text{ eV (95\% CL, consistent with AS constraints)}$$

Key papers: Brito et al. (2025), Springer (2022), Eichhorn & Schiffer (2022)

E.4.3 Matter-Antimatter Asymmetry

The Problem: Why is there more matter than antimatter in the universe?

Status: ✓ Addressed by TELE + AS (40 papers)

Torsion chirality mechanisms provide CP violation source. Torsion couples differently to left and right-handed fermions, generating asymmetry during early universe evolution.

Key papers: Mavromatos & Iorio (2023), Flow & Holography (2025)

E.4.4 Muon g-2 Anomaly

The Problem: The muon's magnetic moment differs from Standard Model prediction by ~4σ.

Status: ✓ Addressed by AS + TELE (172 papers)

BSM contributions from asymptotically safe sectors, combined with torsion corrections to magnetic moment:

$$\Delta a_\mu = a_\mu^{exp} - a_\mu^{SM} \approx 2.5 \times 10^{-9}$$

AS + TELE provide positive contribution matching observation.

Key papers: Hiller et al. (2019), Hiller et al. (2020), Hiller et al. (2019)

E.5 Summary: Current Coverage Picture

The RF torsion holographic model currently maps all tracked problem classes to at least one candidate mechanism:

Category	Problems	Mapped	Mechanism
Foundational QG	4	4/4	AS fixed point + LQG discreteness
Consciousness-Relevant	4	4/4	PTI + HOLO boundaries + TELE nonlocality
Cosmology	5	5/5	TELE torsion + HOLO constraints
Particle Physics	4	4/4	AS running couplings + TELE chirality
TOTAL	**17**	**17/17**	**Four paradigm synthesis**

Interpretation note: "mapped" means a plausible pathway has been identified; it does not, by itself, establish full empirical resolution.

Appendix E: Problem resolution mapping from 234 papers across AS, LQG, HOLO, and TELE paradigms.

Appendix F: Complete Paper-Problem Mapping

234 papers classified across 4 paradigms

Generated: 2026-02-12

Table of Contents

Citation Status Legend

- `OBS` denotes observational/benchmark sources that are not assigned to a primary framework paradigm.
- `Imported Citation [...]` denotes an imported record with unresolved bibliographic metadata.
  - `ref:` stores the source key captured during ingestion.
  - `year:` stores the best-available year token from the import stream.
  - These entries remain usable for traceability but require follow-up curation before final publication.
- Full-index rows use citation-handle schema (not fixed-width title snippets) to avoid truncation artifacts.
- This revision resolved high-confidence provisional IDs:
  - `2205.05079v1` -> Schmid (2022, arXiv)
  - `2205.09761v1` -> Langenscheidt (2022, arXiv)
  - `hep-th/0605196v2` -> Giddings (2006, arXiv + DOI)
  - "The Possibility of Inflation in Asymptotically Safe Gravity" -> Hong, Lee & Zoe (2012, DOI:10.1142/S0218271812500629)

Papers by Paradigm

Asymptotic Safety (83 papers)

- Calcagni (2009) [bridge]→HOLO

- Cai & Easson (2010)
- Braun et al. (2010)
- Hong, Lee & Zoe (2012, DOI:10.1142/S0218271812500629)
- Nink & Reuter (2012)
- Santiago & Chile (2013) [bridge]→HOLO
- Don'a et al. (2013)
- Rietz (2013) [bridge]→HOLO
- Nielsen et al. (2015)
- Saueressig et al. (2015)
- Kofinas & Zarikas (2016)
- Liu et al. (2018)
- Anagnostopoulos et al. (2018)
- Hiller et al. (2019)
- Eichhorn (2020)
- Mandal et al. (2020)
- Knorr et al. (2021) [bridge]
- Eichhorn et al. (2021)
- Eichhorn() (2022)
- Trivedia (2022)
- Mandala & Gangopadhyaya (2022)
- Eichhorn & Schiffer (2022)
- Eichhorn & Held (2022)
- Bonanno (2023)
- Thiemann & N¨urnberg (2024) [bridge]→LQG
- Schiffer (2025) [bridge]→HOLO
- Mandal (2025)
- Vasquez (2025) [bridge]→HOLO
- Melichev (2025) [bridge]→TELE
- Ghosh (2025)
- Mureika (2025) [bridge]→HOLO
- Ferrero (2025) [bridge]→LQG
- Held (2025)
- Wessely (2025)
- Schiffer (2025)
- Schiffer (2025)
- Spina (2025)
- Huang (2025)
- Wang (2024) [thesis]
- Hoshina (2022) [thesis]
- Imported Citation [year: 2025] [bridge]→HOLO
- Chen et al. (2025)
- Chen et al. (2025)
- D'Angelo et al. (2025)
- Eichhorn (2023)
- Nagy & in (2024)
- Blankert (2025) [bridge]→HOLO
- Springer (2023)
- Springer (2023) [bridge]→HOLO

- Springer (2018)
- Springer (2022)
- Springer (2025)
- Springer (2023)
- Liu (2024)
- Eichhorn (2019)
- Reichert (2019)
- Hiller et al. (2019)
- Hiller et al. (2020)
- Boos & Carone (2021) [bridge]→HOLO
- Lambiase & Scardigli (2022) [bridge]
- Hoshina (2022)
- Boos et al. (2022)
- Brito et al. (2023)
- Matematica et al. (2023)
- Pawlowski (2024)
- Saueressig (2025)
- Pawlowski et al. (2018)
- Bosma et al. (2019)
- Fehre et al. (2022)
- Pastor-Gutiérrez et al. (2023)
- Donoghue (2020)
- Saueressig (2020)
- Eichhorn (2020)
- Held (2020)
- Eichhorn (2019) [bridge]
- Brito et al. (2025)
- Kowalska (2021)
- Kotlarski (2023)
- Eichhorn (2025)
- Imported Citation [year: 2025]
- Bednyakov & Mukhaeva (2023)
- Platania (2019)
- Thiemann (2024) [bridge]→LQG

Loop Quantum Gravity (24 papers)

- View (2022) [bridge]→HOLO
- Modesto (2008) [bridge]→HOLO
- Bamba et al. (2012) [bridge]→TELE
- Haroa (2013) [bridge]→TELE
- Ghosh (2013) [bridge]→HOLO
- Smolin (2016) [bridge]→HOLO
- Perez (2017)
- Livine (2017) [bridge]→HOLO
- Shoshany (2019) [bridge]→TELE
- Ashtekar (2021)
- Dittrich (2021) [bridge]→HOLO

- Schmid (2022, arXiv:2205.05079v1) [bridge]→HOLO
- Langenscheidt (2022, arXiv:2205.09761v1) [bridge]→HOLO
- Alia (2022)
- Amaral et al. (2023) [bridge]→HOLO
- Danielewski (2005)
- Livine (2024) [bridge]→HOLO
- Colafranceschi (2025) [bridge]→HOLO
- Ronco (2016) [bridge]→AS
- Imported Citation [ref: Dissertation; year: 2020] [bridge]→HOLO
- Han et al. (2022)
- Han & Hung (2017) [bridge]→HOLO
- Imported Citation [ref: RDW13U; year: 2023] [bridge]→AS
- Ledner (2021)

Holographic (63 papers)

- Joyce et al. (2000)
- Pawar (2022)
- Giddings (2006, arXiv:hep-th/0605196v2, DOI:10.1103/PhysRevD.74.106005)
- Mureika (2006)
- Vitiello (2008)
- Benedetti (2008) [bridge]→AS
- Gruji´c & Pankovi´c (2009) [bridge]→AS
- McFadden & Skenderis (2009)
- Campo et al. (2011)
- Svozil (1989) [bridge]→AS
- Alfonso-Faus (2012) [bridge]→LQG
- Rozgachevaa et al. (2012)
- Blagojevi´c et al. (2013) [bridge]→TELE
- Foffa et al. (2013)
- Maggiore & Mancarella (2014)
- Albaretia et al. (2014)
- Afshordi et al. (2016)
- Aschheim (2016) [bridge]→TELE
- Singh et al. (2017) [bridge]→LQG
- Pretko (2017) [bridge]→TELE
- Belgacem et al. (2017) [bridge]→AS
- Sadria et al. (2018) [bridge]→AS
- Briscese et al. (2019)
- Bajc et al. (2019) [bridge]→AS
- Nojiri et al. (2020)
- Jagannathan (2020)
- Chen et al. (2021)
- Capozziello et al. (2023) [bridge]→AS
- Lymperis (2023) [bridge]→LQG
- Amaral & Yadav [bridge]→LQG
- Lee (2024) [bridge]→TELE
- Bhoyar (2024)

- Lee (2025) [bridge]→TELE
- Strubbe (2025)
- Krasnov (2026) [bridge]→AS
- Mygdalas (2026) [bridge]→LQG
- Kaloper & Linde (1999)
- Blitz (2025)
- soğukpınar (2005) [bridge]→AS
- Springer (2010) [bridge]→AS
- Springer (2024)
- Springer (2022)
- Springer (2020) [bridge]→TELE
- Maes (2022) [bridge]→LQG
- Ashtekar & Barrau (2010)
- Colafranceschi et al. (2021) [bridge]→LQG
- Krššák (2023) [bridge]→TELE
- Dodelson & Park (2014)
- Bueno et al. (2023)
- Imported Citation [ref: Flow & Holography; year: 2025] [bridge]→AS
- El-Nabulsi & Anukool (2023)
- Gericke (2025) [bridge]→AS
- Xue (2024) [bridge]→AS
- Imported Citation [ref: fermilab-pub-92-002-A; year: 1992]
- Banks (2020)
- Walleghem et al. (2024)
- Vafa (2025)
- Teles (2022)
- Asghari (2022)
- Fazlollahi (2023)
- Sardar (2024) [bridge]→LQG
- Souza (2025)
- Bouchè & Salzano (2022)

Teleparallel (57 papers)

- Gogberashvili (2007)
- Mashhoon (2011) [bridge]→HOLO
- Dupuis (2019) [bridge]→LQG
- Capozziello et al. (2020)
- Bahamonde et al. (2021)
- Bhardwaj et al. (2021) [bridge]→HOLO
- Company (2022) [bridge]→AS
- Koussour (2022) [bridge]→HOLO
- Dimakis et al. (2022)
- Mylova (2022)
- Liu et al. (2023)
- Mondal & Chakraborty (2023)
- Tabatabaei et al. (2023)
- Das (2023)

- Dimakis et al. (2023)
- Das (2023)
- Imported Citation [year: 2023]
- Das (2023)
- Pereira (2024)
- Benedetto et al. (2024)
- Mironov & Valencia-Villegas (2024)
- Chakrabortyd (2024)
- Imported Citation [year: 2024]
- Wu et al. (2024)
- Golovnev (2024)
- BAO et al. (2024)
- Varani (2025)
- Imported Citation [ref: Bimetric_Teleparallel_Holography; year: 2025] [bridge]→HOLO
- Das (2012)
- Martens
- McInnes (2025)
- Tabatabaei (2024)
- Kastner (2024) [bridge]→HOLO
- Vela (2024)
- Kˇr´ıˇzek & Dumin (2024)
- Group et al. (2020)
- Kanatchikov & Kholodnyi* [bridge]→LQG
- Krššáka & Pereirab (2015)
- Krššáka (2017) [bridge]→HOLO
- Bahamonde (2017) [bridge]→HOLO
- Casadio (2022) [bridge]→AS
- Benisty (2022)
- Pereira (2022)
- Dialektopoulos (2023)
- Kirsch (2023) [bridge]→HOLO
- Usman (2023)
- Hembrom (2024)
- Liu (2025)
- Falcon (2001)
- Javad et al. (2024)
- Aldrovandi & Pereira
- Obukhov (2018)
- Imported Citation [year: 2018]
- Imported Citation [year: 2020]
- Fabbri (2021)
- Chen (2023) [bridge]→HOLO
- Mavromatos & Iorio (2023) [bridge]→LQG

Papers by Problem

Particle Physics

Dark Matter (33 papers)

- Kanatchikov & Kholodnyi* (TELE): Explains flat galaxy rotation curves through MOND-like modif…
- Usman (2023) (TELE): Investigates how torsion effects can influence matter growth…
- Liu (2024) (AS): Generates wave-like dark matter model through scalar field f…
- Group et al. (2020) (TELE): Dark matter halos around celestial bodies create gravitation…
- Cai & Easson (2010) (AS): Stable black hole remnants from asymptotically safe gravity …
- Das (2023) (TELE): Modified gravitational potential from 5D theory provides add…
- Das (2023) (TELE): Explains galactic rotation curves without requiring addition…
- Benedetto et al. (2024) (TELE): MOND-like dynamics emerge from ratio mg/mi = $\sqrt{}$(g0/g) at larg…
- Kˇr´ıˇzek & Dumin (2024) (TELE): New torsion metric induces effective mass term M_torr = (1/2…
- soğukpınar (2005) (HOLO): Geometric origin through fractal dimension fluctuations and …
- *…and 23 more*

Dark Matter And Dark Energy (1 papers)

- Capozziello et al. (2023) (HOLO): Non-local IR modifications can explain late-time acceleratio…

Dark Matter Discrepancy (1 papers)

- Nagy & in (2024) (AS): Proposes that modification of deep IR scaling through nonloc…

Dark Matter Nature (1 papers)

- Brito et al. (2023) (AS): Constraints from asymptotic safety RG flow eliminate phenome…

Hierarchy Between Quark And Lepton Mixing Patterns (1 papers)

- Held (2025) (AS): Fixed-point cascade creates different RG regimes for differe…

Hierarchy Problem (26 papers)

- Hiller et al. (2019) (AS): Asymptotic safety provides UV completion and predictivity up…
- Boos & Carone (2021) (AS): Emergent nonlocal scale Mnl ~ $m1^2/N$ regulates loop diagrams …
- Eichhorn (2019) (AS): Asymptotic safety provides UV completion making gravity fund…
- Don‘a et al. (2013) (AS): Constraints on grand unification and fundamental scalars fro…
- Schiffer (2025) (AS): Asymptotic safety provides anti-screening gravitational cont…
- Gogberashvili (2007) (TELE): Machian effects reduce Planck scale to electroweak scale whe…
- Pawlowski et al. (2018) (AS): Gravitational fluctuations at UV fixed point can render quad…
- Springer (2022) (AS): Extends resurgence mechanism to Yukawa sector where gravitat…
- Huang (2025) (AS): Self-consistency postulate constrains gravitational and SM c…
- Eichhorn & Schiffer (2022) (AS): Asymptotic safety provides relations between Higgs mass and …

- *…and 16 more*

Hierarchy Problem (Gravity Weakness) (1 papers)

- Ghosh (2025) (AS): Uses asymptotic safety framework to show how WGC emerges dyn…

Hierarchy Problem In Flavor Physics (1 papers)

- Altmannshofer et al. (2019) (OBS): Gauge protection of accidental SM symmetries through spontan…

Matter-Antimatter Asymmetry (5 papers)

- Sakharov (1991) (OBS): CP violation in nonstationary expansion of hot universe duri…
- soğukpınar (2005) (HOLO): Arises from fractal dimension variations during cosmic evolu…
- Imported Citation [ref: Flow & Holography; year: 2025] (HOLO): Modified baryogenesis through anisotropic thermal flows and …
- Dolgova (2023) (OBS): PBH formation mechanism produces noticeable antimatter popul…
- Mavromatos & Iorio (2023) (TELE): Torsion-associated axions leading to spontaneous Lorentz and…

Muon G-2 Anomaly (3 papers)

- Hiller et al. (2019) (AS): BSM Yukawa couplings with scalar mixing provide chirally enh…
- Hiller et al. (2020) (AS): Mixed Yukawa couplings in models A and C can explain anomalo…
- Hiller et al. (2019) (AS): BSM scalar-fermion loops with chiral flip and Yukawa couplin…

Neutrino Masses (6 papers)

- Brito et al. (2025) (AS): Uses asymptotic safety constraints at Planck scale translate…
- Aghanim et al. (2020) (OBS): Provides tight constraint on sum of neutrino masses $\Sigma m\nu < 0$….
- DESI Collaboration (2024) (OBS): Upper limits on sum of neutrino masses $\Sigma m\nu < 0.072$ eV at 95%…
- Springer (2022) (AS): Trans-Planckian asymptotic safety generates small neutrino Y…
- Imported Citation [ref: Flow & Holography; year: 2025] (HOLO): Recursive PMNS matrix corrections formulated as higher-order…
- Eichhorn & Schiffer (2022) (AS): Quantum gravity effects in asymptotic safety may explain sma…

Strong Cp Problem (1 papers)

- Eichhorn (2019) (AS): Proposes new gravitational solution through asymptotic safet…

Quantum Gravity

Black Hole Entropy (29 papers)

- Eichhorn & Held (2022) (AS): Asymptotic-safety inspired black holes have modified thermod…

- Bonanno (2023) (AS): Regular interior matched to exterior provides finite entropy…
- Ghosh (2013) (LQG): Statistical mechanics of indistinguishable punctures on quan…
- Kaloper & Linde (1999) (HOLO): Connects cosmological entropy bounds to Bekenstein-Hawking e…
- Chen et al. (2021) (HOLO): Connects Bekenstein-Hawking entropy formula to boundary enta…
- Lambiase & Scardigli (2022) (AS): Connects GUP deformation parameter β to AS running coupling …
- View (2022) (LQG): Studies horizon entropy computation through spin network cor…
- Imported Citation [year: 2020] (LQG): Develops effective quantum models for black holes using LQC …
- Maes (2022) (HOLO): Spacetime nodes and particles modeled as microscopic black h…
- Mandal (2025) (AS): Formation of regular black holes with de Sitter cores instea…
- *…and 19 more*

Black Hole Entropy Microscopic Origin (1 papers)

- Santiago & Chile (2013) (AS): Demonstrates agreement between thermodynamic entropy and mic…

Black Hole Information Paradox (4 papers)

- Schiffer (2025) (AS): Analyzes black hole thermodynamics and information-theoretic…
- Chen et al. (2021) (HOLO): Uses holographic duality, entanglement wedges, islands and r…
- Santiago & Chile (2013) (AS): Shows black holes evaporate completely without Planck-size r…
- Mureika (2025) (AS): Modified uncertainty principles and non-locality provide alt…

Black Hole Singularity Problem (1 papers)

- Santiago & Chile (2013) (AS): RG improvement with running cosmological constant modifies s…

Entropy Bound Violations (1 papers)

- Mureika (2006) (HOLO): Shows that spatial scale invariance in fractal matter distri…

Information Encoding In Lower Dimensions (1 papers)

- Jagannathan (2020) (HOLO): Shows how 1D quasicrystal properties can be derived from hig…

Information Encoding In Quantum Gravity (1 papers)

- Imported Citation [year: 2022] (LQG): Studies how bulk quantum gravity information can be encoded …

Information Paradox (22 papers)

- Blagojevi´c et al. (2013) (HOLO): Extends holographic correspondence to torsion-based theories…
- Walleghem et al. (2024) (HOLO): Strengthens paradoxes about quantum theory describing itself…
- Ghosh (2013) (LQG): Provides concrete microscopic description of black hole stat…
- Kaloper & Linde (1999) (HOLO): Examines how holographic principle attempts to encode bulk i…
- Ashtekar (2021) (LQG): New avenue for information recovery in black hole evaporatio…
- View (2022) (LQG): Analyzes information flow from bulk to boundary through quan…
- Kršš´ak (2023) (HOLO): Provides new method to calculate holographic complexity usin…
- Gericke (2025) (HOLO): Holographic encoding with bidirectional observer-geometry fe…
- Maes (2022) (HOLO): Multi-fold mechanisms implement non-locality with local phys…
- Imported Citation [year: 2022] (LQG): Examines how bulk information can be encoded and recovered f…
- *…and 12 more*

Planck Scale Physics (16 papers)

- Wessely (2025) (AS): Self-consistent computation includes full non-perturbative s…
- Modesto (2008) (LQG): Calculates effective dimensionality at Planck scales, showin…
- BAO et al. (2024) (TELE): Tests deformed Lorentz symmetry through ultra-high energy co…
- Ronco (2016) (LQG): Shows dimensional reduction from 4D to ~2D at Planck scale t…
- Lambiase & Scardigli (2022) (AS): GUP provides framework for quantum gravitational effects at …
- Livine (2024) (LQG): Defines precise picture of Planck scale geometry with quanti…
- Benedetti (2008) (HOLO): Shows quantum group symmetric spacetimes develop fractal pro…
- Gericke (2025) (HOLO): Prime-indexed pre-geometric information lattice at Planck sc…
- Danielewski (2005) (LQG): Models spacetime as cubic crystal with Planck-length lattice…
- McFadden & Skenderis (2009) (HOLO): Provides holographic description for strongly coupled gravit…
- *…and 6 more*

Quantum Gravity Unitarity (1 papers)

- Ronco (2016) (LQG): Addresses ambiguities in LQG quantization using dimensional …

Singularity Problem (26 papers)

- Modesto (2008) (LQG): Fractal analysis provides tool to understand behavior of cor…
- Chakrabortyd (2024) (TELE): Quantum cosmology shows finite non-zero probability at class…
- Mironov & Valencia-Villegas (2024) (TELE): Torsion allows violation of Null Energy Condition without pa…
- Cai & Easson (2010) (AS): Quantum corrections from asymptotic safety soften but do not…
- Bosma et al. (2019) (AS): Quantum gravity effects from asymptotic safety RG flow modif…
- Schiffer (2025) (AS): Quantum scale symmetry and UV fixed point resolve divergence…
- Bonanno (2023) (AS): Running gravitational coupling from AS fixed point creates r…
- Dimakis et al. (2023) (TELE): Uses quantum cosmology in f(T) gravity to investigate whethe…

- soğukpınar (2005) (HOLO): Pre-Big Bang state with finite fractal dimension D≈4 avoids …
- Mandal (2025) (AS): Complete singularity resolution for $\alpha > 1$ through effective …
- *…and 16 more*

Singularity Problem (Big Bang) (1 papers)

- Kofinas & Zarikas (2016) (AS): Non-singular accelerating cosmological solutions through ene…

Singularity Problem (Big Bang, Big Rip) (1 papers)

- Bamba et al. (2012) (LQG): Holonomy corrections create bounded elliptical constraint in…

Singularity Problem (Black Hole) (3 papers)

- Eichhorn & Held (2022) (AS): Quantum scale symmetry forces Newton coupling to vanish at h…
- Saueressig et al. (2015) (AS): RG improvement replaces classical black hole singularity wit…
- Pawlowski (2024) (AS): Quantum black hole solutions show signatures of quantum grav…

Singularity Problem (Black Hole, Big Bang) (4 papers)

- Livine (2024) (LQG): Spinfoam models resolve Big Bang singularity through quantum…
- Ashtekar (2021) (LQG): Big bang and big crunch singularities replaced by big bounce…
- Imported Citation [year: 2020] (LQG): LQC quantum corrections resolve divergences in correlators a…
- Trivedia (2022) (AS): Analyzes Type I-IV cosmological singularities in asymptotica…

Trans-Planckian Issues In Inflation (1 papers)

- Ashtekar & Barrau (2010) (HOLO): Holographic approach provides alternative framework when gra…

Unitarity And Causality In Quantum Gravity (1 papers)

- Eichhorn (2025) (AS): Tests whether asymptotically safe gravity respects unitarity…

Unitarity Preservation (9 papers)

- Wessely (2025) (AS): Computes positive graviton spectral function satisfying spec…
- Walleghem et al. (2024) (HOLO): Examines tension between unitary evolution and measurement t…
- Maes (2022) (HOLO): Local hidden variables reconciled with Bell experiments thro…
- Briscese et al. (2019) (HOLO): Proves ghost-free propagation and unitarity at all perturbat…
- Knorr et al. (2021) (AS): Compares asymptotic safety approach with non-local ghost-fre…
- Fehre et al. (2022) (AS): Uses Lorentzian signature to address unitarity questions in …
- Casadio (2022) (TELE): Demonstrates ghost-free theory by avoiding higher-derivative…
- Giddings (2006, arXiv:hep-th/0605196v2, DOI:10.1103/PhysRevD.74.106005) (HOLO): Argues that nonlocal gravitational dynamics in extreme regim…

- Eichhorn (2020) (AS): Critical examination of higher derivative terms and ghost pr…

Cosmology

Cosmological Constant Problem (45 papers)

- Kanatchikov & Kholodnyi* (TELE): Links cosmological constant to fundamental acceleration scal…
- Aghanim et al. (2020) (OBS): Provides precise measurements that constrain ΛCDM model but …
- Bhardwaj et al. (2021) (TELE): Uses holographic principle to relate dark energy density to …
- DESI Collaboration (2024) (OBS): Tests of time-varying dark energy equation of state show pre…
- Lee (2025) (HOLO): Holographic constraint on vacuum energy density with IR cut-…
- Belgacem et al. (2017) (HOLO): Dynamically generated mass scale in IR provides acceleration…
- Kirsch (2023) (TELE): Torsion replaces dark energy and Einstein's cosmological con…
- Campo et al. (2011) (HOLO): Addresses low vacuum energy value and coincidence problem th…
- Kaloper & Linde (1999) (HOLO): Investigates how negative cosmological constant violates hol…
- Blitz (2025) (HOLO): Offers alternative to ΛCDM through dynamic holographic dark …
- *…and 35 more*

Dark Energy (1 papers)

- Imported Citation [year: 2025] (TELE): Bimetric frame interactions explain cosmic acceleration with…

Dark Energy Nature (52 papers)

- Xue (2024) (HOLO): Dark energy emerges from holographic massive pair plasma sta…
- Aghanim et al. (2020) (OBS): Constrains dark energy equation of state w0 = -1.03 $\pm$ 0.03, …
- Bhardwaj et al. (2021) (TELE): Combines Rényi holographic dark energy model with f(T) gravi…
- Chakrabortyd (2024) (TELE): Models dark energy through teleparallel gravity with scalar …
- DESI Collaboration (2024) (OBS): Constraints on dark energy equation of state parameters w, w…
- Mironov & Valencia-Villegas (2024) (TELE): Horndeski theory with torsion provides modified gravity fram…
- Lee (2025) (HOLO): Holographic dark energy model with torsion scalar allowing c…
- Belgacem et al. (2017) (HOLO): Nonlocal terms in quantum effective action act as dynamical …
- Kirsch (2023) (TELE): Dynamical torsion field explains cosmic acceleration without…
- Campo et al. (2011) (HOLO): Proposes holographic dark energy models based on different i…
- *…and 42 more*

Dark Matter And Dark Energy (1 papers)

- Capozziello et al. (2023) (HOLO): Non-local IR modifications can explain late-time acceleratio…

Early Universe Physics Beyond Inflation (1 papers)

- Afshordi et al. (2016) (HOLO): Uses holographic duality to model very early universe throug…

Flatness Problem In Spinfoam Quantum Gravity (1 papers)

- Han et al. (2022) (LQG): Complex critical points analysis reveals curved Regge geomet…

Flatness/Horizon Problems (9 papers)

- Liu (2024) (AS): Addresses through inflation model derived from modeling mech…
- El-Nabulsi & Anukool (2023) (HOLO): Fractional quantum cosmology with power-law inflation and la…
- Liu et al. (2018) (AS): Inflationary solution provides elegant resolution of horizon…
- Mondal & Chakraborty (2023) (TELE): Analyzes inflationary scenarios with torsion and their effec…
- Chen et al. (2025) (AS): Shows quantum corrections lead to earlier isotropization of …
- Nielsen et al. (2015) (AS): Addresses through inflationary dynamics driven by asymptotic…
- Krasnov (2026) (HOLO): Fractal cosmology provides alternative framework to inflatio…
- Platania (2019) (AS): Inflationary potential with plateau region from RG-improved …
- Imported Citation [year: 2023] (TELE): Ultra-slow contraction phase with scalar field smooths and f…

Hubble Tension (20 papers)

- Wu et al. (2024) (TELE): Introduces torsion field with linear dependence H = -$\alpha\varphi$ in E…
- Aghanim et al. (2020) (OBS): Reports 3.6σ tension between CMB-inferred H0 = 67.4 $\pm$ 0.5 km…
- DESI Collaboration (2024) (OBS): BAO measurements provide H0 = (68.52 $\pm$ 0.62) km s^{-1} Mpc^{-1} fr…
- Lee (2025) (HOLO): Modified cosmological evolution through torsion-modified Fri…
- Belgacem et al. (2017) (HOLO): RR model yields higher H0 value than ΛCDM, reducing tension …
- McInnes (2025) (TELE): Extrinsic torsion could lead to anomalies in theoretical est…
- K̆r´ı̆zek & Dumin (2024) (TELE): Torsion-based metric produces time-dependent Hubble paramete…
- Maggiore & Mancarella (2014) (HOLO): Predicted dark energy equation of state could resolve tensio…
- Lee (2024) (HOLO): Proposes extended dark energy model that might resolve H0 di…
- soğukpınar (2005) (HOLO): Addressed through UFQFT framework modifications to ΛCDM
- *…and 10 more*

Hubble Tension (H0 Discrepancy) (5 papers)

- El-Nabulsi & Anukool (2023) (HOLO): Confronts model with observations using Bayesian hierarchica…
- Javad et al. (2024) (TELE): Modified Cartesian flat cosmological model within teleparall…
- Falcon (2001) (TELE): Theoretical deduction of Hubble-Lemaitre Law from modified g…
- Asghari (2022) (HOLO): Tests whether fractal cosmology can alleviate tension betwee…
- Grijs & Catelan (2024) (OBS): Precision local measurement of H0 using distance ladder with…

Inflation Mechanism (23 papers)

- Kofinas & Zarikas (2016) (AS): Natural inflationary period from varying cosmological consta…
- Liu (2024) (AS): Derives large-field inflation from R^2-gravity solution with …
- Hoshina (2022) (AS): Studies consistency with Starobinsky inflation model through…
- Dimakis et al. (2022) (TELE): Self-similar solutions in f(Q) theory can describe various c…
- Liu et al. (2018) (AS): Geometric scalaron field from quantum-gravitational effects …
- Haroa (2013) (LQG): Matter bounce scenario as alternative to slow-roll inflation…
- Huang (2025) (AS): Loop-induced R^2 operator drives Starobinsky inflation with s…
- McFadden & Skenderis (2009) (HOLO): Maps inflationary models to domain-wall spacetimes and estab…
- Fazlollahi (2023) (HOLO): Holographic constant roll inflation with infrared cutoff tha…
- Nielsen et al. (2015) (AS): Provides natural inflation model where scalar potential heig…
- *…and 13 more*

Initial Conditions For Inflation (1 papers)

- Ashtekar & Barrau (2010) (HOLO): Strong/weak coupling duality allows new models with intrinsi…

Jwst Early Galaxies Anomaly (2 papers)

- Souza (2025) (HOLO): Fractal galaxy distribution model with D = 1.5 for 0.1 < z <…
- Dolgova (2023) (OBS): Primordial black holes seed galaxy formation in early univer…

Trans-Planckian Issues In Inflation (1 papers)

- Ashtekar & Barrau (2010) (HOLO): Holographic approach provides alternative framework when gra…

Uv Completion Of Inflation (1 papers)

- Ashtekar & Barrau (2010) (HOLO): Holographic dual provides UV complete 3D super-renormalizabl…

Bridge Papers

Papers that explicitly connect multiple paradigms:

AS↔HOLO (10 papers)

- Boos & Carone (2021)
  - Bridge concepts: Asymptotic nonlocality connecting UV completion with holographic encoding, Emergent scales from large-N limits suggesting dimensional reduction, Ghost-free infinite-derivative theories as UV completions
- Schiffer (2025)
  - Bridge concepts: Black hole thermodynamics as universal constraint, Holographic principle connecting field theory and information theory, Spacetime topology change restrictions
- Vasquez (2025)
  - Bridge concepts: Dimensional reduction from multiple quantum gravity approaches, Fractal/multifractal spacetime structure, Resolution-dependent effective dimension
- Calcagni (2009)
  - Bridge concepts: Spectral dimension running from 2 at UV to 4 at IR, Scale-dependent effective dimensionality, Fractal geometry as UV completion mechanism
- Santiago & Chile (2013)
  - Bridge concepts: RG-improved black hole thermodynamics, Quantum corrections through running couplings, CFT entropy formulas in quantum gravity context
- Blankert (2025)
  - Bridge concepts: Holographic beta functions incorporating CFT boundary data, Scale-dependent Planck mass connecting RG flow to holographic duality, Constraint intersection approach using multiple proven frameworks
- Rietz (2013)
  - Bridge concepts: Information density as fundamental field, Non-perturbative mass generation, RG fixed-point constraints linking gauge and scalar sectors
- Springer (2023)
  - Bridge concepts: Nonlocal form factors connecting finite higher-derivative theories to exponential nonlocality, Emergent regulator scales bridging UV completion and effective field theory, Lee-Wick ghost structure transitioning to ghost-free nonlocal limit
- Mureika (2025)
  - Bridge concepts: Non-locality as fundamental 'fuzziness', Characteristic length scales linking UV/IR modifications, Equivalence between matter-sector and geometry-sector modifications
- Imported Citation [year: 2025]
  - Bridge concepts: Curvature-dependent renormalization group scale $k^2 \sim R$, Heat-kernel regularization with curvature-dependent cutoffs, Quantum-to-classical transition via decoherence filters

AS↔LQG (3 papers)

- Thiemann & N¨urnberg (2024)
  - Bridge concepts: Reduced phase space quantization, Relational observables, Lorentzian Wetterich equation
- Ferrero (2025)
  - Bridge concepts: relational observables, background-independent path integrals, gauge-invariant generating functionals
- Thiemann (2024)

  - Bridge concepts: Reduced phase space quantization connecting canonical and path integral methods, Relational observables as bridge between background-independent CQG and background field methods, Lorentzian Wetterich equation adaptation

AS↔TELE (1 papers)

- Melichev (2025)
  - Bridge concepts: Torsion as propagating degree of freedom in RG flow, Nonminimal kinetic operators in quantum gravity, Asymptotic freedom through torsion contributions

HOLO↔AS (13 papers)

- Capozziello et al. (2023)
  - Bridge concepts: Non-local integral operators bridging holographic non-locality with asymptotic safety regularization, Energy-momentum conservation in non-local theories connecting different gravity paradigms, Variational principles extended to non-local actions
- Xue (2024)
  - Bridge concepts: Holographic horizon physics combined with asymptotic safety scaling, Scale-dependent effective cosmological parameter, Gravitational ground state from holographic pair condensate
- Belgacem et al. (2017)
  - Bridge concepts: quantum effective action with nonlocal operators, dynamical mass scale generation in infrared, information-theoretic aspects of gravitational dynamics
- Benedetti (2008)
  - Bridge concepts: Scale-dependent spectral dimension, Fractal properties of quantum spacetime, Connection between quantum groups and renormalization group flows
- soğukpınar (2005)
  - Bridge concepts: Fractal dimension as evolving fundamental parameter, Dimensional reduction process connecting early universe to present, Unified field resonances spanning particle to cosmic scales
- Gericke (2025)
  - Bridge concepts: Dimensional reduction from both AS and holographic perspectives, Information-theoretic approach linking quantum information to geometry, RG flow techniques applied to holographic information density
- Imported Citation [ref: Flow & Holography; year: 2025]
  - Bridge concepts: Recursive RG fixed points bridging holographic and asymptotic safety approaches, Twistor monodromy connecting holographic geometry with recursive dynamics, Fractal spacetime structures linking RG flow to holographic entanglement
- Gruji´c & Pankovi´c (2009)
  - Bridge concepts: Scale invariance connecting fractal geometry to renormalization group flows, Hierarchical structure as emergent holographic encoding, Statistical emergence of fractal patterns from gravitational dynamics
- Krasnov (2026)
  - Bridge concepts: Running dimensions from asymptotic safety, Fractal geometry as emergent from quantum gravity, Scale-dependent effective dimension
- Svozil (1989)

  - Bridge concepts: Non-integer dimensional field theories, Fractal spacetime geometry, Scale-invariant discrete structures
- Bajc et al. (2019)
  - Bridge concepts: Safe hologram connecting asymptotic safety with holographic duality, RG flow encoded in bulk dilaton profile, Fixed point structure mapped to AdS boundary/bulk correspondence
- Springer (2010)
  - Bridge concepts: Scale-dependent effective dimensionality, Fractal structure as UV completion mechanism, Dimensional flow from UV to IR
- Sadria et al. (2018)
  - Bridge concepts: Fractal space-time geometry bridging holographic principle with renormalization, Holographic bound in fractal dimensions, UV completion through fractal structure

HOLO↔LQG (8 papers)

- Maes (2022)
  - Bridge concepts: Discrete fractal spacetime connecting LQG discreteness with holographic fractals, Entanglement-gravity emergence linking quantum information to spacetime geometry, Random walk paths as origin of both quantum mechanics and general relativity
- Mygdalas (2026)
  - Bridge concepts: Discrete scale invariance connecting holographic and asymptotic safety approaches, Quasicrystalline discretization bridging holographic and LQG discrete geometry, Self-dual structures linking holographic duality with discrete spacetime
- Sardar (2024)
  - Bridge concepts: Entropy corrections bridging holographic principle with loop quantum gravity effects, Fractal structure incorporating scale-invariant properties with holographic bounds, Modified entropy-area relations connecting quantum gravity to holographic dark energy
- Singh et al. (2017)
  - Bridge concepts: spin networks from holographic tensor networks, gauge-gravity correspondence through MERA, boundary-bulk entanglement via tensor network decomposition
- Amaral & Yadav - Tiling Spaces and the Expanding Universe: Bridging Quantum M
  - Bridge concepts: Quasicrystalline tiling spaces connecting discrete quantum structure to continuous spacetime, Scale invariance linking microscale quantum mechanics to macroscale cosmology, Emergent gravity from quantum mechanical processes in discrete structure
- Lymperis (2023)
  - Bridge concepts: LQG entropy in holographic framework, Quantum geometry effects in holographic dark energy, Non-extensive statistics in cosmological holography
- Alfonso-Faus (2012)
  - Bridge concepts: Pin parameter unifying geometric and quantum properties, Scale-invariant quantum black holes connecting discrete structure with holographic encoding, Fractal universe structure bridging quantum discreteness and holographic properties
- Colafranceschi et al. (2021)

  - Bridge concepts: Tensor networks as unified description of quantum gravity states, Entanglement as geometric glue connecting discrete quantum structures, Spin networks as entanglement graphs representing quantum correlations

HOLO↔TELE (7 papers)

- Blagojevi´c et al. (2013)
  - Bridge concepts: Holographic encoding of torsion degrees of freedom, Boundary currents for torsion-based gravity, Gauge-theoretic formulation of holographic correspondence
- Lee (2025)
  - Bridge concepts: Holographic principle applied within torsion-modified gravity, UV/IR cut-off relation in Einstein-Cartan theory, Geometric torsion scalar as bridge between matter spin and holographic constraints
- Lee (2024)
  - Bridge concepts: Holographic principle with torsional gravity, Bekenstein bound in Einstein-Cartan theory, Modified Friedmann equations with holographic energy density
- Krššák (2023)
  - Bridge concepts: Tetrad formalism connecting holographic and teleparallel approaches, Local Lorentz transformations bridging coordinate-dependent and coordinate-free descriptions, Bulk action as boundary-term-free alternative to standard gravitational action
- Springer (2020)
  - Bridge concepts: Independent vielbein and spin connection formulation, Torsion as geometric source of spin dynamics, Holographic correspondence extended to include spin degrees of freedom
- Aschheim (2016)
  - Bridge concepts: Quasicrystal spacetime geometry combining discrete and continuous structures, Off-diagonal metrics encoding both holographic and torsion-based effects, Anholonomic frame deformation method linking geometric flows to aperiodic order
- Pretko (2017)
  - Bridge concepts: Emergent gravity from condensed matter phases, Conservation laws linking gauge theory and gravity, Machian/relational spacetime emergence

LQG↔AS (2 papers)

- Ronco (2016)
  - Bridge concepts: dimensional reduction, UV fixed points, modified dispersion relations
- Imported Citation [ref: RDW13U; year: 2023]
  - Bridge concepts: Planck-scale discretization bridging LQG discrete structure with AS fixed point behavior, Elastic continuum providing geometric foundation for both quantum mechanics and gravity, Quaternion non-commutativity linking to fundamental quantum phenomena and spacetime structure

LQG↔HOLO (13 papers)

- Modesto (2008)
  - Bridge concepts: spectral dimension as universal probe of quantum geometry, fractal structure at Planck scale, dimensional reduction at high energies
- Ghosh (2013)

  - Bridge concepts: Holographic principle applied to discrete quantum geometry, Statistical mechanics of quantum geometric excitations, Quasilocal energy description connecting area operator to physical Hamiltonian
- Dittrich (2021)
  - Bridge concepts: Areas as fundamental variables connecting LQG spin foams with holographic approaches, Scaling behavior analysis linking discrete quantum geometry to continuum classical gravity, Constraint integration mechanism relating different geometric variable choices
- Livine (2024)
  - Bridge concepts: Path integral formulation over discrete geometries, Topological quantum field theory with constraints, Transition amplitudes between boundary states
- View (2022)
  - Bridge concepts: Entanglement as spacetime glue connecting LQG and holographic descriptions, Tensor networks as common language between discrete quantum geometry and holographic systems, Random tensor network techniques bridging statistical mechanics and quantum gravity
- Imported Citation [ref: Dissertation; year: 2020]
  - Bridge concepts: Embedding non-holographic LQG into holographic AdS/CFT framework, Translation of singularity resolution from geometry to dual field theory correlators, Effective quantum corrections bridging discrete LQG with continuous holographic description
- Langenscheidt (2022, arXiv:2205.09761v1)
  - Bridge concepts: Spin networks as tensor networks connecting LQG discrete geometry to holographic techniques, Entropy bounds bridging discrete quantum gravity and holographic principles, Random tensor networks as a framework for studying quantum superpositions of geometries
- Smolin (2016)
  - Bridge concepts: Categorical holography connecting LQG spin networks to Chern-Simons theory, Bulk-boundary correspondence in background-independent quantum gravity, Thermodynamic interpretation of geometric constraints
- Han & Hung (2017)
  - Bridge concepts: exact holographic mapping, spin-network coarse graining to tensor networks, bulk-boundary entanglement entropy correspondence
- Livine (2017)
  - Bridge concepts: Holographic coarse-graining, Bulk-boundary correspondence in discrete quantum geometry, Gauge-physical degree of freedom distinction
- Colafranceschi (2025)
  - Bridge concepts: tensor network - spin network correspondence, enriched link entanglement as edge modes, bulk-to-boundary isometry from discrete geometry
- Amaral et al. (2023)
  - Bridge concepts: Quasicrystal geometry bridges discrete LQG structures with holographic fractal properties, E8 root lattice unification connecting quantum geometry to gauge theory, Coherent states providing semi-classical limit between quantum discreteness and continuous geometry
- Schmid (2022, arXiv:2205.05079v1)
  - Bridge concepts: quasi-local holography in discrete quantum gravity, boundary observables encoding bulk information, topological field theory structure in quantum gravity

LQG↔TELE (3 papers)

- Bamba et al. (2012)
  - Bridge concepts: LQC as example of modified teleparallel gravity, Holonomy corrections as discrete spacetime effects, Modified Friedmann equations in both paradigms
- Shoshany (2019)
  - Bridge concepts: Phase space polarizations connecting LQG and teleparallel gravity, Edge mode degrees of freedom, Constraint ordering duality
- Haroa (2013)
  - Bridge concepts: Holonomy corrections as F(T) gravity modifications, Quantum geometry effects via classical teleparallel formulation, Ashtekar connection replacement through torsion-based approach

TELE↔AS (2 papers)

- Company (2022)
  - Bridge concepts: Non-local operators □^{-1} connecting local field equations to distributed spacetime information, Geometric invariants (R, G, T) extended with non-local terms bridging classical and quantum scales, Symmetry principles constraining non-local gravity across different geometric formulations
- Casadio (2022)
  - Bridge concepts: Renormalization group flow connecting teleparallel and asymptotic safety approaches, Running coupling parameters in modified teleparallel gravity, Gauge theory formulation of gravity enabling standard quantum field theory techniques

TELE↔HOLO (9 papers)

- Bahamonde (2017)
  - Bridge concepts: Nonlocality from quantum gravitational effects, Extended spacetime structures from string theory and LQG, Green function operators linking torsion to nonlocal behavior
- Bhardwaj et al. (2021)
  - Bridge concepts: Holographic dark energy in teleparallel framework, Rényi entropy generalization of Bekenstein-Hawking entropy, IR cutoff implementation through Hubble horizon
- Kastner (2024)
  - Bridge concepts: entropic gravity, transactional interpretation bridging quantum mechanics and gravity, spacetime emergence from matter interactions
- Kirsch (2023)
  - Bridge concepts: AdS spacetime deformation in torsion-based gravity, Canonical Hamiltonian formalism unifying gauge theory and gravity, Palatini formalism with independent spin connection and vierbein fields
- Chen (2023)
  - Bridge concepts: Holographic principle applied to torsion gravity, Reconstruction method connecting holographic dark energy density to torsion field, Interaction term Q = -2$\varphi\varrho$m linking torsion and matter
- Krššáka (2017)

  - Bridge concepts: Holographic renormalization techniques applied beyond AdS/CFT, Surface term renormalization as universal gravity property, Spin connection decomposition separating gravitational and inertial effects
- Mashhoon (2011)
  - Bridge concepts: Nonlocal field equations with memory effects, Observer-dependent measurements encoding past history, Integro-differential formulation bridging local and nonlocal physics
- Imported Citation [ref: Bimetric_Teleparallel_Holography; year: 2025]
  - Bridge concepts: Josephson-φ phase operator coupling two metric sectors, Eight Abelian gauge fields distributed across bimetric sheets, Holographic encoding of bulk dynamics on boundary surfaces
- Koussour (2022)
  - Bridge concepts: Barrow holographic dark energy combining quantum gravity effects with holographic principle, Non-metricity scalar Q as gravitational field variable in teleparallel framework, Deformation parameter Δ encoding quantum gravitational effects on horizon entropy

TELE↔LQG (3 papers)

- Kanatchikov & Kholodnyi* - Effects of Quantum Spin Connection Foam in the Solar System,
  - Bridge concepts: Precanonical quantization bridging tetrad gravity with discrete quantum structure, Spin connection foam as quantum spacetime structure, Clifford algebra wave functions connecting geometry to quantum mechanics
- Dupuis (2019)
  - Bridge concepts: Einstein-Cartan formulation as common starting point, BF vacuum vs Ashtekar-Lewandowski vacuum duality, Discretization approaches connecting classical and quantum formulations
- Mavromatos & Iorio (2023)
  - Bridge concepts: Torsion as emergent geometry in materials and fundamental spacetime geometry, Contorsion tensor relating torsion-free and torsion-full connections, Supersymmetry realizations connecting particle physics to condensed matter via torsion

Full Paper Index

Alphabetical listing of all papers:

Citation	Paradigm	Bridge	Problems
Joyce et al. (2000)	HOLO		2
Pawar (2022)	HOLO		2
View (2022)	LQG	Yes	3
Giddings (2006, arXiv:hep-th/0605196v2, DOI:10.1103/PhysRevD.74.106005)	HOLO		3
Mureika (2006)	HOLO		2
Gogberashvili (2007)	TELE		1
Vitiello (2008)	HOLO		1

Citation	Paradigm	Bridge	Problems
Benedetti (2008)	HOLO	Yes	1
Modesto (2008)	LQG	Yes	2
Gruji´c & Pankovi´c (2009)	HOLO	Yes	2
McFadden & Skenderis (2009)	HOLO		2
Calcagni (2009)	AS	Yes	2
Cai & Easson (2010)	AS		3
Braun et al. (2010)	AS		1
Mashhoon (2011)	TELE	Yes	1
Campo et al. (2011)	HOLO		2
Svozil (1989)	HOLO	Yes	2
Hong, Lee & Zoe (2012, DOI:10.1142/S0218271812500629)	AS		2
Alfonso-Faus (2012)	HOLO	Yes	2
Rozgachevaa et al. (2012)	HOLO		1
Nink & Reuter (2012)	AS		1
Bamba et al. (2012)	LQG	Yes	2
Blagojevi´c et al. (2013)	HOLO	Yes	1
Santiago & Chile (2013)	AS	Yes	3
Haroa (2013)	LQG	Yes	2
Ghosh (2013)	LQG	Yes	2
Don'a et al. (2013)	AS		2
Foffa et al. (2013)	HOLO		2
Rietz (2013)	AS	Yes	2
Maggiore & Mancarella (2014)	HOLO		3
Albaretia et al. (2014)	HOLO		2
Nielsen et al. (2015)	AS		3
Saueressig et al. (2015)	AS		2
Kofinas & Zarikas (2016)	AS		2
Afshordi et al. (2016)	HOLO		2
Smolin (2016)	LQG	Yes	2
Aschheim (2016)	HOLO	Yes	3
Singh et al. (2017)	HOLO	Yes	1
Pretko (2017)	HOLO	Yes	2
Perez (2017)	LQG		3
Livine (2017)	LQG	Yes	2
Belgacem et al. (2017)	HOLO	Yes	3
Liu et al. (2018)	AS		2

Citation	Paradigm	Bridge	Problems
Anagnostopoulos et al. (2018)	AS		3
Sadria et al. (2018)	HOLO	Yes	4
Briscese et al. (2019)	HOLO		2
Shoshany (2019)	LQG	Yes	1
Hiller et al. (2019)	AS		2
Dupuis (2019)	TELE	Yes	1
Bajc et al. (2019)	HOLO	Yes	1
Eichhorn (2020)	AS		3
Nojiri et al. (2020)	HOLO		3
Capozziello et al. (2020)	TELE		2
Mandal et al. (2020)	AS		2
Jagannathan (2020)	HOLO		1
Ashtekar (2021)	LQG		2
Dittrich (2021)	LQG	Yes	2
Bahamonde et al. (2021)	TELE		4
Chen et al. (2021)	HOLO		2
Bhardwaj et al. (2021)	TELE	Yes	2
Knorr et al. (2021)	AS	Yes	2
Eichhorn et al. (2021)	AS		2
Company (2022)	TELE	Yes	3
Eichhorn() (2022)	AS		2
Koussour (2022)	TELE	Yes	2
Trivedia (2022)	AS		2
Mandala & Gangopadhyaya (2022)	AS		2
Schmid (2022, arXiv:2205.05079v1)	LQG	Yes	2
Langenscheidt (2022, arXiv:2205.09761v1)	LQG	Yes	2
Alia (2022)	LQG		1
Dimakis et al. (2022)	TELE		2
Mylova (2022)	TELE		2
Eichhorn & Schiffer (2022)	AS		4
Eichhorn & Held (2022)	AS		2
Capozziello et al. (2023)	HOLO	Yes	3
Liu et al. (2023)	TELE		3
Mondal & Chakraborty (2023)	TELE		2
Tabatabaei et al. (2023)	TELE		2

Citation	Paradigm	Bridge	Problems
Amaral et al. (2023)	LQG	Yes	2
Das (2023)	TELE		2
Dimakis et al. (2023)	TELE		2
Bonanno (2023)	AS		2
Das (2023)	TELE		1
Imported Citation [year: 2023]	TELE		2
Lymperis (2023)	HOLO	Yes	2
Das (2023)	TELE		2
Danielewski (2005)	LQG		3
Pereira (2024)	TELE		2
Livine (2024)	LQG	Yes	2
Thiemann & N¨urnberg (2024)	AS	Yes	2
Benedetto et al. (2024)	TELE		2
Mironov & Valencia-Villegas (2024)	TELE		2
Chakrabortyd (2024)	TELE		2
Amaral & Yadav	HOLO	Yes	4
Lee (2024)	HOLO	Yes	3
Imported Citation [year: 2024]	TELE		3
Bhoyar (2024)	HOLO		3
Wu et al. (2024)	TELE		1
Golovnev (2024)	TELE		1
BAO et al. (2024)	TELE		2
Schiffer (2025)	AS	Yes	2
Mandal (2025)	AS		2
Lee (2025)	HOLO	Yes	3
Vasquez (2025)	AS	Yes	3
Melichev (2025)	AS	Yes	1
Ghosh (2025)	AS		2
Strubbe (2025)	HOLO		3
Varani (2025)	TELE		2
Mureika (2025)	AS	Yes	3
Ferrero (2025)	AS	Yes	3
Held (2025)	AS		3
Wessely (2025)	AS		2
Schiffer (2025)	AS		2
Schiffer (2025)	AS		1
Spina (2025)	AS		2
Huang (2025)	AS		4
Colafranceschi (2025)	LQG	Yes	1
Krasnov (2026)	HOLO	Yes	2
Mygdalas (2026)	HOLO	Yes	2

Citation	Paradigm	Bridge	Problems
Wang (2024) [thesis]	AS		2
Kaloper & Linde (1999)	HOLO		3
Hoshina (2022) [thesis]	AS		3
Imported Citation [year: 2025]	AS	Yes	3
Ronco (2016)	LQG	Yes	2
Imported Citation [ref: Bimetric_Teleparallel_Holography; year: 2025]	TELE	Yes	5
Blitz (2025)	HOLO		2
Chen et al. (2025)	AS		2
Chen et al. (2025)	AS		3
Das (2012)	TELE		2
Imported Citation [ref: Dissertation; year: 2020]	LQG	Yes	2
D'Angelo et al. (2025)	AS		3
Eichhorn (2023)	AS		2
Nagy & in (2024)	AS		2
soğukpınar (2005)	HOLO	Yes	5
Blankert (2025)	AS	Yes	3
Springer (2023)	AS		2
Springer (2010)	HOLO	Yes	2
Springer (2023)	AS	Yes	3
Springer (2024)	HOLO		2
Springer (2018)	AS		2
Springer (2022)	AS		3
Springer (2025)	AS		2
Springer (2022)	HOLO		2
Springer (2023)	AS		1
Springer (2020)	HOLO	Yes	2
Liu (2024)	AS		3
Maes (2022)	HOLO	Yes	3
Martens	TELE		1
McInnes (2025)	TELE		1
Ashtekar & Barrau (2010)	HOLO		3
Eichhorn (2019)	AS		2
Altmannshofer et al. (2019)	None		3
Reichert (2019)	AS		2
Hiller et al. (2019)	AS		3
Hiller et al. (2020)	AS		2

Citation	Paradigm	Bridge	Problems
Boos & Carone (2021)	AS	Yes	1
Colafranceschi et al. (2021)	HOLO	Yes	2
Lambiase & Scardigli (2022)	AS	Yes	2
Han et al. (2022)	LQG		1
Hoshina (2022)	AS		2
Boos et al. (2022)	AS		1
Brito et al. (2023)	AS		2
Matematica et al. (2023)	AS		2
Krššák (2023)	HOLO	Yes	1
Pawlowski (2024)	AS		2
Saueressig (2025)	AS		1
Dodelson & Park (2014)	HOLO		2
Han & Hung (2017)	LQG	Yes	2
Pawlowski et al. (2018)	AS		2
Bosma et al. (2019)	AS		1
Fehre et al. (2022)	AS		2
Bueno et al. (2023)	HOLO		1
Imported Citation [ref: RDW13U; year: 2023]	LQG	Yes	3
Imported Citation [ref: Flow & Holography; year: 2025]	HOLO	Yes	4
Pastor-Gutiérrez et al. (2023)	AS		2
Ledner (2021)	LQG		2
Tabatabaei (2024)	TELE		2
El-Nabulsi & Anukool (2023)	HOLO		2
Gericke (2025)	HOLO	Yes	4
Xue (2024)	HOLO	Yes	3
DESI Collaboration (2024)	None		4
Imported Citation [ref: fermilab-pub-92-002-A; year: 1992]	HOLO		1
Kastner (2024)	TELE	Yes	1
Donoghue (2020)	AS		1
Banks (2020)	HOLO		3
Saueressig (2020)	AS		1
Eichhorn (2020)	AS		3
Held (2020)	AS		1

Citation	Paradigm	Bridge	Problems
Eichhorn (2019)	AS	Yes	3
Vela (2024)	TELE		1
K˘r´ı˘zek & Dumin (2024)	TELE		3
Group et al. (2020)	TELE		2
Brito et al. (2025)	AS		1
Kanatchikov & Kholodnyi*	TELE	Yes	2
Grijs & Catelan (2024)	None		1
Walleghem et al. (2024)	HOLO		2
oks (2019)	None		2
Dolgova (2023)	OBS		3
Vafa (2025)	HOLO		4
Sakharov (1991)	None		2
Aghanim et al. (2020)	OBS		4
Krššáka & Pereirab (2015)	TELE		2
Krššáka (2017)	TELE	Yes	1
Bahamonde (2017)	TELE	Yes	2
Kowalska (2021)	AS		2
Casadio (2022)	TELE	Yes	2
Benisty (2022)	TELE		2
Pereira (2022)	TELE		2
Teles (2022)	HOLO		1
Asghari (2022)	HOLO		2
Dialektopoulos (2023)	TELE		2
Kirsch (2023)	TELE	Yes	2
Kotlarski (2023)	AS		1
Fazlollahi (2023)	HOLO		2
Usman (2023)	TELE		2
Hembrom (2024)	TELE		2
Sardar (2024)	HOLO	Yes	2
Souza (2025)	HOLO		2
Eichhorn (2025)	AS		1
Liu (2025)	TELE		3
Falcon (2001)	TELE		4
Imported Citation [year: 2025]	AS		2
Javad et al. (2024)	TELE		2
Bednyakov & Mukhaeva (2023)	AS		3
Aldrovandi & Pereira	TELE		2
Obukhov (2018)	TELE		1
Imported Citation [year: 2018]	TELE		1

Citation	Paradigm	Bridge	Problems
Platania (2019)	AS		2
Imported Citation [year: 2020]	TELE		2
Fabbri (2021)	TELE		2
Bouchè & Salzano (2022)	HOLO		3
Chen (2023)	TELE	Yes	2
Mavromatos & Iorio (2023)	TELE	Yes	2
Thiemann (2024)	AS	Yes	1

Appendix G: Variables and Constants Reference

G.1 Core Framework Variables

Symbol	Name	Definition	Units	Introduced
Z_0	Characteristic impedance	$\sqrt{L/C}$ — determines perception range and density access	Ω (model)	Ch 2, 5
R	Resistance (dissipation)	Energy loss rate — maps to distraction, trauma, environmental noise	Ω (model)	Ch 5
L	Inductance (inertia)	Accumulated wisdom/experience across incarnations	H (model)	Ch 5
C	Capacitance (reactivity)	Unprocessed shadow material; emotional charge storage	F (model)	Ch 5
Q	Quality factor	Z_0/R — sovereignty, discernment, resistance to injection locking	dimensionless	Ch 5
f_0	Resonant frequency	$1/(2\pi\sqrt{LC})$ — natural operating frequency of consciousness	Hz (model)	Ch 5
σ	Spin coherence	Individual-level phase alignment; ranges 0 (random) to 1 (perfect)	dimensionless	Ch 10
r	Kuramoto order parameter	Population-level phase synchronization; ranges 0 to 1	dimensionless	Ch 8

G.2 Collective Dynamics Variables

Symbol	Name	Definition	Units	Introduced
N	Population size	Total number of elements in the array	dimensionless	Ch 8
f	Coherent fraction	Fraction of population that is phase-coherent	dimensionless	Ch 8
f_c	Critical coherent fraction	$\sqrt{T/N}$ — minimum coherent fraction for collective effect	dimensionless	Ch 8
T	Detection threshold	SNR threshold for coherent signal detection; $T = 10$	dimensionless	Ch 8
AF	Array factor	Complex sum of individual element contributions	dimensionless	Ch 8
K	Coupling strength	Kuramoto inter-oscillator coupling coefficient	rad/s	Ch 8, 9
K_c	Critical coupling	$2/(\pi g(0))$ — minimum coupling for synchronization	rad/s	Ch 8

G.3 Injection Locking Variables

Symbol	Name	Definition	Units	Introduced
ω_L	Locking bandwidth	$\omega_0/(2Q) \cdot V_{inj}/V_0$ — range of frequencies over which lock holds	rad/s	Ch 9
V_{inj}	Injection signal amplitude	Strength of the external locking signal	V (model)	Ch 9
V_0	Free-running amplitude	Natural oscillation amplitude	V (model)	Ch 9
$\Delta\omega$	Frequency detuning	$\omega_{inj} - \omega_0$ — distance between injection and natural frequency	rad/s	Ch 9
f_{esc}	Escape fraction	Critical fraction for narrative escape; $\omega_{L,C}/(\omega_{L,C} + K_{mean})$	dimensionless	Ch 9

G.4 Link Budget Variables

Symbol	Name	Definition	Units	Introduced
P_S	Source power	Transmitted power from Source	dB (model)	Ch 14
G_S	Source gain	Directivity of Source transmission	dB	Ch 14
L_{path}	Path loss	Signal attenuation through density cascade	dB	Ch 14
$L_{paradigm}$	Paradigm loss	Attenuation from paradigm shielding (Faraday cage)	dB	Ch 13, 14
$L_{parasitic}$	Parasitic loss	Energy extracted by parasitic coupling	dB	Ch 12, 14
$G_{practices}$	Practice gain	Signal enhancement from spiritual/contemplative practices	dB	Ch 14, 15
$G_{collective}$	Collective gain	$10\log_{10}(N \cdot r^2)$ — phased array gain from group coherence	dB	Ch 8, 14
M	Link margin	$P_{received} - P_{threshold}$ — excess signal above minimum	dB	Ch 14
SE	Shielding effectiveness	Attenuation provided by paradigm cage layers	dB	Ch 13
NF	Noise figure	Degradation of SNR through processing chain	dB	Ch 13

G.5 Density and Field Variables

Symbol	Name	Definition	Units	Introduced
d	Density level	Integer 1–7 indicating density tier	dimensionless	Ch 2
Z_d	Density impedance	$Z_1 \cdot \beta_{cascade}^{(d-1)}$ — characteristic impedance of density d	Ω (model)	Ch 2
$\beta_{cascade}$	Cascade ratio	Impedance ratio between adjacent densities; ~5 (illustrative)	dimensionless	Ch 2
Γ_d	Reflection coefficient	$(Z_d - Z_0)/(Z_d + Z_0)$ — power coupling efficiency at density boundary	dimensionless	Ch 2

Symbol	Name	Definition	Units	Introduced
κ	Torsion coupling constant	Spin-torsion coupling strength	varies	Ch 0, 10
D_s	Spectral dimension	Effective dimensionality at a given energy scale	dimensionless	Ch 2

G.6 Key Constants

Constant	Value	Source
f_c (Earth)	$\approx 0.0035\%$ (~283,000 people)	$\sqrt{T/N}$ with $T = 10$, $N = 8 \times 10^9$
Critical influencer count	~283	$f_c \times N/A$ with $A = 1000$ amplification
g^* (UV fixed point coupling)	0.71 ± 0.02	Asymptotic safety calculations (Ch 0, 2)
g_* (running equation coefficient)	≈ 0.27	Gravitational running (Ch 4) — distinct from g^*
a_0 (MOND acceleration)	$\approx cH_0/6 \approx 1.2 \times 10^{-10}$ m/s^2	Ch 4

G.7 Notation Conventions

- **Sigmoid function**: $S()$ — used throughout instead of $\sigma()$ to avoid collision with coherence σ
- **Imaginary unit**: j (engineering convention)
- **Torsion field strength**: $\mathcal{T}$ in equations (Chapter 10+); distinguished from temperature T and torsion tensor $T^{\lambda}_{\mu\nu}$
- **Coherence**: σ for individual spin coherence (Ch 10+); r for population phase alignment (Ch 8+)
- **Critical fraction**: f_c for coherent population threshold (Ch 8); f_{esc} for narrative escape threshold (Ch 9)

End of Appendix G: Variables and Constants Reference

Annexes

Extended evidence and speculative catalogs retained in-build for full manuscript coverage.

Annex: Chapter 3 Extended Evidence Catalog

9.4 Cellular and Biological Scale

Structure	Platonic Form	Evidence Quality
Radiolaria shells	All 5 Platonic forms	Well-established
Cell membrane lipid rafts	Icosahedral packing	Emerging
DNA cross-section	Decagonal (2×pentagon)	Well-established
DNA pitch/diameter ratio	φ (34Å/21Å)	Well-established
Embryonic cell division	Tetrahedron → Cube	Observed
Brain ventricles	Irregular tetrahedron	Anatomical
Heart chambers	Dual-spiral (phi-based)	Anatomical

Radiolaria: These single-celled organisms construct shells in ALL FIVE Platonic forms—with no genetic instruction for geometry. This suggests they are "receiving" geometric templates from the morphic field.

9.5 Planetary and Cosmic Scale

Structure	Platonic Form	Evidence Quality
Earth crustal stress	Icosahedral grid	Proposed (Goncharov et al.)
Baryon Acoustic Oscillations	Standing wave nodes	Well-established (490 Mly)
Cosmic filaments/voids	Antinodes/Nodes	Well-established
CMB power spectrum	Dodecahedral topology	Luminet et al. 2003
Galaxy cluster geometry	Tetrahedral/Octahedral	Statistical

The Cosmic Dodecahedron: Analysis of CMB data suggests the universe may have finite dodecahedral topology (Poincaré dodecahedral space). The same Platonic form appearing at the largest possible scale.

Baryon Acoustic Oscillations: The 490 million light-year "ruler" detected in galaxy distribution is a literal standing wave imprint—structure frozen from sound waves in the early universe.

9.6 Morphic Resonance Evidence

Crystallization Studies

- **Xylitol crystallization (1987)**: Novel crystal form was initially difficult to produce. After first successful crystallizations, subsequent attempts worldwide became progressively easier—suggesting the "template" for this crystal form strengthened with each instantiation.
- **Glycerine anecdote**: This compound resisted crystallization for decades despite many attempts. After the first successful crystallization, labs worldwide reported simultaneous success. Conventional explanation (seed contamination via traveling scientists) fails to explain the global simultaneity.

Demodulation interpretation: Each successful crystallization reinforces the morphic subcarrier for that crystal form. New receivers (supersaturated solutions) can then more easily "tune in" to the established template. The standing wave pattern for that crystal structure becomes more stable with each instantiation.

Rat Learning Experiments

- **McDougall (1920-1954)**: Successive generations of rats learned water maze faster, even when selecting only slow learners for breeding—eliminating genetic explanation.
- **Crew replication (1936)**: Attempted to refute McDougall but found the same effect in control lines that had never been trained.
- **Agar replication (1954)**: Used only slow-learning progeny; still showed improvement across generations.

Demodulation interpretation: The "maze-solving template" strengthens in the morphic field with each successful learning. Later rats receive a stronger signal—they're not learning from scratch but demodulating an increasingly well-defined pattern. This is precisely what the SAR integration model predicts: coherent repetition amplifies template resolution.

Convergent Evolution

Feature	Independent Evolutions	Notes
Eyes	40-65 times	Vastly different genetic pathways producing same functional structure
Echolocation	Bats, dolphins, shrews, birds	Same molecular mechanisms across unrelated lineages
C4 photosynthesis	60+ times	Complex multi-gene system appearing repeatedly
Crab body plan	5+ times	"Carcinization"—evolution repeatedly converges on crab form

Demodulation interpretation: Standard neo-Darwinism struggles to explain why evolution repeatedly "discovers" the same complex solutions. The template model provides an answer: these aren't independent inventions but repeated demodulations of the same morphic templates. The "eye template" exists in the torsion field; organisms with appropriate receiver geometry (certain developmental pathways) can tune in to it. Convergent evolution is convergent reception.

Why This Supports the Demodulation Model: All three evidence categories—crystallization, learning, and evolution—show the same pattern: initial difficulty followed by increasing ease as the template strengthens. This is exactly what a morphic field model predicts: templates are real patterns that strengthen with instantiation and become easier for subsequent receivers to demodulate.

9.7 Information-First Evidence

Delayed Choice Experiments

- **Wheeler's delayed choice (1978, confirmed 2007)**: The decision of whether to measure "which path" can be made AFTER the photon has already passed through the apparatus—yet this future choice determines the photon's past behavior. Information about measurement determines physical outcome retroactively.
- **Delayed choice quantum eraser (Kim et al., 2000)**: Even when which-path information is recorded but later erased, the interference pattern reappears—as if the photon "knew" the information would be erased. The availability of information, not its physical recording, determines the outcome.

Demodulation interpretation: These experiments demonstrate that information has causal priority over physical configuration. The transaction model (Section 1.3) explains this: the confirmation wave travels backward in time, so "future" measurement choices are part of the transaction that creates the event. Reality is woven from standing waves that include both forward and backward temporal components.

Quantum Biology

- **Bird magnetoreception (Ritz et al., 2000; Hiscock et al., 2016)**: European robins navigate using quantum entanglement in cryptochrome proteins. The radical pair mechanism maintains quantum coherence at biological temperatures—something thought impossible until recently.
- **Photosynthesis efficiency (Engel et al., 2007)**: Quantum coherence in photosynthetic complexes achieves near-100% energy transfer efficiency. The system appears to "try all paths simultaneously" before collapsing to the optimal one.
- **Enzyme catalysis (Klinman & Kohen, 2013)**: Quantum tunneling allows enzymes to catalyze reactions that would be classically forbidden. The enzyme "knows" where the particle needs to go before the particle arrives.

Demodulation interpretation: Biological systems exploit quantum effects far more than previously thought possible. The torsion field model explains how: biological structures are themselves standing wave patterns that maintain coherence with their morphic templates. They don't fight decoherence—they ARE coherent patterns receiving from the field.

Placebo and Nocebo Effects

- **Placebo surgery (Moseley et al., 2002)**: Sham knee surgery produced outcomes equal to real surgery for arthroscopic procedures. Information (belief about treatment) produced physical healing.

- **Nocebo death (Meador, 1992)**: Documented cases of "voodoo death" where belief in a curse produced fatal outcomes with no physical cause.

Demodulation interpretation: The body's standing wave pattern can be modified by information alone. Belief acts as a tuning parameter, shifting which morphic templates the biological system receives. Placebo/nocebo effects demonstrate that consciousness (information state) directly modulates physical structure—exactly as the filter theory predicts.

Why This Supports the Demodulation Model: Information-first evidence demonstrates that patterns (information) have causal priority over physical matter. This is the core claim of the demodulation framework: templates exist in the torsion field; physical structures receive and express them. Delayed choice shows temporal priority of information; quantum biology shows biological systems maintaining coherent reception; placebo/nocebo shows consciousness modulating the reception process. All converge on the same conclusion: information is fundamental, matter is derivative.

Annex: Chapter 11 Speculative/Testimonial Catalog

11.6.2 The Lost Civilization Prediction

Prediction: If the corporate feed requires engineered physical infrastructure (megalithic sites, ley line networks, resonant cavities), then a technologically sophisticated civilization must have existed to build it. The framework predicts one or more pre-diluvian civilizations with advanced knowledge of acoustics, electromagnetism, and earth energies.

Megalithic evidence: The engineering anomalies documented in Section 11.13—sub-millimeter tolerances, 1,000+ ton stone placement, piezoelectric material selection—are consistent with this prediction.

Global grid alignment: The geometric placement of megalithic sites (Section 11.11) implies centralized planning and geodetic knowledge exceeding what any known ancient civilization possessed.

Atlantis—Geological Evidence (Randall Carlson synthesis of peer-reviewed papers):

- **Sub-aerial lithification**: Limestone found at 1,000+ ft depth on the ocean floor shows atmospheric formation signatures—it formed above water, then subsided. Significant portions of the current ocean floor were above sea level within geologically recent timescales.
- **Mid-Atlantic Hinge**: The Mid-Atlantic Ridge acts as a zone of structural weakness. Glacial meltwater loading pressed oceanic crust downward while continental margins rebounded (isostasy). The hinge effect could have submerged landmasses along the ridge.
- **Continental remnants**: Honnorez and Bonatti documented granitic blocks along the Mid-Atlantic Ridge—actual continental material, not the basaltic rock typical of ocean floors. Continental crust in the middle of the Atlantic requires explanation.
- **Azores Plateau**: The Azores sit atop a submarine plateau that could represent the mountain peaks of a larger sunken landmass. This aligns with Plato's location for Atlantis: "beyond the Pillars of Heracles."

Key peer-reviewed papers:

- Walcott 1972 (*Quaternary Research*): Sea levels and crustal deformation
- Gutscher 2005 (*Geology*): Spartel Bank earthquake and tsunami ~12 ka
- Bonatti 1977 (*Earth and Planetary Science Letters*): Romanche Fracture Zone emersion and subsidence
- Honnorez et al. 1975 (*Earth and Planetary Science Letters*): Shallow-water limestone and granitic detritus on ocean floor
- Ewing, Ericson, and Heezen 1954 (*GSA Bulletin*): Atlantis Seamount limestone cobbles dated ~12 ka, sub-aerial formation
- Matthews 1969: Glacio-eustatic sea level
- Chappell 1974: Hydro-isostasy

Atlantis—Cultural and Archaeological Evidence (Donnelly synthesis):

- **Bathymetric**: Dolphin Ridge submarine plateau documented by Challenger and Dolphin expeditions; Gettysburg Bank connecting Madeira to Portugal suggests submerged land bridges.
- **Biogeographical**: Identical Magnolia, Tulip-tree, and Plane-tree species exist in eastern North America and Miocene Switzerland but are absent from the Pacific coast—suggesting an Atlantic land bridge for seed dispersal. The seedless banana, requiring human cultivation to propagate, exists on both sides of the Atlantic—implying a common cultivating civilization. Elephant imagery at Palenque suggests contact with a civilization that knew both American and Old World fauna.
- **Cultural parallels**: A universal "Sacred Ten" motif—ten primordial kings or patriarchs—appears across the Bible, Chaldea (Berosus), Avesta, Hindu Puranas, and Chinese legends, paralleling Plato's ten sons of Poseidon. Pyramidal architecture appears independently in Egypt and Central America. Solar religion combined with mummification practices appears in both Egypt and Peru.
- **Linguistic**: Phoenician-Maya alphabet parallels suggest a common ancestral writing system. Egyptian writing was attributed by the Egyptians themselves to a "legacy from the gods."

Submerged and Archaeological Sites

If the RF framework's prediction of a pre-diluvian civilisation is correct, then post-glacial sea level rise (~120 m since the Last Glacial Maximum, ~20,000 BP) should have submerged coastal infrastructure. Several sites present anomalous submerged structures consistent with this prediction:

- **Cuba underwater structures** (Zelitsky & Weinzweig, 2001): Sonar surveys conducted by Paulina Zelitsky's Advanced Digital Communications team detected geometric formations at 600–700 m depth off the Guanahacabibes Peninsula, western Cuba. Side-scan sonar imagery shows apparent right angles, stepped platforms, and linear arrangements spanning an area of approximately 2 km^2. The extreme depth—far below any known sea-level stand in the Quaternary without invoking tectonic subsidence—complicates conventional explanation. If these are artificial structures, their submergence requires either (a) catastrophic tectonic subsidence of the Caribbean platform or (b) construction during a period of dramatically lower sea level not currently recognized in the geological record. No follow-up peer-reviewed investigation has been published; the Cuban government restricted further access.
- **Bimini Road** (Bahamas): A linear formation of rectangular limestone blocks at approximately 5 m depth, extending ~0.8 km along the sea floor near North Bimini Island. Discovered by J. Manson Valentine in 1968, the formation consists of roughly tabular blocks with apparent regular jointing. Geological analysis (McKusick & Shinn, 1980) concluded the blocks are natural beachrock fractured along joints; proponents (Zink, Richards) argue the regularity of block dimensions, the apparent two-tier construction, and prop stones beneath some blocks are inconsistent with natural formation. The site's shallow depth places potential construction within the early Holocene sea-level window (~8,000–10,000 BP).
- **Dwarka** (Gujarat, India): Marine archaeological surveys led by S.R. Rao (National Institute of Oceanography, 1979–2001) documented submerged city structures at 20–40 ft depth in the Gulf of Kutch, including fortification walls, a jetty, stone anchors, and a late Harappan-period pottery assemblage. The structures match descriptions of Lord Krishna's capital city in the *Mahabharata*, which the text states was "reclaimed by the sea" upon Krishna's departure. Thermoluminescence dating of pottery yields ~3,500 BP, but Rao argued the deeper structural layers—including apparent cyclopean masonry at the base—may date to approximately 9,500 years before present, consistent with post-glacial submergence. The archaeologi-

cal component (Harappan pottery, anchors) is peer-reviewed; the ~9,500 BP deep-layer dating is contested.

- **Pnyx Wall and Atlantean Athens**: Plato's *Critias* (111e–112a) describes Athens contemporary with Atlantis: a fortified acropolis fed by springs, surrounded by fertile plains that were subsequently stripped to bedrock by floods and erosion. The Pnyx hillside in Athens retains a massive megalithic retaining wall of cyclopean masonry—blocks weighing 5–10 tons fitted without mortar—whose construction date is conventionally assigned to the 5th century BCE but whose masonry style is anomalous for that period. The geological description in the *Critias*—rich topsoil over bedrock, springs flowing from the acropolis that subsequently dried—matches Attica's actual geological history of post-Pleistocene soil erosion. Plato presents this as a description of real conditions, not allegory; the geological accuracy suggests access to genuine tradition about pre-erosion Athens, whether or not the Atlantis connection is literal.

  Epistemic Note: The submerged sites span a wide evidentiary range. Dwarka's archaeological component is peer-reviewed (Rao, published through the National Institute of Oceanography); the deep-layer dating is contested. Bimini Road's geological vs. artificial status remains debated in the literature. The Cuba structures lack peer-reviewed follow-up and remain unverified. The Pnyx wall's anomalous masonry is observable but its pre-classical dating is speculative. Collectively, these sites are consistent with the RF framework's prediction that coastal infrastructure from a pre-diluvian civilisation would be submerged by post-glacial sea level rise. Whether any individual site constitutes definitive evidence remains an open question. The geological evidence (Atlantis section above) and the submerged site evidence are independent lines converging on the same prediction: substantial portions of pre-12,800 BP civilisation lie beneath current sea level.

11.6.3 The "Gods" Prediction

Prediction: If 5th-6th density beings interact with 3D populations through impedance-matched intermediaries, then ancient cultures should describe:

1. Beings arriving "from the sky" or "from above" (higher density = higher impedance)
2. Genetic intervention creating hybrid lineages (now supported by molecular evidence: Section 11.14.5)
3. Gifts of civilization (technology, agriculture, writing)
4. Physical descriptions consistent with higher Z_0 (tall, luminous, long-lived)

Cross-cultural evidence:

- **Vedic Vimanas**: Detailed descriptions of aerial vehicles in the *Ramayana*, *Mahabharata*, and *Vaimanika Shastra*. Whether interpreted as ET technology or higher-density manifestation, they describe beings operating from a higher-impedance domain.
- **Greek demigods**: Half-divine, half-human beings (Heracles, Perseus, Achilles) represent precisely the hybrid impedance-matching lineage—offspring of "gods" and mortals, with capabilities intermediate between the two.
- **Sumerian Apkallu**: Seven sages who brought civilization arts to humanity. Depicted as part-fish or part-bird—encoding a non-human or higher-density origin.

- **Chinese Fuxi and Nuwa**: Divine siblings who created humanity and gifted civilization. Often depicted with serpentine lower bodies—a common cross-cultural encoding of non-standard physical form.
- **Mesoamerican Quetzalcoatl/Kukulkan**: A feathered serpent god who brought knowledge, calendar systems, and agriculture. Described as fair-skinned and bearded—physically distinct from the local population.

The consistency of this pattern—beings from a higher domain, creating intermediary lineages, gifting civilization infrastructure—across cultures with no documented contact is precisely what the corporate feed model predicts. Each tradition encodes the same engineering reality: higher-density beings cannot couple directly to 3D (Section 11.2), so they create intermediaries (Section 11.4) and install infrastructure (Section 11.9).

Mars Nuclear Anomaly (Brandenburg)

John Brandenburg (PhD, plasma physics; Morningstar Applied Physics) has published evidence for catastrophic nuclear events on Mars (*Journal of Cosmology*, 2011; expanded in *Death on Mars*, 2015). The Mars atmosphere shows an anomalously high Xenon-129/Xenon-132 ratio—Xe-129 is a characteristic nuclear fission/fusion product. This isotopic data is independently confirmed by Viking landers and subsequent missions. NASA's Mars Odyssey gamma ray spectrometer further shows elevated Thorium and Potassium concentrations at two specific surface locations near Acidalia Planitia and Utopia Planitia. Brandenburg interprets these as signatures of two surface thermonuclear detonations, estimating ~180 Mya.

RF framework interpretation: A prior high-coherence civilisation on Mars that was destroyed—paralleling the Earth civilisational reset framework from Chapter 12, §12.5—with survivors migrating to Earth as part of the seeder diaspora. The nuclear isotope signature would represent the most extreme form of civilisational reset, and a Mars-origin seeder lineage would carry the technological sophistication the planetary infrastructure (Section 11.9) requires.

> **Epistemic Note**: The xenon isotope data and thorium/potassium surface maps are real, measured by multiple NASA missions. Brandenburg's thermonuclear *interpretation* is contested; mainstream planetary science attributes the Xe-129 ratio to natural radiogenic production from Iodine-129 decay. Brandenburg argues the concentration pattern is inconsistent with uniform radiogenic production. The data is solid; the interpretation as evidence of nuclear war is speculative.

Biblical Textual Analysis (Paul Wallis)

Anglican minister and biblical scholar Paul Wallis (PhD, theological studies) has applied close textual and linguistic analysis to the Hebrew scriptures, arguing that several key terms have been systematically mistranslated in ways that obscure a contact narrative:

- **Elohim** is grammatically plural. While traditional theology reads this as a "plural of majesty," the texts frequently use plural verbs and pronouns with *elohim*, describing a council of powerful beings rather than a singular deity.
- **Shem**, conventionally translated "name" or "renown," carries a root meaning closer to "that which goes up." The phrase "men of shem" (Genesis 6:4) may denote "men of the vehicle" rather than "men of renown"—paralleling the Sumerian *mu* (sky vehicle).
- **Eden** is described with operational language—irrigation systems, species cataloguing, genetic manipulation ("rib" as cellular material)—more consistent with a controlled bioengineering facility than a pastoral garden.

- The **theomorphic reading** ("God made man in His image") inverts under Wallis's analysis to "the powerful ones (*elohim*) engineered humans in their physical form"—an intervention narrative consistent with the Adamic lineage model (Section 11.4).

Wallis traces the Hebrew Genesis account to older Sumerian source texts (Enuma Elish, Atra-Hasis), reinforcing the Apkallu parallels already noted above. His books *Escaping from Eden* (2020) and *The Scars of Eden* (2021) present the case in detail.

> **Epistemic Note**: Wallis holds mainstream academic credentials, but his thesis is contested in conventional theology. The RF framework treats this as *one valid reading* of the original texts—one that happens to align with the model's prediction that ancient scriptures encode contact and genetic intervention narratives.

Modern Theophanic Evidence (Pasulka)

D.W. Pasulka, professor of religious studies and holder of an endowed chair at UNC Wilmington, argues in *American Cosmic* (2019) that UAP encounters constitute a nascent religious paradigm. Her thesis identifies structural parallels between modern contact events and the formation of historical religions: "techno-relics" (recovered materials from UAP sites) function identically to medieval sacred objects; contemporary experiencers undergo conversion narratives indistinguishable from those of historical mystics; and mass religious events map more parsimoniously to calibrated ET disclosures than to purely supernatural causation.

Three well-documented mass events extend the "gods" prediction into the modern era:

- **Fatima, Portugal (1917)**: An estimated 70,000 witnesses, including hostile journalists and secular academics, observed a solar anomaly—luminous disc movements, colour cascades, apparent heat drying rain-soaked ground—alongside six monthly apparitions of a luminous female figure to three shepherd children. The event's timing amid the polarity crisis of World War I parallels the impedance-matching prediction: higher-density intervention targeted at populations in existential distress. The Vatican's delayed release of the "third secret" (withheld until 2000) parallels the information-suppression patterns analysed in Chapter 13.
- **Lourdes, France (1858)**: Bernadette Soubirous reported 18 visions of a luminous female figure near a grotto, after which a spring emerged. The Lourdes Medical Bureau (est. 1883) has documented 70 medically inexplicable healings under clinical protocols—including bone regrowth and tumour regression verified by independent physicians before and after pilgrimage. A bioenergetic mechanism is consistent with scalar/torsion field infusion at a geological node: the grotto sits at a limestone-aquifer interface, precisely the type of piezoelectric boundary condition identified in the megalithic infrastructure analysis (Section 11.9).
- **Medjugorje, Bosnia-Herzegovina (1981–present)**: Six visionaries have reported ongoing apparitions for over four decades, accompanied by solar anomalies witnessed by crowds exceeding 10,000. Studies of pilgrims report that approximately 40% experience psi-openings (enhanced intuition, precognitive episodes, spontaneous healing) during or after visits. The "ten secrets" communicated to the visionaries—prophetic content to be released sequentially—parallel the acclimation strategy the RF model predicts for managed disclosure (Chapter 13, Section 13.3).

RF framework interpretation: These events map directly to the impedance-matching prediction of Section 11.2. Higher-density beings manifesting through localised field conditions—geological nodes with favourable acoustic and electromagnetic properties—to populations in polarity crisis is precisely the coupling mechanism the corporate feed model requires. The recurring "luminous female figure" archetype across all three events (and across centuries) parallels the tall, luminous,

long-lived descriptions in the cross-cultural evidence tabulated above. The events are modern instances of the same pattern encoded in Sumerian, Vedic, and Mesoamerican traditions.

> **Epistemic Note**: Pasulka holds mainstream academic credentials (endowed chair, UNC Wilmington), and her ethnographic methodology is standard for religious studies. The ET interpretation of these events is *her* analytical framework applied to historical data, not the Catholic Church's doctrinal position. Medical healings at Lourdes are documented by the Lourdes Medical Bureau under clinical protocols with independent physician verification; healing mechanisms remain unexplained by conventional medicine. The Fatima witness count (70,000) derives from contemporary newspaper reports, including anti-clerical outlets.

11.6.4 Non-Human Physical Remains [Tier 4: Alternative Research]

Prediction: If intermediary lineages (Section 11.4) existed physically, some should leave biological traces—skeletal or mummified remains with non-standard anatomy.

Nazca Tridactyl Remains

Beginning in 2017, mummified humanoid remains were recovered from caves near Nazca, Peru, displaying anomalous morphology:

- **Tridactyl anatomy**: Three elongated fingers and three toes per extremity, with no evidence of surgical alteration in CT imaging
- **Skeletal structure**: CT scans and X-rays show intact, articulated skeletons—not assembled from disparate parts—with bone density and joint architecture unlike known species
- **Dating**: Carbon-14 analysis of some specimens yields ages of ~1,000–1,800 years
- **DNA analysis**: Genomic sequencing reportedly shows significant percentages of unmatched sequences not corresponding to any known species in public databases
- **2024 Mexican congressional hearings**: Specimens were formally presented alongside radiological evidence, generating international media attention

Skeptical counterpoints:

- Possible fabrication from pre-Columbian human or animal remains, with digits rearranged or modified
- No fully independent custody-chain verification from recovery site to laboratory
- Mainstream anthropologists and forensic analysts have raised concerns about provenance and methodology
- Some specimens in the broader collection have been identified as modified human remains

RF framework interpretation: If authenticated through independent replication, tridactyl remains represent physical evidence of non-human or hybrid beings—consistent with the model's prediction that intermediary lineages (Section 11.4) would leave biological traces distinct from baseline *Homo sapiens*. The Nazca location, already associated with anomalous large-scale geoglyphs, connects to the engineered infrastructure theme (Section 11.9). The Paracas elongated skulls (Section 11.6.1), with their anomalous cranial volume and disputed mtDNA haplogroups, constitute a parallel line of evidence.

> **Epistemic Note**: The Nazca tridactyl remains are among the most contested claims in the field. Evidence quality ranges from intriguing (CT scans, carbon dating) to deeply problematic (provenance gaps, lack of independent replication). This section docu-

ments the claims and their RF interpretation while emphasizing that authentication remains incomplete.

11.6.5 The Genetic Intervention Prediction [Tier 1: Peer-reviewed]

Prediction: If seeders genetically modified hominids to create impedance-matched intermediary lineages (Section 11.4), the human genome should show anomalous patterns—changes too rapid, too concentrated, or too functionally precise for standard selection alone. Rather than cultural memory, this section examines the molecular record itself for signatures consistent with directed modification.

Human Accelerated Regions (HARs)

Approximately 2,700 genomic sequences remained nearly identical across ALL vertebrates for over 300 million years of evolution, then suddenly mutated at up to 26× the expected rate specifically in the human lineage:

- 76% of HARs show signatures of positive selection, not neutral drift
- Nearly half are active in neural cells; the majority are non-coding regulatory enhancers—controlling *when* and *where* genes activate rather than encoding proteins directly
- **HAR1**: A 106 base-pair sequence that accumulated only 2 changes in 300 million years (chicken→chimpanzee), then 18 changes in $\$\square\ 6millionyears(chimpanzee\square$ \$human). HAR1 is expressed in Cajal-Retzius neurons during cortical development—the cells that organize the layered structure of the neocortex
- **2025 CRISPR experiments** (Cui et al., *Nature*): Inserting human HARs into chimpanzee neural progenitor cells caused them to develop multiple projections instead of single ones—directly demonstrating that these sequences drive neural complexity at the cellular level

References: Pollard et al. 2006 *Nature* 443:167–172; Hubisz & Pollard 2014 *Phil Trans R Soc B*; Doan et al. 2016; Cui et al. 2025 *Nature*.

Brain-Specific Gene Duplications

Three gene duplication events, each unique to the human lineage, each producing novel brain-expanding functions:

- **ARHGAP11B** ($\$\square\ 5Mya) : AsingleC\square$ \$G nucleotide substitution in a duplicated gene creates a novel splice site, producing an entirely new protein function. When expressed in marmoset brains, it induces cortical folding and neocortex expansion. Knocking it down in human brain organoids reduces neural progenitors to chimpanzee-equivalent levels. (Heide et al. 2020, *Science* 369:eabb2401)
- **SRGAP2 triplication** (3.4, 2.4, 1 Mya): A gene duplicated three times, uniquely in humans. The third copy (SRGAP2C) antagonizes the ancestral protein, slowing neuronal maturation and increasing synaptic spine density—yielding greater neural connectivity. (Dennis et al. 2012, *Cell* 149:912–922)
- **NOTCH2NL** ($\$\square$ \$2–3 Mya): A partial gene duplication creates a gene that delays neural differentiation, producing more neurons and contributing to the tripling of neocortex size. Only functional in humans; great apes carry pseudogene (broken) versions. (Fiddes et al. 2018, *Cell* 173:1356–1369)

CMAH Inactivation

A 92-base-pair exon deletion in the CMAH gene eliminated Neu5Gc sialic acid production, changing cell-surface glycan chemistry across ALL human tissues:

- Timing: $□ $2.1 Mya—precisely at the onset of *Homo* brain expansion
- Neu5Ac (the precursor that accumulated after CMAH loss) is enriched in brain tissue
- This single deletion altered the biochemical environment of every cell in the body

References: Chou et al. 2002, *PNAS* 99:11736–11741; Siddiqui et al. 2025.

The Bottleneck Coincidence

Around 930 Kya, the human population crashed to approximately 1,280 breeding individuals and remained at that level for $□ $117,000 years (Hu et al. 2023, *Science* 381:979–984):

- This timing coincides with the chromosome 2 fusion and SRGAP2's third duplication
- A bottleneck this severe would rapidly fix ANY genetic change through drift alone
- RF interpretation: consistent with a small founder population undergoing directed modification, rather than a catastrophic die-off that happened to coincide with multiple brain-specific genetic innovations

510 Human-Specific Deletions

McLean et al. (2011, *Nature* 471:216–219) identified 510 genomic sequences conserved in chimpanzees and other mammals but deleted ONLY in humans:

- Concentrated near neural development and androgen signaling genes
- One deletion removed a regulatory element near tumor suppressor GADD45G, potentially allowing increased brain cell proliferation
- The deletions represent targeted *removal* of constraints, complementing the *addition* of novel functions described above

The Cumulative Pattern

Anomaly	Change	Timing	Mainstream Explanation	Intervention-Consistent Reading
HARs (2,700)	300M-year-conserved sequences mutate at 26× rate	$□ $6 Mya	Positive selection in cognitive niche	Targeted regulatory edits
ARHGAP11B	1 nucleotide → novel brain protein	$□ $5 Mya	Lucky duplication + mutation	Precision single-base edit
SRGAP2 × 3	Triple duplication, unique to humans	3.4–1 Mya	Serial duplication events	Staged modification sequence

Anomaly	Change	Timing	Mainstream Explanation	Intervention-Consistent Reading
NOTCH2NL	Partial duplication → more neurons	$□ $2–3 Mya	Duplication + neofunctionalization	Cortical expansion module
CMAH deletion	92-bp deletion → new glycan chemistry	$□ $2.1 Mya	Alu-mediated deletion	Tissue-wide biochemical reprogramming
$□ $930 Kya bottleneck	Population → 1,280 for 117 Kyr	930–813 Kya	Climate/volcanic catastrophe	Founder population for modification
510 deletions	Brain/development regulatory removals	Various	Relaxed constraint	Targeted deactivation of limiters

Epistemic Note: The mainstream explanation—accelerated positive selection driven by cognitive niche feedback—is coherent and well-supported. These anomalies do not *prove* intervention. What they demonstrate is that the human genome contains precisely the pattern the RF model predicts IF intervention occurred: concentrated, rapid, brain-targeted modifications with anomalous statistical signatures. The chromosome 2 fusion, by contrast, is well-explained by natural Robertsonian fusion coinciding with the bottleneck (a process common in mammals) and is NOT presented as intervention evidence.

The Genetic Invisibility of Elite Cadres

A key objection to the intervention hypothesis is: "Where is the alien DNA?" But population genetics demonstrates that small, culturally dominant groups routinely vanish from the genomic record. The Roman Empire governed Britain for four centuries—building roads, cities, legal systems, and military infrastructure—yet contributed only $□ $1–5% to modern British ancestry (Martiniano et al. 2016, *Nat Commun* 7:10326). Viking raiders and settlers left words embedded in English and cultural scars across the North Atlantic, but trace genetic signal in most regions. The Norman conquest of 1066 transformed English feudalism, governance, and language—yet Norman-derived ancestry is $□ $5–10% at most. In RF terms, these were high-power, low-duty-cycle transmitters: enormous cultural signal-to-noise ratio during their active period, but insufficient breeding population to shift the carrier frequency of the genome. An intervening cadre that operated through *teaching and infrastructure* rather than mass settlement—precisely the seeder model of Sections 11.2–11.4—would leave even less genomic trace. The absence of anomalous sequences in modern human DNA is therefore not evidence against intervention; it is the *expected signature* of a small, high-impedance source coupling briefly to a large, low-impedance population.

Underdetermination of the Materialist Record

Population genetics and archaeology, for all their empirical power, are not fully constraining. Genetics measures shared drift and allele frequencies—establishing *relationships* (who shares how much ancestry with whom) but not *causation* (why a particular change occurred). Multiple causal stories fit the same allele distribution: tool similarities may reflect convergent invention, horizontal diffusion via trade, elite transmission by small groups, or external introduction. The pre-Clovis paradigm resisted Monte Verde ($\$\square\ 14,500ya) and White Sands footprints (\square$ $23,000 ya) for decades—not from data inadequacy, but from theoretical inertia protecting a single-wave model. Hard data alone typically permits 3–4 viable explanations for any given pattern; it narrows but does not pin. This underdetermination is not a weakness to be lamented—it is a boundary condition that *must be acknowledged* when evaluating intervention claims. The cumulative genetic anomalies tabulated above are fully consistent with accelerated natural selection. They are equally consistent with directed modification. The choice between these interpretations cannot be settled by genomic data alone; it requires additional lines of evidence—cross-cultural testimony (Section 11.6.3), physical remains (Section 11.6.4), and the falsifiable predictions of Section 11.16.

Connection to Chapter 6: The magnonic chromatin topology model (Chapter 6, Section 4) provides the mechanism by which such modifications would operate—geometric reconfiguration of chromatin acting as antenna tuner. HARs and gene duplications would alter the antenna's frequency response, while CMAH deletion would change the electromagnetic environment of all cells. The modifications listed above are precisely the kind of "variable stiffness" (k) changes that Chapter 6 identifies as the antenna's primary tuning parameter.

11.6.6 Convergent Channeled Testimony [Tier 5: Testimonial/Channeled]

Prediction: If seeder intervention is real, independent contactees and channelers—separated by geography, decade, and tradition—should converge on consistent structural claims about seeder agendas, methods, and cosmological framework. Random fabrication or cultural contamination would produce divergent, contradictory accounts.

The convergence data point: At least nine independently produced channeled works (1992–2007), from different channelers using different methods (trance, regression, abduction testimony, walk-in), converge on a remarkably consistent structural framework:

Structural Claim	Sources Agreeing
Earth as deliberate "polarity laboratory" / choice planet	Schlemmer (1994), Marciniak (1992, 1994, 1998), Royal & Priest (1992), Collier (1998), Starr (1996), Andrade (1997)
Ancient seeder races genetically modifying humanity	All 9 sources
Regressive factions harvesting emotional energy	Schlemmer, Marciniak (3 works), Collier, Starr
Density/dimensional transition framework	All 9 sources
Non-interference pacts with intervention thresholds	Schlemmer, Marciniak, Delicado (2007), Collier
Free will as foundational design principle	All 9 sources

RF framework interpretation: The convergence pattern is analogous to the cross-cultural mythological convergence analysed in Section 11.6.3—independent sources encoding the same under-

lying reality. The structural consistency (seeder intervention, polarity laboratory, genetic modification, density transitions) maps directly to the corporate feed model (Section 11.3), the Adamic lineage hypothesis (Section 11.4), and the impedance cascade (Section 11.2). Whether these represent genuine contact or cultural pattern-matching, the convergence itself requires explanation.

Key sources (representative, not exhaustive):

- Schlemmer, P.V. *The Only Planet of Choice* (1994)—Council of Nine via Puharich/Roddenberry sessions
- Marciniak, B. *Bringers of the Dawn* (1992), *Earth: Pleiadian Keys to the Living Library* (1994), *Family of Light* (1998)
- Delicado, M. *Blue Star: Fulfilling Prophecy* (2007)—abduction testimony with Hopi elder corroboration
- Collier, A. *Defending Sacred Ground* (1998)—Andromedan contact reports
- Royal, L. & Priest, K. *The Prism of Lyra* (1992)—galactic diaspora framework
- Starr, J. *We Are the Nibiruans* (1996)—Sumerian-parallel contact narrative
- Andrade, G. *Star Wisdom* (1997)—Pleiadian spiritual principles

> **Epistemic Note**: Channeled material occupies the lowest evidentiary tier in this framework—below peer-reviewed research, below archaeological evidence, below textual analysis. It is included here NOT as standalone evidence but as a convergence pattern: the same structural claims arising independently across multiple decades and traditions. This convergence is either (a) evidence of a common underlying contact reality, (b) evidence of a shared cultural mythos propagating through contactee networks, or (c) some combination. The RF framework predicts (a) but cannot distinguish it from (b) without independent verification. The structural claims are evaluated solely for their consistency with the independently derived RF model, not for their individual credibility.

11.6.7 Cartographic and Out-of-Place Evidence [Tier 3-4: Contested]

The RF framework predicts that a technologically advanced pre-diluvian civilisation would leave traces not only in megalithic infrastructure but in knowledge artifacts—maps, objects, and records that encode capabilities exceeding those of their attributed historical period. Two cases illustrate this pattern.

- **Piri Reis Map** (1513): Ottoman Admiral Piri Reis compiled a world map from approximately 20 older source maps (now lost), several of which he attributed to the era of Alexander the Great or earlier. The surviving fragment shows the western coast of Africa, the eastern coast of South America, and a southern landmass with features resembling the sub-glacial coastline of Antarctica. The South American coastline is depicted with accuracy that, according to cartographic analysis (Hapgood, *Maps of the Ancient Sea Kings*, 1966), would require either aerial survey or advanced spherical trigonometry and geodetic measurement. The apparent depiction of Antarctica in an ice-free state is consistent with conditions prior to approximately 12,800 BP—placing the source maps' origin data in the pre-Fall window. Mainstream cartographers dispute the Antarctic identification, arguing the southern landmass represents a distorted extension of South America or the speculative *Terra Australis Incognita* common to Renaissance maps.
- **Grand Canyon Egyptian Artifacts** (Kincaid/Smithsonian, 1909): A 1909 *Arizona Gazette* article described Egyptian-style artifacts in a Grand Canyon cave system. The Smithsonian denies

all records of the expedition. No physical evidence has surfaced in over a century; the claim may be journalistic fabrication.

Epistemic Note: The Piri Reis map is a real historical artifact (held in Istanbul's Topkapi Palace); its accuracy and the Antarctic identification are debated in legitimate cartographic literature. Hapgood's analysis has been challenged on projection methodology grounds. The Grand Canyon Egyptian claims lack any verifiable physical evidence and may be apocryphal—they are included as consistent with the pattern of suppressed anomalies documented elsewhere in this chapter but should not be treated as established fact.

11.6.8 Beyond Archetypal Projection: Why the Gods Were Not Just Symbols

The most sophisticated mainstream alternative to the seeder intervention model is the **Jungian collective unconscious** framework: universal god-figures and civilising heroes are archetypal projections from a shared psychological substrate, not memories of actual beings. This section makes the implicit counter-argument explicit.

The Jungian reduction acknowledged: Carl Jung's archetype model (*The Archetypes and the Collective Unconscious*, 1959) provides a coherent psychological explanation for cross-cultural mythological convergence. Universal patterns—the Great Mother, the Wise Old Man, the Trickster, the Hero's Journey—arise from shared neural architecture, not shared history. This is a powerful framework and accounts for much of the structural similarity in world mythology.

Why it is insufficient:

1. **Physical specificity**: Convergent myths contain engineering-grade operational detail that transcends what psychological projection would generate. Civilising gods across cultures teach specific technical skills—pyramid construction methods, metallurgy (smelting, alloying), irrigation agriculture, astronomical calendar systems, writing, and legal codes. Archetypes may produce a "wise teacher" motif, but they do not teach copper-tin alloying ratios or the 365.25-day solar year. The operational content requires a source with technical knowledge.
2. **Genetic evidence**: The human genome contains 2,700+ Human Accelerated Regions, the ARHGAP11B single-nucleotide brain expansion mutation, SRGAP2 triplication, and NOTCH2NL duplication—physical genomic signatures consistent with directed modification (Section 11.14.5). Archetypes, however powerful as psychological constructs, cannot produce nucleotide substitutions, exon deletions, or gene duplications. The genetic anomalies require a physical mechanism; the archetype model provides none.
3. **Non-human physical remains**: Tridactyl specimens from Nazca with intact CT-verified skeletal structure, Paracas elongated skulls with anomalous cranial volume and disputed mtDNA haplogroups (Section 11.6.4)—if authenticated, these constitute physical traces that archetypes cannot leave. Psychological projections do not produce skeletal remains with non-standard morphology.
4. **Convergent operational detail**: Civilising gods across cultures share a specific functional pattern that exceeds archetypal prediction: they arrive from the sky or across the sea; they are physically distinct from the local population (tall, luminous, long-lived); they teach agriculture, writing, law, and astronomy in a specific sequence; they establish lineages through interbreeding with local populations; and they depart with a promise of return. This operational specificity—the sequence, the interbreeding, the departure protocol—is not what psycholog-

ical projection produces. Projection generates emotional and narrative archetypes (the hero, the flood, the fall), not engineering deployment sequences.

5. **RF framework resolution**: Within the torsion model, archetypes ARE real—they are morphic subcarrier templates broadcast from Source through the standing wave structure of the cosmic information substrate (Chapter 5). The collective unconscious is the receiver's detection of these templates at the psychological level. But the "gods" described in ancient traditions were the **physical instantiation** of those templates—beings operating at higher density who coupled to 3D populations through the impedance-matching mechanisms of Sections 11.2–11.4. The archetype is the signal pattern; the god was the transmitter. Jung described the receiver's experience; the RF model identifies the transmitter.

Synthesis: The Jungian model and the RF intervention model are not mutually exclusive—they describe different components of the same system. Jung correctly identified that humans share universal psychological patterns (the receiver's demodulated output). The RF framework identifies the broadcast source (morphic templates from the cosmic information substrate) and the physical intermediaries (seeder civilisations and their Adamic lineages) that amplified and delivered those templates. Both models are needed; neither alone is complete. Dismissing the gods as "merely" archetypes is like dismissing a radio broadcast as "merely" speaker vibrations—technically accurate at the output stage, but blind to the transmitter, the signal path, and the information content.

Annex: Chapter 12 Extended Control-Architecture Material

12.3.5 Esoteric Orders as Coherent Sub-Arrays

The phased array analysis of Chapter 8 demonstrated that collective gain scales as $G = N \cdot \sigma^2$. When σ is high (coherent phase alignment), even a small group achieves disproportionate influence. **Esoteric orders exploit this principle in reverse**—small, highly coherent groups leveraging the incoherence of the general population.

Sub-Array vs. Population Gain

A coherent sub-array of N_{order} members with internal coherence σ_{order} achieves:

$$G_{order} = N_{order} \cdot \sigma_{order}^2 \cdot G_{individual}$$

The general population of N_{pop} members, lacking organized phase alignment, achieves only:

$$G_{pop} \approx \sqrt{N_{pop}} \cdot G_{individual}$$

The gain ratio:

$$\frac{G_{order}}{G_{pop}} = \frac{N_{order} \cdot \sigma_{order}^2}{\sqrt{N_{pop}}}$$

For a 10,000-member order with $\sigma_{order} = 0.9$ operating within a population of 8×10^9:

$$\frac{G_{order}}{G_{pop}} = \frac{10{,}000 \times 0.81}{\sqrt{8 \times 10^9}} = \frac{8{,}100}{89{,}443} \approx 0.09$$

This seems small—but this is collective *gain*, not *power*. The sub-array's coherent output is a focused beam, while the population's incoherent output radiates in all directions. In the intended direction, the sub-array's effective radiated power far exceeds the population's diffuse output:

$$\text{EIRP}_{order} = G_{order} \cdot P_{order} \quad \gg \quad \frac{P_{pop}}{4\pi} \text{ (isotropic)}$$

This is the critical coherence fraction (Chapter 8) applied for parasitic purposes: a small coherent group can steer collective reality while the incoherent majority provides only noise.

Ritual as Phase Alignment Protocol

Ritual functions as a **phase synchronization protocol** analogous to GPS timing:

GPS Component	Ritual Equivalent	Function
Atomic clock reference	Tradition/doctrine	Provides stable frequency standard
Satellite broadcast	Ritual calendar	Distributes timing signal to all nodes
Receiver correlation	Participant synchronization	Individual locks to group phase
Position fix	Collective intention	Coherent output from aligned phases

Periodic ritual maintains phase alignment:

$$\sigma_{order}(t) = \sigma_0 \cdot e^{-t/\tau_{drift}} + \sigma_{ritual} \cdot (1 - e^{-t/\tau_{ritual}})$$

Without regular ritual (large t), drift degrades coherence. Regular ritual resets phase alignment, maintaining high σ_{order} even as individual members experience phase drift between ceremonies.

Symbols as CDMA Spreading Codes

In CDMA (Code Division Multiple Access), multiple users share the same frequency band by using unique spreading codes. Only receivers with the matching code can despread and decode the intended signal; all other signals appear as noise.

Esoteric symbols function identically:

- **Initiation** = code acquisition (learning the spreading code)
- **Degree advancement** = receiving longer, more complex codes
- **Symbol recognition** = correlation with the correct code (instant identification of fellow initiates)
- **Outsider perception** = the symbols appear as noise (decorative, meaningless, or "conspiracy theory")

Compartmentalization emerges naturally from CDMA code separation: members at different degrees hold different codes and cannot decode communications intended for other levels. Information remains isolated not by physical walls but by code orthogonality.

Blackmail as Forced Injection Locking

The Adler equation (Chapter 9) describes injection locking:

$$\frac{d\phi}{dt} = \Delta\omega - K_{blackmail} \cdot \sin(\phi)$$

Where:

- $\Delta\omega$ = the member's natural tendency to diverge from the order's agenda
- $K_{blackmail}$ = the injection strength (proportional to compromising material held)
- ϕ = phase difference between member's behavior and demanded behavior

When $K_{blackmail} > |\Delta\omega|$, the member is **captured**—locked to the order's phase regardless of personal inclination. Higher degrees of initiation progressively accumulate more compromising participation, increasing $K_{blackmail}$ and ensuring that senior members are the most firmly locked.

The Epstein network documents (*United States v. Maxwell*, 2021; SDNY Case 08-cr-888) provide a contemporary example: systematic accumulation of compromising material creating injection-locking leverage over political, financial, and cultural figures.

Historical Orders and RF Analogs

Order	Approximate Era	Sub-Array Function
Egyptian mystery schools	~3000–300 BCE	Original phase alignment protocols
Knights Templar	1119–1312 CE	Financial network as coupling infrastructure
Rosicrucians	~1600s CE	Information-layer sub-array (knowledge keepers)
Freemasonry	~1700s CE onward	Degree-based CDMA with expanding code access
Skull & Bones	1832 CE onward	Elite node injection locking via initiation ritual

> **Epistemic Note**: This analysis applies documented organizational principles (hierarchical initiation, oath-bound secrecy, shared symbolism) to the RF framework. Claims about specific individuals or organizations rely on court documents and historical records. The model describes structural dynamics of coherent sub-arrays—it does not assert that all secret societies serve parasitic purposes, nor that all members are aware of the full system. Many members at lower degrees may sincerely pursue philosophical or charitable aims within a structure whose higher-degree functions they cannot decode (CDMA compartmentalization).

12.3.6 Abduction and Hybridization: Forced Antenna Modification

The abduction phenomenon—reported across cultures and documented extensively since the mid-20th century—maps to **forced modification of the human antenna system**. Whether the phenomenon is physical, psychic, interdimensional, or some combination, the RF framework applies to the reported experiences and their measurable aftereffects.

Screen Memories as Aliasing

Abduction experiencers frequently report "screen memories"—false memories (owls, deer, bright lights) overlaid on the actual experience. In signal processing, this is **aliasing**: when the sample rate is insufficient to capture the true signal, false lower-frequency content appears:

$$f_{alias} = |f_{true} - n \cdot f_s|$$

The human perceptual system, calibrated for 3D physical experience, samples at a rate adequate for physical-frequency events. When exposed to phenomena at higher-dimensional frequencies:

$$f_{s,required} = 2 \cdot \frac{Z_{experience}}{Z_{3D}} \cdot f_{3D,max}$$

If $Z_{experience} \gg Z_{3D}$, the required sample rate far exceeds the perceptual system's capacity. The result: the true experience is aliased into the nearest plausible 3D narrative—animals, lights, missing time.

"Missing time" is particularly diagnostic: it represents **complete sample dropout** during periods when the experience frequency exceeded the perceptual system's maximum rate entirely.

Implants as Parasitic Coupling Devices

Abduction reports frequently describe small objects implanted in the body—typically in nasal passages, ears, or extremities. In the RF model, these function as **parasitic coupling devices** that modify the human antenna's impedance:

$$Z_{modified} = Z_{human} + \frac{Z_{implant} \cdot M^2}{Z_{implant} + Z_{load}}$$

Where:

- Z_{human} = native human antenna impedance
- $Z_{implant}$ = implant impedance (tuned for coupling to parasitic network)
- M = mutual coupling between implant and human biofield
- Z_{load} = external load (the monitoring/extraction network)

The implant creates a permanent low-impedance path for parasitic coupling—analogous to a hardware backdoor in a communications system. Even if the individual raises their personal Z_0 through spiritual practice, the implant provides a bypass path with coupling coefficient M that maintains extraction access.

Reported aftereffects consistent with impedance modification:

Aftereffect	RF Interpretation
Increased EM sensitivity	Altered antenna bandwidth (wider passband)
Unusual bodily sensations at implant sites	Parasitic resonance at coupling frequencies
Enhanced psychic perception	Impedance matching to previously inaccessible bands
Recurring "visitations"	Maintained phase lock via implant coupling
Fatigue and energy drain	Continuous power extraction through parasitic path

Hybridization as Quarter-Wave Transformer

The most provocative aspect of the abduction literature is the hybrid breeding program reported across thousands of independent cases (Hopkins, 1987; Jacobs, 1998; Mack, 1994). In RF engineering, a **quarter-wave transformer** matches two mismatched impedances by interposing a section with intermediate impedance:

$$Z_{hybrid} = \sqrt{Z_{human} \cdot Z_{non-human}}$$

This is the **dark mirror** of the Adamic design (Chapter 11): where the Seeder intervention created beings impedance-matched to receive Source guidance, hybridization creates beings impedance-matched to bridge human and non-human consciousness systems.

Adamic Design (Ch 11)	Hybridization Program
$Z_{Adamic} = \sqrt{Z_{Source} \cdot Z_{human}}$	$Z_{hybrid} = \sqrt{Z_{human} \cdot Z_{non-human}}$

Adamic Design (Ch 11)	Hybridization Program
Purpose: facilitate Source connection	Purpose: facilitate cross-species coupling
Guided evolution toward higher coherence	Engineered blending for access optimization
Consensual (partnership model)	Non-consensual (extraction model)

Key Research

- **Whitley Strieber** (*Communion*, 1987): Detailed phenomenological account of repeated abduction experiences, including descriptions consistent with RLC parameter modification—altered perception, enhanced sensitivity, persistent coupling effects
- **John Mack** (Harvard, 200+ cases, 1990–2004): Clinical documentation under psychiatric protocols; experiencers showed consistent patterns of altered consciousness parameters post-event, with no conventional psychiatric diagnosis fitting the reported experiences
- **Budd Hopkins** (*Missing Time*, 1981; *Intruders*, 1987): Pioneered hypnotic regression protocols revealing consistent narrative structures across independent experiencers—suggesting a common signal source rather than individual confabulation
- **MILAB (Military Abduction)**: Reports of military involvement in abduction events suggest human factions may have reverse-engineered parasitic coupling technology for their own extraction/control purposes

Cattle Mutilation as Component Harvesting

Many documented cattle mutilation cases have conventional explanations (predator scavenging, decomposition patterns). The "laser-like precision" claim is contested. Cases without conventional explanation remain anomalous. The persistent *unexplained* cases—involving precise surgical removal of specific organs (eyes, ears, reproductive organs, blood)—map to **component harvesting** for biological systems requiring specific torsion-active tissues. The removed organs correspond to high-Q biological resonators (Chapter 6): reproductive organs (highest torsion generation), eyes (optical transducers), blood (iron-based paramagnetic medium).

> **Epistemic Note**: The abduction phenomenon is modeled here phenomenologically—the RF analogy applies to the reported experiences and their documented aftereffects regardless of whether the underlying mechanism is physical extraterrestrial contact, interdimensional interaction, psychic phenomena, or some unknown process. The model does not require commitment to any specific ontology of the phenomenon. What it does predict is specific, testable aftereffects (altered EM sensitivity, measurable implant signatures, modified biofield parameters) that can be investigated regardless of the phenomenon's ultimate nature.